Alteration of the metabolite spectrum of myxobacteria through alternative cultivation and extraction techniques

Dissertation
zur Erlangung des Grades
des Doktors der Naturwissenschaften
der Naturwissenschaftlich-Technischen Fakultät
der Universität des Saarlandes

von

Markus Neuber

Saarbrücken
2022

Tag des Kolloquiums:	02.09.2022
Dekan:	Prof. Dr. Jörn Walter
Berichterstatter:	Prof. Dr. Rolf Müller
	Prof. Dr. Christoph Wittmann
Vorsitz:	Prof. Dr. Claus-Michael Lehr
Akad. Mitarbeiter:	Dr. Marc Stierhof

Die vorliegende Arbeit wurde von Mai 2018 bis Juni 2022 unter der Anleitung von Herrn Prof. Dr. Rolf Müller am Helmholtz-Institut für Pharmazeutische Forschung Saarland (HIPS) angefertigt.

„Ohne Spekulation gibt es keine neue Beobachtung.“

Charles Darwin, Brief an Alfred Russel Wallace, 22. Dezember 1857

Danksagungen

Hiermit möchte ich allen danken, die zur Verwirklichung dieser Doktorarbeit beigetragen haben. In erster Line möchte ich meinem Doktorvater Rolf Müller danken, für die Chance die er mir eingeräumt hat, durch verschiedene Projekte in seiner Arbeitsgruppe meine Promotion erfolgreich zu absolvieren. Zahlreiche Gespräche und inspirierende Diskussionen unterstützten mich auf meinem Weg zum Wissenschaftler und führten gelichzeitig zu neuen wissenschaftlichen Erkenntnissen.

Ebenfalls möchte ich mich bei Prof. Dr. Christoph Wittmann für die ausgiebigen Diskussionen während der Promotionskomitees und für die Unterstützung als wissenschaftlicher Begleiter bedanken.

Ein großes Dankeschön geht an meinen wissenschaftlichen Betreuer Dr. Daniel Krug für seine Einsatzbereitschaft und Engagement. Seine Tür stand jederzeit während der Promotion für fachliche Gespräche, hilfreiche Ratschläge und auch für neue Projektideen offen.

Mein ausdrücklicher Dank gilt vor allem meinen Familien, die mich zum einen während des gesamten Vorhabens des Studiums stetig unterstützten und auf der anderen Seite meine neu dazu gewonnene Familie die mich herzlichst in ihren Kreis aufgenommen haben. Allerdings ohne meine Frau Stefanie, die mich in so mancher verrückten Stunde während des Schreibens immer tatkräftig unterstützt hat und meiner Tochter Elena der ich hiermit sagen möchte „Ich kann es kaum erwarten, dich im Arm zu halten“, hätte ich diese Herausforderung nicht gemeistert.

Ein besonderes Lob gilt ebenfalls der gesamten Arbeitsgruppe mit ihrer fachlichen Kompetenz, ohne die es nicht möglich gewesen wäre in den letzten 4 Jahren dies Doktorarbeit fertigzustellen. Insbesondere danke ich meinen guten Kollegen Joachim Hug, Sebastian Adam und Sebastian Walesch für das Korrekturlesen dieser Arbeit. Ebenfalls einen herzlichen Dank an das komplette TA-Team welche eine tolle Arbeit machen um das Labor am Laufen zu halten. Natürlich möchte ich mich auch bei allen anderen Kollegen und Kolleginnen für die schöne Zeit bedanken, die wir nicht nur ausschließlich im Labor hatten, sondern auch für die vielen schönen Stunden die wir alle zusammen mit abwechslungsreichen Unternehmungen verbracht haben.

Summary

Myxobacteria are a vast group of soil-living bacteria that have the ability to form extraordinary natural products with unique structures and bioactive properties. Natural products are synthesised by a number of biosynthetic pathways. The genetic information for these biosyntheses are encoded in biosynthetic gene clusters (BGC) found in the bacterial genome. Recent genome sequencing of myxobacteria indicated that a discrepancy exists between the annotated BGCs and the resulting natural products, suggesting that not every biosynthetic pathway are expressed under the chosen cultivation conditions. With the aim to identify more of the potential natural products, this thesis aimed to develop a co-cultivation strategy, establish a new solid-liquid cultivation platform and utilise an alternative extraction technique to exploit the hidden potential of further myxobacterial natural products. The formation of natural products was investigated using metabolome and bioactivity studies together with genome-based approaches, including the analysis of mass spectroscopic data by statistical data analysis and spectroscopic methods for structure elucidation. These achievements have generated a new set of secondary metabolites and led to the discovery of a novel myxobacterial class of natural products with remarkable antimycobacterial activity.

Zusammenfassung

Myxobakterien sind eine große Gruppe von im Boden lebenden Bakterien, die in der Lage sind, außergewöhnliche Naturstoffe mit einzigartigen Strukturen und bioaktiven Eigenschaften zu bilden. Naturstoffe werden über eine Reihe von verschiedenen Biosynthesewegen synthetisiert. Die genetische Information für solche eine Biosynthese sind in biosynthetischen Genclustern (BGC) im bakteriellen Genom lokalisiert. Genomsequenzierungen von Myxobakterien haben gezeigt, dass eine Diskrepanz zwischen den annotierten BGCs und den daraus resultierenden Naturstoffen besteht, was darauf hindeutet, dass nicht alle Biosynthesewege unter den gewählten Kultivierungsbedingungen exprimiert werden. Mit dem Ziel, weitere potenzielle Naturstoffe zu identifizieren, wurde in dieser Arbeit eine Co-Kultivierungsstrategie entwickelt, eine neue Fest-Flüssig-Kultivierungsplattform entwickelt und eine alternative Extraktionstechnik angewandt, um das verborgene Potenzial weiterer myxobakterieller Naturstoffe zu erschließen. Die Bildung von Naturstoffen wurde durch Metabolom- und Bioaktivitätsstudien zusammen mit genombasierten Ansätzen untersucht, einschließlich der Analyse massenspektroskopischer Daten mittels statistische Datenanalyse und spektroskopische Methoden zur Strukturaufklärung. Diese Errungenschaften haben eine Reihe von neuen sekundär Metaboliten hervorgebracht und zur Entdeckung einer neuen myxobakteriellen Klasse von Naturstoffen mit bemerkenswerter antimykobakterieller Aktivität geführt.

Veröffentlichungen

Die folgende Publikation ist während des Zeitraums dieser Arbeit entstanden:

Bader, Chantal D.; **Neuber, Markus**; Panter, Fabian; Krug, Daniel; Müller, Rolf (2020): Supercritical Fluid Extraction Enhances Discovery of Secondary Metabolites from Myxobacteria. In: *Anal. Chem.* 92 (23), S. 15403–15411. DOI: 10.1021/acs.analchem.0c02995.

Conference Contributions (Posters and oral presentations)

Markus Neuber; Daniel Krug and Rolf Müller; Development of co-cultivation strategies to access novel secondary metabolites from myxobacteria. **Poster presentation** International VAAM Workshop 2019; Jena, Germany

Markus Neuber; Development of co-cultivation strategies to access novel secondary metabolites from myxobacteria. **Oral presentation** 8th Summer Symposium of Interdisciplinary Graduate School Symposium 2019, Saarbrücken, Germany

Markus Neuber; Daniel Krug and Rolf Müller; Development of co-cultivation strategies to access novel secondary metabolites from myxobacteria. **Poster presentation** 10th International HIPS Symposium 2020; Jena, Germany

Table of Contents

Chapter 1

1. Introduction

1.1 Natural products

Natural products (NPs) are small molecules produced by living organisms, such as plants, algae, fungi and bacteria. NPs feature structurally diverse chemical scaffolds and unique pharmacological or biological activities due to natural selection and evolutionary processes that have shaped their utility over hundreds of thousands of years[1]. Generally, NPs are often subdivided in two main classes: primary and secondary metabolites. The difference between primary and secondary metabolites is not clearly defined, as many intermediates originating from primary metabolism overlap with intermediates from secondary metabolism[2]. However, primary metabolites are components of basic metabolic pathways that are essential for living organisms. They are involved in fundamental cellular functions such as nutrient uptake, energy production, development and cell growth[3]. Primary metabolites include building blocks required to make the four major macromolecules within living organisms: carbohydrates, lipids, proteins, and nucleic acids[4,5]. Secondary metabolites originate from different nodes of core primary metabolic pathways, suggesting that the developing enzymatic activities different from primary metabolism may result in new compounds that could improve the adaptation of organisms to their specific environment[6]. Secondary metabolites serve also as a buffering zone into which excessive carbon (C) and nitrogen (N) can be temporarily deposited. When required, the stored C and N can be converted back into primary metabolism through metabolic degradation of secondary metabolites[7]. There is a delicate balance between the activities of primary and secondary metabolism being influenced by cell growth and development, tissue differentiation and also other external influences[8]. Therefore, NPs or secondary metabolites can be defined as a heterogeneous group of metabolites that are not essential for vegetative growth of the producing organism. Nevertheless, NPs can be considered as differentiation compounds conferring adaptive roles, for example, by functioning as defence compounds or signalling molecules in ecological interactions with other living organisms, *via* symbiosis, nutrient acquisition, metal transport or competition[9,10].

SM are commonly used in research and biotechnology due to their broad spectrum of physiological properties and unique ecological or biological effects. Therefore many microbial

NPs, their semisynthetic derivatives and synthetic analogues are usually used in medicine for the treatment of a range of clinical disorders, e.g. infectious diseases and cancer[11] including the usage as antibiotics[10], antifungals[12], siderophores[13], antivirals[14], quorum-sensing molecules[15], and immunosuppressants[16]. Although pharmaceutical companies have reduced their efforts in NP drug discovery and development significantly in recent years, NPs are still an important source of clinically-used drugs and novel lead structures comprising very small molecules such as acetylsalicylic acid, but also larger chemical structures, such as Taxol.

Despite the benefits and numerous successful examples of drug discovery, pharmaceutical companies have downscaled their NP-based drug discovery programmes as it has led to several drawbacks, such as the rediscovery of known NPs[17]. To avoid replicate discovery as a typical workflow mistake while screening libraries of extracts from natural sources, dereplication tools can help to identify in earlier stage the known bioactive compound[18]. The use of an appropriate method to isolate and characterise bioactive NPs from different biological materials can also be challenging. Nevertheless, NPs remain a reliable source of potential drug candidates derived from the biologically enormous diverse flora and fauna of the earth. NPs are thought to be produced as a consequence of millions of years of evolution of terrestrial and marine organisms adapting to various environmental conditions for example by biotic and abiotic stress factors[19,20]. History has shown that NPs have played a crucial role in drug discovery, especially for infectious diseases and cancer[17,21], but also in other therapeutic fields, such as cardiovascular diseases (e.g. statins) or multiple sclerosis (e.g. fingolimod)[22,23]. Compared to conventional synthetic molecules, NPs offer special properties such as their enormous scaffold diversity and structural complexity that provide both advantages and challenges for the drug discovery process[24]. NPs are in this respect regarded as "privileged" chemical scaffolds that could also have either a biological function or bioactivity against infectious pathogens.

NPs derived from plants have always played an essential role in human healthcare and their use in traditional medicine of different cultures is documented[25]. Some relevant example is the sesquiterpene lactone endoperoxide named artemisinin, from the plant *Artemisia annua*, which is highly effective in the treatment of malaria against multi-drug-resistant *Plasmodium spp.*. In addition, plants are also used in the treatment of cancer diseases[26]. One of the most intriguing plant-derived anticancer drugs is paclitaxol, discovered in 1962, which is produced together with several key precursors (baccatins) in the leaves of various *Taxus*

species[27,28]. The success of paclitaxel led to extensive studies on the synthesis of analogues, resulting in docetaxel as the first developed close chemical relative[29].

A fruitful source of structurally diverse biologically active molecules are terrestrial microorganisms, which have yielded some of the most important products for the pharmaceutical industry, especially for the treatment of human infectious diseases. The serendipitous discovery of penicillin from the filamentous fungus *Penicillium notatum* by Fleming in 1929 and its widespread therapeutic usage in the 1940s launched a new era termed "Golden Age of Antibiotics"[8,29]. Furthermore, other antibacterial agents such as cephalosporins (from *Cephalosporium acremonium*), aminoglycosides, tetracyclines and other polyketides with different chemical scaffolds (from the order *Actinomycetales*), and anthelmintics and antiparasitic drugs, such as the ivermectins (from *Streptomyces sp.*)[30] have been discovered and implemented in clinical usage during the “Golden Age of Antibiotics ". Cyclosporins (from *Trichoderma* and *Tolypocladium sp.*) and rapamycin (from *Streptomyces sp.*) with their immunosuppressive properties were also identified in this era[31].

The aforementioned examples of crucial pharmaceuticals demonstrate the relevance of NPs in the treatment against life-threating pathogens and diseases. The successes of the "Golden Age of Antibiotics" has been followed by a considerable period of disruption in the identification of new chemical scaffolds, which started in the 1960s and lasted until the early 1990s[32]. Unfortunately, the increase in global antimicrobial resistance has been accompanied by a failure to discover antibacterial agents. However, also high-throughput biochemical screenings of large chemical libraries were often unable to find promising compounds with the required physical and chemical properties. If promising lead compounds were found, they failed mainly due to the difficulty of developing antibacterial agents with a suitable product profile with efficacy against a broad spectrum of pathogens or against Gram-negative organisms that are difficult to treat. Despite all undertakings, the introduction of novel antibiotics or chemical scaffolds was not as effective as expected in more than two decades[32].

In particular, Gram-negative bacteria cause two-thirds of the infections in intensive care units and resistance of these microorganisms to certain antibiotics is a serious problem[33]. A number of multidrug-resistant, Gram-negative microorganisms such as carbapenem-resistant *Acinetobacter baumannii*, *Pseudomonas aeruginosa* and Enterobacterales are ranked in the latest WHO list of high-priority pathogens[34].

The crisis in novel antibiotic discovery is also leading to a resurgence of NP research. Some chemical scaffolds already known but abandoned in the past are now being revived with some success[35]. This topic indicates that NPs synthesised by microorganisms are an excellent source for researchers to discover. On the one hand, the isolation of new microbial taxa from underexplored environments is beneficial and needed, as is the successful cultivation in the laboratory of possibly innovative organisms in order to expand the diversity of accessible secondary metabolites. On the other hand, developing approaches to diversify the metabolome of already cultured bacteria by activating non-expressed biosynthetic gene clusters (BGCs) can lead to various SMs or new chemical moieties.

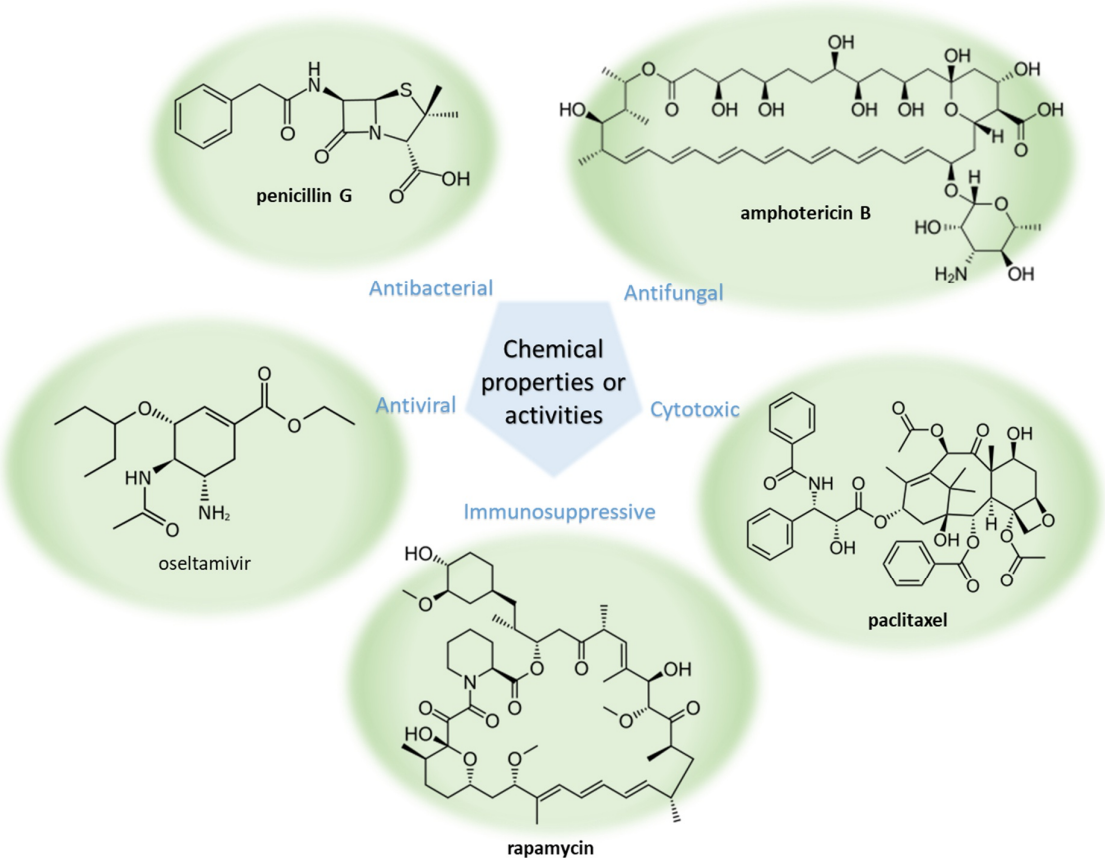

Figure 1.1: Drugs in medical application und their corresponding chemical properties/activities.

1.2 Classification of natural products

So far, over one million compounds[36] are already known and there is no rigid scheme of classifying NPs – their remarkable diversity in function, structure and biosynthesis is too complex to fit into a few simple categories. However, scientists in that field defined five main classes of SMs: terpenes, terpenoids and steroids, alkaloids, fatty acid-derived substances and polyketides, non-ribosomal polypeptides and enzyme cofactors[37] (Figure 1.2).

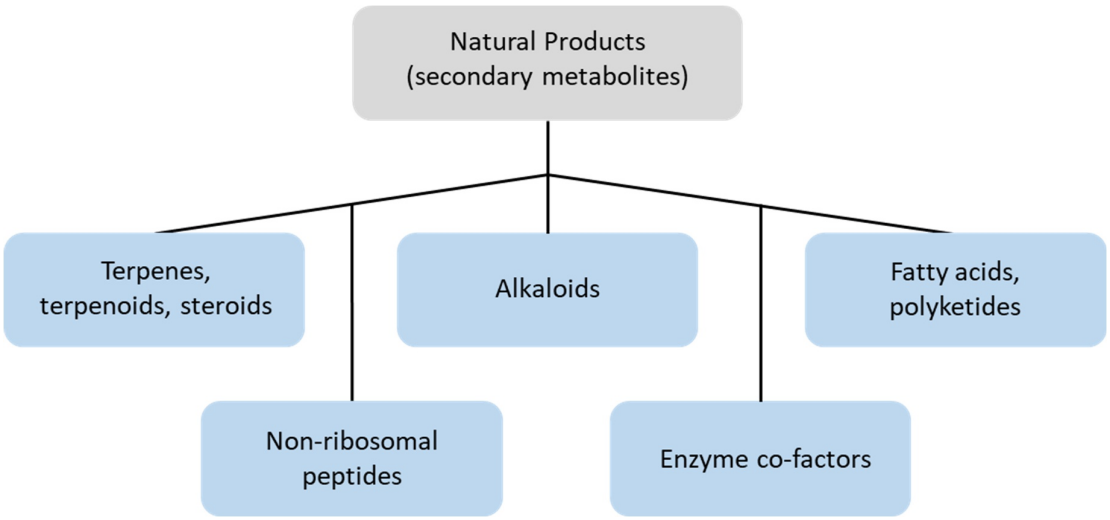

Figure 1.2: Classification of natural products.

Terpenes, terpenoids & steroids

Terpenes, terpenoids and steroids comprise a vast group of more than 30.000 known substances, which derive biosynthetically from isopentenyl diphosphate[38]. Terpenes belong to the biggest class of secondary metabolites and they consist of relatively simple five-carbon isoprene units (Figure 1.3), which are connected to each other in numerous ways. Terpenes are simple hydrocarbons, while terpenoids are a modified class of terpenes with different functional groups and oxidized methyl group moved or removed at various positions. Terpenoids are distinguished according to their number of carbon units into monoterpenes, sesquiterpenes, diterpenes, sesterpenes and triterpenes[39]. These terpenoids also have immense variety of apparently unrelated structures, while steroids have a common tetracyclic carbon moiety and are modified terpenoids that are biosynthesized from the triterpene lanosterol.

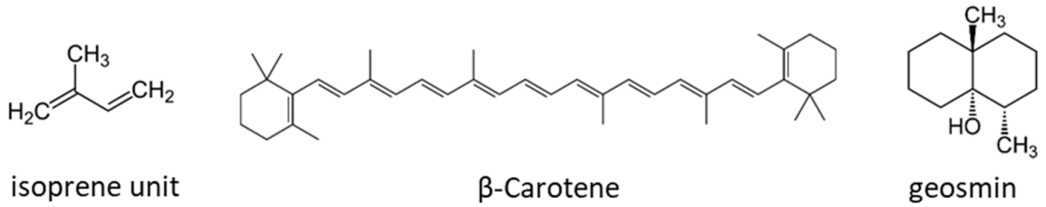

Figure 1.3: Chemical structures of isoprene unit, terpenoids and steroids[40].

Geosmin is a naturally occurring bicyclic alcohol produced, as one example, by the Gram-positive soil bacterium *Streptomyces avermitilis*[41]. The substance has a distinct earthy-musty smelling and is partly responsible for the typical soil smell in the forest after rainfalls[42,43]. A majority of terpenoids, which differ in structure, are biologically active compounds and have been used worldwide for the treatment of various diseases[44,45].

Alkaloids

About 20.000 alkaloids are known[46], which group into organic, nitrogenous and mostly alkaline NPs. They contain an amine group in their structure, which is biosynthetically derived from amino acids. Due to these nitrogen subunits, these compounds behave alkaline. Usually, the nitrogen atoms are located in a cyclic ring system. Such compounds play a major role in living organisms and can be synthetized as secondary metabolites by plants and some animals.

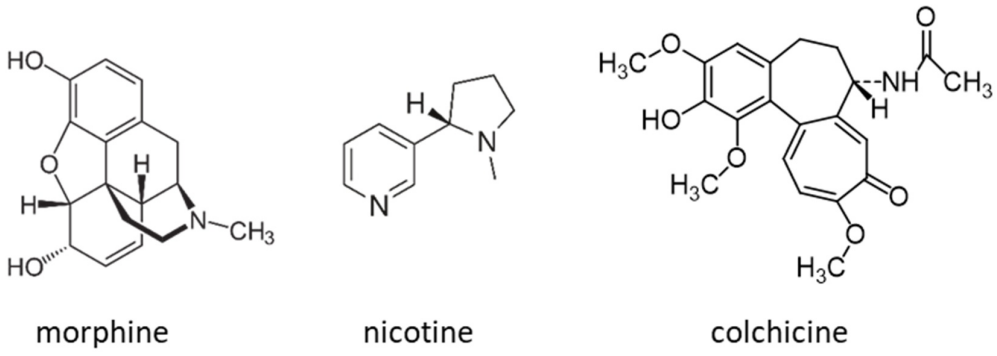

Figure 1.4: Chemical structures of alkaloids.

In general, alkaloids can be classified based on their chemical structure into classes such as indoles, quinolines, isoquinolines, pyrrolidines, pyridines, pyrrolizidines, tropanes, and terpenoids and steroids[47,48]. Morphine was isolated from the plant *Papaver somniferum* in 1804[49] and is one of the most popular alkaloids in use for medicinal purposes. This alkaloid is a potent narcotic used for pain relief, but its usefulness is limited due to its addictive properties[50].

Fatty acids & polyketides

About 10.000 known compounds are fatty acid-derived substances and polyketides (Figure 1.5), which are biosynthesized out of simple acyl precursors such as acetyl coenzyme A (CoA), methylmalonyl CoA and propionyl CoA[51]. In the case of NPs derived from fatty acids, the oxygen atoms are usually removed during their synthesis. In contrast, polyketides, such as the antibiotic erythromycin A isolated from soli bacterium *Saccharopolyspora erythraea*[52], often have more than one oxygen substituents incorporated[53,54].

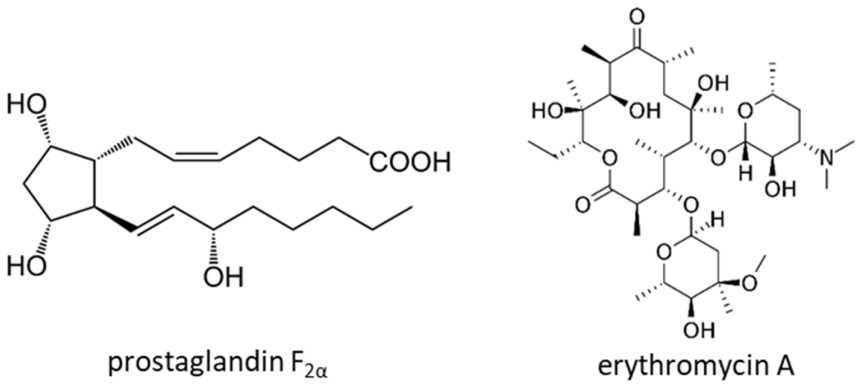

Figure 1.5: Chemical structures of a fatty acid derived compound and a polyketide.

Non-ribosomal peptides

Non-ribosomal peptides are synthesized from amino acids by a multifunctional enzyme complex without a direct RNA description/template. The vast diversity of non-ribosomal peptides can be attributed to their ability to integrate a more diverse range of monomers than ribosomal peptide biosynthesis and to extensively modify the peptide both during and after chain assembly[55,56].

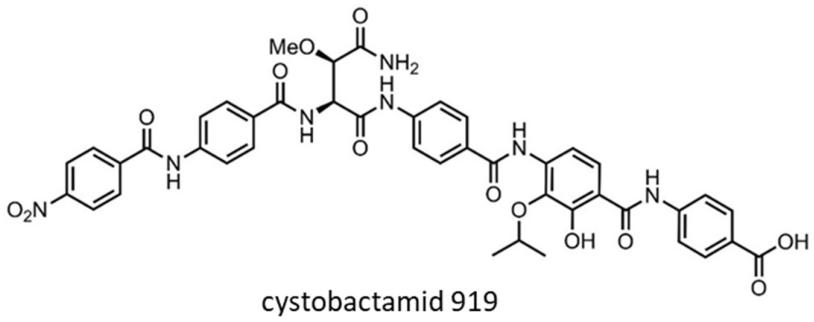

Figure 1.6: Chemical structure of the non-ribosomal peptide cystobactamid.[57]

For example, cystobactamid 919 (Figure 1.6) is biosynthesized by an non-ribosomal peptide synthetases (NRPS) and is a newly discovered natural product isolated from *Cystobacter* sp., which exhibits strong antibacterial activity against *E. coli* and other Gram-negative bacteria in the submicromolar range[57].

Enzyme cofactors

Enzyme cofactors are non-protein chemical compounds or metallic ions, which are required for catalytic activity of specific proteins. Cofactors can be divided in two major groups: organic co-factors, such as biotin; and inorganic co-factors, such as metal ions. Organic cofactors such as vitamins (vitamin K) and non-vitamins (adenosine triphosphate) are small organic molecules, which feature typically a molecular mass less than 1000 Da. Metal ions are essential trace elements that include for example iron, magnesium, manganese, cobalt, copper, zinc, and molybdenum.

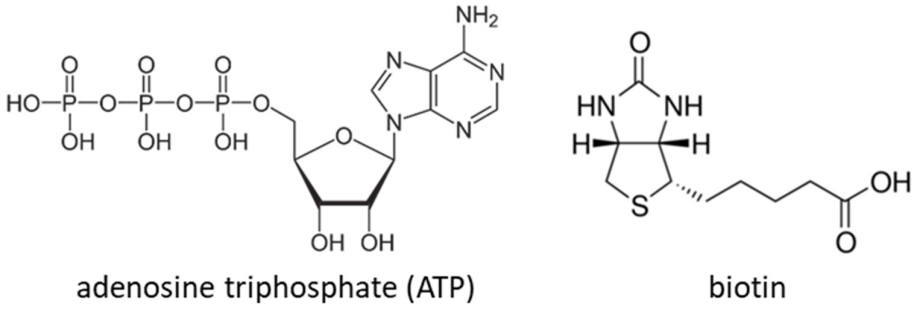

Figure 1.7: Chemical structures of cofactors from enzymes.

Biotin is the major enzymatic cofactor involved in carbon dioxide metabolism; it serves as cofactor and is required for the transfer of CO_2[58]. In fact, biotin-dependent enzymes in nature are ubiquitous and participate in a vast number of metabolic processes, which include fatty acid synthesis and gluconeogenesis[59].

1.3 Bacteria as source for natural products

About 6000 antibiotics have been described, 4000 from *Actinobacteria*[60,61] but there are additional members of *Proteobacteria*[62] and *Firmicutes* that produce antibiotics. In recent years, myxobacteria and cyanobacteria have also joined these important organisms as productive species.

As early as 1892, Roland Thaxter recognised that myxobacteria represent an independent and extraordinary group of bacteria[63]. Myxobacteria belong to the δ-group of proteobacteria, which are phylogenetically related to the order *Myxococcales*[64,65]. This order is subdivided into *Cystobacterineae*, to which *Stigmatella aurantiaca* belongs, *Sorangineae* to which *Sorangium cellulosum* belongs, and *Nannocystineae*[66] of which *Nannocystis exedens* is a member. Myxobacteria are Gram-negative unicellular microorganisms, strictly aerobic, chemoheterotrophic soil bacteria with a rod-shaped cell structure and a length of 3 to 12 µm[67]. Myxobacteria usually live in the topmost layer of soil, but they can also be found in freshwater or marine environments [68].

These extraordinary Gram-negative bacteria feature an exceptional life cycle that involves the development of fruiting bodies. This procedure is reminiscent of fruiting body development in slime molds and can be seen as an example of convergent evolution[69]. The nutrient deficiency-induced process first leads to an aggregation of vegetative cells into mounds, which then subsequently lead to forming fruiting bodies in which the rod-shaped cells will undergo morphogenesis to form spherical myxospores[70–72]. The shape and colours of the cells and fruiting bodies vary from milky, yellow, orange, red, and brown to black are the result of carotenoid and melanoid pigments that provide protection against photooxidation[73,74].

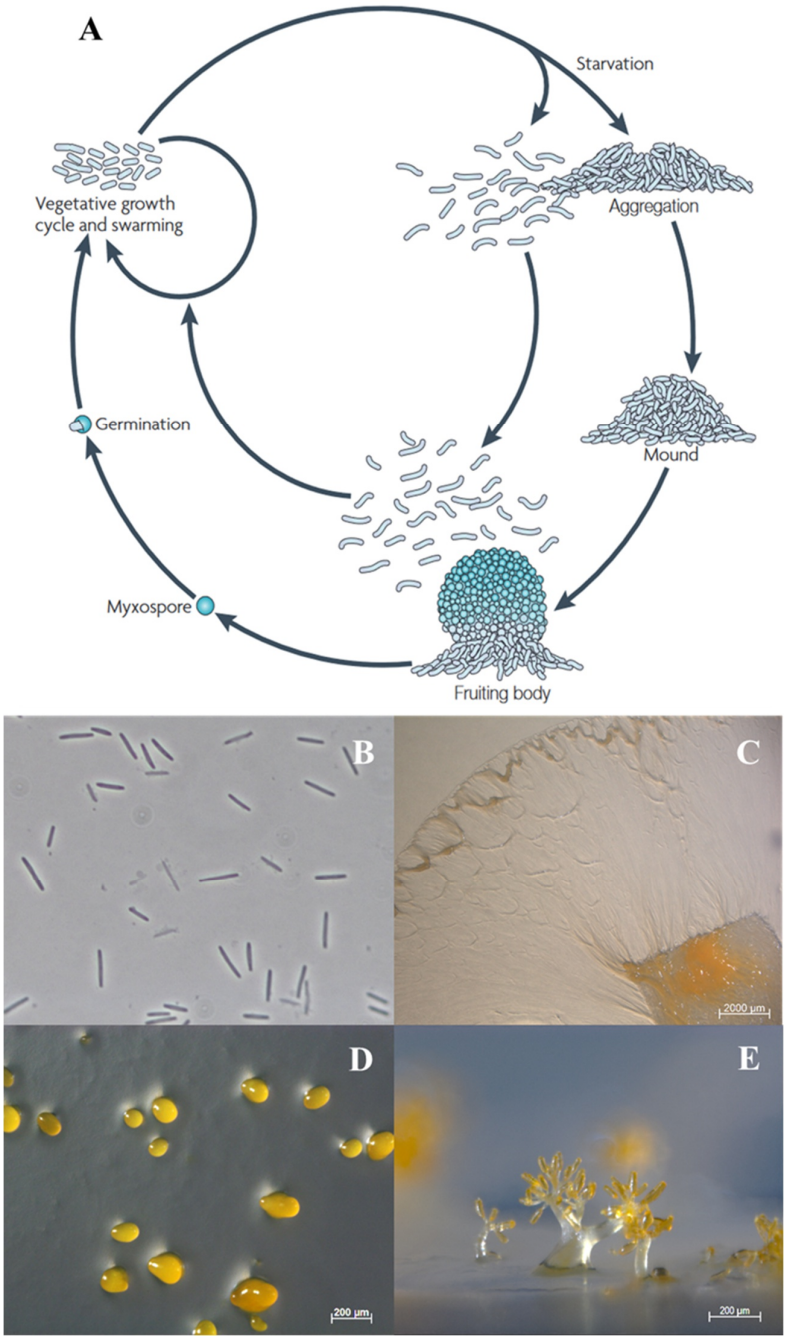

Figure 1.8: (**A**) *Myxococcus xanthus* life cycle described by Zusman, Scott *et al.*[75]. Upon starvation, cells aggregate into microscopic mounds, and forming fruiting bodies in which the rod-shaped cell will undergo morphogenesis to spherical myxospores. These myxospores can germinate under nutrient-rich conditions. (B-E) Stages of development from myxobacteria. (**B**) Vegetative cells of *Myxococcus fulvus* Mxf50 in liquid media. (**C**) Swarming cells of *Sorangium sp.* on agar. Fruiting bodies of (**D**) *Myxococcus sp.* and (**E**) *Chondromyces apiculatus* on solid agar. Figures provided by Dr. Ronald Garcia.

In addition to their particular life cycle, myxobacteria feature other unique characteristics such as gliding motility on solid surfaces and their social behaviour like for example synchronized selective swarming based on chemical communication[76]. These underlying complex physiological and morphological processes are enabled only by distinct cell-cell communication, which finally led to the term "social bacteria" after studying these communication pathways[77]. Their social behaviour also apparent itself in foraging, when they prey as united cell structure. *Myxococcus xanthus* have the ability to lyse bacteria and yeasts by secreting *exo*-enzymes in order to metabolise the achieved lysates as nutrients[78,79]. *Exo*-enzymes may also be employed to degrade biopolymers like cellulose in order to use them as a carbon source[80].

Another outstanding feature of myxobacteria is the size of their chromosomes, which ranges from 9 to 16 Mb. The myxobacterium *Minicystis rosea* DSM 24000 currently has one of the largest bacterial chromosomes published to date[81]. Several studies already indicating there are tight correlations between the production of secondary metabolites and cellular development in myxobacteria[82]. Myxobacterial species are significantly less studied compared to other bacteria such as actinomycetes, but nevertheless, these microorganisms already contributed to the discovery of more than hundred families of bioactive compounds. Myxobacterial secondary metabolites displays numerous new modes of action with various biologically activities e.g. antifungal (ambruticin[83]), immunomodulatory (argyrin[84]), antiviral (aetheramide[85]), antibacterial (cystobactermid[57], myxovalargin[86], myxopyronin[87]), cytotoxic (epothioline[88]), antiplasmodial (chlorotonil[89]) and antifilarial (corallopyronin[90]). Ambruticin is a cyclopropyl-polyene, which exhibits antifungal activity and was one of the first isolated compounds from myxobacteria[83]. Corallopyronin and myxopyronin represent a promising class of α-pyron antibiotics for further development as antibacterial agents including therapeutic applications against *Wolbachia* bacteria. These potential antibiotics are particularly important for the treatment of rifampicin-resistant bacteria because they bind to a novel target site of bacterial RNA polymerase[91].

In summary, the NPs synthesised by myxobacteria, with their diverse range of bioactivities and novel chemical scaffolds, provide a unique opportunity to engineer them into potential lead structures for future therapeutics. It is encouraging to note that the potential of myxobacteria as a source of natural products has not yet been exhausted, as new strains are still frequently isolated from environmental niches[92]. A taxonomic study highlighting the cor-

relation between genetic distance and the production of certain NP families therefore supports efforts to focus on insufficiently studied natural product producers that are phylogenetically as distant as possible from other myxobacteria in order to obtain new compounds[93]. Especially, the exploration of myxobacterial organisms from novel genera as well as additional representatives within an already characterised genus seems to be a superb starting point to identify new NPs.

1.4 The biosynthesis of natural products

In the biosynthesis of NPs, a limited number of monomeric building blocks from primary metabolism is used to assemble a variety of different secondary metabolites as part of the biosynthetic pathway. Therefore, a biosynthetic gene cluster (BGCs) consists of a group of co-located genes within the genome, which is involved in a common, discrete metabolic pathway. BGCs are a common characteristic of bacterial[94] and most fungal genomes[95], and their expression is often co-regulated. The spectrum of substances produced ranges from numerous pharmaceutical drugs, natural toxins, and compounds involved in chemical communication or chemical warfare of competing organisms. Non-ribosomal peptide synthetases (NRPSs) and polyketide synthases (PKSs) are two of the main classes of biosynthetic machineries and are particularly unique multifunctional enzymes that exhibit modular organization. These enzymes act as biosynthetic protein machines that identify specific substrates through their unique three-dimensional structures and catalyse the transformation of these substrates towards novel biomolecules[96]. These two classes of BGCs, encompass most of the known antibiotics, antifungals, and other potential clinical agents[97,98].

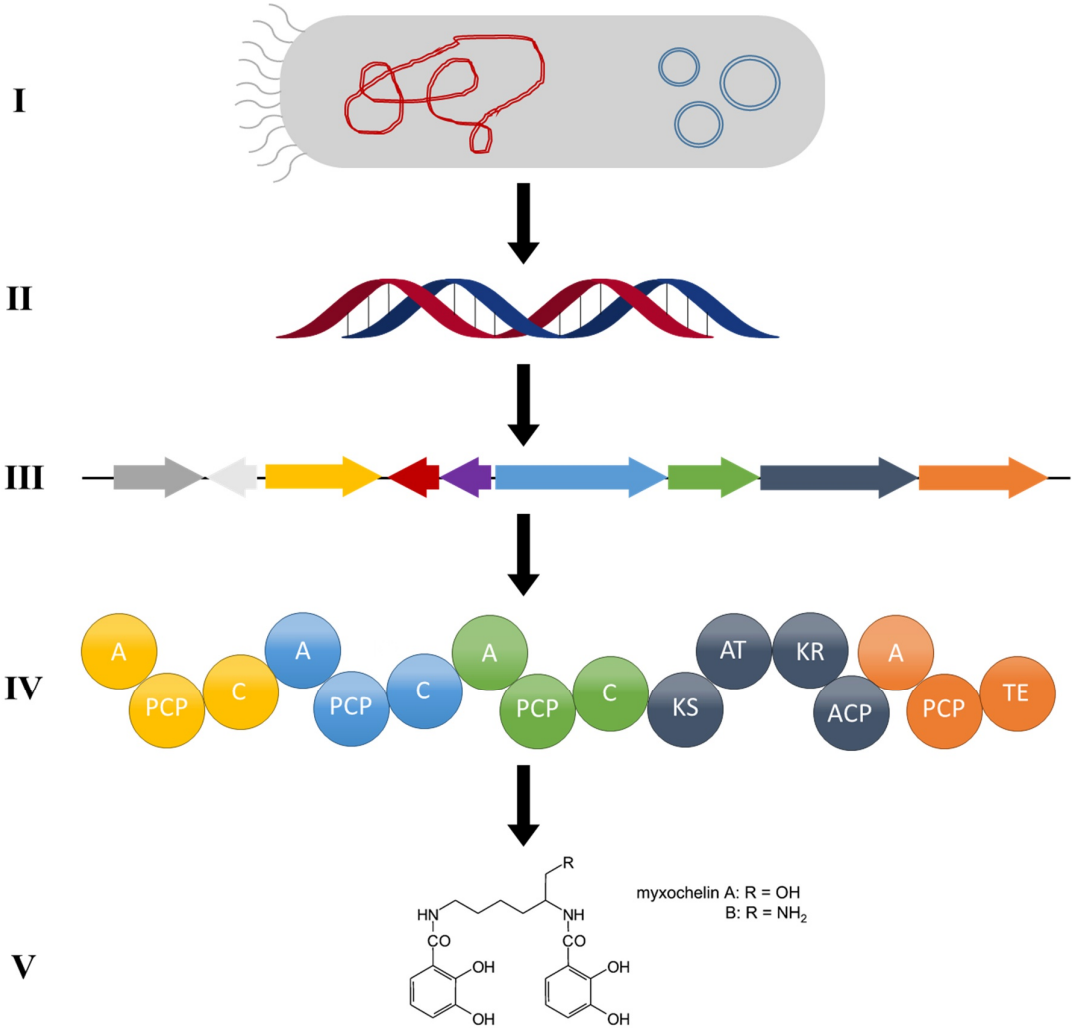

Figure 1.9: General scheme of elements required for the biosynthesis of NPs. (**I**) Bacterium containing genomic DNA (red) and circular plasmids (blue). (**II**) Genomic DNA encoding for BGCs. (**III**) Construction of biosynthetic gene cluster located in the genome that codes for distinct PKS and/or NRPS modules. (**IV**) Exemplary hierarchical architecture of non-ribosomal multi-modular enzyme machinery in combination with PKS module for the synthesis (**V**) of myxochelin as natural product in several chemical reaction steps[99]. A – adenylation domain ;ACP – acyl carrier protein; AT – acyltransferase, C – condensation domain ; KR – ketoreductase, KS – ketosynthase, PCP – peptidyl carrier protein, TE – thioesterase.

In the past years, genome studies on actinomycetes[100] and myxobacteria[101] indicated that many secondary metabolites are biosynthesized through PKS/NRPS hybrid systems. The research on actinomycetes resulted in the discovery of some PKS/NRPS hybrid system responsible for the synthesis of rapamycin[102,103] and naphthomycin[104]. Myxothiazol[105,106] and the myxalamids[107] represent two electron transport inhibitors, which are produced by a number of strains of myxobacterium *Stigmatella aurantiaca* and both molecules are biosynthesized by a PKS/NRPS hybrid assembly line as mentioned above.

Polyketide synthases

Polyketide synthases (PKS) can be classified into three types (I, II, and III) according to their organization and catalytic mechanisms; however numerous exceptions and variations of PKS-based assembly lines are known and impede a simple classification into three types[108]. For example, a modular type I PKS is an enzyme assembly line for the biosynthesis of chemically versatile polyketide NPs, which are the basis for almost one-third of medicinal products [109]. This type I PKS system is similar to fatty acid synthases in the way that both catalyse the assembly of several acetate-derived building blocks through Claisen condensation[110] to form a long polyketide chain. Therefore, type I PKS modules act successively in polyketide chain in three steps: elongation, processing and termination. Modular type I PKSs of this kind are hierarchical, i.e. the entire enzyme complex consists of several subunits, each subunit consists of several modules, and a module consists of several domains[111].

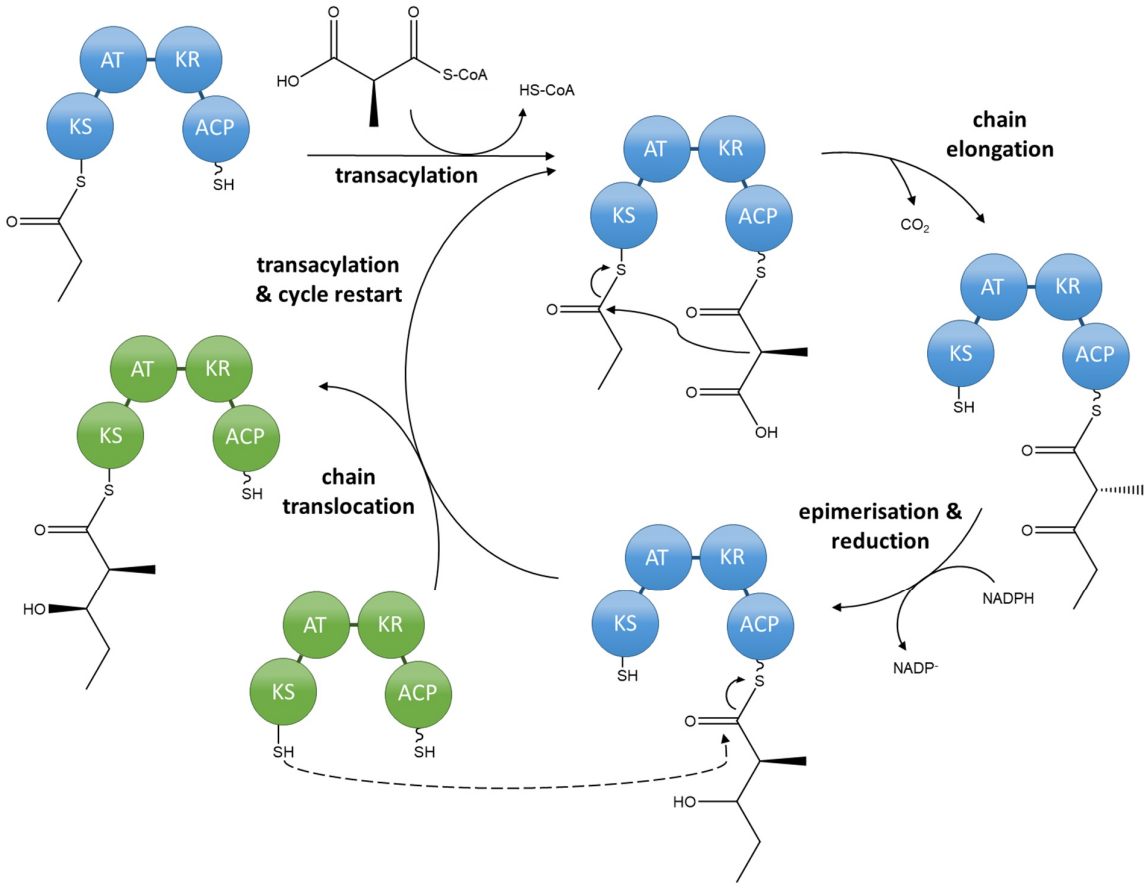

Figure 1.10: Domain architectures and mechanisms of polyketide chain extension in modular PKS. Catalytic cycle of polyketide chain extension exemplified by two elongation modules (blue & green). AT-catalyzed

transacylation with (2*S*)-methylmalonyl-CoA, followed by KS-mediated decarboxylative Claisen condensation (chain elongation) to get the (2*R*)-2-methyl-3-ketoacyl-ACP[53]. The KR (blue module) catalyzes the epimerization of the C2 methyl group, followed by diastereospecific reduction to obtain the product (2*S*,3*R*)-2-methyl-3-hydroxydiketide. The translocation of the diketide to the KS domain (green module) in the downstream direction to the substrate-accepting module, from which the next round of reactions can initiate[112]. ACP, acyl carrier protein; AT, acyltransferase; KR, ketoreductase; KS, ketosynthase.

The minimal PKS module contains three domains: (i) an acyltransferase (AT), (ii) an acyl carrier protein (ACP), and (iii) a ketosynthase (KS) that extend the linear sequence of an intermediate by two carbon atoms. The AT domain loads the chain extender moiety (usually malonyl- or methylmalonyl-CoA) and ACP for tethering and transporting the extension unit or polyketide intermediate. Afterwards, the KS domain catalyses the condensation reaction between the extender unit of the downstream of the ACP domain and the polyketide intermediate, which are bound to the active KS site, displaced from the ACP domain of the upstream module[113]. In PKS assembly lines, ketoreductase (KR) domains are the most abundant processing domains located between the AT and ACP domain acting as a reductive loop. Such KR domain executes the NADPH-mediated reduction reaction of β-keto group to β-hydroxyl group and thus determines the stereochemistry of α- substituent and β-hydroxyl group[114]. In addition, the dehydratase (DH) domain for the production of a double bond and the enoyl reductase (ER) domain for the production of a saturated C2 unit can also be part of a PKS module.

Non-ribosomal peptide synthetases

Non-ribosomal peptide synthetases (NRPS) are multi-modular megaenzymes catalysing the synthesis of a broad range of NPs of bacterial or fungal origin. NRPS contain multiple active sites (domains) and can be classified into two types depending on their organisation and catalytic mechanisms: modular type I NRPS and independent type II NRPS[115]. Type I modular NRPS are similar to type I modular PKS, with a hierarchical structure of the enzyme complex: subunit, module and domain. The minimal module to perform substrate selection, binding and elongation of the growing polypeptide chain comprises three domains, namely an adenylation (A), a thiolation (T or PCP) and a condensation (C) domain[116] (Figure 1.11).

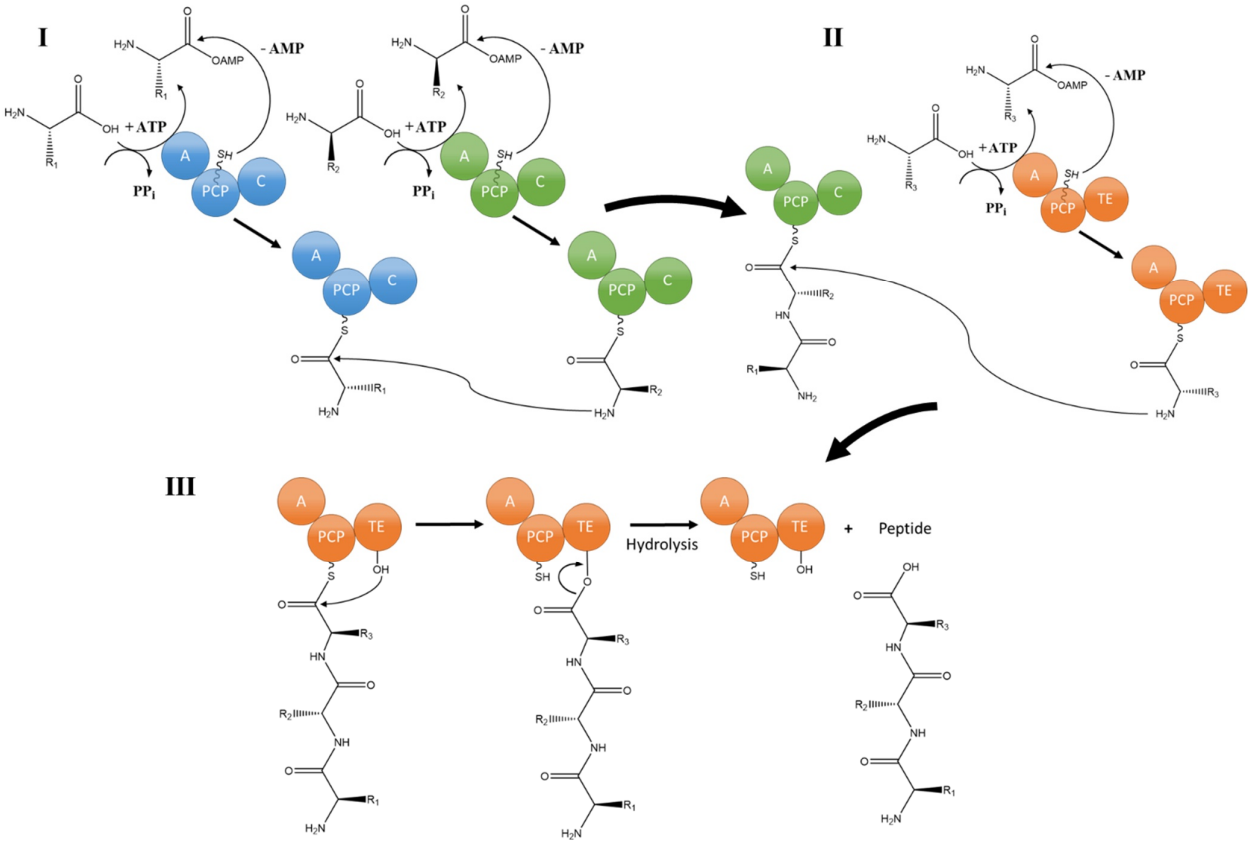

Figure 1.11: Domain architectures and polypeptide biosynthesis in type I modular NRPS. (**I**) Amino acid substrates are activated through reaction with ATP to from an aminoacyl-AMP intermediate, catalyzed by an adenylation domain (A). The aminoacyl-AMP intermediate is then captured by the thiol group attached to the PCP domain. Condensation domain (C) successively catalyses the formation of peptide bonds between the thioester intermediates loaded onto adjacent PCP domains. The first module (blue) is known as the initiation module and subsequent modules (green, orange) are the elongation modules. (**II**) C domain performs the condensation reaction of the peptide bond through nucleophilic attack to the next loaded extender unit for the elongation of the peptide chain by one amino acid. Each module incorporates a single amino acid, hence, depending on the structure; many modules are required to form the final peptide product. (**III**) The final module (orange) contains an additional thioesterase domain (TE) which catalyses hydrolysis or cyclisation to release the peptide from the NRPS. The released peptide can subsequently modified by tailoring enzymes, thus further increasing structural diversity.

A cycle of catalysed reactions within prototypical NRPS modules starts with the recognition of an amino acid substrate by the upstream module, followed by adenosine triphosphate (ATP)-dependent activation as aminoacyl adenylate. The A domain selects the first amino acid of the peptide chain, which can incorporate both proteinogenic and non-proteinogenic amino acids[117] as extender unit. The covalent linkage of the A-domain facilitates transfer of adenosine monophosphate (AMP)-activated amino acid to a PCP domain as a thioester. As the last step, the C domain catalyses the condensation reaction of the peptide

bond through nucleophilic attack of the next loaded extender unit on the acyl thioester of the growing peptide chain to elongate the non-ribosomal peptide with one amino acid[118]. The unloaded PCP domain can now be tethered with a successive substrate molecule after elongation of the peptide backbone. A terminal module is usually located downstream of the last elongation module to release the full-length peptide chain from the enzyme by a terminal thioesterase (TE) domain[119,120]. There are two ways for the TE domain to release the tethered peptide backbone. On one site by simply hydrolysis to a linear polypeptide or through a cyclisation as a macrolactone depending on the reaction catalysed by the TE domain[121].

1.5 Pipeline of natural product discovery

Microbial NP research depends on an interdisciplinary teamwork in the field of natural sciences. In the field of microbiology, traditional approaches start with the isolation of microorganisms from the different environments in order to find new secondary metabolites, e.g. by screening crude extracts for bioactivity against certain pathogens. The recent revolution of affordable whole-genome sequencing has immensely changed the process of discovering new bacterial NPs, and bioinformatics is becoming increasingly important for NPs research.

In general, the development of new medicines ranges between 10 and 18 years and is a highly complex procedure consisting of several steps, in particular the hit identification, the hit to lead optimization and subsequently followed by clinical trials[122]. The estimated average cost varies widely, depending on the therapeutic area for treatment, from $161 million to $4.54 billion[123]. Notably, academic research institutions do not usually have the financial capacity in contrast to pharmaceutical companies to finance all development steps; therefore, they usually focus on basic research to identify hits.

As mentioned in the previous sections, NPs are a noteworthy source of new pharmaceuticals. Before a natural product can be identified as a potential hit, this potential drug candidate needs to be studied in detail and purified from a complex mixture of primary and secondary metabolites contained in the bacterial broth after cultivation. Once the pure natural product is isolated, the structure has to be elucidated in detail to permit in-depth studies on the mode of action, the identification of possible BGCs and the development of synthetic pathways for better access to the compound. The following part deals with the identification of novel NPs from bacteria, in particular the commonly used bioactivity-guided screening

and recently developed genome mining approach, the limitations of both concepts, and new technological devices and strategies to overcome these bottlenecks.

1.5.1 Instrumentation for natural products discovery

A central component of NP discovery is the analytical setup for identification, isolation and structural elucidation of the NP. Therefore, the basic physical method for the analysis and purification of NP is based on the separation of molecules from a crude extract mixture according to the principle of chromatography. Usually, a combination of liquid chromatography coupled with mass spectrometry (LC-MS) is utilised for monitoring, dereplication, and statistical data evaluation on large datasets for metabolic profiles. For the purification of sufficient amounts of a substance, e.g. to determine the chemical structure, semi-preparative HPLC is suited because of the higher throughput of extracts under standard conditions. Nuclear magnetic resonance (NMR) spectroscopy is usually performed for structure elucidation of NPs as a result of 1D and 2D experiments and derivatisation techniques to determine the absolute configuration of a molecule[124]. The following subsection is intended to provide a brief outline of the analytical techniques and fundamental instrumentations used in the field of NP research and the methods applied in the context of this work.

1.5.2 Liquid chromatography coupled with mass spectrometry

A successful approach in natural product discovery mostly depends on sufficient production of the NP of interest for reliable detection. The produced complex mixture of primary and secondary metabolites of bacteria makes it necessary to separate the metabolites in a bacterial extract from each other. For this purpose, the ultra-high performance liquid chromatography (U-HPLC) and related separation techniques were a milestone for the reproducible identification and isolation of NPs from crude extracts. For a long period of time the discovery of NPs was only carried out using LC-based separation and UV/Vis-specific detection of the respective natural product. After the combination of LC with *hr*MS detectors it was possible to provide an accurate mass-to-charge ratio (m/z) information on the eluting molecule, which revolutionised the natural product research by supporting the calculation of proposed molecular sum formula. In addition, significant improvements in chromatographic separation materials allowed highly efficient separation of even complex samples in very short time. Furthermore, data analysis of *hr*MS provides the exact molecular formula and predicted structure of the metabolites by analysing and comparing the fragmentation patterns of the building blocks generated via tandem mass spectrometry (MS^2)

with molecular libraries using advanced commercial software tools such as MetaboScape. Each software tool possesses unique advantages in different steps of pre-processing, data analysis, visualization, and interpretation[125]. That is helpful to create a molecular network of all existing metabolites from extracts by comparing them to molecular libraries, which can help to detect new metabolites from bacterial extracts. In particular, a molecular network of annotated metabolites supports identification of derivatives or analogues belonging to known and unknown compound families produced by the organism. In addition, dereplication is becoming essential as the number of NPs discovered by scientists has increased tremendously in the last two decades[126]. In order to avoid this rediscovery, it is crucial to quickly identify known secondary metabolites in the crude extract[127]. For correct dereplication, information on all described NPs or a subset of the natural product class of interest is essential. Databases like Dictionary of Natural Products[128] (DNP) or Scifinder[129] can provide this information including the sum formula, structure and spectroscopic data of the most NPs described today.

For the bioactivity-guided identification of NPs, fractionation of the crude extract is the method of choice. Based on the performance of LC-MS chromatography, direct fractionation for a bioactivity assay is possible by splitting the LC flow after elution, using a portion for MS detection (as in LC-MS analysis) and passing the remaining flow into a 96-well plate; thus, each well of the 96-well plate can be associated with a small retention time range. After incubation with the respective test organism, the entire bioassay readout is combined into an activity chromatogram and correlated with MS data obtained in parallel to identify bioactive compounds.

1.5.3 Nuclear magnetic resonance (NMR) spectroscopy

After the identification and isolation of an NP, the determination of its chemical structure is fundamental for the characterisation of a new molecule. Spectroscopic techniques such as infrared (IR) or UV-VIS spectroscopy, which are widely used in organic chemistry, provide information about certain structural properties. However, this molecular information is often not sufficient for *de novo* structural elucidation of a new natural product. High-resolution mass spectrometry can deliver the molecular formula and with the help of MS^2 fragmentation, a partial structural elucidation of the molecule is achievable. Nevertheless, structural elucidation of new NPs can rarely be achieved by MS only, but it is a helpful

technique and offers additional information for X-ray and nuclear magnetic resonance (NMR) spectroscopy.

Today, two techniques are commonly employed for the *de novo* elucidation of complex NPs. The first is X-ray diffraction spectroscopy, which is based on the diffraction pattern of a crystal in which an electron density map can be created that reflects the spatial structure of a molecule. A prerequisite for the success of this method is the ability to grow sufficiently large crystals of a molecule, which in most cases is a major obstacle for NPs.

The second one is the nuclear magnetic resonance spectroscopy that can be used with fewer restrictions. However, the low sensitivity requires a considerable amount of sample (which is also the case with X-ray crystallography), and the data sets obtained must be extensively analysed for *de novo* structure elucidation. Due to their easy sample preparation and universal applicability, NMR spectroscopy is the most powerful technique for structure elucidation in natural product research.

Measurement of 1D proton NMR spectra is widely used to identify changes in more abundant metabolites due to the large dynamic range of metabolite concentrations in biological fluids. Therefore, the one-dimensional (1D) proton (^{1}H) NMR has been extensively used since 1985 in the field of study biofluids and tissue types[130]. For metabolic NMR profiling studies[131], 1D proton spectra are used in combination with statistical pattern recognition methods. Mainly two-dimensional (2D) proton-proton experiments are used for structure determination. The use of carbon (^{13}C) as a second dimension in 2D experiments with indirect detection can significantly improve the solution. Thus, various experiments such as correlation spectroscopy (COSY), heteronuclear single quantum correlation (HSQC) and heteronuclear multiple bond correlation (HMBC) can be performed with high-resolution NMR spectroscopy[132]. NMR experiments have been used to determine most NP structures in recent decades, which underlines the efficiency of this technique. In addition, NMR can be applied to elucidate biosynthetic pathways (e.g. in the study of incorporation profiles of isotope labelled precursors) and in target binding analysis to determine the mode of action of a natural product.

1.5.4 Genome mining approach

The realisation that many microorganisms possess "silent" BGCs and have the potential to produce microbial metabolites not seen under standard conditions lead to the development of a range of experimental methods for identifying the small-molecule products of such gene clusters[133]. Hence, new strategies and approaches have been developed based on the more accessible whole genome sequences data. The application of bioinformatic-based approaches to guide NP discovery and investigation have been termed "genome mining". In general, genome mining comprises a huge field of molecular (e.g. genome sequences, cloning and heterologous expression) and cellular (test bioactive NP on bacteria and cell lines) biology techniques, as well as chemical (MS and NMR spectroscopy) and bioinformatic (BLAST search, antiSMASH annotation) analysis to predict associated BGCs[134] (Figure 1.12).

With regard to bacteria, genome mining helps to more specifically identify new SMs that might be used for drug development. In particular, genome mining approaches can be used to connect uncharacterized identified BGC its natural product within the genomes of sequenced organisms. The development of next-generation sequencing (NGS) technology have accelerated the rate and reduced the cost of genomic data acquisition[135]. It is becoming a routine to use NGS to obtain a draft genome sequence of the secondary metabolite producing microbe[136], in order to identify the underlying BGC.

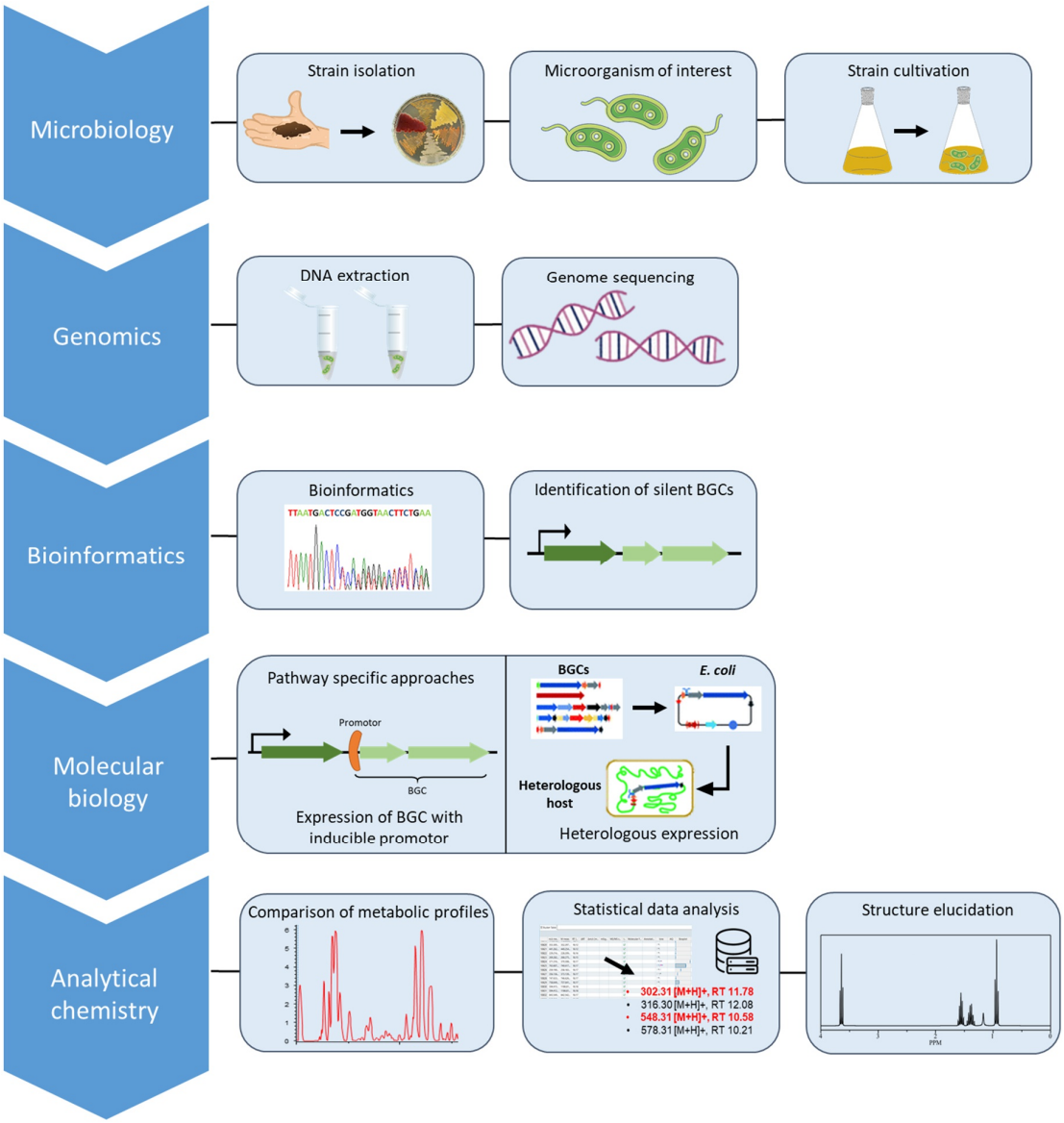

Figure 1.12: Genome mining approach for natural product discovery in microorganisms. Isolation and growth of a microorganism of interest is followed by DNA extraction and genome sequencing. Bioinformatic tools are then applied to analyse the genome and identify silent biosynthetic gene clusters (BGCs). Non-expressed BGCs are activated using pathway specific strategies e.g. gene activation with inducible promoter or heterologous expression. New metabolites are identified in crude extracts or supernatants, followed by their purification and characterization, usually using a combination of high-resolution mass spectrometry, and 1D NMR spectroscopy. Scheme adapted from Rutledge *et al.*[137].

The genome mining approach is entirely dependent on computing capacity and bioinformatic tools such as BLAST[138]. Beyond this, huge datasets consisting mainly of DNA sequences and their annotations are now being deposited in publicly accessible databases. Once all the genes in a new genome have been sequenced, they can be compared with the

sequence of annotated genes, sequences of proteins encoding enzymes, and with their functions as known in public databases[134]. Nevertheless, it is important to keep in mind that the similarity of sequences between multimodular enzymes does not mean that they have to follow the same chemistry, but that it may occur that they lead to a different pathway or a completely different natural product. The central role of the genome mining approach is to identify new BGCs within the genome sequence of a microorganism, which cannot be associated to the production of any known secondary metabolite. Therefore exploiting this information by any means such as the induced expression of the BGC via genetic manipulation of the host strain, heterologous expression of the identified BGC or the through fully investigation of the secondary metabolome of the host strain might lead to the discovery of new NPs. The exceptional modular architecture of the PKS and NRPS classes are well suited for genome-mining-based discovery, as these two major biosynthetic pathways for the production of NPs can be easily identified *in silico*[139]. That provides the opportunity to compare the target gene cluster to known gene cluster, which are useful for predicting their function and structure using several associated web tools[140]. The scientific progress considering DNA and amino acid sequences, enzymes, gene cluster architecture and biological function of NPs lead to the development of different web tools. A widely used computer-based tool for BGC identification is "antibiotics and Secondary Metabolite Analysis SHell" (antiSMASH), which was introduced in 2011 and allows simultaneous input of multiple related sequences, direct analysis of protein sequences and detection of additional classes of BGCs that can encode different SMs. The Conserved Domain Database (CDD) is an additional tool for predictive sequence analysis of BGCs encoding for NRPS and modular PKS assembly lines. It can provide considerable insight into the structure of metabolites and enable *in silico* dereplication by comparison with databases of already known metabolites.

Molecular biology focuses on characterising the biosynthetic machinery producing NPs. (Figure 1.12). Therefore, pathway specific strategies enable a more targeted approach, but that need knowledge about the regulation of particular gene clusters and generate a lower throughput as metabolome-based strategies. Such methods including the expression of pathway specific activator genes, deleting genes encoding pathway repressors, reorganisation of a BGC to replace the natural promoter with a putative or inducible one, or the de-

velopment of a heterologous expression platform in a different host. Afterward, the analytical chemistry is following with different methods like metabolic profiling workflow, statistical data replication and structure elucidation.

Recently, a genome mining survey of myxobacterial type III PKS has resulted in the identification of unusual alkypyrones as products derived from type III PKS biosynthesis from the model organism *Myxococcus xanthus* DK1622[141]. The pyxidicyclines as topoisomerase inhibitors were identified by activation of an unusual type II PKS gene cluster in the native producer *Pyxidicoccus fallax* An d48 and their heterologous expression guided using a comprehensive genome mining approach[142]. In another genome-directed approach on the same strain, the first myxobacterial biarylitide, called myxarylin, was identified from *Pyxidicoccus fallax* An d48[143].

1.5.5 Bioactivity-guided approach

The most prominent method for identifying chemical lead structures for the development of new drugs and agrochemicals is the bioactivity-guided approach by screening of plant and microbial extracts for novel SMs with particular biologically effects towards living organisms (Figure 1.13). Thus, it is not remarkable that it has been used as a discovery strategy for many chemical compounds[144]. For this purpose, the isolated microorganisms have to be cultivated either on solid or liquid environment under optimal conditions to produce a broad mixture of secondary metabolites. This is followed by the preparation of the crude extract from the culture broth using various polar and non-polar solvents. The crude extract obtained can be used directly for *in vitro* assays to determine the bioactivity that occurs, or it can be further treated using chemical methods such as liquid-liquid partitioning to test of each solvent phase separately. In addition, time-dependent fractionation of the crude extract by HPLC in 96-well plates allows the screening of the activity of small compound fractions from the abundant metabolite mixture.

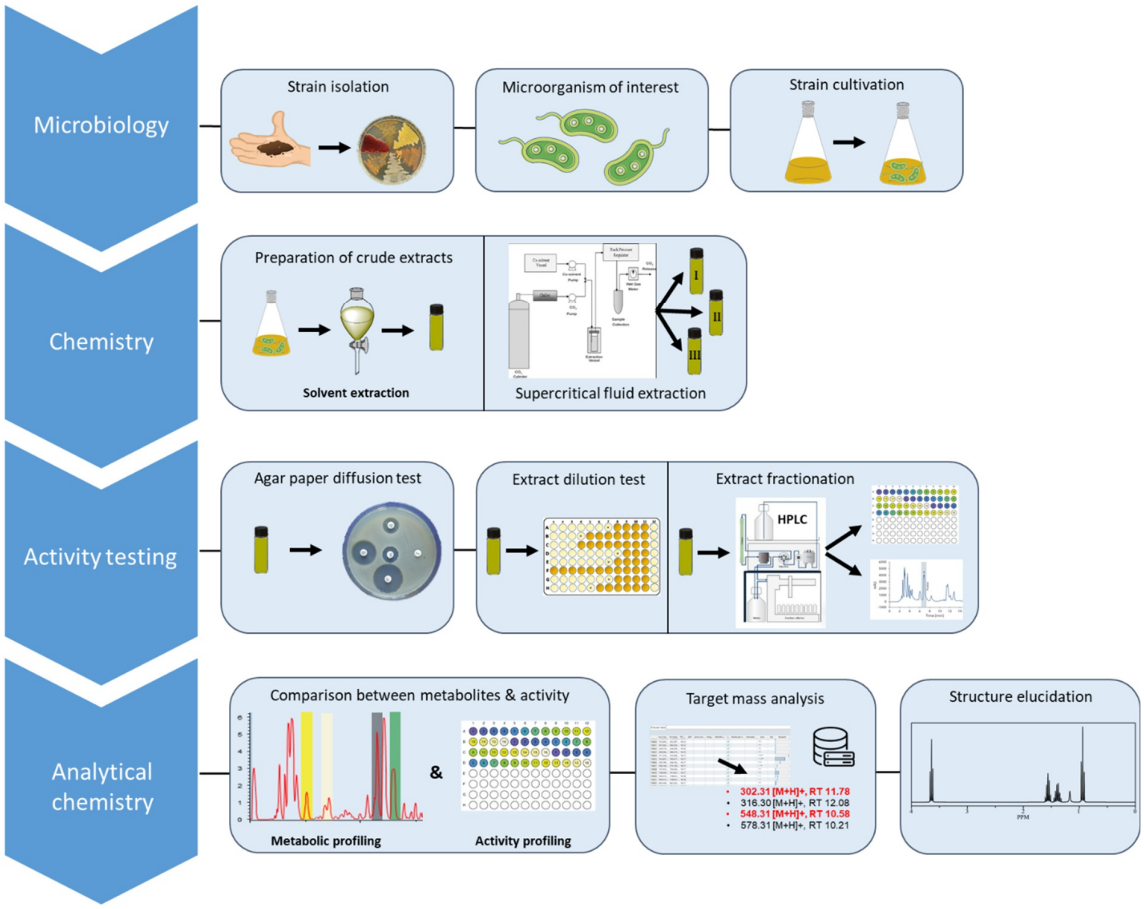

Figure 1.13: Bioactivity-guided approach for natural product discovery in microorganisms. Following the isolation and growth of a microorganism of interest, the crude extract is prepared. Solvent extraction can performed on the conventional matter in combination with liquid-liquid partitioning or by supercritical fluid extraction (SFE). Biologically activities are typically investigated by agar paper diffusion test and extract dilution test of the corresponding crude extract. Extract fractionation is helpful to identify certain metabolites in dependence on the retention time. New identified metabolites in crude extracts or supernatants, followed by their purification and characterization, usually using a combination of high-resolution mass spectrometry, and NMR spectroscopy. Scheme adapted from Rutledge *et al.*[137].

There are several methods for *in vitro* assay of crude extracts and pure compounds for use in antimicrobial testing as potential active agents. The most known and fundamental methods are the agar disk diffusion and the dilution testing. To study the antimicrobial effect of a substance in depth, time-killing test and flow cytofluorometric techniques are also useful, providing information on the inhibitory effect (bactericidal or bacteriostatic) and the cell damage inflicted on the test organism.

The agar paper disk diffusion test, developed in 1940[145], is one of the common method used many clinical microbiology laboratories for routine antimicrobial susceptibility testing and

is still performed today for bacteria and yeast. For this procedure, agar plates are inoculated with a standardized inoculum of the test microorganism. Then, filter paper discs, containing the crude extract or test compound at a desired concentration, are placed on the surface of the agar followed by incubation under suitable conditions. The antimicrobial compounds diffuses into the agar and inhibits germination and growth of the test organism. The diameter of the inhibition zone is determined, which allows conclusions to be drawn about the bioactivity of the crude extracts. However, the agar disk diffusion procedure is not appropriate to determine the minimum inhibitory concentration (MIC), as it is impossible to quantify the concentration of the antimicrobial substance diffused into the agar medium. The mentioned advantages of the disk diffusion test is mainly its simple procedure and the low cost, which have contributed to its extensive use for antimicrobial screening of bacterial and plant extracts.

Dilution methods are the most applicable for the determination of MIC values as they offer the possibility to estimate the concentration of the tested crude extract or antimicrobial compound in a liquid milieu. The dilution procedure consists of preparing a serial dilution of the crude extract or a compound in a liquid growth medium dissolved in a 96-well microtiter plate. Each well has then been inoculated with a bacterial solution prepared with the same medium of a standardised amount of the microbial suspension after dilution. Then the well-mixed 96-well plates are incubated under appropriate conditions depending on the microorganism tested. The MIC value corresponds to the lowest concentration of the extract or compound that completely inhibits the microbial growth in the microtiter wells detected by visualisation. In addition, several colorimetric methods have been developed based on the use of dye reagents, such as Alamar blue (resazurin)[146], which is an effective growth indicator to determine the MIC endpoint.

Following the conventional bioactivity-guided approach to identify bioactive metabolites from Sorangium strains, chlorotonil A was isolated from *Sorangium cellulosum* So ce1525[89]. However, bioactivity-based screening of crude extracts from microbial cultures that are known to be potent producers of bioactive NPs, such as actinobacteria and filamentous fungi, has provided disappointing results, because these approaches tend to rediscover known metabolites[147]. In order to prevent this, it is recommended to couple the bioactivity-guided approach with an LC-MS system and use a metabolic profiling workflow to identify the active fractions/target mass over the specific retention time. This is helpful to identify already known compounds at an earlier stage by comparing them with public or in-house

databases. Subsequently, the identified compounds can be reviewed for pre-existing bioactive metabolites in the literature. This has prompted the development of alternative approaches to identifying novel lead compounds, which combine the different working fields for complementary workflow, such as high-throughput screening of compound libraries, microbial genomic and fragment-based design[148].

1.5.6 Metabolome-based approaches

Over the past three decades, a number of genetic engineering strategies were developed for strain engineering, including pre-cursor development, deletion of competing metabolic pathways, development of translational or transcriptional mechanisms, and manipulation of pathway-specific regulators[149,150]. Metabolome-based approaches encompass many different methods (such as variation of growth conditions, co-cultivation, manipulation of global regulators and epigenetic perturbation), which can have multiple effects on more than one gene by triggering global changes in the regulation of specialised metabolic pathways (Figure 1.14). The goal of such approach is the manipulation of pathway-specific regulators to discover novel metabolites with or without knowledge about their regulation of specific BGCs works. Hence, they allow higher throughput than more targeted strategies for organisms that are not genetically accessible[137].

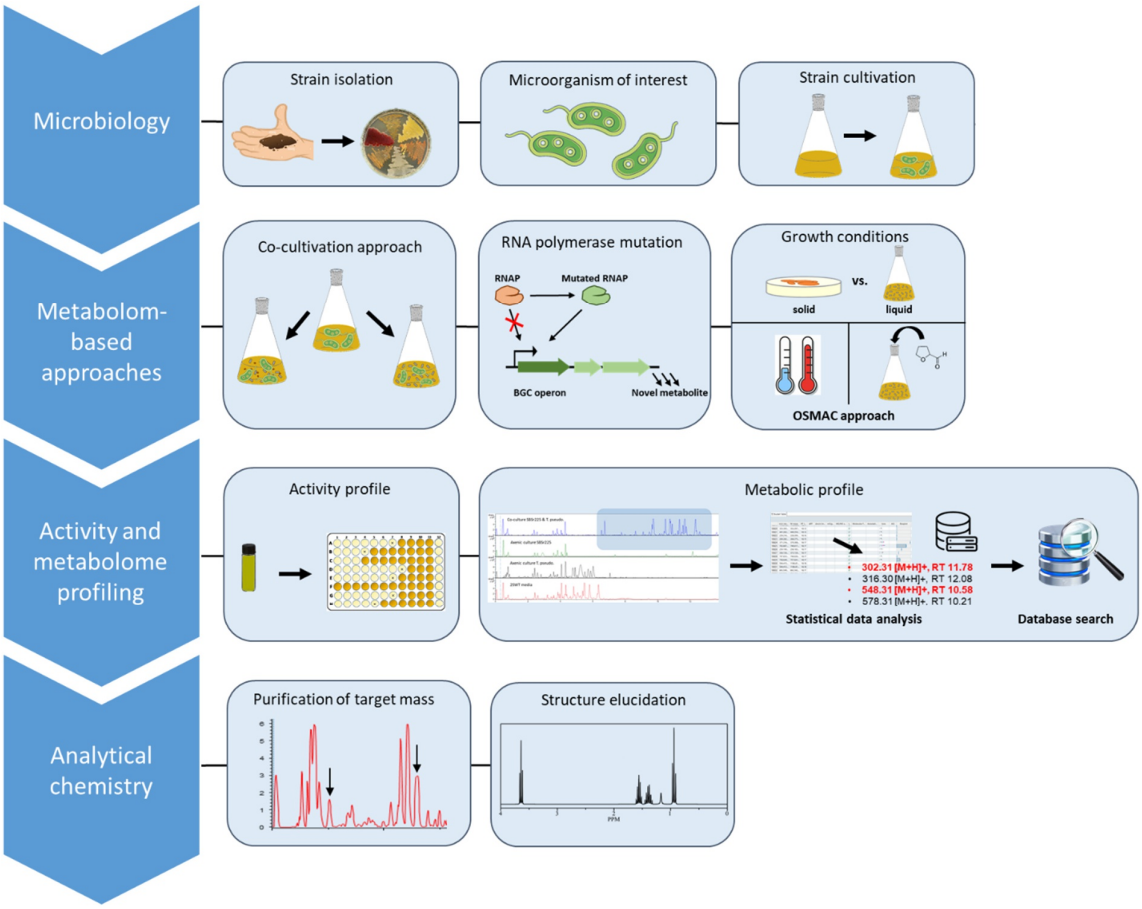

Figure 1.14: Metabolome-based approaches for the natural product discovery in microorganisms (MOs). Isolation and growth of a microorganism of interest is followed by different metabolome-based approaches. Co-culturing of microorganisms to induce the microbial crosstalk, which has the potential to activate non-expressed biosynthetic gene clusters BGCs. Engineering of the transcriptional and translational machinery attempts to induce mutations in RNA polymerase (RNAP) and ribosomal proteins to cause upregulation of BGC expression[151]. The RNAP approach is based on the selection of rifampicin resistance in actinobacteria, which leads to a mutation of the RNA polymerase β-subunit and results in an increased affinity of RNAP to the promoters of BGCs encoding particular metabolites[152]. Variation of growth conditions aims to change the environment in which the MO grows (e.g. by adding chemical triggers, physical parameters or modifying the culture method) to induce changes in BGC expression. Computerised data analysis by comparing metabolic profiles (blank, untreated and treated) are used for the identification of known and novel target masses in crude extracts. New identified metabolites in crude extracts or supernatants, followed by their purification and characterization, usually using a combination of high-resolution mass spectrometry, and NMR spectroscopy. Scheme adapted from Rutledge *et al.*[137].

However, metabolome-based approaches are basically rather empirical, which makes it difficult to predict the outcome. In addition, the co-induction of multiple BGCs can compromise the identification and isolation of particular chemical compounds from a more complex mixture of new metabolites. Compared to metabolome-based approaches, pathway-

specific strategies offer a more targeted control and better prediction of the natural product outcome. Nevertheless, theses targeted approaches offer generally lower throughput than metabolome-based methods, since a specific strategy has to be developed and implemented for the activation of each BGC.

As an example of the manipulation of global regulators, alleles of the pleiotropic regulatory gene *abs*A1 of *S. coelicolor*, which together with *abs*A2 are responsible for regulating the transcription of several BGCs, were introduced into *S. flavopersicus* as a heterologous host. This triggered the production of pulvomycin and revealed a broader spectrum of antimicrobial activity than had previously been reported[153].

To summarise, an obvious trend is to combine methods from bioactivity-guided, metabolome- and genome-based approaches to improve the overall information on the theoretical and observed biosynthetic strength of a strain[144]. Since the biosynthesis of NPs cannot be thoroughly assessed with a single method alone, these synergies are both useful and critical to success in the field of NP discovery. They offer an approach to investigate both the observable under laboratory conditions and the genome inscribed and thus theoretical but "secret" secondary metabolome. Metagenomics is starting to uncover the tremendous untapped potential of uncultured microorganisms as a bountiful source of structurally complex bioactive NPs. A key challenge for the future is to utilise the metabolic potential of still untapped bacteria and to transfer the information from BGCs found through metagenomics to heterologous hosts, which are engineered by rational genetic manipulation to induce their expression. These drawbacks are expected to improve with the development of a more progressive understanding of the many aspects that regulate the expression of specific BGCs encoding secondary metabolites.

1.6 Co-culture & OSMAC approach for enhancing the diversity of SM

The following section introduces the most common approaches to enhance the secondary metabolite diversity, especially focused on co-cultivation methods and OSMAC (one strain many compounds) approach including the Transwell system (petri dish) as well as solid support cultivation systems.

With the beginnings of microbiology in the late 19th century, scientists have grown microorganisms almost exclusively in axenic cultures, leading to a limited awareness of the microbial world[154]. Recent metagenomics studies have revealed the diversity of uncultivated microorganisms from extremophile habitats and the existing potential for the production of

NPs[155]. Implemented sequencing of hundreds of microbial genomes, in particular bacteria and fungi, revealed that most of the identified genes connected to secondary metabolism are not expressed under laboratory cultivation conditions[156]. In natural habitats, microorganisms process signals from both abiotic and biotic environments. One obvious explanation for this are the standard cultivation conditions for axenic microorganisms, which never exposed the natural environmental conditions at the isolated habitat. Thus, a significant proportion of microbial secondary metabolites, especially those that enable them to interact, communicate, form alliances or engage in conflict with or against other species, are not produced.

Given the importance of microbial communication for the production of SMs, microorganism communities represent a treasure trove for the discovery of NPs. The remarkable momentum that co-cultivation studies are currently gaining shows that the first study on "mixed cultures" between *E. coli* and *Bacillus paratyphosus* with special interest in biochemical and physiological processes was published as early as 1918[157]. One century later, researchers in various fields of microbiology, biotechnology, and natural product discovery still explore mixed or co-cultivation experiments to address the regulation of NP production.

One strategy consists of exploiting biosynthetic pathways that are not expressed under standard laboratory growth conditions in known producers. Therefore, various techniques for activating BGCs already known, ranging from the genome to the metabolome level (Figure 1.15). In particular, approaches like co-culture or one strain many compounds (OSMAC) have multiple effects and thus global changes permit more interventions on the regulation of SM pathways. In contrast, other methods, e.g. heterologous expression, require prior knowledge of the genome sequence. In the first instance, a BGC of interest must to be identified via bioinformatic tools. Moreover, the genetic engineering of certain BGCs by modification in the gene arrangement need well-characterized pathways, including the overall transcriptomic regulatory mechanism of the encoded genes.

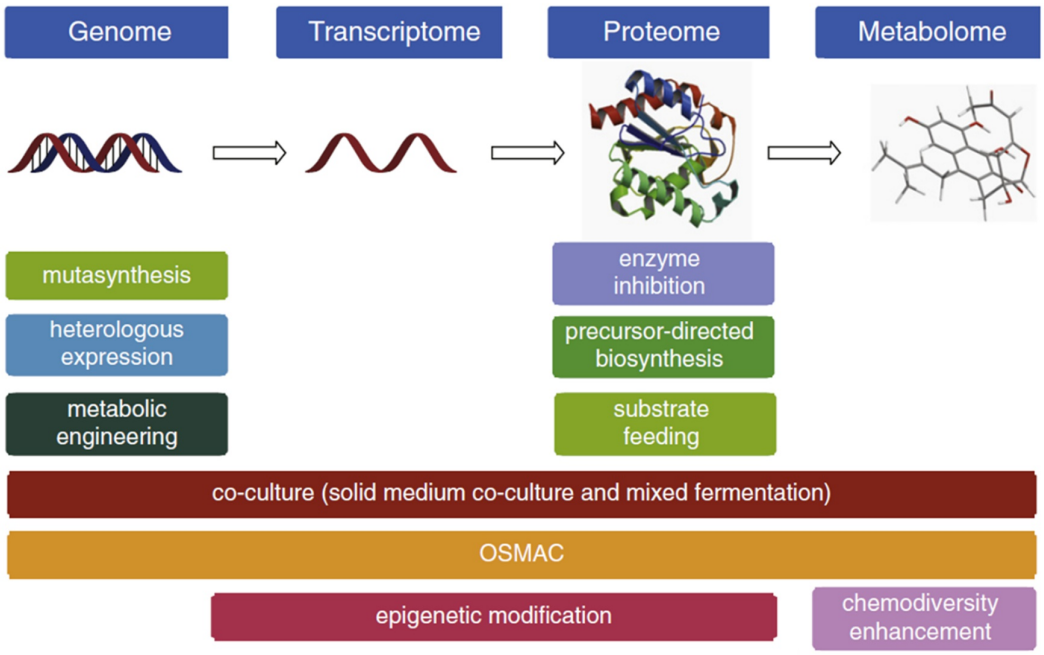

Figure 1.15: Overview about methods for influencing the biosynthesis of secondary metabolites in microorganisms. Possible methods to alter the production of SMs or to enhance their chemical diversity. (OSMAC: one strain-many compounds approach). Scheme from Bertrand *et al.*[158]

Additionally, the chemical-ecological relationships that occur in microorganism interspecies interactions can be utilized to activate not expressed BGCs to discover novel secondary metabolites without the requirement for further knowledge. Imitation of the natural environment with the interspecies interactions occurring in microorganism communities can be exploited under laboratory conditions. Interspecies crosstalk leading to chemical diversity has also been successfully employed to study the biosynthesis of previously undescribed metabolites[159,160]. In this respect, the novel approach in which microorganisms are growing together (co-cultivation) has increasingly gained attention for the potential discovery of novel NPs.

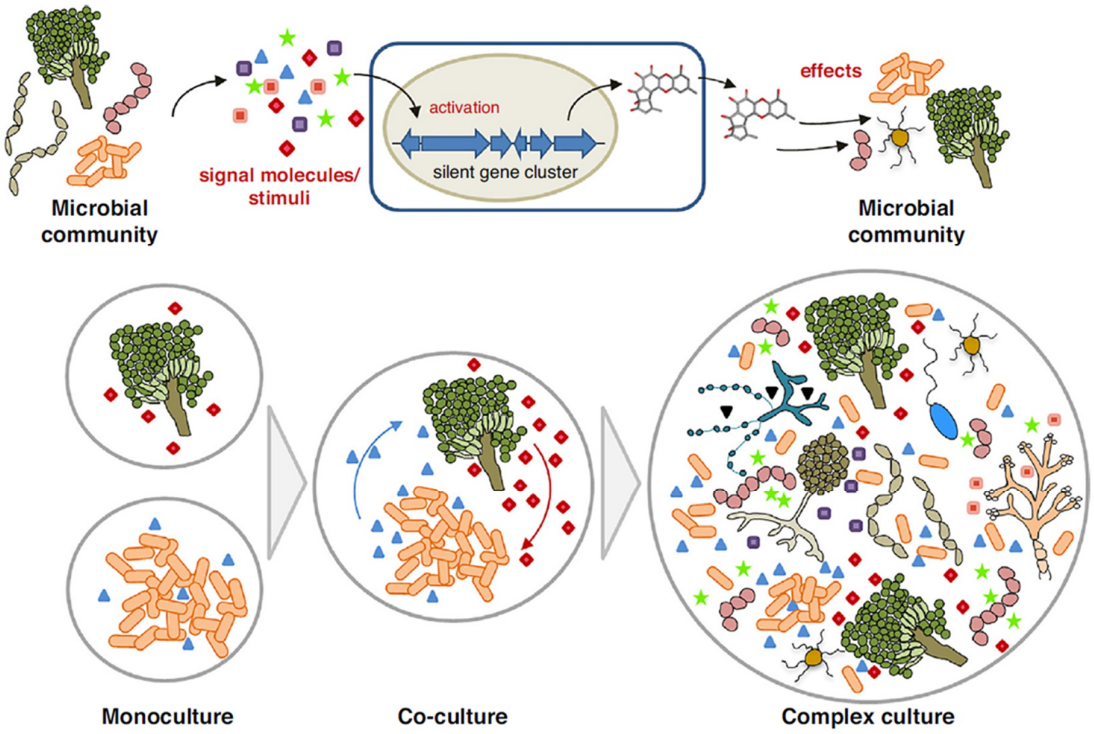

Figure 1.16: Production of secondary metabolites by microorganisms in monoculture, co-culture or by complex consortia leading to activation of silent biosynthetic gene clusters and production of potentially novel secondary metabolites. Scheme adapted from Netzker *et al.*[161]

During traditional discovery of microbial NPs, a selected strain is often grown in a nutrient-rich axenic culture[162]. Specific BGCs encoding biosynthetic enzyme machineries are involved in the production of microbial NPs. However, in the vast majority of cases, only a small percentage of the biosynthetic gene clusters present in the organism are actively expressed under laboratory conditions. The "silent" or "cryptic" gene cluster that are not expressed represent a potential treasure trove for the discovery of novel SMs. However, it should be obvious that not all BGCs predicted in an organism by bioinformatic tools are naturally functional and lead to the production of metabolites after their possible activation. Co-cultivation of microorganisms is designed to stimulate environmental interactions that are absent in microbial monocultures (Figure 1.16). Microorganisms excrete a wealth of NPs that act as chemical signalling molecules such as antibiotics or as potential inducers of silent gene clusters in adjacent species. Thereby produced compounds might influence other microorganisms [161]. These interactions can be induced by diffusible small molecules or by direct cell-cell contact between different strains and can influence the cellular machinery through initiated processes aimed at increasing competitiveness and fitness, which

often translates into the production of biologically active metabolites. Hence, the stimulation of microbial communication can lead to the production of compounds that cannot be produced in monoculture, which may help to "awakening" cryptic and poorly expressed secondary metabolites.

A number of novel SMs have been already isolated from co-cultivated microorganisms [163]. Co-cultivation experiments are not only interesting as an approach to identify novel compounds, but also to understand the underlying molecular mechanisms and the role of SMs in nature. In previous studies, such mixed fermentations have already been executed between bacteria-bacteria, fungi-bacteria[164], and terrestrial-marine organisms[165]. Furthermore, the elicitation of the interaction partners was conducted with living cells, cell lysates and heat-inactivated cells, respectively[164].

One early example is the mixed culture of the fungus *Aspergillus nidulans* and the bacterium *Streptomyces rapamycinicus*, which resulted in the activation of a silent fungal BGC followed by the production of the archetypal polyketide orsellinic acid[166]. The same streptomycetes species was also capable to trigger a silent gene cluster in *A. fumigatus*, leading to the identification of fumicyclines[167]. Co-culturing of *Streptomyces sp.* MA37 with *Pseudomonas sp.* resulted in the discovery and induction of cryptic indole alkaloid BGC in MA37 and to the characterisation of the known pyrroloindolocarbazole alkaloid metabolite with strong anti-proliferative activity against HT- 29 cells[168]. Serratiochelin A, a siderophore with bioactivity against *S. aureus* was purified from the marine microbes *Shewanella sp.* and *Serratia sp.* after co-cultivation[169]. In particular, direct co-cultivation requires the physical cell-cell contact between two or more microorganisms in an environment. It was previously reported, that bacteria containing mycolic acids (MACB) in their outer membrane could induce secondary metabolism in a wide range of *Streptomyces* strains[170]. Mycolic acids are fatty acids that are important components in forming the highly impermeable outer barrier in *Corynebacterineae*[171]. The results of the study show only the direct cell-cell interactions between *Streptomyces sp.* and MACB induce the natural product biosynthesis of alchivemycin A[172]. These examples illustrate the benefit of co-cultivation technique over axenic cultures for the mining of valuable NPs.

Despite some promising results, additional work needs to be done to verify whether the chemical scaffolds produced in co-culture are innovative or derivatives of known compounds. Study of induction related phenomena within interacting microbes is challenging

due to the complex nature and chemical diversity of their metabolites. Therefore, sophisticated and sensitive analytical techniques are mandatory, primarily based on high-resolution mass spectrometry for metabolome profiling or direct MS imaging of the co-cultures. In particular, the identification of specific biomarkers can be achieved through metabolome mining and efficient data dereplication, but depending on the strains being studied, the quality of annotation and biomarker identification can vary greatly.

Another way, the global alteration of microbial physiology can be a useful tool in changing the SM profile of a microorganism. Those approaches are based on the modifications of the growth conditions without co-cultivation or genetically manipulation of the host organism. The general concept for this was designed by Zeeck *et al.*[173], which termed that as "one strain many compounds" (OSMAC) approach. However, the underlying idea behind this approach is that every microorganism has the potential to synthesise different compounds, but only a subset of these compounds will be produced under particular growth conditions. The underlying assumption is that the variation in cultivation parameters can trigger the production and discovery of novel SMs. Zeeck *et al.* demonstrated by changing the parameters for cultivation e.g. temperature, salinity, aeration, and even the shape of flasks that the fungus *Aspergillus ochraceus* was able to produce 15 additional metabolites[173]. The past 20 years have revealed that modification of parameters such as the supplementation of nutrients, trace elements, chemical elicitors (communication molecules, antibiotics, e.g. *N*-acetylglucosamine) and physical parameters affect the diversity of SM production in microbes.

An optimal range for the production of possibly all secondary metabolites in these living microbes depends on the selected culture conditions and cultivation platform, which can be difficult to figure out. In general, the cultivation of microorganisms can be executed either in liquid or solid media, or in bioreactors. During a systematic OSMAC approach for antibiotic identification in *Streptomyces* sp. USC-633 isolated from an intertidal environment, examining over 50 different media formulations and each media was prepared as a liquid and as a solid medium with the addition of agar. They observed antagonistic activities against *E. faecalis* and *E. coli* ATTC 13706 from the solid medium but the bioactivity from the liquid broth was only determined against the similar *E. coli* strain[174]. Further OSMAC-based experiments are indicating a drastic change in the produced SMs by the deep-sea-derived fungus *Penicillium* sp. F23-2 when the cultivation switched from complex liquid media to rice-based solid medium. That cultivation led to the isolation of five ambuic acid

analogues (penicyclones A–E), which exhibit antibacterial activity against *S. aureus*[175]. It is important to clarify that in the latter example it is unclear whether the changes in the metabolic production were caused by cultivation on solid medium. In fact, variations on the composition of complex media can often have enormous effects on the production of microbial SMs.

It appears that understanding the underlying mechanisms of co-cultivation induced SM production remains crucial and should be further investigated in the near future. However, the identification of potential pharmaceutical agents or lead structures via co-cultivation should be prioritised in the interest of combating antimicrobial resistance. Nevertheless, it is clear from such preliminary experiments that further investigations into these effects of solid vs. liquid environment or a combination with other parameter variations on SM production are warranted.

1.7 Outline of this work

The general aim of this thesis was the discovery and characterisation of novel myxobacterial natural products through the variation of cultivation and extraction methods. To achieve the intended goals, a co-cultivation procedure and a new cultivation device for myxobacteria had to be developed. Furthermore, supercritical fluid extraction should be employed to obtain a broader spectrum of myxobacterial metabolites. As part of this effort, genome and metabolome mining and bioactivity-guided approaches were to be extensively used to address the topic of this thesis (Figure 1.17).

Chapter 2 presents the first development of a co-cultivation procedure for myxobacteria in liquid environment. For this purpose, the well-known myxobacterium *M. xanthus* DK1622 was chosen as a model organism to investigate the influence on the metabolic profile using physical cell-cell contact, addition of filtered supernatant and heat-inactivated cells of Gram-negative, Gram-positive and eukaryotic partner strains. In addition, this study aimed to apply statistical data analysis at the metabolome level using mass spectrometry data to identify known and unknown families of compounds.

In the chapter 3 of this thesis, a more sophisticated co-cultivation approach was planned with so-called *Streptomyces*-like myxobacteria that have recently been isolated. In particular, the group of mycolic acid-containing bacteria have previously shown an enormous potential to alters the production of secondary metabolites after co-cultivation. In order to

investigate their ability to change the myxobacterial metabolome, *hr*MS and MS^2 measurements were devised to enable the identification of newly produced metabolites using statistical data analysis and molecular networks.

Chapter 4 focuses on the development and implementation of a combined solid-liquid cultivation system. Myxobacteria have a complex life cycle and regulatory system for cell development, which also influences the repertoire of secondary metabolites produced due to growth in solid or liquid environments. This study aims to access the underrepresented SMs formed exclusively in solid environments using a combined solid-liquid cultivation device called “Flow Plate”.

In chapter 5, the extraction process of the supercritical fluid extraction is evaluated in comparison to a conventional solvent procedure to generate bacterial crude extracts. The central aim of this part was to determine the extraction efficiency on SM with different chemical properties derived from three different myxobacterial producer strains and their antimicrobial activity profiles in the crude extract. To achieve the objectives, a targeted and non-targeted metabolomic workflow was applied to identify the unique myxobacterial metabolic features.

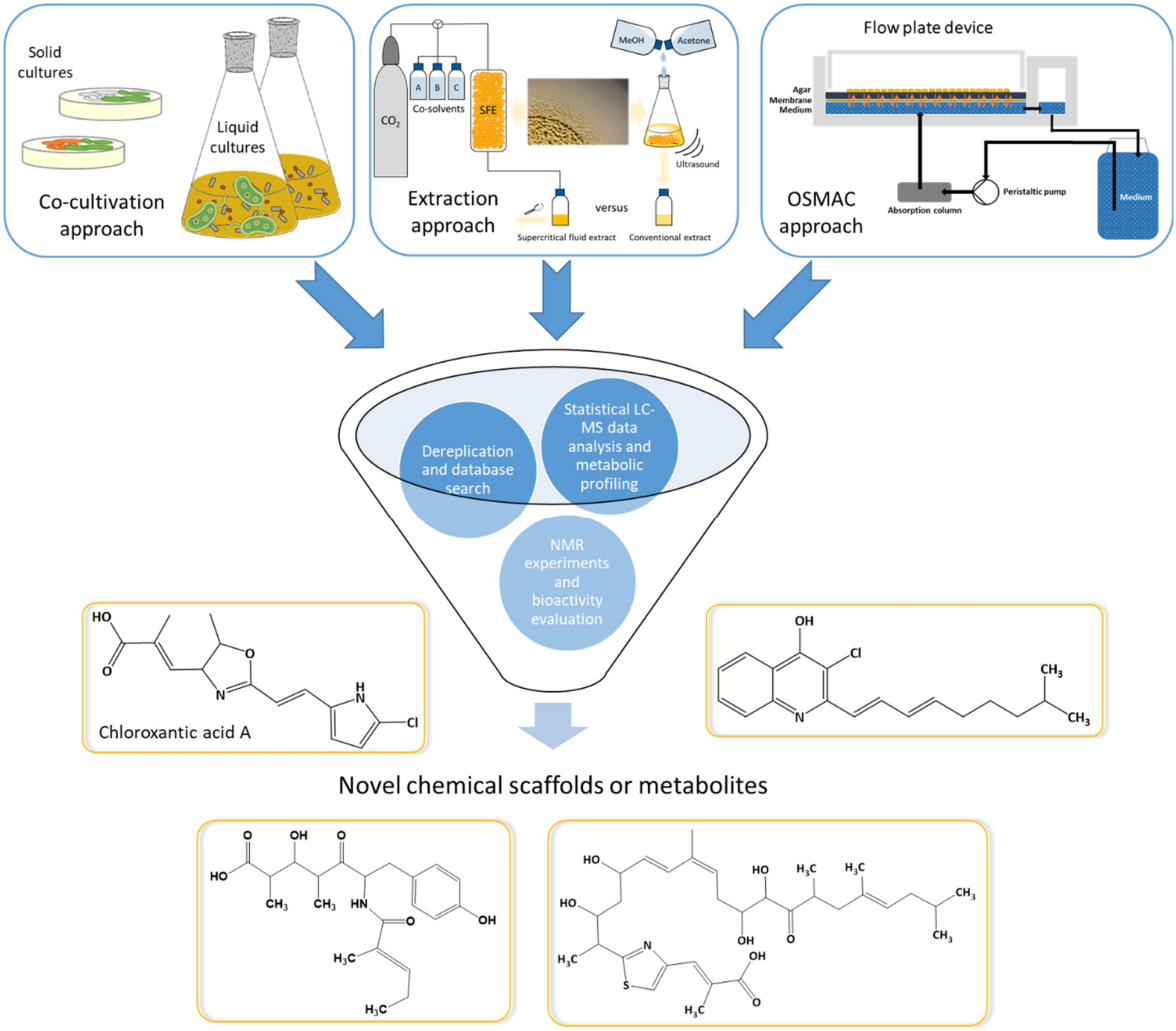

Figure 1.17: Illustrated overview about the applied approaches to discover myxobacterial natural products in this thesis.

1.8 References

(1) Jarvis, B. B. The Role of Natural Products in Evolution. In *Evolution of metabolic pathways*; Romeo, J. T., Ed.; Recent Advances in Phytochemistry v. 34; Pergamon: Amsterdam, Oxford, 2000; pp 1–24.

(2) Verpoorte, R.; van der Heijden, R.; Memelink, J. Engineering the plant cell factory for secondary metabolite production. *Transgenic Res* **2000**, *9*, 323–343.

(3) Sanchez, S.; Demain, A. L. Metabolic regulation and overproduction of primary metabolites. *Microb. Biotechnol.* **2008**, *1*, 283–319.

(4) Pott, D. M.; Osorio, S.; Vallarino, J. G. From Central to Specialized Metabolism: An Overview of Some Secondary Compounds Derived From the Primary Metabolism for Their Role in Conferring Nutritional and Organoleptic Characteristics to Fruit. *Front. Plant Sci.* **2019**, *10*.

(5) Carrington, Y.; Guo, J.; Le, C. H.; Fillo, A.; Kwon, J.; Tran, L. T.; Ehlting, J. Evolution of a secondary metabolic pathway from primary metabolism: shikimate and quinate biosynthesis in plants. *Plant J* **2018**, *95*, 823–833.

(6) Weng, J.-K. The evolutionary paths towards complexity: a metabolic perspective. *New Phytol* **2014**, *201*, 1141–1149.

(7) Ruiz, B.; Chávez, A.; Forero, A.; García-Huante, Y.; Romero, A.; Sánchez, M.; Rocha, D.; Sánchez, B.; Rodríguez-Sanoja, R.; Sánchez, S.*; et al.* Production of microbial secondary metabolites: regulation by the carbon source. *Crit. Rev. Microbiol.* **2010**, *36*, 146–167.

(8) Liu, W.; Zhu, D.-W.; Liu, D.-H.; Geng, M.-J.; Zhou, W.-B.; Mi, W.-J.; Yang, T.-W.; Hamilton, D. Influence of nitrogen on the primary and secondary metabolism and synthesis of flavonoids in *Chrysanthemum morifolium Ramat*. *Journal of Plant Nutrition* **2010**, *33*, 240–254.

(9) Demain, A. L.; Fang, A. The natural functions of secondary metabolites. *Adv. Biochem. Eng. Biotechnol.* **2000**, *69*, 1–39.

(10) Hibbing, M. E.; Fuqua, C.; Parsek, M. R.; Peterson, S. B. Bacterial competition: surviving and thriving in the microbial jungle. *Nat Rev Micro* **2010**, *8*, 15–25.

(11) Demain, A. L.; Sanchez, S. Microbial drug discovery: 80 years of progress. *J. Antibiot.* **2009**, *62*, 5–16.

(12) Aldholmi, M.; Marchand, P.; Ourliac-Garnier, I.; Le Pape, P.; Ganesan, A. A Decade of Antifungal Leads from Natural Products: 2010–2019. *Pharmaceuticals* **2019**, *12*, 182.

(13) Miethke, M.; Marahiel, M. A. Siderophore-based iron acquisition and pathogen control. *Microbiol. Mol. Biol. Rev.* **2007**, *71*, 413.

(14) Ho, T.; Wu, S.; Chen, J.; Li, C.; Hsiang, C. Emodin blocks the SARS coronavirus spike protein and angiotensin-converting enzyme 2 interaction. *Antiviral Res.* **2007**, *74*, 92–101.

(15) Keller, L.; Surette, M. G. Communication in bacteria: an ecological and evolutionary perspective. *Nat. Rev. Microbiol.* **2006**, *4*, 249–258.

(16) Vaishnav, P.; Demain, A. L. Unexpected applications of secondary metabolites. *Biotechnol. Adv.* **2011**, *29*, 223–229.

(17) Harvey, A. L.; Edrada-Ebel, R.; Quinn, R. J. The re-emergence of natural products for drug discovery in the genomics era. *Nat. Rev. Drug Discov.* **2015**, *14*, 111–129.

(18) Henrich, C. J.; Beutler, J. A. Matching the power of high throughput screening to the chemical diversity of natural products. *Nat. Prod. Rep.* **2013**, *30*, 1284–1298.

(19) Mishra, B. B.; Tiwari, V. K. Natural products: An evolving role in future drug discovery. *Eur. J. Med. Chem.* **2011**, *46*, 4769–4807.

(20) Colegate, S. M.; Molyneux, R. J., Eds. *Bioactive natural products: Detection, isolation, and structural determination / edited by Steven M. Colegate, Russell J. Molyneux*, 2nd ed.; CRC Press: Boca Raton, 2008.

(21) Newman, D. J.; Cragg, G. M. Natural Products as Sources of New Drugs from 1981 to 2014. *J. Nat. Prod.* **2016**, *79*, 629–661.

(22) Waltenberger, B.; Mocan, A.; Šmejkal, K.; Heiss, E.; Atanasov, A. Natural Products to Counteract the Epidemic of Cardiovascular and Metabolic Disorders. *Molecules* **2016**, *21*, 807.

(23) Tintore, M.; Vidal-Jordana, A.; Sastre-Garriga, J. Treatment of multiple sclerosis — success from bench to bedside. *Nat Rev Neurol* **2019**, *15*, 53–58.

(24) Feher, M.; Schmidt, J. M. Property Distributions: Differences between Drugs, Natural Products, and Molecules from Combinatorial Chemistry. *J. Chem. Inf. Compu. Sci.* **2003**, *43*, 218–227.

(25) Johnson, T. *CRC Ethnobotany Desk Reference*, 1st Edition; CRC Press: Boca Raton, Fla., 1999.

(26) Hartwell, J. L. Plants used against cancer. A survey. *Lloydia* **1971**, *34*, 204–255.

(27) Kingston, D. G. Tubulin-Interactive Natural Products as Anticancer Agents (1). *J. Nat. Prod.* [Online early access]. DOI: 10.1021/np800568j.

(28) Cragg, G.; Kingston, D.; Newman, D., Eds. *Anticancer agents from natural products*; Taylor & Francis: Boca Raton, 2005.

(29) Donnellan, P. P.; Crown, J. P. The development of docetaxel (Taxotere) in non-small cell lung cancer--docetaxel in new combinations and new schedules: an overview of ongoing and future developments. *Semin. Oncol.* **1997**, *24*, S14-18-S14-21.

(30) Buss, A. D.; Cox, B.; Waigh, R. D. Natural Products as Leads for New Pharmaceuticals. In *Burger's medicinal chemistry, drug discovery and development,* 7th ed. / edited by Donald J. Abraham, David P. Rotella; Abraham, D. J., Rotella, D. P., Burger, A., Eds.; Wiley: Oxford, 2010; pp 847–900.

(31) Sehgal, S. N.; Baker H.; Vézina, C. Rapamycin (AY-22,989), a new antifungal antibiotic. II. Fermentation, isolation and characterization. *J. Antibiot.* **1975**, *28*, 727–732.

(32) Brown, E. D.; Wright, G. D. Antibacterial drug discovery in the resistance era. *Nature* **2016**, *529*, 336–343.

(33) Vincent, J.-L.; Rello, J.; Marshall, J.; Silva, E.; Anzueto, A.; Martin, C. D.; Moreno, R.; Lipman, J.; Gomersall, C.; Sakr, Y.*; et al.* International study of the prevalence and outcomes of infection in intensive care units. *JAMA* **2009**, *302*, 2323–2329.

(34) Tacconelli, E.; Carrara, E.; Savoldi, A.; Harbarth, S.; Mendelson, M.; Monnet, D. L.; Pulcini, C.; Kahlmeter, G.; Kluytmans, J.; Carmeli, Y.*; et al.* Discovery, research, and development of new antibiotics: the WHO priority list of antibiotic-resistant bacteria and tuberculosis. *Lancet Infect. Dis.* **2018**, *18*, 318–327.

(35) Theuretzbacher, U.; van Bambeke, F.; Cantón, R.; Giske, C. G.; Mouton, J. W.; Nation, R. L.; Paul, M.; Turnidge, J. D.; Kahlmeter, G. Reviving old antibiotics. *J Antimicrob Chemother* **2015**, *70*, 2177–2181.

(36) Thirumurugan, D.; Cholarajan, A.; Raja, S. S.; Vijayakumar, R. An Introductory Chapter: Secondary Metabolites. In *Secondary metabolites: Sources and applications / edited by Ramasamy Vijayakumar and Suresh S.S. Raja*; Vijayakumar, R., Raja, S. S. S., Eds.; IntechOpen: London, United Kingdom, 2018.

(37) McMurry, J. *Organic chemistry with biological applications: Secondary Metabolites: An Introduction to Natural Products Chemistry*, 3rd; Cole: Stamford CT, 2015.

(38) Ullah, H.; Khan, H. Epigenetic drug development for autoimmune and inflammatory diseases. In *Histone modifications in therapy*; Castelo-Branco, P., Jeronimo, C., Eds.; Translational epigenetics 20; Academic Press: Amsterdam, 2020; pp 395–413.

(39) Perveen, S. Introductory Chapter: Terpenes and Terpenoids. In *Terpenes and terpenoids*; Perveen, S., Al-Taweel, A., Eds.; IntechOpen: London, 2018.

(40) Fugmann, B.; Lang-Fugmann, S.; Steglich, W.; Schick, H.; Adam, G. *Naturstoffe*; Römpp Lexikon; Thieme: Stuttgart, New York, 1997.

(41) Cane, D. E.; He, X.; Kobayashi, S.; Ōmura, S.; Ikeda, H. Geosmin Biosynthesis in *Streptomyces avermitilis* . Molecular Cloning, Expression, and Mechanistic Study of the Germacradienol/Geosmin Synthase. *J Antibiot* **2006**, *59*, 471–479.

(42) Dickschat, J. S.; Bode, H. B.; Mahmud, T.; Müller, R.; Schulz, S. A novel type of geosmin biosynthesis in myxobacteria. *J. Org. Chem.* **2005**, *70*, 5174–5182.

(43) Nawrath, T.; Dickschat, J. S.; Müller, R.; Jiang, J.; Cane, D. E.; Schulz, S. Identification of (8*S*,9*S*,10*S*)-8,10-dimethyl-1-octalin, a key intermediate in the biosynthesis of geosmin in bacteria. *J. Am. Chem. Soc.* **2008**, *130*, 430–431.

(44) Chadwick, M.; Trewin, H.; Gawthrop, F.; Wagstaff, C. Sesquiterpenoids lactones: benefits to plants and people. *Int. J. Mol. Sci.* **2013**, *14*, 12780–12805.

(45) Cox-Georgian, D.; Ramadoss, N.; Dona, C.; Basu, C. Therapeutic and Medicinal Uses of Terpenes. In *Medicinal plants: From farm to pharmacy / Nirmal Joshee, Sadanand A. Dhekney, Prahlad Parajuli, editors*; Joshee, N., Dhekney, S. A., Parajuli, P., Eds.; Springer: Cham, Switzerland, 2019; pp 333–359.

(46) Verpoorte, R. ALKALOIDS. *Encyclopedia of Analytical Science*; Elsevier, 2005; pp 56–61.

(47) Misra, N.; Luthra, R.; Singh, K. L.; Kumar, S. Recent Advances in Biosynthesis of Alkaloids. In *Comprehensive Natural Products Chemistry*; Barton, D. e., Meth-Cohn, O. e., Eds.; Elsevier, 1999; page: 25–59.

(48) Prithipalsingh. *Plant taxonomy: Past, present, and future Dr Prithipalsingh fest-schrift*; The Energy and Resources Institute: New Delhi, 2012.

(49) Schmitz, R. Friedrich Wilhelm Sertürner and the discovery of morphine. *Pharmacy in history* **1985**, *27*, 61–74.

(50) Wicks, C.; Hudlicky, T.; Rinner, U. Morphine alkaloids: History, biology, and synthesis; The Alkaloids: Chemistry and Biology; Elsevier, 2021; pp 145–342.

(51) Koskinen, A. M. P.; Karisalmi, K. Polyketide stereotetrads in natural products. *Chem Soc.Rev.* **2005**, *34*, 677–690.

(52) Oliynyk, M.; Samborskyy, M.; Lester, J. B.; Mironenko, T.; Scott, N.; Dickens, S.; Haydock, S. F.; Leadlay, P. F. Complete genome sequence of the erythromycin-producing bacterium *Saccharopolyspora erythraea* NRRL23338. *Nat. Biotechnol.* **2007**, *25*, 447–453.

(53) Cane, D. E. Programming of Erythromycin Biosynthesis by a Modular Polyketide Synthase. *J. Biol. Chem.* **2010**, *285*, 27517–27523.

(54) Rawlings, B. J. Type I polyketide biosynthesis in bacteria (Part A - erythromycin biosynthesis). *Nat. Prod. Rep.* **2001**, *18*, 190–227.

(55) Cryle, M.; Izore, T.; Ho, Y. T.; Kaczmarski, J.; Gavriilidou, A.; Chow, K.; Steer, D.; Goode, R.; Schittenhelm, R.; Tailhades, J.*; et al. Understanding condensation domain selectivity in non-ribosomal peptide biosynthesis: structural characterization of the acceptor bound state*, 2021.

(56) Izoré, T.; Candace Ho, Y. T.; Kaczmarski, J. A.; Gavriilidou, A.; Chow, K. H.; Steer, D. L.; Goode, R. J. A.; Schittenhelm, R. B.; Tailhades, J.; Tosin, M.*; et al.* Structures of a non-ribosomal peptide synthetase condensation domain suggest the basis of substrate selectivity. *Nat Commun* **2021**, *12*, 2511.

(57) Trauner, D.; Cheng, B.; Müller, R. Total syntheses of cystobactamids and structural confirmation of cystobactamid 919-2. *Angew. Chem. Int. Ed.* **2017**, *56*, 7407–7410.

(58) Wakil, S. J.; Titchener, E. B.; Gibson, D. M. Evidence for the participation of biotin in the enzymic synthesis of fatty acids. *Biochimica et biophysica acta* **1958**, *29*, 225–226.

(59) Waldrop, G. L.; Holden, H. M.; St Maurice, M. The enzymes of biotin dependent CO_2 metabolism: what structures reveal about their reaction mechanisms. *Protein Sci.* **2012**, *21*, 1597–1619.

(60) Schumacher, R. W.; Talmage, S. C.; Miller, S. A.; Sarris, K. E.; Davidson, B. S.; Goldberg, A. Isolation and structure determination of an antimicrobial ester from a marine sediment-derived bacterium. *J. Nat. Prod.* **2003**, *66*, 1291–1293.

(61) Maskey, R. P.; Helmke, E.; Laatsch, H. Himalomycin A and B: isolation and structure elucidation of new fridamycin type antibiotics from a marine *Streptomyces* isolate. *J Antibiot* **2003**, *56*, 942–949.

(62) Le Marrec, C.; Hyronimus, B.; Bressollier, P.; Verneuil, B.; Urdaci, M. C. Biochemical and genetic characterization of coagulin, a new antilisterial bacteriocin in the pediocin family of bacteriocins, produced by *Bacillus coagulans* I4. *Appl. Environ. Microbiol.* **2000**, *66*, 5213–5220.

(63) Thaxter, R. On a Myxobacteriaceae, a new order of Schizomycetes. *Botanical Gazette* **1892**, *17*, 389–406.

(64) Reichenbach, H.; Höfle, G. Production of bioactive secondary metabolites. In *Myxobacteria II*; Dworkin, M., Kaiser, D., Eds.; ASM Press: Washington, D.C., 1993; pp 347–397.

(65) Reichenbach, H. Order VIII. *Myxococcales*. Tchan, Pochon and Prévot 1948, 398AL. In *Bergey's manual of systematic bacteriology,* 2nd; Brenner, D., Krieg, N., Staley, J., Eds.; Springer, 2005; pp 1059–1144.

(66) Garcia, R.; Müller, R. The Family *Nannocystaceae*. In *The Prokaryotes*; Rosenberg, E., DeLong, E., Lory, S., Stackebrandt, E., Thompson, F., Eds.; Springer-Verlag: Berlin Heidelberg, 2014; pp 213–229.

(67) Reichenbach, H.; Höfle, G. Myxobacteria as producers of secondary metabolites. In *Drug Discovery from Nature*; Grabley, S., Thiericke, R., Eds.; Springer: Berlin, 1999; pp 149–179.

(68) Garcia, R.; Krug, D.; Müller, R. Discovering natural products from myxobacteria with emphasis on rare producer strains in combination with improved analytical methods. In *Methods in Enzymology: Complex Enzymes in Microbial Natural Product Biosynthesis* Part A: Overview Articles and Peptides; David A. Hopwood, Ed. 458, 2009; pp 59–91.

(69) Roane, T. M.; Reynolds, K. A.; Maier, R. M.; Pepper, I. L. Microorganisms. In *Environmental microbiology,* 2nd ed.; Maier, R. M., Pepper, I. L., Gerba, C. P., Eds.; Elsevier/Academic Press: Amsterdam, Boston, 2009; pp 9–36.

(70) Shimkets, L. J. Intercellular signaling during fruiting-body development of *Myxococcus xanthus*. *Annu. Rev. Microbiol.* **1999**, *53*, 525–549.

(71) O'Connor, K. A.; Zusman, D. R. Development in *Myxococcus xanthus* involves differentiation into two cell types, peripheral rods and spores. *J. Bacteriol.* **1991**, *173*, 3318–3333.

(72) Weissman, K. J.; Müller, R. Myxobacterial secondary metabolites: bioactivities and modes-of-action. *Nat. Prod. Rep.* **2010**, *27*, 1276–1295.

(73) Dawid, W. Biology and global distribution of myxobacteria in soils. *FEMS Microbiol. Rev.* **2000**, *24*, 403–427.

(74) Burchard, R. P.; Dworkin, M. Light-Induced Lysis and Carotenogenesis in *Myxococcus xanthus*. *J. Bacteriol.* **1966**, *91*, 535–545.

(75) Zusman, D. R.; Scott, A. E.; Yang, Z.; Kirby, J. R. Chemosensory pathways, motility and development in *Myxococcus xanthus*. *Nat. Rev. Microbiol.* **2007**, *5*, 862 EP -.

(76) Mauriello, E. M. F.; Mignot, T.; Yang, Z.; Zusman, D. R. Gliding motility revisited: how do the myxobacteria move without flagella? *Microbiol. Mol. Biol. Rev.* **2010**, *74*, 229–249.

(77) Koch, A. L.; White, D. The social lifestyle of myxobacteria. *Bioessays* **1998**, *20*, 1030–1038.

(78) Sudo, S.; Dworkin, M. Bacteriolytic enzymes produced by *Myxococcus xanthus*. *J. Bacteriol.* **1972**, *110*, 236–245.

(79) Wenzel, S. C.; Müller, R. The biosynthetic potential of myxobacteria and their impact on drug discovery. *Curr. Opin. Drug Discov. Devel.* **2009**, *12*, 220–230.

(80) Muñoz-Dorado, J.; Marcos-Torres, F. J.; García-Bravo, E.; Moraleda-Muñoz, A.; Pérez, J. Myxobacteria: Moving, Killing, Feeding, and Surviving Together. *Front. Microbiol.* **2016**, *7*.

(81) Pal, S.; Sharma, G.; Subramanian, S. Complete genome sequence and identification of polyunsaturated fatty acid biosynthesis genes of the myxobacterium *Minicystis rosea* DSM 24000T. *BMC Gen.* **2021**, *22*, 655.

(82) Hoffmann, M.; Auerbach, D.; Panter, F.; Hoffmann, T.; Dorrestein, P. C.; Müller, R. Homospermidine Lipids: A compound class specifically formed during fruiting body formation of *Myxococcus xanthus* DK1622. *ACS Chem. Biol.* **2018**, *13*, 273–280.

(83) Ringel, S. M.; Greenough, R. C.; Roemer, S.; Connor, D.; Gutt, A. L.; Blair, B.; Kanter, G.; von Strandtmann. Ambruticin (W7783), a new antifungal antibiotic. *J. Antibiot.* **1977**, *30*, 371–375.

(84) Sasse, F.; Steinmetz, H.; Schupp, T.; Petersen, F.; Memmert, K.; Hofmann, H.; Heusser, C.; Brinkmann, V.; Matt, P. von; Höfle, G.*; et al.* Argyrins, immunosuppressive cyclic peptides from myxobacteria. I. Production, isolation, physico-chemical and biological properties. *J. Antibiot.* **2002**, *55*, 543–551.

(85) Plaza, A.; Garcia, R.; Bifulco, G.; Martinez, J. P.; Hüttel, S.; Sasse, F.; Meyerhans, A.; Stadler, M.; Müller, R. Aetheramides A and B, potent HIV-inhibitory depsipeptides from a myxobacterium of the new genus "Aetherobacter". *Organic letters* **2012**, *14*.

(86) Irschik, H.; Gerth, K.; Kemmer, T.; Steinmetz, H.; Reichenbach, H. The Myxovalargins, new peptide antibiotics from *Myxococcus fulvus* (Myxobacterales) I. Cultivation, isolation, and some chemical and biological properties. *J. Antibiot.* **1983**, *36*, 6–12.

(87) Irschik, H.; Gerth, K.; Höfle, G.; Kohl, W.; Reichenbach, H. The myxopyronins, new inhibitors of bacterial RNA synthesis from *Myxococcus fulvus (*Myxobacterales). *J. Antibiot.* **1983**, *36*, 1651–1658.

(88) Höfle, G.; Bedorf, N.; Steinmetz, H.; Schomburg, D.; Gerth, K.; Reichenbach, H. Epothilone A and B: Novel 16-membered macrolides with cytotoxic activity: Isolation, crystal structure, and conformation in solution. *Angew. Chem. Int. Ed. Engl.* **1996**, *35*, 1567–1569.

(89) Gerth, K.; Steinmetz, H.; Höfle, G.; Jansen, R. Chlorotonil A, a macrolide with a unique gem-dichloro-1,3-dione functionality from *Sorangium cellulosum*, So ce1525. *Angew. Chem. Int. Ed. Engl.* **2008**, *47*, 600–602.

(90) Schäberle, T. F.; Schiefer, A.; Schmitz, A.; König, G. M.; Hoerauf, A.; Pfarr, K. Corallopyronin A – A promising antibiotic for treatment of filariasis. *Int. J. Med. Microbiol.* **2014**, *304*, 72–78.

(91) Mukhopadhyay, J.; Das, K.; Ismail, S.; Koppstein, D.; Jang, M.; Hudson, B.; Sarafianos, S.; Tuske, S.; Patel, J.; Jansen, R.*; et al.* The RNA polymerase "switch region" is a target of inhibitors. *Cell* **2008**, *135*, 295–307.

(92) Landwehr, W.; Wolf, C.; Wink, J. Actinobacteria and Myxobacteria-Two of the Most Important Bacterial Resources for Novel Antibiotics. *Curr. Top. Microbiol. Immunol.* [Online early access]. DOI: 10.1007/82_2016_503.

(93) Hoffmann, T.; Krug, D.; Bozkurt, N.; Duddela, S.; Jansen, R.; Garcia, R.; Gerth, K.; Steinmetz, H.; Müller, R. Correlating chemical diversity with taxonomic distance for discovery of natural products in myxobacteria. *Nat. Commun.* **2018**, *9*, 803.

(94) Cimermancic, P.; Medema, M. H.; Claesen, J.; Kurita, K.; Wieland Brown, Laura C; Mavrommatis, K.; Pati, A.; Godfrey, P. A.; Koehrsen, M.; Clardy, J.*; et al.* Insights into secondary metabolism from a global analysis of prokaryotic biosynthetic gene clusters. *Cell* **2014**, *158*, 412–421.

(95) Slot, J. C. Fungal Gene Cluster Diversity and Evolution. *Adv. Genet.* **2017**, *100*, 141–178.

(96) Agarwal, P. K. Enzymes: An integrated view of structure, dynamics and function. *Microb. Cell Fact.* **2006**, *5*.

(97) Newman, D. J.; Cragg, G. M. Natural Products as Sources of New Drugs over the Nearly Four Decades from 01/1981 to 09/2019. *J. Nat. Prod.* **2020**, *83*, 770–803.

(98) Staunton, J.; Weissman, K. J. Polyketide biosynthesis: a millennium review. *Nat. Prod. Rep.* **2001**, *18*, 380–416.

(99) Li, Y.; Weissman, K. J.; Müller, R. Myxochelin biosynthesis: direct evidence for two- and four-electron reduction of a carrier protein-bound thioester. *J. Am. Chem. Soc.* **2008**, *130*, 7554–7555.

(100) Hopwood, D. A. Genetic Contributions to Understanding Polyketide Synthases. *Chemical reviews* **1997**, *97*, 2465–2498.

(101) Silakowski, B.; Schairer, H. U.; Ehret, H.; Kunze, B.; Weinig, S.; Nordsiek, G.; Brandt, P.; Blöcker, H.; Höfle, G.; Beyer, S.*; et al.* New lessons for combinatorial biosynthesis from myxobacteria. The myxothiazol biosynthetic gene cluster of *Stigmatella aurantiaca* DW4/3-1. *J. Biol. Chem.* **1999**, *274*, 37391–37399.

(102) Park, S. R.; Yoo, Y. J.; Ban, Y.-H.; Yoon, Y. J. Biosynthesis of rapamycin and its regulation: past achievements and recent progress. *J. Antibiot.* **2010**, *63*, 434–441.

(103) Gregory, M. A.; Hong, H.; Lill, R. E.; Gaisser, S.; Petkovic, H.; Low, L.; Sheehan, L. S.; Carletti, I.; Ready, S. J.; Ward, M. J.*; et al.* Rapamycin biosynthesis: elucidation of gene product function. *Org. Biomol. Chem.* **2006**, *4*, 3565–3568.

(104) Chen, S.; Bamberg, D. von; Hale, V.; Breuer, M.; Hardt, B.; Müller, R.; Floss, H. G.; Reynolds, K. A.; Leistner, E. Biosynthesis of ansatrienin (mycotrienin) and naphthomycin. Identification and analysis of two separate biosynthetic gene clusters in *Streptomyces collinus* Tü 1892. *Eur. J. Biochem.* **1999**, *261*, 98–107.

(105) Gerth, K.; Irschik, H.; Reichenbach, H.; Trowitzsch, W. Myxothiazol, an antibiotic from *Myxococcus fulvus* (myxobacterales). I. Cultivation, isolation, physico-chemical and biological properties. *J. Antibiot.* **1980**, *33*, 1474–1479.

(106) Thierbach, G.; Reichenbach, H. Myxothiazol, a new antibiotic interfering with respiration. *Antimicrob. Agents Chemother.* **1981**, *19*, 504–507.

(107) Silakowski, B.; Nordsiek, G.; Kunze, B.; Blöcker, H.; Müller, R. Novel features in a combined polyketide synthase/non-ribosomal peptide synthetase: the myxalamid biosynthetic gene cluster of the myxobacterium *Stigmatella aurantiaca* Sga15. *Chem. Biol.* **2001**, *8*, 59–69.

(108) Müller, R. Don't classify polyketide synthases. *Chem. Biol.* **2004**, *11*, 4–6.

(109) Cragg, G. M.; Newman, D. J. Natural products: a continuing source of novel drug leads. *Biochim. Biophys. Acta* **2013**, *1830*, 3670–3695.

(110) Hauser, C. R.; Hudson, B. E. The Acetoacetic Ester Condensation and Certain Related Reactions. In *Organic reactions*; Adams, R., Ed.; John Wiley & Sons: New York, 1942-; pp 266–302.

(111) Fischbach, M. A.; Walsh, C. T. Assembly-line enzymology for polyketide and nonribosomal Peptide antibiotics: logic, machinery, and mechanisms. *Chem. Rev.* **2006**, *106*, 3468–3496.

(112) Klaus, M.; Buyachuihan, L.; Grininger, M. The Ketosynthase Domain Constrains the Design of Polyketide Synthases. *ACS Chem. Biol.* [Online early access]. DOI: 10.1021/acschembio.0c00405.

(113) Bayly, C.; Yadav, V. Towards Precision Engineering of Canonical Polyketide Synthase Domains: Recent Advances and Future Prospects. *Molecules* **2017**, *22*, 235.

(114) Reid, R.; Piagentini, M.; Rodriguez, E.; Ashley, G.; Viswanathan, N.; Carney, J.; Santi, D. V.; Hutchinson, C. R.; McDaniel, R. A model of structure and catalysis for ketoreductase domains in modular polyketide synthases. *Biochemistry* **2003**, *42*, 72–79.

(115) Jaremko, M. J.; Davis, T. D.; Corpuz, J. C.; Burkart, M. D. Type II non-ribosomal peptide synthetase proteins: structure, mechanism, and protein-protein interactions. *Nat. Prod. Rep.* [Online early access]. DOI: 10.1039/c9np00047j. http://dx.doi.org/10.1039/c9np00047j (accessed October 16, 2019).

(116) Sieber, S. A.; Marahiel, M. A. Molecular mechanisms underlying nonribosomal peptide synthesis: approaches to new antibiotics. *Chem Rev* **2005**, *105*, 715–738.

(117) Marahiel, M. A.; Stachelhaus, T.; Mootz, H. D. Modular Peptide Synthetases Involved in Nonribosomal Peptide Synthesis. *Chem. Rev.* **1997**, *97*, 2651–2674.

(118) Winn, M.; Fyans, J. K.; Zhuo, Y.; Micklefield, J. Recent advances in engineering nonribosomal peptide assembly lines. *Nat. Prod. Rep.* **2016**, *33*, 317–347.

(119) Schwarzer, D.; Finking, R.; Marahiel, M. A. Nonribosomal peptides: from genes to products. *Nat. Prod. Rep.* **2003**, *20*, 275–287.

(120) Trauger, J. W.; Kohli, R. M.; Mootz, H. D.; Marahiel, M. A.; Walsh, C. T. Peptide cyclization catalysed by the thioesterase domain of tyrocidine synthetase. *Nature* **2000**, *407*, 215–218.

(121) Trauger, J. W.; Kohli, R. M.; Walsh, C. T. Cyclization of backbone-substituted peptides catalyzed by the thioesterase domain from the tyrocidine nonribosomal peptide synthetase. *Biochemistry* **2001**, *40*, 7092–7098.

(122) Mohs, R. C.; Greig, N. H. Drug discovery and development: Role of basic biological research. *Alzheimer Dement (N Y)* **2017**, *3*, 651–657.

(123) Schlander, M.; Hernandez-Villafuerte, K.; Cheng, C.-Y.; Mestre-Ferrandiz, J.; Baumann, M. How Much Does It Cost to Research and Develop a New Drug? A Systematic Review and Assessment. *PharmacoEconomics* **2021**, *39*, 1243–1269.

(124) Seco, J. M.; Quiñoá, E.; Riguera, R. Assignment of the absolute configuration of polyfunctional compounds by NMR using chiral derivatizing agents. *Chem. Rev.* **2012**, *112*, 4603–4641.

(125) Sugimoto, Y.; Camacho, F. R.; Wang, S.; Chankhamjon, P.; Odabas, A.; Biswas, A.; Jeffrey, P. D.; Donia, M. S. A metagenomic strategy for harnessing the chemical repertoire of the human microbiome. *Science (New York, N.Y.)* **2019**, *366*.

(126) Dinan, L. Dereplication and Partial Identification of Compounds. In *Natural products isolation,* 2nd ed. / edited by Satyajit D. Sarker, Zahid Latif, Alexander I. Gray; Sarker, S. D., Latif, Z., Gray, A. I., Eds.; Methods in biotechnology 20; Humana Press: Totowa, N.J., 2006; pp 297–321.

(127) Beutler, J. A.; Alvarado, A. B.; Schaufelberger, D. E.; Andrews, P.; McCloud, T. G. Dereplication of Phorbol Bioactives: *Lyngbya majuscula* and *Croton cuneatus*. *J. Nat. Prod.* **1990**, *53*, 867–874.

(128) Dictionary of Natural Products. http://dnp.chemnetbase.com/faces/chemical/ChemicalSearch.xhtml.

(129) Gabrielson, S. W. SciFinder. *J. Med. Libr. Assoc.* **2018**, *106*.

(130) Yamaguchi, S.; Koda, N.; Eto, Y.; Aoki, K. Quick screening and diagnosis of organic acidemia by NMR urinalysis. *J. Pediatr.* **1985**, *106*, 620–622.

(131) Deborde, C.; Fontaine, J.-X.; Jacob, D.; Botana, A.; Nicaise, V.; Richard-Forget, F.; Lecomte, S.; Decourtil, C.; Hamade, K.; Mesnard, F.*; et al.* Optimizing 1D ^{1}H-NMR profiling of plant samples for high throughput analysis: extract preparation, standardization, automation and spectra processing. *Metabolomics* **2019**, *15*, 28.

(132) Dass, R.; Grudzia Ż, K.; Ishikawa, T.; Nowakowski, M.; Dębowska, R.; Kazimierczuk, K. Fast 2D NMR Spectroscopy for In vivo Monitoring of Bacterial Metabolism in Complex Mixtures. *Front. Microbiol.* **2017**, *8*, 1306.

(133) Zerikly, M.; Challis, G. L. Strategies for the discovery of new natural products by genome mining. *ChemBioChem* **2009**, *10*, 625–632.

(134) Albarano, L.; Esposito, R.; Ruocco, N.; Costantini, M. Genome Mining as New Challenge in Natural Products Discovery. *Marine drugs* **2020**, *18*.

(135) Metzker, M. L. Sequencing technologies - the next generation. *Nat. Rev. Genet.* **2010**, *11*, 31–46.

(136) Izawa, M.; Kawasaki, T.; Hayakawa, Y. Cloning and Heterologous Expression of the Thioviridamide Biosynthesis Gene Cluster from *Streptomyces olivoviridis*. *Appl. Environ. Microbiol.* **2013**, *79*, 7110–7113.

(137) Rutledge, P. J.; Challis, G. L. Discovery of microbial natural products by activation of silent biosynthetic gene clusters. *Nat. Rev. Microbiol.* **2015**, *13*, 509–523.

(138) Boratyn, G. M.; Camacho, C.; Cooper, P. S.; Coulouris, G.; Fong, A.; Ma, N.; Madden, T. L.; Matten, W. T.; McGinnis, S. D.; Merezhuk, Y.*; et al.* BLAST: a more efficient report with usability improvements. *Nucleic Acids Res.* **2013**, *41*, W29-33.

(139) Timmermans, M. L.; Paudel, Y. P.; Ross, A. C. Investigating the Biosynthesis of Natural Products from Marine Proteobacteria: A Survey of Molecules and Strategies. *Marine drugs* **2017**, *15*.

(140) Boddy, C. N. Bioinformatics tools for genome mining of polyketide and non-ribosomal peptides. *J. Ind. Microbiol. Biotechnol.* **2014**, *42*, 443–450.

(141) Hug, J. J.; Panter, F.; Krug, D.; Müller, R. Genome mining reveals uncommon alkylpyrones as type III PKS products from myxobacteria. *J. Ind. Microbiol. Biotechnol.* **2019**, *46*, 319–334.

(142) Panter, F.; Krug, D.; Baumann, S.; Müller, R. Self-resistance guided genome mining uncovers new topoisomerase inhibitors from myxobacteria. *Chem. Sci.* **2018**, *9*, 4898–4908.

(143) Hug, J. J.; Frank, N. A.; Walt, C.; Šenica, P.; Panter, F.; Müller, R. Genome-Guided Discovery of the First Myxobacterial Biarylitide Myxarylin Reveals Distinct C–N Biaryl Crosslinking in RiPP Biosynthesis. *Molecules* **2021**, *26*, 7483.

(144) Bader, C. D.; Panter, F.; Müller, R. In depth natural product discovery - Myxobacterial strains that provided multiple secondary metabolites. *Biotechnol. Adv.* **2020**, *39*, 107480.

(145) Heatley, N. G. A method for the assay of penicillin. *Biochem. J.* **1944**, *38*, 61–65.

(146) Monteiro, M. C.; La Cruz, M. de; Cantizani, J.; Moreno, C.; Tormo, J. R.; Mellado, E.; Lucas, J. R. de; Asensio, F.; Valiante, V.; Brakhage, A. A.*; et al.* A new approach to drug discovery: high-throughput screening of microbial natural extracts against *Aspergillus fumigatus* using resazurin. *J. Biomol. Screen.* **2012**, *17*, 542–549.

(147) Tulp, M.; Bohlin, L. Rediscovery of known natural compounds: nuisance or goldmine? *Bioorg. Med. Chem.* **2005**, *13*, 5274–5282.

(148) Hajduk, P. J.; Greer, J. A decade of fragment-based drug design: strategic advances and lessons learned. *Nat. Rev. Drug Discov.* **2007**, *6*, 211–219.

(149) Palazzotto, E.; Tong, Y.; Lee, S. Y.; Weber, T. Synthetic biology and metabolic engineering of actinomycetes for natural product discovery. *Biotechnol. Adv.* **2019**, *37*, 107366.

(150) Baltz, R. H. Genetic manipulation of secondary metabolite biosynthesis for improved production in *Streptomyces* and other actinomycetes. *J. Ind. Microbiol. Biotechnol.* **2016**, *43*, 343–370.

(151) Hosaka, T.; Ohnishi-Kameyama, M.; Muramatsu, H.; Murakami, K.; Tsurumi, Y.; Kodani, S.; Yoshida, M.; Fujie, A.; Ochi, K. Antibacterial discovery in actinomycetes strains with mutations in RNA polymerase or ribosomal protein S12. *Nat. Biotechnol.* **2009**, *27*, 462–464.

(152) Gomez-Escribano, J. P.; Song, L.; Fox, D. J.; Yeo, V.; Bibb, M. J.; Challis, G. L. Structure and biosynthesis of the unusual polyketide alkaloid coelimycin P1, a metabolic product of the *cpk* gene cluster of *Streptomyces coelicolor* M145. *Chem. Sci.* **2012**, *3*, 2716.

(153) McKenzie, N. L.; Thaker, M.; Koteva, K.; Hughes, D. W.; Wright, G. D.; Nodwell, J. R. Induction of antimicrobial activities in heterologous streptomycetes using alleles of the *Streptomyces coelicolor* gene *absA1*. *J. Antibiot.* **2010**, *63*, 177–182.

(154) Nai, C.; Meyer, V. From axenic to mixed cultures: technological advances accelerating a paradigm shift in microbiology. *Trends Microbiol.* [Online early access]. DOI:

10.1016/j.tim.2017.11.004. http://dx.doi.org/10.1016/j.tim.2017.11.004 (accessed March 27, 2018).

(155) Waschulin, V.; Borsetto, C.; James, R.; Newsham, K. K.; Donadio, S.; Corre, C.; Wellington, E. Biosynthetic potential of uncultured Antarctic soil bacteria revealed through long-read metagenomic sequencing. *ISME J.* **2022**, *16*, 101–111.

(156) Brakhage, A. A. Regulation of fungal secondary metabolism. *Nat. Rev. Microbiol.* **2013**, *11*, 21–32.

(157) Fischer, A. Acid production graphically registered as an indicator of the vital processes in the cultivation of bacteria. *J. Exp. Med.* **1918**, *28*, 529–545.

(158) Bertrand, S.; Bohni, N.; Schnee, S.; Schumpp, O.; Gindro, K.; Wolfender, J.-L. Metabolite induction via microorganism co-culture: a potential way to enhance chemical diversity for drug discovery. *Biotechnol. Adv.* **2014**, *32*, 1180–1204.

(159) Scherlach, K.; Hertweck, C. Triggering cryptic natural product biosynthesis in microorganisms. *Org. Biomol. Chem.* **2009**, *7*, 1753–1760.

(160) Oh, D. C.; Kauffman, C. A.; Jensen, P. R.; Fenical, W. Induced production of emericellamides A and B from the marine-derived fungus Emericella sp in competing co-culture. *J. Nat. Prod.* **2007**, *70*, 515–520.

(161) Netzker, T.; Flak, M.; Krespach, M. K.; Stroe, M. C.; Weber, J.; Schroeckh, V.; Brakhage, A. A. Microbial interactions trigger the production of antibiotics. *Curr. Opin. Microbiol.* **2018**, *45*, 117–123.

(162) Okada, B. K.; Seyedsayamdost, M. R. Antibiotic dialogues: induction of silent biosynthetic gene clusters by exogenous small molecules. *FEMS Microbiol. Rev.* **2017**, *41*, 19–33.

(163) Molloy, E. M.; Hertweck, C. Antimicrobial discovery inspired by ecological interactions. *Curr. Opin. Microbiol.* **2017**, *39*, 121–127.

(164) Abdelmohsen, U. R.; Grkovic, T.; Balasubramanian, S.; Kamel, M. S.; Quinn, R. J.; Hentschel, U. Elicitation of secondary metabolism in actinomycetes. *Biotechnol. Adv.* **2015**, *33*, 798–811.

(165) Oppong-Danquah, E.; Budnicka, P.; Blümel, M.; Tasdemir, D. Design of Fungal Co-Cultivation Based on Comparative Metabolomics and Bioactivity for Discovery of Marine Fungal Agrochemicals. *Mar. Drugs* **2020**, *18*.

(166) Schroeckh, V.; Scherlach, K.; Nutzmann, H. W.; Shelest, E.; Schmidt-Heck, W.; Schuemann, J.; Martin, K.; Hertweck, C.; Brakhage, A. A. Intimate bacterial-fungal interaction triggers biosynthesis of archetypal polyketides in *Aspergillus nidulans*. *Proc. Natl. Acad. Sci. USA* **2009**, *106*, 14558–14563.

(167) König, C. C.; Scherlach, K.; Schroeckh, V.; Horn, F.; Nietzsche, S.; Brakhage, A. A.; Hertweck, C. Bacterium induces cryptic meroterpenoid pathway in the pathogenic fungus *Aspergillus fumigatus*. *ChemBioChem* **2013**, *14*, 938–942.

(168) Maglangit, F.; Fang, Q.; Kyeremeh, K.; Sternberg, J. M.; Ebel, R.; Deng, H. A Co-Culturing Approach Enables Discovery and Biosynthesis of a Bioactive Indole Alkaloid Metabolite. *Molecules (Basel, Switzerland)* **2020**, *25*.

(169) Schneider, Y.; Jenssen, M.; Isaksson, J.; Hansen, K. Ø.; Andersen, J. H.; Hansen, E. H. Bioactivity of Serratiochelin A, a Siderophore Isolated from a Co-Culture of *Serratia* sp. and *Shewanella* sp. *Microorganisms* **2020**, *8*.

(170) Onaka, H.; Ozaki, T.; Mori, Y.; Izawa, M.; Hayashi, S.; Asamizu, S. Mycolic acid-containing bacteria activate heterologous secondary metabolite expression in *Streptomyces lividans*. *J. Antibiot.* **2015**, *68*, 594–597.

(171) Marrakchi, H.; Laneelle, M. A.; Daffe, M. Mycolic Acids: Structures, Biosynthesis, and Beyond. *Chem. Biol.* **2014**, *21*, 67–85.

(172) Onaka, H.; Mori, Y.; Igarashi, Y.; Furumai, T. Mycolic acid-containing bacteria induce natural-product biosynthesis in *Streptomyces* species. *Appl. Environ. Microbiol.* **2011**, *77*, 400–406.

(173) Bode, H. B.; Bethe, B.; Höfs, R.; Zeeck, A. Big Effects from Small Changes: Possible Ways to Explore Nature's Chemical Diversity. *ChemBioChem* **2002**, *3*, 619.

(174) English, A. L.; Boufridi, A.; Quinn, R. J.; Kurtböke, D. I. Evaluation of fermentation conditions triggering increased antibacterial activity from a near-shore marine intertidal environment-associated *Streptomyces* species. *Synth. Syst. Biotechnol.* **2017**, *2*, 28–38.

(175) Guo, W.; Zhang, Z.; Zhu, T.; Gu, Q.; Li, D. Penicyclones A-E, Antibacterial Polyketides from the Deep-Sea-Derived Fungus *Penicillium* sp. F23-2. *J. Nat. Prod.* **2015**, *78*, 2699–2703.

Chapter 2

A co-cultivation approach to alter the myxobacterial secondary metabolome

Markus Neuber, Alexander Popoff, Daniel Krug and Rolf Müller

Manuscript in preparation

Contributions to the presented work

Author's contribution

The author contributed to the concept of this study, designed and performed experiments, evaluated and interpreted resulting data. The author developed and performed co-cultivation experiments and analysed the corresponding LC-MS data using statistical methods. In the course of this, the author identified derivatives of phenylethylamine as a previously unknown myxobacterial compound class. In addition, the author contributed to the conception and writing of this manuscript.

Contribution by others

Alexander Popoff performed the NMR-based structure elucidation. Daniel Krug and Rolf Müller contributed by supervision of the project and conceiving, editing and proofreading of this manuscript.

2. Development of a myxobacterial co-cultivation approach

2.1 Abstract

Recent genomic studies indicate that the majority of biosynthetic gene clusters (BGCs) of many bacteria and fungi are not expressed under standard laboratory cultivation conditions. One approach to access the metabolic diversity of microbes is co-cultivation, where the presence of co-habiting microbes may induce the expression of "silent or cryptic" BGCs. In this study, a co-cultivation strategy was developed and implemented for the model myxobacterium *Myxococcus xanthus* DK1622. Direct and indirect co-cultivation setups revealed that the production of new metabolic features was triggered by Gram-positive bacteria, Gram-negative bacteria as well as eukaryotic microorganisms. From a co-culture of DK1622 and *S. carnosus* various phenylethylamines were identified as a previously unknown myxobacterial substance class. Our work clearly demonstrates that myxobacterial co-cultivation of DK1622 with direct cell-cell contact in liquid environment leads to the detection of a number of new secondary metabolites.

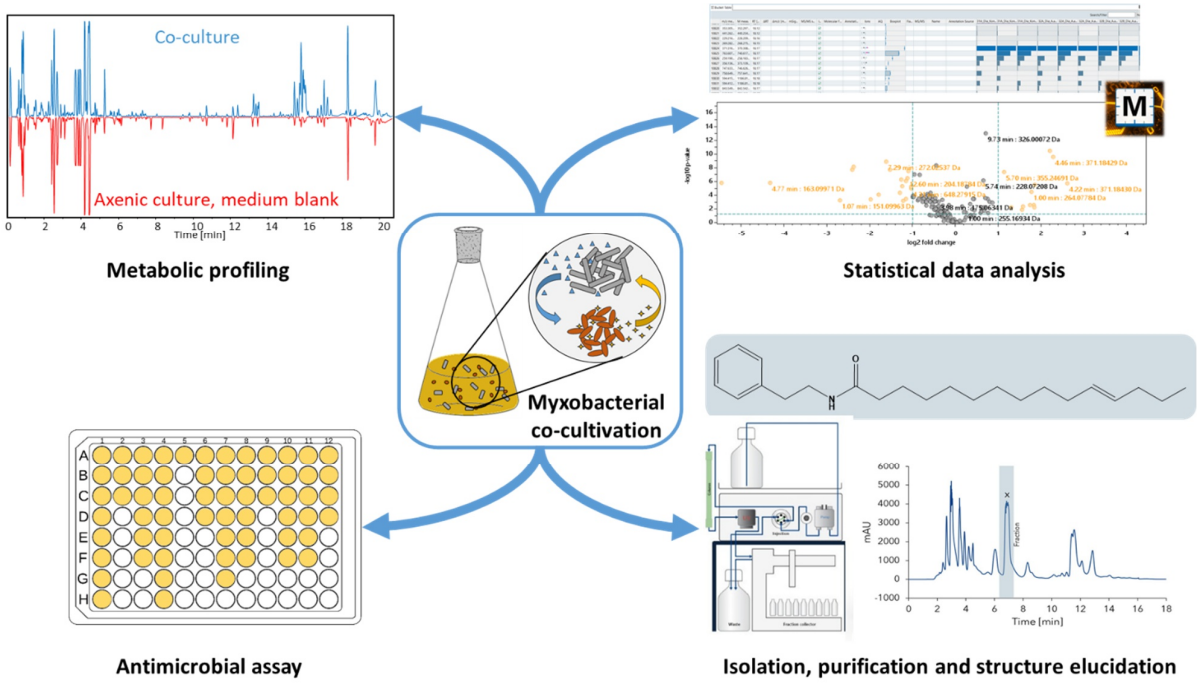

Graphical Abstract

2.2 Introduction

Bacteria and fungi are a valuable and indispensable source for the development of human medicine, veterinary health as well as plant crop protection[1]. Therefore, compared to other natural resources, microbes are considered a highly attractive source of NPs in drug discovery, in particular because of their ubiquitous existence, their enormous biodiversity and the vast chemical diversity that can be found within a given species[2,3]. Besides these general considerations for the utility of microorganisms in NP research, an important aspect is the possibility of discovering new scaffolds for the generation of new bioactive compounds. In this context, several biotechnological approaches in which microorganisms are typically grown in axenic culture have attracted interest for the potential discovery of new lead compounds and the study of underlying biosynthetic pathways.

Myxobacteria are Gram-negative, unicellular rod shaped delta-proteobacteria that occur ubiquitously in soils[4]. They show unique cooperative social behaviour, based on a communication system of cell-to-cell interaction[5]. Myxobacteria move by gliding on solid surfaces and use exoenzymes to lyse different biological macromolecules as well as whole organisms, such as bacteria or yeasts[6]. Another extraordinary feature of myxobacteria is their enormous potential to produce low-molecular but structurally complex molecules, so-called secondary metabolites (SMs)[7]. Natural products (NPs) have traditionally served as a viable source for therapeutic agents and have been used as antibiotics, antitumor agents, and anti-fungal compounds[8,9]. The responsible genes for the biosynthesis of SMs are often clustered in microbial genomes. For the synthesis of most myxobacterial SMs, the polyketide synthases (PKS) or non-ribosomal peptide synthetases (NRPS) play a key role, as demonstrated by genetic and biochemical characterisation of their gene clusters[10]. For example, the reported myxothiazol biosynthesis was one of the first NP assembly lines which contained both PKS and NRPS modules in a single multienzyme[11]. Recent genomic studies indicate that the majority of biosynthetic gene clusters of certain groups of microorganisms are not expressed under standard laboratory cultivation conditions[12,13].

One approach to access the metabolic diversity of microbes which has been rarely used to date with myxobacteria is the co-cultivation or mixed fermentation[14,15], where the presence of cohabiting microbes may induce the expression of so-called “silent” or non-expressed biosynthetic gene clusters (BGCs). Microbial co-cultivation, where two or multiple organisms are grown together in a confined environment, has been discussed as an effective strategy to increase the chemical diversity of secondary metabolites, mainly related to competition. In such cases, it is assumed that the presence of diffusible, low-molecular-weight signalling molecules results in the biosynthesis

of diverse NPs by triggering the non-expressed BGCs [16]. These signal molecules can elicit positive or negative effects and initiate chemical interactions, which results in the production of NPs that are not detectable in axenic cultures. However, conventional co-cultivation approaches require vast screening to identify the suitable microbial combinations, which is difficult and often tedious to apply on a larger scale. One scientific advance has been the steady development of analytical techniques especially in the field of high-resolution mass spectrometry, which considerably improves the detection limits for analytes[17]. This enables more sophisticated monitoring of chemical induction, leading to more convincing studies to investigate novel NPs formed by e.g. using advanced spectral similarity networks[18].

Several novel chemical substances such as siderophores, defense molecules or secondary metabolites have already been isolated from co-cultivated microorganisms in the past[19–22]. This approach has been successful due to affecting the metabolome and can lead to increased yield in the discovery of known and novel compounds, including bioactive molecules or lead structures[16,23–26]. For example, the co-cultivation of two actinomycetes associated with marine sponges, namely *Actinokineospora sp.* EG49 and *Nocardiopsis sp.* RV163, resulted in the production of three metabolites that were not produced when the strains were cultivated independently. The compound phenazine displays considerable biological activity against *Bacillus sp.* p25 and *Trypanosoma brucei*, as well as against *Actinokineospora sp.* EG49 themselves[27]. Interaction between the predatory myxobacterium *M. xanthus* with antibiotic producer *S. coelicolor* was investigated and resulted in an up to 20-fold increased production of the antibiotic actinorhodin by *S. coelicolor* in liquid medium[28].

In this study, an attempt was conducted for the first time to enhance the individual metabolomic profiles of *Myxococcus xanthus* DK1622 in combination with six different partner strains (*E. coli, P. putida, B. subtilis, S. carnosus, Y. lipolytica, S. cerevisiae*) by direct and indirect liquid co-cultivation to generate novel SMs. Through LC-*hr*MS techniques, the similarities and the differences among the produced secondary metabolites in direct and indirect co-cultured fermentation were detected depending on the Gram-positive, Gram-negative or eukaryotic partner strain. The phenylethylamines were identified as unique features for the first time after direct co-cultivation between *M. xanthus* DK1622 and *Staphylococcus carnosus*.

2.3 Results and discussion

For co-cultivation, we designed an experimental setup of the well-studied model myxobacterium *M. xanthus* DK1622[29] with six different partner strains derived from Gram-positive, Gram-negative and eukaryotic origins. Each partner strain was co-cultivated with *M. xanthus* DK1622 in three different runs using direct and indirect methods. To investigate the influence on secondary metabolite production by our model organism, we decided to perform a direct (cell-cell contact) and two indirect (filtrated supernatant and heat-inactivated cells) co-cultivation approaches. The corresponding crude extracts of the co-culture, axenic culture and medium blank were analysed by LC-MS, compared and processed using statistical data analysis software.

2.3.1 Developing co-culture procedures for the model organism *M. xanthus* DK1622

During the ongoing research for novel biologically active metabolites from microorganisms, several studies carried out mainly within the last few years proved the potential of co-cultivation with two or more different microbes as an experimental tool for either enhancing the production of constitutively present compounds and/or to investigate non-expressed BGCs. In this study, the liquid direct and indirect co-cultivation of *M. xanthus* DK1622 with Gram-positive (*B. subtilis*, *S. carnosus*), Gram-negative (*E. coli*, *P. putida*) and eukaryotic (*S. cerevisiae*, *Y. lipolytica*) microorganisms was attempted for the first time.

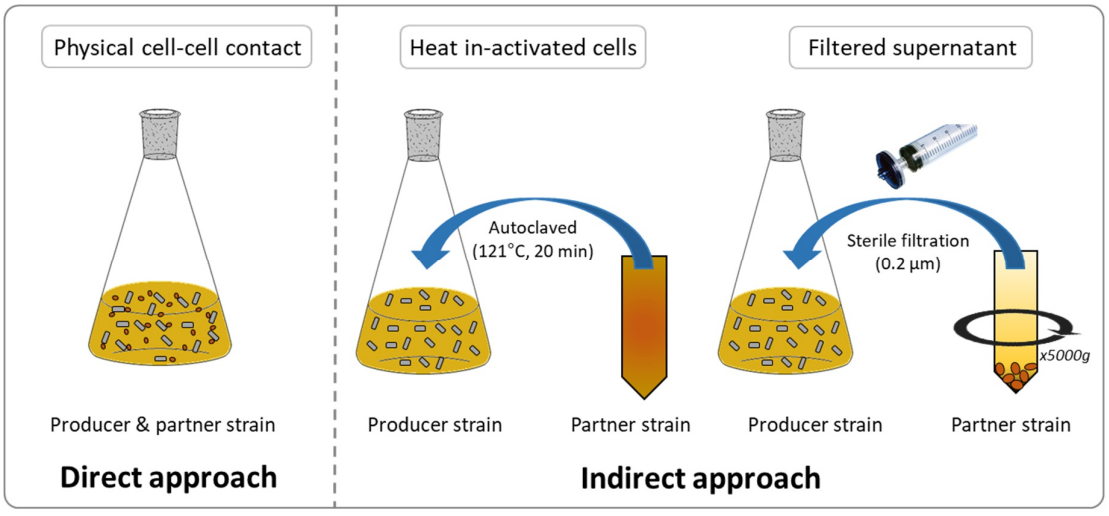

Figure 2.1: Developed direct and indirect co-culturing approaches for myxobacterium *M. xanthus* DK1622. Direct approach consists of a physical cell-cell contact between DK1622 and a partner strain in liquid media. Indirect approaches involve the addition of either heat inactivated cells (through autoclaving) or filtered (0.2 µm) supernatant from the partner strain after centrifugation at 5000 g.

The direct co-cultivation setup aims to explore the influence of physical cell-cell contacts between producer and partner strain on the production of SMs. The indirect cultivation with filtered supernatant (fSN) and heat inactivated cells (hCells) allows us to identify changes in the metabolome due to produced small molecules and/or cell components from the partner strain.

It was observed that after 7 days of direct co-cultivation, the culture broth exhibited a mixture of producer and partner strain under the microscope. This observation indicates the inoculation ratio between *M. xanthus* DK1622 and the partner strains calculated on the basis of optical density was properly selected to avoid overgrowth by the partner strain. In addition, all co-cultures display changes in the density and colour in comparison with the respective axenic cultivations. All cultures from the indirect co-cultivation approaches, which did not contain living partner strains, showed no visible changes in culture colour after addition of filtered supernatant or heat-inactivated cells. In a next step, we evaluated the detected metabolites from all extracts of the different approaches and partner strains using a statistical annotation workflow to clarify differences between the co-cultures.

2.3.2 Non-targeted metabolomics investigation of the extracts from direct and indirect co-cultivation approaches

Beyond the targeted metabolomics study of the myxobacterial extracts, we aimed to assess the overall chemical complexity of the three approaches in order to fully characterise overlaps and differences as well as the influence of different partner strains. Therefore, all crude extracts were analysed in a non-targeted metabolomics workflow (threshold intensity of $5x10^3$), and data was evaluated on alterations in SM profiles of direct and indirect co-cultures compared to axenic culture counterparts. A statistically annotated feature table of metabolites was created using a principal component analysis (PCA) in conjunction with t-Test/ANOVA and significant differences in the metabolic profiles were found. Therefore, features found in at least two out of three biological replicates were considered as a significant hit. In addition, we only compared the occurrence of newly detected features after the elimination of axenic culture controls and medium blanks. The differences between newly appearing metabolites were characterised by seven combinations of detected features: the only appearance by direct; fSN or hCells co-cultivation, the appearance by direct/fSN; direct/hCells; or fSN/hCells co-cultivation, and appearance by direct/fSN/hCells co-cultivation. The compared results were visualised for the respective partner strain in combination with *M. xanthus* DK1622 in Venn diagrams (Figure 2.2).

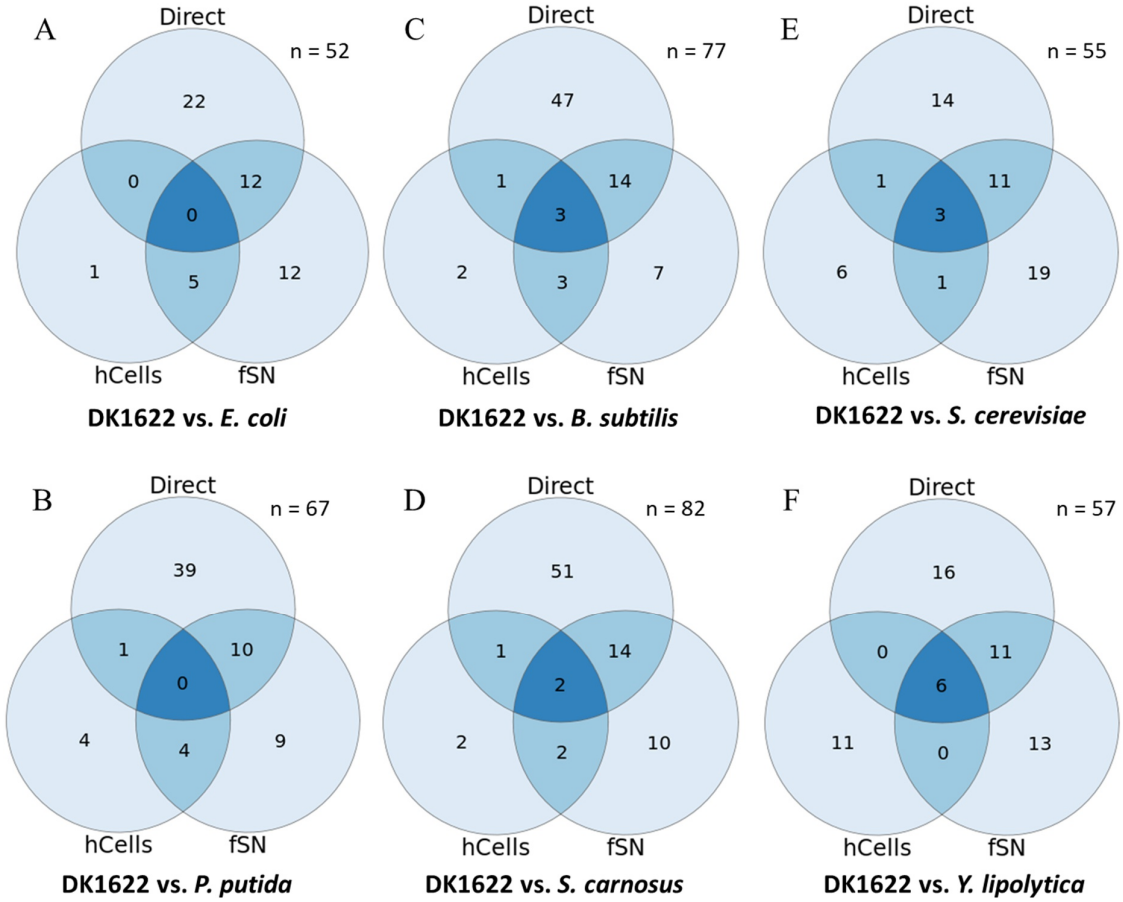

Figure 2.2: Venn diagrams showing the influence of co-cultivation (Direct), filtrated supernatant (fSN) and heat-inactivated cells (hCells) with Gram-negative (**A–B**), Gram-positive (**C–D**) and eukaryotic (**E–F**) partner strains on the production of novel secondary metabolites of *M. xanthus* DK1622. The numbers represent the appearance of new metabolites in comparison to axenic culture of DK1622. All annotated metabolites in the media were classified as blank.

In general, the metabolomic study of all extracts has shown that each approach can generate a different number of new metabolites that are not detectable in axenic cultures. Interestingly, we observe that the direct approach yielded almost always the highest number of newly identified features, independently of the type of partner strain that was used for co-cultivation. In addition, direct co-cultivation always revealed more unique features than the comparable indirect approaches combined, but only in the Gram-negative and Gram-positive partner strains. The eukaryotic microorganisms did not show such an effect on *M. xanthus* DK1622. The second most powerful approach was the addition of filtered supernatant, followed by the heat-inactivated cells according to the total number of identified features. In addition, the investigation of newly appearing metabolites also reveals distinct differences between the used Gram-negative, Gram-positive and

eukaryotic partner strains themselves. For example, the total number of novel features ranges from 52 (vs. *E. coli*) to 82 (vs. *S. carnosus*), depending on the partner strain employed.

These results indicate that Gram-positive strains such as *B. subtilis* and *S. carnosus* have a greater chance of activating/triggering the production of new SMs in *M. xanthus* DK1622. In addition, direct co-cultivation has also been shown to be more efficient in generating a greater variety of SMs. Observations on increasing the production or expanding the diversity of metabolites of biological organisms using the co-culture method have already been reported as a strategy for current biotechnological purposes[30,31]. In particular, microbial communication through the secretion of small molecules or defence substances such as antimicrobials is encouraged by competition in the same environment. An obvious result is that most of the partner strains treated with heat inactivation are significantly less able to initiate the production of new metabolites of DK1622, which was probably caused by the degradation of cells and small molecules due to autoclaving.

After the non-targeted metabolomics evaluation, the effect of the different partner strains and co-cultivation approaches on production levels of known SMs from *M. xanthus* DK1622 was analysed. Therefore, intensities of known compounds were determined from LC-MS measurements, which can be related to the production levels of certain metabolites of different compound classes.

2.3.3 Influence of the direct and indirect co-cultivation approaches on the production of myxobacterial secondary metabolites

All extracts were investigated in a targeted metabolomics workflow and known myxobacterial secondary metabolites were annotated from our in-house database (myxobase). Three different families of natural compounds, namely cittilins, DKxanthen and myxalamides, were detected in axenic *M. xanthus* DK1622 extracts. We were only able to detect cittilin A, myxalamid A and myxalamid B in all extracts above the threshold of 5 x 10^3 which allowed a comparison of the respective intensities. Comparison of intensities of these natural product families are shown in Figure 2.3 and Figure 2.4. Results for myxalamid B can be found in the supporting information (Figure S2.1). On the other hand, myxovirescin, myxochromids, myxochelins and myxoprincomides are four additional natural product families known from *M. xanthus* DK1622[32,33], which were not produced under the chosen cultivation conditions. Cittilin A (Figure 2.3) could be detected in all approaches of each partner strain, with the highest intensities found in extracts with added filtered supernatant[33,34]. Furthermore, treatment with heat-inactivated cells or direct co-cultivation resulted in a higher intensity than in the axenic extract for some partner strains. Direct co-cultivation with Gram-negative partner strains *E. coli* and *P. putida* led to slightly reduced intensities of cittilin A, whereas in both indirect methods the intensities were increased. Up to now, no antimicrobial activity of cittilin A has been published.

The compound family of Myxalamides consists of a number of derivatives, of which the two main derivatives (A and B) were detectable in our targeted metabolomic workflow[35,36]. The highest intensities of Myxalamid A (Figure 2.4) were found in the indirect co-cultivation procedure using filtered supernatant. These results are observed independently of the partner strain employed. Interestingly, similar effects were observed for the production levels of cittilin A. All co-cultivation approaches increased the detected Myxalamid A concentrations or at least maintained them in a comparable level to the control, excluding direct co-cultivation with Gram-negative strains, where a negative effect was observed. Myxalamid A and B are known for their moderate bioactivity against various Gram-positive and Gram-negative pathogens such as *B. subtilis*, *S. aureus* Newman and *E. coli* TolC[37], which can be considered as a possible reason for the higher production levels in particular crude extracts after co-cultivation. It can also be speculated that the increased production of active molecules against potential pathogens is due to competition in the liquid environment and quorum signalling[38,39]. When co-cultivation was performed directly in the same liquid environment, the nutrient supply required for growth between producer and partner strain was limited, which might also influence the production of myxobacterial secondary metabolites.

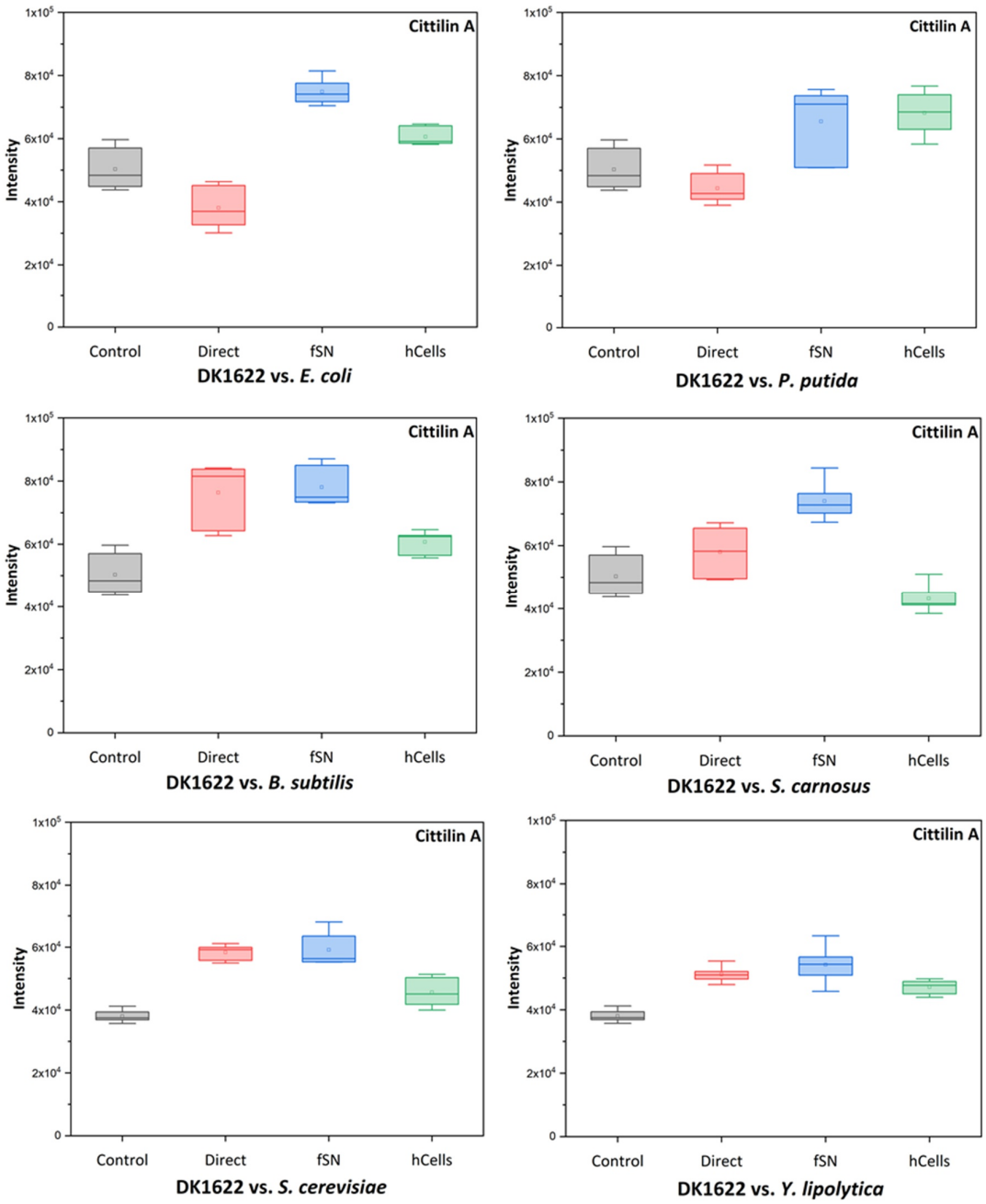

Figure 2.3: Influence of co-culturing approaches (direct – cell-cell contact, fSN – filtrated supernatant, hCells – heat-inactivated cells) on the production level of Cittilin A from *M. xanthus* DK1622 (**A–F**). Detected intensities of Cittilin A in respective crude extract are shown as a box plot.

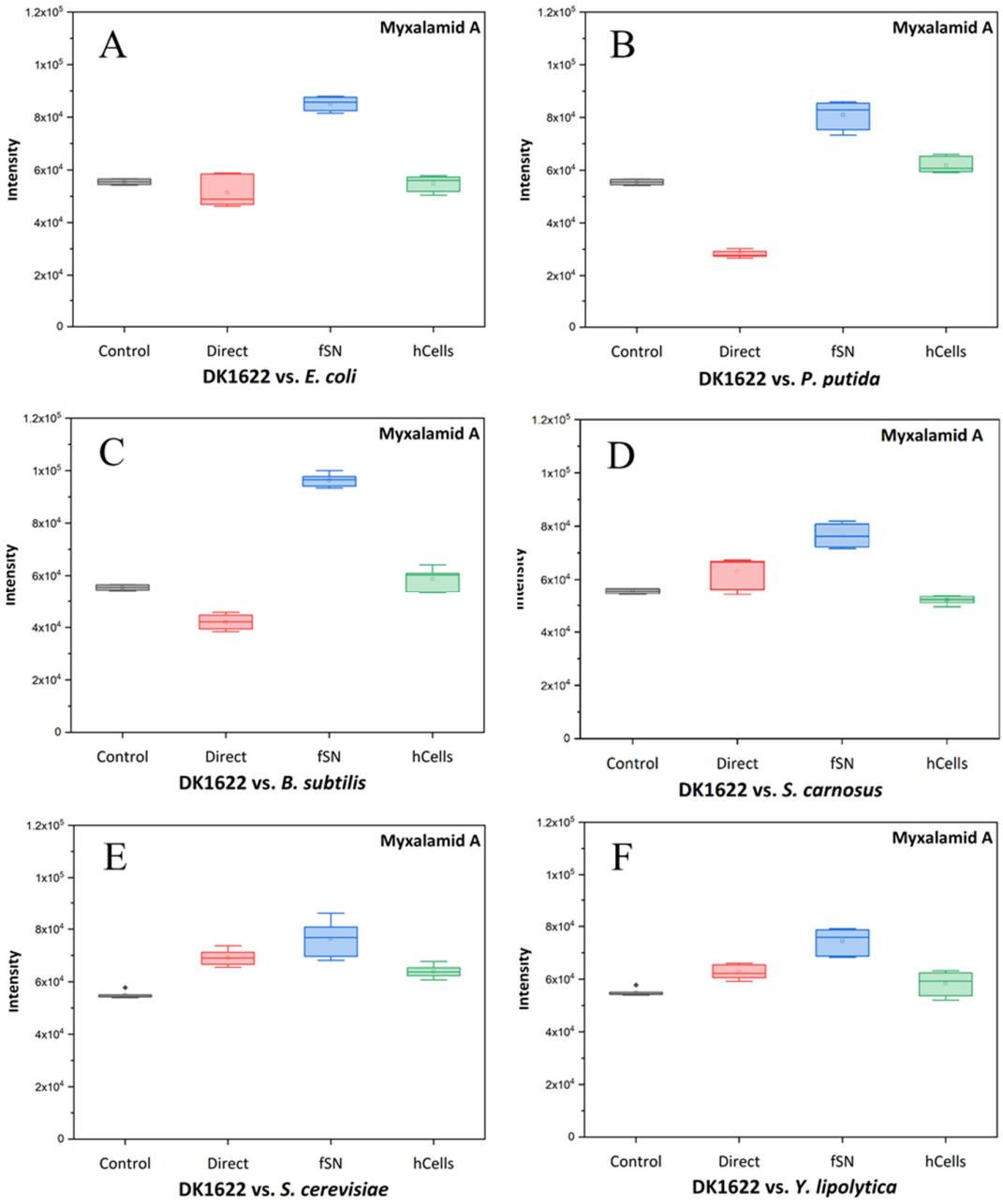

Figure 2.4: Influence of co-culturing approaches (direct – cell-cell contact, fSN – filtrated supernatant, hCells – heat-inactivated cells) on the production level of myxalamid A from *M. xanthus* DK1622 depending on different partner strains (**A–F**). Detected intensities of myxalamid A in respective crude extract are shown as a box plot.

The next experiment focused on the structural elucidation of the major derivative of phenylethyl-amine, which was identified as a new myxobacterial metabolite induced by direct co-cultivation between DK1622 and *S. carnosus*.

2.3.4 Isolation of phenylethylamine derivative-357

We were able to identify the class of phenylethylamine compounds by their increased intensity in non-targeted metabolomics and then to correlate the respective LC-MS chromatograms. To investigate the chemical structure of a newly appearing compound due to co-cultivation, we isolated one of the main derivatives and named it phenylethylamine-357. Therefore, a large scale co-cultivation between *M. xanthus* DK1622 and *S. carnosus* was carried out to obtain the required quantity for NMR experiments. Comparison of 1-D (^{1}H and ^{13}C) and 2-D (COSY, HSQC, HMBC) NMR data of phenylethylamin-357 confirmed that we isolated a representative of the already reported class of phenylethylamine compounds[40–42]. NMR spectra and the assignment table can be found in the supplementary information (Figure S2.2 – Figure S2.7; Table S2.1). According to the signals, the molecular sum formula and the other derivatives detected, we concluded that it is indeed the phenylethylamine derivative-357 ($C_{24}H_{39}NO$, $M_W = 357.58$)[43]. Additional derivatives of phenylethylamine (Figure S2.8 and Table S2.2) were identified using LC-*hr*MS, but not isolated or verified by NMR.

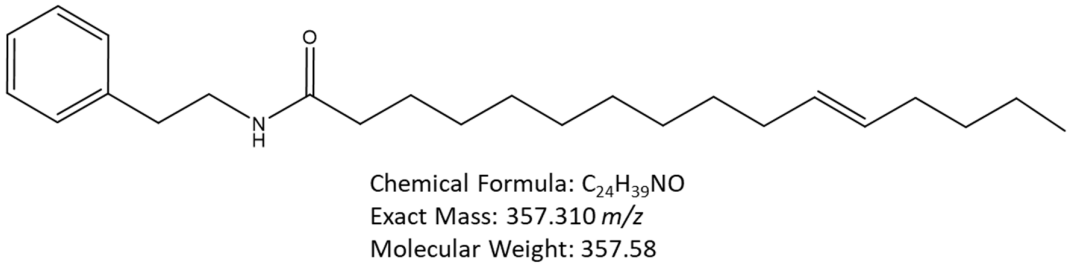

Figure 2.5: Chemical structure of phenylethylamine derivative-357.

In this co-cultivation study, we have discovered four different phenylethylamine analogues as a new class of compounds produced by the myxobacterium *M. xanthus* DK1622. We were able to identify and isolate the compound class of phenylethylamine from the well-known model organism DK1622, even though many classes of compounds have already been published[34,44,45]. Bacteria of the genus Xenorhabdus are so far the only producers of bioactive compounds of the phenylethylamine class that have already been published[40,41]. This class of compounds, also known as cytotoxic fatty acid amides, exhibit cytotoxic effects on L929 and HL-60 cells, with their cytotoxicity dependent on the acyl chain length[43].

The production of particular compounds from the chemical class of phenylethylamines have been used to the assessment of direct and indirect co-cultivation approaches. For the next investigation, we screened the respective extracts for the occurrence of target masses after treatment with different co-cultivation procedures.

2.3.5 Co-cultivation study between DK1622 and *S. carnosus* for the induced production of phenylethylamine

To evaluate and compare different co-culturing approaches for the production of a specific metabolite, we decided to choose the newly identified compound class of phenylethylamines produced by DK1622 as a target metabolite within the crude extracts. The targeted co-cultivation study reveals that phenylethylamin-357 was produced exclusively in the direct co-cultures with living cells of *S. carnosus*, as shown in Figure 2.6A. Cultures grown without living cells of *S. carnosus* like the axenic (control) and filtered supernatant (fSN) approach, did not produce the phenylethylamine after 7 days of cultivation. In the co-culture (direct) and in the solely centrifuged supernatant (SN) attempt, phenylethylamin-357 was detected in different concentrations after 7 days of growth. The presence of viable *S. carnosus* cells could be determined by the sudden changes in cell turbidity and by microscopy.

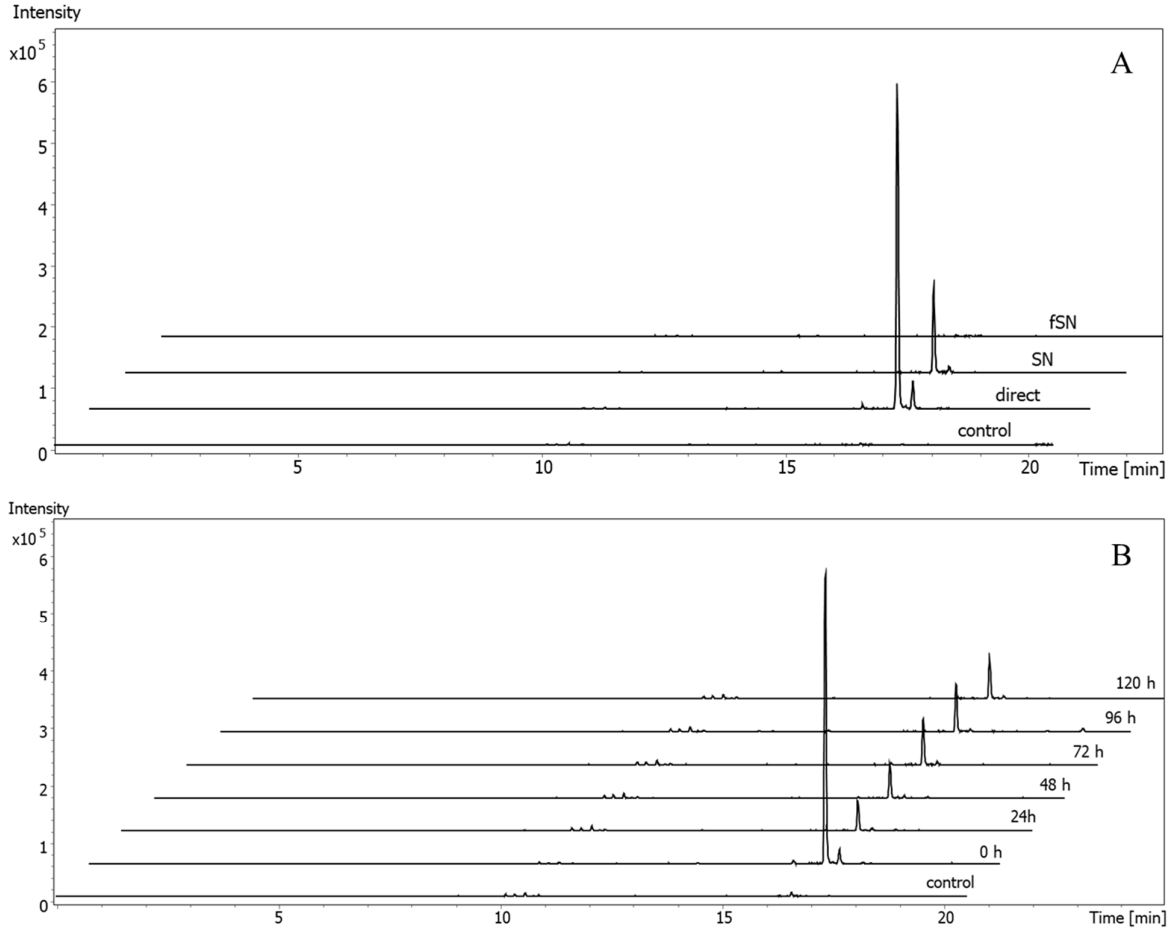

Figure 2.6 Extracted ion chromatogram of phenylethylamin-357 (EIC 358.308 +/- 0.01 m/z) derived from crude extracts after co-cultivations of *M. xanthus* DK1622 and *S. carnosus*. (**A**) Investigation of the effect on production of direct co-cultivation and indirect cultivation approaches by addition of centrifuged *S. carnosus* supernatant (SN) and

centrifuged + filtered supernatant (fSN) to DK1622 cultures. (**B**) Time-dependent experiment with addition of partner strain *S. carnosus* for the direct co-cultivation with DK1622.

Furthermore, a time-dependent experiment with specific addition times of viable *S. carnosus* cells showed that phenylethylamin-357 was detectable in all extracts from the co-cultures, except in the control culture (Figure 2.6 B). The highest intensity of phenylethylamin-357 was observed in the co-culture extract when the partner strain was added at the beginning of the experiment. This can be explained by a specific cell number of the living partner strain, which is necessary to exchange or produce small molecules to trigger the production of unspecific and specific metabolites.

Previously, several co-cultivation studies have shown that an interspecies communication/interaction of bacteria with other bacterial or fungal genera can increase the concentration of novel metabolites and expand the diversity of secondary metabolites[25,46]. The model organism DK1622 was capable of producing various phenylethylamine derivatives in a co-culture with *S. carnosus* as a previously unknown compound class from myxobacteria. Therefore, we assume that physical cell-cell contact between both bacteria seems to be required as a trigger for product formation.

In addition to the known cytotoxic effects of fatty acid amides, we have screened the extracts that we obtained from direct and indirect co-cultivation approaches, including the respective controls and medium blanks, for their antimicrobial activity. The following part aims to rate the biological activity using an activity score to distinguish either an increase, decrease or no change at all.

2.3.6 Antimicrobial assays of crude extracts from direct and indirect co-cultivation approaches

All methanol extracts from co-cultivation approaches were tested against a panel of Gram-negative (*E. coli, P. putida*), Gram-positive pathogens (*B. subtilis, S. carnosus*) and eukaryotic organisms (*Y. lipolytica, S. cerevisiae*), which were the partner strains used for co-cultivation. The activity score (Figure 2.7 B) was calculated from the raw data of the antimicrobial assay (Table S2.3).

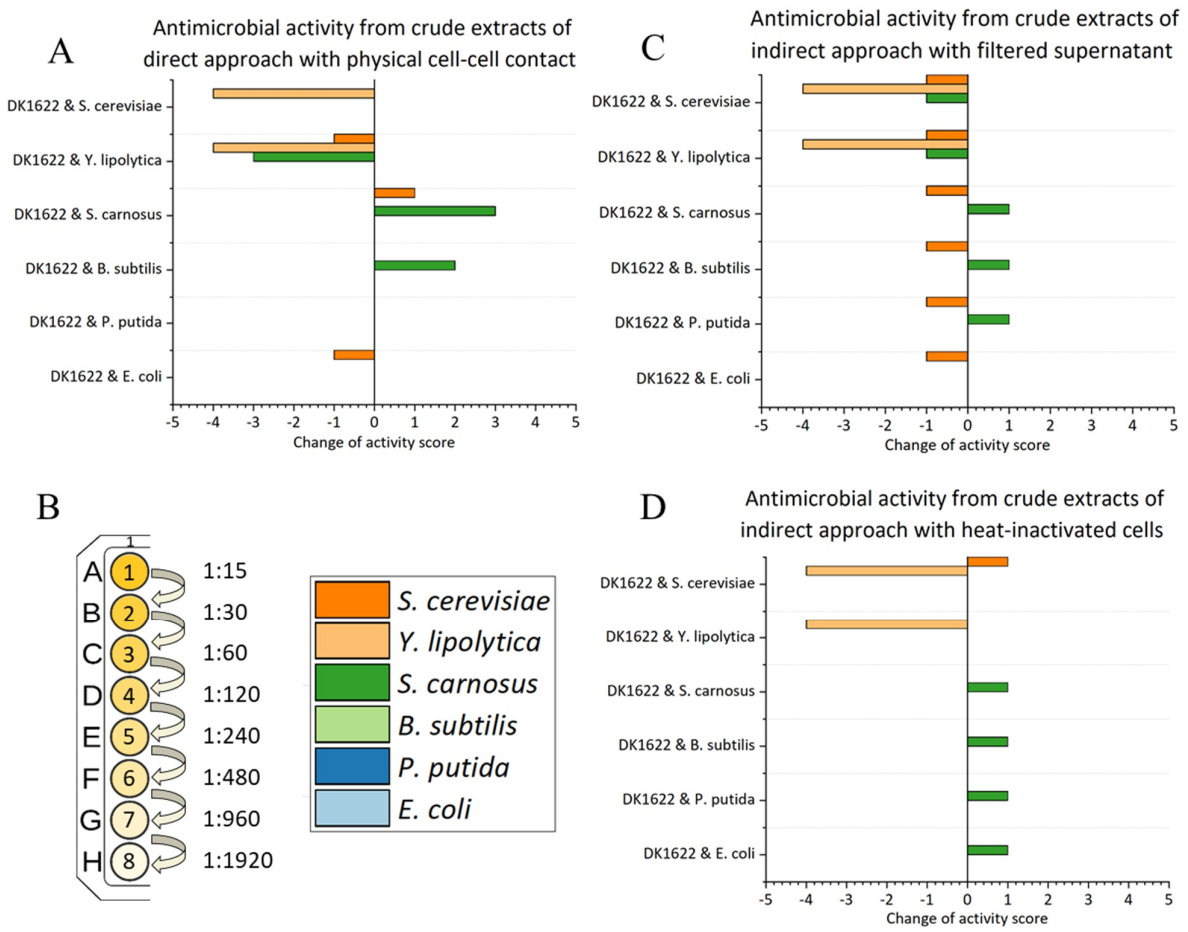

Figure 2.7 Change of activity scores of the crude extracts from direct (**A**) and indirect co-cultivation with filtered supernatant (**C**) and heat-inactivated cells (**D**). Controls were subtracted from all activity data to represent the change in activity. Positive score implies an increase in biological activity, a negative score a decrease in biological activity against the tested organisms. Activity rating (**B**) shows the resulting dilution of saturated crude extract.

None of the co-cultivation approaches performed showed a strong increase in antimicrobial activities towards the test organisms, except for a slightly improved activity against *S. carnosus*. In particular, the extracts of *B. subtilis* and *S. carnosus* from the direct co-cultivation approach display a positive change in activity scores by more than one order of magnitude. The overall moderate improvement in activity against Gram-positive organisms can be attributed to the increased concentration of myxalamid[47,48]. Moreover, the concentration of these secondary metabolites in the extracts reached higher concentrations, which were mainly detected from the indirect approaches. We also found that activity changes of more than one order of magnitude due to manual assessment of the inhibitory effect through visualisation are only considered significant. Furthermore, we observe a significant negative change in the antifungal activity of extracts from co-cultures of *Y. lipolytica* and *S. cerevisiae* against themselves. This suggests that a specific interaction or an elicitor with *M. xanthus* DK1622, especially in combination with *Y. lipolytica*, leads

to a reduction of the previously detected weak activity independent of a direct or indirect approach. None of these antifungal activities can be correlated with known secondary metabolites detectable in the crude extract. However, this shows that the potential for discovery of secondary metabolites is far from exhausted, even in well-described strains such as *M. xanthus* DK1622.

2.4 Conclusion

We were able to demonstrate the potential of the developed co-cultivation approach for the model myxobacterium *M. xanthus* DK1622 in a liquid environment. We consid it as a straight-forward approach to diversify this strain's secondary metabolome. There is an evidence for the production of novel myxobacterial metabolites depending on the used partner strain and method. In addition, when the Gram-positive partner strain *S. carnosus* is inoculated together with *M. xanthus* DK1622, the co-cultivation induces the biosynthesis of various phenylethylamine derivatives. Physical cell-cell contact during co-cultivation was necessary to initiate the formation of this unknown compound class from myxobacteria. Furthermore, the production yield of known myxobacterial secondary metabolites such as cittilin and myxalamid A was enhanced during co-culturing. We conclude that direct co-cultivation approaches are more effective due to the promoted competition, which may be related to the exchange of small molecules in liquid environments.

2.5 References

(1) Berdy, J. Thoughts and facts about antibiotics: Where we are now and where we are heading. *J. Antibiot.* **2012**, *65*, 441.

(2) Wilson, Z. E.; Brimble, M. A. Molecules derived from the extremes of life. *Nat. Prod. Rep.* **2009**, *26*, 44–71.

(3) Akondi, K. B.; Lakshmi, V. V. Emerging trends in genomic approaches for microbial bioprospecting. *Omics* **2013**, *17*, 61–70.

(4) Reichenbach, H.; Höfle, G. Myxobacteria as producers of secondary metabolites. In *Drug Discovery from Nature*; Grabley, S., Thiericke, R., Eds.; Springer: Berlin, 1999; pp 149–179.

(5) Koch, A. L.; White, D. The social lifestyle of myxobacteria. *Bioessays* **1998**, *20*, 1030–1038.

(6) Dawid, W. Biology and global distribution of myxobacteria in soils. *FEMS Microbiol. Rev.* **2000**, *24*, 403–427.

(7) Weissman, K. J.; Müller, R. Myxobacterial secondary metabolites: bioactivities and modes-of-action. *Nat. Prod. Rep.* **2010**, *27*, 1276–1295.

(8) Neelam Gurnani; D. Mehta; M. Gupta; B.K. Mehta. Natural Products: Source of Potential Drugs. *Afr. J. Basic Appl. Sci.* **2014**, *6*, 171–186.

(9) Lahlou, M. The Success of Natural Products in Drug Discovery. *PP* **2013**, *04*, 17–31.

(10) Baral, B.; Akhgari, A.; Metsä-Ketelä, M. Activation of microbial secondary metabolic pathways: Avenues and challenges. *Synth. Syst. Biotechnol.* **2018**, *3*, 163–178.

(11) Silakowski, B.; Schairer, H. U.; Ehret, H.; Kunze, B.; Weinig, S.; Nordsiek, G.; Brandt, P.; Blöcker, H.; Höfle, G.; Beyer, S.*; et al.* New lessons for combinatorial biosynthesis from myxobacteria. The myxothiazol biosynthetic gene cluster of *Stigmatella aurantiaca* DW4/3-1. *J. Biol. Chem.* **1999**, *274*, 37391–37399.

(12) Okada, B. K.; Seyedsayamdost, M. R. Antibiotic dialogues: induction of silent biosynthetic gene clusters by exogenous small molecules. *FEMS Microbiol. Rev.* **2017**, *41*, 19–33.

(13) Nett, M.; Ikeda, H.; Moore, B. S. Genomic basis for natural product biosynthetic diversity in the actinomycetes. *Nat. Prod. Rep.* **2009**, *26*, 1362–1384.

(14) Caudal, F.; Tapissier-Bontemps, N.; Edrada-Ebel, R. A. Impact of Co-Culture on the Metabolism of Marine Microorganisms. *Marine drugs* **2022**, *20*.

(15) Pettit, R. K. Mixed fermentation for natural product drug discovery. *Appl. Microbiol. Biotechnol.* **2009**, *83*, 19–25.

(16) Goodwin, C. R.; Covington, B. C.; Derewacz, D. K.; McNees, C. R.; Wikswo, J. P.; McLean, J. A.; Bachmann, B. O. Structuring Microbial Metabolic Responses to Multiplexed Stimuli via Self-Organizing Metabolomics Maps. *Chem. Biol.* **2015**, *22*, 661–670.

(17) Bertrand, S.; Bohni, N.; Schnee, S.; Schumpp, O.; Gindro, K.; Wolfender, J.-L. Metabolite induction via microorganism co-culture: a potential way to enhance chemical diversity for drug discovery. *Biotechnol. Adv.* **2014**, *32*, 1180–1204.

(18) Oppong-Danquah, E.; Budnicka, P.; Blümel, M.; Tasdemir, D. Design of Fungal Co-Cultivation Based on Comparative Metabolomics and Bioactivity for Discovery of Marine Fungal Agrochemicals. *Mar. Drugs* **2020**, *18*.

(19) Schneider, Y.; Jenssen, M.; Isaksson, J.; Hansen, K. Ø.; Andersen, J. H.; Hansen, E. H. Bioactivity of Serratiochelin A, a Siderophore Isolated from a Co-Culture of *Serratia* sp. and *Shewanella* sp. *Microorganisms* **2020**, *8*.

(20) Molloy, E. M.; Hertweck, C. Antimicrobial discovery inspired by ecological interactions. *Curr. Opin. Microbiol.* **2017**, *39*, 121–127.

(21) Netzker, T.; Fischer, J.; Weber, J.; Mattern, D. J.; Konig, C. C.; Valiante, V.; Schroeckh, V.; Brakhage, A. A. Microbial communication leading to the activation of silent fungal secondary metabolite gene clusters. *Front. Microbiol.* **2015**, *6*, 299.

(22) Jones, J. A.; Wang, X. Use of bacterial co-cultures for the efficient production of chemicals. *Curr. Opin. Biotechnol.* **2018**, *53*, 33–38.

(23) Ola, A. R. B.; Thomy, D.; Lai, D.; Brötz-Oesterhelt, H.; Proksch, P. Inducing Secondary Metabolite Production by the Endophytic Fungus *Fusarium tricinctum* through Coculture with *Bacillus subtilis*. *J. Nat. Prod.* **2013**, *76*, 2094–2099.

(24) Zhu, F.; Chen, G.; Chen, X.; Huang, M.; Wan, X. Aspergicin, a new antibacterial alkaloid produced by mixed fermentation of two marine-derived mangrove epiphytic fungi. *Chem. Nat. Compd.* **2011**, *47*, 767–769.

(25) Kurosawa, K.; Ghiviriga, I.; Sambandan, T. G.; Lessard, P. A.; Barbara, J. E.; Rha, C.; Sinskey, A. J. Rhodostreptomycins, antibiotics biosynthesized following horizontal gene transfer from *Streptomyces padanus* to *Rhodococcus fascians*. *J. Am. Chem. Soc.* **2008**, *130*, 1126–1127.

(26) Sonnenbichler, J.; Dietrich, J.; Peipp, H. Secondary Fungal Metabolites and Their Biological Activities, V. Investigations Concerning the Induction of the Biosynthesis of Toxic Secondary Metabolites in Basidiomycetes. *Biol. Chem. Hoppe. Seyler* **1994**, *375*, 71–80.

(27) Dashti, Y.; Grkovic, T.; Abdelmohsen, U. R.; Hentschel, U.; Quinn, R. J. Production of Induced Secondary Metabolites by a Co-Culture of Sponge-Associated Actinomycetes, *Actinokineospora* sp. EG49 and *Nocardiopsis* sp. RV163. *Mar. Drugs* **2014**, *12*, 3046–3059.

(28) Pérez, J.; Muñoz-Dorado, J.; Braña, A. F.; Shimkets, L. J.; Sevillano, L.; Santamaría, R. I. *Myxococcus xanthus* induces actinorhodin overproduction and aerial mycelium formation by *Streptomyces coelicolor*. *Microb. Biotechnol.* **2011**, *4*, 175–183.

(29) Wenzel, S. C.; Muller, R. Myxobacteria—''microbial factories' for the production of bioactive secondary metabolites. *Molecular bioSystems* **2009**, *5*, 567–574.

(30) Goers, L.; Freemont, P.; Polizzi, K. M. Co-culture systems and technologies: taking synthetic biology to the next level. *J. R. Soc. Interface* **2014**, *11*.

(31) Padmaperuma, G.; Kapoore, R. V.; Gilmour, D. J.; Vaidyanathan, S. Microbial consortia: a critical look at microalgae co-cultures for enhanced biomanufacturing. *Crit. Rev. Biotechnol.* **2018**, *38*, 690–703.

(32) Cortina, N. S.; Krug, D.; Plaza, A.; Revermann, O.; Muller, R. Myxoprincomide: a natural product from *Myxococcus xanthus* discovered by comprehensive analysis of the secondary metabolome. *Angew. Chem.* **2012**, *51*, 811–816.

(33) Krug, D.; Zurek, G.; Revermann, O.; Vos, M.; Velicer, G. J.; Müller, R. Discovering the Hidden Secondary Metabolome of *Myxococcus xanthus*: a Study of Intraspecific Diversity. *Appl. Environ. Microbiol.* **2008**, *74*, 3058–3068.

(34) Hug, J. J.; Dastbaz, J.; Adam, S.; Revermann, O.; Koehnke, J.; Krug, D.; Müller, R. Biosynthesis of Cittilins, Unusual Ribosomally Synthesized and Post-translationally Modified Peptides from *Myxococcus xanthus*. *ACS Chem. Biol.* **2020**, *15*, 2221–2231.

(35) Bode, H. B.; Meiser, P.; Klefisch, T.; Cortina, N. S.; Krug, D.; Göhring, A.; Schwär, G.; Mahmud, T.; Elnakady, Y. A.; Müller, R. Mutasynthesis-derived myxalamids and origin of the isobutyryl-CoA starter unit of myxalamid B. *ChemBioChem* **2007**, *8*, 2139–2144.

(36) Trowitzsch, W.; Wray, V.; Gerth, K.; Höfle, G. Structure of Myxovirescin A, a new macrocyclic antibiotic from gliding bacteria. *J. Chem. Soc., Chem. Commun.* **1982**, 1340–1341.

(37) Charousova, I.; Steinmetz, H.; Medo, J.; Javorekova, S.; Wink, J. Soil myxobacteria as a potential source of polyketide-peptide substances. *Folia microbiologica* [Online early access]. DOI: 10.1007/s12223-017-0502-2.

(38) Zhao, X.; Yu, Z.; Ding, T. Quorum-Sensing Regulation of Antimicrobial Resistance in Bacteria. *Microorganisms* **2020**, *8*.

(39) Bhardwaj, A. K.; Vinothkumar, K.; Rajpara, N. Bacterial quorum sensing inhibitors: attractive alternatives for control of infectious pathogens showing multiple drug resistance. *Recent Patents Anti-Infect. Drug Disc.* **2013**, *8*, 68–83.

(40) Bode, E.; He, Y.; Vo, T. D.; Schultz, R.; Kaiser, M.; Bode, H. B. Biosynthesis and function of simple amides in *Xenorhabdus doucetiae*. *Environ. Microbiol.* **2017**, *19*, 4564–4575.

(41) Dreyer, J.; Malan, A. P.; Dicks, L. M. T. Bacteria of the Genus *Xenorhabdus*, a Novel Source of Bioactive Compounds. *Front. Microbiol.* **2018**, *9*, 3177.

(42) Zhou, Q.; Grundmann, F.; Kaiser, M.; Schiell, M.; Gaudriault, S.; Batzer, A.; Kurz, M.; Bode, H. B. Structure and biosynthesis of xenoamicins from entomopathogenic *Xenorhabdus*. *Chem. Eur. J.* **2013**, *19*, 16772–16779.

(43) Proschak, A.; Schultz, K.; Herrmann, J.; Dowling, A. J.; Brachmann, A. O.; ffrench-Constant, R.; Müller, R.; Bode, H. B. Cytotoxic fatty acid amides from *Xenorhabdus*. *ChemBioChem* **2011**, *12*, 2011–2015.

(44) Cortina, N. S.; Krug, D.; Plaza, A.; Revermann, O.; Müller, R. Myxoprincomide: a natural product from *Myxococcus xanthus* discovered by comprehensive analysis of the secondary metabolome. *Angew. Chem. Int. Ed. Engl.* **2012**, *51*, 811–816.

(45) Meiser, P.; Bode, H. B.; Müller, R. The unique DKxanthene secondary metabolite family from the myxobacterium *Myxococcus xanthus* is required for developmental sporulation. *Proc. Natl. Acad. Sci. U.S.A.* **2006**, *103*, 19128–19133.

(46) Zuck, K. M.; Shipley, S.; Newman, D. J. Induced production of *N*-formyl alkaloids from *Aspergillus fumigatus* by co-culture with *Streptomyces peucetius*. *J. Nat. Prod.* **2011**, *74*, 1653–1657.

(47) Beyer, S.; Kunze, B.; Silakowski, B.; Müller, R. Metabolic diversity in myxobacteria: identification of the myxalamid and the stigmatellin biosynthetic gene cluster of *Stigmatella aurantiaca* Sg a15 and a combined polyketide-(poly)peptide gene cluster from the epothilone producing strain *Sorangium cellulosum* So ce90. *Biochim. Biophys. Acta* **1999**, *1445*, 185–195.

(48) Gerth, K.; Jansen, R.; Reifenstahl, G.; Höfle, G.; Irschik, H.; Kunze, B.; Reichenbach, H.; Thierbach, G. The myxalamids, new antibiotics from *Myxococcus xanthus* (Myxobacterales) I. production, physico-chemical and biological properties, and mechanism of action. *J. Antibiot.* **1983**, *36*, 1150–1156.

Supporting Information

A co-cultivation approach to alter the myxobacterial secondary metabolome

Markus Neuber, Alexander Popoff, Daniel Krug and Rolf Müller

Methods

Strains and Media

The partner strains *E. coli* DSM 1116, *P. putida* DSM 6125, *B. subtilis* DSM 10, *S. carnosus* DSM 4600, *Y. lipolytica* DSM 3286 and *S. cerevisiae* DSM 70449 were purchased from German Collection of Microorganisms and Cell Cultures (DSMZ). The myxobacterial producer strain *M. xanthus* DK1622 (MCy9151) was obtained from our internal strain collection.

CTT medium (1% casiton, 10 mM TRIS hydrochloride, 1 mM potassium dihydrogen phosphate, 8 mM magnesium sulphate, pH 7.6) was used as a growth medium for the producing strain *M. xanthus* DK1622. Both Gram-positive and Gram-negative partner strains *E. coli*, *P. putida*, *B. subtilis*, *S. carnosus* were incubated in LB medium (1% tryptone, 0.5% yeast extract, 0.5% sodium chloride, pH 7.0). The eukaryotic partner organisms *Y. lipolytica* and *S. cerevisiae* were grown in YPAD medium (1% yeast extract, 2% peptone, 2% glucose monohydrate, 0.01% adenine hemisulfate, pH 7.0 adjusted with KOH). Amberlite resin XAD-16 (Sigma) was added to all blanks, controls and co-culture mixtures at a volume concentration of 1% [v/v].

Preparation of filtrated supernatant and heat inactivated cells

300 mL shaking flasks containing 50 mL LB or YPAD medium were inoculated with 50 µL cryo stock of each partner strain and incubated at 30 °C and 180 rpm shaking for 2 days. To obtain a filtered supernatant, the culture broth was centrifuged at 5.000 g and 4 °C for 10 min and the supernatants were filtered through a 0.2 µM PTFE membrane (Sartorius) for removal of remaining cells. For the preparation of the heat inactivated partner strain, the whole culture broth was autoclaved at 121 °C and one bar overpressure for 20 min.

Direct and indirect co-cultivation

Liquid CTT medium was used in this study for axenic culture and all co-cultivations of *M. xanthus* DK1622. Optical density was used to seed a defined number of cells between the producer and partner strain prior to a direct co-cultivation approach. Optical density was determined with a Bio Photometer plus 6132 (Eppendorf) at λ = 600 nm. The samples were diluted to be in the linear range of the photometer.

300 mL shake flask containing 50 mL CTT medium was inoculated with 200 µL cryo stock of *M. xanthus* DK1622 and incubated at 30 °C and 180 rpm for 2 days. After determination of OD_{600}, the required volume of pre-culture of DK1622 was calculated to achieve an optical density of 0.15

(OD_{600}) in 50 mL CTT medium. For the direct co-cultivation, the required volume of DK1622 was transferred into a 300 mL shake flask with 50 mL CTT medium and the calculated volume of the cell suspension of the corresponding partner strain was added and the co-culture incubated at 30 °C and 180 rpm for 7 days. All partner strains were seeded for the direct co-cultivation in a final optical density of 0.01 (OD_{600}).

For the indirect co-cultivation approach, 3% [v/v] of the filtered supernatant or heat inactivated cells were added to DK1622 instead of the cell suspension of the partner strain. LB and YPAD medium were added in equal volume as control to an axenic culture of DK1622. To adsorb the metabolites, an aqueous solution of Amberlite XAD16 resin was added to all co-cultivations, controls and blanks at a volumetric concentration of 2% [v/v] after 6 days of cultivation. At the end of the fermentation after 7 days, both resin and cells were harvested together by centrifugation (5.000 g, 4 °C, 15 min). All co-cultivations, controls and blanks were conducted in biological triplicates.

Large-scale direct co-cultivation of *M. xanthus* DK1622 and *S. carnosus*

The large-scale co-culture of M. *xanthus* DK1622 and *S. carnosus* were grown in 5 L shaking flask containing 1.5 L CTT media for 7 days at 30 °C and 180 rpm. All production co-cultures were inoculated with the same conditions for the producer and partner strain as in the small scale cultures. Autoclaved aqueous suspension of Amberlite XAD-16 resin was added at a volumetric concentration of 2% [v/v] to all large cultures after 6 days. After the end of the fermentation, both cell pellets and resin were harvested by centrifugation (5.000 g, 4 °C, 15 min) and lyophilised prior to further processing. A total volume of 9 L of culture broth was harvested to obtain a sufficient quantity for successful isolation.

Generation of crude extracts for statistical analysis and bioactivity profiling

The resin XAD16 and cell pellet were frozen at -20 °C and lyophilised. Subsequently, the metabolites were extracted twice with 50 mL MeOH/acetone (1:1 [v/v]) under constant stirring at 300 rpm with a magnet bar for 90 min. The supernatant was filtered into a round bottom flask and the solvent was evaporated under reduced pressure until it was completely dry. The residue was dissolved in 1 mL MeOH, transferred into 1.5 mL glass vial and stored at 4 °C. All extracts were diluted 1:10 prior to the UHPLC-MS measurements.

MS and NMR Analysis of crude extracts and pure compound

UHPLC-qTOF measurements were performed in duplicates as technical replicates on a Dionex Ultimate 3000 SL system coupled to a Bruker maXis 4G UHR-qTOF. This system was used for high resolution LC-MS measurements. Following template method was used: Column: ACQUITY BEH 100 x 2.1 mm 1.7 µm 130 Å, a flow rate of 0.6 mL/ min and a column temperature of 45 °C. Following gradient was applied with H_2O + 0.1% FA as eluent A and ACN + 0.1% FA as eluent B. 0-0.5 min: 5% Eluent B; 0.5-18.5 min: linear increase of eluent B to 95%; 18.5-20.5 min: 95% eluent B; 20.5-20.8 min: linear decrease of eluent B; 20.8-22.5 min: re-equilibration with 5% eluent B. The detection was usually performed in positive MS mode or MS^2 mode, using a scan range from 150-2500 *m/z*. Capillary voltage was set to +4000 V for measurements in positive ionization mode. Dry gas was set to a flow rate of 5 L/ min at 200 °C.

NMR spectra were recorded on a Bruker Ascend 700 spectrometer equipped with a 5 mm TCI cryoprobe (^1H at 700 MHz, ^{13}C at 175 MHz). All observed chemical shift values (δ) are given in ppm and coupling constant values (J) in Hz. Standard pulse programs were used for HMBC, HSQC and COSY experiments. The spectra were recorded in methanol-d4, and chemical shifts of the solvent signals at δH 3.31 ppm and δC 49.2 ppm were used as reference signals for spectra calibration. To increase sensitivity, the measurements were conducted in a 5 mm Shigemi tube (Shigemi Inc., Allison Park, PA 15101, USA).

Statistical LC-MS data analysis and annotations of crude extracts

For the statistical interpretation of the LC-MS data for targeted and non-targeted metabolomics, analysis was carried out with MetaboScape 2021b (Bruker). The minimal intensity threshold for feature detection by the built-in T-Rex 3D algorithm was set to 5 x 10^3, and the maximum charge was set to three. The minimal group size for creating batch features was set to four. Known myxobacterial secondary metabolites were annotated using our in-house database containing myxobacterial secondary metabolites (myxobase). Overlaps of the direct and indirect co-cultivation approach as well as features uniquely found in one analysis were calculated via *t*-Test analysis in MetaboScape 2021b.

Isolation Procedure

Phenylethylamine-357 was isolated by semi-preparative HPLC following a fractionation of the crude extract by liquid−liquid partitioning and reverse-phase chromatography. The cell pellet together with XAD was shaken with 500 mL methanol/acetone (1:1) for 90 minutes and then the supernatant were poured through a filter paper into a round bottom flaks. This process was carried

out 3 times and the solvents were completely evaporated under vacuum. The residue was resolved in 200 mL methanol mixed with 20 mL water. Afterwards, 300 mL hexane was added to carry out for liquid-liquid partitioning for 3 times. The obtained hexane residue (~43 mg) was unitised for the normal-phase chromatography. Afterwards, the concentrated hexane phase was separated with normal-phase chromatography (column volume = 7 ml) with silica gel (pore size: 60Å; 70-230 mesh, 63-200 µm) using a linear gradient from the solvent mixture of hexane (20 %) and ethylacetate (80 %) over 40 column volumes to the solvent mixture of hexane (80 %) and ethylacetate (20 %). Purification was performed on a Dionex Ultimate 3000 SDLC low pressure gradient system equipped with a Phenomenex Luna 5 *µm* C18(2) 100 Å LC Column (250 × 10 mm) tempered at 45 °C. Separation was achieved using a linear gradient from 95% ddH_2O/acetonitrile with 0.1% formic acid to 5% ddH_2O/acetonitrile with 0.1% formic acid over 20 min. The compound was detected by UV absorption at 210 and 280 nm.

Antimicrobial assays

For the determination of antimicrobial activities of each crude extract (co-culture, axenic cul-ture and media blank), all three biological replicates were combined, 20 µL of the saturated methanolic extract was mixed with 130 µL microbial test medium and serially diluted by transferring 75 µL of mixed sample solution into the 96 well plate[1]. Afterwards, 75 µL of the microbial test culture was added to each well of the microtitre plate. The microbial test panel consisted of *E. coli* DH5α, *P. aeruginosa* PA14, *S. aureus* Newman, *B. subtilis* and fungus *C. albicans*. Growth inhibition was assessed by visual inspection and given activity score (minimal dilution of inhibition) in the lowest concentration of extract at which no visible growth was observed.

Supplementary Figures & Tables

In the box plots, the detected intensities of myxalamid B after direct and indirect co-cultivation in corresponding crude extracts are shown.

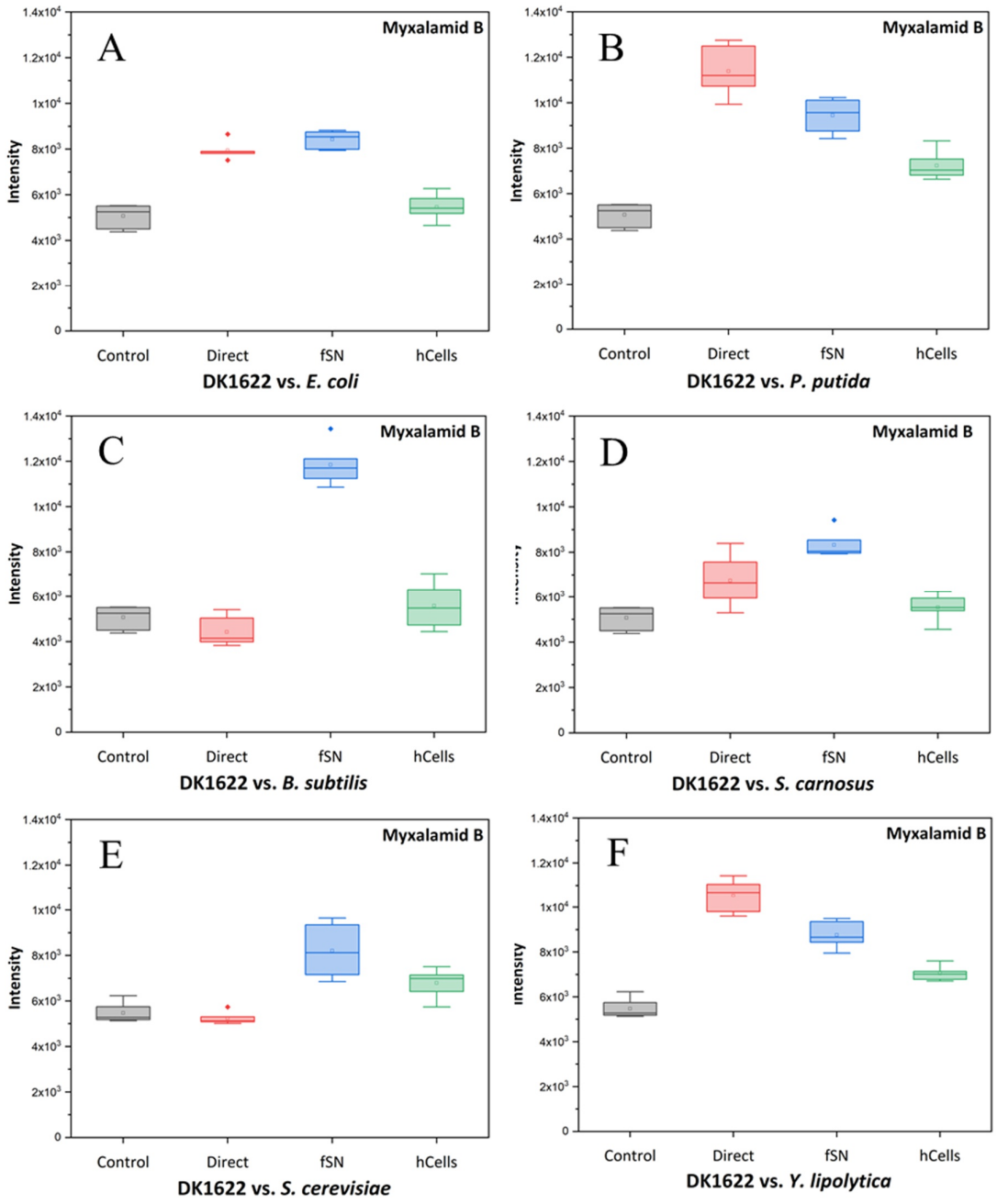

Figure S2.1: Influence of the co-culturing approach (direct – cell-cell contact, fSN – filtrated supernatant, hCells – heat-inactivated cells) on the production level of Myxalamid B from *M. xanthus* DK1622 depending on different partner strains (**A**–**F**). Detected intensities of Myxalamid B in respective crude extract are shown as a box plot.

NMR data of phenylethylamine derivative-357:

Figure S2.2: Chemical structure of phenylethylamine derivative-357.

Table S2.1: Spectroscopic data of phenylethylamine derivative-357 acquired at 700 MHz in MeOD.

Position	C Shift	H Shift	H Multiplicity	COSY	C to H HMBC
1	127.5	7.18	m		
2, 6	129.6	7.27	m		4
3, 5	130	7.21	br d (7.16)	2, 6	7, 1
4	140.6				
7	36.7	2.79	t (7.40, 7.40)	8	8, 3, 5, 4
8	42.1	3.4	t (7.40, 7.40)	7	7, 4, 10
10	176.5				
11	37.3	2.13	t (7.40, 7.40)	13	13, 10
13	27.2	1.55	dt (14.51, 7.44, 7.44)	19, 18, 17, 16, 15, 14, 11	10
19, 18, 17, 16, 15, 14	30.6	1.29	m	13	
22, 21	131	5.34	t (5.34, 5.34)	23, 20	
23, 20	28.3	2.04	m	25, 22, 21	24, 22, 21
24	33.3	1.33	m		25, 25
25	23.6	1.33	m	26, 23, 20	24, 24
26	14.5	0.91	br t (7.30, 7.30)	25	25, 24

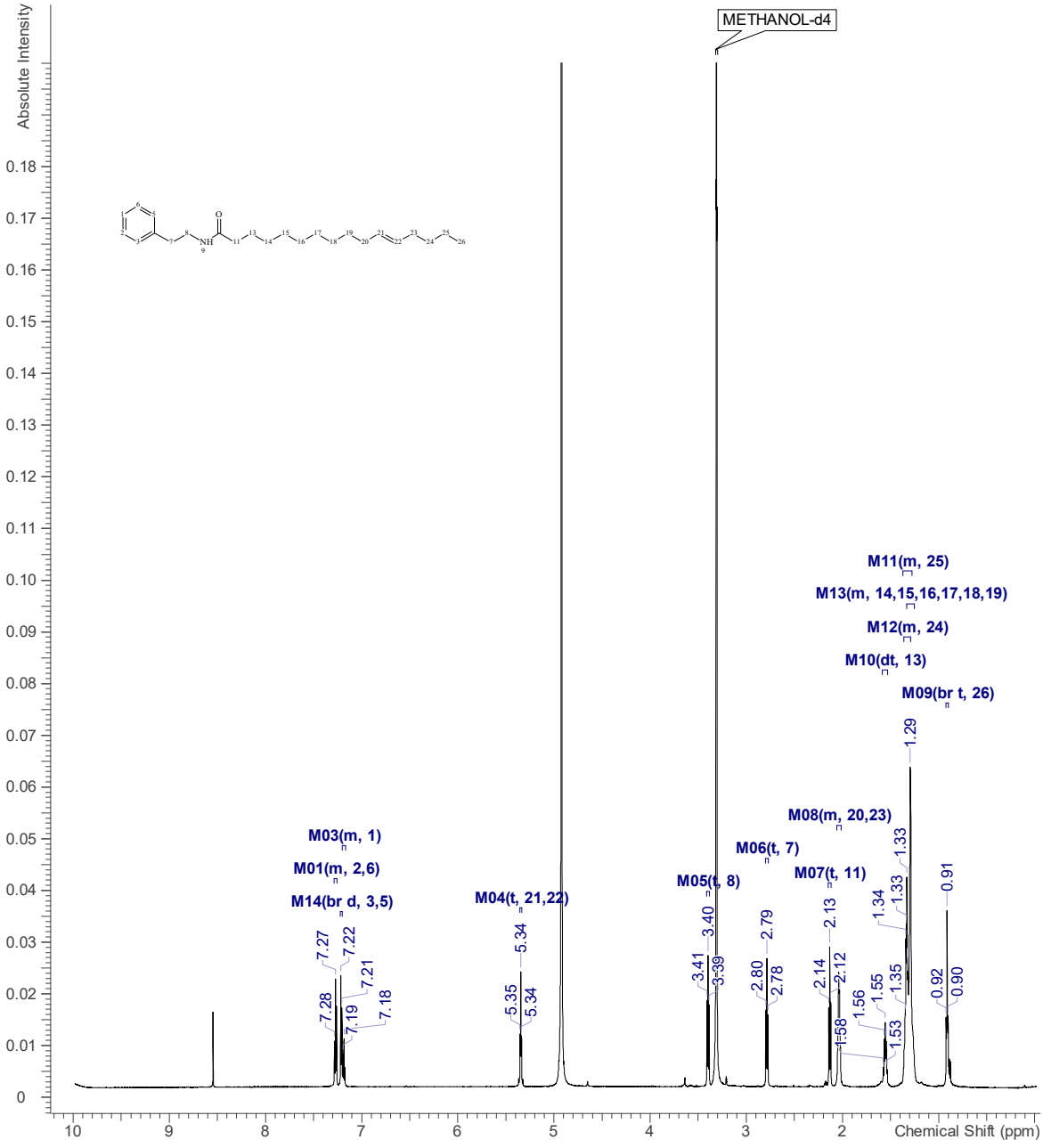

Figure S2.3: ^{1}H-NMR spectrum of phenylethylamine derivative-357 acquired at 700 MHz in MeOD.

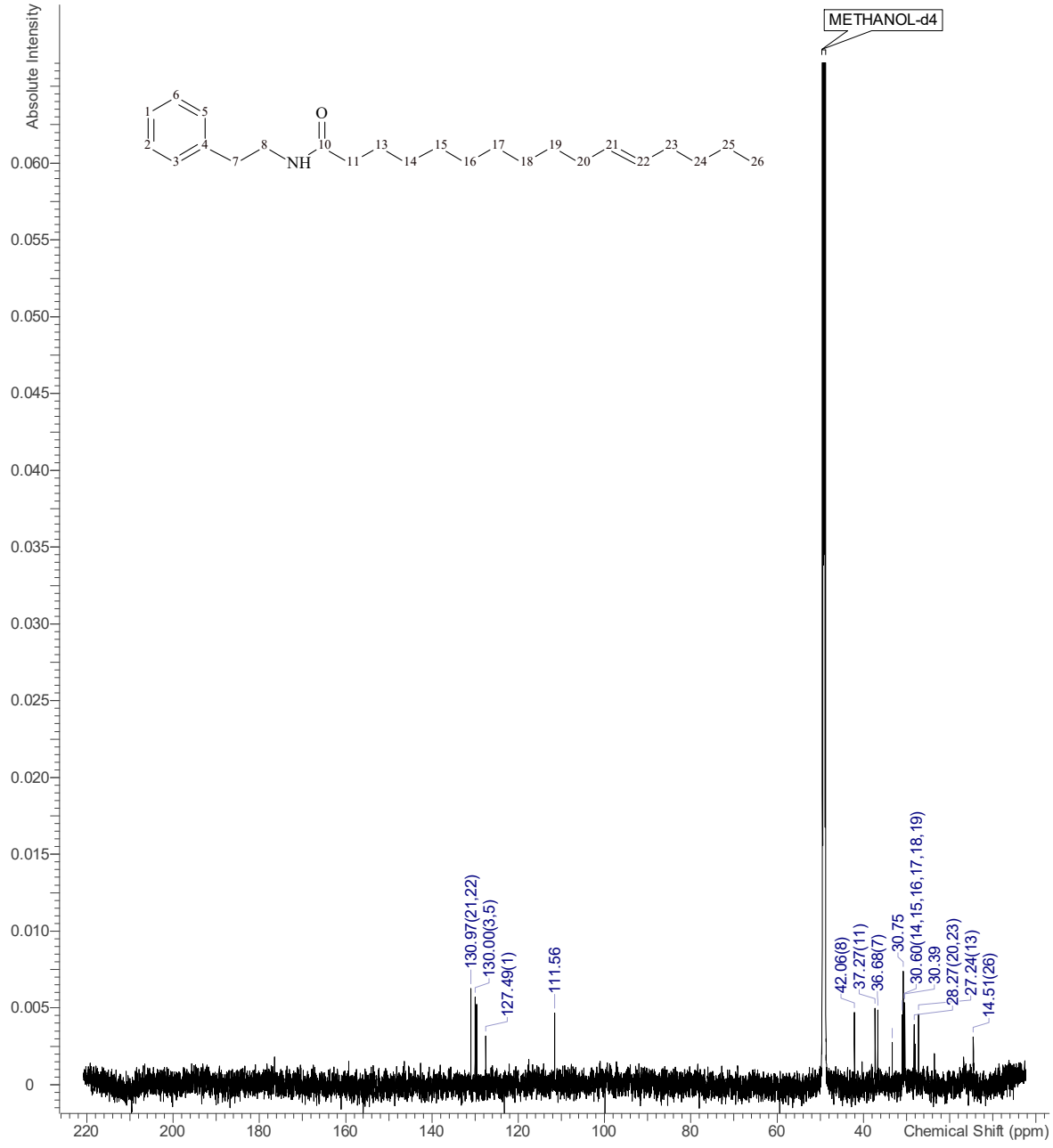

Figure S2.4: ^{13}C-NMR spectrum of phenylethylamine derivative-357 acquired at 175 MHz in MeOD.

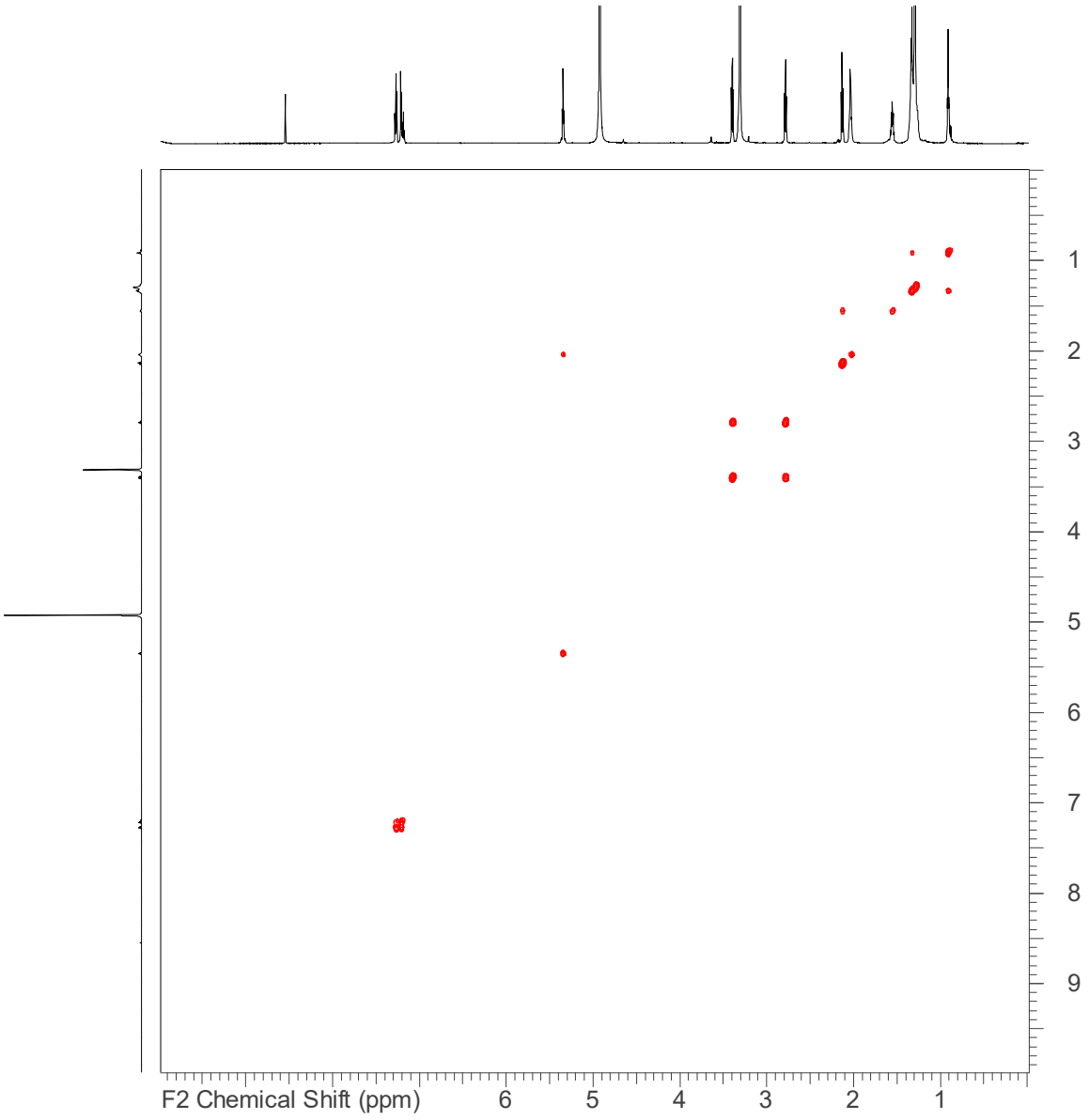

Figure S2.5: ^{1}H-^{1}H-COSY-spectrum of phenylethylamine derivative-357 acquired at 700 MHz in MeOD.

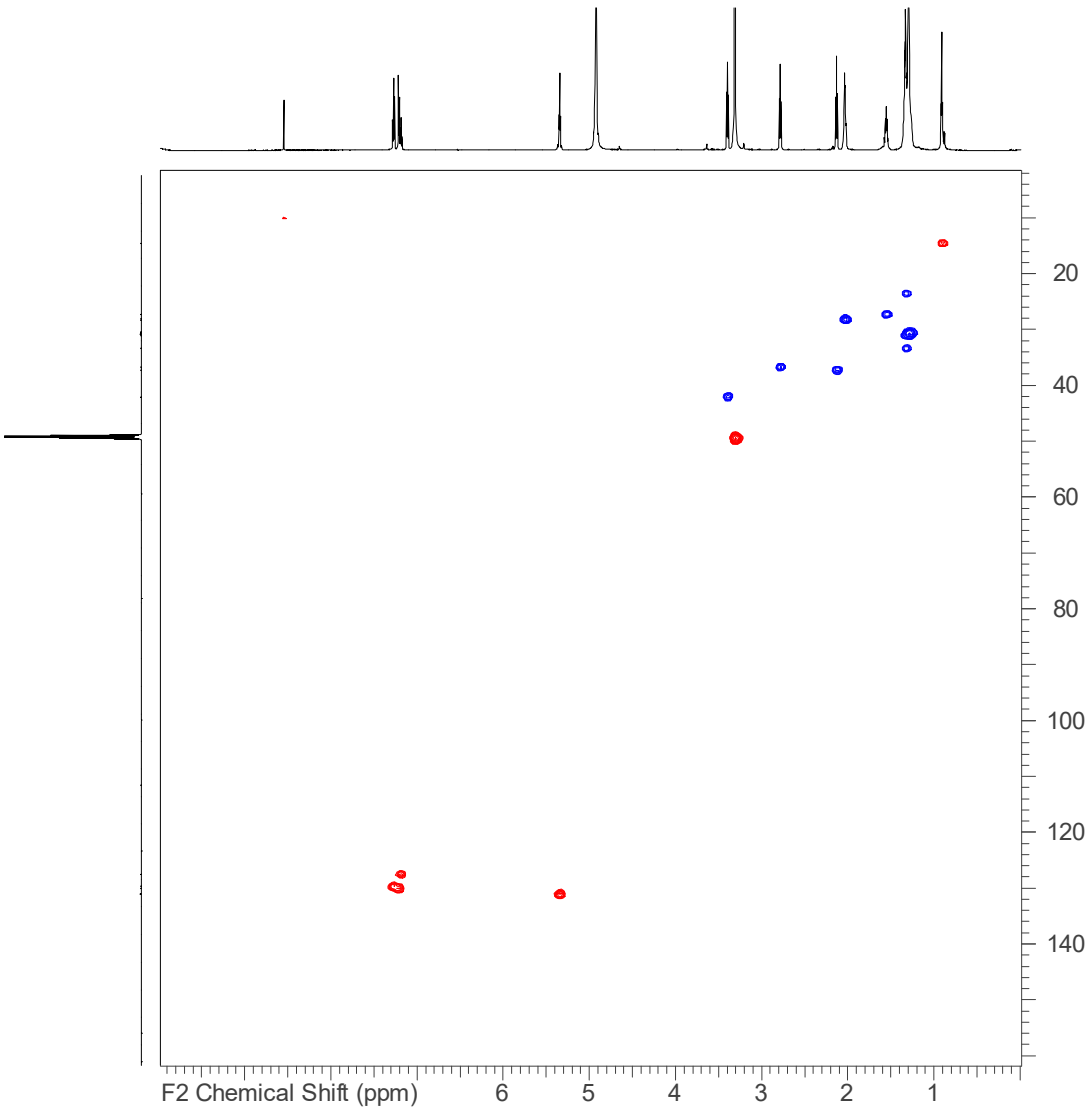

Figure S2.6: HSQC-spectrum of phenylethylamine derivative-357 acquired at 175/700 (F1/F2) MHz in MeOD.

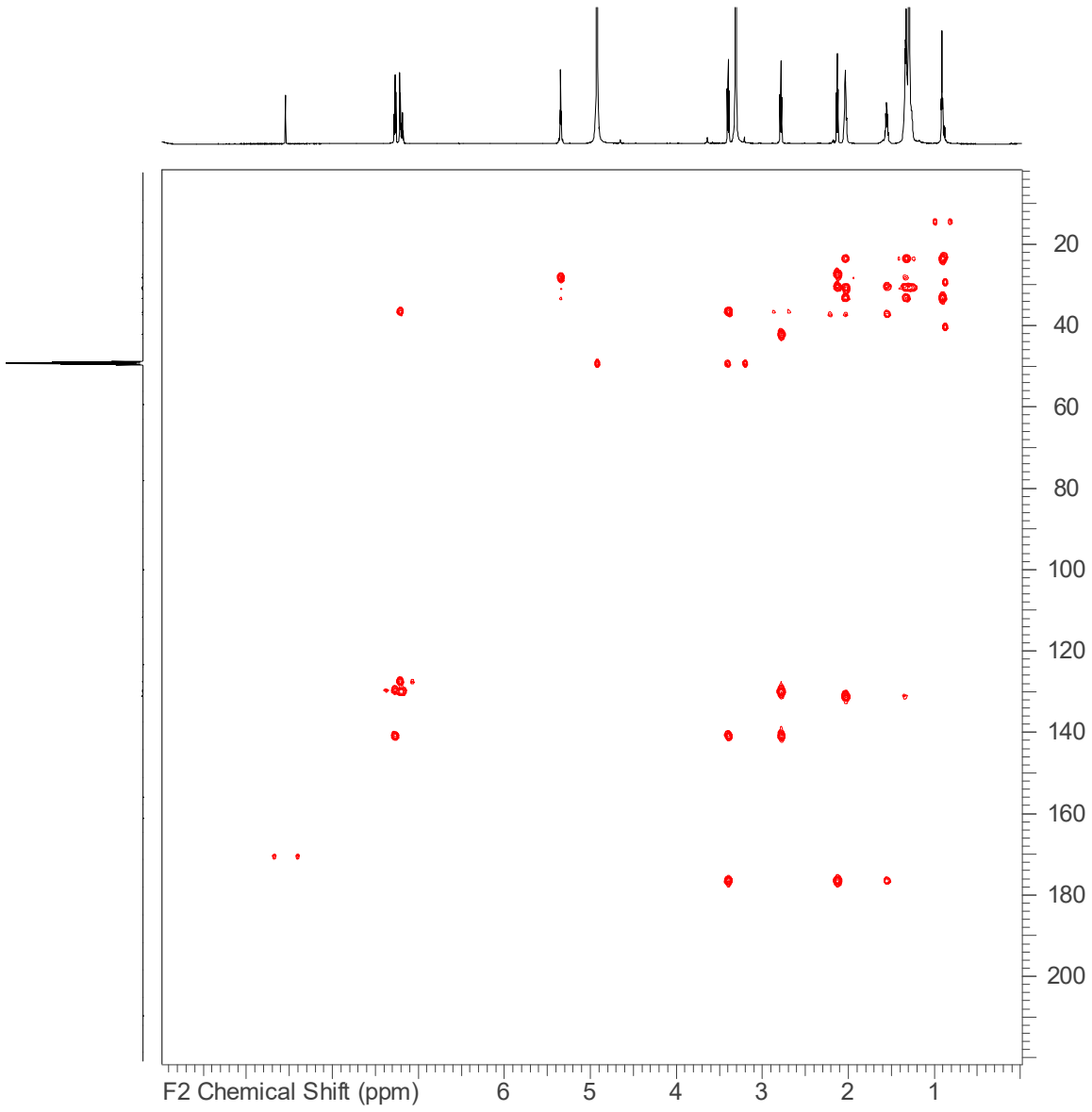

Figure S2.7: HMBC-spectrum of phenylethylamine derivative-357 acquired at 175/700 (F1/F2) MHz in MeOD.

LC-hrMS data of phenylethylamine derivatives

Identification of further derivatives from phenylethylamines in the crude extract after co-cultivation between DK1622 and *S. carnosus*.

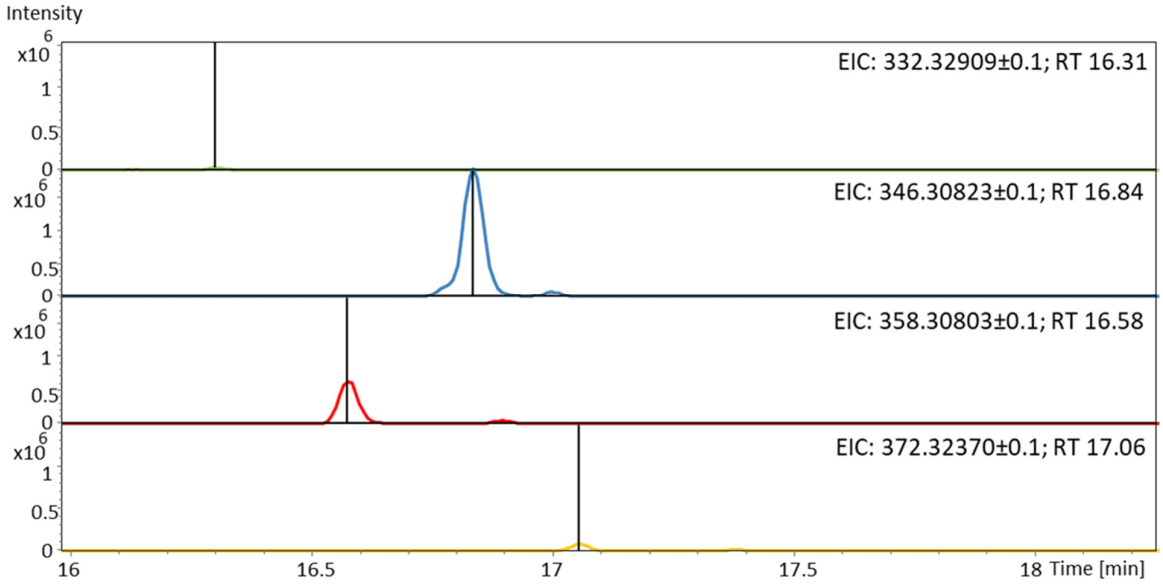

Figure S2.8: Extracted ion chromatograms (EICs) of phenylethylamine derivatives-331, -345, -357 and -371 in the crude extract via LC-*hr*MS system.

Overview about the four detected phenylethylamine derivatives in the crude extract after co-cultivation between DK1622 and *S. carnosus*.

Table S2.2: Further phenylethylamine derivatives observed in crude extract via LC-*hr*MS system. Derivatives were identified after comparison with previously published fatty acid amides.[2]

Phenylethylamide M_W	**Sum formula**	**Retention time**	**$[M+H]^+$**	**Phenyl-ethylamine building block** 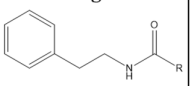	**Predicted Rest**
331	$C_{22}H_{37}NO$	16.31	332.350	•	
345	$C_{23}H_{39}NO$	16.84	346.309	•	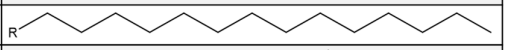
357	$C_{24}H_{39}NO$	16.58	358.310	•	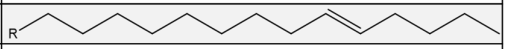
371	$C_{25}H_{41}NO$	17.06	372.370	•	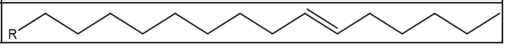

Co-cultivation study of DK1622 and *S. carnosus*

To evaluate and compare different co-culturing approaches for the production of a specific metabolite, we identified phenylethylamine-345 as a target mass to study the behaviour depending on the respective treatment (Figure S2.9).

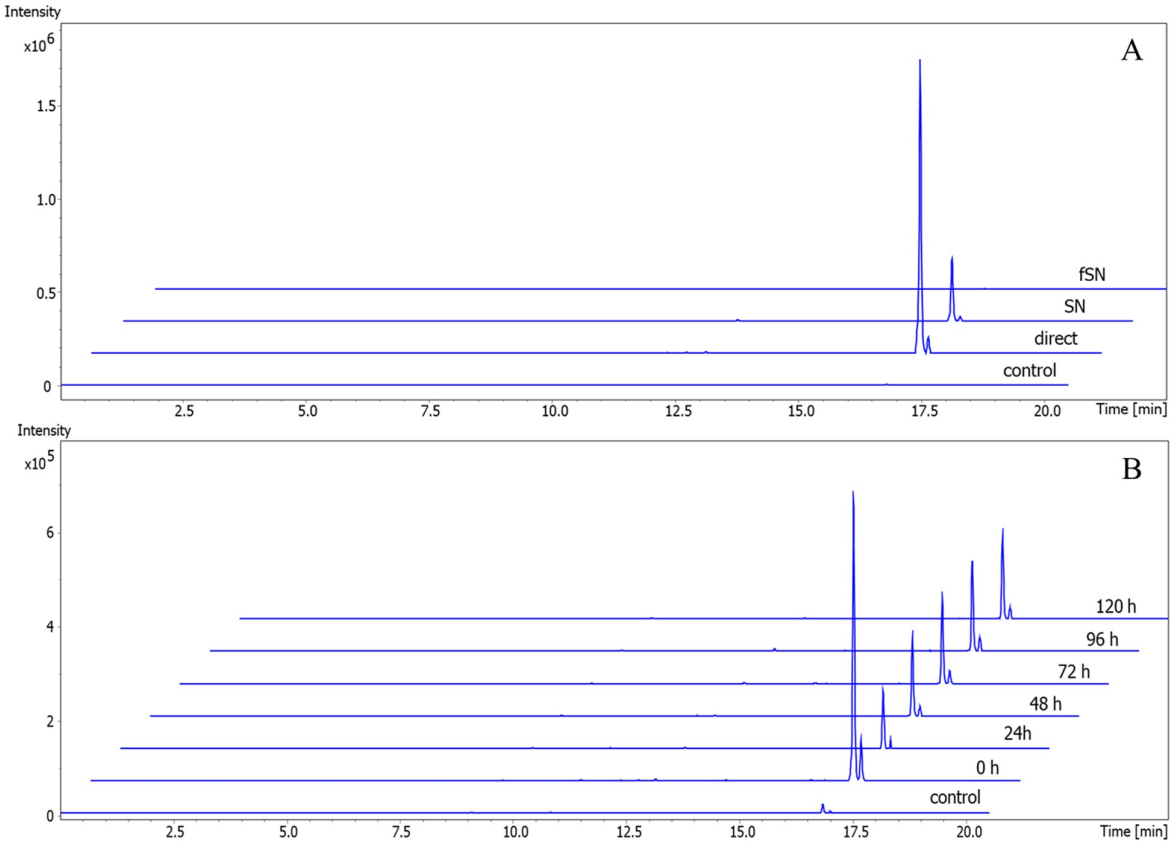

Figure S2.9: Extracted ion chromatogram of phenylethylamin-345 (EIC 346.310 +/- 0.01 m/z) derived from crude extracts after cultivations of *M. xanthus* DK1622 and *S. carnosus*. (**A**) Investigation of the effect on induction of direct co-cultivation and indirect co-cultivation by addition of centrifuged *S. carnosus* supernatant (SN) and centrifuged and filtered supernatant (fSN) to DK1622. (**B**) Time-dependent experiments with addition of partner strain *S. carnosus* for the direct co-cultivation with DK1622.

Antimicrobial assay

All corresponding crude extracts of co-cultures, axenic cultures, medium blank, filtered supernatant and heat-inactivated cells were tested to determine the activity score against Gram-positive, Gram-negative and eukaryotic organisms (Table S2.3).

Table S2.3: Activity score results of the crude extracts from media blanks, axenic cultures and co-culture of *M. xanthus* DK1622 and six partner strains in direct and indirect approach fSN - filtered supernatant and hCells - heat-inactivated cells).

Crude Extract	Activity score					
	E. coli	*P. putida*	*B. subtilis*	*S. carnosus*	*Y. lipolytica*	*S. cerevisiae*
Blank CTT Medium	0	0	0	0	0	0
Control-DK1622_CTT+LB	0	0	0	1	0	1
Control-DK1622_CTT+YPAD	0	0	0	3	4	1
Control-E.coli_LB	0	0	0	0	0	0
Control-P.putida_LB	0	0	0	0	1	0
Control-B.subtilis_LB	2	3	2	4	0	0
Control-S.carnosus_LB	0	0	0	0	0	0
Control-Y.lipo_YPAD	0	0	0	0	0	0
Control-S.cerevisiae_YPAD	0	0	0	0	1	0
Direct-DK1622_E.coli_CTT	0	0	0	1	0	0
Direct-DK1622_P.putida_CTT	0	0	0	1	0	1
Direct-DK1622_B.subtilis_CTT	0	0	0	3	0	1
Direct-DK1622_S.carnosus_CTT	0	0	0	4	0	2
Direct-DK1622_Y.lipo_CTT	0	0	0	0	0	0
Direct-DK1622_S.cerevisiae_CTT	0	0	0	3	0	1
Control-fSN_E.coli_LB	0	0	0	0	0	0
Control-fSN_P.putida_LB	1	0	0	0	0	0
Control-fSN_B.subtilis_LB	0	0	0	4	0	0
Control-fSN_S.carnosus_LB	1	0	0	0	0	0

Control-fSN_Y.lipo_YPAD	1	0	0	0	0	0
Control-fSN_S.cerevisiae_YPAD	1	0	0	1	0	0
fSN-DK1622_E.coli_CTT	0	0	0	1	0	0
fSN-DK1622_P.putida_CTT	0	0	0	2	0	0
fSN-DK1622_B.subtilis_CTT	0	0	0	2	0	0
fSN-DK1622_S.carnosus_CTT	0	0	0	2	0	0
fSN-DK1622_Y.lipo_CTT	0	0	0	2	0	0
fSN-DK1622_S.cerevisiae_CTT	0	0	0	2	0	0
Control-CL_E.coli_LB	1	0	0	0	0	0
Control-hCells_P.putida_LB	0	0	0	0	0	0
Control-hCells_B.subtilis_LB	0	0	0	0	0	0
Control-hCells_S.carnosus_LB	0	0	0	1	0	0
Control-hCells_Y.lipo_YPAD	0	0	0	0	0	0
Control-hCells_S.cerevisiae_YPAD	0	0	0	0	0	0
hCells-DK1622_E.coli_CTT	0	0	0	2	0	1
hCells-DK1622_P.putida_CTT	0	0	0	2	0	1
hCells-DK1622_B.subtilis_CTT	0	0	0	2	0	1
hCells-DK1622_S.carnosus_CTT	0	0	0	2	0	1
hCells-DK1622_Y.lipo_CTT	0	0	0	3	0	1
hCells-DK1622_S.cerevisiae_CTT	0	0	0	3	0	2

References

(1) Herrmann, J.; Hüttel, S.; Müller, R. Discovery and biological activity of new chondramides from *Chondromyces* sp. *ChemBioChem* **2013**, *14*, 1573–1580.

(2) Proschak, A.; Schultz, K.; Herrmann, J.; Dowling, A. J.; Brachmann, A. O.; ffrench-Constant, R.; Müller, R.; Bode, H. B. Cytotoxic fatty acid amides from *Xenorhabdus*. *ChemBioChem* **2011**, *12*, 2011–2015.

Chapter 3

Co-cultivation of *Streptomyces*-like myxobacteria enables discovery of bioactive secondary metabolites

Markus Neuber, Sebastian Walesch, Chantal Bader, Daniel Krug and Rolf Müller

Manuscript in preparation

Contributions to the presented work

Author's contribution

The author contributed to the concept of this study, planned and executed experiments, evaluated and interpreted resulting data. The author developed and performed co-cultivation experiments and analysed the corresponding LC-MS data using statistical methods and molecular networks. In the course of this, the author identified and isolated two new compound families the alkyl-quinolones (268, 282, 302, and 316) and the thuggacin-analogues (564, 566, and 578), which are not present in axenic cultures. In addition, the author contributed to the conception and writing of this manuscript.

Contribution by others

Sebastian Walesch planned and executed cultivation and purification experiments, evaluated and interpreted resulting data. He purified thuggacin-analogue 548, performed most NMR-based structure elucidations and carried out genetic analyses to identify the BGCs. Chantal Bader performed the NMR-based structure elucidation of alkyl-quinolone 316. Daniel Krug and Rolf Müller contributed by supervision of the project and conceiving, editing and proofreading of this manuscript.

3. Myxobacterial co-cultivation leads to the discovery of novel alkyl-quinolones and thuggacin derivatives

3.1 Abstract

Co-cultivation of Streptomyces-like myxobacteria with another taxonomically unrelated microbial species resulted in increased production of constitutively produced compounds and/or accumulation of new compounds that are not detectable in axenic cultures. In our study, the myxobacterium *Sorangium sp.* MSr12523 was co-cultivated together with mycolic acid-containing bacteria (MACB), *C. glutamicum*, *R. erythropolis*, *T. soli* and *T. pseudospumae*. Examining the unique molecular features from the metabolomic data, we found notable changes in metabolite profiles due to an increased number of new metabolites. In addition, bioactivity screening revealed an expanded antimicrobial activity profile against Gram-positive and Gram-negative pathogens inclusive *M. tuberculosis* 7H37Ra. Moreover, two compound families consisting of alkyl-quinolones and thuggacins were isolated and structurally characterised. Remarkable antimycobacterial activity was found for the myxobacterial alkyl quinolones.

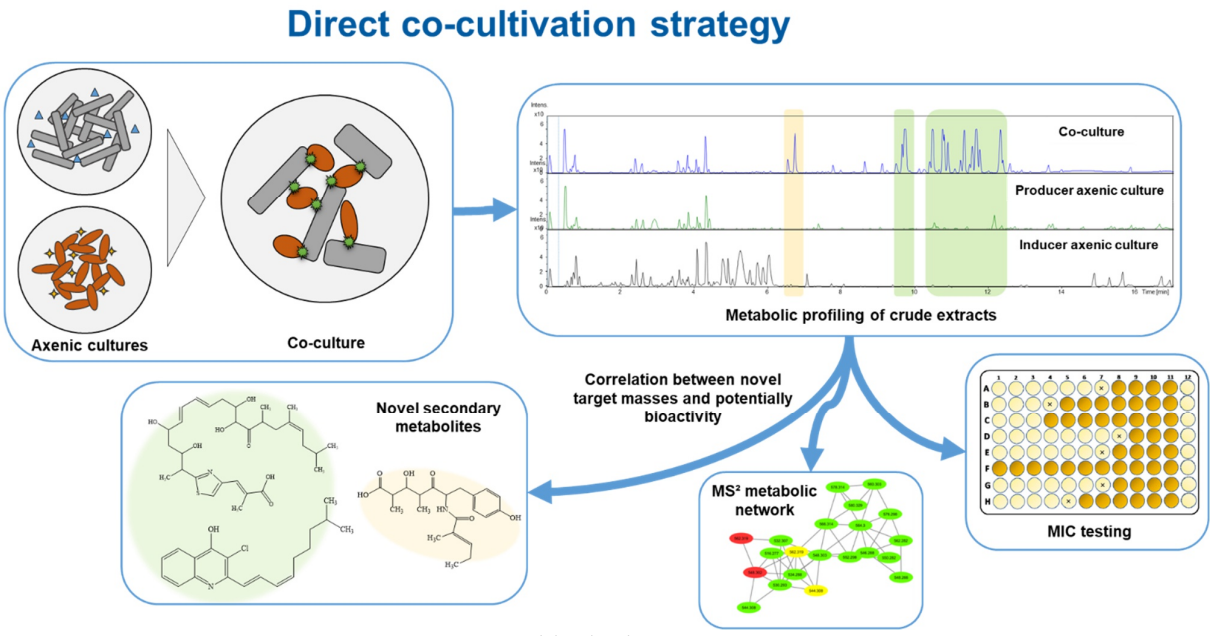

Graphical Abstract

3.2 Introduction

Natural products as well as their derivatives represent one of the foundations for the development of medications effective against a widespread range of human diseases[1,2]. Myxobacteria belong to the δ-proteobacteria subgroup and therefore are Gram-negative bacteria[3]. They are ubiquitous in soil and are an excellent source of new classes of secondary metabolites[4]. One unique feature of myxobacteria is their ability to generate a diverse range of secondary metabolites including polyketides, non-ribosomal polypeptides or hybrids thereof[5].

The genus *Sorangium* is a particularly promising source, as 48,8% of myxobacterial secondary metabolites[6], including macrolide chlorotonil A active against malaria[7], epothilone[8] as a potent anti-tumour compound as well as the antibacterial thuggacins A-C[8] have been isolated from this genus. In addition, *Sorangium* strains exhibit remarkable biological properties, such as the ability to form biofilms, gliding cell movement and complex morphological cell differentiation including ascending fruiting bodies under starving conditions[9]. Comparison of genome sequences of *Sorangium* strains with other members of the δ-proteobacteria allows an in-depth look into the complex regulatory mechanisms related to the lifecycle and secondary metabolism of myxobacteria[10].

Recent genomic studies indicate that the majority of biosynthetic gene clusters of certain groups of microorganisms are not expressed under standard laboratory cultivation conditions[11,12]. Different strategies for the activation of silent/cryptic genes include chemical, biological and molecular modification and have already been proven to be remarkably successful[13–15]. Confronting the bacteria with external small signal molecules, namely "elicitors", is a recognised strategy for the generation of new, bioactive secondary metabolites[16]. Co-cultivation-based elicitation can therefore be used to access the metabolic diversity of microbes not produced in axenic cultures, which may help to unmask silent/cryptic biosynthetic gene clusters (BGCs) and poorly expressed secondary metabolites (SMs)[17].

Several previous studies reported the potential to activate silent/cryptic BGCs by co-cultivation of the host strain with other microorganisms, due to the *in situ* mimicking of microbial interactions in the original environment[18–21]. In recent years, it has become apparent that mycolic acid-containing bacteria (MACB) stimulate the biosynthesis of silent/cryptic natural products in co-cultures with members of *Streptomycetaceae*[22]. Mycolic acids are fatty acids that are essential components of the highly impermeable outer barrier of the

bacterial cell wall. They are a characteristic feature of bacteria belonging to the suborder *Corynebacterineae*[23]. Remarkably, physical contact between MACB and *Streptomyces sp.* was required for induction in almost all cases[24]. Such co-cultivation setup involving the actinobacteria *Streptomyces padanus* and the MACB *Rhodococcus fascians* 307CO has resulted in the discovery of two isomers of a new class of aminoglycosides [25]. The resulting Rhodostreptomycins A and B exhibited potent antibiotic activities against a wide range of Gram-positive and Gram-negative bacteria. Another example is the co-cultivation of *Actinosynnema mirum* NBRC 14064, a producer of the monocyclic polyene macrolactam mirilactam A, with the MACB *Tsukamurella pulmonis* TP-B0596, which led to the identification of three novel compounds (mirilactams C–E) produced only in the co-culture[26].

After the myxobacterial isolation of a new phylogenetically characterised clade and so called *Streptomyces*-like myxobacteria. These isolates show a high phenotypic similarity to *Streptomyces* and possess a substantial number of BGCs with considerable potential for new SMs. To activate additional non-expressed BGCs of *Streptomyces*-like myxobacteria for natural product discovery, we selected three novel myxobacterial isolates with previously determined bioactivity profile and cultured them in a paired manner with four different MACB species. All co-culture extracts were subjected to LC-*hr*MS for a metabolomics workflow, which revealed that MACB strains can successfully activate the secondary metabolism of the investigated myxobacteria. We were able to identify a novel compound family, an increased number of derivatives of known compound classes and an enhanced production yield of an already known metabolite by co-cultivation. In addition, bioactivity assays showed a remarkable increase in activity against Gram-positive pathogens as well as high potent inhibition of purified alkyl-quinolones against *M. tuberculosis* 7H37Ra. The results of this study provide insights into the potential of *Streptomyces*-like myxobacteria for natural product discovery.

3.3 Results and discussion

We used a direct co-cultivation setup for myxobacteria and mycolic acid-containing bacteria (MACB), in which both bacteria grow together in a liquid environment. In previous studies, members of MACB have been shown to induce the expression of BGCs from various actinobacteria, but only by interacting with mycolic acids located in their outer cell membrane[24]. Therefore, we decided to employ the co-cultivation procedure using a similar setup (Figure 3.1).

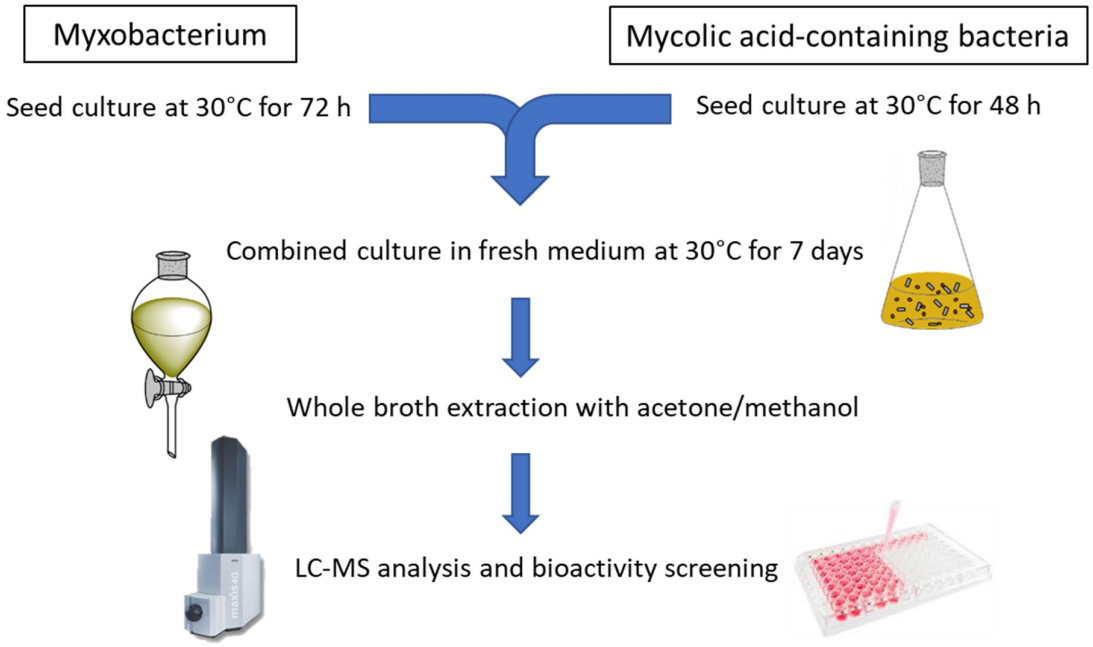

Figure 3.1: Flowchart of the co-cultivation procedure.

After cultivation of co-cultures, controls and blanks, we performed a comprehensive metabolomics-based workflow on the crude extracts to identify changes in the secondary metabolome as well as antibacterial activities using bioactivity assays. Co-cultivation experiments have demonstrated that direct cultivation of the myxobacterial producer together with a partner strain in the same liquid environment was more effective because it resulted in the detection of additional SMs.

The obtained metabolomic data from each co-cultivation were evaluated through a statistical data workflow to distinguish the unique molecular features within the different MACB approaches. Accordingly, we analysed in detail the appearance or disappearance of metabolites, an increase or decrease in metabolite production, and metabolites that showed no change.

3.3.1 Comprehensive metabolomic data analysis from co-cultures between *Sorangium sp.* MSr12523 and different MACB

We determined whether all four MACB species influence the secondary metabolism of not only MSr12523, (Figure 3.2) but also two other *Sorangium species* MSr11954 and MSr11367 (Figure S3.1 & Figure S3.2). For this, we compared the molecular features of the secondary metabolite profiles between the co-culture and axenic crude extracts using an LC-MS system. Afterwards, a statistical metabolomic data workflow was used to identify significant features by *t*-Test/ANOVA analysis, which allowed the comparison of detected features in order to identify their increased or decreased production level, appearance of new metabolites, disappearance of some SMs, as well as lack of change (within +/- 30 % of intensity). Therefore, features found in at least two out of three biological replicates were considered as a significant compound. All co-culturing approaches with MACB *C. glutamicum*, *R. erythropolis*, *T. soli*, and *T. pseudospumae* showed a considerable effect on the SM production of MSr12523 (Figure 3.2A-D).

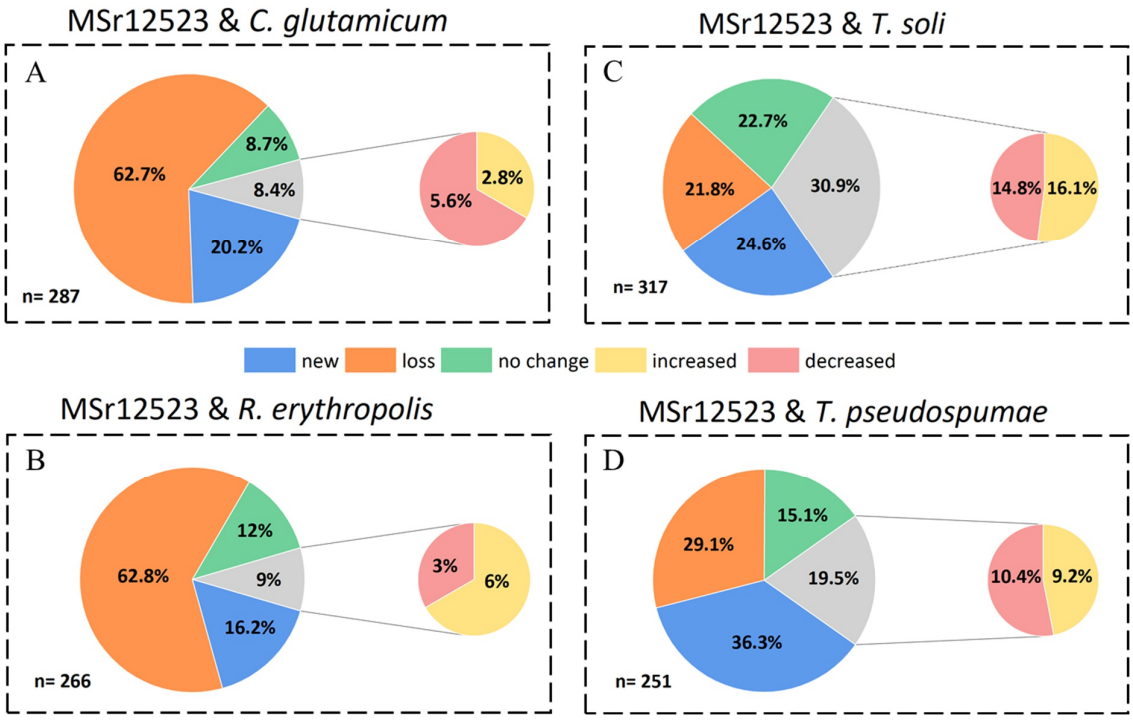

Figure 3.2: (**A - D**) Results of the comparison of secondary metabolite profiles of MSr12523 axenic culture and co-cultures with *C. glutamicum* (A), *R. erythropolis* (B), *T. soli* (C) and *T. pseudospumae* (D) are shown in pie charts. The chart represents the total number of molecular features identified by the MetaboScape features (metabolites) in the crude extract that exceed a threshold value of $1x10^5$. The axenic culture was used as a control. Each extract was classified in terms of increase/decrease or no change in metabolite production, appearance of new metabolites, and disappearance of some secondary metabolites. New: New secondary

metabolites appeared in co-culture. Loss: Secondary metabolite production was absent in the co-culture. No change: There was a lower change than +/- 30% of intensity between the SM level of the axenic culture and the co-culture. Increase/decrease: There was a higher change then +/- 30% of intensity between SM level of the axenic and the co-culture.

Interestingly, we could observe an almost similar percentage of ~62% disappearing molecular features by co-cultivation with *C. glutamicum* and *R. erythropolis*. In contrast to that, co-culture extracts with MACB using *Tsukamurella sp.* only show a disappearance of metabolites by ~ 20-30%. The highest number of new metabolic features was detected in *T. pseudospumae* (Figure 3.2D) extracts with 36.6%, the lowest ability to generate new metabolites was observed for *R. erythropolis* (Figure 3.2B). *T. soli* (Figure 3.2C) showed the greatest effect on the general production by increasing (16.1%) and decreasing (14.8%) the intensity of metabolites. In all of the examined crude extracts, it was found that a proportion from 9% to 22% of the secondary metabolites remained unchanged after co-cultivation. Our results suggest that the utilised MACB significantly influenced the metabolome, leading to an increase of the number of produced SMs from *Sorangium* sp. MSr12523 by 15% to 36% depending on the partner strain.

Similar observations were reported for the co-cultivation between the actinobacteria *Streptomyces cinnamoneus* NBRC 13823 and MACB *T. pulmonis*, leading to a change in secondary metabolism and the isolation of a new cytotoxic indolocarbazole alkaloid[27]. The order Corynebacteriales consists of a large number of different MACB, which exhibit a variety of mycolic acid features, including a diverse number of carbon atoms in their outer cell membrane[23]. For this reason, the different number or length of the mycolic acids could explain the different induction ability of the secondary metabolism by particular MACB. Furthermore, an intense phenotypic change of *Sorangium sp.* MSr12523 in the contact zone with *T. pseudospumae* was observed by co-cultivation on agar plates. These results indicate that the MACB and MSr12523 intertwine under co-culture conditions, whereby the cell-cell interactions via mycolic acids can influence the secondary metabolism[28].

As a result, we were able to recognise the strongest influence on the occurrence of new metabolites for *T. pseudospumae* as a partner strain during co-cultivation with MSr12523. Because of this, this particular combination of co-cultivation was studied in depth. Furthermore, the effects of the colour change on the culture broth were to be pursued.

3.3.2 HPLC-*hr*MS spectra of co-culture- and axenic-culture-derived extracts from strain MSr12523 and *Tsukamurella pseudospumae* DSM 44118

Towards the end of cultivation, the culture colour of each co-cultivation setup was observed to change from light yellow to dark reddish. This phenomenon occurs irrespective of the type of solid (Figure 3.3A) or liquid (Figure 3.3B) cultivation conditions. However, only co-cultivation with myxobacterium MSr12523 and *T. pseudospumae* leads to this discovery.

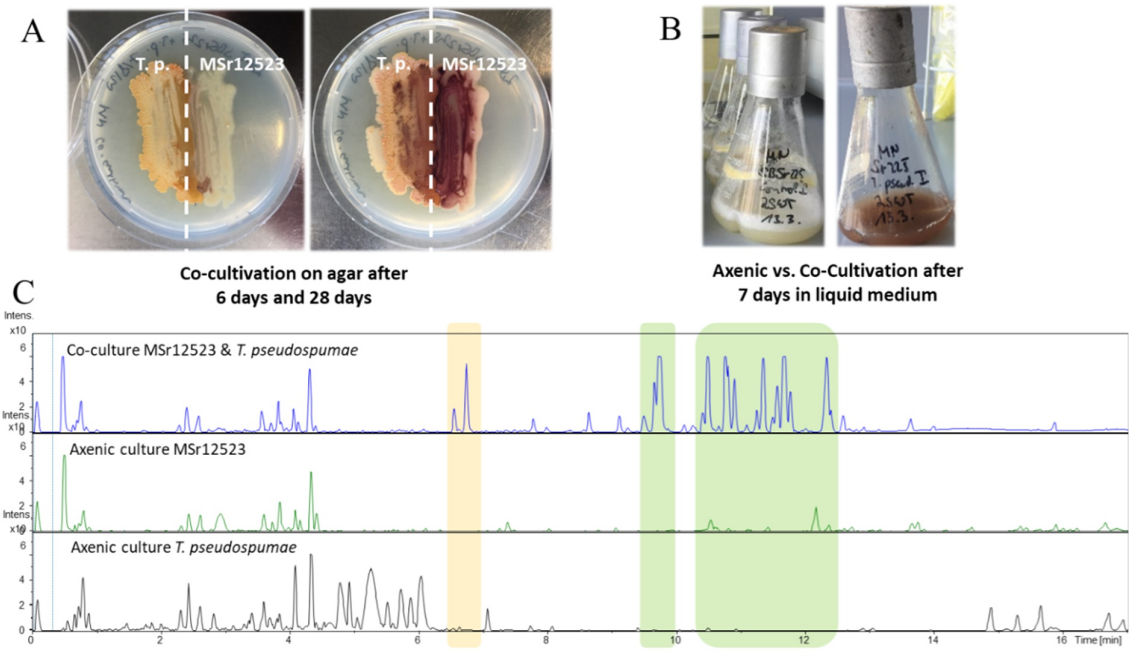

Figure 3.3: (**A**) Co-cultivation between *Tsukamurella pseudospumae* (left site, *T.p.*) and *Sorangium sp.* MSr12523 (right site) on a 2SWT agar plate after 6 and 28 days. (**B**) Axenic culture of MSr12523 (left flask) and co-culture of MSr12523 and *T. pseudospumae* (right flask) in 2SWT medium after 7 days of cultivation. (**C**) Base peak chromatogram with mass scan range from 150-2500 m/z of the crude extracts of *Sorangium sp.* MSr12523 cultured with *T. pseudospumae*, showing metabolites that are upregulated (highlighted yellow) and expressed only in co-cultures (highlighted green). Comparison between co-culture (top), *Sorangium sp.* MSr12523 axenic culture (middle), and *Tsukamurella pseudospumae* axenic culture (bottom).

Crude extracts of both axenic culture and co-culture were analysed using an LC-MS-system to determine changes in the metabolome related to the co-cultivation. Metabolite profiling of these extracts demonstrated that several myxobacterial metabolites in axenic culture were upregulated in the co-culture extract (Figure 3.3C, highlighted yellow). Moreover, a high number of metabolites that were not previously observed in axenic cultures were detected in the co-culture (Figure 3.3C, highlighted green). Thus, in the box highlighted in green (Figure 3.3C) several peaks belonging to the same compound class can be observed.

This class of compounds consists of several isomers, which are shown in Figure S3.3 - Figure S3.5. These metabolites are therefore specific to the co-culture extract and are probably produced due to microbial interactions between MACB *T. pseudospumae* and *Sorangium sp.* MSr12523[28,29]. Similar observations have previously been published, whereby dialysed cultures and the addition of some components prepared from MACB to *Streptomyces* cultures revealed no inducing ability[24].

As next step, we utilised molecular networking for comprehensive identification and visualisation of new occurring metabolites, additional derivatives and connections between existing metabolite clusters.

3.3.3 Molecular network from co-culture between *Sorangium sp.* MSr12523 and *T. pseudospumae*

For the identification of the chemical space in axenic- and co-cultures comparatively, a global molecular network (MN) based on LC-hrMS² data was created using the GNPS platform[30]. This approach allows us to capture diverse chemical structure classes and analogues and arrange them into different clusters based on MS² spectral alignment algorithms. This enables rapid identification of putative new molecules and derivatives thereof and map them to known or unknown molecular families out of different libraries. Global MN displays all features from axenic-, co-culture and their combinations present in crude extracts of myxobacterium MSr12523 and *T. pseudospumae* (*T. p.*).

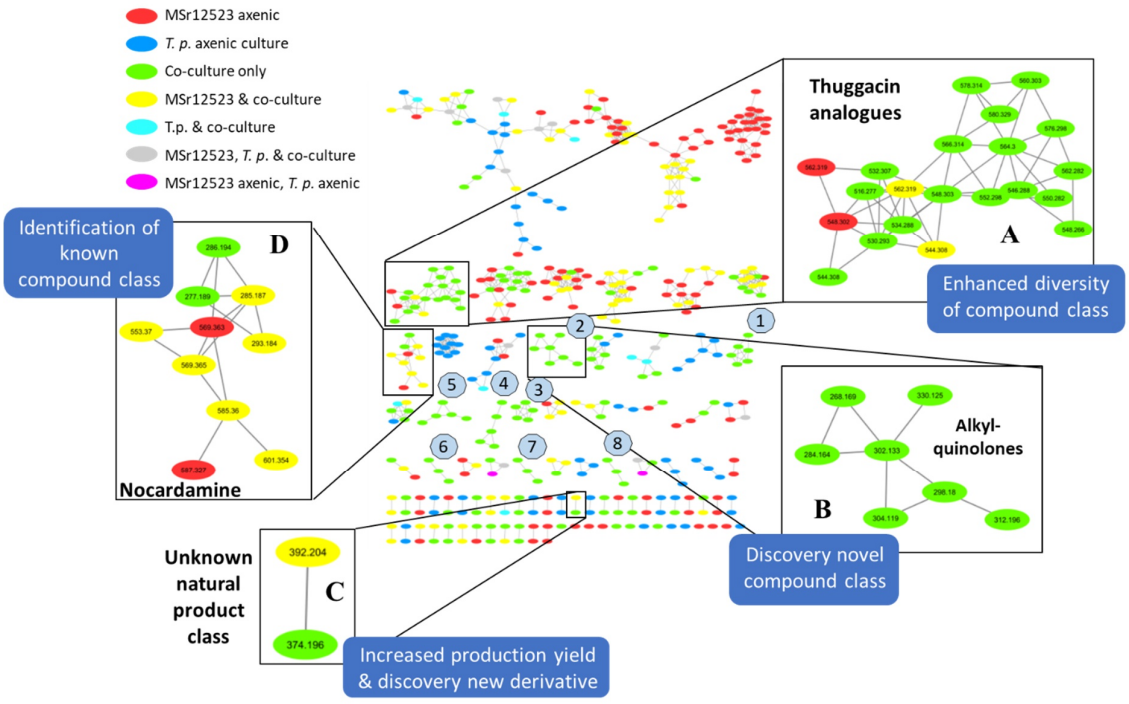

Figure 3.4: Global molecular network based on MS² data from the co-cultivation of *Sorangium sp.* MSr12523 and *T. pseudospumae* (*T. p.*) and their respective axenic-cultures. Red nodes: axenic-culture of Msr12523; blue nodes: axenic-culture of *T. p.*; green nodes: co-culture; yellow nodes: combination of MSr12523 & co-culture; turquoise nodes: combination of *T. p.* & co-culture; grey nodes: combination of MSr12523 & *T. p.* & co-culture; magenta nodes: combination of MSr12523 & *T. p.* axenic culture. The MN boxes highlight that co-culture increased the chemical diversity in comparison to axenic culture and allowed for the identification of a known compound family. Numbers (1-8) show the newly introduced molecular clusters that only occur in co-cultivation.

The generated MN of all three extracts (co-culture MSr12523 & *T. pseudospumae* (*T. p.*), axenic MSr12523, axenic *T. p.*) consisted of 604 nodes with a total number of 936 edges, which were grouped into 36 clusters (two or more nodes per cluster). Some nodes are representing adducts, thereby, not all existing network nodes correspond to a unique metabolite. As shown in Figure S3.6, some chemical families/compounds were annotated including anthraquinone[31] (cyclic polyketide), corallopyronin[32] (polyketide), DKxanthen[33] (linear PKS-NRPS peptide), myxothiazol[34] (linear PKS-NRPS peptide), myxochromids[35] (cyclic lipopeptide), sorangicins[36] (polyketide), nocardamine (cyclic ferrioxamine siderophore) and thuggacin[37] (macrolide antibiotic). In total, 139 known chemical molecules/substances from our internal data base (Myxobase) could be annotated. Since the molecular network annotations organised by MS² data are based on chemical similarity, false positive annotation cannot be avoided, in particular for large datasets. However, successful dereplication

with molecular networks requires high-quality MS^2 spectra of the extract together with MS/MS spectra of known natural products or well-characterised organisms, preferably organised in robust databases[38]. Nevertheless, in order to facilitate the recognition of other derivatives or new representatives of the compound class from the abundant mixture of metabolites, these approaches are helpful and can be carried out quickly.

The global MN showed that 8 molecular clusters (green nodes) were exclusively identified in the co-culture extract of MSr12523 and *T. p.* (numbered 1 – 8, SI). We were able to discover a novel compound class of myxobacteria (Figure 3.4, Box B), which was later identified as alkyl-quinolones and only present in co-culture. The other molecular clusters (numbered: 1, 3 - 8) comprised of 30 nodes with precursor masses ranging from m/z 284 to 1223 Da and could not be annotated, which suggests their potential novelty. Still, we were able to annotate the known chemical families of thuggacin (Figure 3.4, Box A) and nocardamine (Figure 3.4, Box D). Interestingly, it was possible to enhance the chemical diversity of the already produced thuggacins due to co-cultivation, which lead to the identification of six new analogues. In contrast to that, we were not able to identify additional derivatives of nocardamine in co-cultivated extracts in comparison to axenic culture. In addition to the expression of new molecular clusters, we observed altered production levels of some compounds in the co-cultures (Figure 3.4, Box C). For example, the integrated area of compound-392 exhibited a 70-fold increase in production while the additional new derivative (Cpd-374) was exclusively expressed in co-culture of MSr12523 and *T. pseudospumae*. This result indicates that the corresponding BGC was intensively expressed as a reaction to the competition by partner strains, which confirms our hypothesis of interaction between myxobacteria and mycolic acid-containing bacteria.

About 30 % of the molecular network nodes analysed in this study were produced in the co-culture only. The chemical novelty of the as of yet unidentified molecules still needs to be confirmed through their purification and characterisation. We could again underline the effectiveness of co-cultivation due to the increased number and size of the molecular network by the biosynthesis of new derivatives of known clusters or observation of completely new nodes/clusters.

In addition to that, the discovered novel myxobacterial compound class of alkyl-quinolones as well as further derivatives of known thuggacin analogues have been isolated and structurally characterised by LC-MS and NMR experiments. Hence, we carried out large scale

co-cultivations between *Sorangium sp.* Msr12523 and mycolic acid-containing *T. pseudo-spumae* to receive sufficient amounts for purification.

3.3.4 Discovery of secondary metabolites produced from co-culture with MACB of *Sorangium sp.* MSr12523

All shown structures were characterized using several spectrometric and spectroscopic analyses including liquid chromatography mass spectrometry (LC-*hr*MS), 1D and 2D nuclear magnetic resonance spectroscopy (NMR).

3.3.4.1 Compound-392

Compound-392 (cpd-392) was obtained with a molecular formula of $C_{21}H_{29}NO_6$ using high-resolution electrospray ionisation mass spectrometry (observed $[M+H]^+ = 392.20667$, m/z calculated $[M+H]^+ = 392.20676$; $\Delta = 0.23$ ppm, Figure S3.8) and was determined to consist of incorporated polyketide building blocks and the amino acid tyrosine (Figure 3.5).

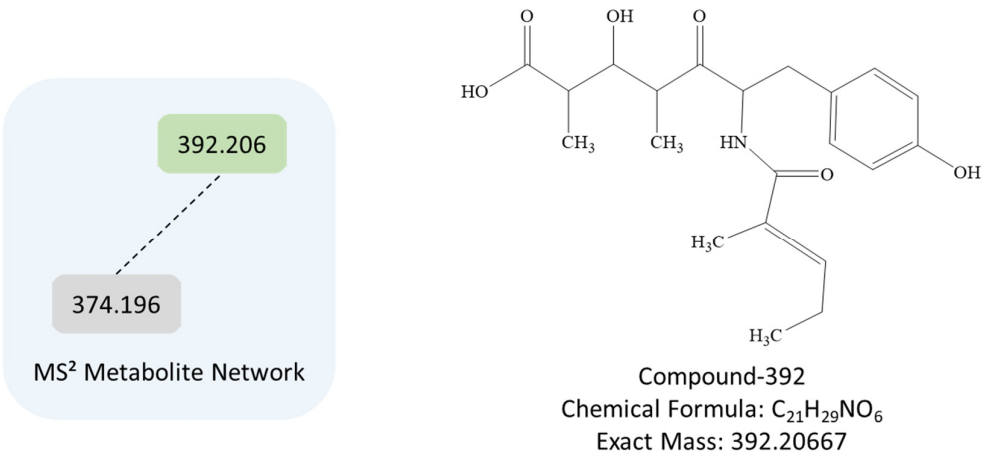

Figure 3.5: Structure of PKS-NRPS hybrid compound-392 isolated after co-cultivation of MSr12523 with *T. pseudospumae*. The molecular network shows the elucidated metabolite (green) and the remaining derivative (grey).

Analysis of the 1-D (^1H and ^{13}C) and 2-D (COSY, HMBC and HSQC) NMR data are shown in supporting information (Figure S3.11 - Figure S3.15, and Table S3.2). Using NPAtlas, we were unable to find similar compounds or partial structures of previously described natural products of cpd-392 in this database[39]. After co-cultivation, we identified another derivative of the cpd-392 compound class by a molecular network not present in extract of the axenic culture. Furthermore, cpd-392 was also detectable in the crude extract of the

axenic culture of *Sorangium sp.* MSr12523, but at a significantly lower intensity, thus not allowing prior isolation. Based on the structure, we suppose that cpd-392 consists of a PKS part (four methylmalonyl-CoA units) in combination with an incorporated NRPS moiety in the form of a tyrosine amino acid. Unfortunately, the corresponding gene cluster of this compound in the genome of MSr12523 has not yet been identified.

3.3.4.2 Alkyl-quinolones

Evaluation of LC-*hr*MS (Figure S3.9) and NMR (1-D and 2-D) data revealed that we isolated compounds from the class of bacterial alkyl-4-quinolones[40] after co-cultivation of MSr12523 and *T. pseudospumae*. Overall, we were able to identify five novel derivatives of alkyl-quinolones (AQs) from myxobacterium *Sorangium sp.* MSr12523, but only four of them could be isolated. NMR data of 1-D (^{1}H and ^{13}C) and 2-D (HMBC, HSQC and COSY) analysis can be found in the supporting information (Figure S3.16 - Figure S3.35, and Table S3.3 - Table S3.8).

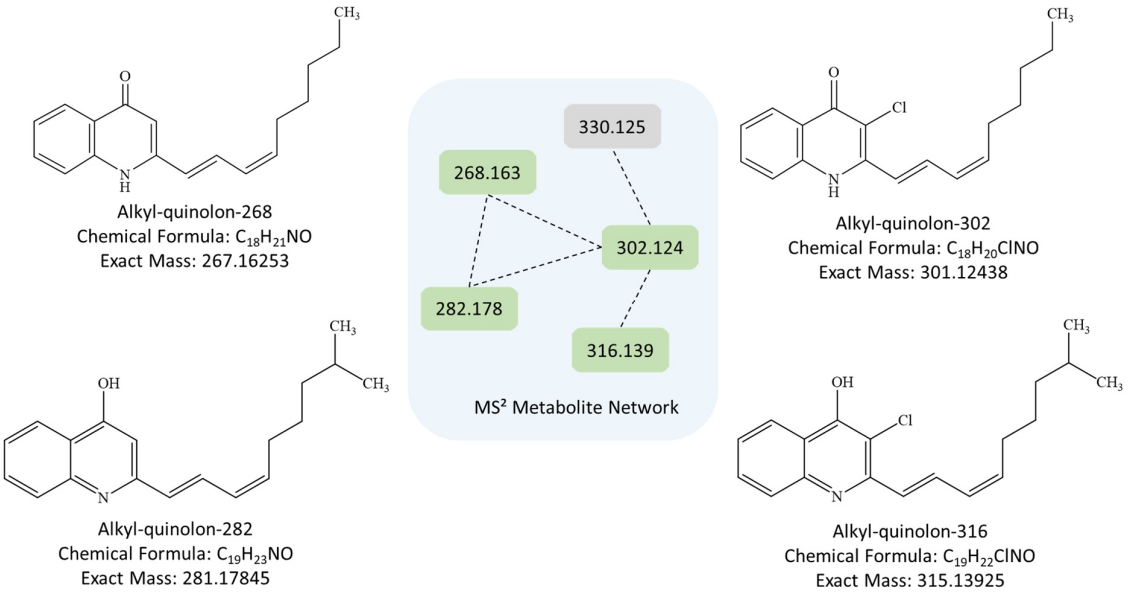

Figure 3.6: Structures of four alkyl-quinolones isolated from co-cultivation of MSr12523 with *T. pseudospumae*. The molecular network shows the elucidated metabolites (green) and the remaining derivative (grey).

The microbial metabolite class of AQs is mainly produced by bacterial strains belonging to the genera *Pseudomonas* and *Burkholderia*[41,42]. These compounds consist of a 4-quinolone core structure substituted with a number of pendant groups, usually at the C-2 position. Recently, it has been discovered that one alkyl-quinolone derivative in particular, the Pseu-

domonas Quinolone Signal (PQS), plays an important role in the communication of bacteria and quorum sensing of *P. aeruginosa*[43]. We isolated four different metabolites that structurally consist of the AQ motif with the 4-quinolone core, an aromatic nitrogen-containing heterocyclic compound substituted by an alkyl side chain with two conjugated double bonds (Figure 3.6). In addition to that, we determined that two AQ derivatives (302 and 316) are substituted by chlorination on C-3 position of the heterocycle by both isotopic pattern and NMR analysis. We should mention that such structural features of AQs as the conjugated double bonds as well as chlorination have not so far been encountered in nature in this class of compounds.

Due to the high structural diversity of AQs, a considerable number of biological effects have already been discovered, including antimicrobial, antifungal and anti-algal activities[40]. Therefore, we tested our isolated AQs on a panel of different Gram-negative and Gram-positive pathogens.

3.3.4.3 Thuggacin analogues

All isolated thuggacin analogues-548, -564, -566, and -578 (Figure 3.7) were characterized using spectrometric and spectroscopic analyses including liquid chromatography mass spectrometry (Figure S3.10), 1-D and 2-D NMR. In the course of another project regarding *Sorangium sp*. MSr12523, additional cyclic thuggacin analogues-548 and-662 were isolated (data not shown). Closer inspections of the 1-D (^{1}H and ^{13}C) and 2-D (COSY, HSQC and HMBC) NMR data sets of the thuggacin analogues-548, -564, -566, and -578 confirmed that we isolated new representatives of the thuggacin family[44]. All NMR data are shown in the Supplementary information (Figure S3.36 - Figure S3.55, and Table S3.9 - Table S3.12).

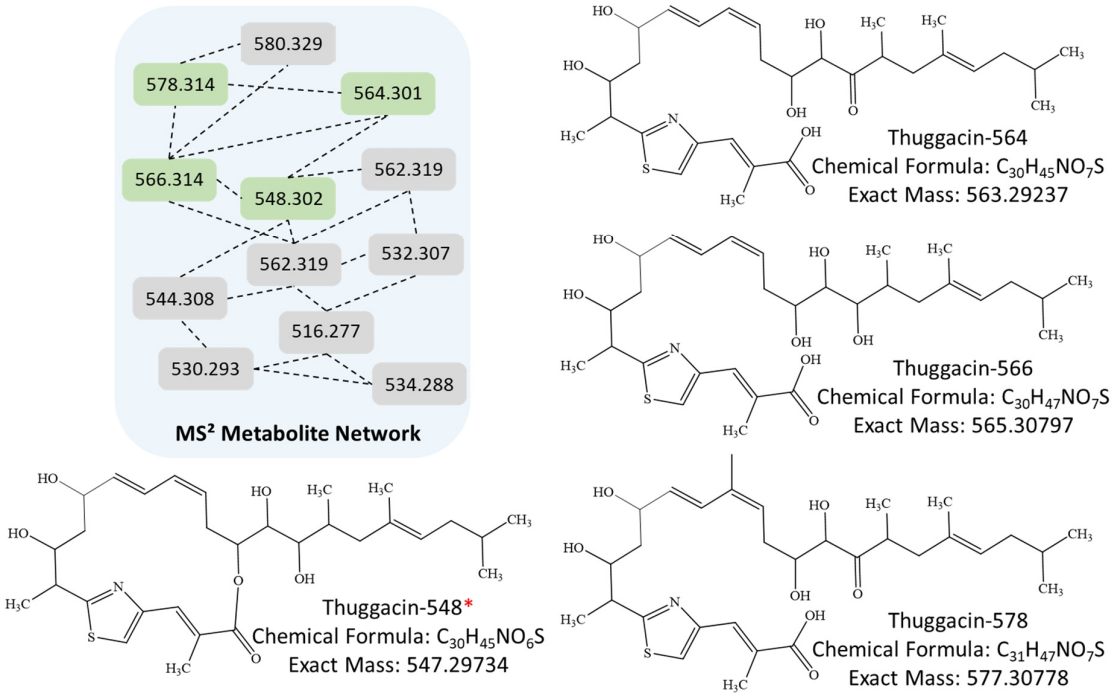

Figure 3.7: Structures of the thuggacin analogues-548, -564, -566, and -578 isolated from co-cultivation of MSr12523 with *T. pseudospumae*. The cyclic thuggacin analogue-548 was isolated from axenic culture of MSr12523 grown under different experimental setup (Red star marking). The molecular network shows the elucidated new metabolites (green) and the remaining derivative (grey).

Three of the thuggacin analogues (564, 566, and 578) possess a difference in their macrocyclic lactone moiety compared to the major analogue-548. We could determine the open chain structure in the region of the initial macrocyclic ring moiety instead of the chemical lactone bond. This structural feature distinguishes these thuggacin analogues from the already reported members of the known thuggacin family[37]. Generally, the compounds of the thuggacin family target the bacterial respiratory chain and show mediocre to strong antibacterial activity against a range of microorganisms, e.g. *Mycobacterium tuberculosis*, depending on the tested derivative[45]. Therefore, we investigated our isolated and purified thuggacin analogues for biological activity against *M. tuberculosis* 7H37Ra, which is shown in sub-chapter 3.3.5.3.

Subsequently, all extracts from axenic and co-cultivation were screened in a dilution assay to obtain an overview of the antimicrobial activity and their alterations. Additionally, the isolated and pure compounds which were mentioned above have been tested for their potentially occurring biological activity against various Gram-negative and Gram-positive pathogens.

3.3.5 Biological activity testing of crude extracts and purified compounds from co-cultivation of *Sorangium sp.* MSr12523 with MACB

Three out of four examined extracts after myxobacterial co-cultivation showed potent or at least increased activities against six test organisms of our antimicrobial test panel (Figure 3.8).

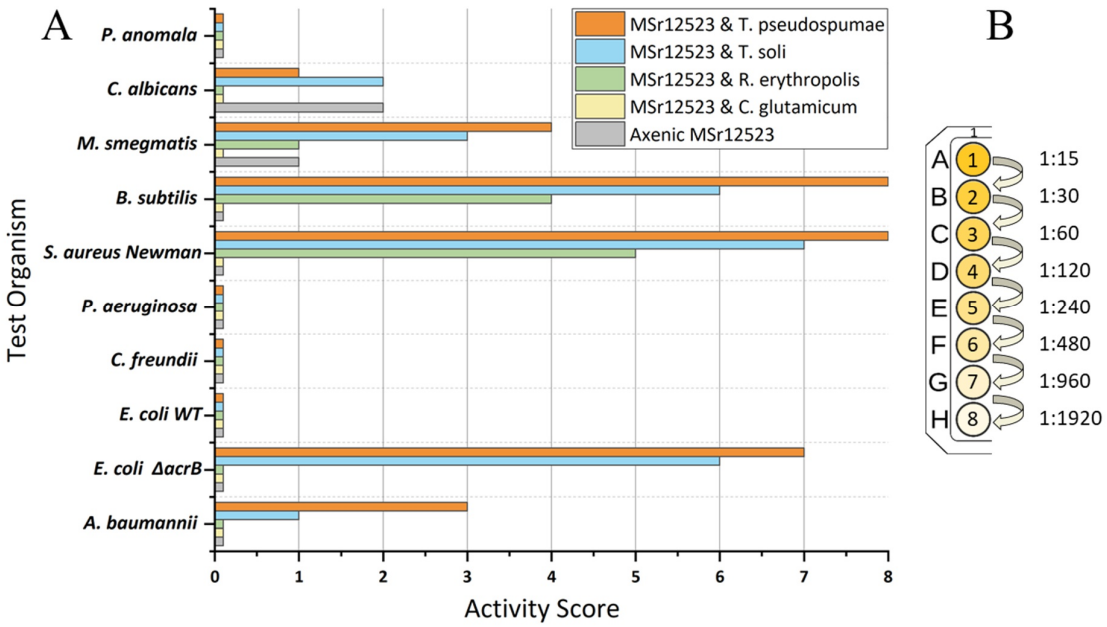

Figure 3.8: (**A**) Antimicrobial activity scores of crude extracts after co-cultivation of MSr12523 with *C. glutamicum, R. erythropolis, T. soli* and *T. pseudospumae* in comparison to axenic culture (grey) as control. (**B**) Activity scores with correlation between the concentration of the crude extract by serial dilution and biological inhibition of the test organism.

The co-cultivation extract of MSr12523 and *T. pseudospumae* exhibits the highest and broadest antimicrobial activities, with inhibition of Gram-negative and Gram-positive organisms as well as at least of one fungus from the test panel. There was a remarkably strong activity of this extract with the maximum score of eight by inhibiting growth of both *B. subtilis* and *S. aureus* up to the highest dilution. In addition, we could also observe Gram-negative activity against *A. baumannii* (moderate) and *E. coli* ΔacrB (potent) of the same extract. Interestingly, it was found that co-cultivation by both *Tsukamurella sp.* resulted in a similar spectrum of antifungal and antimicrobial activities, with only a few differences in activity scores, hinting at a similar influence of both organisms. In comparison, the extract from the co-culture of *R. erythropolis* shows only selective activity against Gram-positive test organisms. In contrast to the other myxobacterial MSr12523 extracts, we were not able

to detect any antimicrobial activities after co-cultivation with *C. glutamicum*. In addition, the extract from axenic culture of MSr12523 displays a slight activity against *M. smegmatis* and *C. albicans* in our antimicrobial assay.

In summary, we were able to enhance the antimicrobial activities of almost all myxobacterial co-cultures with MACB by co-cultivation, with the exception of *C. glutamicum*. Furthermore, we were also able to extend the spectrum of antimicrobial activity, which was not observed for the axenic culture of MSr12523. These results suggest that this type of co-culture approach can stimulate the production of new secondary metabolites that were not previously expressed. The remaining antimicrobial activities of the crude extracts from the co-cultivation of myxobacteria MSr11367 and MSr11954 together with MACB can be found in the supporting information (Figure S3.56 and Figure S3.57). For an in-depth study of this observed bioactivity, we further screened purified compounds isolated from this crude extract to determine their potential activities.

3.3.5.1 Antimicrobial assay for Compound-392

Compound-392 was tested against a panel of Gram-positive (*M. smegmatis*, *S. aureus*, *B. subtilis*), Gram-negative pathogens (*E. coli* BW25113*, E. coli* WT JW0451-2 (ΔacrB), *A. baumannii, P. aeruginosa, C. freundii*) and fungi (*M. hiemalis*, *C. albicans*, *C. neoformans, P. anomala*) for determination of minimum inhibitory concentrations (MICs).

Table 3.1: Determination of antimicrobial activity of compound-392 against a panel of bacterial pathogens.

Pathogen	**Minimum Inhibitory Concentration [µg/mL]**
	392
E. coli BW25113	>64
E. coli JW0451-2 ΔacrB	>64
A. baumannii DSM-30008	>64
P. aeruginosa PA14	>64
C. freundii DSM-30039	>64
M. smegmatis mc² 155	>64
S. aureus Newman	>64

B. subtilis DSM-10	>64
M. hiemalis DSM-2656	>64
C. albicans DSM-1665	>64
C. neoformans DSM-11959	>64
P. anomala DSM-6766	>64

Table 3.1 indicates that we could not detect any significant antimicrobial activity of the investigated crude extracts at the highest concentration tested (>64 µg/mL). However, we have not tested compound-392 for cytotoxicity or ran further assays yet.

3.3.5.2 Antimicrobial assay for alkyl-quinolones

The isolated AQs were tested against a panel of Gram-positive (*S. aureus* Newman, *M. tuberculosis* 7H37Ra) and Gram-negative pathogens (*E. coli*, *E. coli* ΔacrB, *A. baumannii*, *P. aeruginosa*) to determine the respective MIC values.

Table 3.2: Determination of antimicrobial activity of AQs against a panel of bacterial pathogens. Abbreviations: n. t. - not tested

Pathogen	**Minimum Inhibitory Concentration [µg/mL] or IC_{50} [µM]**			
	268	**282**	**302**	**316**
E. coli WT	>64	n. t.	>64	>64
E. coli ΔacrB	>64	n. t.	>64	>64
A. baumannii DSM-30008	>64	n. t.	>64	>64
P. aeruginosa PA14	>64	n. t.	>64	>64
S. aureus Newman	>64	n. t.	32	>64
M. tuberculosis 7H37Ra	1 - 0.5	>64	4 - 2	32
CHO-K1 (IC_{50})	3.28 ± 0.59	n. t.	1.45 ± 0.13	8.51 ± 5.21

AQ-268 and -302 showed strong anti-mycobacterial activity against *M. tuberculosis* 7H37Ra in the lower 0.5 - 4 µg/mL range. Another tested AQ derivative-316, showed only

moderate (32 µg/mL) antimycobacterial activity. In contrast to that, no biological activity was detected in the assay for AQ derivative-282. Additionally, we were unable to detect further antimicrobial activities of all four alkyl-quinolones, except for AQ-302 (32 µg/mL), which showed moderate biological activity against *S. aureus*. Unfortunately, the AQs that were tested showed significant cytotoxicity against the CHO-K1 cell line. The bioactivity results show that there is no evident correlation between the chlorinated (302, 316) and the non-chlorinated (268, 282) AQ derivatives regarding their antimycobacterial activity. For this reason, it looks like the activity is related to the branched part of the alkyl-chain instead of the chlorination of the C-3 position of the heterocycle.

3.3.5.3 Antimicrobial assay of thuggacin analogues

Four thuggacin analogues were tested to determine the minimum inhibitory concentration (MIC) against *M. tuberculosis* 7H37Ra.

Table 3.3: Determination of antimicrobial activity of thuggacin analogues as pure compounds and published thuggacin A against *M. tuberculosis* 7H37Ra.

Pathogen	**Minimum Inhibitory Concentration [µg/mL]**				
	548	**564**	**566**	**578**	**Thuggacin A**
M. tuberculosis 7H37Ra	16	>64	>64	>64	32

In the antimicrobial MIC assay, we detected a moderate inhibitory effect thuggacin analogue-548 against *M. tuberculosis* 7H37RA. At the highest concentration tested, no antimicrobial effect of the thuggacin analogues -564, -566 and -578 were observed. For comparability, thuggacin A was used as a reference, whose antimycobacterial activity with a determined MIC of 8 µg/mL against *M. tuberculosis* H37RV had already been reported in the literature[45]. In the respective paper, the authors have shown that thuggacin A inhibited the growth of some Gram-positive bacteria, especially of *Micrococcus luteus* and of other species from the genera *Corynebacterium* and *Mycobacterium*[37]. In our study, we were only able to demonstrate the antimycobacterial activity of thuggacin analogue-548, which differs structurally from the other derivatives. This result suggests that the closed ring moiety of the thuggacin structure is essential for their biological activity[45]. Therefore, we did not observe activity against *M. tuberculosis* 7H37Ra for the analogues-564, -566, and -578 in our assay.

Next, we were able to identify the putative BGC for the synthesis of our thuggacin analogues based on the genome sequence of *Sorangium sp.* MSr12523 compared to the previously reported thuggacin clusters.

3.3.6 Proposed biosynthetic pathways

In silico analysis of the sequenced genome of *Sorangium sp.* MSr12523 have been carried out using antiSMASH 6.0[46] and MIBiG[47]. In the following section, we presented a putative BGC, what is likely to be involved in the myxobacterial alkyl-quinolone biosynthesis, as well as the already known *tga* BGC for the thuggacin analogues.

3.3.6.1 Biosynthetic pathway of the myxobacterial alkyl-quinolone from *Sorangium sp.* MSr12523

The bacterial groups of *Burkholderia* and *Pseudomonas* producing 4-hydroxy-2-alkyl-quinolines (HAQs) as part of their secondary metabolism, which are known to be implicated in bacterial interspecies competition, cell-cell signalling, iron acquisition and virulence, among other biological functions[48–50]. A putative biosynthetic gene cluster has been identified by *in silico* analysis with antiSMASH in the genome of *Sorangium sp.* MSr12523. These are likely to be involved in the biosynthesis of alkyl-quinolone, representing homology to the biosynthesise of HMAQ (4-hydroxy-3-methyl-2-alkenylquinolones), HHQ (4-hydroxy-2-heptylquinoline), and PQS (2-heptyl-3,4-dihydroxyquinoline, Pseudomonas quinolone signal) by various *Burkholderia sp.*[51] and *P. aeruginosa*[52,53].

Our proposed *maq* BGC (Figure 3.9A) contains approximately 11.8 kb of genomic DNA including open reading frames (ORFs) with derived functions which have been associated on the basis of database comparisons and sequence alignment (Table 3.4).

Table 3.4. Deduced functions of open reading frames (ORFs) in alkyl-quinolone biosynthetic gene cluster in the *Sorangium sp.* MSr12523.

Protein	aa	Proposed function of the homologues protein	Source of the homologues protein	Percent Identity	Accession Number
Orf1	109	Hypothetical protein	*Nothing found*	-	-
MaqA	307	MBL-fold metallohydrolase	*Burkholderia thailandensis*	40.6 %	WP_019256095.1
MaqB	484	Tryptophan 7-halogenase	*Chondromyces apiculatus*	56.5 %	WP_044251132.1

MaqC	290	Hypothetical protein	*Arcicella aurantiaca*	37 %	WP_109744980.1
MaqD	347	Ketoacyl-ACP synthase III	*Burkholderia sp.* BDU5	49.5 %	WP_059471366.1
Orf2	76	Acyl carrier protein	*Alphaproteobacteria bacterium*	42.2 %	MCB9681280.1
Orf3	584	AMP-binding protein	*Myxococcales bacterium*	55.9 %	MCA9541850.1
MaqE	356	3-oxoacyl-ACP synthase III family protein	*Hymenobacter rubripertinctus*	46.5 %	WP_119656068.1
Orf4	563	Acyl-CoA dehydrogenase	*Burkholderia singularis*	52.2 %	WP_089339373.1
Orf5	582	Acyl-CoA dehydrogenase	*Streptomyces rimosus*	54.4 %	WP_107066188.1

BLAST search using the amino acid sequences from aurachin, PQS and HMAQ biosynthesis revealed that the coding genes share some similarities with MAQ (myxobacterial alky- quinolone) synthesis. For this reason, we assume that a comparable biosynthetic pathway most likely occurs in the biosynthesis of the various alkyl-quinolone derivatives in MSr12523. Besides biosynthesis, we also proposed the gene organisation of *maq* gene cluster in MSr12523 based on amino acid sequence alignment.

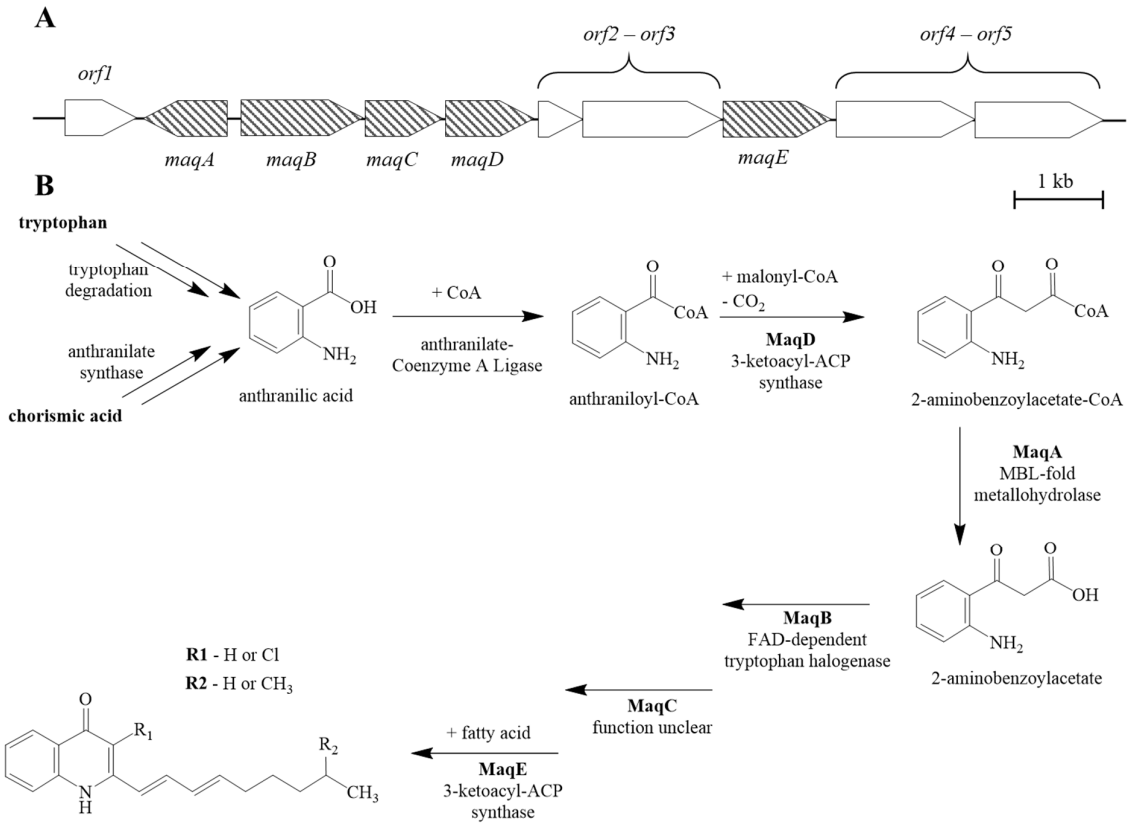

Figure 3.9: Schematic representation of the proposed MAQ genes in *Sorangium sp.* MSr12523 (**A**). Hatched: genes *maq*A – E likely involved in the biosynthetic pathways; white: genes might be not involved in biosynthesis. Proposed biosynthesis of hydroxyl-alkyl-quinolone in myxobacterium *Sorangium sp.* MSr12523 (**B**).

The *maqABCDE* genes showing slight similarities (about ~20%) to *pqsABCDE* and *maqA-BCDE* genes sequences that are involved in the biosynthesis of *Pseudomonas aeruginosa* PQSs and *Burkholderia thailandensis* HMAQs[41,51]. Nevertheless, it can be assumed that the synthesis of MAQs follows the same biological rationale even in the case of slight gene similarity. Anthranilic acid is the precursor of HAQ biosynthesis by Burkholderia and Pseudomonas, formed either by the degradation of tryptophan by the kynurenine pathway or by the formation of chorismic acid via TrpEG anthranilate synthase[54]. Next, anthranilic acid is synthesised to anthraniloyl-CoA by anthranilate coenzyme A ligase, which is not part of the MAQ gene cluster. MaqD then transferred malonyl-CoA to anthraniloyl-CoAto from 2-aminobenzoylacetate-CoA[55]. A MBL-fold metallo-hydrolase (maqA) can remove the CoA from 2-aminobenzoylacetate-CoA to obtain (2-ABA). Then, 2-aminobenzoyl acetate is modified by *maqBCE* incorporating a chlorine atom as a halogen and an alkyl group derived from a fatty acid to form 4-hydroxy-2-alkylquinoline[56]. On the other hand, in *P.*

aeruginosa, 2-ABA is converted to 2-hydroxyl-ABA by *pqsL*. 2-Hydroxyl-ABA is then alkylated with *pqsBC* to obtain derivatives of HAQs[57].

In addition, we were able to show that MSr12523, MSr11367 and MSr11368 are closely related by comparing the genome sequences in a phylogenetic tree of the suborder Sorangiineae (Figure S3.58). The three strains belonging to this clade produced derivatives of myxobacterial AQs also in axenic cultures using different cultivation media (data not shown). In contrast, we observed no production of such AQs in *Sorangium sp.* MSr11954, even using different axenic or co-cultivation conditions.

3.3.6.2 Putative BGC for the thuggacin analogues from *Sorangium sp.* MSr12523

In silico analysis of the *Sorangium sp.* MSr12523 genome using antiSMASH and MIBiG[47] identified the *tga* BGC likely to be involved in the biosynthesis of our thuggacin analogues, showing homology to thuggacin A–C from *Sorangium cellulosum* So ce895[58] (GQ981380.1) and thuggacin cmc–A from *Chondromyces crocatus* Cm c5[58] (GQ981381.1) BGCs. The *tga* BGC spans about ~5.6 kb containing five open reading frames (ORFs) with derived functions assigned on the basis of database comparisons and sequence analyses (Figure S3.59 and Table S3.13). The entire thuggacin BGC (T1PKS, NRPS, 90.05 kb) from MSr12523 was used for a sequence alignment to identify similar known BGCs from the internal antiSMASH database. We found several other ORFs that are spatially close to this cluster, their function is still unclear. We observed that the nucleotide sequence of particular genes with the corresponding ORFs of the BGCs of spirangien O, Cmc-thuggacin–A / –B, and thuggacin A are in a range of 33% - 21% similarity, coloured genes are putative homologues due to significant blast hits (Figure S3.60).

Based on gained knowledge from the thuggacin biosynthetic locus in *S. cellulosum* So ce895, the arrangement of our identified thuggacin BGC showed the corresponding organisation of respective genes (Figure S3.59). They showed roughly 42% of identical residues with *tga* and *tug* BGCs in the sequence after a direct alignment (Figure S3.61, Table S3.14). We assume that the biosynthesis of our thuggacin core structure follows a comparable assembly line as has already been shown for the Soce-*tga* and Cmc-*tug* biosynthetic machineries[58]. These biosynthetic pathways comprise the required number of modules to incorporate 10 polyketide building blocks and one amino acid to assemble the thuggacin backbone.

Such types of PKS/NRPS hybrid biosynthetic machinery have been observed in other myxobacterial BGCs, e.g. epothilone and myxalamide[59].

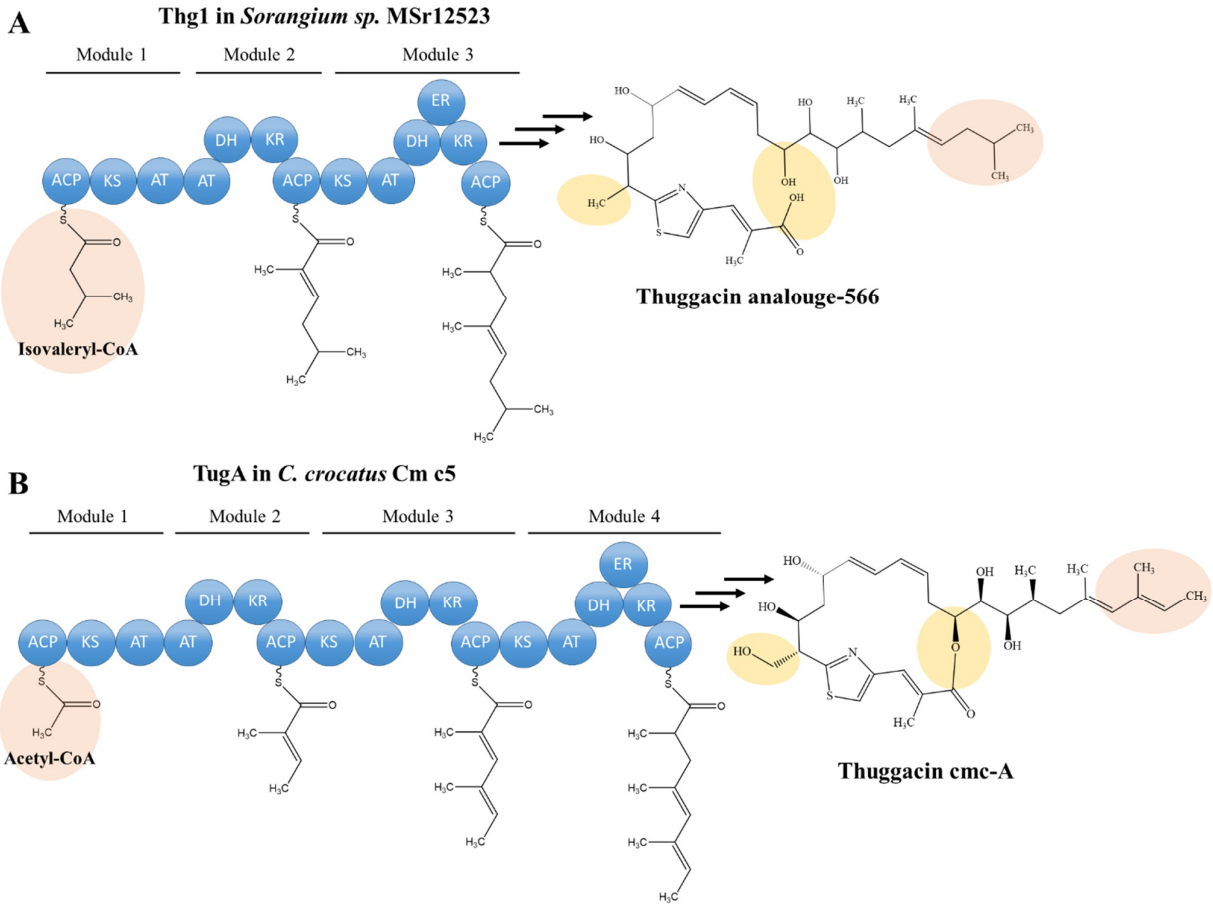

Figure 3.10 Schematic representation of PKS modules of the respective thuggacin biosynthesis found in proteins from *Sorangium sp.* MSr12523 and *C. crocatus* Cm c5. (A) The Thg1 and the first isovaleryl-CoA starter unit (highlighted orange) illustrate the initial assembly line for the biosyntheses of thuggacin analogue-566. (B) The TugA and the first acetyl-CoA starter unit (highlighted orange) shown the initial assembly line of thuggacin cmc–A. Both thuggacins structures are highlighted yellow to show individual characteristics. ACP: acyl carrier protein; AT: acyl transferase; DH: dehydratase; ER: enoyl reductase; KS: ketosynthase; KR: ketoreductase.

One isolated thuggacin analogue-548 (Figure 3.7) from axenic culture of MSr12523 structurally showed the greatest similarity to thuggacin cmc–A[45]. However, our representatives of the thuggacin family demonstrate several structural characteristics, which are highlighted in Figure 3.10. The main difference among the thuggacin assembly lines are the starter units that are incorporated into this biosynthesis. Presumably, isovaleryl-CoA (Figure 3.10A) is recognised by the additional AT domain for the formation of thuggacin analogue-566, whereas an acetyl-CoA (Figure 3.10B) starter unit is involved for thuggacin

cmc–A synthesis. Further modification can be observed in comparison to the macrocyclic part due to an additional hydroxylation (highlighted yellow, Figure 3.10A) of thuggacin cmc–A. In particular, only the isolated thuggacin analogues-564, -566, and -578 from the co-cultivation between MSr12523 and *T. pseudospumae* exhibited an open-chain structure of the core motif that was not observed before in any axenic culture. In addition, the hydrolysis of the macrocyclic core structure or the hydrolytic release from the assembly line could be the reason for the loss of their biological activity against *M. tuberculosis* 7H37Ra. Macrocycle cleavage could only be observed after co-cultivation with a member of *Tsukamurella sp* MACB, suggesting a potential involvement. However, further experiments should be carried out to substantiate such a hypothesis. Due to their phylogenetic origin in the same genus as *M. tuberculosis*, it is considered plausible that some MACB species could secrete exoenzymes that can hydrolyse the thuggacin macrocycle structure as a defence mechanism against the natural product.

3.4 Conclusion

The co-cultivation of *Sorangium sp.* MSr12523 and *T. pseudospumae* enabled the production of four alkyl-quinolone derivatives and several new representatives of the thuggacin family. These compounds were not observed in the bacterial axenic cultures; therefore, this is an effect specific for the co-cultures. We postulate that cell-cell interactions between these two bacterial species in the same environment trigger the silent alkyl-quinolones and thuggacin BGCs in MSr12523, leading to the respective biosynthesis of these NPs. The alkyl-quinolones show strong antimycobacterial activity against *M. tuberculosis* 7H37Ra with a MIC of 0.5–32 µg/mL depending of the derivative and a cytotoxic effect on CHO-K1 cells at an IC_{50} of 1.4–8.5 µM. Further antimicrobial assays of the alkyl-quinolone compound class did not demonstrate significant activities (> 64µg/mL) towards certain Gram-positive and negative bacteria. Only the thuggacin analogue-548 exhibited a moderate activity of 16 µg/mL against *M. tuberculosis* 7H37Ra. Additionally, the putative thuggacin BGC responsible for production of our analogues was identified. Our work also provides additional evidence for the ability of co-cultures to unlock the chemical diversity of novel SM derivatives from every tested strain, an indication of a powerful approach for discovering previously untapped natural product resources.

3.5 References

(1) Neelam Gurnani; D. Mehta; M. Gupta; B.K. Mehta. Natural Products: Source of Potential Drugs. *Afr. J. Basic Appl. Sci.* **2014**, *6*, 171–186.

(2) Lahlou, M. The Success of Natural Products in Drug Discovery. *PP* **2013**, *04*, 17–31.

(3) Reichenbach, H.; Gerth, K.; Irschik, H.; Kunze, B. Myxobacteria: a source of new antibiotics. *Trends Biotechnol.* **1988**, *6*, 115–121.

(4) Gerth, K.; Pradella, S.; Perlova, O.; Beyer, S.; Müller, R. Myxobacteria: proficient producers of novel natural products with various biological activities - past and future biotechnological aspects with the focus on the genus *Sorangium*. *J. Biotechnol.* **2003**, *106*, 233–253.

(5) Weissman, K. J.; Müller, R. Myxobacterial secondary metabolites: bioactivities and modes-of-action. *Nat. Prod. Rep.* **2010**, *27*, 1276–1295.

(6) Landwehr, W.; Wolf, C.; Wink, J. Actinobacteria and Myxobacteria-Two of the Most Important Bacterial Resources for Novel Antibiotics. *Curr. Top. Microbiol. Immunol.* [Online early access]. DOI: 10.1007/82_2016_503.

(7) Held, J.; Gebru, T.; Kalesse, M.; Jansen, R.; Gerth, K.; Müller, R.; Mordmüller, B. Antimalarial activity of the myxobacterial macrolide chlorotonil A. *Antimicrob. Agents Chemother.* **2014**, *58*, 6378–6384.

(8) Gerth, K.; Bedorf, N.; Hofle, G.; Irschik, H.; Reichenbach, H. Epothilons A and B: antifungal and cytotoxic compounds from Sorangium cellulosum (Myxobacteria). Production, physico-chemical and biological properties. *J. Antibiot.* **1996**, *49*, 560–563.

(9) Gerth, K.; Perlova, O.; Müller, R. *Sorangium cellulosum*. In *Myxobacteria: Multicellularity and differentiation*; Whitworth, D., Ed.; ASM Press: Chicago, 2007; pp 329–348.

(10) Schneiker, S.; Perlova, O.; Kaiser, O.; Gerth, K.; Alici, A.; Altmeyer, M. O.; Bartels, D.; Bekel, T.; Beyer, S.; Bode, E.*; et al.* Complete genome sequence of the myxobacterium *Sorangium cellulosum*. *Nat. Biotechnol.* **2007**, *25*, 1281–1289.

(11) Okada, B. K.; Seyedsayamdost, M. R. Antibiotic dialogues: induction of silent biosynthetic gene clusters by exogenous small molecules. *FEMS Microbiol. Rev.* **2017**, *41*, 19–33.

(12) Nett, M.; Ikeda, H.; Moore, B. S. Genomic basis for natural product biosynthetic diversity in the actinomycetes. *Nat. Prod. Rep.* **2009**, *26*, 1362–1384.

(13) Zhu, H.; Sandiford, S. K.; van Wezel, G. P. Triggers and cues that activate antibiotic production by actinomycetes. *J. Ind. Microbiol. Biotechnol.* **2014**, *41*, 371–386.

(14) Luo, Y.; Huang, H.; Liang, J.; Wang, M.; Lu, L.; Shao, Z.; Cobb, R. E.; Zhao, H. Activation and characterization of a cryptic polycyclic tetramate macrolactam biosynthetic gene cluster. *Nat. Commun.* **2013**, *4*, 2894.

(15) Hertweck, C. Hidden biosynthetic treasures brought to light. *Nat. Chem. Biol.* **2009**, *5*, 450–452.

(16) Müller, R.; Wink, J. Future potential for anti-infectives from bacteria - how to exploit biodiversity and genomic potential. *Int. J. Med. Microbiol.* **2014**, *304*, 3–13.

(17) Marmann, A.; Aly, A. H.; Lin, W.; Wang, B.; Proksch, P. Co-cultivation – a powerful emerging tool for enhancing the chemical diversity of microorganisms. *Mar. Drugs* **2014**, *12*, 1043–1065.

(18) Schneider, Y.; Jenssen, M.; Isaksson, J.; Hansen, K. Ø.; Andersen, J. H.; Hansen, E. H. Bioactivity of Serratiochelin A, a Siderophore Isolated from a Co-Culture of *Serratia* sp. and *Shewanella* sp. *Microorganisms* **2020**, *8*.

(19) Ola, A. R. B.; Thomy, D.; Lai, D.; Brötz-Oesterhelt, H.; Proksch, P. Inducing Secondary Metabolite Production by the Endophytic Fungus *Fusarium tricinctum* through Coculture with *Bacillus subtilis*. *J. Nat. Prod.* **2013**, *76*, 2094–2099.

(20) Xu, X.-Y.; Shen, X.-T.; Yuan, X.-J.; Zhou, Y.-M.; Fan, H.; Zhu, L.-P.; Du, F.-Y.; Sadilek, M.; Yang, J.; Qiao, B.*; et al.* Metabolomics Investigation of an Association of Induced Features and Corresponding Fungus during the Co-culture of *Trametes versicolor* and *Ganoderma applanatum*. *Front. Microbiol.* **2017**, *8*, 2647.

(21) Schäberle, T. F.; Orland, A.; König, G. M. Enhanced production of undecylprodigiosin in Streptomyces coelicolor by co-cultivation with the corallopyronin A-producing myxobacterium, *Corallococcus coralloides*. *Biotechnol. Lett.* **2014**, *36*, 641–648.

(22) Onaka, H. Novel antibiotic screening methods to awaken silent or cryptic secondary metabolic pathways in actinomycetes. *J Antibiot* **2017**, *70*, 865–870.

(23) Marrakchi, H.; Laneelle, M. A.; Daffe, M. Mycolic Acids: Structures, Biosynthesis, and Beyond. *Chem. Biol.* **2014**, *21*, 67–85.

(24) Onaka, H.; Mori, Y.; Igarashi, Y.; Furumai, T. Mycolic acid-containing bacteria induce natural-product biosynthesis in *Streptomyces* species. *Appl. Environ. Microbiol.* **2011**, *77*, 400–406.

(25) Kurosawa, K.; Ghiviriga, I.; Sambandan, T. G.; Lessard, P. A.; Barbara, J. E.; Rha, C.; Sinskey, A. J. Rhodostreptomycins, antibiotics biosynthesized following horizontal gene transfer from *Streptomyces padanus* to *Rhodococcus fascians*. *J. Am. Chem. Soc.* **2008**, *130*, 1126–1127.

(26) Hoshino, S.; Ozeki, M.; Wong, C. P.; Zhang, H.; Hayashi, F.; Awakawa, T.; Morita, H.; Onaka, H.; Abe, I. Mirilactams C-E, Novel Polycyclic Macrolactams Isolated from Combined-Culture of *Actinosynnema mirum* NBRC 14064 and Mycolic Acid-Containing Bacterium. *Chem. Pharm. Bull.* **2018**, *66*, 660–667.

(27) Hoshino, S.; Zhang, L.; Awakawa, T.; Wakimoto, T.; Onaka, H.; Abe, I. Arcyriaflavin E, a new cytotoxic indolocarbazole alkaloid isolated by combined-culture of mycolic acid-containing bacteria and *Streptomyces cinnamoneus* NBRC 13823. *J. Antibiot.* **2015**, *68*, 342–344.

(28) Milshteyn, A.; Schneider, J. S.; Brady, S. F. Mining the metabiome: Identifying novel natural products from microbial communities. *Chemistry & biology* **2014**, *21*, 1211–1223.

(29) Jawed, K.; Yazdani, S. S.; Koffas, M. A. Advances in the development and application of microbial consortia for metabolic engineering. *Metab. Eng. Commun.* **2019**, *9*, e00095.

(30) Wang, M.; Carver, J. J.; Phelan, V. V.; Sanchez, L. M.; Garg, N.; Peng, Y.; Nguyen, D. D.; Watrous, J.; Kapono, C. A.; Luzzatto-Knaan, T.*; et al.* Sharing and community curation of mass spectrometry data with Global Natural Products Social Molecular Networking. *Nat. Biotechnol.* **2016**, *34*, 828–837.

(31) Bartel, P. L.; Zhu, C. B.; Lampel, J. S.; Dosch, D. C.; Connors, N. C.; Strohl, W. R.; Beale, J. M.; Floss, H. G. Biosynthesis of anthraquinones by interspecies cloning of actinorhodin biosynthesis genes in Streptomycetes - clarification of actinorhodin gene functions. *J. Bacteriol.* **1990**, *172*, 4816–4826.

(32) Schiefer, A.; Hübner, M. P.; Krome, A.; Lämmer, C.; Ehrens, A.; Aden, T.; Koschel, M.; Neufeld, H.; Chaverra-Muñoz, L.; Jansen, R.*; et al.* Corallopyronin A for short-course anti-wolbachial, macrofilaricidal treatment of filarial infections. *PLoS Negl. Trop. Dis.* **2020**, *14*, e0008930.

(33) Meiser, P.; Bode, H. B.; Müller, R. The unique DKxanthene secondary metabolite family from the myxobacterium *Myxococcus xanthus* is required for developmental sporulation. *Proc. Natl. Acad. Sci. U.S.A.* **2006**, *103*, 19128–19133.

(34) Perlova, O.; Fu, J.; Kuhlmann, S.; Krug, D.; Stewart, A. F.; Zhang, Y.; Muller, R. Reconstitution of the myxothiazol biosynthetic gene cluster by Red/ET recombination and heterologous expression in *Myxococcus xanthus*. *Appl. Environ. Microbiol.* **2006**, *72*, 7485–7494.

(35) Wenzel, S. C.; Kunze, B.; Höfle, G.; Silakowski, B.; Scharfe, M.; Blöcker, H.; Müller, R. Structure and Biosynthesis of Myxochromides S_{1-3} in *Stigmatella aurantiaca*: Evidence for An Iterative Bacterial Type I Polyketide Synthase and for Module Skipping in Nonribosomal Peptide Biosynthesis. *ChemBioChem* **2005**, *6*, 375–385.

(36) Irschik, H.; Kopp, M.; Weissman, K. J.; Buntin, K.; Piel, J.; Muller, R. Analysis of the sorangicin gene cluster reinforces the utility of a combined phylogenetic/retrobiosynthetic analysis for deciphering natural product assembly by trans-AT PKS. *ChemBioChem* **2010**, *11*, 1840–1849.

(37) Irschik, H.; Reichenbach, H.; Höfle, G.; Jansen, R. The thuggacins, novel antibacterial macrolides from *Sorangium cellulosum* acting against selected Gram-positive bacteria. *J Antibiot.* **2007**, *60*, 733–738.

(38) Yang, J. Y.; Sanchez, L. M.; Rath, C. M.; Xueting, L.; Boudreau, P. D.; Bruns, N.; Glukhov, E.; Wodtke, A.; Felicio, R. de; Fenner, A.*; et al.* Molecular networking as a dereplication strategy. *J. Nat. Prod.* **2013**, *76*, 1686–1699.

(39) Linington, R. G. npatlas - The Natural Products Atlas. https://www.npatlas.org/.

(40) Saalim, M.; Villegas-Moreno, J.; Clark, B. R. Bacterial Alkyl-4-quinolones: Discovery, Structural Diversity and Biological Properties. *Molecules (Basel, Switzerland)* **2020**, *25*.

(41) Coulon, P. M. L.; Groleau, M.-C.; Déziel, E. Potential of the *Burkholderia cepacia* Complex to Produce 4-Hydroxy-3-Methyl-2-Alkyquinolines. *Front. Cell. Infect. Microbiol.* **2019**, *9*, 33.

(42) Dubern, J. F.; Diggle, S. P. Quorum sensing by 2-alkyl-4-quinolones in *Pseudomonas aeruginosa* and other bacterial species. *Mol. Biosyst.* **2008**, *4*, 882–888.

(43) Pesci, E. C.; Milbank, J. B.; Pearson, J. P.; McKnight, S.; Kende, A. S.; Greenberg, E. P.; Iglewski, B. H. Quinolone signaling in the cell-to-cell communication system of *Pseudomonas aeruginosa*. *Proc Natl Acad Sci USA* **1999**, *96*, 11229–11234.

(44) Tsutsumi, T.; Matsumoto, M.; Iwasaki, H.; Tomisawa, K.; Komine, K.; Fukuda, H.; Eustache, J.; Jansen, R.; Hatakeyama, S.; Ishihara, J. Total Synthesis of Thuggacin cmc-A and Its Structure Determination. *Org. Lett.* **2021**, *23*, 5208–5212.

(45) Steinmetz, H.; Irschik, H.; Kunze, B.; Reichenbach, H.; Höfle, G.; Jansen, R. Thuggacins, macrolide antibiotics active against *Mycobacterium tuberculosis*: Isolation from myxobacteria, structure elucidation, conformation analysis and biosynthesis. *Chem. Eur. J.* **2007**, *13*, 5822–5832.

(46) Blin, K.; Shaw, S.; Kloosterman, A. M.; Charlop-Powers, Z.; van Wezel, G. P.; Medema, M. H.; Weber, T. antiSMASH 6.0: improving cluster detection and comparison capabilities. *Nucleic Acids Res.* **2021**, *49*, W29-W35.

(47) Epstein, S. C.; Charkoudian, L. K.; Medema, M. H. A standardized workflow for submitting data to the Minimum Information about a Biosynthetic Gene cluster (MIBiG) repository: Prospects for research-based educational experiences. *Stand. Genomic Sci.* **2018**, *13*, 16.

(48) Diggle, S. P.; Lumjiaktase, P.; Dipilato, F.; Winzer, K.; Kunakorn, M.; Barrett, D. A.; Chhabra, S. R.; Camara, M.; Williams, P. Functional genetic analysis reveals a 2-alkyl-4-quinolone signaling system in the human pathogen *Burkholderia pseudomallei* and related bacteria. *Chem. Biol.* **2006**, *13*, 701–710.

(49) Kilani-Feki, O.; Culioli, G.; Ortalo-Magné, A.; Zouari, N.; Blache, Y.; Jaoua, S. Environmental *Burkholderia cepacia* strain Cs5 acting by two analogous alkyl-quinolones and a didecyl-phthalate against a broad spectrum of phytopathogens fungi. *Curr. Microbiol.* **2011**, *62*, 1490–1495.

(50) Deziel, E.; Lepine, F.; Milot, S.; He, J.; Mindrinos, M. N.; Tompkins, R. G.; Rahme, L. G. Analysis of *Pseudomonas aeruginosa* 4-hydroxy-2-alkylquinolines (HAQs) reveals a role for 4-hydroxy-2-heptylquinoline in cell-to-cell communication. *Proc. Natl. Acad. Sci. USA* **2004**, *101*, 1339–1344.

(51) Vial, L.; Lepine, F.; Milot, S.; Groleau, M. C.; Dekimpe, V.; Woods, D. E.; Deziel, E. *Burkholderia pseudomallei*, *B. thailandensis*, and *B. ambifaria* produce 4-hydroxy-2-alkylquinoline analogues with a methyl group at the 3 position that is required for quorum-sensing regulation. *J. Bacteriol.* **2008**, *190*, 5339–5352.

(52) Kim, K.; Kim, Y. U.; Koh, B. H.; Hwang, S. S.; Kim, S. H.; Lepine, F.; Cho, Y. H.; Lee, G. R. HHQ and PQS, two *Pseudomonas aeruginosa* quorum-sensing molecules, down-regulate the innate immune responses through the nuclear factor-kB pathway. *Immunology* **2010**, *129*, 578–588.

(53) Diggle, S. P.; Matthijs, S.; Wright, V. J.; Fletcher, M. P.; Chhabra, S. R.; Lamont, I. L.; Kong, X.; Hider, R. C.; Cornelis, P.; Camara, M.*; et al.* The *Pseudomonas aeruginosa* 4-quinolone signal molecules HHQ and PQS play multifunctional roles in quorum sensing and iron entrapment. *Chem. Biol.* **2007**, *14*, 87–96.

(54) Farrow, J. M.; Pesci, E. C. Two Distinct Pathways Supply Snthranilate as a Precursor of the *Pseudomonas* Quinolone Signal. *Journal of bacteriology* **2007**, *189*, 3425–3433.

(55) Drees, S. L.; Ernst, S.; Belviso, B. D.; Jagmann, N.; Hennecke, U.; Fetzner, S. PqsL uses reduced flavin to produce 2-hydroxylaminobenzoylacetate, a preferred PqsBC substrate in alkyl quinolone biosynthesis in *Pseudomonas aeruginosa*. *J. Biol. Chem.* **2018**, *293*, 9345–9357.

(56) Klaus, J. R.; Coulon, P. M. L.; Koirala, P.; Seyedsayamdost, M. R.; Déziel, E.; Chandler, J. R. Secondary metabolites from the *Burkholderia pseudomallei* complex: structure, ecology, and evolution. *J. Ind. Microbiol. Biotechnol.* **2020**, *47*, 877–887.

(57) Lépine, F.; Milot, S.; Déziel, E.; He, J.; Rahme, L. G. Electrospray/mass spectrometric identification and analysis of 4-hydroxy-2-alkylquinolines (HAQs) produced by *Pseudomonas aeruginosa*. *J. Am. Soc. Mass Spectrom.* **2004**, *15*, 862–869.

(58) Buntin, K.; Irschik, H.; Weissman, K. J.; Luxenburger, E.; Blöcker, H.; Müller, R. Biosynthesis of thuggacins in myxobacteria: comparative cluster analysis reveals basis for natural product structural diversity. *Chem. Biol.* **2010**, *17*, 342–356.

(59) Wenzel, S. C.; Müller, R. Myxobacterial natural product assembly lines: fascinating examples of curious biochemistry. *Nat. Prod. Rep.* **2007**, *24*, 1211–1224.

Supporting Information

Co-cultivation of *Streptomyces*-like myxobacteria enables discovery of bioactive secondary metabolites

Markus Neuber, Sebastian Walesch, Chantal Bader, Daniel Krug and Rolf Müller

Materials and Methods

Strains and Media

The mycolic acid-containing bacteria *R. erythropolis* DSM 44235, *T. soli* DSM 45046 and *T. pseudospumae* DSM 44118 were purchased from German Collection of Microorganisms and Cell Cultures (DSMZ). The bacterium *C. glutamicum* ATCC 13032 was provided by the Wittmann working group at Saarland University. The myxobacterial producer strain *Sorangium sp.* MSr12523, MSr11954 and MSr11367 was obtained from our internal strain collection.

The 2SWT medium (0.3% Bacto tryptone, 0.1% Bacto Soytone, 0.2% glucose, 0.2% soluble starch, 0.1% maltose monohydrate, 0.2% Cellobiose, 0.05% calcium chloride dihydrate, 0.1% magnesium sulphate heptahydrate, 10 mM HEPES buffer, pH 7.0 adjusted with KOH) was used for all myxobacterial producer strains (MSr12523, MSr11954, MSr11367). All mycolic acid-containing bacteria *C. glutamicum* ATCC 13032, *R. erythropolis* DSM 44235, *T. soli* DSM 45046 and *T. pseudospumae* DSM 44118 were incubated in TSB medium (3% Trypticase Soy Broth, pH 7.3 adjusted with KOH). The absorber Amberlite resin XAD-16 (Sigma) was added to all blanks, controls and co-culture mixtures at a volume concentration of 2% [v/v].

Myxobacterial co-cultivation

All co-cultivations and axenic cultivations of *Sorangium sp.* MSr12523 were performed in 2SWT media. 300 mL shake flask containing 50 mL 2SWT media was inoculated with 150 µL of prepared cryo stock of MSr12523 and incubated at 30 °C and 180 rpm for 72 h. The MACB were grown in 100 mL shaking flasks containing 25 mL of TSB media for 48 h at 30 °C and 180 rpm. For co-cultivation, 5% [v/v] of MSr12523 (producer strain) was transferred into a 300 mL shake flask with 50 mL 2SWT medium, 2% [v/v] of the corresponding mycolic acid-containing bacteria (partner strain) was added and the culture incubated at 30 °C and 180 rpm for 7 days. To adsorb the metabolites, Amberlite XAD-16 resin suspension was added to all co-cultivations, controls and blanks at a volumetric concentration of 2% [v/v] after 6 days of cultivation. At the end of the fermentation after 7 days, both resin and cells were harvested together by centrifugation (5.000 g, 4 °C, 15 min). All co-cultivations, controls and blanks were performed as biological triplicates.

Extraction procedure of crude extracts for metabolic workflow and bioassay

The resin XAD-16 and cell pellets were frozen at -20 °C and lyophilised. Subsequently, the metabolites were extracted twice with 50 mL MeOH/acetone (1:1 [v/v]) under constant stirring at 300 rpm with magnet bar for 90 min. The supernatant was filtered into a round bottom flask and the solvent was evaporated under reduced pressure until completely dry. The residue was dissolved in 1 mL MeOH, transferred into a 1.5 mL glass vial and stored at 4 °C. All extracts were diluted 1:5 prior to the UHPLC-MS measurements.

MS and NMR Analysis of crude extracts and purified compound

UHPLC-qTOF measurements were performed in duplicates as technical replicates on a Dionex Ultimate 3000 SL system coupled to a Bruker maXis 4G UHR-qTOF. This system was used for high resolution LC-MS measurements. The following template method was used: Column: ACQUITY BEH 100 x 2.1 mm 1.7 µm, 130 Å, a flow rate of 0.6 mL/ min and a column temperature of 45 °C. The following gradient was applied with H_2O + 0.1% FA as eluent A and ACN + 0.1% FA as eluent B. 0-0.5 min: 5% Eluent B; 0.5-18.5 min: linear increase of eluent B to 95%; 18.5-20.5 min: 95% eluent B; 20.5-20.8 min: linear decrease of eluent B; 20.8-22.5 min: re-equilibration with 5% eluent B. The detection was usually performed in the positive MS mode or MS^2 mode, using a scan range from 150-2500 *m/z*. Capillary voltage was set to 4000 V for measurements in positive ionization mode. Dry gas was set to a flow rate of 5 L/ min at 200 °C.

NMR spectra were recorded on a Bruker Ultra Shield 500 spectrometer equipped with a 5 mm TCI probe head (^1H at 500 MHz, ^{13}C at 125 MHz). All observed chemical shift values (δ) are given in ppm and coupling constant values (J) in Hz. Standard pulse programs were used for HMBC, HSQC and COSY experiments. The spectra were recorded in methanol-d4, and chemical shifts of the solvent signals at δH 3.31 ppm and δC 49.15 ppm were used as reference signals for spectra calibration. To increase sensitivity, the measurements were conducted in a 5 mm Shigemi tube (Shigemi Inc., Allison Park, PA 15101, USA).

Statistical LC-MS data analysis and annotations of crude extracts

As a basis for the statistical assessment of the generated LC-MS data for both targeted and non-targeted metabolomic workflows, the analysis was conducted by MetaboScape 2021b (Bruker). The intensity threshold for feature detection by the integrated T-Rex 3D algorithm was set at least to 1 x 10^5, and the charge was set to maximum three. The minimum

group size for batch feature creation was set to two. Features found in at least two out of three biological replicates (measured as technical duplicates) were considered as a significant hit, as long as no appearance could be detected in media blank. All metabolites of co-cultivation experiments as well as metabolites uniquely found in axenic and control extracts were calculated via *t*-Test/ANOVA analysis.

MS² experiments and molecular networking

All LC-MS² measurements were based on the already described 18 min gradient separation using the U3000-maXis 4G setup. Fragmentation spectra were achieved either by auto-MS² measurements or by targeted precursor selection. Fixed MS² parameters were an m/z-adjusted precursor isolation width and fragmentation energy. Values are interpolated in between the set points [300 m/z /4 m/z / 30 eV], [600 m/z / 6 m/z / 35 eV], [1000 m/z / 8 m/z / 45 eV], and [2000 m/z /10 m/z / 55 eV]. The precursor intensity threshold is always set to 5000.

A molecular network was created using the online workflow at GNPS (Global Natural Products Social Molecular Networking). The data was then clustered with MS-Cluster with a parent mass tolerance of 0.05 Da and a MS/MS fragment ion tolerance of 0.1 Da to create consensus spectra. Further, consensus spectra that contained less than 1 spectra were discarded. A network was then created where edges were filtered to have a cosine score above 0.65 and more than 4 matched peaks. Data were visualized with Cytoscape (Version 3.9.1).

Isolation Procedures

The large-scale co-culture of MSr12523 and the MACB *T. pseudospumae* were grown in 2 L shaking flask containing 500 mL 2SWT media for 7 days at 30 °C and 180 rpm. All production co-cultures were inoculated with the same volumetric concentration of producer and partner strain as in the small scale. Autoclaved aqueous suspension of Amberlite XAD-16 resin was added at a volumetric concentration of 2% [v/v] to all large cultures after 6 days. After the end of the fermentation, both cell pellets and resin were harvested by centrifugation (5.000 g, 4 °C, 15 min) and lyophilised prior further processing.

Isolation of compound-392

Compound-392 was isolated by semi-preparative HPLC following a fractionation of the crude extract by liquid−liquid partitioning. The dried resin and cell pellet were extracted three times with 300 mL of Acetone/MeOH (1:1) mixture. After that, the supernatant was

poured through folded paper filter and the solvent was evaporated under reduced pressure. This extract was re-dissolved in 400 mL Hexane and 400 mL MeOH/H_2O (95:5) and transferred into a separating funnel. Both layers were separated and the liquid/liquid extraction was repeated with 400 mL Hexane. The MeOH/H_2O layer was dried and re-dissolved in 300 mL H_2O and 300 mL DCM. The layers were separated and the liquid/liquid extraction was repeated with 300 mL DCM. The aqueous layer was directly used for the liquid/liquid extraction with 300 mL EtOAc. Both phases were separated and the liquid/liquid extraction was repeated with 300 mL EtOAc. Compound-392 was present in the EtOAc layer. Afterwards, the EtOAc phase was dried and dissolved in MeOH. As a further purification step, semi-preparative HPLC was performed on a Dionex Ultimate 3000 SDLC low pressure gradient system equipped with a Phenomenex Luna 5 µm C18(2), 100 Å LC Column (250 × 10 mm) tempered at 45 °C. Separation was achieved using a linear gradient from 95% ddH_2O/acetonitrile with 0.1% formic acid to 5% ddH_2O/acetonitrile with 0.1% formic acid over 30 min. The compound was detected by UV absorption at 230 nm and 280 nm. The collected fraction was evaporated under reduced pressure, and the residue was dissolved in MeOH.

Isolation of alkyl-quinolones (268, 282, 302, 316) and thuggacin analogues (564, 566, 578)

Supercritical fluid extraction (SFE) was used for the extraction procedure of alkyl-quinolones and thuggacin analogues out of the large scale co-cultivation of MSr12523 and *T. pseudospumae*. This SFE system (Waters MV-10 ASFE) was equipped with 10 mL analytical extraction cartridges. At first, the lyophilised cell pellets and resin were pulverised and packed tightly into the cartridges (~3 g). Afterwards, the whole extraction process was carried out at 200 bar pressure and 40 °C with a total flow rate of 10 mL/min. The process of extraction was done in four steps, each one performed with an initial dynamic extraction phase for 5 min followed by a static extraction phase for 5 min and a second dynamic extraction phase for another 5 min. The filled cartridge was first extracted with 100% CO_2 as solvent. Afterwards, the pellet was extracted with 20% EtOAc as co-solvent, followed by 20% MeOH and as a final step, the pellet was flushed with 50% MeOH. This extraction procedure was carried out twice for each cartridge to archive the maximum yield of extracted product. The make-up flow of MeOH was set to a total organic solvent flow of 3 mL/min. All generated phases were collected and treated separately. All solvents were evaporated under reduced pressure, and the residues were re-dissolved in 4 mL MeOH.

The highest amount of target compounds were obtained in the 20% and 50% MeOH phase of the SFE extracts. Both extracts were fractionated using size exclusion chromatography with Sephadex LH-20 resin and MeOH as eluent. A total flow rate of 90 drops/ min was carried out and 600 drops were collected for each fraction in a glass tube. An aliquot of each fraction was measured using LC-MS to screen for the target compounds. The thuggacin analogues (-564, -566, -578), which were identified in fraction 6-9, were pooled and the solvent evaporated under reduced pressure, after which the residue was re-dissolved in 1 mL of MeOH. In contrast, the alkyl-quinolones (-268, -282, -302, -316) were detected in fraction 10-15, pooled, the solvent evaporated and the residue was re-dissolved in MeOH.

For purification of the alkyl-quinolones, semi-preparative HPLC was performed on a Dionex Ultimate 3000 SDLC low pressure gradient system equipped with a Waters Xselect CSH130 5 *µm* C18 130 Å LC Column (250 × 10 mm) tempered at 45 °C. Separation was achieved using a linear gradient from 60% ddH_2O/acetonitrile to 30% ddH_2O/acetonitrile without formic acid over 40 min. The compound was detected by UV absorption at 230 nm and 280 nm. The collected fractions were evaporated under reduced pressure, and the residues were re-dissolved in MeOH.

To purify the different thuggacin analogues, semi-preparative HPLC was performed on a Dionex Ultimate 3000 SDLC low pressure gradient system equipped with a Waters Xbridge BEH 5 *µm* C18(2) 130 Å LC Column (250 × 10 mm) tempered at 45 °C. Separation was achieved using a linear gradient from 60% ddH_2O/acetonitrile to 30% ddH_2O/acetonitrile without formic acid over 40 min. The compound was detected by UV absorption at 230 nm and 280 nm. The collected fractions were evaporated under reduced pressure, and the residues were re-dissolved in MeOH.

Antimicrobial assays

For the determination of the antimicrobial activities of each crude extract (co-culture, axenic culture and media blank), all three biological replicates were combined. 20 µL of the saturated methanolic extract was mixed with 130 µL microbial test medium and serially diluted by transferring 75 µL of mixed sample solution into the 96 well plate[1]. Afterwards, the 75 µL of the microbial test culture was added to each well of the microtiter plate. The microbial test panel consisted of *E. coli* WT JW0451-2 (ΔacrB), *E. coli* BW25113, *P. aeruginosa* PA14, *C. freundii* DSM-30039, *A. baumannii* DSM-30008, *S. aureus* Newman, *B. subtilis* DSM-10, *M. smegmatis* mc² 155 and fungus *P. anomala* DSM-6766 as well as

C. albicans DSM-1665. Growth inhibition was assessed by visual inspection and given activity score or MIC (minimum inhibitory concentration) values as the lowest concentration of extract or compound at which no visible growth was observed.

Cytotoxic activity

Cell lines were obtained from the German Collection of Microorganisms and Cell Cultures (Deutsche Sammlung für Mikroorganismen und Zellkulturen, DSMZ) or were part of our internal collection and were cultured under the conditions recommended by the depositor. Cells were seeded at 6 x 10^3 cells per well of 96-well plates in 120 µl complete medium and treated with purified compounds in serial dilution after 2 h of equilibration. Each compound was tested in duplicate as well as the internal solvent control. After 5 d incubation, 20 µl of 5 mg/mL MTT (thiazolyl blue tetrazolium bromide) in PBS was added per well and it was further incubated for 2 h at 37°C. The medium was then discarded and before adding 100 µl 2-propanol/10 N HCl (250:1) in order to dissolve formazan granules. The absorbance at 570 nm was measured using a microplate reader (Tecan Infinite M200Pro), and cell viability was expressed as percentage relative to the respective methanol control. IC_{50} values were determined by sigmoidal curve fitting.

Supplementary Figures & Tables

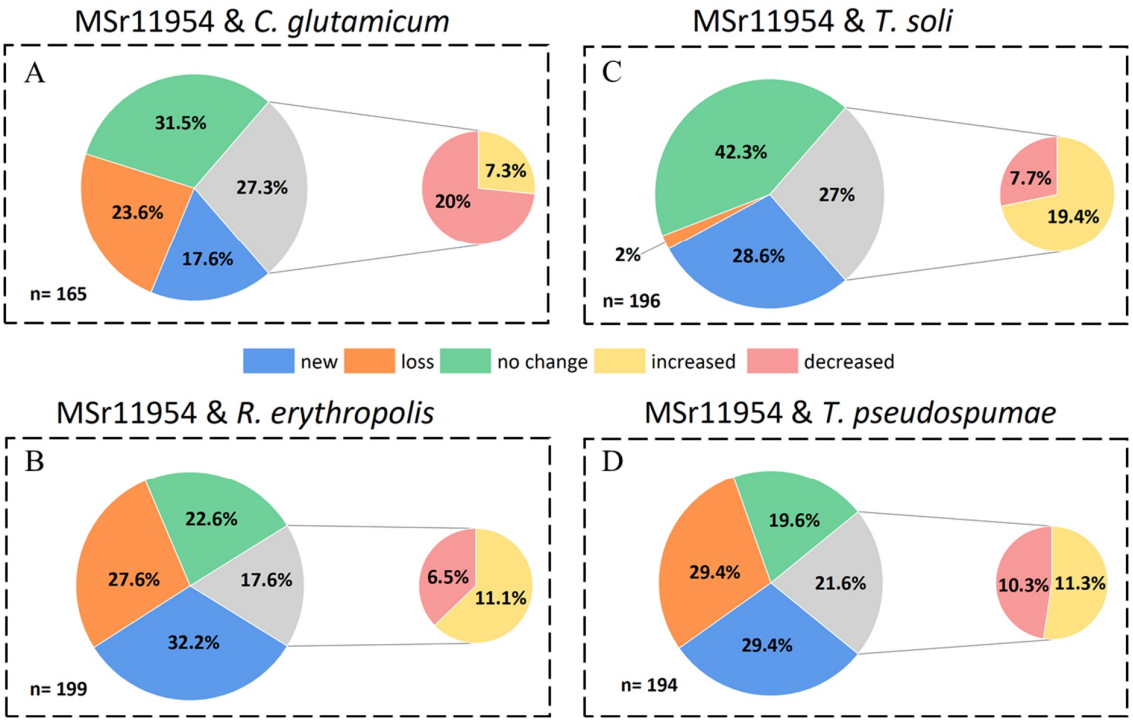

Figure S3.1: (**A - D**) Results of the comparison of secondary metabolite profiles of MSr11954 axenic culture and co-cultures with *C. glutamicum* (**A**), *R. erythropolis* (**B**), *T. soli* (**C**) and *T. pseudospumae* (**D**) are shown in a pie chart. The chart represents the total number of molecular features identified by the MetaboScape features (metabolites) in the crude extract that exceed a threshold value of $1x10^5$. The medium blank was used as a control. Each extract was classified according to the increase/decrease or no change in metabolite production, appearance of new metabolites, and disappearance of some secondary metabolites. New: New secondary metabolites appeared in the co-culture. Loss: Secondary metabolite production was absent in the co-culture. No change: There was a lower change of +/- 30% of intensity between the SM level of the axenic culture and the co-culture. Increase/decrease: There was a higher change of +/- 30% of intensity between SM level of the axenic and the co-culture.

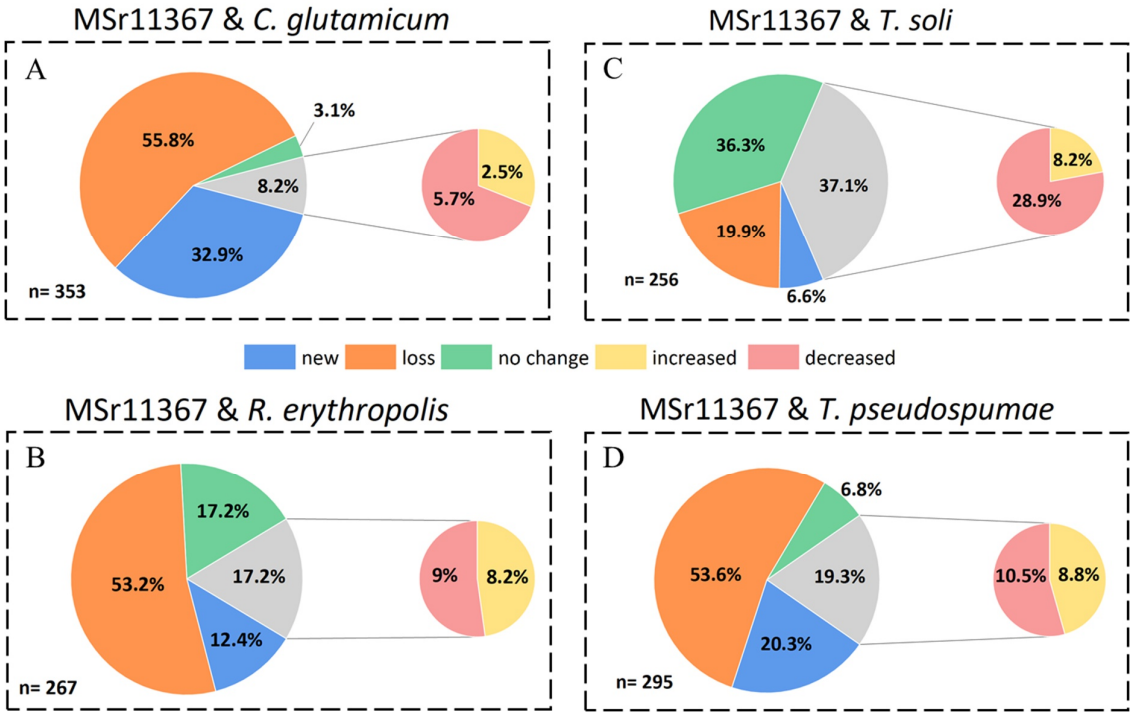

Figure S3.2: (**A - D**) Results of the comparison of secondary metabolite profiles of MSr11367 axenic culture and co-cultures with *C. glutamicum* (**A**), *R. erythropolis* (**B**), *T. soli* (**C**) and *T. pseudospumae* (**D**) are shown in a pie chart. The chart represents the total number of molecular features identified by the MetaboScape features (metabolites) in the crude extract that exceed a threshold value of $1x10^5$. The medium blank was used as a control. Each extract was classified according to the increase/decrease or no change in metabolite production, appearance of new metabolites, and disappearance of some secondary metabolites. New: New secondary metabolites appeared in the co-culture. Loss: Secondary metabolite production was absent in the co-culture. No change: There was a lower change of +/- 30% of intensity between the SM level of the axenic culture and the co-culture. Increase/decrease: There was a higher change of +/- 30% of intensity between SM level of the axenic and the co-culture.

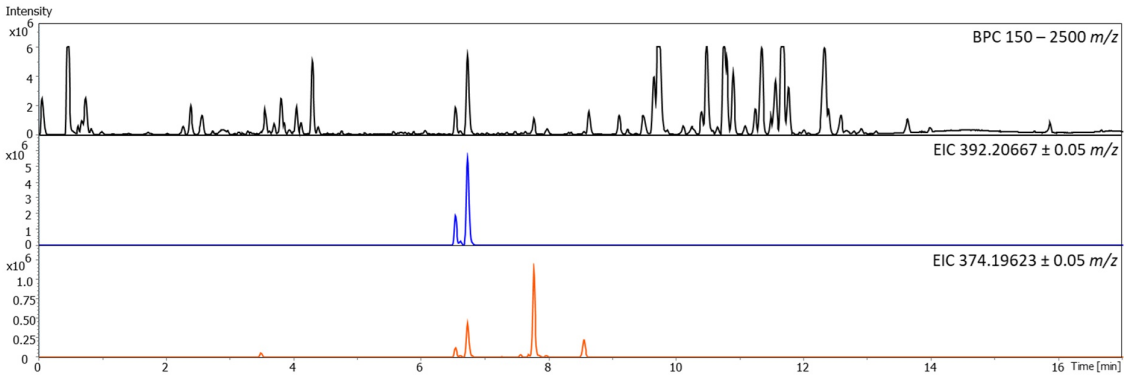

Figure S3.3: The based peak and extracted ion chromatograms are showing all detected target masses of compound- 392 in the crude extract after co-cultivation of MSr12523 and *T. pseudospumae.*

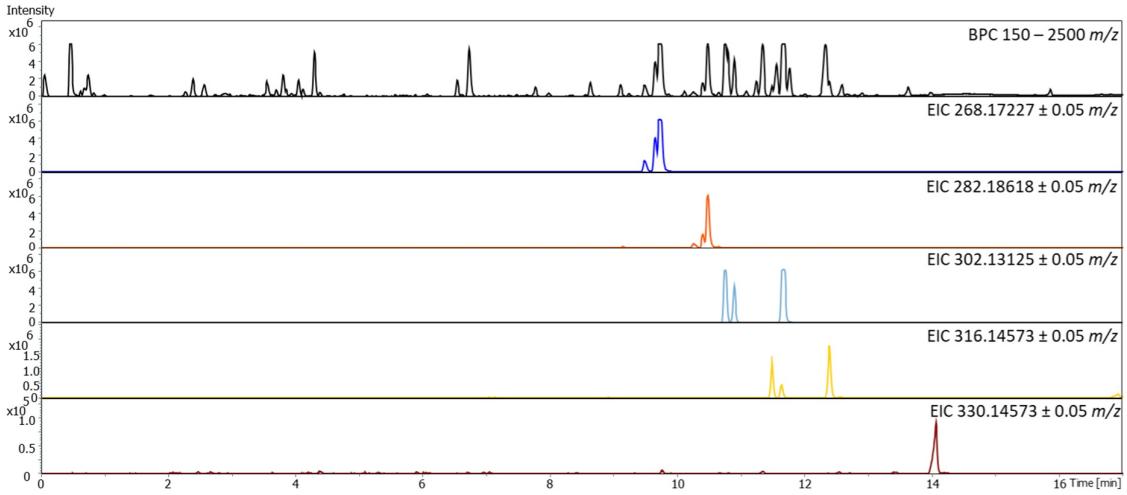

Figure S3.4: The based peak and extracted ion chromatograms are showing all detected target masses of alkyl-quinolones in the crude extract after co-cultivation of MSr12523 and *T. pseudospumae*.

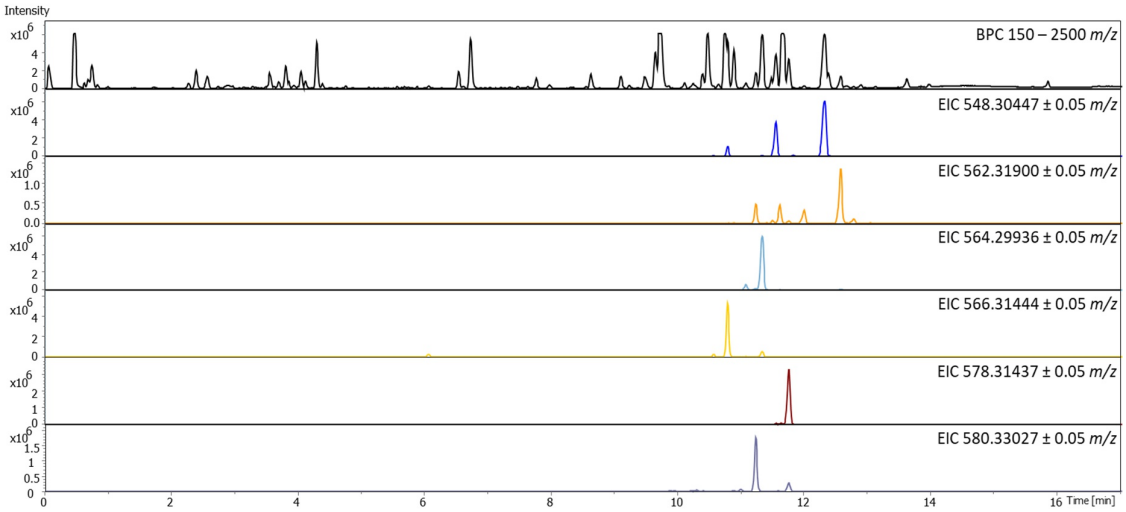

Figure S3.5: The based peak and extracted ion chromatograms are showing all detected target masses of thuggacin analogues in crude extract after co-cultivation of MSr12523 and *T. pseudospumae*.

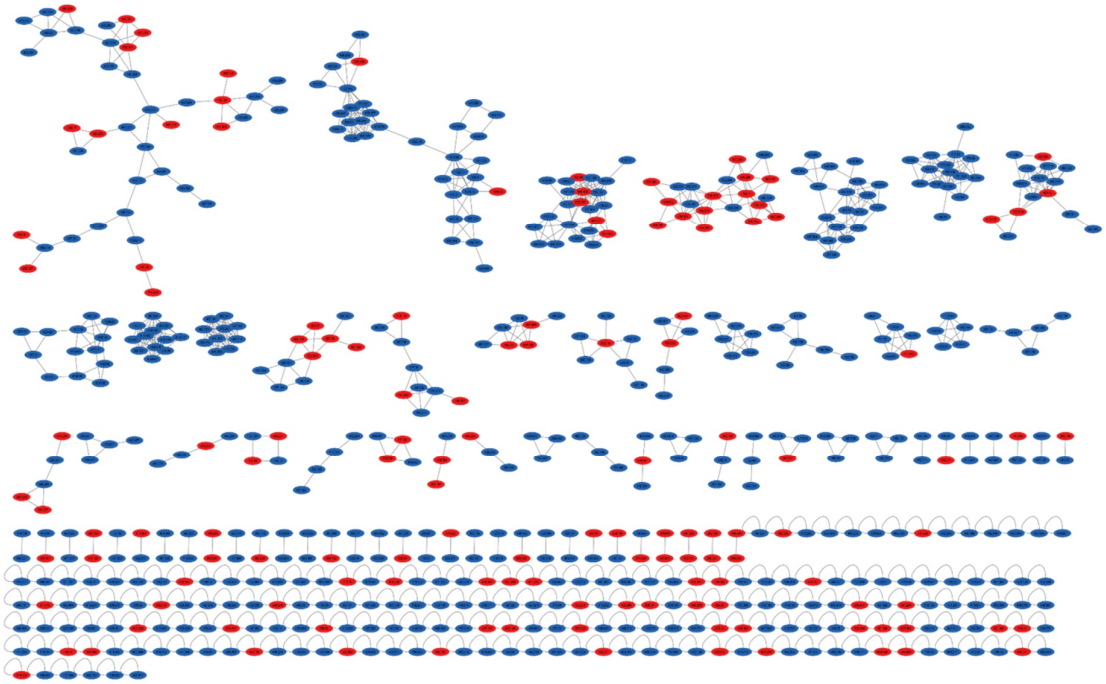

Figure S3.6: Global molecular network based on MS² data of co-culture from MSr12523 and *T. pseudospumae* and their respective axenic cultures. Red nodes were annotated using our internal data base (Myxobase); Blue nodes could not be annotated.

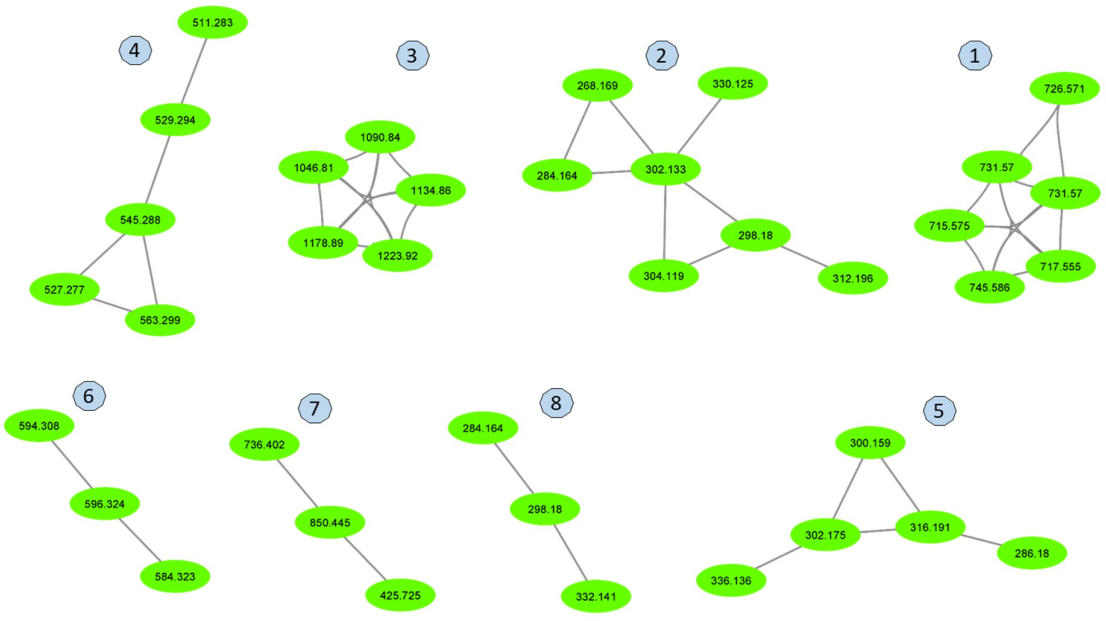

Figure S3.7: Unique molecular clusters extracted from global molecular network of MSr12523 and *T. pseudospumae* co-culture. Green nodes are existing exclusively in the co-culture extracts.

Table SI 3.1 List with annotated myxobase entries of precursor ion mass of MS² fragmentation from molecular network (Figure S3.6) generated from crude extracts of MSr12523 and *T. pseudospumae*.

RT [min]	Precursor ion mass	ΔMz [ppm]	Sum formula	Analyte name [Myxobase]
0,55	685,24	17,410	C34H42N3O7Br1	Miuraenamide A
1,16	490,191	16,626	C24H31N3O4S2	Myxothiazol F
1,71	285,135	6,067	C14H20O6	Aspinolide B
1,8	393,222	13,148	C22H32O6	Jerangolid C
1,87	582,325	19,972	C27H43N5O9	Myxoprincomide-582
2,35	261,124	2,489	C14H16N2O3	cyclo(Tyr-Pro)
2,43	521,238	2,782	C28H32N4O6	Dkxanthen-520
2,89	313,16	14,593	C16H24O6	Pyrenophorol [Helmidiol]
3,07	571,309	3,956	C29H44O11	Soraphen M (HZI)
3,25	501,22	16,061	C27H32O9	And48_501_FP
3,3	377,145	1,458	C17H20N4O6	Riboflavin
3,38	385,244	17,210	C24H32O4	Chlorotonil C2
3,38	702,356	4,172	C35H51N5O8S1	N-Desmethyl 11-hydroxy 12-keto pretubulysin A
3,43	709,349	0,959	C42H48N2O8	Disorazol A2
3,46	547,296	9,775	C29H42N2O8	And48_546_FP
3,59	553,37	1,355	C27H48N6O6	Nocardamine_Derivative_D6
3,61	553,334	4,428	C20H40N16O1S1	CYH_med_CMP553
3,68	417,212	19,727	C22H33O5K1	Aurafuron A
3,73	499,259	0,601	C46H69N12O13	Medium-peptide997
3,76	411,26	17,094	C26H34O4	Preussilide F
3,77	400,208	7,746	C43H55N6O9	mz799_LKJ
3,89	569,365	1,317	C27H48N6O7	Nocardamine_Derivative_D5
3,91	480,282	3,435	C51H75N8O10	Myxochromid B3
3,91	502,265	9,656	C32H31N5O1	AP9003_502
3,94	569,363	4,830	C27H48N6O7	SbSr044_Compound_569

4,18	245,129	2,162	C14H16N2O2	Aureusimine A
4,18	576,351	8,762	C31H50N3O5P1	Phosphomandanidin
4,18	585,36	1,110	C27H48N6O8	Nocardamine_Derivative_D4
4,22	635,339	7,823	C35H46N4O7	cda562
4,24	546,293	1,373	C27H39N5O7	MCy9101_546_NF
4,31	374,228	1,470	C17H31N3O6	SH-Myxo-373_1
4,38	848,449	7,437	C44H65O15N1	Ipomoeassin F -Isomer
4,42	601,354	2,578	C27H48N6O9	Nocardamine
4,43	301,181	3,951	C19H24O3	Maracin A
4,51	627,358	18,123	C41H46N4O2	CcG34_Comp.15
4,54	521,307	7,424	C29H44O8	2.4-Di-epi-Soraphen A1Î±
4,56	686,396	2,083	C36H55N5O6S1	Pretubulysin A
4,63	755,395	17,011	C34H54N6O13	Cystomanamide D
4,76	365,181	17,115	C23H24O4	CBD_Cpd365
4,77	408,212	2,205	C20H29N3O6	SH-Cm7-407
4,81	489,233	2,780	C24H32N4O7	SH_MxDK1622_488
4,84	489,233	2,780	C24H32N4O7	SH_MxDK1622_488
4,99	558,328	18,895	C27H47N3O9	MCy9049_557_FP
5,03	659,34	10,996	C38H46N2O8	Disorazol Z11
5,15	751,366	12,670	C42H51N2O9Na1	Disorazol F2
5,2	376,187	0,665	C19H25N3O5	MCy9101_376_NF
5,2	530,297	4,243	C31H39N5O1S1	SWA_12523_547_a
5,31	470,239	10,208	C49H63N8O11	Cyclic Thaxteramide A
5,38	314,178	9,390	C19H23N1O3	CBD_Cpd314
5,55	398,17	11,176	C18H27N3O5S1	Lipothiazole A
5,6	255,065	0,666	C15H10O4	Aloesaponarin II
5,68	758,408	0,461	C37H55N7O10	Media_CyS_758
5,7	669,36	13,819	C31H56O15	SoCe836_669_NF
5,73	500,343	2,498	C24H45N5O6	SbSr044_Compound_500

5,87	536,343	13,667	C31H43N4O4	AP11954_535b
5,92	634,324	2,759	C33H47N1O11	Noricumazol B
6,01	550,359	1,762	C28H47N5O6	Compound-3648
6,03	664,333	0,376	C34H49N1O12	Noricumazol C
6,09	566,354	1,324	C28H47N5O7	Compound-3649
6,1	887,468	9,093	C44H66N6O13	Soce1112_Tartrolonvariante 1
6,12	319,14	18,550	C19H23O2Cl1	Maracen A
6,18	536,307	11,825	C32H41N1O6	Icumazol A
6,22	855,498	12,192	C45H62N10O7	Soce1112_Tartrolonvariante 9
6,3	501,216	8,080	C27H32O9	And48_501_FP
6,34	273,16	0,915	C16H20N2O2	Indiacene precursor
6,58	623,341	1,684	C29H46N6O9	Cystomanamide E
6,75	487,291	1,026	C52H77N8O10	Myxochromid B4
6,78	301,998	2,152	C11H11N1O3S3	Compound301_MCy10636_CBD
6,86	966,53	0,569	C48H71N9O12	Crocapeptin A2
6,94	299,091	1,170	C17H14O5	SWA_12523_299
7,14	529,265	9,012	C32H36N2O5	Chaetoglobosin A
7,22	613,427	2,201	C30H56N6O7	SbSr044_Compound_613
7,67	341,065	1,613	C18H12O7	Anthraquinone 340
7,79	339,086	0,796	C19H14O6	Rabelomycin
7,83	747,385	13,473	C40H58O13	4-[H2]-Ipomoeassin B
7,87	449,239	9,906	C27H32N2O4	PH449
8,01	797,549	0,564	C39H72N8O9	SbSr044_Compound_797
8,15	323,102	7,645	C17H19Cl1O4	Strobilurin B
8,43	332,141	1,355	C17H18F1N3O3	Ciprofloxacin
8,91	569,31	1,528	C33H44O8	Hyafurone 4
9,02	285,076	0,807	C16H12O5	Medium_M284_Soce487_Comp.13
9,05	254,063	14,288	C10H11N3O3S1	SEA-XI-55B
9,44	943,527	2,809	C51H74N8O5S2	RG2 media compound-943

9,64	584,323	2,105	C33H45N1O8	Icumazol M+16
9,68	582,308	9,222	C27H43N5O9	Myxoprincomide-582
9,77	535,331	5,884	C31H42N4O4	AP11954_535
9,8	753,463	7,605	C44H64O10	Compound-4045
9,91	569,31	1,528	C33H44O8	Hyafurone 4
10,25	423,201	3,946	C23H26N4O4	Sevadicin
10,56	332,141	1,355	C17H18F1N3O3	Ciprofloxacin
10,64	605,425	8,143	C39H56O5	3-O-Caffeoyl-betulin
10,7	550,282	8,087	C30H40N1O7Na1	Corallopyronin A2
10,95	424,135	2,287	C19H25N3O4S2	Myxothiazol Y
11,22	564,3	8,488	C59H83N8O14	Cc003E_10_2
11,26	603,253	3,896	C40H35O4Na1	MNa9317_291E_LKJ
11,29	302,133	7,712	C18H20Cl1N1O1	Sr044_302_b
11,49	548,303	4,286	C31H41N5O2S1	SWA_12523_547_a
11,58	548,302	6,110	C31H41N5O2S1	SWA_12523_547_b
11,64	562,282	2,259	C30H43N1O7S1	Thuggacin cmc-A
11,76	578,314	0,640	C23H43N7O10	Malleobactin F
11,79	560,303	8,692	C28H41N5O7	MCy9049_560_NF
11,79	605,426	9,795	C39H56O5	3-O-Caffeoyl-betulin
11,96	530,293	3,300	C31H39N5O1S1	SWA_12523_547_a
12,04	576,298	8,386	C32H42N1O7Na1	Icumazol M-14
12,07	544,308	2,113	C31H45N1O5S1	SWA_12523_562-b
12,07	562,319	1,334	C31H47N1O6S1	SWA_12523_562-a
12,1	546,288	7,780	C27H39N5O7	MCy9101_546_NF
12,1	562,319	1,334	C31H47N1O6S1	SWA_12523_562-a
12,18	397,331	0,680	C24H44O4	Rickiol E
12,36	1095,6	3,149	C62H82N10O4S2	SWA_12523_547_b
12,41	797,426	0,063	C48H60O10	SWA_12523_797-a
12,49	510,284	2,058	C30H39N1O6	Corallopyronin A2

12,53	387,195	19,757	C20H26N4O4	AP9003_387
12,55	544,308	2,113	C31H45N1O5S1	SWA_12523_562-b
12,67	809,527	0,062	C42H72N4O11	SWA_12523_809
12,72	321,075	2,398	C19H12O5	1.8-Dihydroxy-3-methylbenz[a]an-thracene-7.12-dione
12,84	526,136	7,527	C25H27N5O2S3	Thiangazol B
12,9	508,269	0,728	C30H37N1O6	Xylobovatin
13,62	909,64	3,353	C45H88N4O14	909_potential media cpd
13,65	926,665	1,565	C45H91N5O14	909_potential media cpd
13,69	823,542	7,954	C49H74O10	Etnangien
13,93	511,283	14,023	C27H42O9	Soraphen AÎ³
14,18	325,195	0,308	C10H28N8S2	SR017-325
14,46	563,299	18,001	C31H43N2O6Na1	Crocacin D
14,53	341,19	0,147	C25H24O1	SbSr044_Compound_341
14,69	492,273	9,852	C27H41N1O5S1	Epothilon D
14,7	527,277	2,560	C18H38N8O10	SH-Cm7-526
15,08	801,452	6,576	C48H64O10	Compound-3997
16,3	717,555	7,623	C51H72O2	VitaminK2_So2640
16,35	1189,72	9,019	C61H104O22	Oasomycin B
16,6	307,263	0,488	C20H34O2	SbSr044_Compound_307
18,01	636,533	0,518	C35H74N1O6P1	Etherlipide-PEAGLbb
18,26	338,342	0,739	C22H43N1O1	Erucamide
18,31	560,419	3,622	C31H53N5O4	SH-Xeno-559
18,99	635,488	4,013	C34H62N6O5	SbSr044_Compound_635
19,54	394,346	1,953	C28H43N1	SH-393
20,18	674,51	2,772	C37H72N1O7P1	Etherlipide-PEAGL3d
20,33	674,509	4,255	C37H72N1O7P1	Etherlipide-PEAGL3d
20,52	780,593	6,879	C45H81N1O9	Sphingolipid-GSL1c

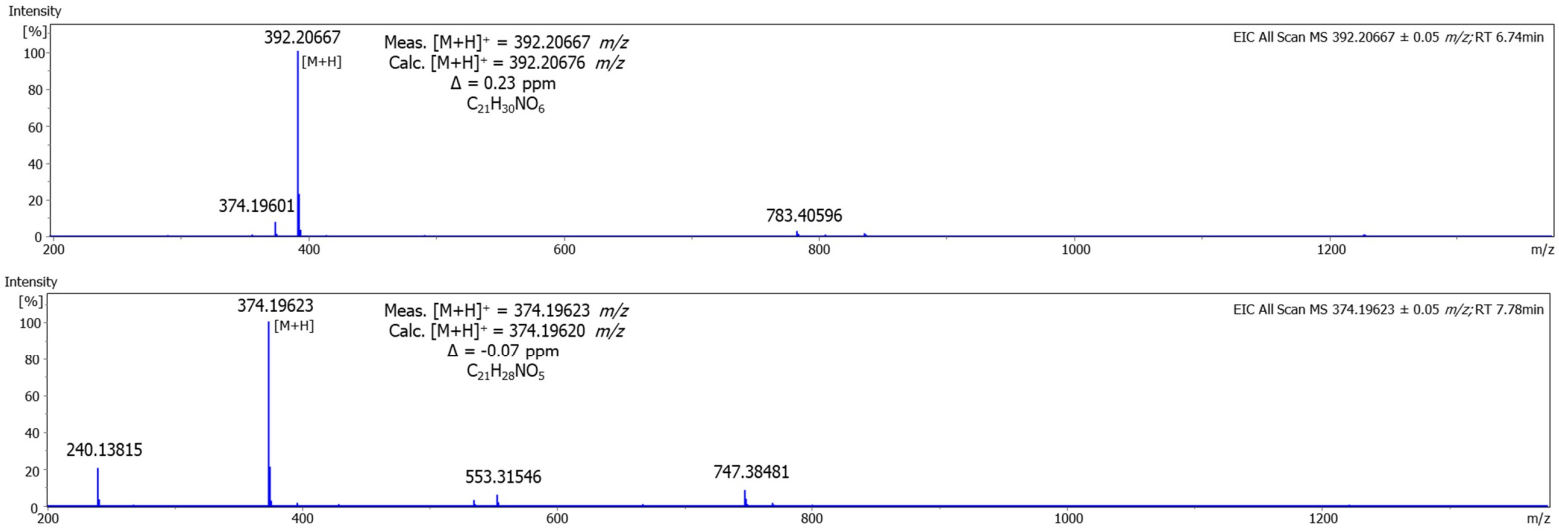

Figure S3.8: High-resolution electrospray ionisation mass spectrometry data of compound-374 and -392.

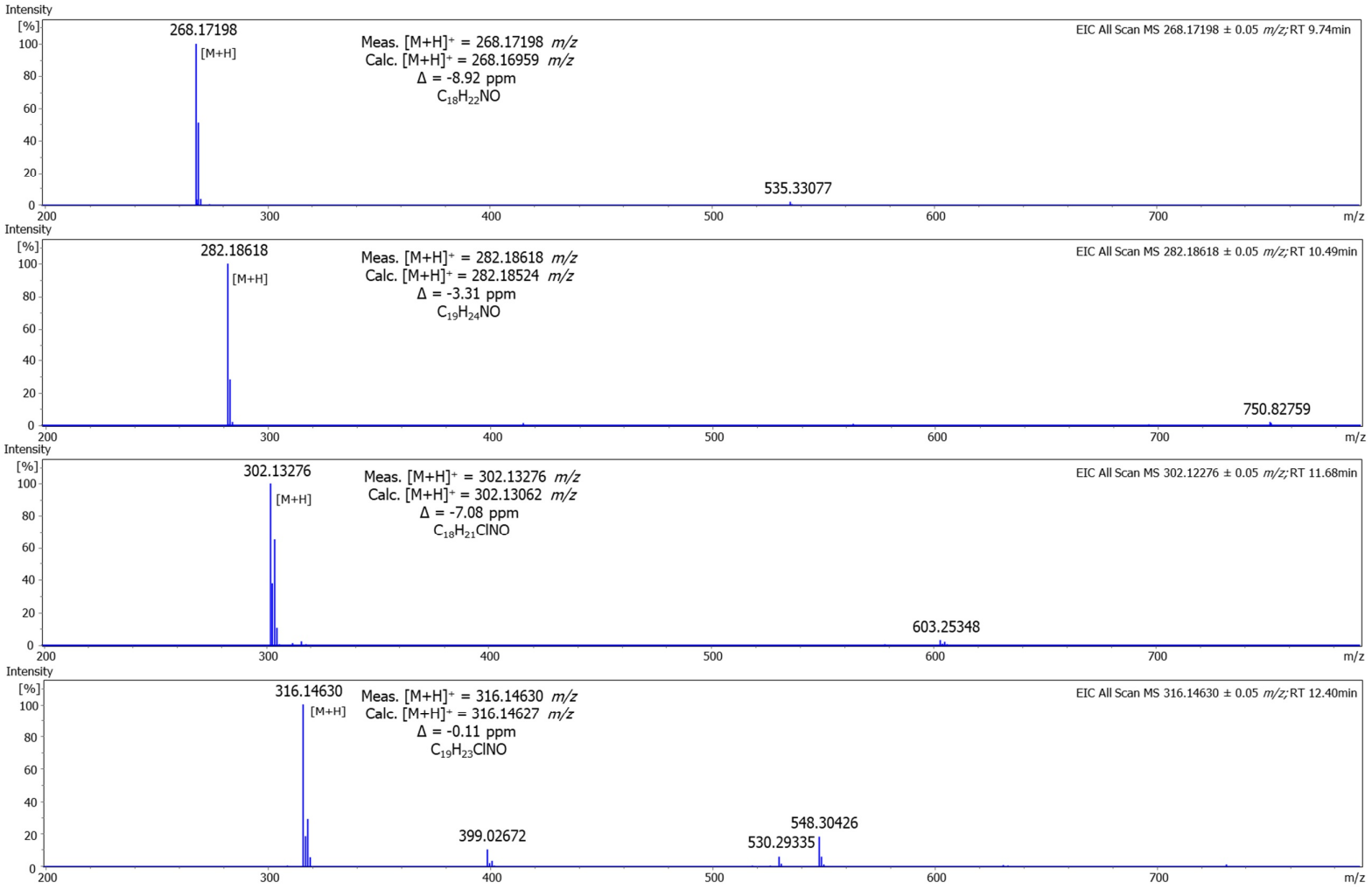

Figure S3.9: High-resolution electrospray ionisation mass spectrometry data of alkyl-quinolones.

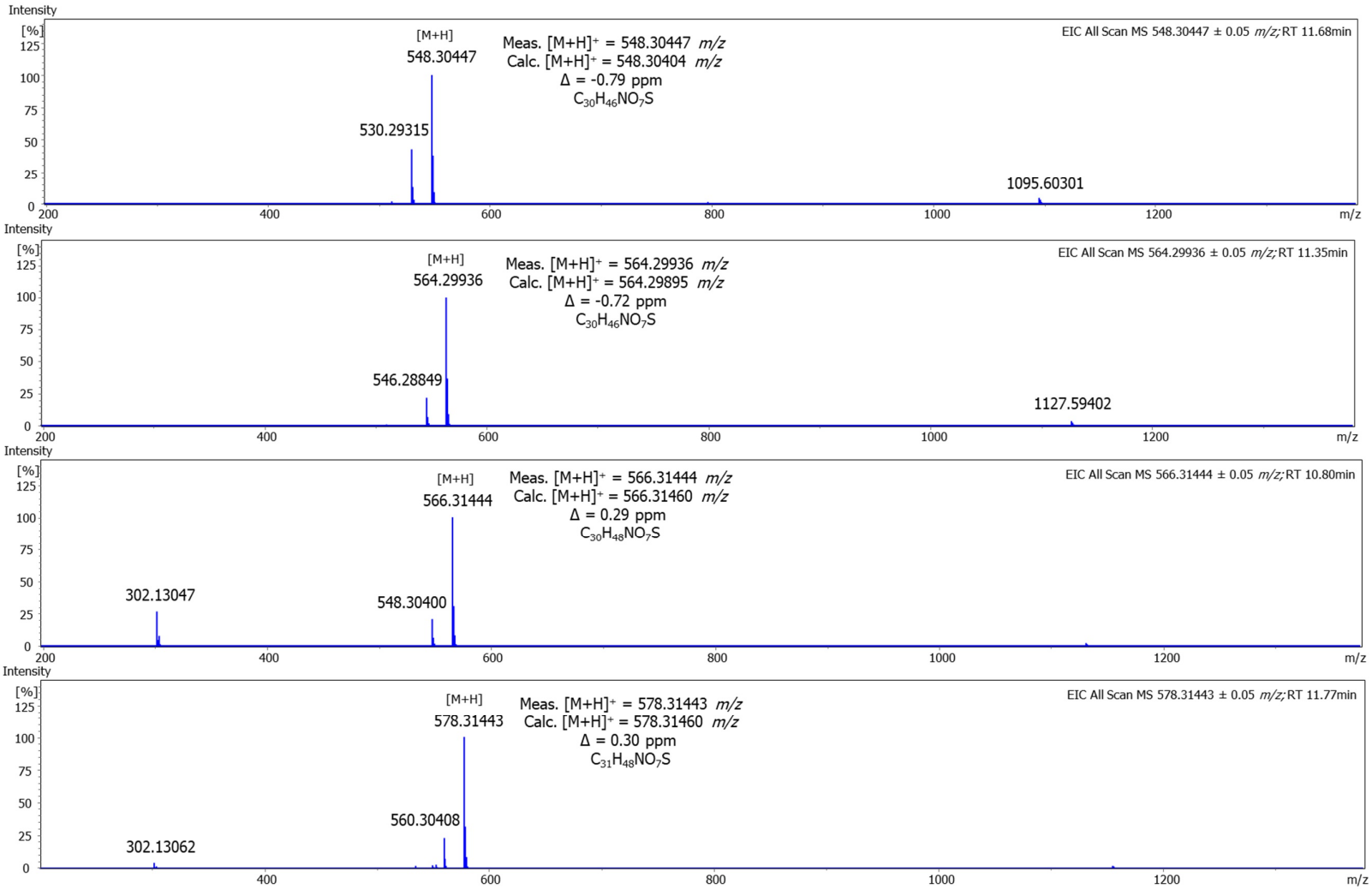

Figure S3.10: High-resolution electrospray ionisation mass spectrometry data of thuggacin analogues.

Table S3.2 NMR spectroscopic data for Cpd-392[a].

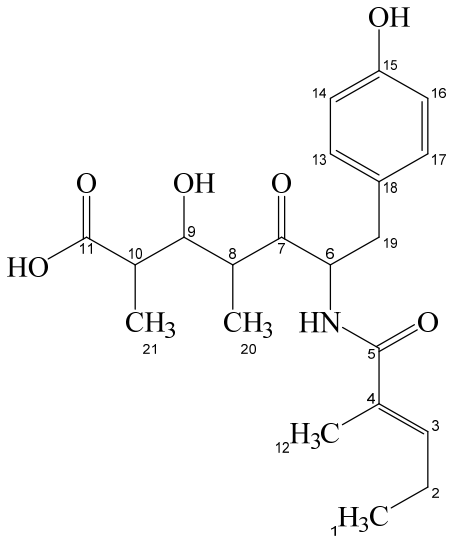

Position	δ ^{13}C[b]	δ ^{1}H[c], mult (J [Hz])	COSY[d]	HMBC[e]
1	13.7	1.02, m	2	2, 3
2	22.7	2.16, m	1, 3, 12	1, 3, 4
3	139.8	6.23, m	2, 12	1, 2, 4, 5, 12
4	131.4			
5	172.5			
6	60.3	4.92, m	19	5, 7, 18, 19
7	213.1			
8	48.1	2.76, m	9, 20	7, 9, 10, 19, 20
9	74.7	4.08, dd (7.27, 4.83)	8, 10	7, 8, 10, 11, 20, 21
10	45.1	2.46, m	9, 21	8, 9, 11, 21
11	179.6			
12	12.7	1.77, d (1.34)	2, 3	1, 2, 3, 4, 5
13, 17	131.4	7.05, m	14, 16, 19	6, 13, 14, 15, 16, 17, 19
14, 16	116.5	6.71, m	13, 17	14, 15, 16, 18
15	157.6			
18	129.4			

19a	37.1	3.03, dd (13.85, 6.69)	6, 13, 17	6, 7, 13, 17, 18
19b	37.1	2.89, dd (13.88, 8.38)	6, 13, 17	6, 7, 13, 17, 18
20	10.2	0.98, d (6.85)	8	7, 8, 9
21	15.3	1.04, d (6.54)	10	9, 10, 11

[a] Recorded in methanol-d_4

[b] Acquired at 125 MHz, referenced to solvent signal CD_3OD at δ 49.15 ppm.

[c] Acquired at 500 MHz, referenced to solvent signal CD_3OD at δ 3.31 ppm.

[d] Proton showing COSY correlations to indicated protons.

[e] Proton showing HMBC correlations to indicated carbons.

NMR spectra were acquired with a Bruker Ultra Shield 500 NMR spectrometer equipped with a 5mm TCI probe head.

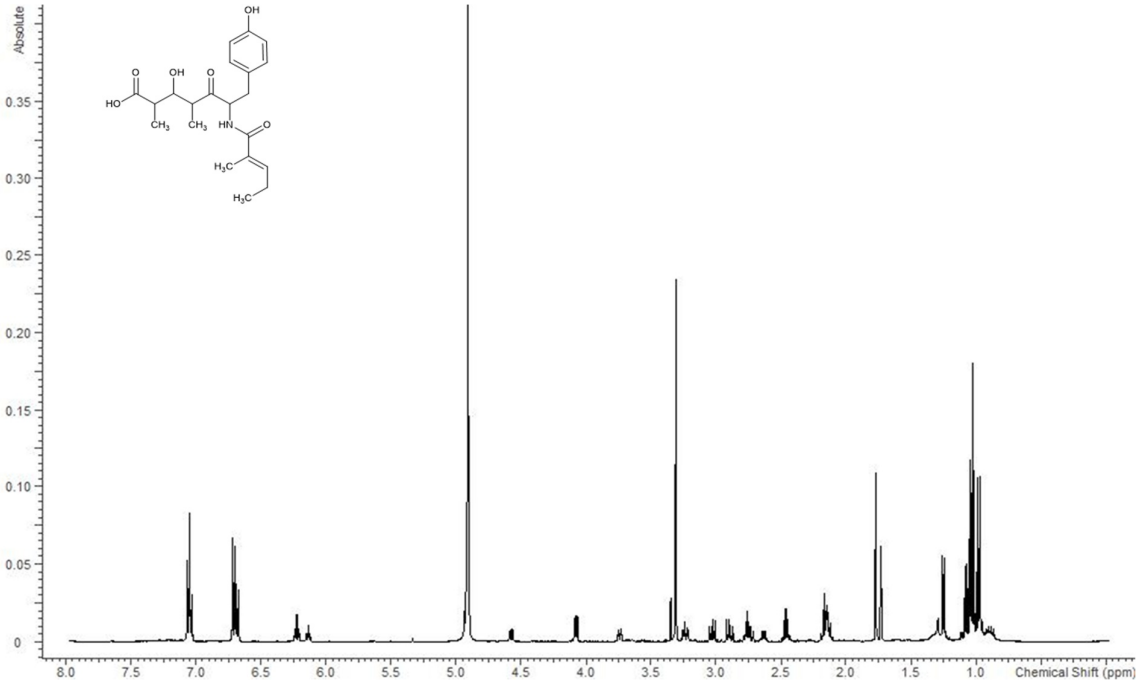

Figure S3.11 ^{1}H spectrum of Cpd-392 acquired in methanol-d_4 at 500 MHz.

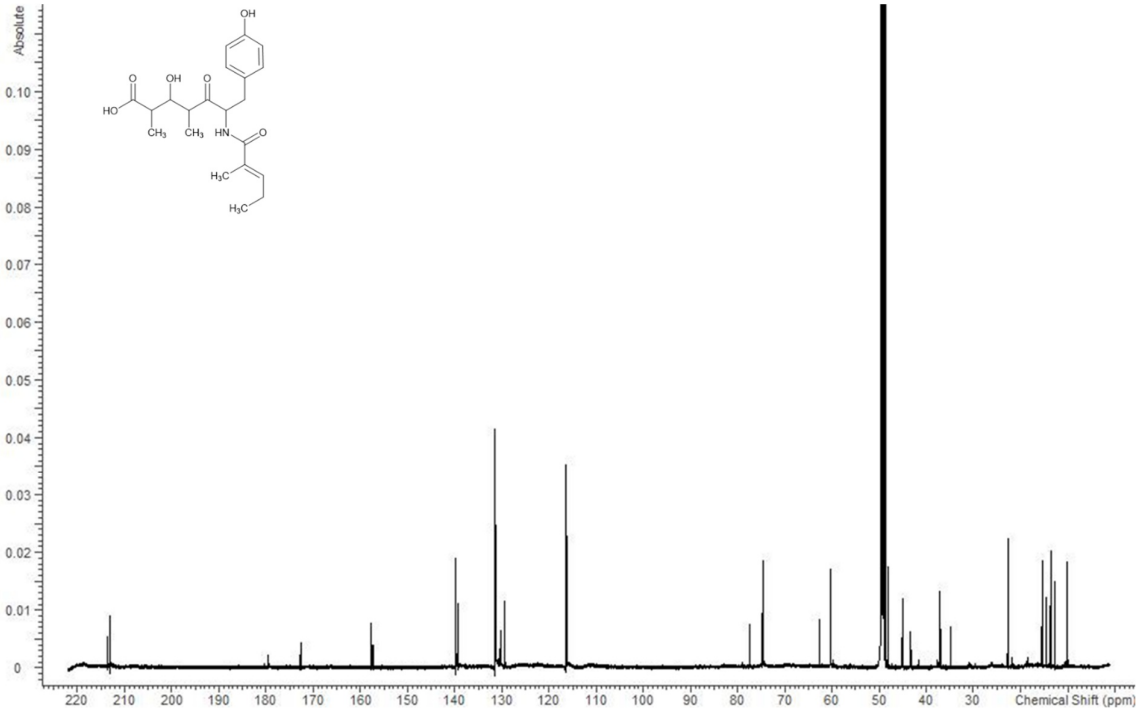

Figure S3.12: ^{13}C spectrum of Cpd-392 acquired in methanol-d_4 at 125 MHz.

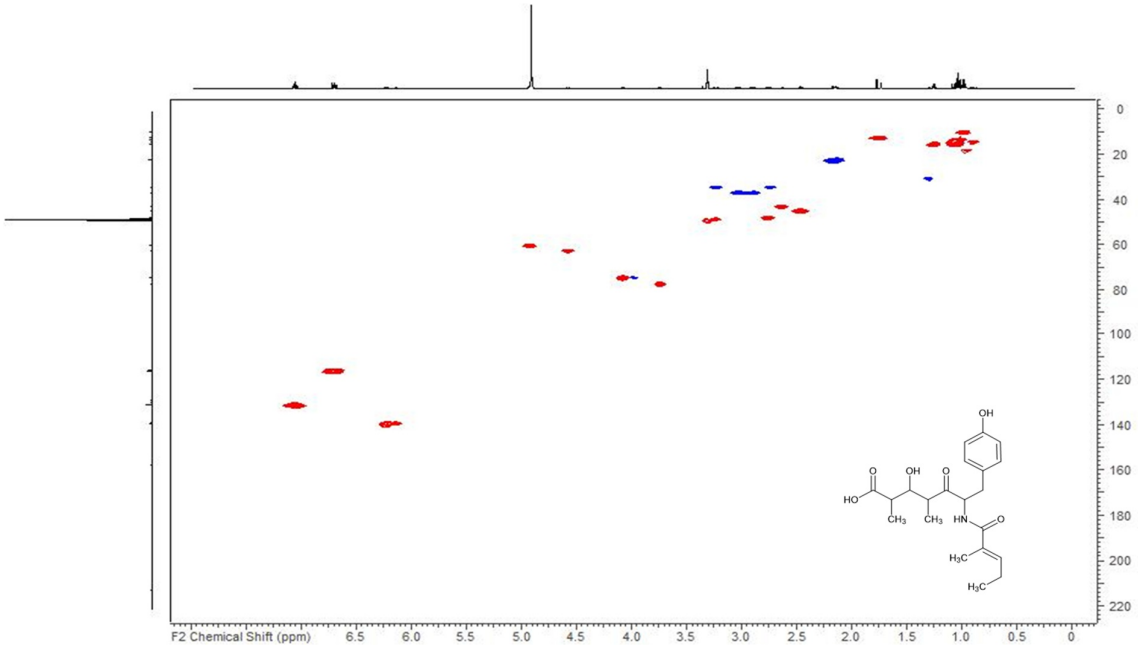

Figure S3.13: HSQC spectrum of Cpd-392 acquired in methanol-d_4 at 125/500 (F1/F2) MHz.

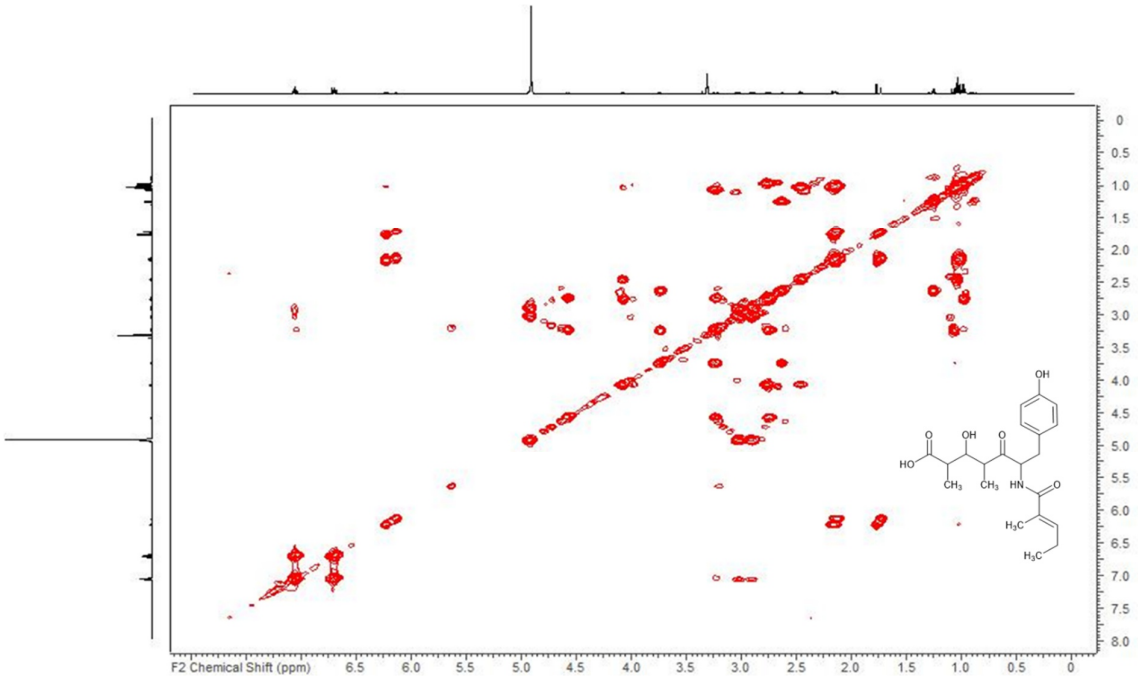

Figure S3.14: COSY spectrum of Cpd-392 acquired in methanol-d_4 at 500 MHz.

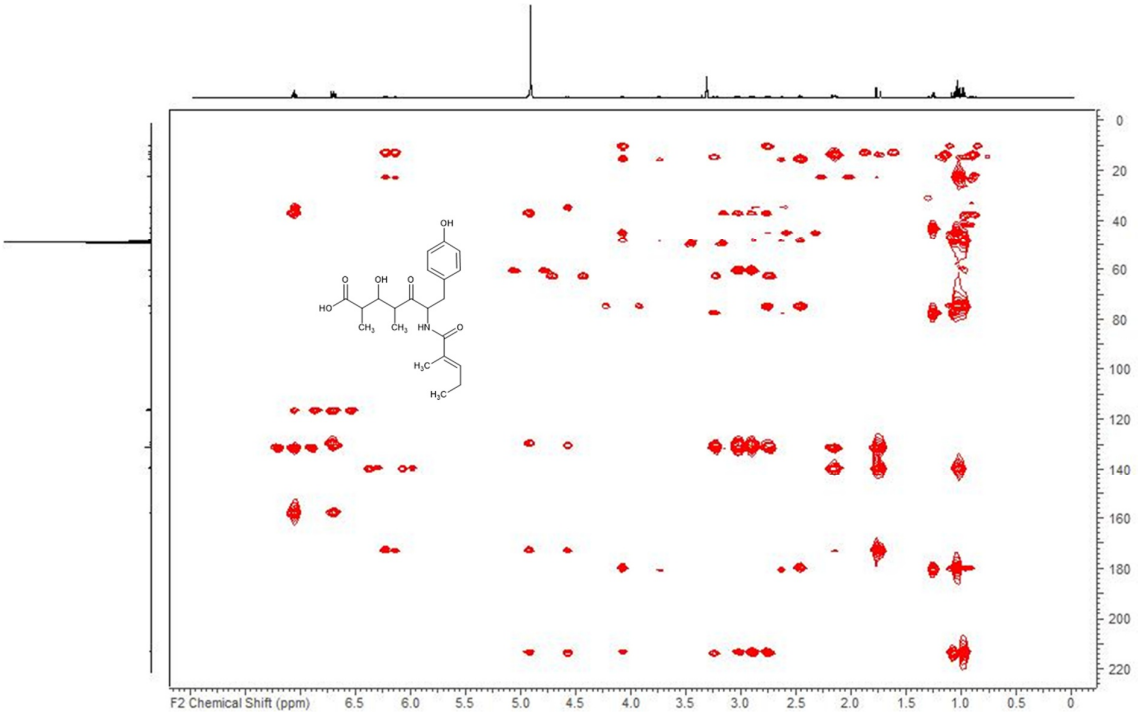

Figure S3.15: HMBC spectrum of Cpd-392 acquired in methanol-d_4 at 125/500 (F1/F2) MHz.

Table S3.3: NMR spectroscopic data for Cpd-268[a].

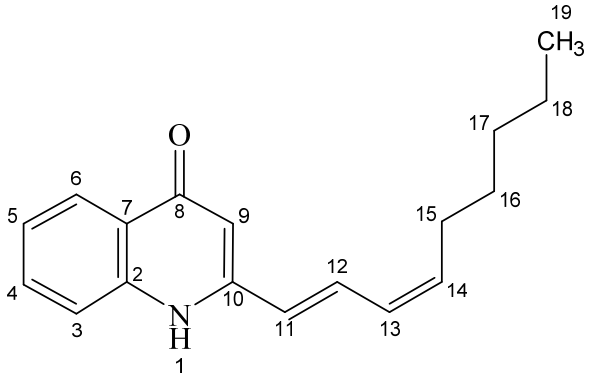

Position	δ ^{13}C[b]	δ ^{1}H[c], mult (J [Hz])	COSY[d]	HMBC[e]
2	141.7			
3	119.4	7.65, m	4	2, 4, 5, 6, 8
4	133.8	7.69, m	3, 5, 6	2, 5, 6
5	125.3	7.39, m	4, 6	2, 3, 4, 6
6	126.0	8.19, ddd (8.16, 4.12, 1.22)	3, 4	2, 3, 4, 5, 7, 8
7	126.1			
8	180.5			
9	106.9	6.45, s		7, 8, 10, 11
10	150.9			
11	123.2	6.38, m	12	9, 10, 12, 13
12	139.3	7.28, br dd (15.72, 10.45)	11, 13	10, 11, 13, 14
13	130.9	6.34, m	12, 14, 15	11, 12, 14, 15, 16
14	143.8	6.18, m	13, 15	12, 13, 15, 16
15	34.2	2.23, q (6.97, 6.97, 6.97)	13, 14, 16	12, 13, 14, 16, 17
16	30.0	1.48, m	15, 17	14, 15, 17, 18
17	32.8	1.35, m	16, 18	15, 16, 18, 19
18	23.7	1.37, m	17, 19	17
19	14.5	0.93, m	18	17, 18

[a] Recorded in methanol-d_4

[b] Acquired at 125 MHz, referenced to solvent signal CD_3OD at δ 49.15 ppm.

[c] Acquired at 500 MHz, referenced to solvent signal CD_3OD at δ 3.31 ppm.

[d] Proton showing COSY correlations to indicated protons.

[e] Proton showing HMBC correlations to indicated carbons.

NMR spectra were acquired with a Bruker Ultra Shield 500 NMR spectrometer equipped with a 5mm TCI probe head.

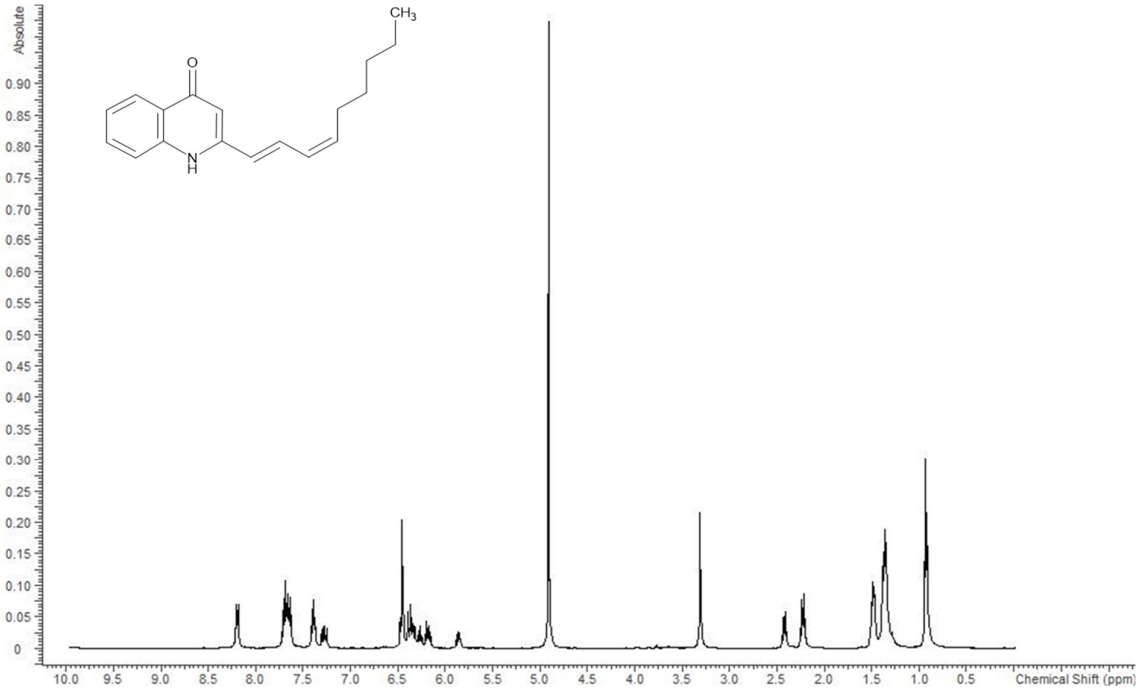

Figure S3.16: ^{1}H spectrum of Cpd-268 acquired in methanol-d_4 at 500 MHz.

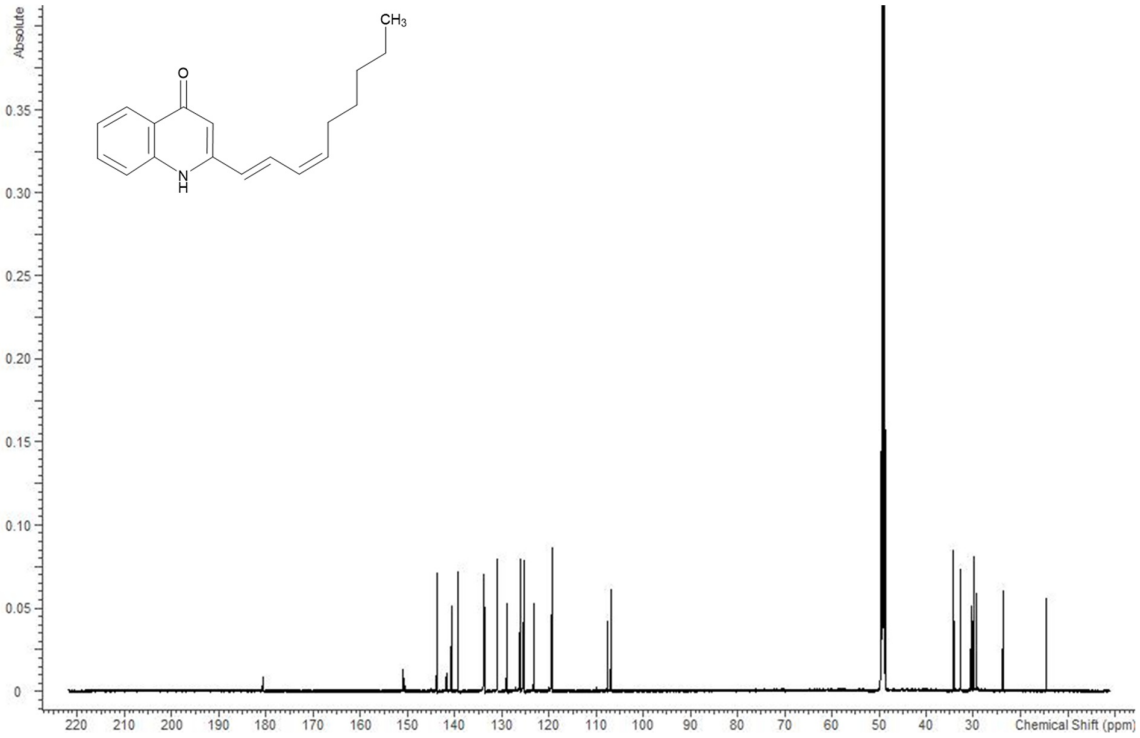

Figure S3.17: ^{13}C spectrum of Cpd-268 acquired in methanol-d_4 at 125 MHz.

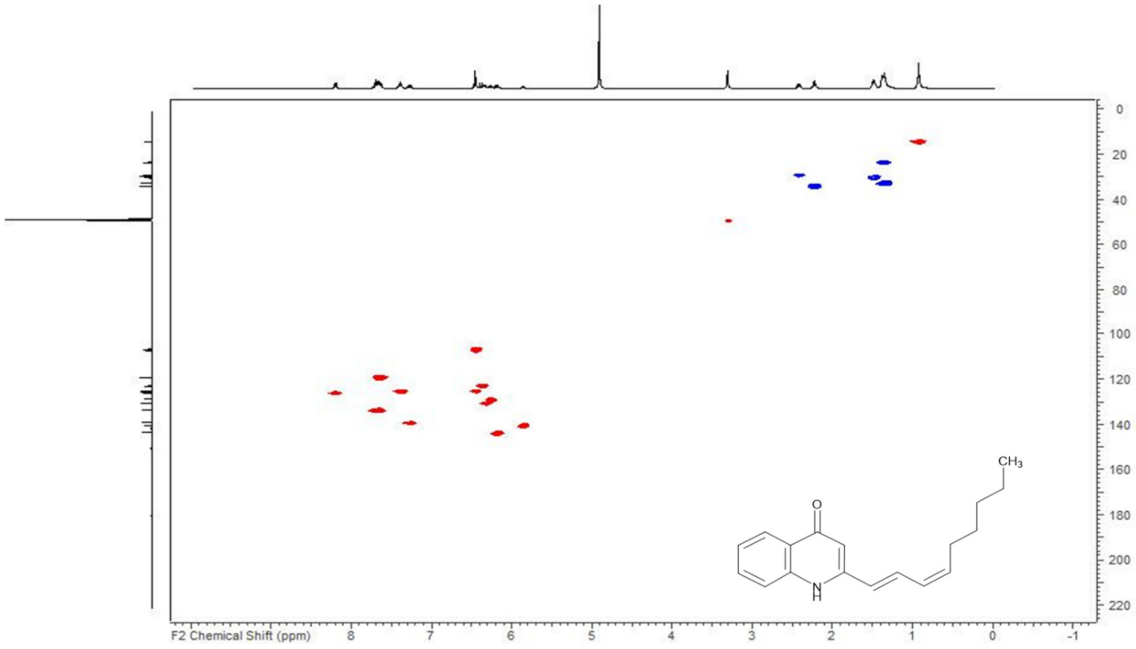

Figure S3.18: HSQC spectrum of Cpd-268 acquired in methanol-d_4 at 125/500 (F1/F2) MHz.

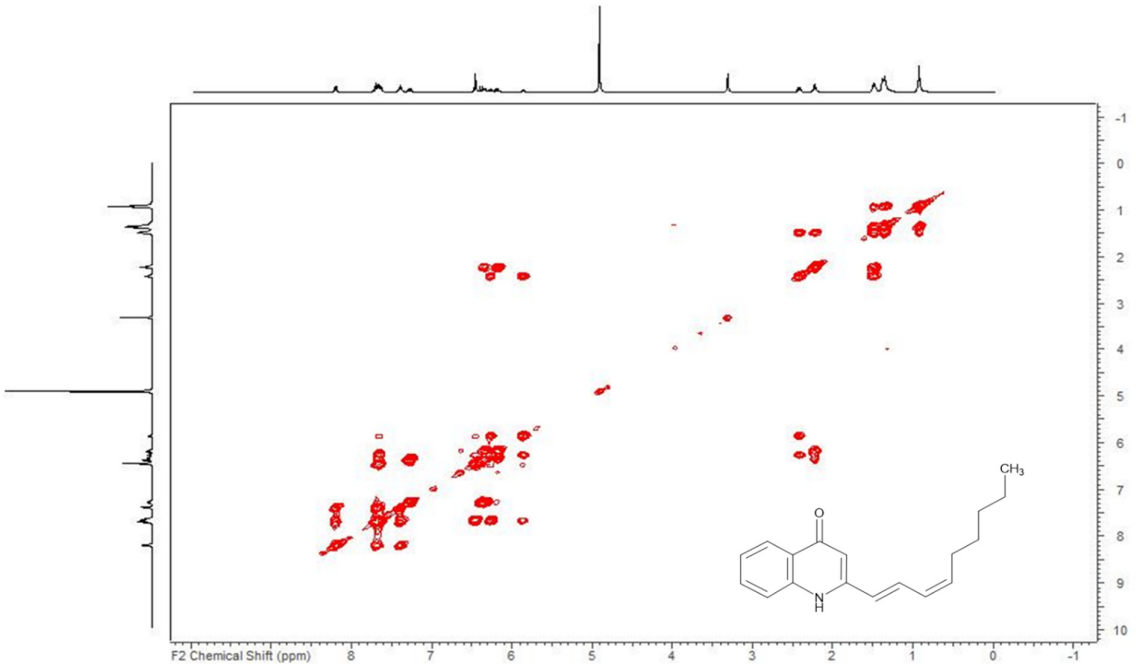

Figure S3.19: COSY spectrum of Cpd-268 acquired in methanol-d_4 at 500 MHz.

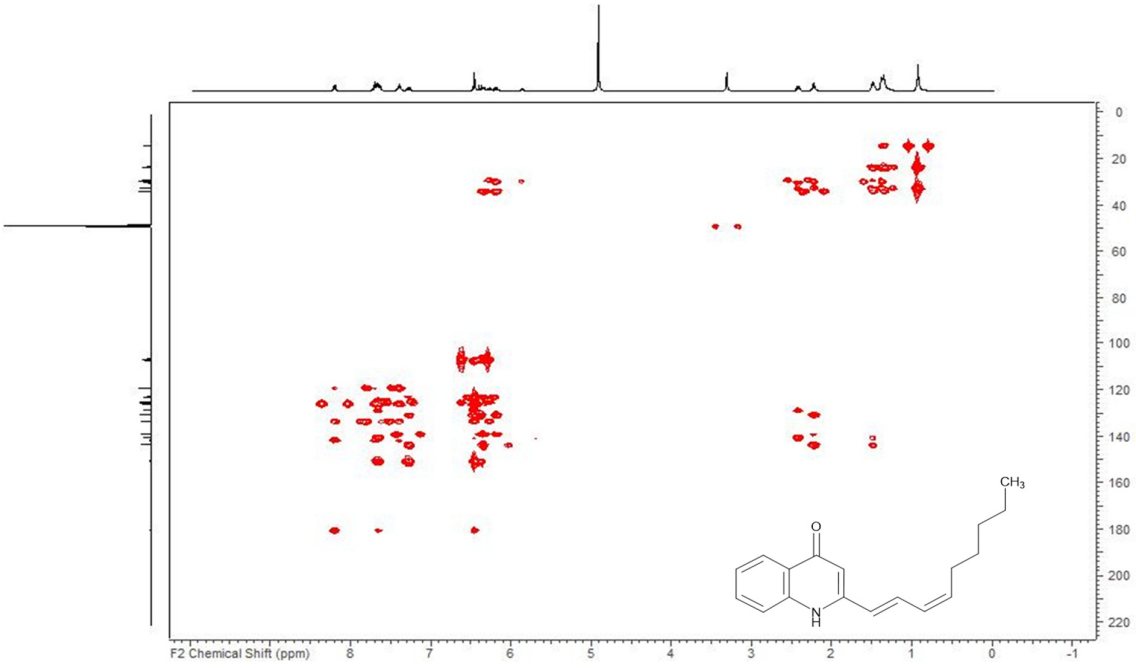

Figure S3.20: HMBC spectrum of Cpd-268 acquired in methanol-d_4 at 125/500 (F1/F2) MHz.

Table S3.4: NMR spectroscopic data for Cpd-282[a] (Component 1).

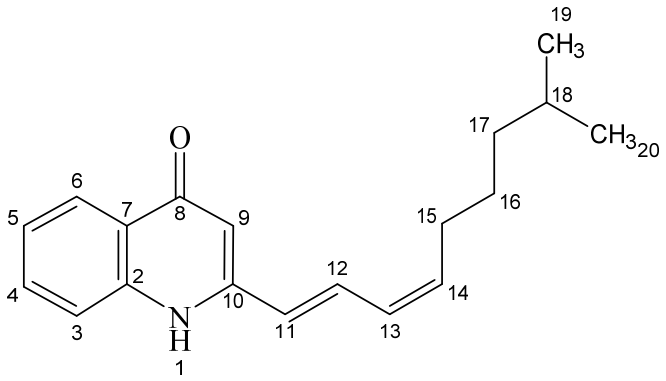

Position	δ ^{13}C[b]	δ ^{1}H[c], mult (J [Hz])	COSY[d]	HMBC[e]
2	140.2			
3	117.9	7.64, m	4, 5	4, 5, 6, 8, 10
4	132.2	7.70, m	3, 5, 6	2, 3, 6
5	123.8	7.39, m	3, 4, 6	3, 4, 6
6	124.5	8.21, dd (4.04, 1.37)	4, 5	2, 3, 4, 5, 7, 8
7	124.5			
8	179.0			
9	105.3	6.45, s		7, 8, 11
10	149.4			
11	121.7	6.38, d (15.72)	12	8, 9, 10, 12, 13, 14
12	137.7	7.28, dd (15.72, 10.45)	11, 13, 14	10, 11, 13, 14
13	129.4	6.34, m	12, 14, 15	11, 12, 14, 15
14	142.3	6.18, m	12, 13, 15	12, 13, 15, 16
15	32.9	2.22, q (7.12, 7.12, 7.12)	13, 14, 16	12, 13, 14, 16, 17, 18
16	26.6	1.49, m	15, 17	14, 15, 17, 18
17	38.3	1.24, m	16, 18	15, 16, 18, 19, 20
18	27.7	1.58, m	17, 19, 20	16, 17, 19, 20
19, 20	21.6	0.91, d (6.64)	18	17, 18, 19, 20

[a] Recorded in methanol-d_4

[b] Acquired at 125 MHz, referenced to solvent signal CD_3OD at δ 49.15 ppm.

[c] Acquired at 500 MHz, referenced to solvent signal CD_3OD at δ 3.31 ppm.

[d] Proton showing COSY correlations to indicated protons.

[e] Proton showing HMBC correlations to indicated carbons.

Table S3.5: NMR spectroscopic data for Cpd-282[a] (Component 2).

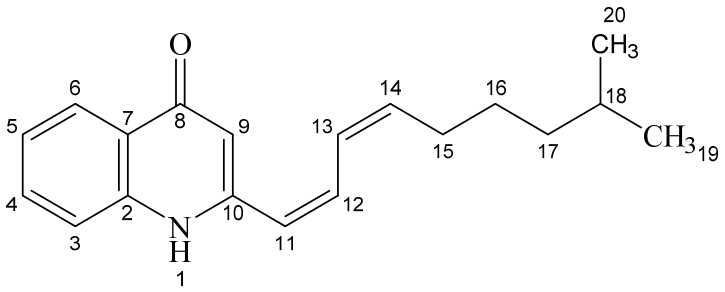

Position	δ ^{13}C[b]	δ ^{1}H[c], mult (J [Hz])	COSY[d]	HMBC[e]
2	140.3			
3	117.9	7.64, m	4, 5	4, 5, 6, 8, 10
4	132.3	7.70, m	3, 5, 6	2, 3, 6
5	123.8	7.39, m	3, 4, 6	3, 4, 6
6	124.5	8.19, dd (4.04, 1.30)	4, 5	2, 3, 4, 5, 7, 8
7	124.6			
8	179.1			
9	106.1	6.46, s		7, 8, 11
10	149.1			
11	124.0	6.46, m	12	8, 9, 10, 12, 13, 14
12	132.1	7.66, m	11, 13, 14	10, 11, 13, 14
13	127.4	6.27, t (10.91, 10.91)	12, 14, 15	11, 12, 14, 15
14	139.1	5.86, dt (10.62, 7.89, 7.89)	12, 13, 15	12, 13, 15, 16
15	28.1	2.41, qd (7.55, 7.55, 7.55, 1.30)	13, 14, 16	12, 13, 14, 16, 17, 18
16	27.1	1.50, m	15, 17	14, 15, 17, 18
17	38.3	1.29, m	16, 18	15, 16, 18, 19, 20
18	27.7	1.58, m	17, 19, 20	16, 17, 19, 20
19, 20	21.6	0.91, br d (6.64)	18	17, 18, 19, 20

[a] Recorded in methanol-d_4

[b] Acquired at 125 MHz, referenced to solvent signal CD_3OD at δ 49.15 ppm.

[c] Acquired at 500 MHz, referenced to solvent signal CD_3OD at δ 3.31 ppm.

[d] Proton showing COSY correlations to indicated protons.

[e] Proton showing HMBC correlations to indicated carbons.

NMR spectra were acquired with a Bruker Ultra Shield 500 NMR spectrometer equipped with a 5mm TCI probe head.

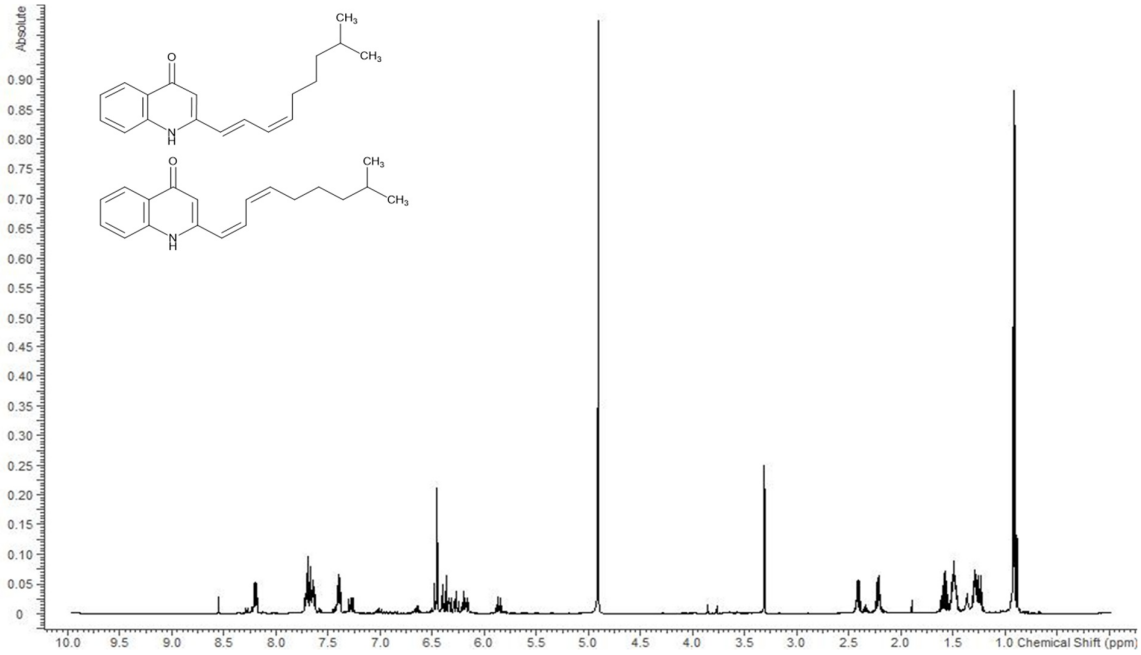

Figure S3.21: ^{1}H spectrum of Cpd-282 acquired in methanol-d_4 at 500 MHz.

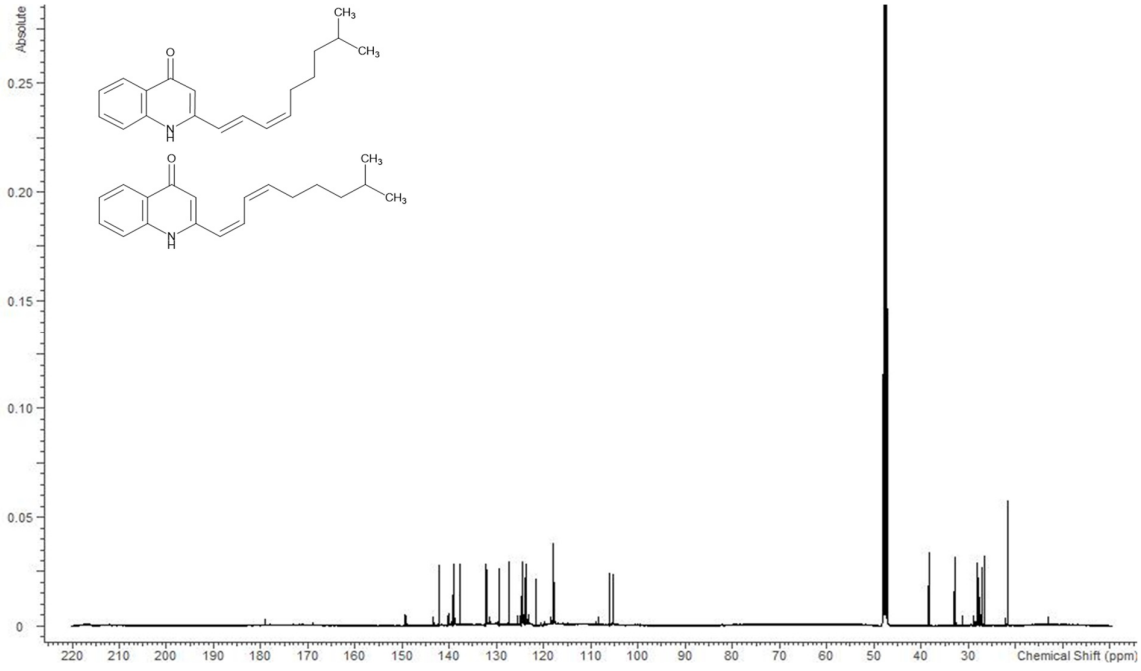

Figure S3.22: ^{13}C spectrum of Cpd-282 acquired in methanol-d_4 at 125 MHz.

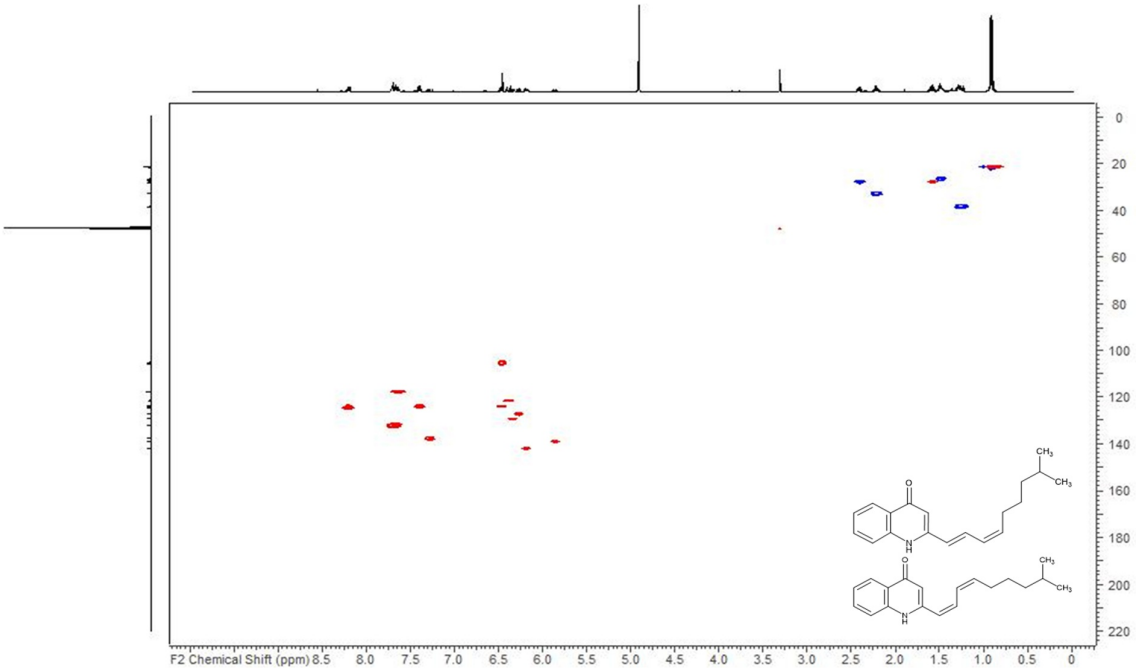

Figure S3.23: HSQC spectrum of Cpd-282 acquired in methanol-d_4 at 125/500 (F1/F2) MHz.

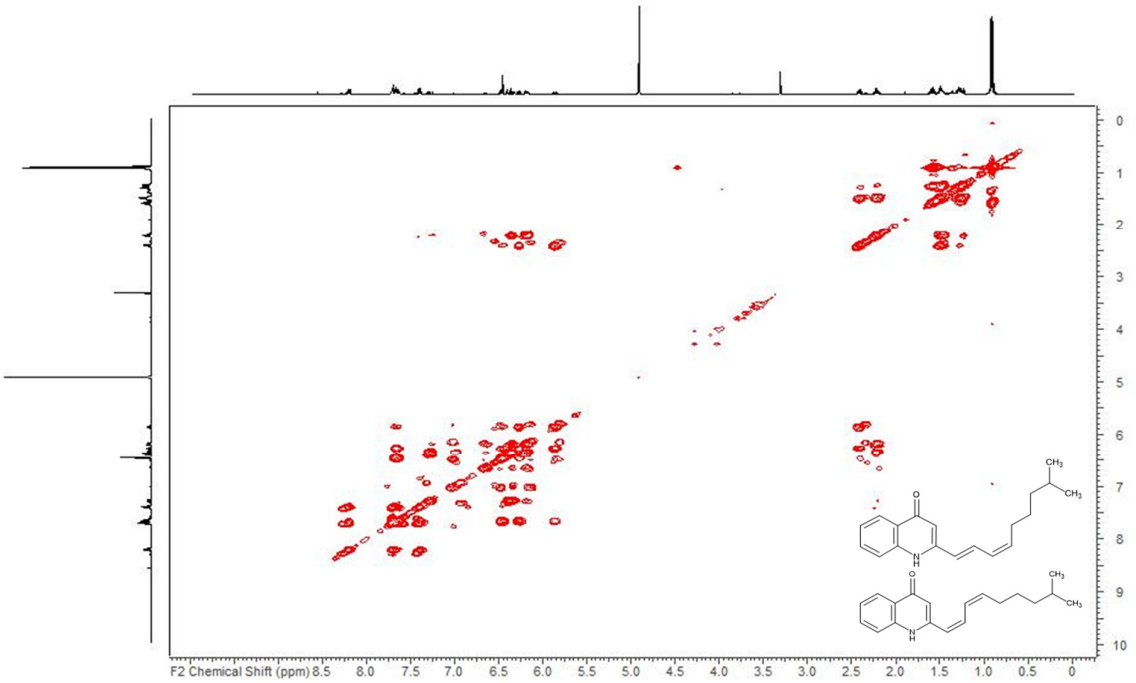

Figure S3.24: HSQC spectrum of Cpd-282 acquired in methanol-d_4 at 500 MHz.

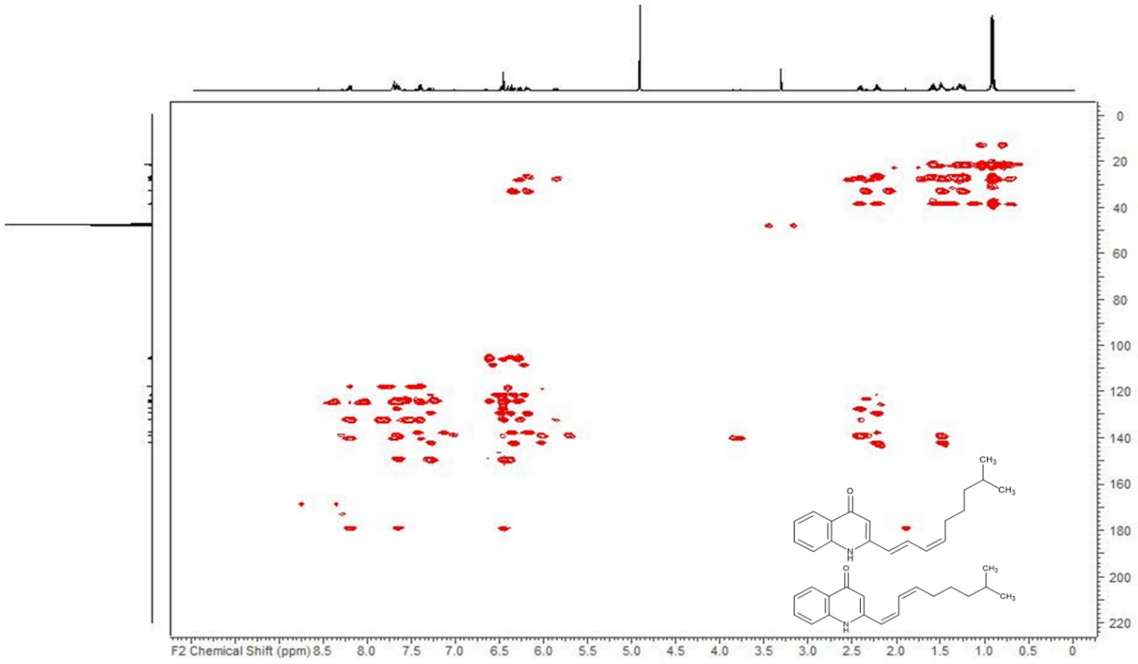

Figure S3.25: HMBC spectrum of Cpd-282 acquired in methanol-d_4 at 125/500 (F1/F2) MHz.

Table S3.6: NMR spectroscopic data for Cpd-302[a] (Major component).

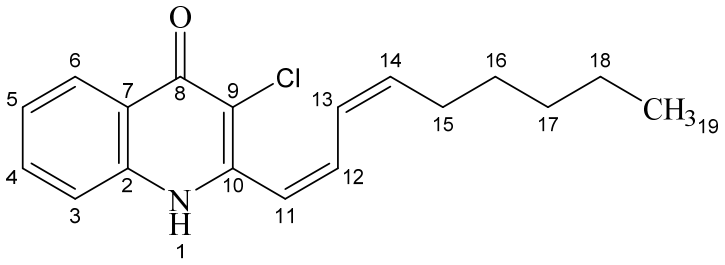

Position	δ ^{13}C[b]	δ ^{1}H[c], mult (J [Hz])	COSY[d]	HMBC[e]
2	140.6			
3	119.7	7.63, m	4, 5	4, 5, 6, 7, 8
4	133.6	7.72, m	3, 5, 6	2, 3
5	125.7	7.45, ddd (8.20, 6.98, 1.14)	3, 4, 6	2, 3, 4, 6, 7, 9
6	126.5	8.29, m	4, 5	2, 3, 4, 5, 8
7	125.2			
8	174.5			
9	115.6			
10	148.0			
11	119.5	6.36, d (11.44)	12	9, 10, 12, 13
12	138.7	6.66, t (11.25, 11.25)	11, 13	9, 10, 13, 14
13	127.1	6.23, m	12, 14, 15	11, 12, 14, 15
14	143.9	6.13, m	13, 15	12, 13, 15, 16
15	34.0	2.14, q (7.30, 7.30, 7.30)	13, 14, 16	12, 13, 14, 16, 17
16	29.8	1.42, m	15, 17	14, 15, 17, 18
17	32.7	1.30, m	16	15, 16, 18, 19
18	23.7	1.30, m	19	16, 17, 19
19	14.5	0.88, s	18	17, 18

[a] Recorded in methanol-*d*$_4$

[b] Acquired at 125 MHz, referenced to solvent signal CD_3OD at δ 49.15 ppm.

[c] Acquired at 500 MHz, referenced to solvent signal CD_3OD at δ 3.31 ppm.

[d] Proton showing COSY correlations to indicated protons.

[e] Proton showing HMBC correlations to indicated carbons.

Table S3.7: NMR spectroscopic data for Cpd-302[a] (Minor component).

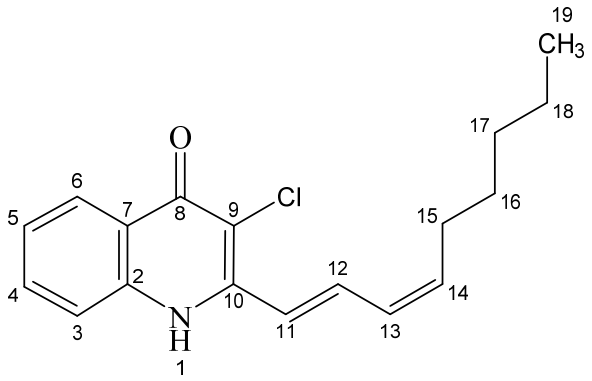

Position	δ ^{13}C[b]	δ ^{1}H[c], mult (J [Hz])	COSY[d]	HMBC[e]
2	140.7			
3	119.5	7.73, m	4, 5	2, 4, 7, 8
4	133.8	7.70, m	3, 5, 6	2, 3, 5, 6
5	125.4	7.40, ddd (8.18, 6.50, 1.56)	3, 4, 6	2, 3, 4, 6, 7
6	126.4	8.24, m	4, 5	2, 3, 4, 7, 8
7	125.4			
8	174.6			
9	115.6			
10	147.0			
11	121.3	6.93, d (15.87)	12, 13	9, 10, 13
12	140.3	7.33, dd (15.83, 10.41)	11, 13, 14	9, 10, 11, 13, 14
13	131.2	6.44, dd (14.72, 10.15)	11, 12, 14	11, 12, 15
14	144.6	6.24, m	12, 13, 15	12, 13, 15, 16
15	34.2	2.26, q (6.92, 6.92, 6.92)	13, 14, 16	12, 13, 14, 16, 17
16	29.9	1.50, m	15, 17	14, 18
17	32.8	1.37, m	16	15, 16, 18 ,19
18	23.7	1.36, m	19	17, 19
19	14.5	0.93, m	18	17, 18

[a] Recorded in methanol-d_4

[b] Acquired at 125 MHz, referenced to solvent signal CD_3OD at δ 49.15 ppm.

[c] Acquired at 500 MHz, referenced to solvent signal CD_3OD at δ 3.31 ppm.

[d] Proton showing COSY correlations to indicated protons.

[e] Proton showing HMBC correlations to indicated carbons.

NMR spectra were acquired with a Bruker Ultra Shield 500 NMR spectrometer equipped with a 5mm TCI probe head.

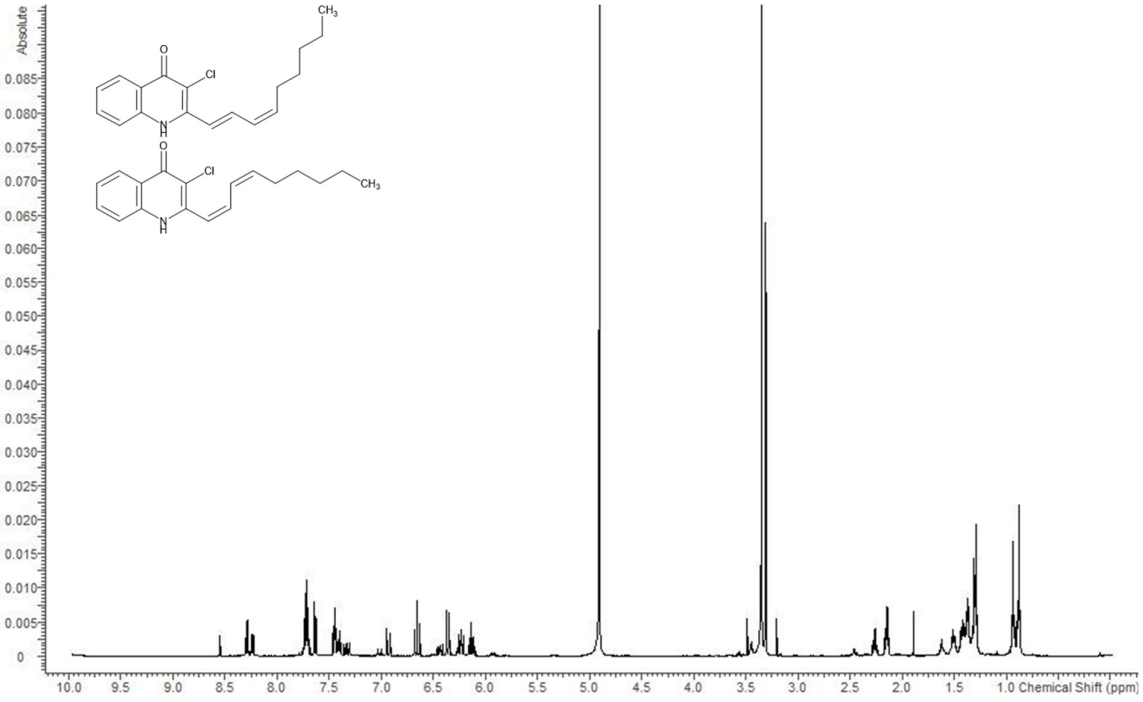

Figure S3.26: ^{1}H spectrum of Cpd-302 acquired in methanol-d_4 at 500 MHz.

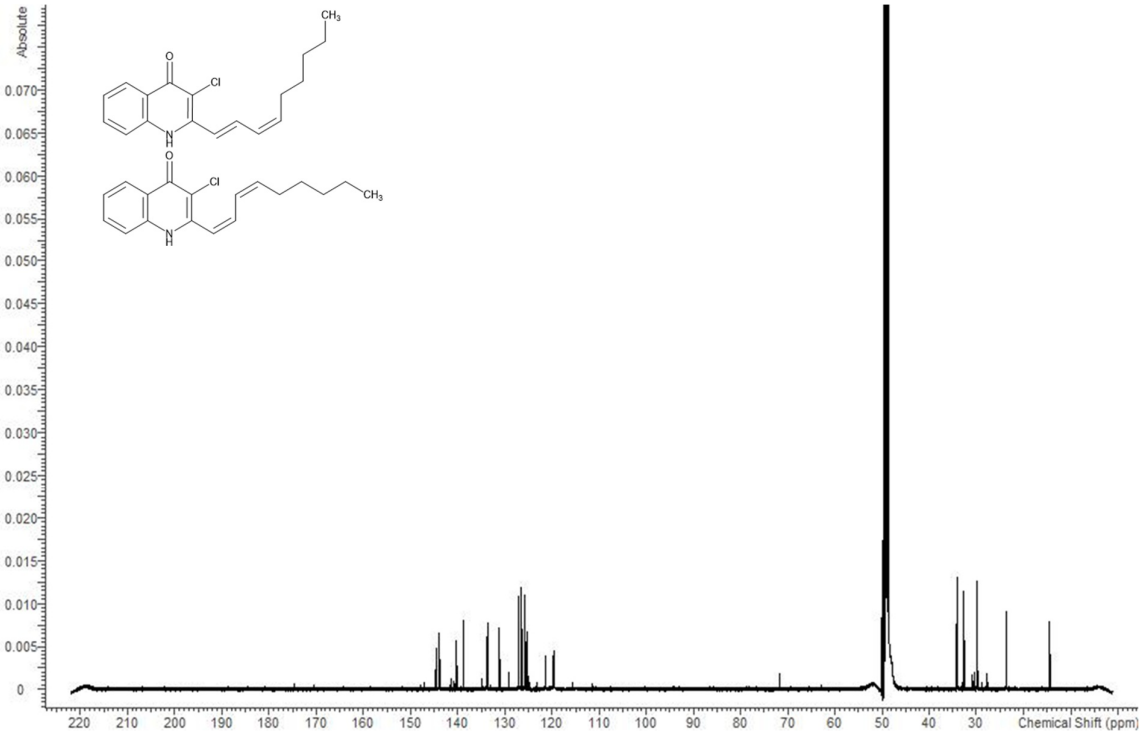

Figure S3.27: ^{13}C spectrum of Cpd-302 acquired in methanol-d_4 at 125 MHz.

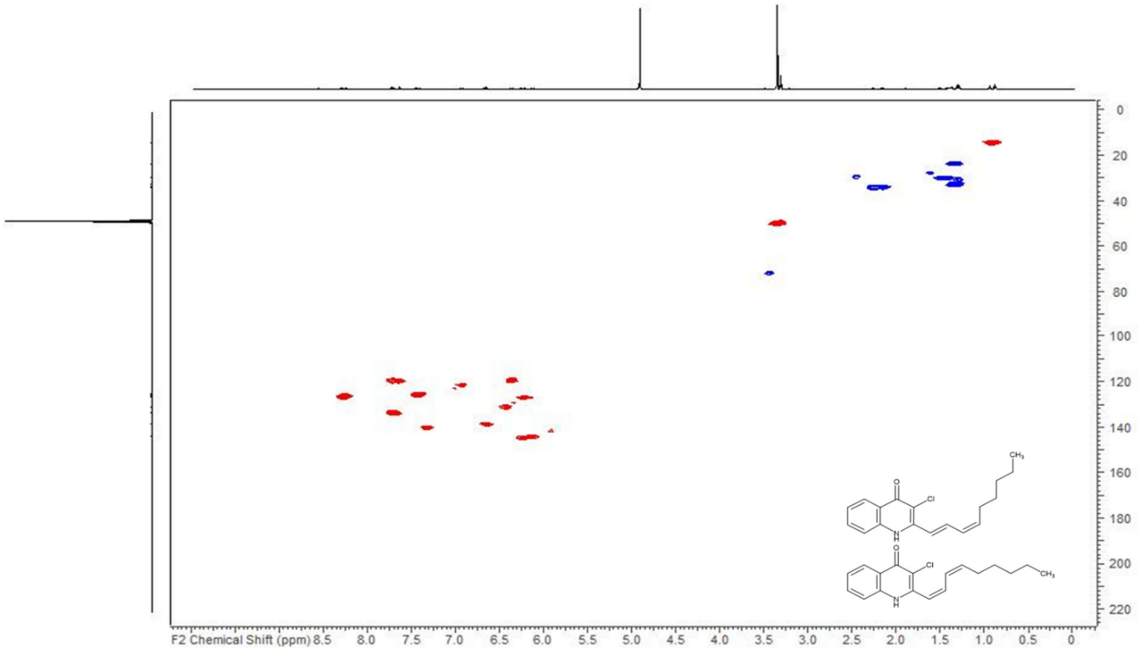

Figure S3.28: HSQC spectrum of Cpd-302 acquired in methanol-d_4 at 125/500 (F1/F2) MHz.

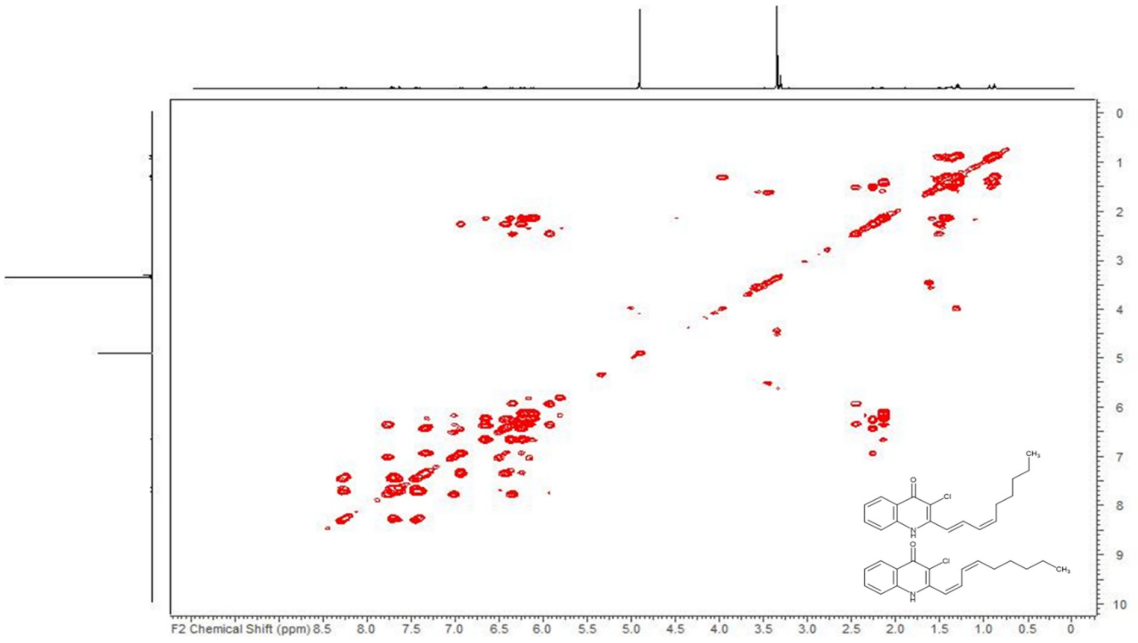

Figure S3.29: COSY spectrum of Cpd-302 acquired in methanol-d_4 at 500 MHz.

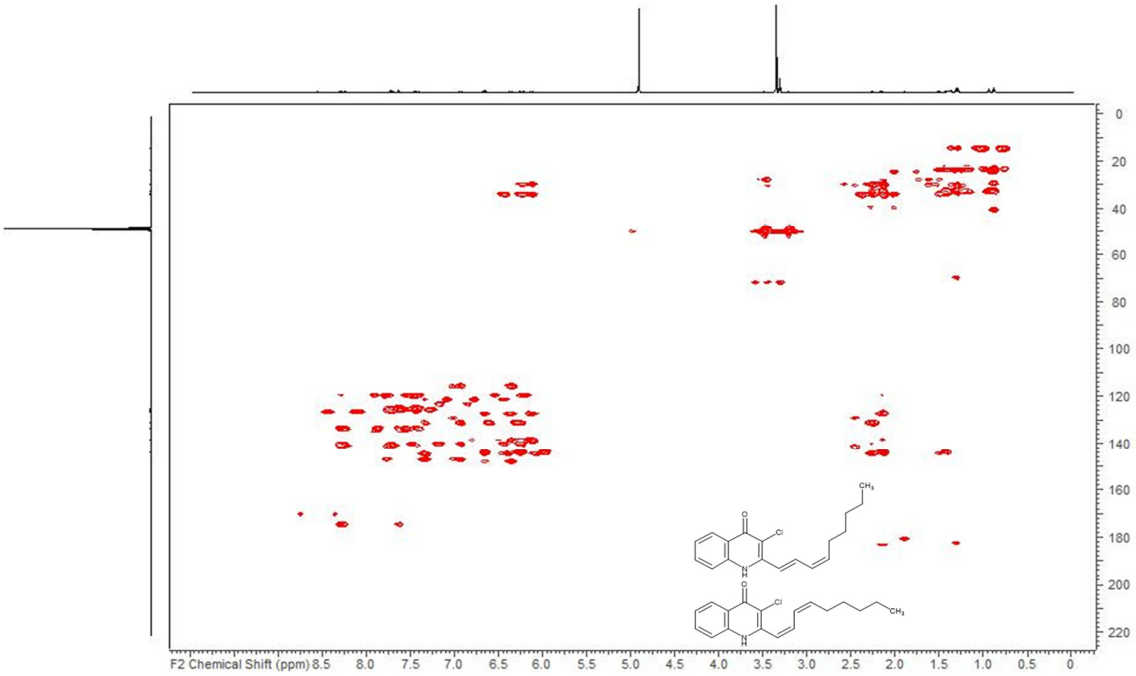

Figure SI 3.30: HMBC spectrum of Cpd-302 acquired in methanol-d_4 at 125/500 (F1/F2) MHz.

Table S3.8: NMR spectroscopic data for Cpd-316[a].

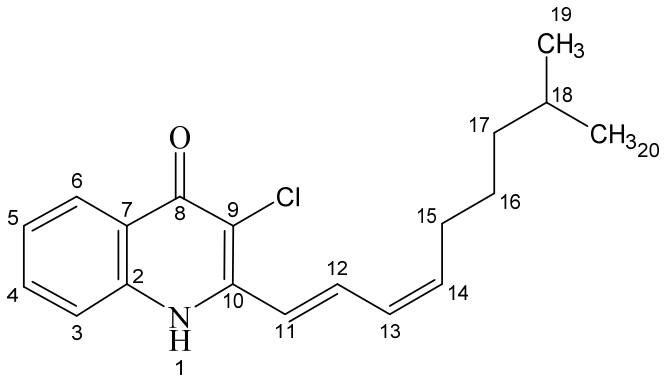

Position	δ ^{13}C[b]	δ ^{1}H[c], mult (J [Hz])	COSY[d]	HMBC[e]
2	140.6			
3	119.4	7.73, m	4, 5	2, 7
4	133.9	7.71, m	3, 5, 6	2, 3, 5, 6
5	125.4	7.41, ddd (8.16, 6.22, 1.87)	3, 4, 6	2, 3, 4, 7
6	126.4	8.24, dd (7.86, 0.92)	4, 5	2, 3, 4, 8
7	124.9			
8	174.7			
9	115.6			
10	146.8			
11	121.2	6.93, d (15.87)	12, 13, 14, 15	9, 10, 12, 13
12	140.4	7.33, dd (15.75, 10.41)	11, 13, 14, 15	10, 11, 13, 14
13	131.2	6.44, ddd (15.11, 10.38, 0.61)	11, 12, 14, 15	11, 12, 14, 15
14	144.7	6.25, m	11, 12, 13, 15	12, 13, 15, 16
15	34.5	2.25, q (7.10, 7.10, 7.10)	11, 12, 13, 14, 16, 17	12, 13, 14, 16, 17
16	28.1	1.51, m	15, 17	14, 15, 17, 18, 19,20
17	39.9	1.26, m	15, 16, 18	15, 16, 18, 19, 20
18	29.2	1.59, dt (13.35, 6.68, 6.68)	17, 19, 20	16, 17, 19, 20
19, 20	23.1	0.92, d (6.64)	18	17, 18

[a] Recorded in methanol-*d*$_4$

[b] Acquired at 125 MHz, referenced to solvent signal CD_3OD at δ 49.15 ppm.

[c] Acquired at 500 MHz, referenced to solvent signal CD_3OD at δ 3.31 ppm.

[d] Proton showing COSY correlations to indicated protons.

[e] Proton showing HMBC correlations to indicated carbons.

NMR spectra were acquired with a Bruker Ultra Shield 500 NMR spectrometer equipped with a 5mm TCI probe head.

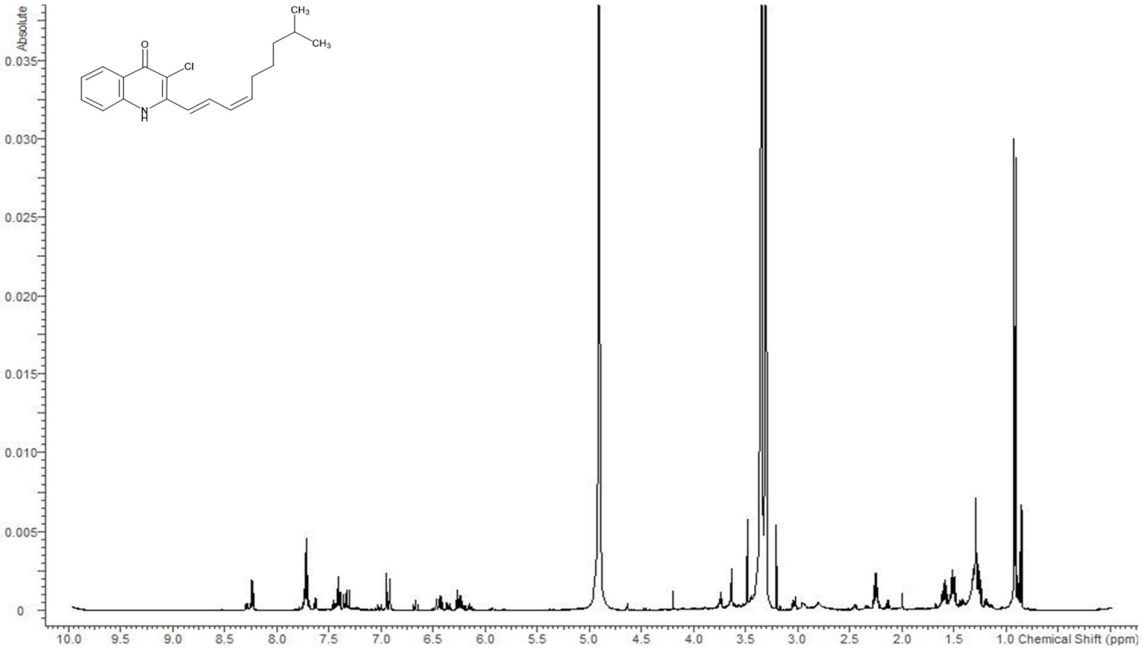

Figure S3.31: ^{1}H spectrum of Cpd-316 acquired in methanol-d_4 at 500 MHz.

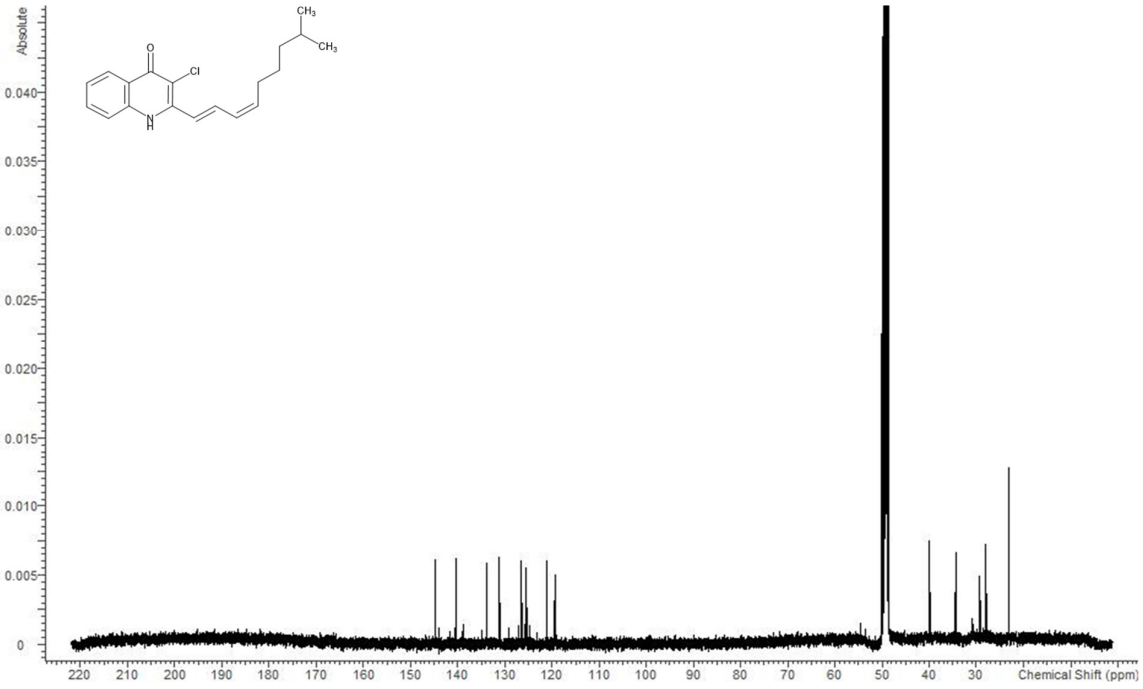

Figure S3.32: ^{13}C spectrum of Cpd-316 acquired in methanol-d_4 at 125 MHz.

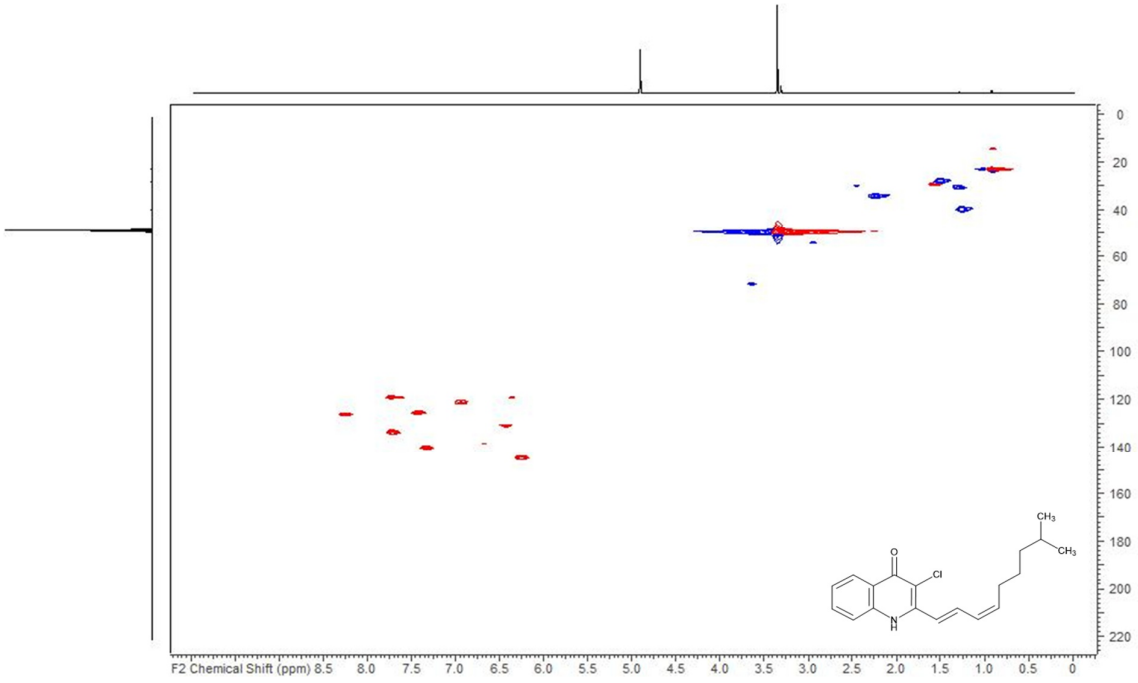

Figure S3.33: HSQC spectrum of Cpd-316 acquired in methanol-d_4 at 125/500 (F1/F2) MHz.

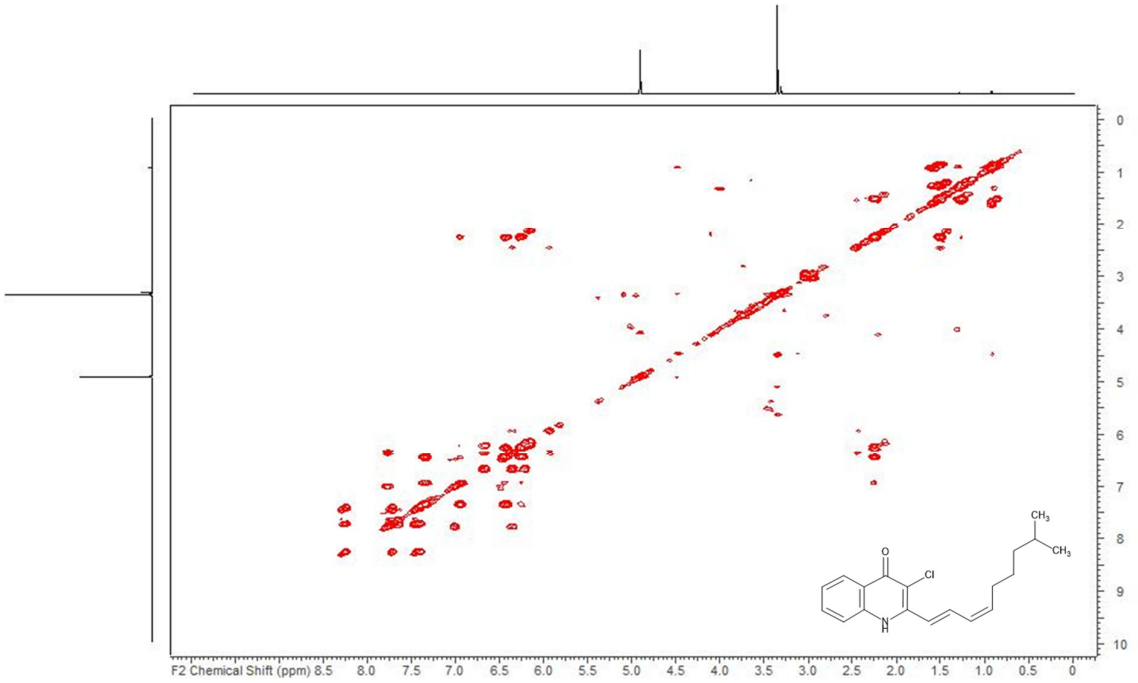

Figure S3.34: COSY spectrum of Cpd-316 acquired in methanol-d_4 at 500 MHz.

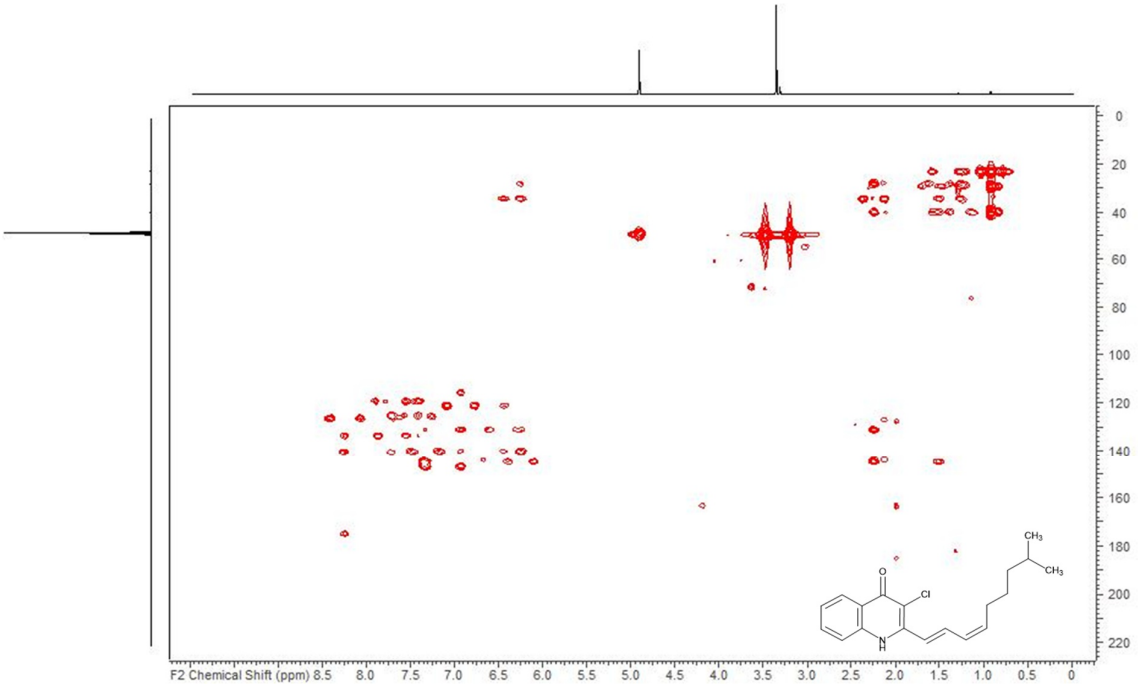

Figure S3.35: HMBC spectrum of Cpd-316 acquired in methanol-d_4 at 125/500 (F1/F2) MHz.

Table S3.9: NMR spectroscopic data for Cpd-548-1[a].

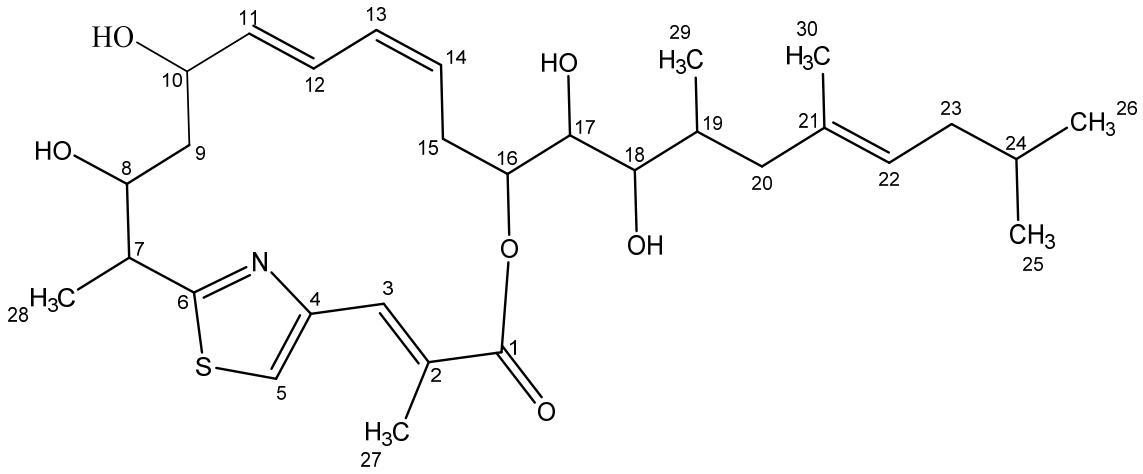

Position	δ ^{13}C[b]	δ ^{1}H[c], mult (J [Hz])	COSY[d]	HMBC[e]
1	169.2			
2	128.0			
3	135.7	8.08, m	5, 27	1, 2, 4, 5, 27
4	151.0			
5	120.5	7.66, s	3, 7, 27	2, 3, 4, 6
6	171.7			
7	42.8	3.71, dd (7.25, 3.43)	5, 8, 28	6, 8, 28
8	71.6	4.10, dt (10.95, 3.60, 3.60)	7, 9	6, 28
9a	44.7	1.57, m	8, 10	7, 8, 10, 11
9b	44.7	0.57, m	8, 10	7, 8, 10, 11
10	70.8	4. 73, br t (9.77, 9.77)	9, 11	8, 9, 11, 12
11	138.4	5.40, m	10, 12	9, 10, 13
12	127.4	6.65, m	11, 13	9, 10, 13, 14
13	132.7	5.92, m	12, 14, 15	11, 12, 15, 16
14	129.0	5.35, m	13, 15	12, 15, 16
15a	31.7	2.99, dt (14.06, 11.36, 11.36)	13, 14, 16	13, 14, 16
15b	31.7	2.30, m	13, 14, 16	13, 14, 16

16	76.2	5.03, dd (9.96, 3.78)	15, 17	1, 14, 15, 18
17	74.4	3.75, dd (5.99, 3.93)	16, 18	15, 16, 18, 19
18	74.5	3.52, dd (5.95, 3.74)	17, 19	16, 17, 19, 20, 29
19	34.1	2.05, m	18, 20, 29	18, 20, 29
20a	46.0	2.19, m	19	18, 19, 21, 22, 30
20b	46.0	1.85, m	19, 30	18, 19, 21, 22, 29, 30
21	135.2			
22	126.9	5.21, br t (6.94, 6.94)	23, 30	19, 20, 23, 24, 30
23	38.5	1.87, m	22, 24	20, 21, 22, 24, 25, 26
24	30.4	1.58, m	23, 25, 26	23, 25, 26
25	23.1	0.87, m	24	23, 24, 26
26	23.0	0.87, m	24	23, 24, 25
27	13.8	2.03, m	3, 5	1, 2, 3, 4, 5
28	16.7	1.51, d (7.25)	7	6, 7, 5
29	14.1	0.86, m	19	18, 19, 20
30	16.4	1.60, m	20, 22	20, 21, 22

[a] Recorded in methanol-d_4

[b] Acquired at 125 MHz, referenced to solvent signal CD_3OD at δ 49.15 ppm.

[c] Acquired at 500 MHz, referenced to solvent signal CD_3OD at δ 3.31 ppm.

[d] Proton showing COSY correlations to indicated protons.

[e] Proton showing HMBC correlations to indicated carbons.

NMR spectra were acquired with a Bruker Ultra Shield 500 NMR spectrometer equipped with a 5mm TCI probe head.

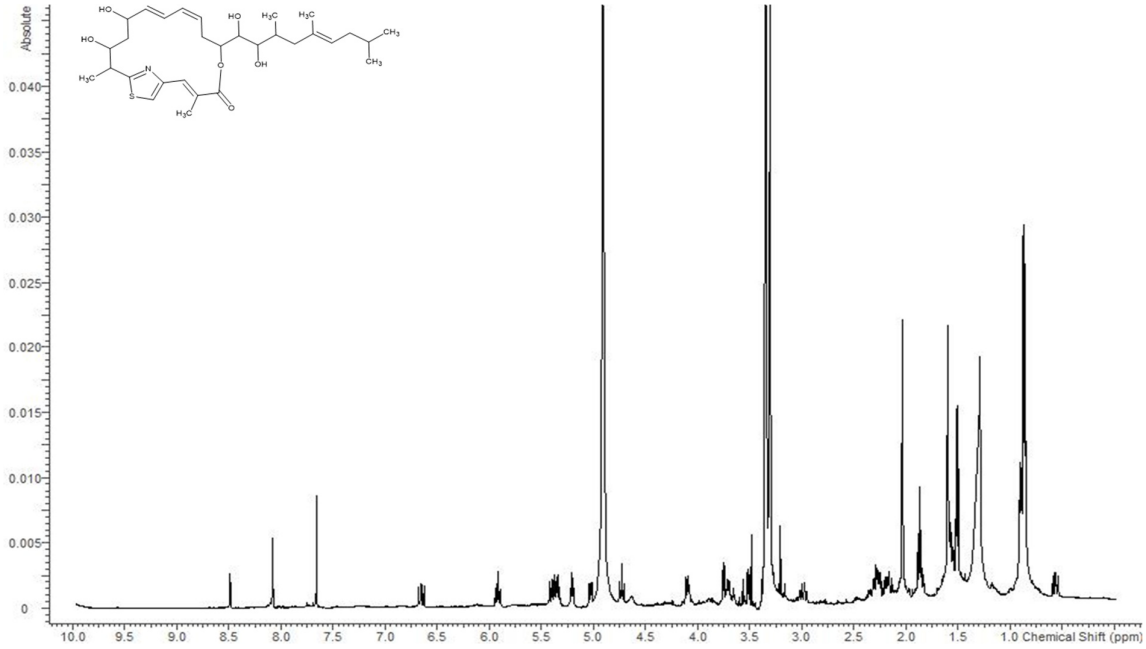

Figure S3.36: ^{1}H spectrum of Cpd-548-1 acquired in methanol-d_4 at 500 MHz.

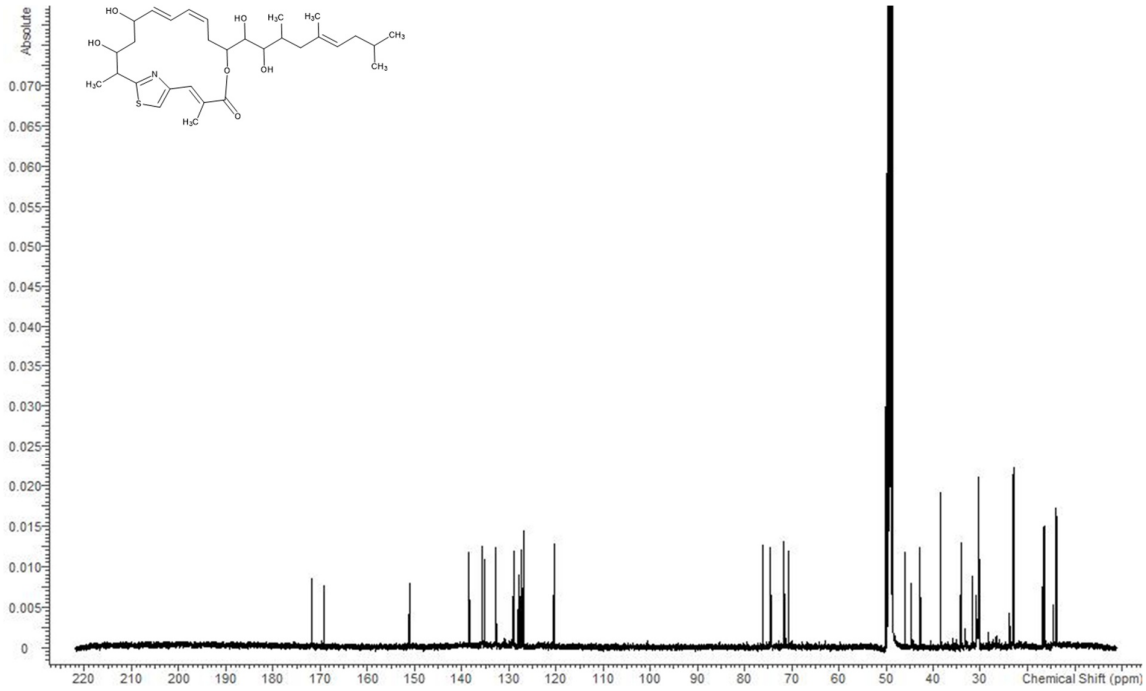

Figure S3.37: ^{13}C spectrum of Cpd-548-1 acquired in methanol-d_4 at 125 MHz.

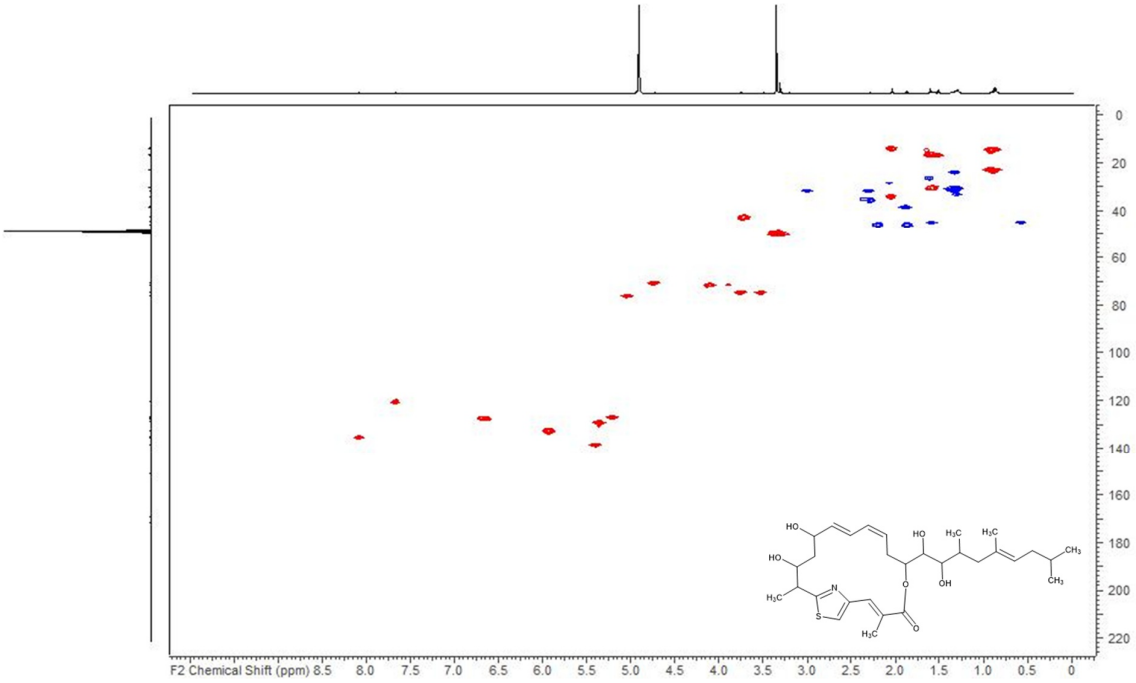

Figure S3.38: HSQC spectrum of Cpd-548-1 acquired in methanol-d_4 at 125/500 (F1/F2) MHz.

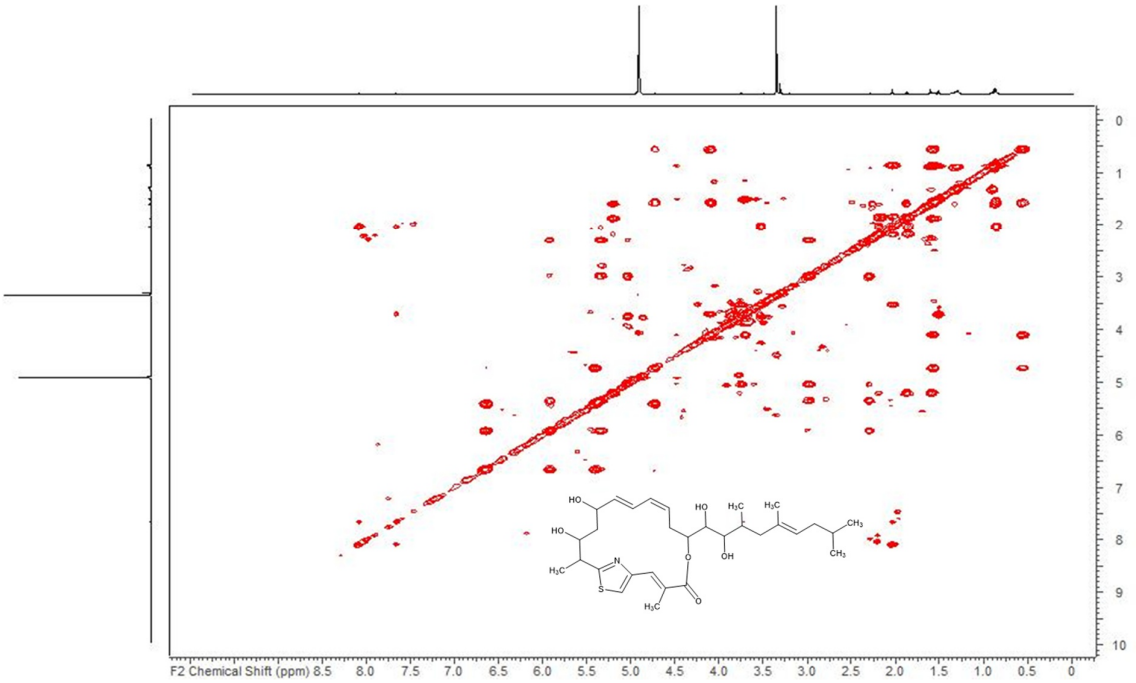

Figure S3.39: COSY spectrum of Cpd-548-1 acquired in methanol-d_4 at 500 MHz.

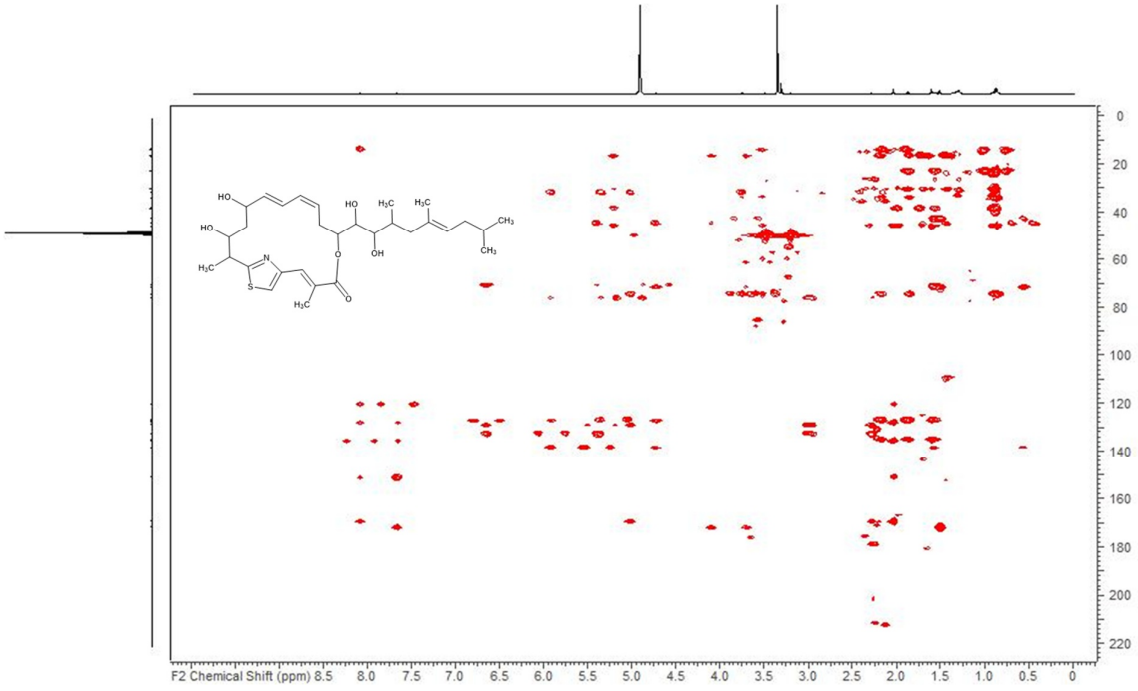

Figure S3.40: HMBC spectrum of Cpd-548-1 acquired in methanol-d_4 at 125/500 (F1/F2) MHz.

Table S3.10: NMR spectroscopic data for Cpd-564[a].

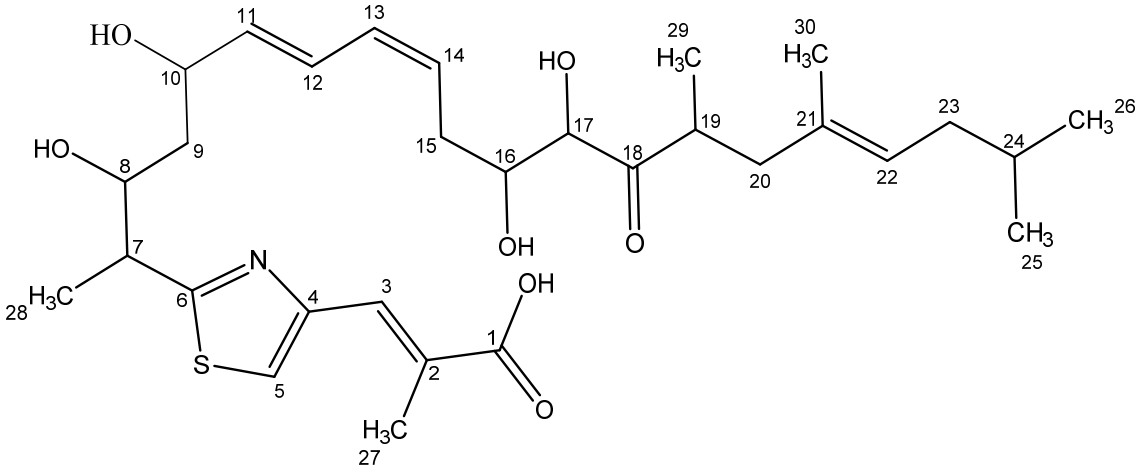

Position	δ ^{13}C[b]	δ ^{1}H[c], mult (J [Hz])	COSY[d]	HMBC[e]
1	172.7			
2	130.7			
3	131.7	7.64, d (0.92)	5, 27	1, 2, 4, 5, 27
4	152.6			
5	123.0	7.62, m	3, 7	3, 6, 7
6	174.4			
7	45.7	3.37, m	5, 8, 28	4, 6, 8, 9, 28
8	73.4	3.97, m	7, 9	6, 7, 9, 10, 28
9	42.4	1.63, m	8, 10	7, 8, 10, 11
10	71.9	4.38, q (6.92, 6.92, 6.92)	9, 11, 12	8, 9, 11, 12
11	137.4	5.62, dd (15.14, 7.13)	10, 12, 13	9, 10, 12, 13, 14
12	127.4	6.59, dd (15.14, 11.10)	10, 11, 13, 14	9, 10, 11, 13, 14, 15
13	131.7	6.11, t (11.06, 11.06)	11, 12, 14, 15	11, 12, 15, 16
14	128.8	5.51, m	12, 13, 15	12, 15, 16
15a	33.4	2.58, m	13, 14, 16	13, 14, 16, 17
15b	33.4	2.43, m	13, 14, 16	13, 14, 16, 17
16	73.4	3.98, m	15, 17	14, 15, 17, 18

17	79.2	4.10, d (2.14)	16	15, 16, 18
18	218.1			
19	40.5	3.23, m	20, 29	18, 20, 21, 29
20a	43.7	2.42, m	19, 22, 29, 30	18
20b	43.7	1.88, m	19, 22	18, 19, 21, 22, 29
21	134.2			
22	127.7	5.20, br t (7.32, 7.32)	20, 23, 30	20, 23, 24, 30
23	38.4	1.90, m	22, 24	21, 22, 24, 25, 26
24	30.3	1.58, m	23, 25, 26	23, 25, 26
25	23.0	0.89, m	24	22, 23, 24, 26
26	22.9	0.89, m	24	22, 23, 24, 25
27	15.0	2.28, d (1.30)	3	1, 2, 3, 4, 5
28	18.1	1.43, d (7.10)	7	6, 7, 8
29	16.2	0.98, d (6.87)	19, 20	18, 19, 20
30	16.2	1.61, m	20, 22	20, 21, 22, 24

[a] Recorded in methanol-d_4

[b] Acquired at 125 MHz, referenced to solvent signal CD_3OD at δ 49.15 ppm.

[c] Acquired at 500 MHz, referenced to solvent signal CD_3OD at δ 3.31 ppm.

[d] Proton showing COSY correlations to indicated protons.

[e] Proton showing HMBC correlations to indicated carbons.

NMR spectra were acquired with a Bruker Ultra Shield 500 NMR spectrometer equipped with a 5mm TCI probe head.

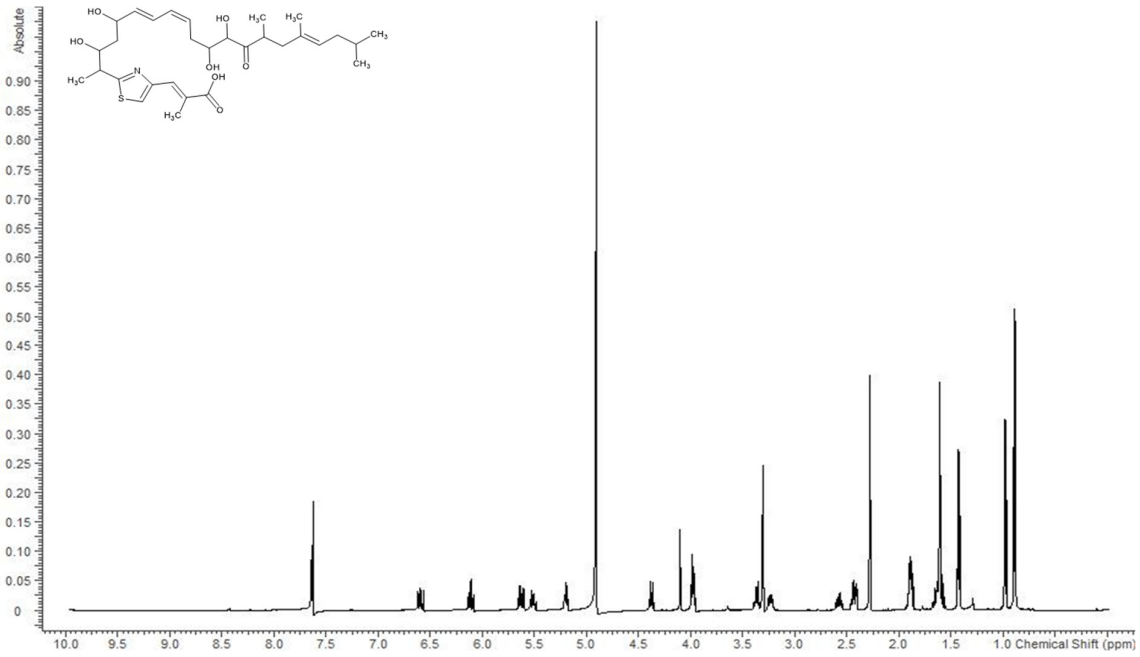

Figure S3.41: ^{1}H spectrum of Cpd-564 acquired in methanol-d_4 at 500 MHz.

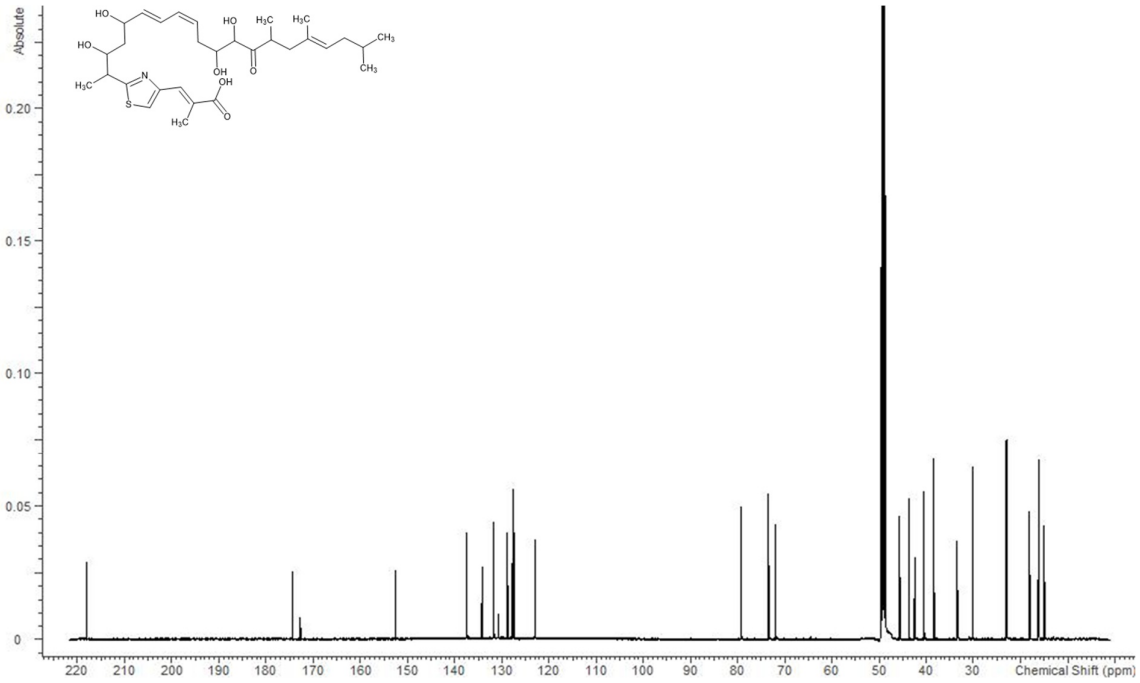

Figure S3.42: ^{13}C spectrum of Cpd-564 acquired in methanol-d_4 at 125 MHz.

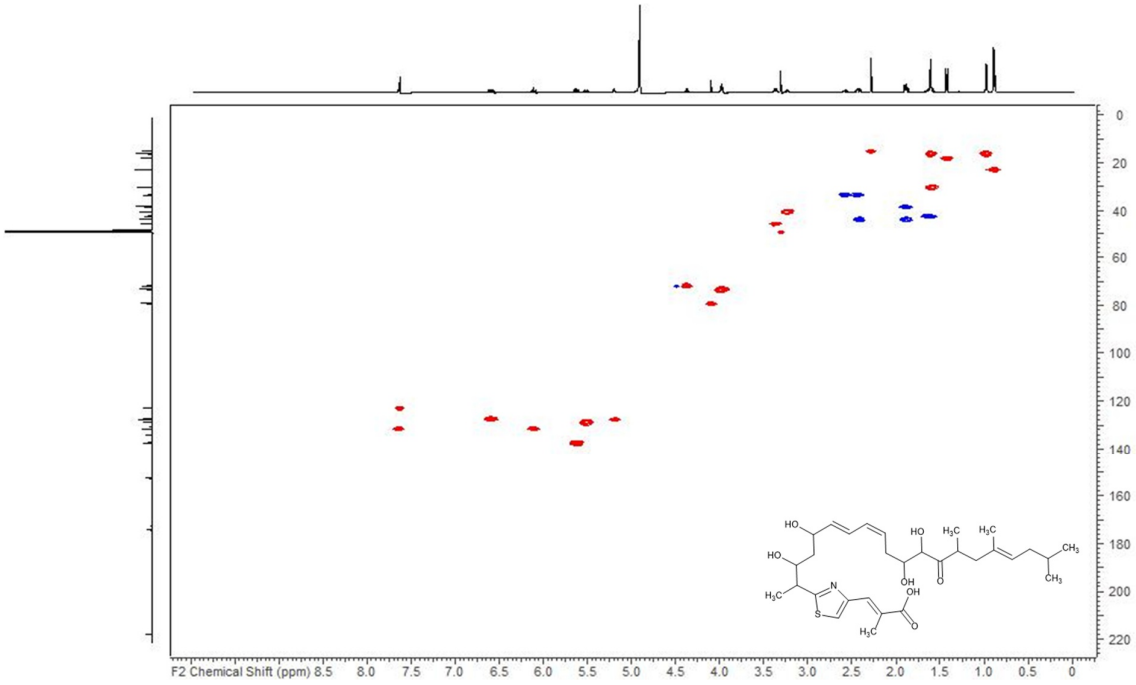

Figure S3.43: HSQC spectrum of Cpd-564 acquired in methanol-d_4 at 125/500 (F1/F2) MHz.

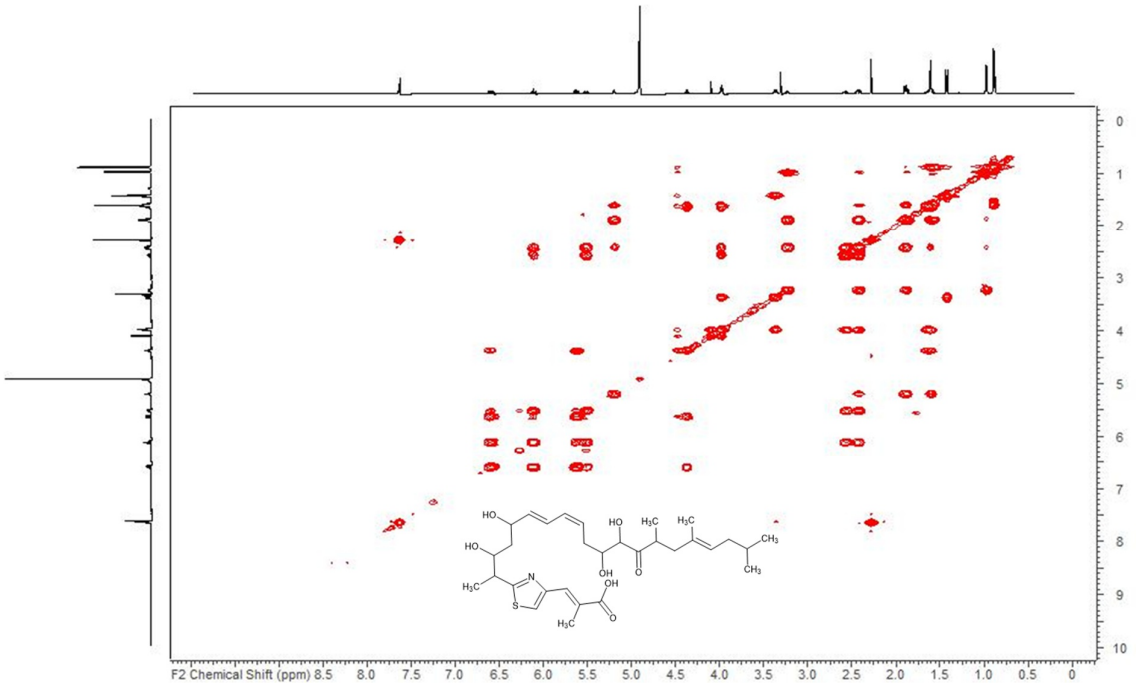

Figure S3.44: COSY spectrum of Cpd-564 acquired in methanol-d_4 at 500 MHz.

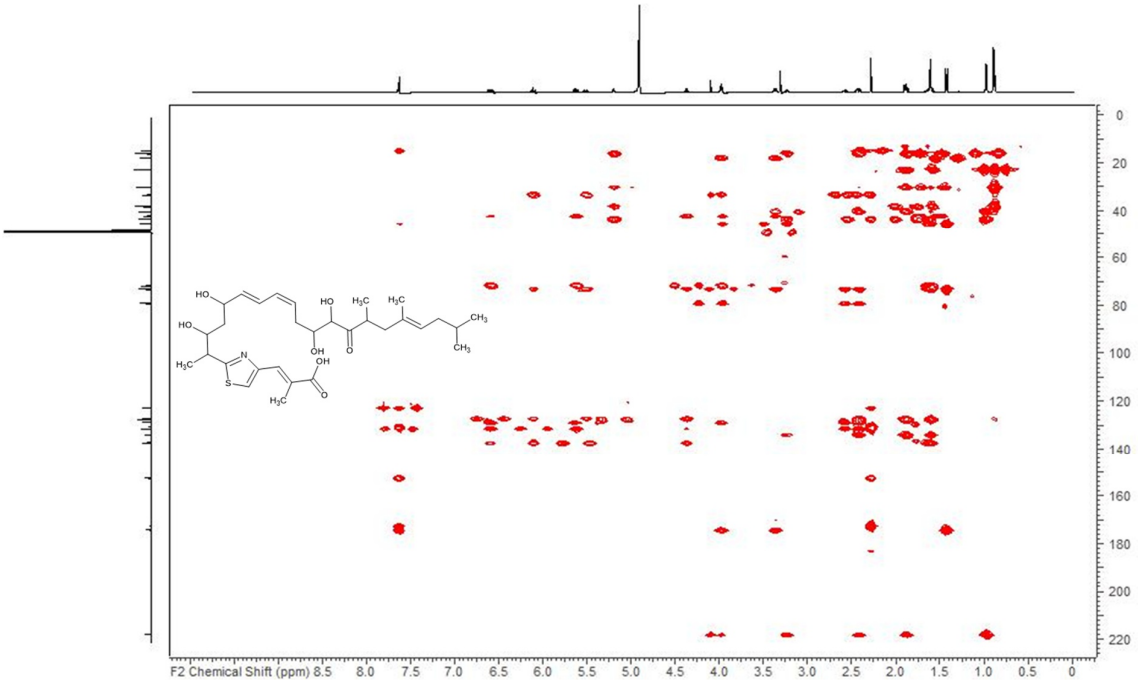

Figure S3.45: HMBC spectrum of Cpd-564 acquired in methanol-d_4 at 125/500 (F1/F2) MHz.

Table S3.11: NMR spectroscopic data for Cpd-566[a].

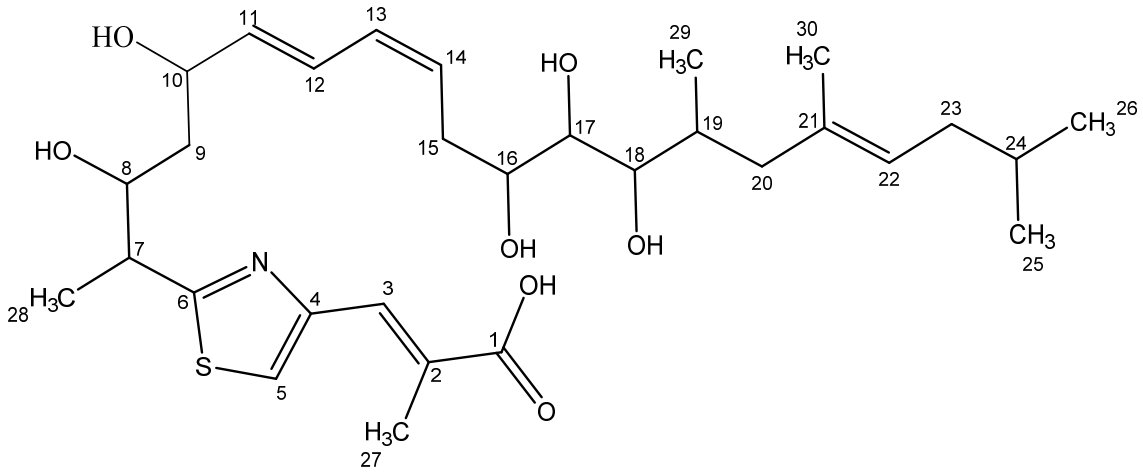

Position	δ ^{13}C[b]	δ ^{1}H[c], mult (J [Hz])	COSY[d]	HMBC[e]
1	173.5			
2	131.7			
3	131.1	7.60, d (0.99)	27	1, 2, 5, 27
4	152.8			
5	122.5	7.59, m	7	3, 4, 6, 7
6	174.3			
7	45.7	3.37, m	5, 8, 28	6, 8, 9, 28
8	73.4	3.98, m	7, 9	6, 7, 9, 10, 28
9	42.4	1.61, m	8, 10	8, 10, 11
10	71.9	4.37, q (6.87, 6.87, 6.87)	9, 11, 12	9, 8, 11, 12, 13
11	137.2	5.61, dd (15.11, 7.10)	10, 12, 13	9, 10, 13, 14
12	127.5	6.58, m	10, 11, 13, 14	9, 10, 11, 13, 14
13	131.3	6.10, m	11, 12, 14 ,15	11, 12, 15, 16
14	129.3	5.53, m	12, 13, 15	12, 15, 16
15a	33.4	2.53, m	13, 14, 16	13, 14, 16, 17
15b	33.4	2.41, m	13, 14, 16	13, 14, 16, 17
16	73.5	3.66, m	15, 17	14, 15

17	74.4	3.45, m	16, 18	15, 18
18	76.6	3.47, m	17, 19	16, 17, 19, 20, 29
19	34.2	1.91, m	18, 20, 29	18, 20, 29
20a	45.7	2.18, br dd (12.78, 5.15)	19, 22, 30	18, 19, 21, 22, 29, 30
20b	45.7	1.82, m	19, 22	18, 19, 21, 22, 23, 29, 30
21	135.3			
22	126.8	5.19, br t (6.98, 6.98)	20, 23, 30	20, 23, 24, 30
23	38.4	1.90, m	22, 24	21, 22, 24 25, 26
24	30.4	1.59, m	23, 25, 26	23, 25, 26, 30
25	23.0	0.90, d (2.06)	24	23, 24, 26
26	23.1	0.89, d (2.06)	24	23, 24, 25
27	15.2	2.28, d (1.22)	3	1, 2, 3, 4, 5
28	18.1	1.42, d (7.10)	7	6, 7, 8
29	14.2	0.82, d (6.71)	19	18, 19, 20
30	16.2	1.58, m	20, 22	20, 21, 22, 24

[a] Recorded in methanol-d_4

[b] Acquired at 125 MHz, referenced to solvent signal CD_3OD at δ 49.15 ppm.

[c] Acquired at 500 MHz, referenced to solvent signal CD_3OD at δ 3.31 ppm.

[d] Proton showing COSY correlations to indicated protons.

[e] Proton showing HMBC correlations to indicated carbons.

NMR spectra were acquired with a Bruker Ultra Shield 500 NMR spectrometer equipped with a 5mm TCI probe head.

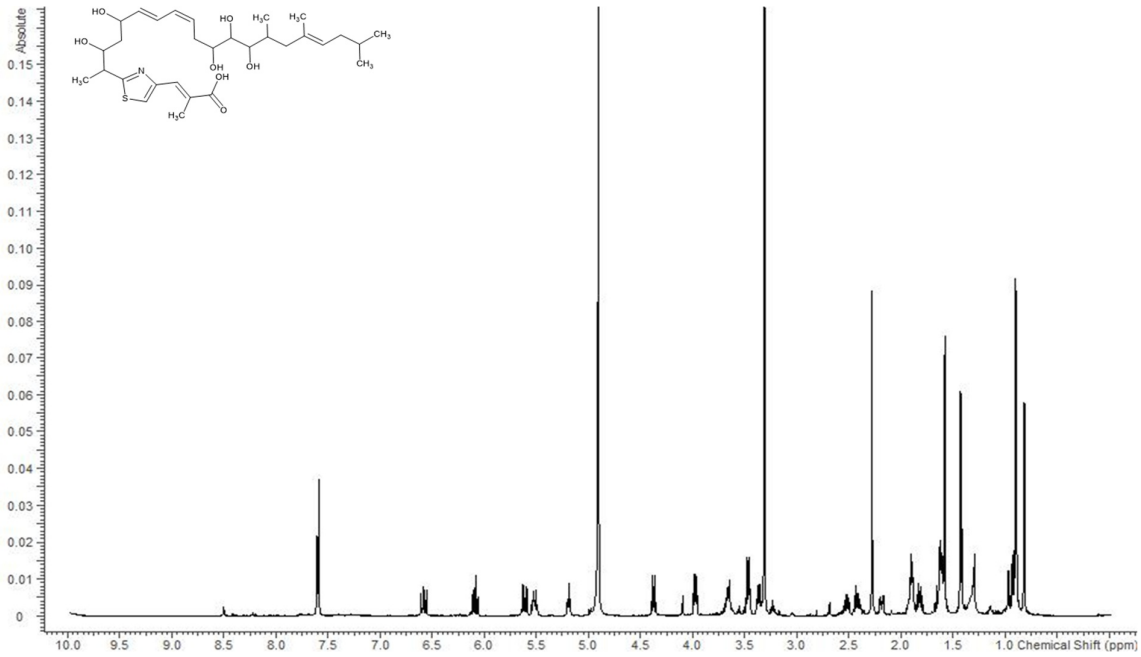

Figure S3.46: ^{1}H spectrum of Cpd-566 acquired in methanol-d_4 at 500 MHz.

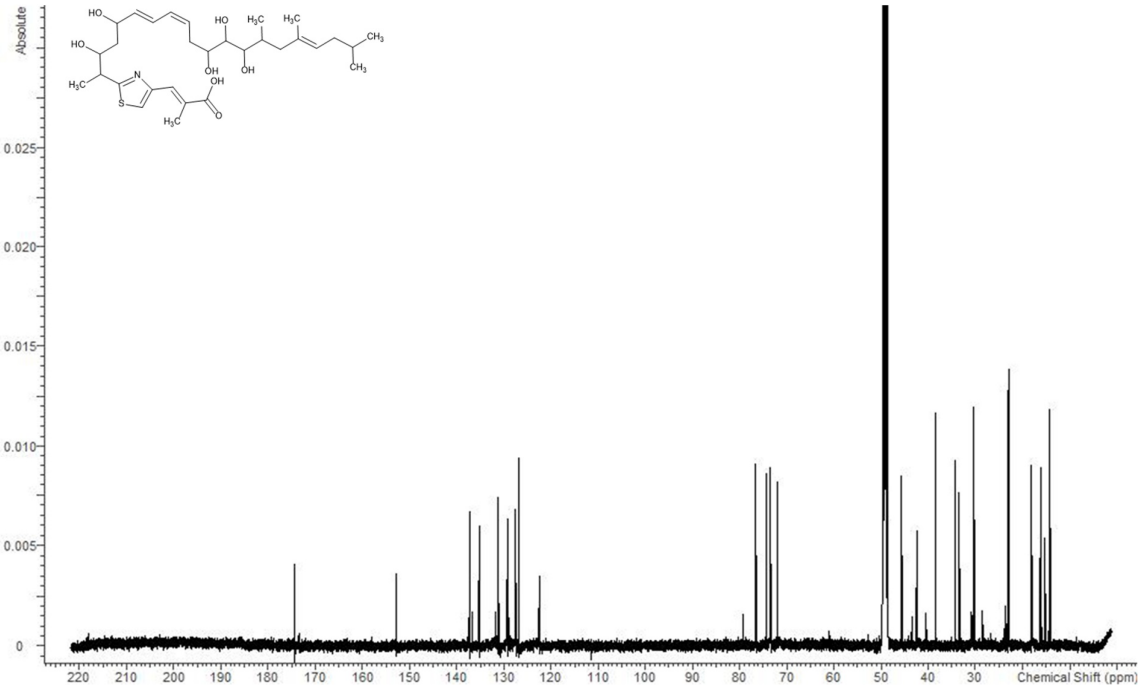

Figure S3.47: ^{13}C spectrum of Cpd-566 acquired in methanol-d_4 at 125 MHz.

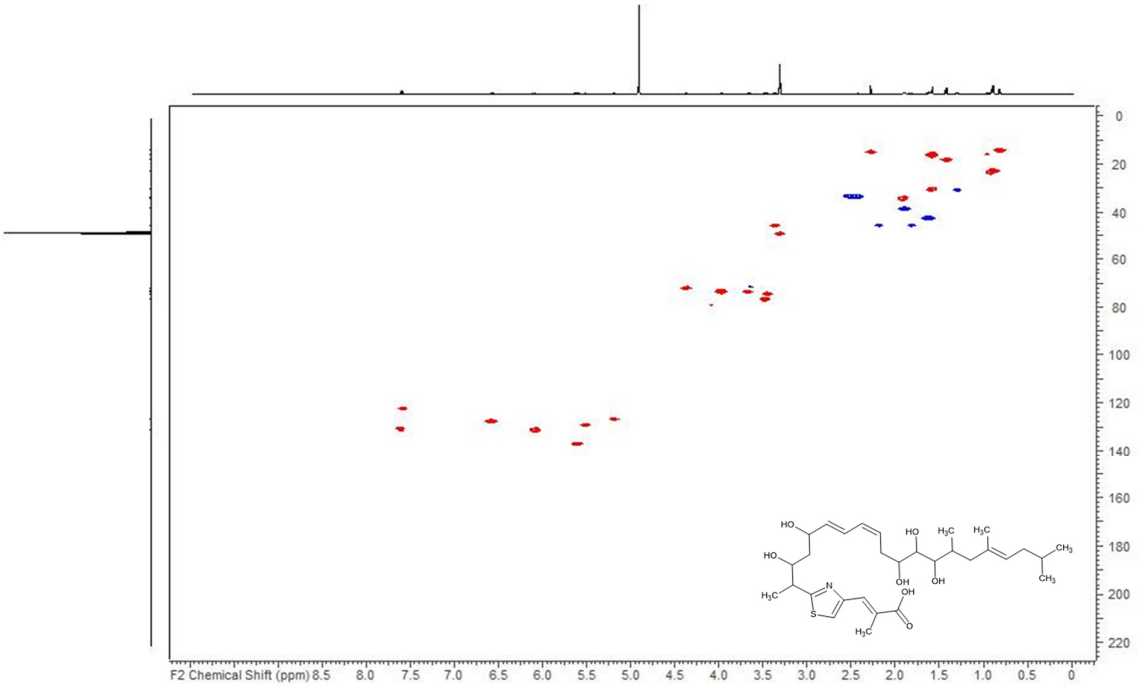

Figure S3.48: HSQC spectrum of Cpd-566 acquired in methanol-d_4 at 125/500 (F1/F2) MHz.

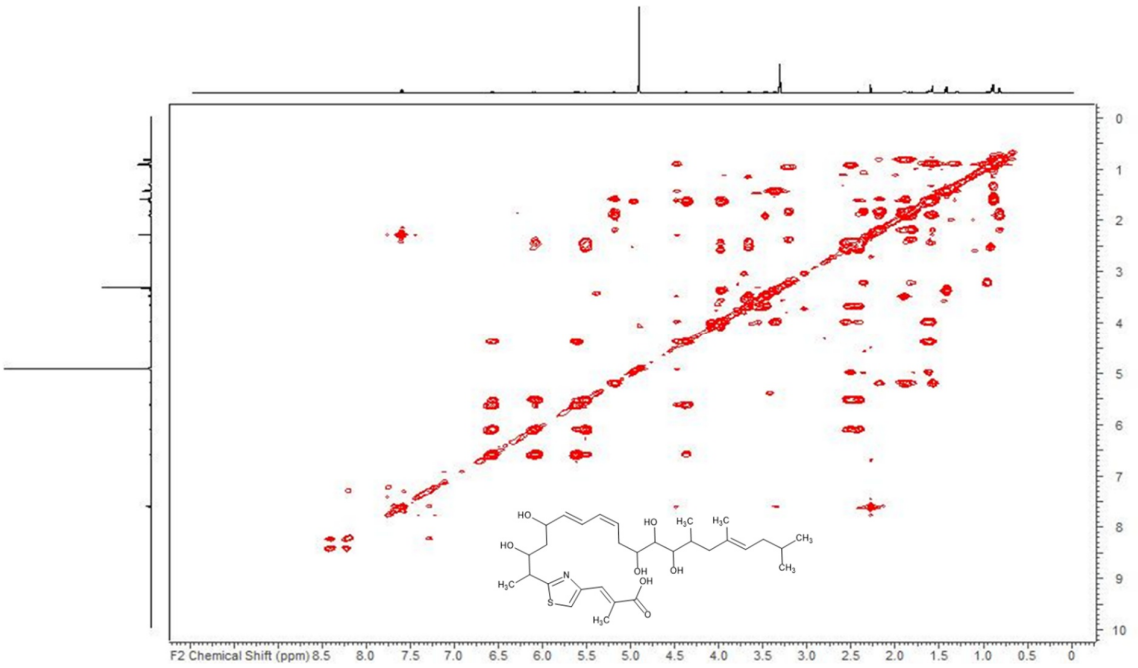

Figure S3.49: COSY spectrum of Cpd-566 acquired in methanol-d_4 at 500 MHz.

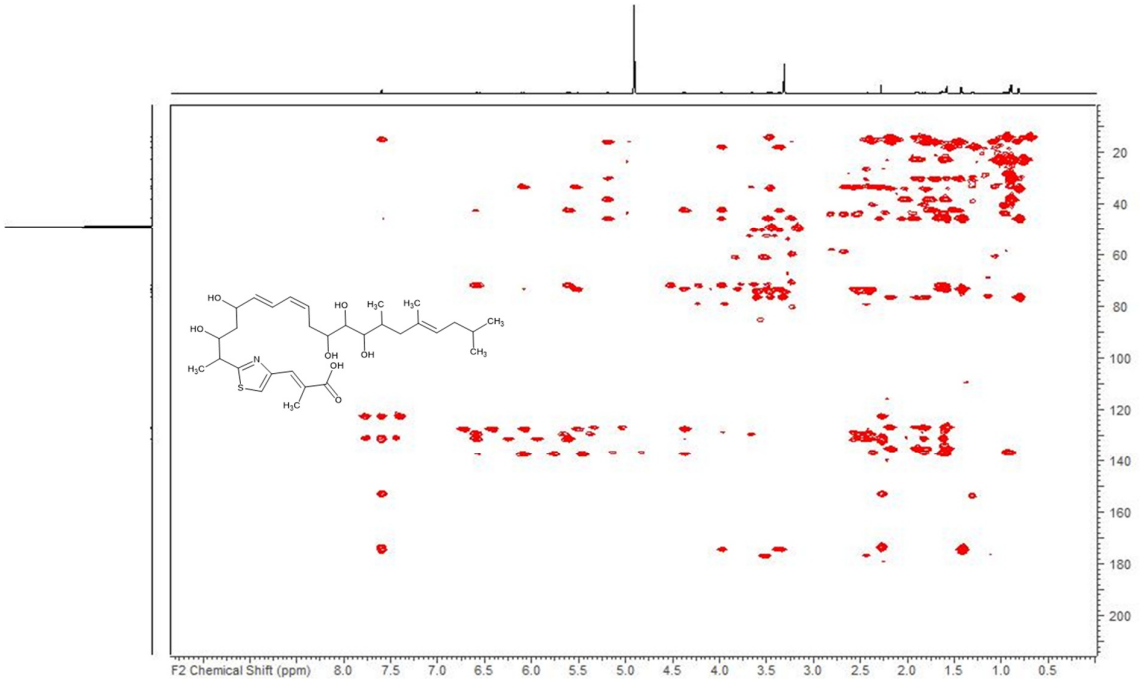

Figure S3.50: HMBC spectrum of Cpd-566 acquired in methanol-d_4 at 125/500 (F1/F2) MHz.

Table S3.12: NMR spectroscopic data for Cpd-578[a].

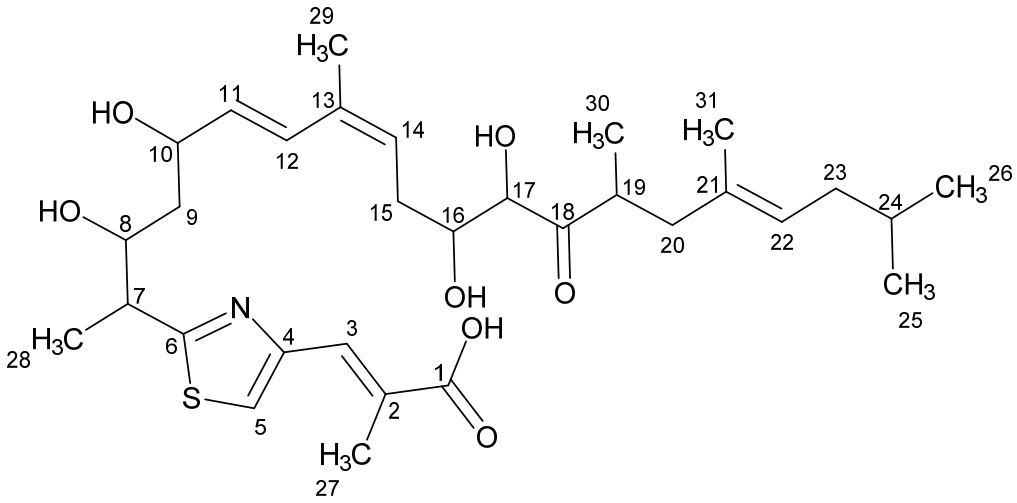

Position	δ ^{13}C[b]	δ ^{1}H[c], mult (J [Hz])	COSY[d]	HMBC[e]
1	175.4			
2	134.5			
3	129.3	7.51, m	27	1, 2, 4, 5, 27
4	153.3			
5	121.2	7.51, m		3, 6, 7
6	174.0			
7	45.6	3.37, dd (7.13, 4.23)	8, 28	6, 8, 28
8	73.5	3.99, m	7, 9	6, 7, 9, 10, 28
9	42.5	1.64, m	8, 10	7, 8, 10, 11
10	72.5	4.40, q (6.87, 6.87, 6.87)	9, 11, 12	9, 8, 11, 12, 13
11	133.6	5.63, dd (15.60, 7.13)	10, 12	9, 10, 12, 13, 14
12	128.9	6.71, d (15.56)	10, 11, 14	9, 10, 11, 13, 14, 29
13	135.2			
14	127.6	5.46, t (7.44, 7.44)	12, 15, 29	12, 13, 15, 16, 29
15a	33.1	2.55, dt (14.44, 7.24, 7.24)	14, 16	13, 14, 16, 17, 29
15b	33.1	2.42, m	14, 16	13, 14, 16, 17, 29

16	73.7	3.97, m	15, 17	14, 15, 7, 18
17	79.3	4.08, d (2.14)	16	15, 16, 18
18	218.3			
19	40.4	3.24, td (4.69, 4.69, 2.14)	20, 30	18, 20, 21, 30
20a	43.7	2.42, m	19, 22, 31	18, 19, 21, 30
20b	43.7	1.88, m	19, 22, 31	18, 19, 21, 30
21	134.2			
22	127.7	5.19, m	20, 23, 31	20, 23, 24
23	38.4	1.89, m	22, 24	21, 22, 24, 25, 26
24	30.3	1.59, m	23, 25, 26	23, 25, 26
25	22.9	0.89, m	24	22, 23, 24, 26
26	23.0	0.89, m	24	22, 23, 24, 25
27	15.7	2.26, d (1.30)	3	1, 2, 3, 4, 5
28	17.9	1.43, d (7.10)	7	6, 7, 8
29	21.1	1.83, s	14	12, 13, 14, 15, 16
30	16.1	0.97, d (6.87)	19	18, 19, 20
31	16.2	1.61, m	20, 22	20, 21, 22, 24

[a] Recorded in methanol-d_4

[b] Acquired at 125 MHz, referenced to solvent signal CD_3OD at δ 49.15 ppm.

[c] Acquired at 500 MHz, referenced to solvent signal CD_3OD at δ 3.31 ppm.

[d] Proton showing COSY correlations to indicated protons.

[e] Proton showing HMBC correlations to indicated carbons.

NMR spectra were acquired with a Bruker Ultra Shield 500 NMR spectrometer equipped with a 5mm TCI probe head.

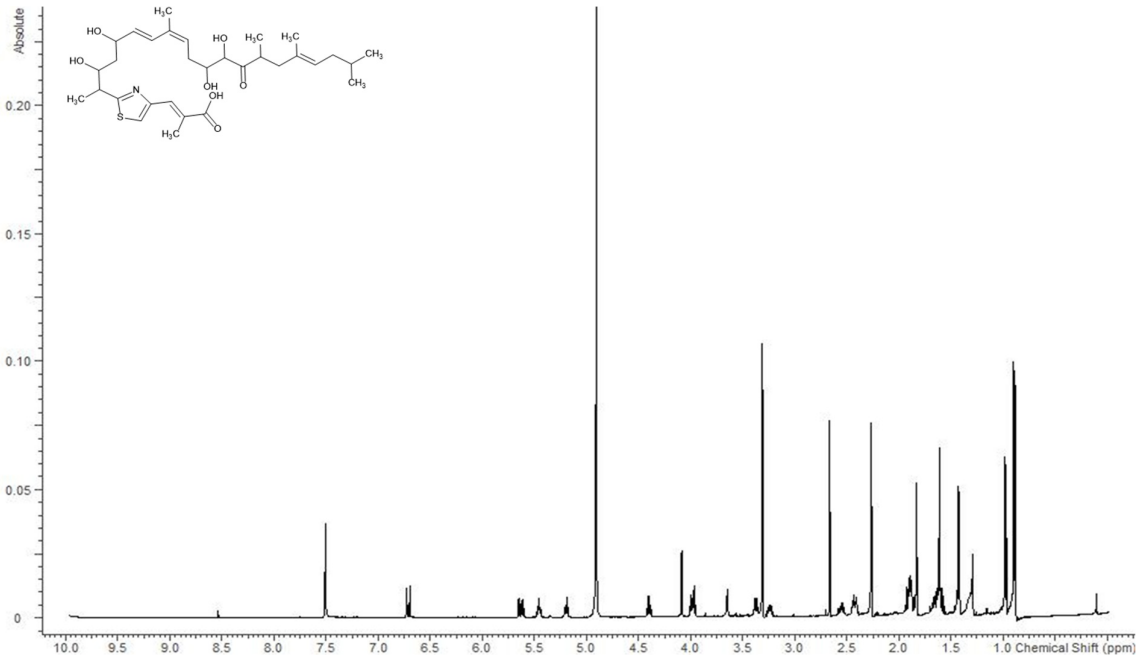

Figure S3.51: ^{1}H spectrum of Cpd-578 acquired in methanol-d_4 at 500 MHz.

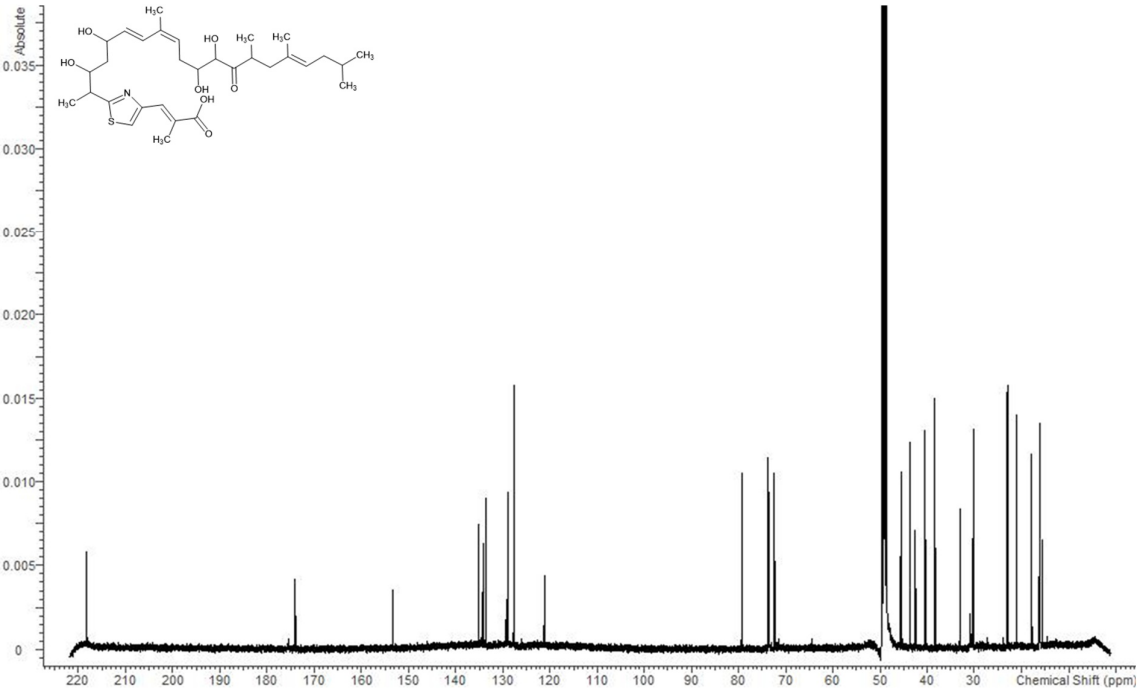

Figure S3.52: ^{13}C spectrum of Cpd-578 acquired in methanol-d_4 at 125 MHz.

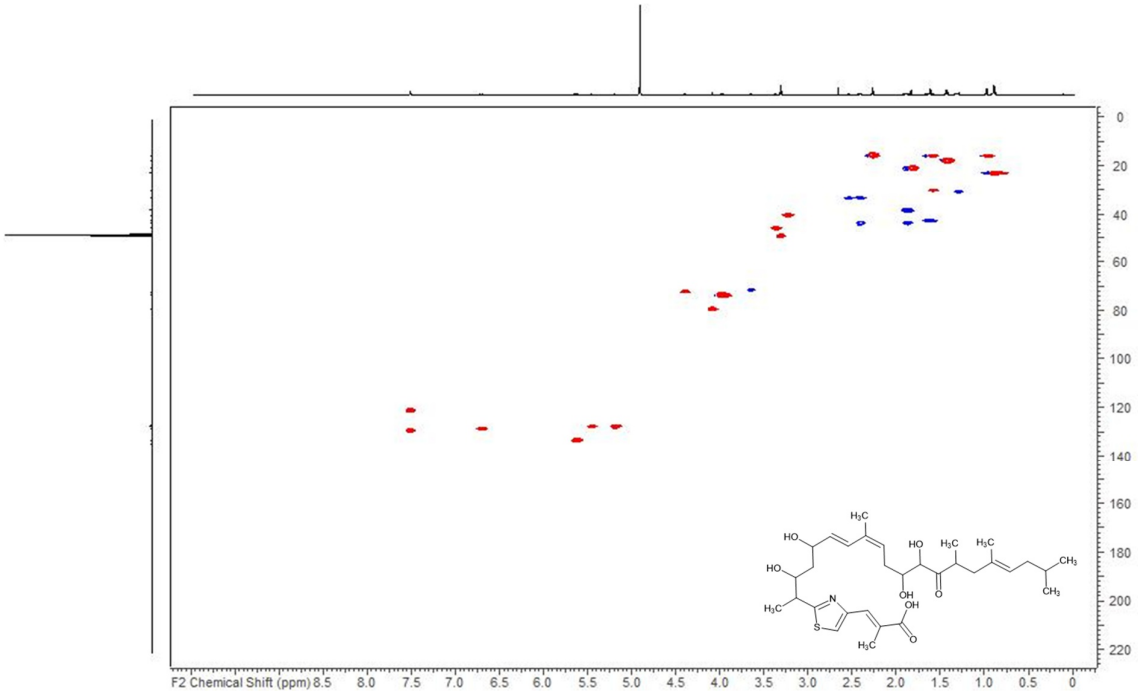

Figure S3.53: HSQC spectrum of Cpd-578 acquired in methanol-d_4 at 125/500 (F1/F2) MHz.

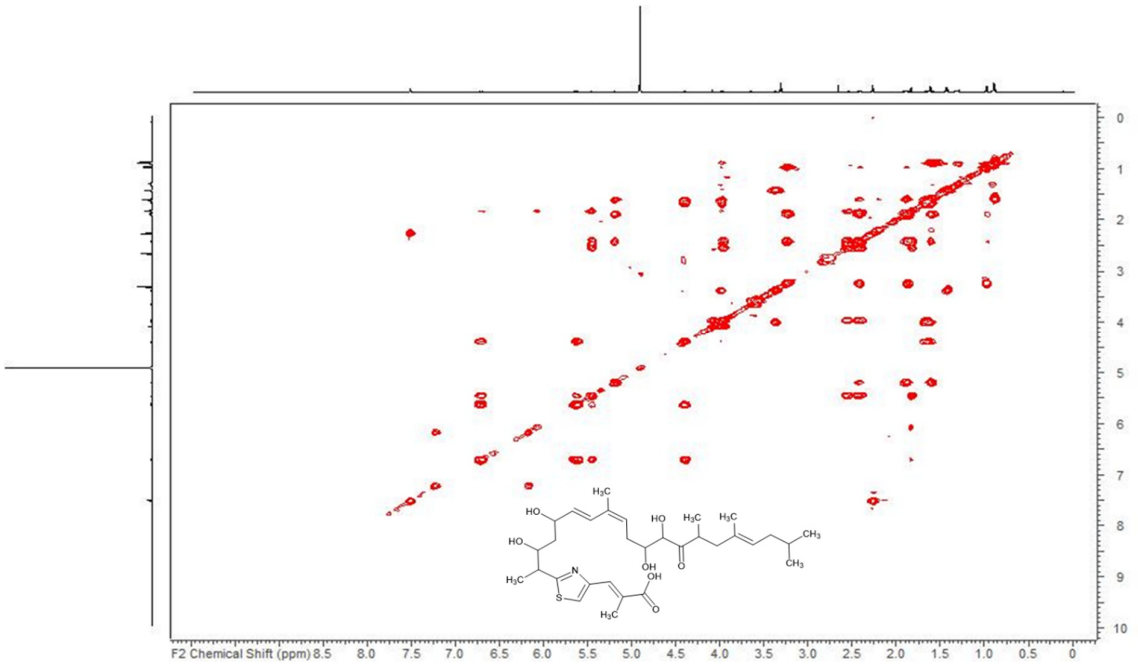

Figure S3.54: COSY spectrum of Cpd-578 acquired in methanol-d_4 at 500 MHz.

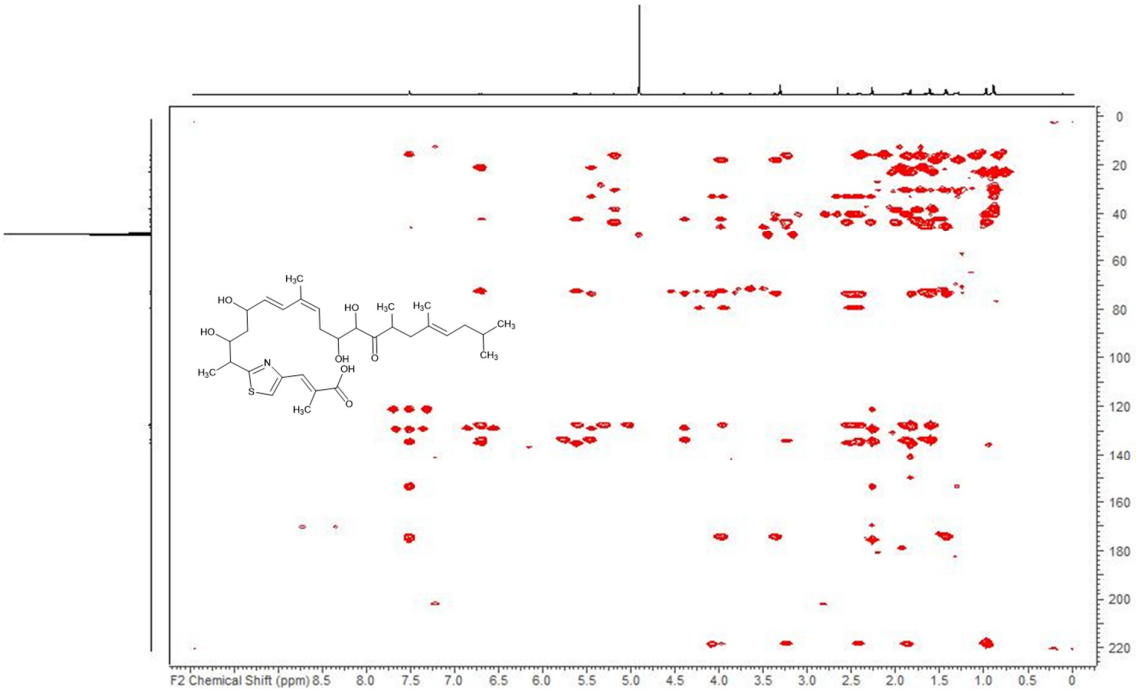

Figure S3.55: HMBC spectrum of Cpd-578 acquired in methanol-d_4 at 125/500 (F1/F2) MHz.

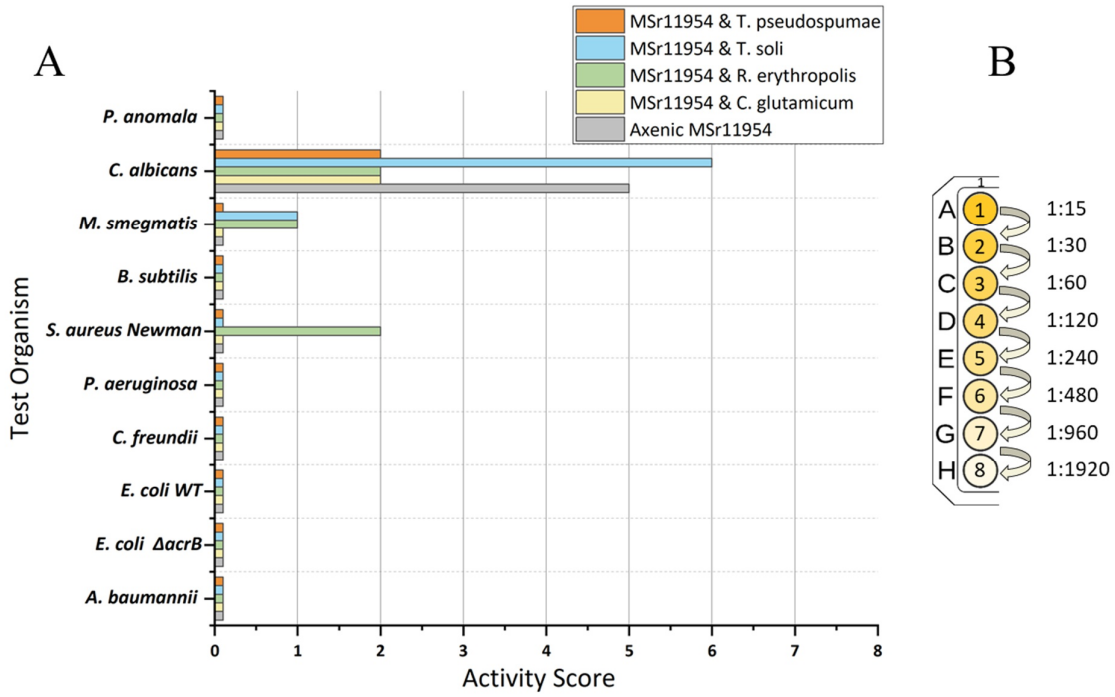

Figure S3.56: (**A**) Antimicrobial activity score of crude extracts after co-cultivation of MSr1954 with *C. glutamicum, R. erythropolis, T. soli* and *T. pseudospumae* in comparison to axenic culture (grey) as control. (**B**) Activity score with correlation between the concentration of the crude extract by serial dilution and biological inhibition of the test organism.

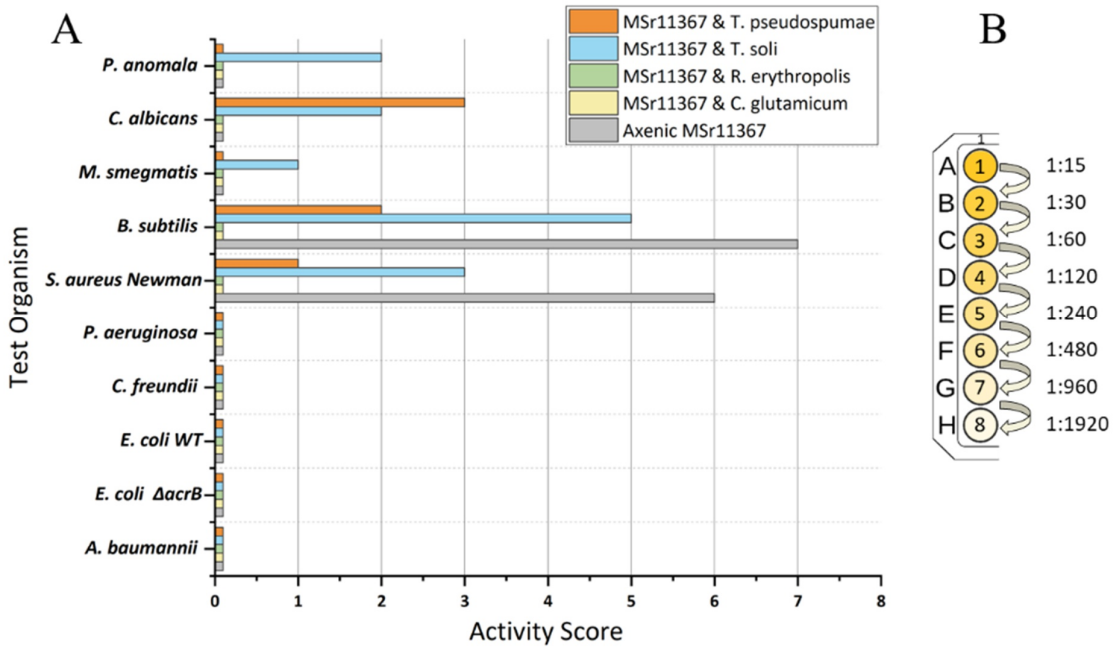

Figure S3.57: (**A**) Antimicrobial activity score of crude extracts after co-cultivation of MSr11367 with *C. glutamicum, R. erythropolis, T. soli* and *T. pseudospumae* in comparison to axenic culture (grey) as control. (**B**) Activity score with correlation between the concentration of the crude extract by serial dilution and biological inhibition of the test organism.

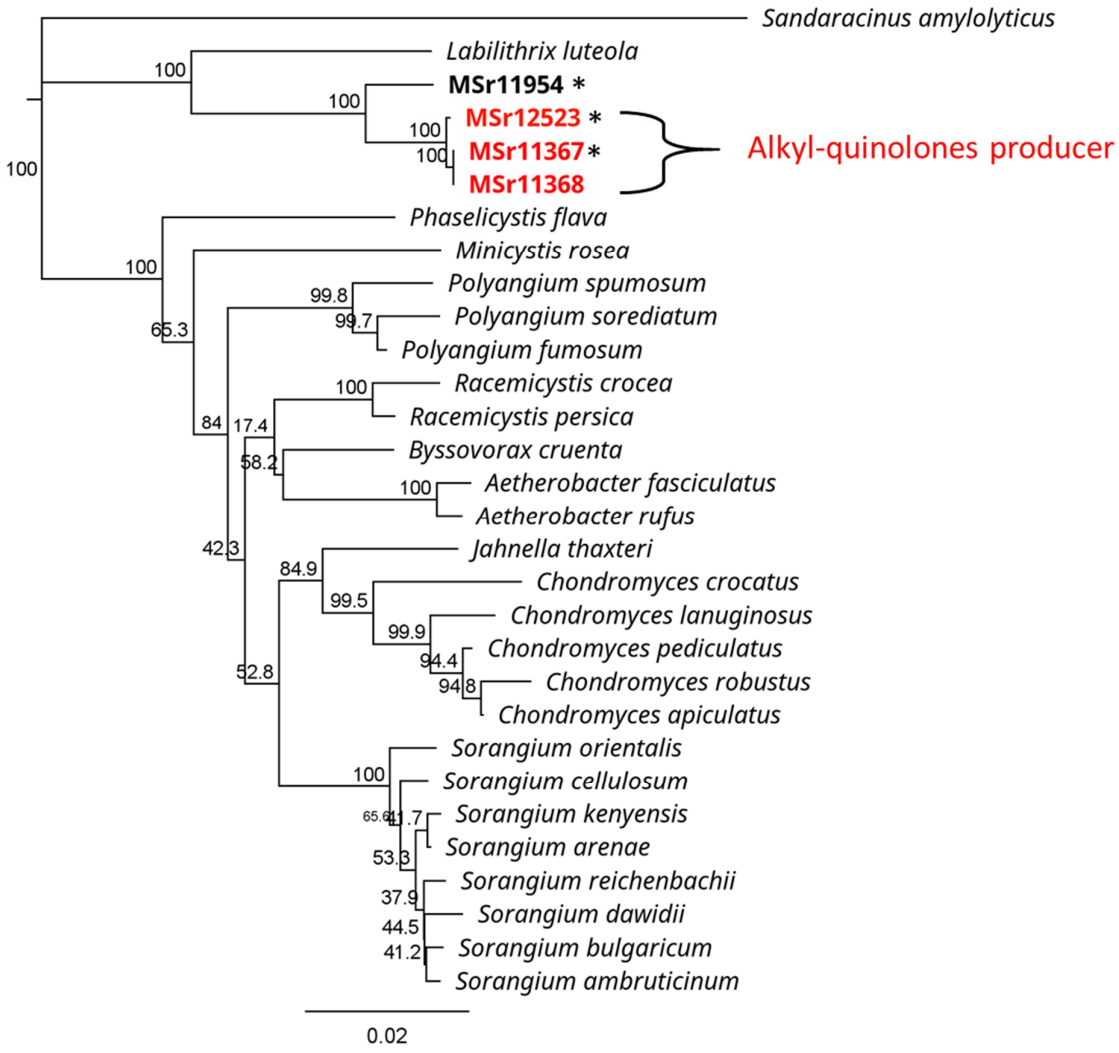

Figure S3.58: Phylogenetic reconstruction of the suborder Sorangiineae based on the neighbour-joining algorithm. Alkyl-quinolone producing *Sorangium sp.* strains are highlighted in red, and the strains used in our study are marked with a star.

Table S3.13: Overview of BLAST search of proteins and their functions from thuggacin BGC in *Sorangium sp.* MSr12523.

Protein	aa	Proposed function of the homologues protein	Source of the homologues protein	Percent Identity	Accession Number
Thg1	4.305	TgaA	*Sorangium cellulosum*	60.2 %	ADH04639.1
Thg2	6.184	type I polyketide synthase	*Kibdelosporangium aridum*	48.2 %	WP_084425507.1
Thg3	6.365	TgaC	*Sorangium cellulosum*	63.5 %	ADH04641.1
Thg4	367	LLM class flavin-dependent oxidoreductase	*Chondromyces crocatus*	78.1 %	WP_063796353.1

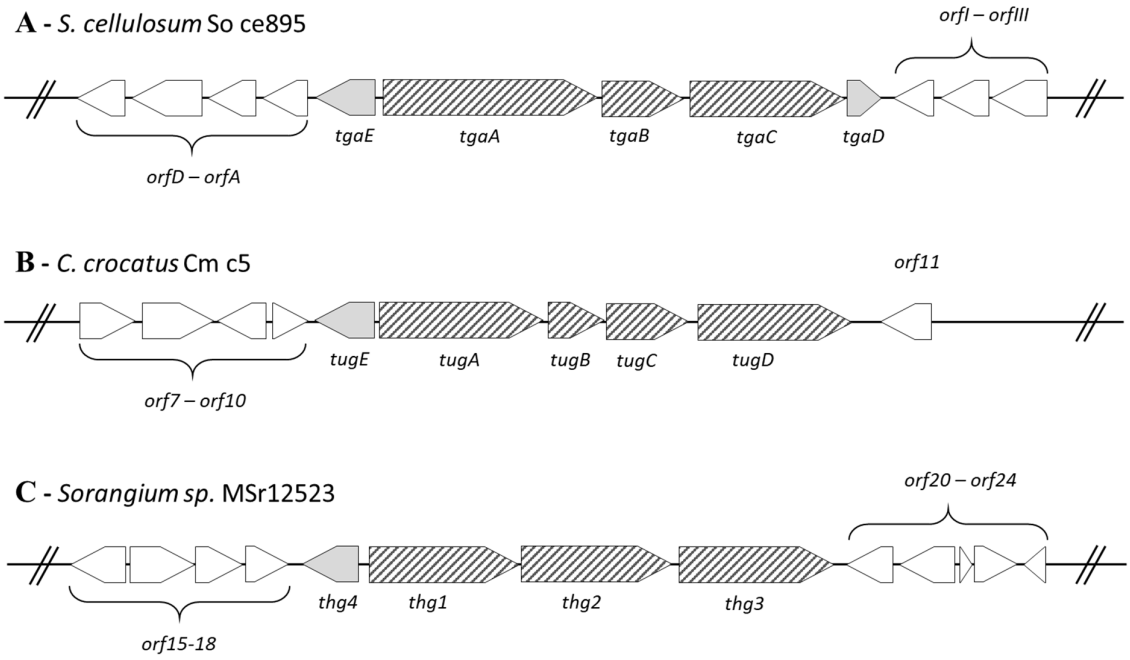

Figure S3.59: Schematic representation of the thuggacin biosynthetic locus in *Sorangium cellulosum* So ce895, *Chondromyces crocatus* Cm c5[2] and the proposed BGC of *Sorangium sp.* MSr12523. Light grey: genes likely involved in the biosynthetic pathways; white: genes not involved in biosynthesis; hatches: PKS and NRPS genes. Scheme adapted and extended from Buntin *et al.*[2].

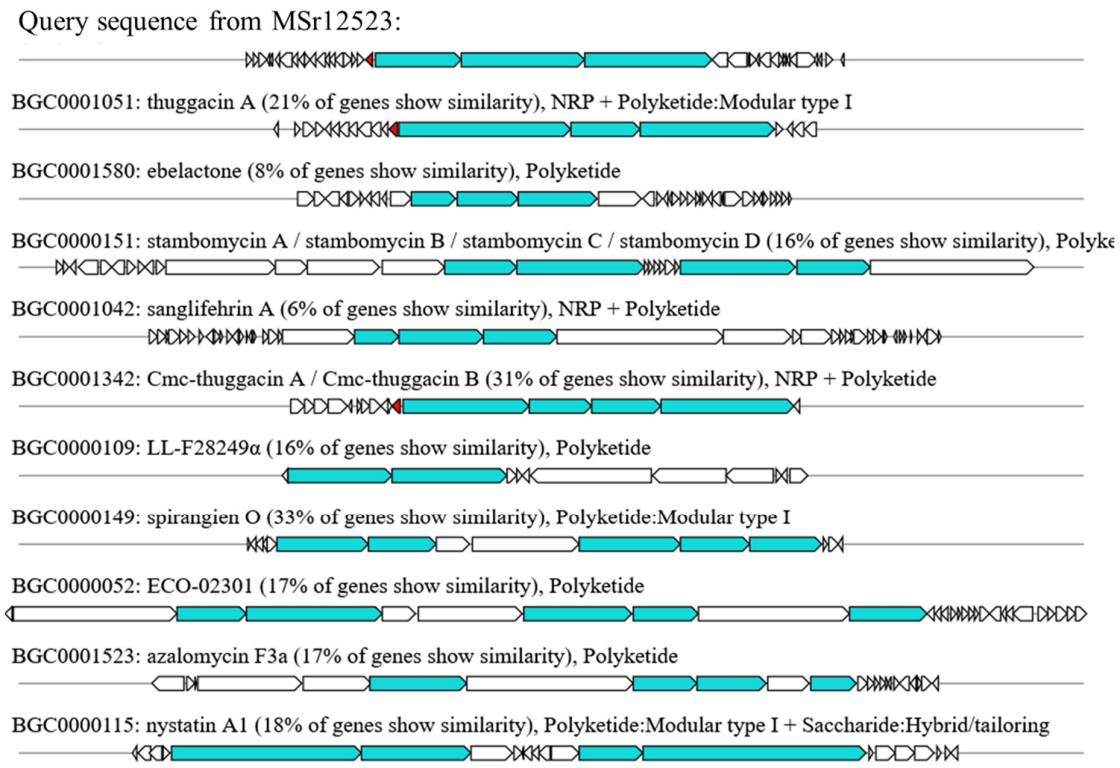

Figure S3.60: Sequence alignment to search for homologues BGCs with "KnownClusterBlast" from the annotated thuggacin BGC of *Sorangium sp.* MSr12523. Coloured genes are the putative homologues due to their blast hits.

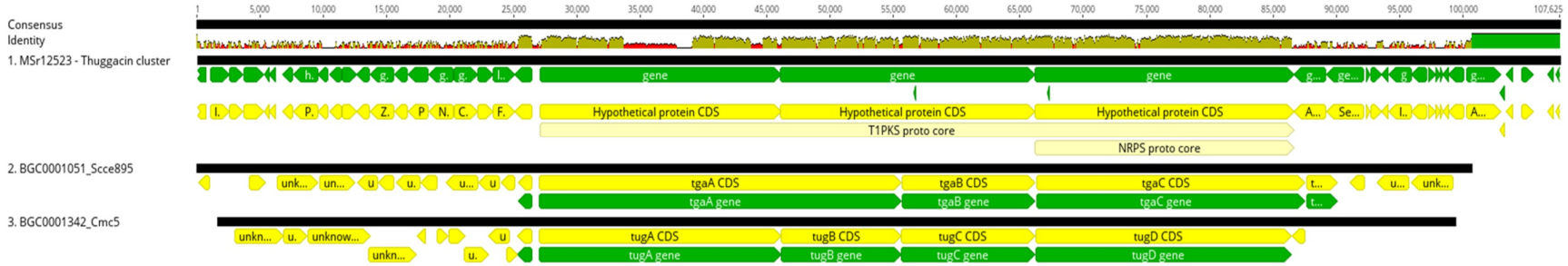

Figure S3.61: Alignment view of sequences from BGC0001051: *tga* (*S. cellulosum* So ce895), BGC0001342: *tug* (*C. crocatus* Cm c5) and thuggacin analogues BGC (*Sorangium sp*. MSr12523). Green: annotated gene sequence; yellow: annotated protein sequence/function.

Table S3.14: Heat map showing the percentage of identical bases/residues in the compared sequences of *tga* (*S. cellulosum* So ce895), *tug* (*C. crocatus* Cm c5) and thuggacin BGC (*Sorangium sp*. MSr12523).

	MSr12523 - Thuggacin BGC	BGC0001051_Scce895	BGC0001342_Cmc5
MSr12523 - Thuggacin BGC		43.2%	41.8%
BGC0001051_Scce895	43.2%		54.9%
BGC0001342_Cmc5	41.8%	54.9%	

References

(1) Herrmann, J.; Hüttel, S.; Müller, R. Discovery and biological activity of new chondramides from *Chondromyces* sp. *ChemBioChem* **2013**, *14*, 1573–1580.

(2) Buntin, K.; Irschik, H.; Weissman, K. J.; Luxenburger, E.; Blöcker, H.; Müller, R. Biosynthesis of thuggacins in myxobacteria: comparative cluster analysis reveals basis for natural product structural diversity. *Chem. Biol.* **2010**, *17*, 342–356.

Chapter 4

Comparison of myxobacterial secondary metabolite profiles from conventional- and innovative solid–liquid cultivation

Markus Neuber, Daniel Krug and Rolf Müller

Manuscript in preparation

Contributions to the presented work

Author's contribution

The author contributed to the concept of this study, designed and performed experiments, evaluated and interpreted resulting data. The author performed solid and liquid cultivation experiments and analysed the corresponding LC-MS data using statistical methods and metabolic networks. First prototype of the solid–liquid cultivation device - "Flow plate" was assembled, tested and optimised by the author. In addition, the author contributed to the conception and writing of this manuscript.

Contribution by others

Daniel Krug designed the first prototype of the solid–liquid cultivation device and named that "Flow plate". Daniel Krug and Rolf Müller contributed by general design and supervision of the project and conceiving, editing and proofreading of this manuscript.

4. Secondary metabolite profiling of myxobacteria applying various cultivation strategies

4.1 Abstract

Secondary metabolite profiles of the model organism *M. xanthus* DK1622 depend on the type of cultivation, e.g. solid–based or liquid environment used for growth. The application of the OSMAC (one strain many compounds) approach on this strain using several techniques for growth resulted in the identification of unique metabolites for each type of cultivation. Besides, the known compound class of homospermidine lipids was utilised as benchmark compound, which is typically only detectable after solid–based growth. In this study, a comprehensive characterisation of secondary metabolite profiles was carried out to determine the complementary metabolome coverage between both conventional cultivation and a new mixed approach. The designed prototype of a "Flow plate" device allows a mixed solid–liquid based cultivation of bacteria combining characteristics of both environments, leading to composite metabolite profiles from solid phase and suspension growth. With this prototype, we were able to cover about 68% of the existing molecular features detected from independent individual solid and liquid cultures of DK1622. In particular, the hitherto underrepresented solid-based metabolite production became more accessible, while simultaneously covering substantial complexity of the bacterial secondary metabolome.

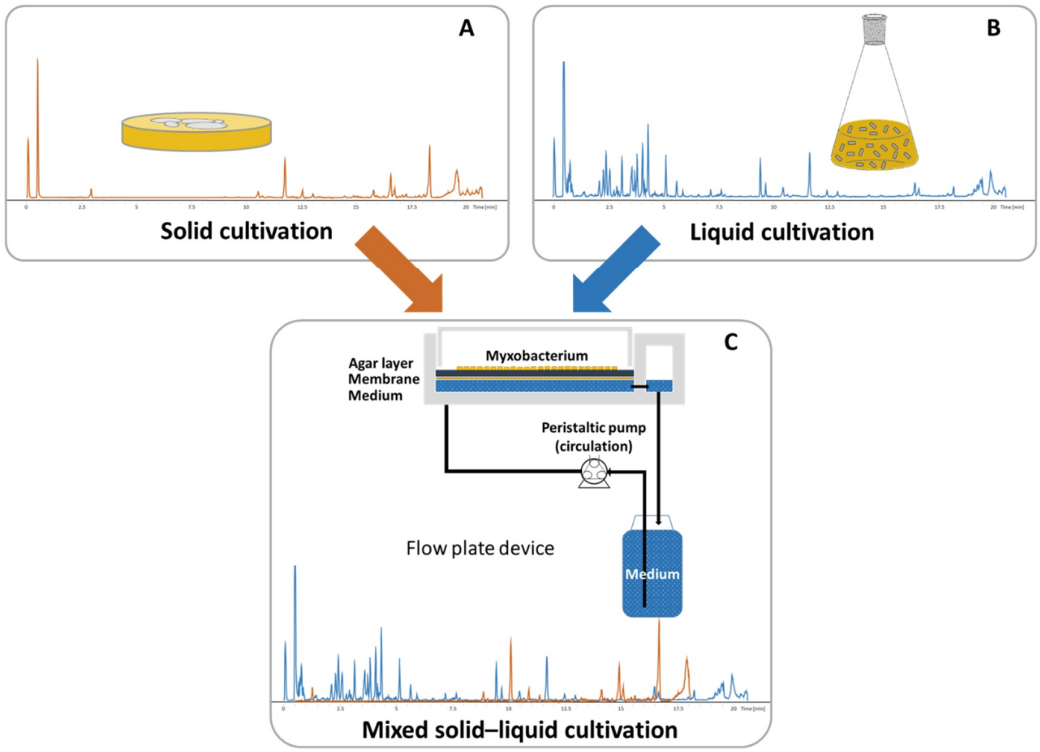

A – Metabolic profile from agar culture; **B** – Metabolic profile from shake flask culture; **C** – Metabolic profile from Flow Plate device

Graphical Abstract

4.2 Introduction

Microbiology is constantly developing in various areas of applied and basic research, e.g. in the fight against antimicrobial resistance and the use of the microorganism in industrial biotechnology, which is based on the successful understanding of biological processes and the engineering of microbes. Therefore, depending on the specific microorganism, one of the biggest challenges is to find optimal cultivation conditions not only to grow the organism but also to produce the largest possible diversity of secondary metabolites (SM). Bacterial SMs are often produced by biosynthetic pathways encoded in contiguous biosynthetic gene clusters (BGCs)[1,2]. Most SMs biosynthetic pathways are non-essential for viability, which implies that such genes can be deleted with little or almost no effect on the producer´s growth[3,4]. However, such formation of SMs are tightly regulated by a variety of abiotic and biotic environmental factors[5].

A number of methods for activating non-expressed BGCs already exist, for example pleiotropic approaches. Therefore, various aspects such as nutrient content, temperature, and rate of aeration can be easily changed, altering the global physiology of a microbial strain and in turn significantly affecting its secondary metabolism[6]. Zeeck and co-workers developed the OSMAC (one strain many compounds) approach in the early 2000s, which led to the isolation of more than 100 metabolites representing 25 structural classes derived only from six different microorganisms[7]. This approach has since been successfully applied to produce new secondary metabolites from single microbial strains during the last 10 years [8,9]. On the other hand, studies aiming at comparison between solid and liquid cultivations are very limited[10]. The metabolome studies of 30 marine actinomycetes in order to compare the differences between growth in solid versus liquid media showed that only 7% of the extracted metabolites overlapped, most of which belonged to known metabolite classes[11]. One can imagine that external signal molecules required to activate particular BGCs, e.g. local high-concentration of quorum sensing stimuli are dissimilar in shake flasks compared to solid cultivation and are thus responsible – at least in part – for the different metabolite profiles.

In recent decades, myxobacteria gained a reputation as excellent producers of SMs[12,13], which are comparable to Streptomyces. They are also known as soil-dwelling organisms known for their rich secondary metabolism, which is due to a vast number of BGCs, and makes these bacteria an excellent research subject[14,15].

Therefore, in this project we envisioned to create a scalable cultivation platform for the integrated solid and liquid cultivation of myxobacteria to alter their secondary metabolite profile and thus provide access to the production of previously unseen SMs. In our study, a membrane separation system in combination with a solid–liquid culturing approach of multiple myxobacteria was studied for its ability to generate diversified profiles of secondary metabolites. The similarities and the differences among the secondary metabolites produced on solid surface, in liquid media and with solid–liquid interface cultivation were determined using LC-*hr*MS techniques. The basic intention was to achieve the diffusion of SMs from two separated compartments through a permeable membrane, which only allows the diffusion of small molecules. In addition, we have developed a solid–liquid cultivation device named "Flow plate" to produce a combined mixed SM profile representing the large number of metabolites from both cultivation methods. This system allows to grow organisms on solid surface separated by semi-permeable membrane supported with circular liquid flow of medium for the diffusion of produced metabolites.

4.3 Results and discussion

In previous studies, fruiting body formation in myxobacteria has been intensively investigated using genomic and transcriptomic methods, leading to a better understanding of the regulatory and signalling mechanisms during cell aggregation and sporulation[16,17]. However, access to chemical diversity at the metabolome level through solid media based growth of myxobacteria are still not well explored, as production yields are often the limiting factor. A previous secondary metabolic study has shown that during fruiting body formation on solid culture medium the occurrence of certain metabolites in myxobacteria changes compared to suspension cultures[18]. In the present study, we have further investigated the differences of SM profiles of *M. xanthus* DK1622 derived from solid surface and liquid suspension growth. Changing the cultivation method not only affected the produced compounds quantitatively but also had particular effects on the activation of biosynthetic pathways leading to the synthesis of unique metabolites from different chemical classes. Thereby, the compound class of homospermidine lipids have been identified in our study as major metabolite class which are only present on solid growth of DK1622. The resulting altered features in crude extracts derived from both growth conditions were analysed by LC-*hr*MS for statistical comparison. As we want to improve production and access to the unique SMs produced during solid growth by myxobacteria, we have attempted to grow

the bacteria under mixed solid–liquid growth conditions similar to their natural habitat by developing a new cultivation device called the "Flow plate".

4.3.1 Solid *versus* liquid growth of *M. xanthus* DK1622

For statistical comparison of different SM profiles, the extraction procedure for both cultivation conditions was identical. The extracts obtained from three biological replicates for both conditions (solid and liquid) were then analysed as two technical replicates by LC-MS to take presumed changes in the secondary metabolism into account. Analysis of solid and liquid growth from DK1622 revealed a clear depiction of the existing dynamic change in the metabolic profiles at the base peak chromatogram (BPC) in Figure 4.1A. Significant additional molecular features with a retention time between 2–5 min could be observed, which are only present in the extract from the liquid growth and originate from the media components absorbed by the XAD-16 resin. Therefore, the solid culture approach was performed differently to reduce the presence of media component residues by scraping the cells off the surface of the agar plate with a cell scraper. Comparison of both base peak chromatograms with matching medium blanks are shown in supporting information (Figure S4.1 and Figure S4.2).

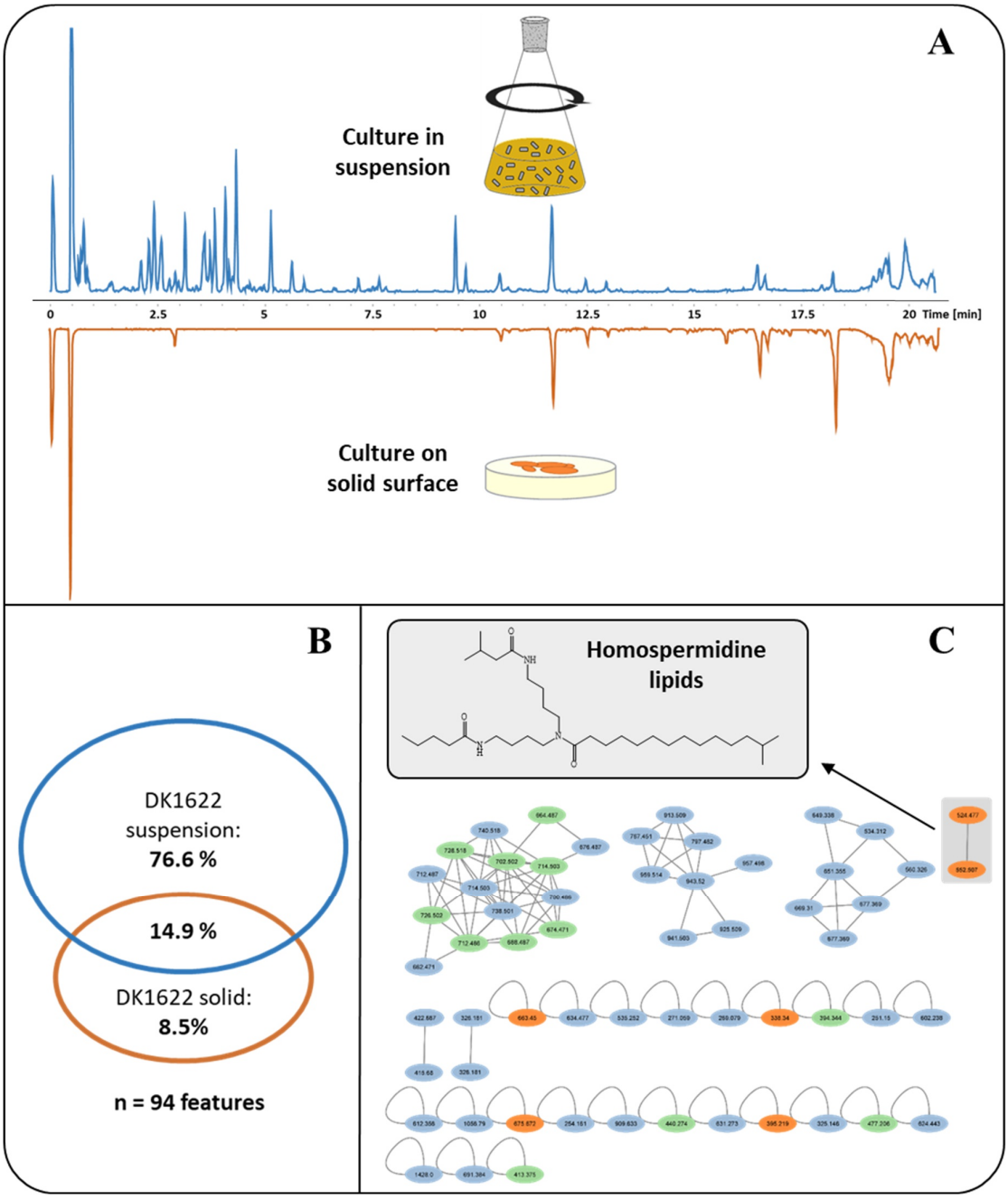

Figure 4.1: Comparison of crude extracts derived from solid surface and suspension growth of *M. xanthus* DK1622 with CYH medium. (**A**) Base peak chromatograms (150−2500 m/z) of both crude extract from DK1622 cultivation each derived from growth in liquid medium with absorber resin (blue) and on an agar plate (orange). (**B**) Number of exclusive features represented in each extract from solid and liquid cultivation. Intensity threshold of 5 x 10^4 was selected. (**C**) Molecular network generated from extracts carried out of solid and liquid cultivation. Blue nodes represent ions detected only from liquid growth; red nodes represent ions detected only from solid growth on agar; green nodes represent ions detected in liquid and solid growth. Members of the molecular family of homospermidine lipids, which are only present on solid growth, are particularly highlighted in the network (grey box, displaying the structure of the most abundant analogue).

A statistically filtered feature table of metabolites was created using principal component analysis (PCA) in conjunction with *t*-Test/ANOVA; significant differences in the metabolic profiles were found (Figure 4.1B). Therefore, features found in at least two out of three biological replicates were considered as a significant hit. The majority of the metabolites have been found in suspension cultures, with 76.6% of the unique features being detected only there. Nevertheless, a small percentage of 8.5% of the entirety of produced metabolites could be identified only from solid growth, and only 14.9% of the 94 features were present in both cultivation methods. In addition, a molecular network (MN) was created from MS^2 datasets consisting of one sample (combination of biological triplicates) for each cultivation method to illustrate connections by nodes and edges (Figure 4.1C). The composite MN of both extracts consisted of 59 nodes, which were grouped into six clusters that form at least two nodes per cluster. The group of homospermidine lipids are myxobacterial metabolites from DK1622, which are only formed during conventional agar plate cultivation[18]. Two derivatives from the homospermidine lipid compound class have been identified and highlighted (grey box) after the comparison of solid and liquid growth at the molecular network. These results provide an indication for the biosynthetic potential that may exist for any secondary metabolite-producing bacterium to alter or activate different metabolic pathways to produce specific metabolic profiles. However, the low production rate and the subsequent efficient extraction of SMs produced by solid cultivation on agar plates are the biggest obstacles and need improved workflows to access such metabolites.

To assess the resulting differences between solid and liquid growth in detail, the production yield of the most abundant myxobacterial SMs were investigated and the ratio calculated (Figure 4.2). Twelve selected metabolites have been divided in three different compound classes of myxalamides (Figure 4.2A), DKxanthenes (Figure 4.2B), and myxovirescin (Figure 4.2C) as well as cittilin B, myxochromids A3, and homospermidine-522 (Figure 4.2D). Interestingly, the class of myxalamides showed almost similar production yields, with the exception of myxalamid A, which showed a 2.5-fold increase in concentration after growing under solid cultivation conditions compared to liquid. Similar observations regarding the production yields of myxochromids can be observed for two derivatives of this substance class. Depending on whether solid or liquid cultivation have been carried out, we were able to achieve different production yields, which increased by a fold of 4 or 2.8 respectively. In contrast, DKxanthen production in liquid medium was about 6–11-fold more efficient, whereas DKxanthen was produced only in small amounts under solid

growth conditions. As expected, homospermidin-522 was only present in the extract from the solid culture with the highest detectable yield.

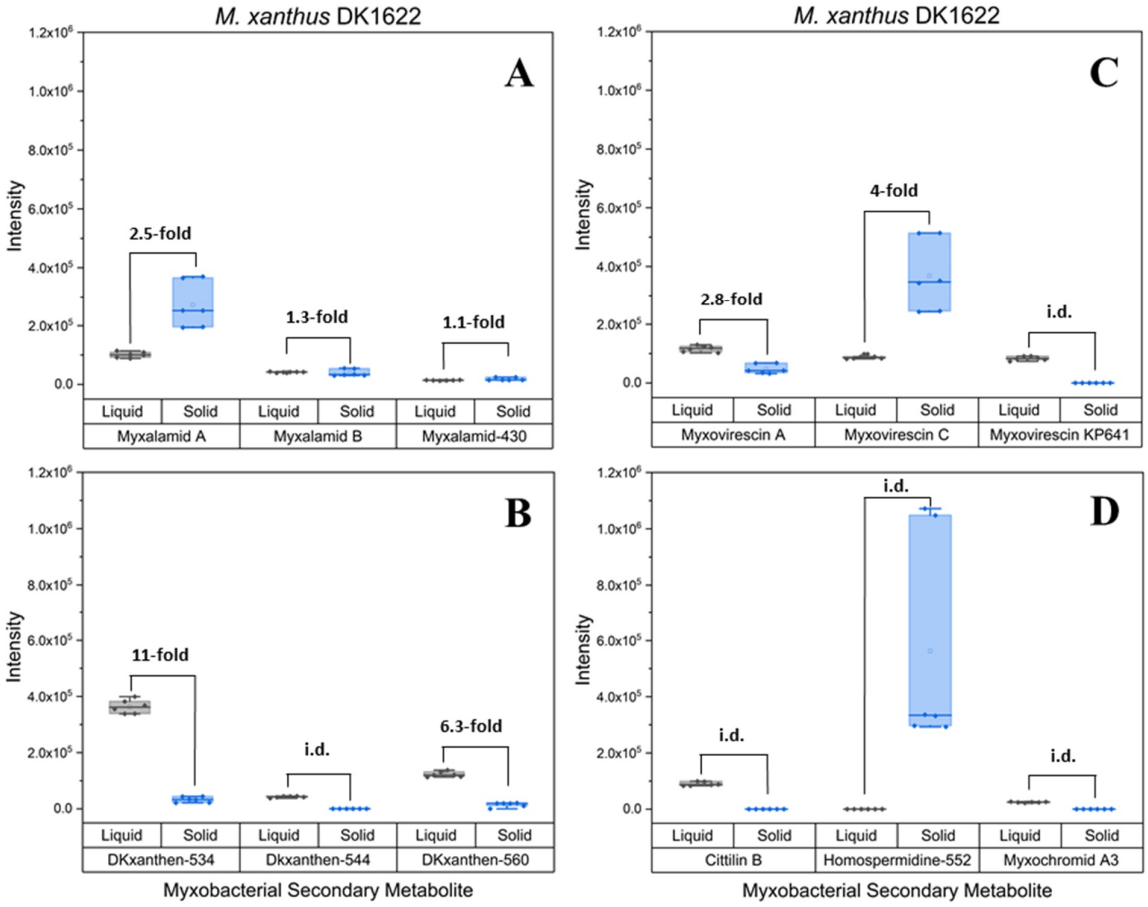

Figure 4.2: Comparison of production yield of different myxobacterial SM (**A**–**D**) based on LC-MS data from crude extracts. Calculation of production ratio by median between liquid and solid cultivation of *M. xanthus* DK1622 from detected intensities obtained from biological triplicates (measured in two technical replicates). The detected intensities of the SMs in the respective crude extract at a concentration of 5 mg/mL are shown as a box plot i.d. - indeterminable

For this we can conclude, there is great variety of synthesised metabolites under the growth of both cultivation conditions, but the SM subset which were produced is highly depending on the environment. Growth of DK1622 in liquid medium provides a higher number of diverse metabolites and generally a higher production yield depending on the compound class. However, the crude extract reveals that a significant amount of media components were captured and isolated from the XAD-16 resin, which could later complicate the purification process. We detected unique metabolites produced exclusively after solid cultivation, indicating that there are still some potentially new SMs to be discovered. Nevertheless,

the production yields and scalability of cultivation platforms based on solid phase are often limited.

We showed that homospermidine lipids as compound class were exclusively found at solid growth of DK1622 on agar. Our next step is to investigate the transfer of particular SM produced on solid media into a liquid phase using a Transwell® inserts for Petri dishes. We thus consider that homospermidine lipids can be used as target features to determine the occurrence by diffusion into a liquid medium connected to the solid agar through a semi-permeable membrane.

4.3.2 Distribution of myxobacterial SMs using a Transwell insert for the cultivation of DK1622

Transwell® permeable units are a convenient and straightforward device that provides independent access to both sides of the membrane layer to study transport and metabolic activities *in vitro* due to continuous exchange across the upper and lower compartments[19]. Standard Transwell insert (75 mm diameter) with membrane area (44 cm^2) was used to determine the spectrum of metabolites produced within the upper compartment and investigate the exchange between the both compartments (Figure 4.3A). For this reason, we used a targeted metabolomics approach to directly identify the known homospermidine lipids to assess metabolite transfer from the solid agar layer (into the Transwell® insert) through the semi-permeable membrane into the underlying liquid phase (lower compartment). Therefore, our myxobacterial model organism *M. xanthus* DK1622 was cultivated on top of the CYH agar layer and compared to liquid growth conditions. In particular, we focused on the metabolites synthesised from the solid growth and their distribution between the two compartments. After analysis from the respective crude extracts, LC-MS data were screened for the presence of homospermidine lipids to evaluate the diffusion through semi-permeable membrane (Figure 4.3B).

The semi-quantitative comparison of the homospermidine-522 production levels from standardised extracts are shown in Figure S4.3.

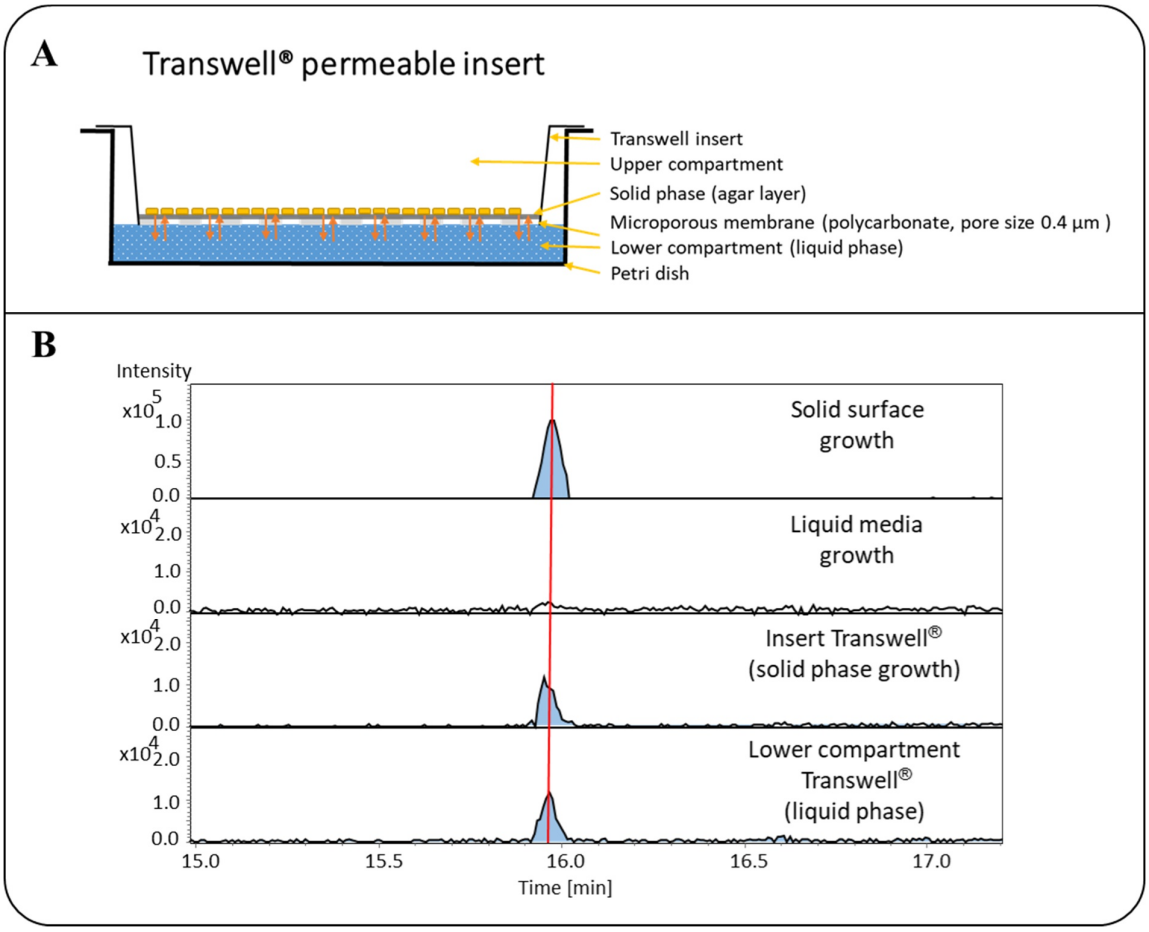

Figure 4.3: (**A**) Schematic illustration of Transwell insert with permeable polycarbonate membrane (0.4 µm pore size) used for Petri dish. (**B**) Homospermidine-522 comparison of the extracted ion chromatogram (EIC) 552.505 ± 0.005 m/z from crude extracts of solid, liquid medium as well as the Transwell device (insert and lower compartment) used to grow *M. xanthus* DK1622.

The homospermidine-522 mentioned above was used to demonstrate the distribution of the substance within the Transwell system compared to conventional agar and shake flask cultures. As expected from previous experiments, we were able to re-identify our produced unique target mass only after cultivation on agar surface. Thus, homospermidine-522 was detected at the control culture as well as the Transwell inset. When DK1622 was cultured in liquid CYH medium, these metabolites could not be found in the control. Remarkably, we observed an enrichment of homospermidine-522 at the lower compartment of the Transwell system. This result suggests that the secondary metabolites can diffuse through the semi-permeable membrane from the upper agar layer into the lower liquid environment. Therefore, it should be possible to apply this so-called hybrid solid–liquid cultivation technique to our designed initial prototype of the "Flow plate" device.

4.3.3 Cultivation of *M. xanthus* DK1622 using Flow plate device

For the first hybrid solid–liquid cultivation of DK1622, we developed a cultivation device named Flow plate (Figure 4.4) which was made of stainless steel and consisted of a chamber (16 x 15 cm) equipped with a perforated metal plate to deposit the agar layer and a lid (Figure 4.4B). A 0.45 µm polyethersulfon (PES) membrane (Sterlitech, US) was used to separate the agar layer from the liquid part. The semi-permeable membrane allows the diffusion of chemical nutrients and exchange of SMs between both environments. Circulation flow of the liquid medium was accomplished by a peristaltic pump connected to a medium reservoir and silicon tubes. The Flow plate device was completely assembled and autoclaved before use.

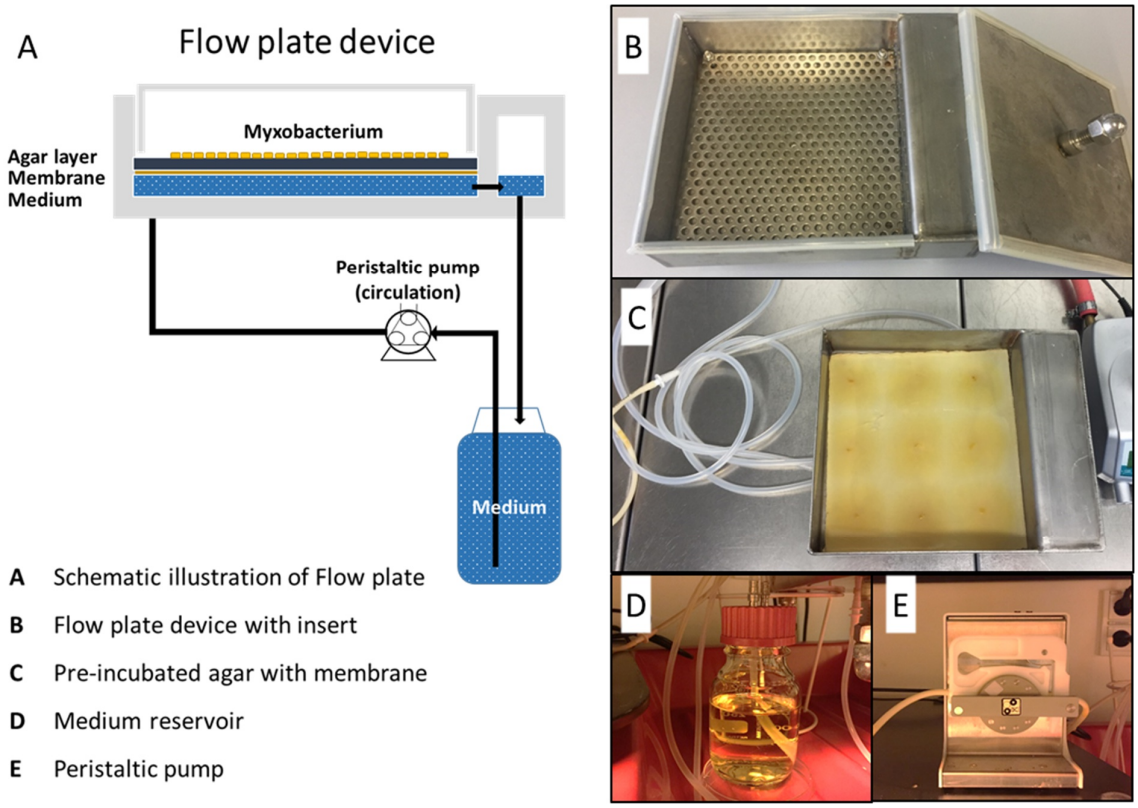

Figure 4.4 (**A**) Schematic illustration of important compartments of Flow Plate device. (**B-E**) Representation of the individual parts of the overall system including the cultivation chamber, pipes, medium bottle and peristaltic pump.

First, the pre-incubation of the solid agar phase was carried out in the chamber (15 x 16 cm) with *M. xanthus* DK1622 for 7 days before the circulation of the liquid phase with the same medium as the solid phase began. Flow rate of 2.8 mL/min was chosen to sustain the circulation for 7 days to exchange nutrients and SMs produced. Furthermore, we performed

the same cultivation with DK1622 without circulation as a control experiment in an identical chamber for 14 days. For a comprehensive assessment, we extracted and analysed the solid and liquid phases separately for improved comparability with the different cultivation methods. In addition, all detected features from the crude extracts that are also present in the respective media blanks were excluded from the statistical data analysis.

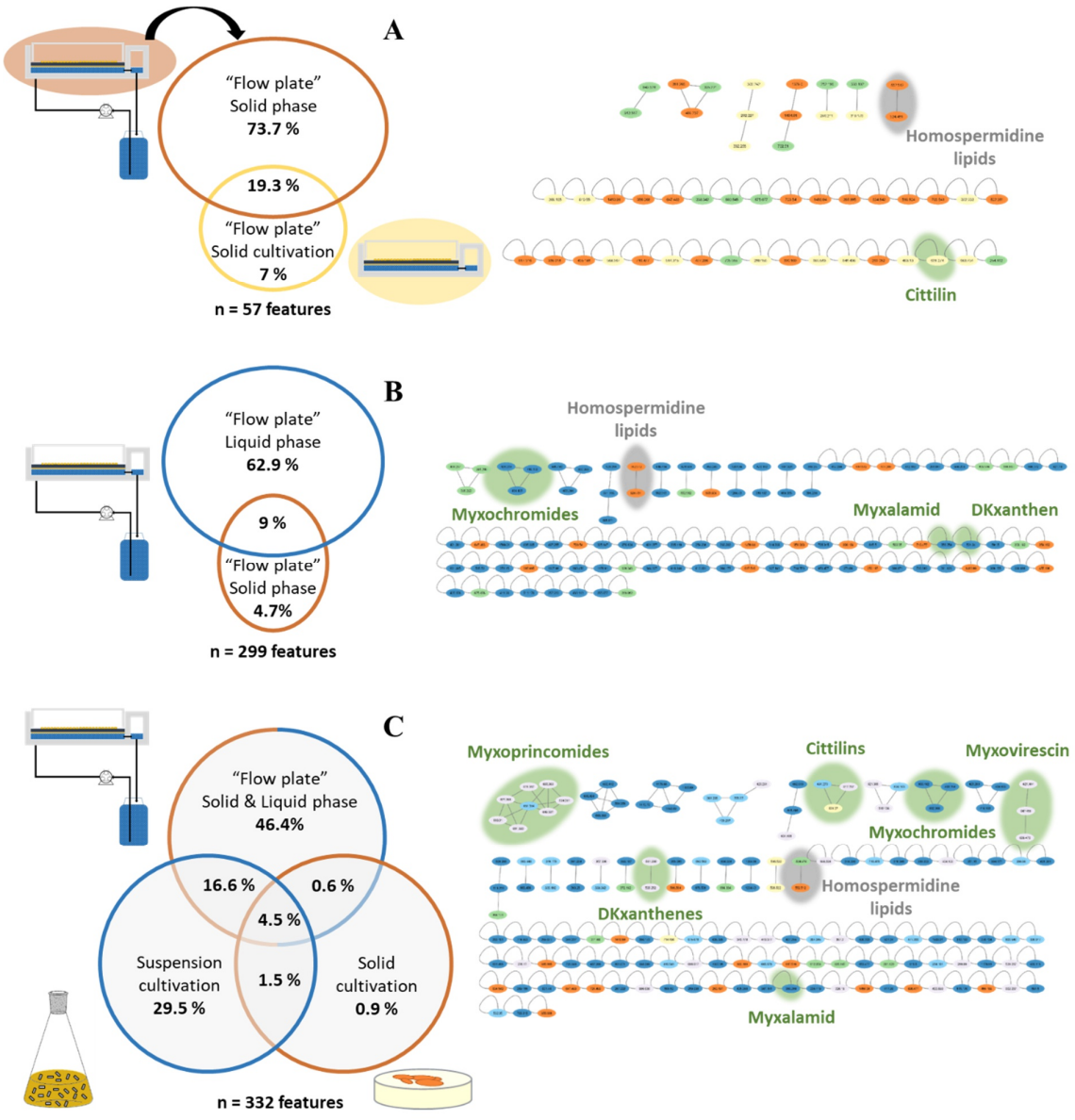

Figure 4.5: Identified molecular features (threshold: 5 x 10^4) in crude extracts after only solid, liquid and Flow plate cultivation of *M. xanthus* DK1622 in CYH medium. (**A**) Distribution of present metabolites between solid phase (agar & circulation flow) and solid cultivation (control) using Flow plate device. (**B**) Distribution of present metabolites between liquid and solid phase of Flow plate cultivation. (**C**) Venn diagram of present metabolites between Flow plate (solid and liquid phase) as well as only solid (control in Flow plate) and suspension (shaking flask) cultivation. Molecular network of the respective comparisons are shown

in addition on the right site. Orange – solid phase (Flow plate); yellow – solid cultivation (control in Flow plate); blue – liquid phase (Flow plate); light blue – suspension cultivation (shaking flask); green – shared metabolites.

Several previous studies have already described how the modification of cultivation conditions/methods, media composition and physical parameters changes the generated metabolic profile for individual organisms[20–22]. Therefore, we were interested in the influence of the three different cultivation methods (Flow plate, solid surface and suspension growth) and the connected changes in the SM profiles (Figure 4.5).

We observed the predominant part of the molecular features with around 73% in the solid phase (Figure 4.5A), which is due to the cultivation in the Flow plate compared to the control without liquid circulation. It can be imagined that the complementary liquid phase provides the overlying agar layer (solid phase) with additional nutrients so that the growing myxobacterium can produce a more abundant amount of SMs. However, as expected, the total number of 57 molecular features was significantly lower than for DK1622 which had been grown in liquid medium.

Next, we analysed the extracts after culturing DK1622 in the Flow plate device to determine the ability to generate a mixed metabolite profile from liquid and suspension (Figure 4.5B). It was demonstrated that a mixed metabolic profile had occurred, but only 9% of the features were detectable in both crude extracts. This relatively small overlap between the metabolites from the cultivation of solid surfaces, which were also found in the liquid part, are rather small from our preliminary study carried out and agree with reported results from Crüsemann *et al.*[11]. However, the data from the Flow plate cultivation showed that we were able to enrich and extract about 72% of the total formed metabolites from DK1622 in the liquid part using this method. Only the small proportion of 4.7% was still exclusively in the solid phase, so that no diffusion of these special metabolites occurs.

Afterwards, we compared the three different methods of cultivation including Flow plate, solid and suspension growth against each other in a Venn diagram (Figure 4.5C). With all three cultivation methods and after subtracting the blank features of the medium, a total of 332 molecular features were detected, of which about majority (46%) were present solely after cultivation with the flow plate. On the one hand, we were lacking about 30% of specific molecular features produced exclusively during growth in suspension, which could be caused by the non-optimal conditions without agitation in the medium reservoir. On the

other hand, these results indicate that just 2.4% of molecular features from solid cultivation were not obtained in the Flow plate cultivation.

For the estimation of the production level of myxobacterial metabolites between Flow plate device and agar plate, the production ratio was compared with the growth area of both cultivation systems (see method: Calculation of the relative quantity of myxobacterial metabolites produced by *M. xanthus* DK1622 and Table S4.1). By using the flow plate device the relative quantity of particular metabolites produced by DK1622 is enlarged due to the increased growth area and the supply of the liquid medium as part of this cultivation system. The ratio of relative quantity of homospermidine-522 on the Flow plate was a 3.1 times higher compared to cultivation on agar plates. Even with a lower production of DK1622 metabolites, the Flow plate extract can provide an almost similar yield of compound, which for example can be demonstrated by the relative amount of myxovirescin C (Table S4.1). It should be noted that these calculations are based on a fixed extract concentration of 5 mg/mL and does not consider the absolute amounts of the extracts obtained. Therefore, it is possible to obtain the required amount of metabolites for structure elucidation and bioactivity tests with the developed flow plate device.

The overall concept of our flow plate was to provide access to the unique SMs that are usually only produced by culturing on solid surface. So we were finally able to show that with the designed Flow plate device, culturing DK1622 can produce a mixed solid–liquid secondary metabolite profile that exhibited molecular features from both cultivation modes.

4.3.4 Conclusion

In this study, we have shown that both solid and liquid cultivation can significantly alter the spectrum profile of myxobacterial SMs produced by DK1622. Besides the total number of molecular features, the production yield of various myxobacterial SMs was found to be dependent on the cultivation method. The compound class of homospermidine lipids were identified as the target group obtained solely after growing on agar as solid medium. Ability to diffuse metabolites from a solid phase to a liquid phase through a polycarbonate membrane was validated using the Transwell® petri dish, using the homospermidine lipids as indicative readout. During cultivation in our flow plate device, metabolome coverage was significantly increased compared to independent single cultures grown in suspension and agar plates. Because of the more than 2-fold increase in the growth area of the flow plate cultivation device in relation to the agar plates, it is possible to obtain a similar or improved quantity of certain metabolites even at a lower production level. We conclude that our cultivation device for mixed solid–liquid cultures provides a practical method to access the hitherto less studied SMs associated with growth on solid media.

4.4 References

(1) Liu, G.; Chater, K. F.; Chandra, G.; Niu, G.; Tan, H. Molecular regulation of antibiotic biosynthesis in *Streptomyces*. *Microbiol. Mol. Biol. Rev.* **2013**, *77*, 112–143.

(2) Bode, H. B.; Müller, R. Analysis of myxobacterial secondary metabolism goes molecular. *J. Ind. Microbiol. Biotechnol.* **2006**, *33*, 577–588.

(3) Komatsu, M.; Komatsu, K.; Koiwai, H.; Yamada, Y.; Kozone, I.; Izumikawa, M.; Hashimoto, J.; Takagi, M.; Omura, S.; Shin-Ya, K.*; et al.* Engineered Streptomyces avermitilis host for heterologous expression of biosynthetic gene cluster for secondary metabolites. *ACS synthetic biology* **2013**, *2*, 384–396.

(4) Myronovskyi, M.; Rosenkranzer, B.; Nadmid, S.; Pujic, P.; Normand, P.; Luzhetskyy, A. Generation of a cluster-free *Streptomyces albus* chassis strains for improved heterologous expression of secondary metabolite clusters. *Metab. Eng.* **2018**, *49*, 316–324.

(5) Meyer, M.; Bourras, S.; Gervais, J.; Labadie, K.; Cruaud, C.; Balesdent, M.-H.; Rouxel, T. Impact of biotic and abiotic factors on the expression of fungal effector-encoding genes in axenic growth conditions. *Fungal Genet. Biol.* **2017**, *99*, 1–12.

(6) Romano, S.; Jackson, S. A.; Patry, S.; Dobson, A. D. W. Extending the "One Strain Many Compounds" (OSMAC) Principle to Marine Microorganisms. *Mar. Drugs* **2018**, *16*.

(7) Bode, H. B.; Bethe, B.; Höfs, R.; Zeeck, A. Big effects from Small Changes: Possible Ways to Explore Nature's Chemical Diversity. *ChemBioChem* **2002**, *3*, 619–627.

(8) Netzker, T.; Fischer, J.; Weber, J.; Mattern, D. J.; Konig, C. C.; Valiante, V.; Schroeckh, V.; Brakhage, A. A. Microbial communication leading to the activation of silent fungal secondary metabolite gene clusters. *Front. Microbiol.* **2015**, *6*, 299.

(9) Wang, Y.; Lu, Z.; Sun, K.; Zhu, W. Effects of high salt stress on secondary metabolite production in the marine-derived fungus *Spicaria elegans*. *Mar. Drugs* **2011**, *9*, 535–542.

(10) Ňancucheo, I.; Rowe, O. F.; Hedrich, S.; Johnson, D. B. Solid and liquid media for isolating and cultivating acidophilic and acid-tolerant sulfate-reducing bacteria. *FEMS microbiology letters* **2016**, *363*.

(11) Crüsemann, M.; O'Neill, E. C.; Larson, C. B.; Melnik, A. V.; Floros, D. J.; da Silva, R. R.; Jensen, P. R.; Dorrestein, P. C.; Moore, B. S. Prioritizing natural product diversity in a collection of 146 bacterial strains based on growth and extraction protocols. *J. Nat. Prod.* **2017**, *80*, 588–597.

(12) Wenzel, S. C.; Muller, R. Myxobacteria—''microbial factories' for the production of bioactive secondary metabolites. *Molecular bioSystems* **2009**, *5*, 567–574.

(13) Wenzel, S. C.; Müller, R. Myxobacteria - unique microbial secondary metabolite factories. In *Comprehensive Natural Products Chemistry II, Vol 2: Structural Diversity II - Secondary Metabolite Sources, Evolution and Selected Molecular Structures*; Moore, B., Ed.; Elsevier: Oxford, 2010; pp 189–222.

(14) Wenzel, S. C.; Müller, R. The biosynthetic potential of myxobacteria and their impact on drug discovery. *Curr. Opin. Drug Discov. Devel.* **2009**, *12*, 220–230.

(15) Zaburannyi, N.; Bunk, B.; Maier, J.; Overmann, J.; Muller, R. Genome Analysis of the Fruiting Body-Forming Myxobacterium *Chondromyces crocatus* Reveals High Potential for Natural Product Biosynthesis. *Appl. Environ. Microbiol.* **2016**, *82*, 1945–1957.

(16) Huntley, S.; Hamann, N.; Wegener-Feldbrügge, S.; Treuner-Lange, A.; Kube, M.; Reinhardt, R.; Klages, S.; Müller, R.; Ronning, C. M.; Nierman, W. C.*; et al.* Comparative Genomic Analysis of Fruiting Body Formation in Myxococcales. *Mol. Biol. Evol.* **2011**, *28*, 1083–1097.

(17) Lloyd, D. G.; Whitworth, D. E. The myxobacterium *Myxococcus xanthus c*an sense and respond to the quorum signals secreted by potential prey organisms. *Front. Microbiol.* **2017**, *8*, 439.

(18) Hoffmann, M.; Auerbach, D.; Panter, F.; Hoffmann, T.; Dorrestein, P. C.; Müller, R. Homospermidine Lipids: A compound class specifically formed during fruiting body formation of *Myxococcus xanthus* DK1622. *ACS Chem. Biol.* **2018**, *13*, 273–280.

(19) Justus, C. R.; Leffler, N.; Ruiz-Echevarria, M.; Yang, L. V. In vitro cell migration and invasion assays. *Journal of visualized experiments : JoVE* [Online early access]. DOI: 10.3791/51046. Published Online: Jun. 1, 2014.

(20) Hewage, R. T.; Aree, T.; Mahidol, C.; Ruchirawat, S.; Kittakoop, P. One strain-many compounds (OSMAC) method for production of polyketides, azaphilones, and an

isochromanone using the endophytic fungus Dothideomycete sp. *Phytochemistry* **2014**, *108*, 87–94.

(21) Sarkara, A.; Funka, A. N.; Scherlach, K.; Horn, F.; Schroeckh, V.; Chankhamjon, P.; Westermann, M.; Roth, M.; Brakhage, A. A.; Hertweck, C.*; et al.* Differential expression of silent polyketide biosynthesis gene clusters in chemostat cultures of Aspergillus nidulans. *J. Biotechnol.* **2012**, *160*, 64–71.

(22) Rateb, M. E.; Houssen, W. E.; Harrison, W. T. A.; Deng, H.; Okoro, C. K.; Asenjo, J. A.; Andrews, B. A.; Bull, A. T.; Goodfellow, M.; Ebel, R.*; et al.* Diverse metabolic profiles of a *Streptomyces* strain isolated from a hyper-arid environment. *J. Nat. Prod.* **2011**, *74*, 1965–1971.

Supporting Information

Comparison of myxobacterial secondary metabolite profiles from conventional- and innovative solid–liquid cultivation

Markus Neuber, Daniel Krug and Rolf Müller

Methods

Strains and media

The myxobacterial strain *M. xanthus* DK1622 (MCy9151) was preserved from our internal strain collection and was used for all cultivations. CYmod medium (0.3% casitone, 0.1% yeast extract, 0.1% calcium chloride dihydrate, pH 7.6) and H medium (0.8% soluble starch, 0.2% soya flour, 0.2% glucose, 0.2% yeast extract, 0.1% calcium chloride dihydrate, 0.1% magnesium sulphate heptahydrate, 50 mM HEPES buffer, 8 mg/L iron(III)-sodium ethylenediaminetetraacetate hydrate, pH 7.4) was prepared for *M. xanthus* DK1622. Therefore, CY and H medium were combined in equal volumes to obtain CYH medium. For the preparation of solid CYH medium was 1.5% [w/v] of agar added.

Cultivation solid versus liquid and extract preparation

Pre-culture of *M. xanthus* DK1622 was grown at 30 °C for three days in shaking flask containing 25 ml CYH medium at 180 rpm. 50 mL liquid cultures were inoculated by the well-grown pre-culture (1% [v/v]) in the same media and cultivation conditions for seven days. Five days after inoculation, aqueous XAD-16 absorber resin solution was added at the volumetric concentration of 2% [v/v] to each liquid culture. Cell suspension and the resin were harvested using centrifugation (10 min, x 5.000 g, RT) following by lyophilisation. For solid culture, 150 µL of the same pre-culture of DK1622 was used and plated out onto the surface of 25 mL CYH agar in a Petri dish. After incubation at 30 °C for seven days, the cells grown on the surface were scraped off with a cell scraper and collected separately from the agar. Both cells and agar were lyophilised before extraction. All liquid and solid cultures and the corresponding controls were performed as biological triplicates, whereby for the solid cultivation each replicate consisted of two agar plates.

Cultivation using Transwell insert for Petri dish

Pre-culture of *M. xanthus* DK1622 grew at 30 °C for three days in shaking flask containing 25 mL CYH medium at 180 rpm. Transwell® inlet (with semi-permeable membrane) were inoculated with 150 µL of DK1622 pre-culture and plated out onto the surface of 25 mL CYH, and pre-cultivated at 30 °C for seven days. Subsequently, 10 mL of CYH medium together with 1 mL of XAD-16 resin were transferred to the lower compartment of the Petri dish and incubated with shaking at 100 rpm at 30 °C for another seven days. After 14 days, the solid phase (Transwell inlet) and the liquid phase (lower compartment) were harvested

separately, lyophilised and extracted. The respective controls of solid/agar and liquid cultivation were carried out accordingly (see section: Cultivation solid versus liquid and extract preparation).

Cultivation with Flow plate device

The Flow plate (FP) device equipped with PSE (polyethersulfon, 0.45 µm pore size,) membrane (Sterlitech) was sterilised for 20 min at 121 °C and one bar overpressure. A preculture of *M. xanthus* DK1622 grew at 30 °C for three days in shaking flask containing 25 mL CYH medium at 180 rpm. Afterwards, 150 mL of CYH agar was poured into the camber (15 x 16 cm) and 750 µL of the well-grown pre-culture of DK1622 was platted out. First, the FP device was pre-incubated at 30 °C for 7 days. The second step is an additional circulation of 500 mL CYH liquid medium using a peristatic pump (2.8 mL/min) for another 7 days. After 14 days, solid phase was separately harvested and dried through lyophilisation. To capture the metabolites in liquid medium, resin XAD-16 (1% [v/v]) was added and stirred for 2 days by 300 rpm. Afterwards, liquid medium and the resin were harvested using centrifugation (10 min, 5.000*g*, RT) following by lyophilisation.

Preparation of crude extracts

Extracts were prepared by extracting the cell pellet including the resin, the scraped cells and agar with acetone/methanol (1:1 [v/v]), evaporating the solvents and re-dissolving the residues in methanol. Therefore, each sample were extracted with 50 mL MeOH/acetone (1:1 [v/v]) under constant stirring at 300 rpm with magnet bar for two times for 90 min. The supernatant was filtered into a round bottom flask and the solvent was evaporated under reduced pressure until the residue was completely dry. The residue was dissolved in 1 mL MeOH, transferred into 1.5 mL glass vial and stored at 4°C. All extracts were diluted 1:5 or a certain concentration prepared prior to the UHPLC-MS measurements.

Determination of the myxobacterial SMs production level

An aliquot was taken from the corresponding crude extracts and the methanol was subsequently evaporated. The dry weight of each crude extract was determined. The required volume of methanol was then added to obtain an extract with a concentration of 5 mg/mL. 1 µL of each extract was injected for LC-MS analysis (see LC-MS Analysis of crude extracts) to compare the production levels of the myxobacterial SMs.

Calculation of the relative quantity of myxobacterial metabolites produced by *M. xanthus* DK1622

To compare of the relative quantity of SMs from two agar plates (growth area, 128 cm²) and Flow plate device (growth area, 272 cm²) , the determined area under the curve (AUC) of the certain metabolites and the growth area of the respective cultivation system was used. Equation 1 and 2 are used to calculate the relative quantity of produced metabolites by DK1622 between Flow plate device and the agar plates.

$$\textbf{Eq. 1}\quad Ratio\ (Metabolite) = \frac{AUC\ of\ Agar\ plates}{AUC\ of\ Flow\ plate}$$

$$\textbf{Eq. 2}\quad rel.Quantity\ of\ Flow\ plate = \ Ratio\ (Metabolite) * \frac{Growth\ area\ of\ Flow\ plate}{Growth\ area\ of\ Agar\ plates}$$

LC-MS Analysis of crude extracts

UHPLC-qTOF measurements were performed in duplicates as technical replicates on a Dionex Ultimate 3000 SL system coupled to a Bruker maXis 4G UHR-qTOF. This system was used for high resolution LC-MS measurements. Following template method was used: Column: ACQUITY BEH 100 x 2.1 mm 1.7 µm 130 Å, a flow rate of 0.6 mL/ min and a column temperature of 45 °C. Following gradient was applied with H2O + 0.1% FA as eluent A and ACN + 0.1% FA as eluent B. 0–0.5 min: 5% Eluent B; 0.5–18.5 min: linear increase of eluent B to 95%; 18.5–20.5 min: 95 % eluent B; 20.5–20.8 min: linear decrease of eluent B; 20.8–22.5 min: re-equilibration with 5% eluent B. The detection was usually performed in the positive MS mode or MS^2 mode, using a scan range from 150-2500 *m/z*. Capillary voltage was set to +4000 V for measurements in positive ionization mode. Dry gas was set to a flow rate of 5 L/ min at 200 °C.

Statistical LC-MS data analysis and annotations of crude extracts

For the statistical interpretation of generated LC-MS data by *t*-Test/ANOVA was carried out with MetaboScape 2021b (Bruker). The minimal intensity threshold for feature detection by the built-in T-Rex 3D algorithm was set to 5 x 10^4, and the maximum charge was set to three[1]. The minimal group size for creating batch features to four. Features found in at least two out of three biological replicates (measured as technical duplicates) were considered as a significant hit, as long as no appearance could be detected in media blanks. Known myxobacterial secondary metabolites were annotated using our in-house database containing myxobacterial secondary metabolites (myxobase)[2]. Overlaps of the direct and

indirect co-cultivation approach as well as features uniquely found in one analysis were calculated via *t*-Test/ANOVA analysis in MetaboScape 2021b.

MS² experiments and molecular networking

All LC-MS² measurements were based on the already described 18 min gradient separation using the U3000-maXis 4G setup. Fragmentation spectra were achieved either by auto-MS² measurements or by targeted precursor selection. Fixed MS² parameters were an m/z-adjusted precursor isolation width and fragmentation energy. Values are interpolated in between the set points [300 m/z /4 m/z / 30 eV], [600 m/z / 6 m/z / 35 eV], [1000 m/z / 8 m/z / 45 eV], and [2000 m/z /10 m/z / 55 eV]. The precursor intensity threshold was set to 5000.

A molecular network was created using the online workflow at GNPS (Global Natural Products Social Molecular Networking). The data was then clustered with MS-Cluster with a parent mass tolerance of 0.05 Da and a MS² fragment ion tolerance of 0.1 Da to create consensus spectra. Further, consensus spectra that contained less than 1 spectra were discarded. A network was then created where edges were filtered to have a cosine score above 0.65 and more than 4 matched peaks[3]. Data were visualized with Cytoscape (Version 3.9.1).

Supplementary Figures & Tables

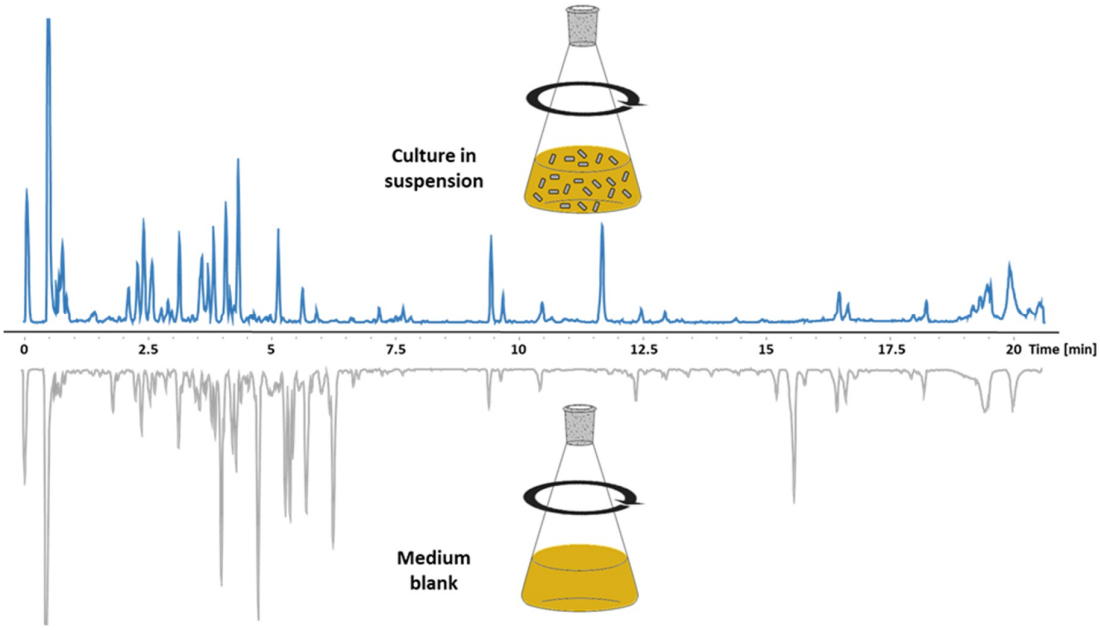

Figure S4.1: Comparing of base peak chromatograms (150−2500 m/z) of crude extracts from DK1622 liquid cultivation (blue) and medium blank (grey) using absorber resin.

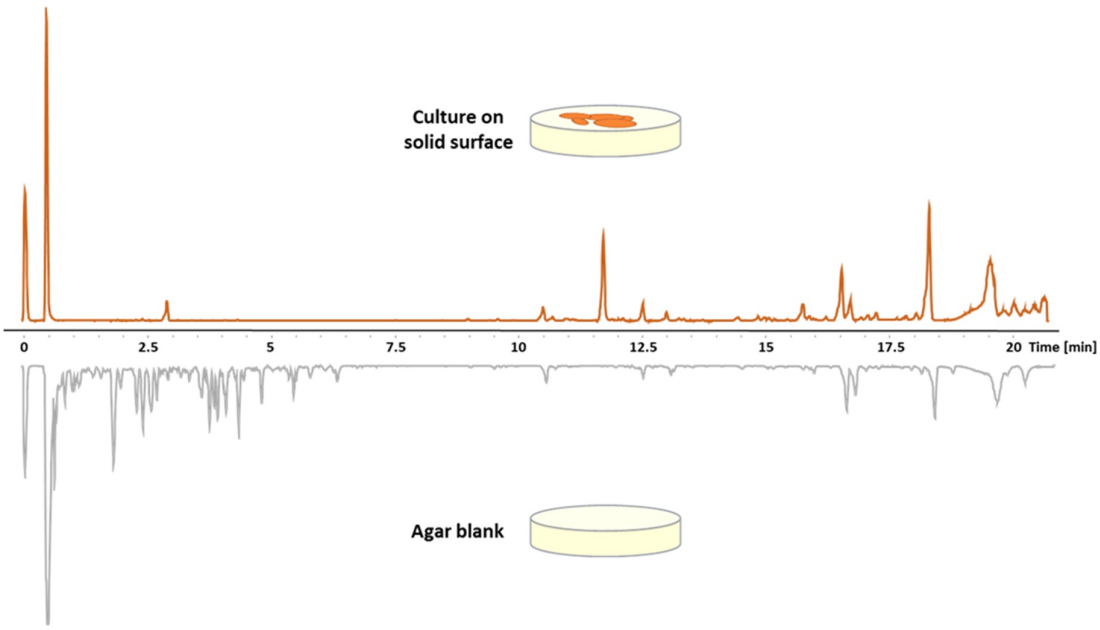

Figure S4.2: Comparing of base peak chromatograms (150−2500 m/z) of crude extracts from DK1622 solid cultivation (orange) and agar blank (grey).

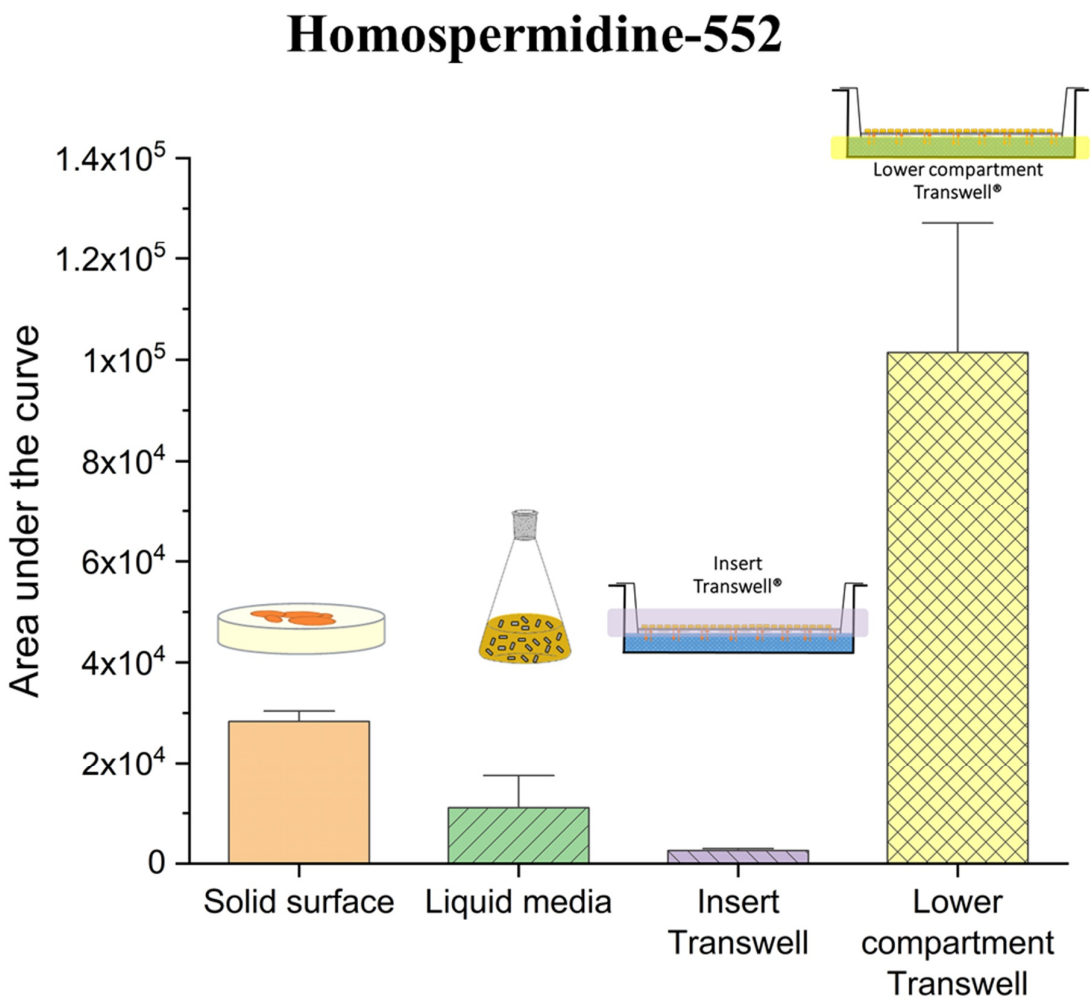

Figure S4.3: Comparison of the production level of homospermidine-522 from the respective crude extracts with a concentration of 5 mg/mL. Whole agar and cells were used for the extraction process of solid surface and Insert Transwell to obtain the crude extracts. For the extraction of liquid media and the lower Transwell compartment, only the liquid fraction was used to obtain the crude extract.

For the comparison of the production amounts of homospermidine-522 (Figure S4.3), the respective extracts were balanced to prepare a defined concentration of 5 mg/mL per extract. Afterwards, 1 µL injection volume of the extract was used for the LC-MS measurement.

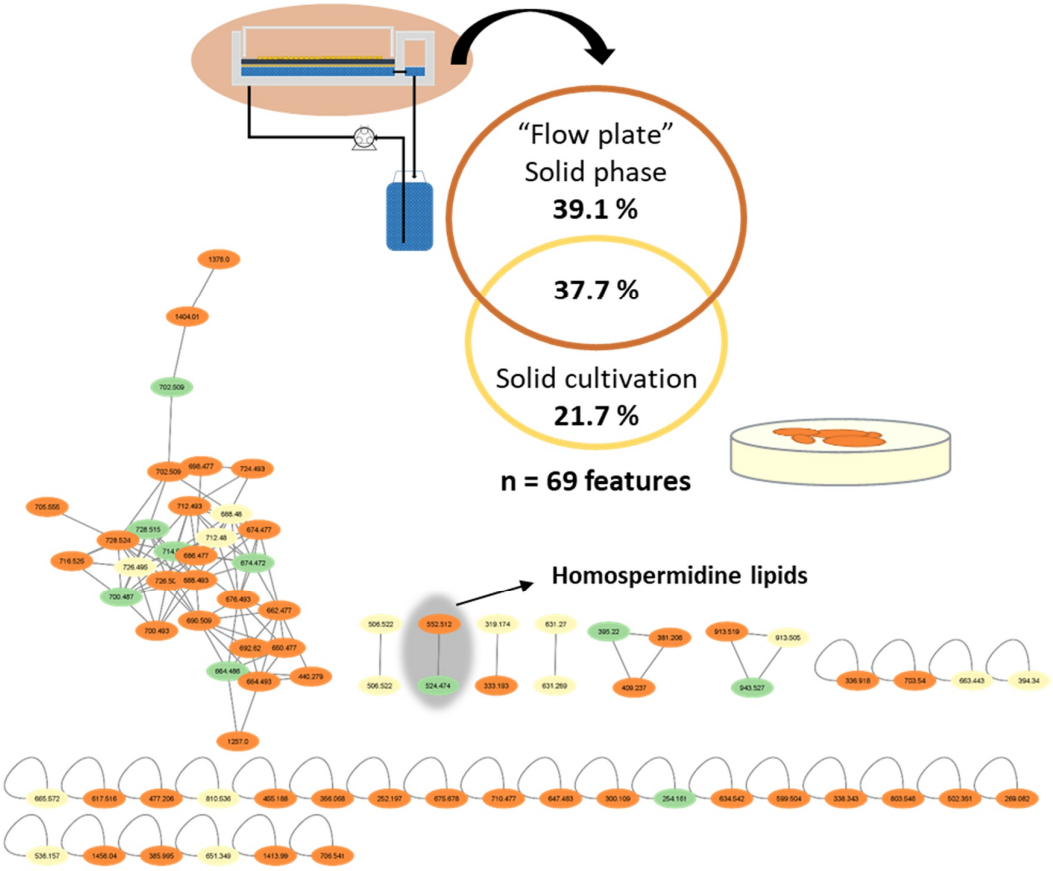

Figure S4.4: Identified molecular features (threshold: 5 x 104) in crude extracts after only solid, liquid and Flow plate cultivation of *M. xanthus* DK1622 in CYH medium. Molecular network consist of nodes: 73 and edges: 133

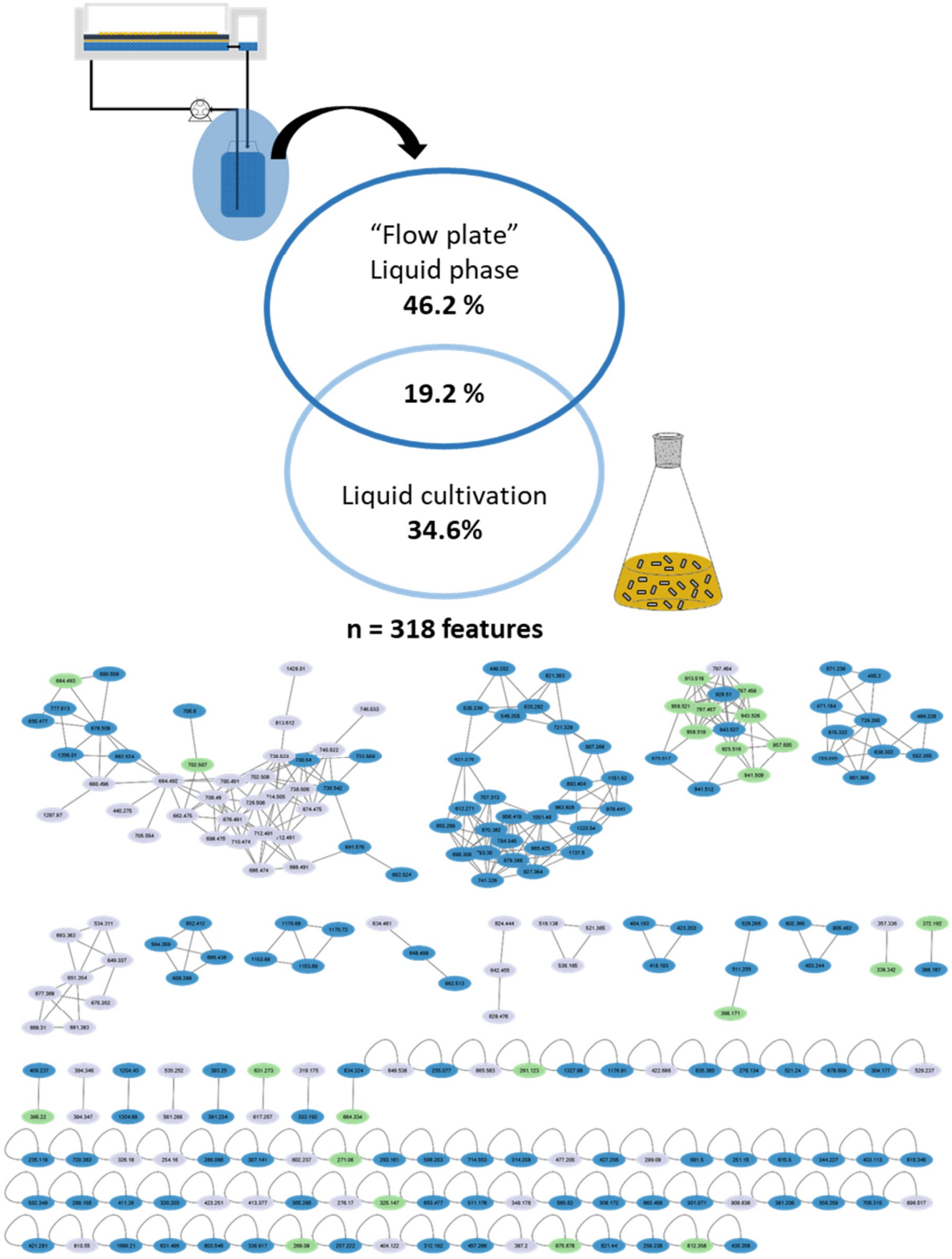

Figure S4.5: Identified molecular features (threshold: 5 x 10^4) in crude extracts after only solid, liquid and Flow plate cultivation of *M. xanthus* DK1622 in CYH medium. Molecular network consist of nodes: 216 and edges: 390.

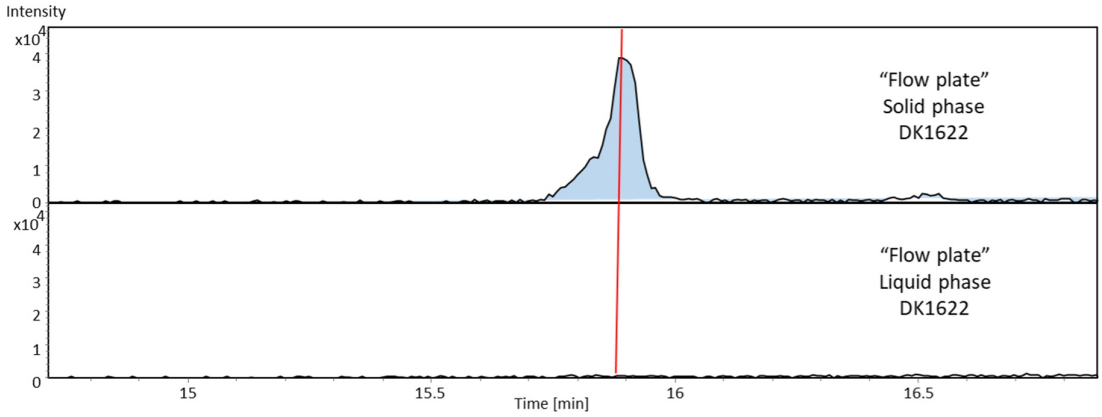

Figure S4.6: Extracted ion chromatogram (EIC) of homospermidine-522 552.505 ± 0.005 m/z from crude extracts with a concentration of 5 mg/mL from solid and liquid phase after Flow plate cultivation with *M. xanthus* DK1622.

Table S4.1 Calculation of the relative quantity of certain metabolites produced by *M. xanthus* DK1622 between Flow plate derive and agar plates. The AUC was determined from crude extracts with a defined concentration of 5 mg/mL.

Myxobacterial secondary metabolite	**Area under the curve (AUC) of metabolite**		**Ratio-Metabolite**	**Relative quantity of FP**
	Agar plates	*Flow plate*		
Myxovirescin C	90.019	39.945	0.4	**0.9**
Homospermidine-522	137.508	198.533	1.4	**3.1**
Cittilin A	160.534	1.035.632	6.5	**13.7**

References

(1) Bader, C. D.; Haack, P. A.; Panter, F.; Krug, D.; Müller, R. Expanding the Scope of Detectable Microbial Natural Products by Complementary Analytical Methods and Cultivation Systems. *J. Nat. Prod.* [Online early access]. DOI: 10.1021/acs.jnatprod.0c00942. Published Online: Jan. 15, 2021.

(2) Hoffmann, T.; Krug, D.; Bozkurt, N.; Duddela, S.; Jansen, R.; Garcia, R.; Gerth, K.; Steinmetz, H.; Müller, R. Correlating chemical diversity with taxonomic distance for discovery of natural products in myxobacteria. *Nat. Commun.* **2018**, *9*, 803.

(3) Hoffmann, M.; Auerbach, D.; Panter, F.; Hoffmann, T.; Dorrestein, P. C.; Müller, R. Homospermidine Lipids: A compound class specifically formed during fruiting body formation of *Myxococcus xanthus* DK1622. *ACS Chem. Biol.* **2018**, *13*, 273–280.

Chapter 5

Supercritical Fluid Extraction Enhances Discovery of Secondary Metabolites from Myxobacteria

Chantal D. Bader[†], **Markus Neuber**[†], Fabian Panter[†], Daniel Krug[†] and Rolf Müller[†*]

Analytical Chemistry

DOI: 10.1021/acs.analchem.0c02995

Accepted manuscript: 30.10.2020

*Corresponding author

[†] Department Microbial Natural Products, Helmholtz-Institute for Pharmaceutical Research Saarland (HIPS), Helmholtz Centre for Infection Research (HZI), German Center for Infection Research (DZIF, Partner site Hannover-Braunschweig) and Department of Pharmacy, Saarland University Campus E8.1, 66123 Saarbrücken (Germany)

Contributions to the presented work

Author's contribution

The manuscript was written through contributions of all authors. All authors have given approval to the final version of the manuscript.

5. Supercritical fluid extraction enhances discovery of secondary metabolites from myxobacteria

5.1 Abstract

Supercritical fluid extraction (SFE) is widely used for the isolation of natural products from plants, but its application in efforts to identify structurally and physicochemically often dissimilar microbial natural products is limited to date. In this study we evaluated the impact of SFE on the extractability of myxobacterial secondary metabolites aiming to improve the prospects of discovering novel natural products. We investigated the influence of different co-solvents on the extraction efficiency of secondary metabolites from three myxobacterial strains as well as the antimicrobial activity profiles of the corresponding extracts. For each known secondary metabolite we found extraction conditions using SFE leading to superior yields in the extracts compared to conventional solvent extraction. Compounds with a logP higher than 3 showed best extraction efficiency using 20% EtOAc as a co-solvent, whereas compounds with logP values lower than 3 were better extractable using more polar co-solvents like MeOH. Extracts generated with SFE showed increased antimicrobial activities including the presence of activities not explained by known myxobacterial secondary metabolites, highlighting the advantage of SFE for bioactivity-guided isolation. Moreover, non-targeted metabolomics analysis revealed a group of chlorinated metabolites produced by the well-studied model myxobacterium *Myxococcus xanthus* DK1622 which were not accessible previously due to their low concentration in conventional extracts. The enriched SF extracts were used for isolation and subsequent structure elucidation of chloroxanthic acid A as founding member of a novel secondary metabolite family. Our findings encourage the increased utilization of SFE as part of future microbial natural products screening workflows.

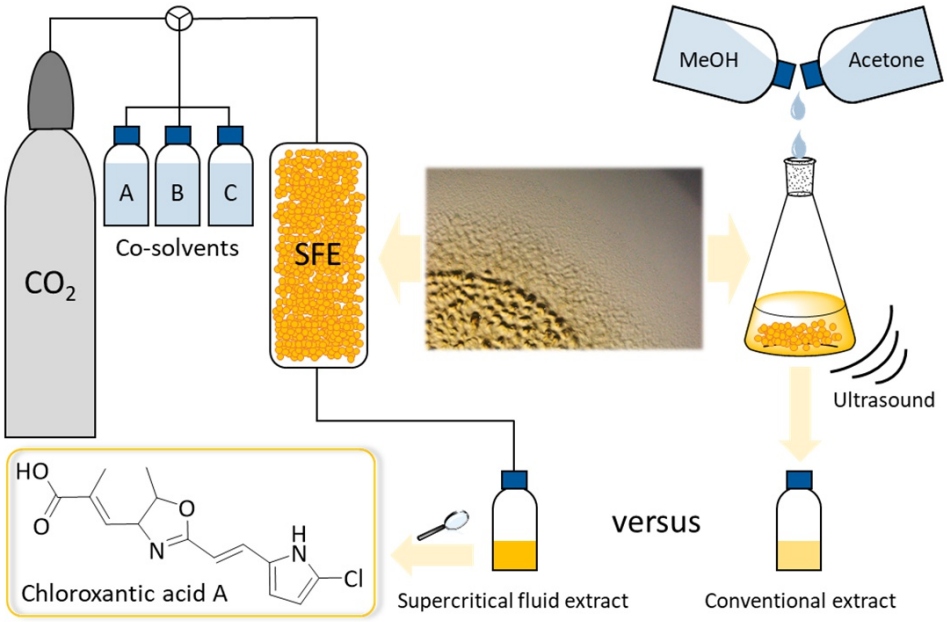

Graphical Abstract

5.2 Introduction

Over the years, supercritical fluid extraction (SFE) has contributed to efficient extraction processes of plant based natural products for pharmaceutical and food applications.[1,2] SFE is often characterized as a "green technology" as its benefits include comparably low energy and liquid solvent consumption, relying mainly on supercritical carbon dioxide (CO_2) as extraction solvent.[3] Furthermore it profits from the unique intrinsic properties of a supercritical fluid, showing liquid–like solvation because of its liquid-like density, combined with increased mass transfer between the extracted material and the supercritical fluid because of its gas–like viscosity and diffusivity.[4] These unique properties allowed extraction and isolation of a diverse set of natural products from plants, such as flavonoids and phenolic acids from *Medicago sativa L.* (Alfalfa)[5] or piperine from *Piper nigrum L.*.[6] In microbial natural product research however, the application of SFE appears limited to the isolation of natural products from cyanobacteria. The structural diversity among cyanobacterial metabolites isolated with SFE is high, comprising the epoxide containing polycyclic natural product chaetoglobosin, the xanthone sydowinin B, the nitrophenyl containing mycolutein and luteoreticuls, the glycosylated macrolactam elaiophylin and the polyunsaturated fatty acid γ-linoleic acid.[7,8] All of these compounds extractable with dichloromethane in a conventional solvent extraction approach can be enriched with alcohol-modified supercritical CO_2 extraction.[8]

Some of the metabolites successfully isolated with SFE from plants or cyanobacteria are not only characterized by their unique chemical properties but exhibit potent biological activities such as the cytotoxic chaetoglobosins.[9,10] The comparison of chemical profiles and biological activities of SF extracts to conventional solvent extracts has also been carried out successfully for various plants like *Satureja montana* or *Sideritis scardica Griseb.*.[11,12] Compared to soxhlet and hydrodistillation extracts of *Satureja montana*, SF extracts of this traditional medicine plant show stronger activities against *Bacillus cereus* and *B. subtilis* as well as unique activities against *Salmonella enteritidis* and *Colletotrichum coffeanum*.[11] These results highlight the potential impact of SFE on natural products research, as SFE was not only able to generate extracts with improved biological activities, but also enabled generation of extracts showing previously undetected biological activities.

In studies by Silva *et al.*, only supercritical CO_2 without the addition of co-solvent was used, which limits the supercritical fluid extraction exclusively to highly non-polar metabolites, as CO_2 itself is highly hydrophobic.[13] Esquivel-Hernández *et al.* have shown for the cyanobacterium *Arthrospira platensis* that from all variable extraction parameters like pressure, temperature, co-solvent and the introduction of static, dispersant and dynamic states during the extraction process, the choice of co-solvent has the highest impact on the extraction efficiency.[14] Pressure and temperature have to be chosen appropriately to exceed the supercritical point of CO_2 at 304.12 K and 73.7 bar.[14,15] Subsequently, they have to be kept high enough, to preserve the CO_2 in supercritical state. For choosing temperature and pressure, it has to be taken into account that increasing percentage of co-solvent increases pressure and temperature required to reach the supercritical point of the mixture.[16] The exact supercritical point of the respective mixture herein is strongly dependent on the chosen co-solvent. The most widely used co-solvents in SFE are alcohols such as ethanol (EtOH) and methanol (MeOH).[3]

For conventional solvent extraction, the choice of extraction solvent is also the most varied parameter. The extraction process can be enhanced by exposing the extraction mixture to microwaves, ultrasound or heat. Microwave-assisted extraction or heat supported extractions like soxhlet extraction, are not applicable for metabolites suffering from poor thermal stability, given for a broad range of natural products.[17] SFE in comparison offers the possibility to keep the temperature relatively low due to the additional pressure applied, without loss in extraction efficiency.[16] On the other hand, conventional solvent extraction methods have one main advantage: they come without expensive instrumentation.

Most microbial natural product isolation protocols rely on maceration as conventional solvent extraction method.[18–20] To access a preferably diverse set of microbial natural products, Ito *et al.* exemplarily used a mixture of dichloromethane:methanol:water (64:36:8).[18] Novel secondary metabolites from myxobacteria isolated in the past years have almost exclusively been extracted with classical solvent extraction methods, using acetone as most commonly used solvent. Besides acetone, only MeOH and ethyl acetate (EtOAc) were used.[21–26]

Despite its many advantages over solvent extraction, SFE is underrepresented in microbial natural product research and has never been described for the extraction of myxobacterial cells. Most publications dealing with SFE furthermore only report its utilization for previously described natural products, like caffeine or capsaicin.[3] As a representative example

for natural product extraction from microbial secondary metabolism we therefore set out to investigate the metabolome of three different myxobacterial strains using SFE in comparison to conventional ultrasound-assisted extraction (UAE) with acetone and MeOH. To study the influence of different co-solvents on the extraction of known myxobacterial metabolites, we performed targeted metabolomics-based examination of the SF extracts. Furthermore, all extracts were compared with regards to detection of antimicrobial activities. As a proof of concept, a novel secondary metabolite only detectable in trace amounts in UA extracts of the well-studied model organism *Myxococcus xanthus* DK1622 was isolated and structurally elucidated.

5.3 Methods and Material

All cultivation conditions, analytical methods and statistical data treatment procedures are described in detail in the Supporting Information.

Cultivation and Sample Preparation. Three myxobacterial strains (*M. xanthus* DK1622, *Sorangium* sp. MSr11367 and *Sandaracinus* sp. MSr10575) were grown in 2 liter shaking flasks containing 400 mL of cultivation medium for 10 days at 30 °C and 180 rpm. An autoclaved aqueous suspension of Amberlite XAD-16 resin was added to all production media to a volumetric concentration of 2% [v/v]. The cell pellets and resin were lyophilized prior to further processing. The combined dry pellet containing cells and resin was then pulverized using an electric coffee grinder and split into two equal batches. One batch was extracted by UAE whilst the other batch was extracted with SFE. Blank extracts were generated by extracting the medium with resin.

Extraction procedure. SFE was carried out on a Waters® MV-10 ASFE® system equipped with 10 mL analytical extraction cartridges. The pulverized pellets were densely packed into the cartridges and topped up with glass beads to avoid pressure drops due to inconsistencies in the packing. The extraction process was carried out at 200 bar and 40 °C using a total flow rate of 10 mL/min. The extraction was done in five steps, each one performed with an initial dynamic extraction step for 5 minutes followed by a static extraction step for 5 minutes and a second dynamic extraction step for another 5 minutes. The pellets were first extracted with 100% CO_2. Afterwards, the pellet was extracted with 20% EtOAc as co-solvent, followed by 20% isopropanol (^{i}PrOH), 20% MeOH and as a final step the pellet was flushed with 50% MeOH. The MeOH make-up flow was set to a total organic solvent

flow of 3 mL/min. All steps were collected and treated separately. The solvents were evaporated under reduced pressure and the residues were dissolved in 4 mL MeOH each. UAE consisted of two subsequent extraction steps, which were adapted from the most common extraction procedures conducted for myxobacterial natural products from 2018−2020 (see Chapter S3.1 Supporting Information)[21–24,27–34].

Firstly, 100 mL MeOH was added and the pellet sonicated for 1 h. After removal of the MeOH, 100 mL acetone was added, and the pellet was sonicated for another 1 h. The two extracts were combined, and the solvent was removed under reduced pressure. The residues were dissolved in 4 mL MeOH each. All extracts were diluted 1:100 prior to UHPLC-MS measurements.

Isolation procedure. Chloroxanthic acid A was isolated by semipreparative HPLC following a fractionation of the crude extract by liquid-liquid partitioning. Purification was performed on a Dionex Ultimate 3000 SDLC low pressure gradient system equipped with a Phenomonex Luna® 5 µm C18(2) 100 Å LC Column (250 x 10 mm) thermostated at 45 °C. Separation was achieved using a linear gradient from 95% (A) ddH_2O with 0.1% formic acid to 70% (B) acetonitrile with 0.1% formic acid over 29 minutes. The compound was detected by UV absorption at 210 and 280 nm.

Analytical analysis of crude extracts and pure compound. UHPLC-qTOF measurements were performed in duplicates as technical replicates on a Dionex Ultimate 3000 SL system coupled to a Bruker maXis 4G UHRqTOF. The mobile phase consisted of (A) ddH_2O with 0.1% formic acid and (B) acetonitrile with 0.1% formic acid. For separation a linear gradient from 5-95% B in A on a Waters Acquity BEH C18 column (100 x 2.1 mm, 1.7 µm d_p) was used. Flow rate was set to 0.6 mL/min and the column heated to 45 °C. The LC flow was split to 75 µL/min before entering the mass spectrometer, which was externally calibrated to a mass accuracy of < 1 ppm. External calibration was achieved with sodium formate clusters. Mass spectra were acquired in centroid mode ranging from 150-2500 m/z at a 2 Hz scan rate. Capillary voltage was set to + 4000 V for measurements in positive ionization mode. Dry gas was set to a flow rate of 5 L/min at 200 °C.

NMR spectra were recorded on a Bruker Ascend 700 spectrometer equipped with a 5 mm TXI cryoprobe (^{1}H at 700 MHz, ^{13}C at 175 MHz). All observed chemical shift values (δ) are given in in ppm and coupling constant values (J) in Hz. Standard pulse programs were used for HMBC, HSQC and COSY experiments. HMBC experiments were optimized for

$^{2,3}J_{C\text{-}H}$ = 6 Hz. The spectra were recorded in methanol-d_4 and chemical shifts of the solvent signals at δ_H 3.31 ppm and δ_C 49.2 ppm were used as reference signals for spectra calibration. To increase sensitivity, the measurements were conducted in a 5 mm Shigemi tube (Shigemi Inc., Allison Park, PA 15101, USA).

Statistical Analysis and Annotations. Statistical interpretation of the LC-MS data for targeted and non-targeted metabolomics analysis was carried out with MetaboScape 4.0 (Bruker). The minimal intensity threshold for feature detection by the built-in T-Rex 3D algorithm was set to 1.5 x 10^4 and the maximum charge was set to three. The minimal group size for creating batch features to five. Known myxobacterial secondary metabolites were annotated using our in-house database containing myxobacterial secondary metabolites (Myxobase). Overlap of the extraction methods as well as features uniquely found in one analysis were calculated via t-Test analysis in MetaboScape 4.0.

Determination of antimicrobial activities. For determination of the extracts' antimicrobial activities, all three biological replicates were combined and 20 µL of the saturated methanolic extract was pipetted to 150 µL microbial test culture and serially diluted in 96 well plates. The microbial test panel consisted of *Staphylococcus aureus* Newman, *Escherichia coli* DSM111, *E. coli* TolC, *Bacillus subtilits*, *Micrococcus luteus*, *Pseudomonas aeruginosa* PA14, *Candida albicans*, *Pichia anomala*, *Mucor hiemalis* and *Mycobacterium smegmatis* Mc2155.

5.4 Results and Discussion

We generated a total number of six different extracts per strain. In case of the SF extraction, the pellet was extracted sequentially with pure CO_2, followed by the addition of 20% EtOAc, ^{i}PrOH and MeOH as co-solvents. The co-solvents were used in ascending polarity. As the last step 50% MeOH was used in addition to the 20% MeOH step. When SF extracts are referred to in the following, this is indicated by the percentage and type of cosolvent used. Conventional extraction is referred to as ultrasound assisted extraction (UAE).

Influence of the co-solvent on the extraction of myxobacterial secondary metabolites. All extracts were investigated in a targeted metabolomics workflow and known myxobacterial secondary metabolites were annotated from our in-house data base (Myxobase). As *Sandaracinus* MSr10575 and *Sorangium* strain MSr11367 are new myxobacterial strains that were recently isolated in our working group, a lower number of metabolites is known

compared to the well-studied model myxobacterium *M. xanthus* DK1622.[35,36] In *M. xanthus* DK1622 extracts, five different natural product families, namely the cittilins, myxovirescins, DKxanthenes, myxalamides and myxochromids, are detected. Representatives of these natural product families are shown in Figure 5.1 (A-E). The remaining derivatives can be found in in the Supporting Information. Myxochelins and myxoprincomides, two additional natural product families known from this strain, are not produced under the chosen cultivation conditions. Besides those secondary metabolites, the strain is found to produce riboflavin. As there is a controversial debate if riboflavin should be taken as primary or secondary metabolite (sometimes classified as pseudo-secondary metabolite), the production and extraction is just mentioned for completeness but not discussed in more detail here.[37] Both described cittilin derivatives (A and B) could be detected in the extracts, with the highest intensity found in the 50% MeOH extracts.[38,39] Cittilins are also extractable with 20% MeOH as well as UAE and cittilin A can also be detected in lower intensities in the ^{i}PrOH extract. The family of myxovirescins contains more than 12 members, whereof six different derivatives (A-C and G-I) are detectable in our analysis.[40] The highest intensities of all myxovirescin derivatives are found in the EtOAc extracts. Contrary to the cittilins that are not extractable with pure CO_2, the myxovirescins are also extractable without the addition of any co-solvent in SFE. They are also present in low amounts in the 20% and 50% MeOH extracts. Due to the serial design of the experiment, this indicates that the myxovirescins could be extracted using MeOH as a co-solvent, but the compounds were already exhaustively extracted during the EtOAc step. Another abundant and derivative-rich family of secondary metabolites are the DKxanthenes (DKx).[41] In our analysis, we detect seven DKx derivatives, DKx 520, 526, 534, 544, 548, 560 and 574. Except for DKx 526 all derivatives show the highest intensities in the 50% MeOH extracts. DKx 526 on the other hand shows highest intensities in the EtOAc extract. All described myxalamide derivatives (A-D and K) are detectable in our extraction analysis, with highest intensities in the EtOAc extracts. The ^{i}PrOH extracts show higher intensities than the UAE as well.[42,43] From the myxochromide compound family, only one derivative (A3) is observed.[44] Here, we find highest intensities in the EtOAc extracts. Myxochromide A3 is also found in the ^{i}PrOH and both of the MeOH extracts. In those extracts the detected intensities of the secondary metabolite are on a similar level as in the UAE, indicating that only SF extraction

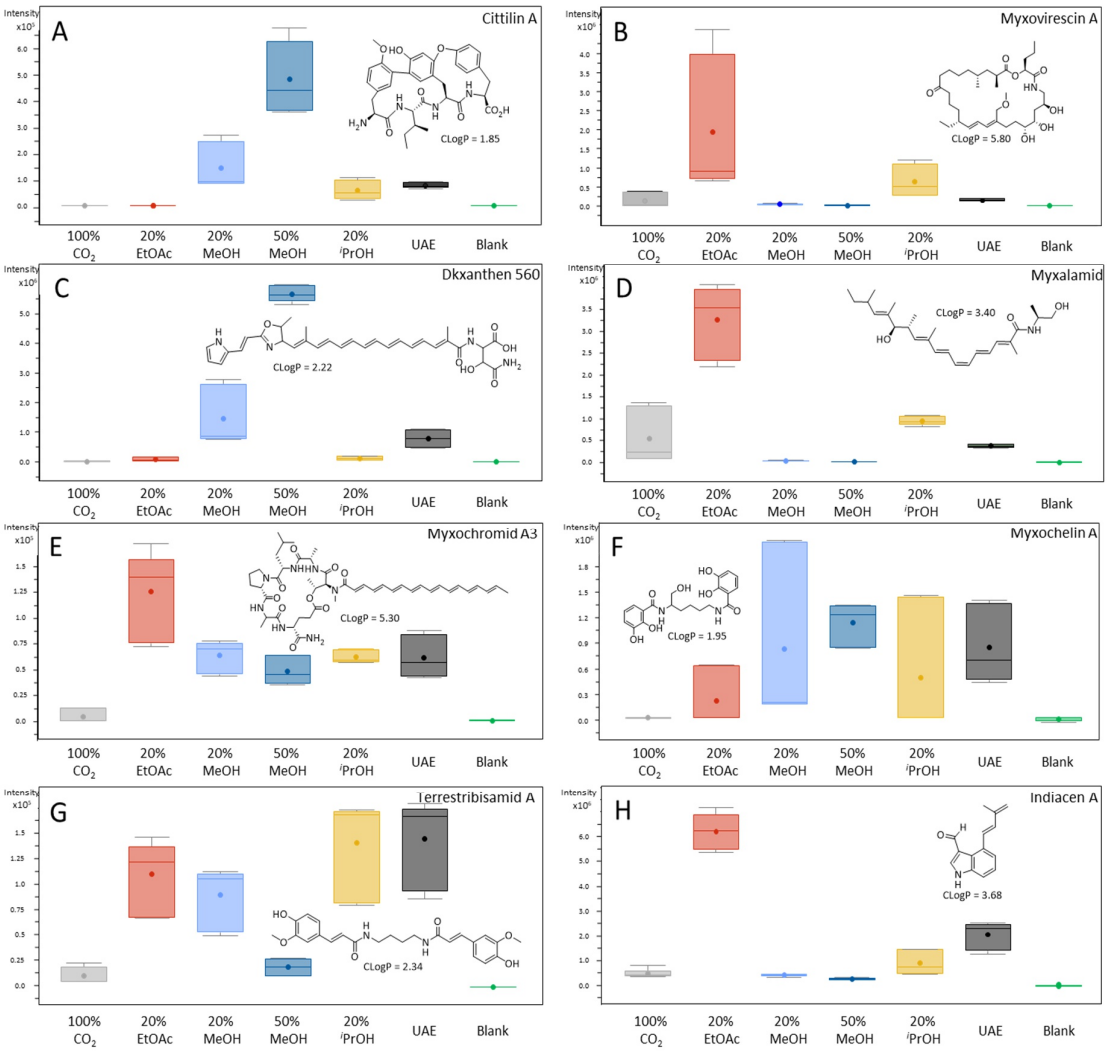

Figure 5.1 Influence of the co-solvent on the supercritical fluid extraction of secondary metabolites from *M. xanthus* DK1622 (**A-E**) and MSr10575 (**F-H**). Detected intensities are shown as box plots. From left to right: gray 100% CO_2, red 20% EtOAc, light blue 20% MeOH, dark blue 50% MeOH, yellow 20% ^{i}PrOH, black UAE and green combined blank (SFE+UAE).

using EtOAc is superior in extraction efficiency compared to UAE in this case. In the *Sandaracinus* MSr10575 extracts, three known myxobacterial secondary metabolite families are detectable (Figure 5.1 F-H). From the two natural myxochelins A and B only myxochelin A is observed in the extracts. Highest intensities are found in the 20% MeOH extracts, but the compound is present in all other extracts except the 100% CO_2 extract. Terrestribisamid A is the only known secondary metabolite in our extracts showing the highest intensity in one of the UA extracts.[45] Nevertheless, this compound is also extractable with SFE, whereby ^{i}PrOH shows the best extraction efficiency. Indiacen A and B, two secondary metabolites originally isolated from the myxobacterial strain *Sandaracinus amylolyticus*

NOSO-4T also belonging to the family of *Sandaracineae* are also found in the extracts of MSr10575.[46] The Indiacens show highest intensities in the EtOAc extracts. As those prenylated indole aldehydes with activity against Gram–positive and Gram–negative bacteria as well as the fungus *Mucor hiemalis* are the only reported secondary metabolites from another *Sandaracinus* strain to date, we wanted to validate our initial hit based on exact mass and retention time and isolated both derivatives. Crystallization followed by X-ray crystallography of the isolated compounds confirms that MSr10575 is indeed able to produce indiacens (see Supporting Information).

All known secondary metabolites described above are extractable with UAE as a conventional extraction method and SFE. Concerning the different co-solvents investigated, EtOAc and MeOH are found to be the most efficient co-solvents for extraction. MeOH-based SF extracts show specificity for more polar myxobacterial secondary metabolites, while EtOAc as a co-solvent leads to increased extraction of more nonpolar secondary metabolites. Furthermore, extraction with 50% MeOH as co-solvent seems to be superior to the extraction with 20% MeOH. Due to the relatively high pressure of 200 bar in our experiments, the CO_2/MeOH mixture remains in the supercritical state even when increasing to an equipotential portion of the co-solvent. This is reflected in the high extraction efficiency for more polar natural products such as the cittilins and the DKxanthenes.[47,48] Our data suggests that secondary metabolites such as myxovirescin A (CLog*P* =5.80), myxalamid A (CLog*P* = 3.40), myxochromid A3 (CLog*P* = 5.30) and indiacen A (CLog*P* = 3.68) exceeding a log*P* of 3 show best extraction using 20% EtOAc as a co-solvent. Secondary metabolites such as cittilin A (CLog*P* = 1.85), DKxanthen 560 (CLog*P* = 2.22), myxochelin A (CLog*P* = 2.34) and terrestribisamid A (CLog*P* = 2.34) with log*P* values below 3 are better extractable using more polar and protic co-solvents such as ^{i}PrOH and MeOH (see Figure 5.1). This log*P* dependency can also be observed during consecutive UA extraction with different solvents (see Supporting Information).

Antimicrobial activities of the SF and UA extracts. All of the three examined myxobacterial strains show potent activities against at least three test organisms of our antimicrobial test panel (see Figure 5.2). Extracts of *Sandaracinus* MSr10575 display the highest and broadest activities, with antimicrobial activities of at least one of the extracts against each of the test organisms. The conventional UA extract shows activities against *S. aureus*, *E. coli*, *E. coli* TolC (representing an efflux deficient *E. coli* strain), *B. subtilis*, *M. luteus*, *P. aeruginosa* and *M. smegmatis*. All of these activities are also found in the 20% MeOH and 50% MeOH SF extracts, indicating that the responsible metabolites are relatively polar. Interestingly, the 100% CO_2 extracts show a selective activity against Gram-positive pathogens as well as *C. albicans*. As those activities do not correlate to the ones observed in other extracts, it is very likely that they are caused by a different family of natural products. Furthermore, we observe activities of the ^{i}PrOH based SF extract against *M. luteus*, *M. smegmatis* and *C. albicans*. The EtOAc extract on the contrary shows a selective activity against *M. smegmatis*. Besides the activities of the ^{i}PrOH extract against *M. luteus* and *C. albicans* all activities are comparably strong, showing an inhibition down to a dilution of the extract to 0.1% of the starting concentration.

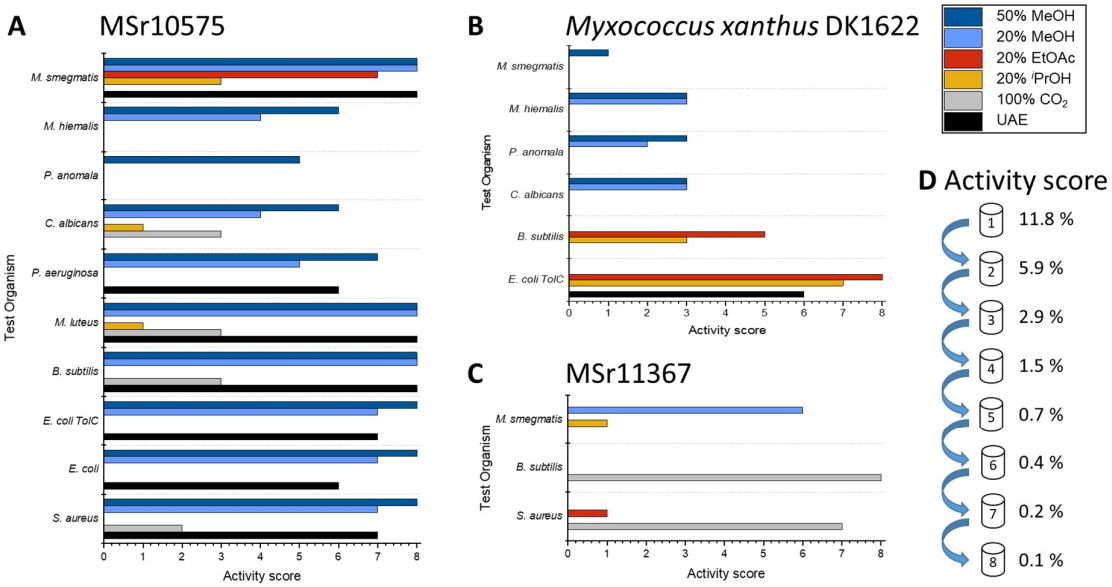

Figure 5.2 Antimicrobial activity score of myxobacterial SF extracts in comparison to conventional UA extraction (black). **A** MSr10575, **B** *M. xanthus* DK1622, **C** MSr11367. Extract with 50% MeOH as co-solvent is shown in dark blue, 20% MeOH in light blue, 20% EtOAc in red, 20% ^{i}PrOH in yellow and 100% CO_2 in grey. **D** Activity score with correlating concentration of the crude extract showing an inhibition of the test organism.

This indicates that the selectivity of antimicrobial activities does not result from the inaccuracy of the assay or the presence of compound yields close to their minimum inhibitory concentration (MIC), but rather the presence of several different antimicrobial natural product classes in the extract. From the known myxobacterial secondary metabolites produced by this strain, only indiacen is known for antimicrobial activity.[46] Although it was not tested against *M. smegmatis* itself, it exhibits activities against two related mycobacterial species. By far the highest intensities of indiacens are measured in our EtOAc extracts. This finding correlates with the selective inhibition of *M. smegmatis* by the EtOAc extract. Nevertheless, the strong other antimicrobial activities cannot be explained by the presence of already described secondary metabolites alone, making this strain a target for further secondary metabolite extraction campaigns.

The UA extract of *M. xanthus* DK1622 shows activities against *E. coli* TolC, explained by the presence of myxovirescins and myxalamids.[49,50] Anti-*E. coli* TolC activity was also found for the EtOAc and ^{i}PrOH extracts where myxovirescins and myxalamids are present in higher intensities than in the UAE. Furthermore, those two extracts show activity against *B. subtilis*, explained by the presence of the same natural product classes. In the UA extract the concentration of those secondary metabolites very likely does not reach the minimal inhibitory concentration, wherefore no activity against *B. subtilis* is detectable. We additionally observe antifungal activities of the SF MeOH extracts as well as antimycobacterial activity only observed for the 50% MeOH extract. None of these activities can be correlated to known secondary metabolites detectable in the crude extract, highlighting that the potential of secondary metabolite discovery even in well-described strains like *M. xanthus* DK1622 is far from exhausted.

MSr11367 only shows few activities compared to the other two strains. Contrary to the other myxobacterial strains we observe no antimicrobial activities in the UA extract at all. The 100% CO_2 extract of this strain, however, shows the highest antimicrobial activities when just comparing the 100% CO_2 extracts of the different strains and represents the only case where we can detect an activity selectively in the extract without co-solvent. Furthermore, we observe a strong activity of the 20% MeOH extract against *M. smegmatis* besides weak activities of the ^{i}PrOH extract against *M. smegmatis* and of the EtOAc extract against *S. aureus*. In all our extracts from MSr11367 we were not able to detect any known myxobacterial natural product, wherefore these activities offer the possibility for bioactivity-guided isolation of novel secondary metabolites.

In summary, for all three myxobacterial strains we were able to enhance the detectability of biological activities using SFE instead of UAE. Furthermore, each of the strains showed additional activities for the SF extracts, not observable for the UA extracts. This increase in detectable antimicrobial activities may stem from extraction of a larger dynamic range as well as enrichment of certain active secondary metabolites by introducing some selectivity to the extraction process. This selectivity can as well be introduced by using solvents with different polarity for UAE (see Supporting Information).

Non-targeted metabolomics investigation of the extracts. Besides the targeted metabolomics investigation of the three myxobacterial strains' extracts as well as their biological characterization, we sought to access the total chemical complexity of the different extracts to fully characterize overlaps and differences of the two extraction systems as well as the influence of the different co-solvents. We therefore performed a non-targeted metabolomics analysis and compared features detected in the UAE with those detected in the SF extracts. Furthermore, we compared features detected in the individual SF extracts resulting from the use of different co-solvents. The results of this investigation for strain MSr10575 are depicted in Figure 5.3 as Euler diagrams. Results for the two other strains can be found in the Supporting Information.

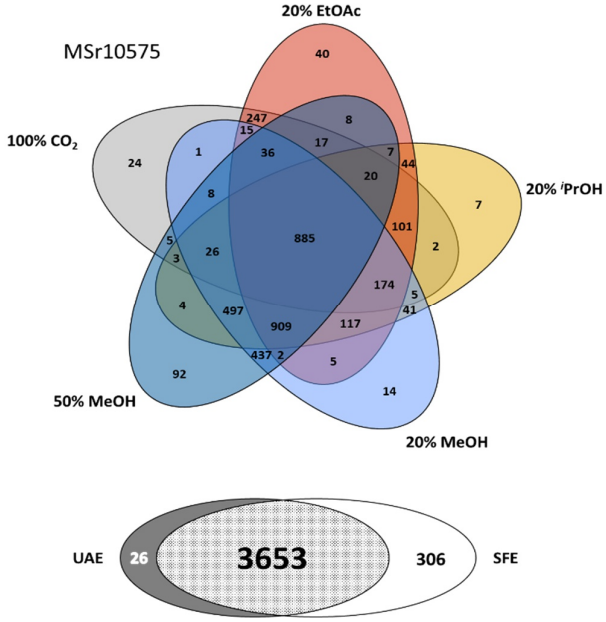

Figure 5.3 Upper part: Euler diagram showing features found in the SF extracts from MSr10575 sorted by co-solvent. Intersections of the extracts generated using different co-solvents are shown in the same colors as used in Fig. 1 and 2. Lower part: Euler diagram showing features unique for UAE or SFE and features extractable with both methods.

The overlap of features found with UAE and SFE is very high. 92% of the total features can be extracted with both methods. Looking at the features uniquely extractable with one of the methods, about 12% more features are only present in the SF extract than in the UA extract. If it is only a matter of accessing as many features as possible with one method, SFE should therefore be the method of choice. The comparison of the different co-solvents used for the extraction shows that the number of metabolites extractable with only one co-solvent is relatively low. Among the different co-solvents, extraction with 50% MeOH yielded the most features. In general, most of the metabolites are detectable in all of the SF extracts (885 features) or in all of the SF extracts except the CO_2 extract (909 features). Omitting the first extraction step with 100% CO_2 would only result in a data loss of less than 1% as all other metabolites are also accessible with the addition of co-solvents and should therefore be preferred if the extraction protocol needs to be shortened.

During the non-targeted investigation of the SF extracts of *M. xanthus* DK1622 a group of metabolites raised our interest. They all show significantly higher intensities in the SF extract using EtOAc as a co-solvent and an isotopic pattern characteristic for chlorination as depicted in Figure 5.4. Halogenated natural products are well-known to exhibit diverse biological activities, making those features particularly interesting for further investigation. The presence of 30 features with characteristic chlorination-indicating isotope pattern furthermore indicated, that they belong to a relatively large family of secondary metabolites (see Supporting Information). According to MS analysis all family members incorporate a minimum of two nitrogen and two oxygen atoms. To investigate the chemical structure of those compounds, we isolated the main derivative, later named chloroxanthic acid A. As the other compounds are only produced in comparably low amounts, they were not accessible to full structure elucidation by NMR.

Structure elucidation of chloroxanthic acid A. HRESIMS of chloroxanthic acid A shows an $[M+H]^+$ peak at *m/z* 295.0848 consistent with the molecular formula $C_{14}H_{15}ClN_2O_3$ (*m/z* calcd for $[M+H]^+$ 295.0844) containing 8 double-bond equivalents (DBE). The ^{1}H-NMR spectrum of chloroxanthic acid A exhibits five signals characteristic for double bond protons at δ = 7.14 (1H, d, J = 16.18 Hz), δ = 6.38 (2H, m), δ = 6.18 (1H, d, J = 16.09 Hz), δ = 6.03 (1H, d, J = 3.66 Hz). Furthermore, two methyl groups at δ = 1.94 (3H, d, J = 1.44 Hz) and δ = 1.43 (3H, dd, J = 7.00 Hz) and two methine groups at δ = 4.55 (1H, dd, J = 9.30 , J = 7.18 Hz) and δ = 4.46 (1H, m) are observed. Their coupling constants as well as

COSY correlations reveal the two protons at $\delta = 7.14$ and $\delta = 6.18$ to be part of an aliphatic double bond in *E*-configuration.

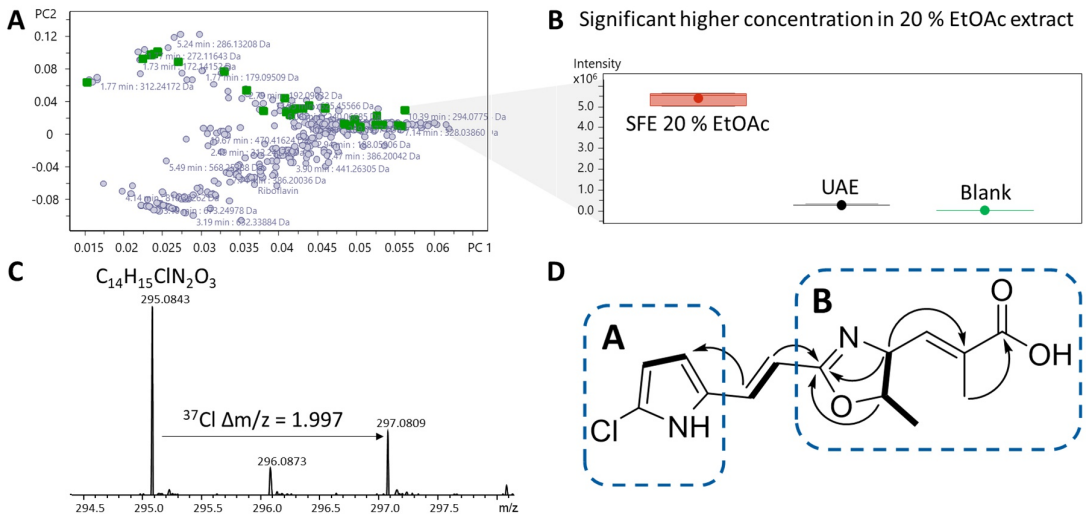

Figure 5.4 Chlorinated metabolites from *M. xanthus* DK1622. **A** PCA plot of the comparison between UAE and SFE 20% EtOAc extracts. Chlorinated features are highlighted in green. **B** Box plot for chloroxanthic acid A highlighting the differences in intensities between UAE and SFE EtOAC extract. **C** Zoom into the isotopic pattern of the $[M+H]^+$ peak of chloroxanthic acid A showing the characteristic mass shift of the ^{37}Cl isotope. **D** Structure of chloroxanthic acid A. Most relevant COSY correlations are marked bold and most relevant HMBC correlations are shown as arrows. Substructures A and B are marked in dashed blue boxes.

Their down-field chemical shift suggests participation in a bigger conjugated π-system. HMBC correlations show their location between two different substructures (substructure A and B) of the molecule (see Figure 5.4). COSY and HMBC correlations reveal, that substructure A consists of the two double bond protons at $\delta = 6.03$ and $\delta = 6.38$ as well as two quaternary carbons at $\delta = 129.8$ and $\delta = 120.2$. Their characteristic chemical shifts suggest that substructure A is a pyrrole ring with chlorination at the quaternary carbon at $\delta = 120.2$ and the quaternary carbon at $\delta = 129.8$ is the linker to the aliphatic double bond. The splitting pattern of the two protons of the pyrrole moiety as well as their COSY correlations confirm their allocation next to each other, leaving only two possibilities for substitution of the pyrrole ring. The downfield shifts of both the chlorine bearing carbon at $\delta = 120.2$ and the quaternary carbon at $\delta = 129.8$ finally reveal chlorination in 5 position of the pyrrole ring. In substructure B the two aliphatic double bond protons only show HMBC correlations to one quaternary carbon at $\delta = 166.8$. Its characteristic chemical shift as well as further HMBC correlations to the two methine groups at $\delta = 4.55$ and $\delta = 4.46$ suggest an oxazoline core structure. COSY correlations reveal a substitution with the methyl group at

δ = 4.46 in the 5 position. The 4 position of the oxazoline moiety is linked to 2-methylacrylic acid, which are confirmed by COSY and HMBC correlations.

Chloroxanthic acid A shows partial structural similarity to the DKxanthenes that were already described from *M. xanthus* DK1622 before.[41] The coupling constant of ^{3}J = 7.2 Hz indicates a Z-configuration of the two protons participating in the chloroxanthic acid A oxazoline ring, which is in line with the configuration determined for DKxanthenes. DKxanthenes are produced by a hybrid polyketide synthase – non-ribosomal peptide synthetase (PKS-NRPS) gene cluster.[51] The two NRP parts of the molecules are linked by a polyketide chain consisting of an aliphatic conjugated double bond system in variable chain lengths. Chloroxanthic acid A only comprises the first NRP part of the DKxanthenes, elongated with one methylmalonyl-CoA unit of the PK part. To the best of our knowledge, halogenated DKxanthene derivatives have not been described previously, nor is a halogenase part of the reported biosynthetic gene clusters of those natural products.[41,51] The isolation and structure elucidation of chloroxanthic acid A highlights the impact of applying deviant analytical chemistry approaches for the discovery of novel natural products from already well-studied bacterial strains. Besides the setup chosen for the detection of secondary metabolites as shown by the discovery of the myxoprincomides by Cortina *et al.,* the extraction method has a tremendous influence on the accessibility of natural products.

5.5 Conclusion

SFE in microbial secondary metabolomics is a promising yet underexplored technique for the discovery and extraction of new natural products. In our study, we were able to show that for each known metabolite in our three myxobacterial strains, supercritical CO_2 extraction efficiency was comparable or superior to conventional ultrasound assisted extraction. We developed an SFE protocol suitable for all metabolites that resulted in higher extraction yields for most target compounds. The choice of co-solvent herein plays an important role. For more polar compounds such as the cittilins or DKxanthenes, MeOH is the best co-solvent for extraction amongst the co-solvents tested in our study. Here we also observe that the use of 50% MeOH is superior to 20% MeOH. For myxobacterial natural products with a log*P* higher than 3, namely, the myxovirescins, myxalamides, indiacens and myxochromids, the most efficient co-solvent for extraction is EtOAc. Estimating the polarity of the secondary metabolite to be extracted therefore is crucial for the choice of a matching co-solvent. SFE offers the possibility to extract secondary metabolites from bacteria while

simultaneously introducing some degree of selectivity, whereas solvent extractions have a much broader extraction scope. Non-targeted analysis of the extracts underpin the notion that the choice of co-solvent (or rather the use of co-solvent at all) plays the most important role in SFE. Only less than one percent of myxobacterial compounds are extractable with pure CO_2 alone. Besides the many compounds extractable under all conditions, most myxobacterial secondary metabolites in this study are extractable when adding a polar co-solvent like ^{i}PrOH or MeOH. In comparison to UAE we find 12% more features uniquely extractable with SFE, highlighting that SFE should be preferred over UAE in order to access as many metabolites as possible. We also observe an increase in antimicrobial activities of the SF extracts compared to the UA extracts. Importantly, some antimicrobial activities could only be seen in the SF extracts indicating that certain bioactive metabolites can only be detected and isolated using the SF-based approach. This is exemplified by strain MSr11367, where we could not observe any bioactivities from the UAE at all.

Our non-targeted analysis of the extracts shows that the overall number of metabolites that are exclusively extractable with SFE is comparably low. Nevertheless, this result highlights that the most powerful feature of SFE is its capability to increase the metabolite concentration in the resulting extract fractions thereby making new metabolites accessible. This finding is also reflected in the increased bioactivities seen in SF extracts. Many secondary metabolites are generally detectable with highly sensitive mass spectrometry but may not give rise to bioactivity in assays as these often suffer from comparably low sensitivity, especially in case of cell based assays aiming to identify antifungals and antibacterials. The use of SFE can therefore help to detect and prioritize new natural products based on their antimicrobial activities. Furthermore, our study shows that SFE can be used to prioritize secondary metabolites for isolation and structure elucidation based on their chemical properties, as demonstrated here for chloroxanthic acid A. In this case, SFE achieved concentrations in the extract at which isolation and structure elucidation became feasible, without the necessity to upscale to very high culture volumes. Especially for myxobacteria – where the change in cultivation conditions during upscaling often results in a decrease of secondary metabolite production – SFE thus paves the way to access secondary metabolites that have not been uncovered to date.[52] Taken together, the advantageous features of SFE encourage its use for a wider range of microbial natural products applications in the future.

Associated content

The Supporting Information is available free of charge at https://pubs.acs.org/doi/10.1021/acs.analchem.0c02995.

Media recipes and detailed cultivation conditions, calculation of analytical GREEnness, evaluation of different solvents for UAE, box plots (targeted metabolomics investigation) of complete natural product families, summary of chlorinated metabolites in *M. xanthus* DK1622 extracts, Euler diagrams for *M. xanthus* DK1622 and MSr11367 (non-targeted metabolomics investigation), and raw data for structure elucidation of indiacene A and chloroxanthic acid A.

Acknowledgments

We thank Viktoria Schmitt and Stefanie Schmidt for performing the antimicrobial assays, Ghaith Zahra for his help with the cultivations, and Alexander Kiefer as well as Jake F.P. Haeckl for proofreading of the manuscript.

Abbreviations

NP	natural product
MS	mass spectrometer
HPLC	high performance liquid chromatography
BGC	biosynthetic gene cluster
SFE	supercritical fluid extraction
UAE	ultrasound-assisted extraction.

5.6 References

(1) Rafińska, K.; Pomastowski, P.; Rudnicka, J.; Krakowska, A.; Maruśka, A.; Narkute, M.; Buszewski, B. Effect of solvent and extraction technique on composition and biological activity of *Lepidium sativum* extracts. *Food Chem.* **2019**, *289*, 16–25.

(2) Manjare, S. D.; Dhingra, K. Supercritical fluids in separation and purification: A review. *Mater. Sci. Technol.* **2019**, *2*, 463–484.

(3) Khaw, K.-Y.; Parat, M.-O.; Shaw, P. N.; Falconer, J. R. Solvent Supercritical Fluid Technologies to Extract Bioactive Compounds from Natural Sources: A Review. *Molecules (Basel, Switzerland)* **2017**, *22*.

(4) Chollet, C.; Boutet-Mercey, S.; Laboureur, L.; Rincon, C.; Méjean, M.; Jouhet, J.; Fenaille, F.; Colsch, B.; Touboul, D. Supercritical fluid chromatography coupled to mass spectrometry for lipidomics. *J. Mass Spectrom.* **2019**, *54*, 791–801.

(5) Wrona, O.; Rafińska, K.; Walczak-Skierska, J.; Możeński, C.; Buszewski, B. Extraction and Determination of Polar Bioactive Compounds from Alfalfa (Medicago sativa L.) Using Supercritical Techniques. *Molecules (Basel, Switzerland)* **2019**, *24*.

(6) Dutta, S.; Bhattacharjee, P. Enzyme-assisted supercritical carbon dioxide extraction of black pepper oleoresin for enhanced yield of piperine-rich extract. *J. Biosci. Bioeng.* **2015**, *120*, 17–23.

(7) Yang, X.; Li, Y.; Li, Y.; Ye, D.; Yuan, L.; Sun, Y.; Han, D.; Hu, Q. Solid Matrix-Supported Supercritical CO_2 Enhances Extraction of γ-Linolenic Acid from the Cyanobacterium Arthrospira (Spirulina) platensis and Bioactivity Evaluation of the Molecule in Zebrafish. *Marine drugs* **2019**, *17*.

(8) Cocks, S.; Wrigley, S. K.; Chicarelli-Robinson, M. I.; Smith, R. M. High-performance liquid chromatograpy comparison of supercritical-fluid extraction and solvent extraction of microbial fermentation products. *J. Chromatogr. A* **1995**, *697*, 115–122.

(9) Knudsen, P. B.; Hanna, B.; Ohl, S.; Sellner, L.; Zenz, T.; Döhner, H.; Stilgenbauer, S.; Larsen, T. O.; Lichter, P.; Seiffert, M. Chaetoglobosin A preferentially induces apoptosis in chronic lymphocytic leukemia cells by targeting the cytoskeleton. *Leukemia* **2014**, *28*, 1289–1298.

(10) Li, B.; Gao, Y.; Rankin, G. O.; Rojanasakul, Y.; Cutler, S. J.; Tu, Y.; Chen, Y. C. Chaetoglobosin K induces apoptosis and G2 cell cycle arrest through p53-dependent pathway in cisplatin-resistant ovarian cancer cells. *Cancer Lett.* **2015**, *356*, 418–433.

(11) Silva, F. V. M.; Martins, A.; Salta, J.; Neng, N. R.; Nogueira, J. M. F.; Mira, D.; Gaspar, N.; Justino, J.; Grosso, C.; Urieta, J. S.*; et al.* Phytochemical profile and anticholinesterase and antimicrobial activities of supercritical versus conventional extracts of *Satureja montana*. *J. Agric. Food Chem.* **2009**, *57*, 11557–11563.

(12) Tadić, V.; Bojović, D.; Arsić, I.; Dorđević, S.; Aksentijevic, K.; Stamenić, M.; Janković, S. Chemical and antimicrobial evaluation of supercritical and conventional *Sideritis scardica* Griseb., Lamiaceae extracts. *Molecules (Basel, Switzerland)* **2012**, *17*, 2683–2703.

(13) Wrona, O.; Rafińska, K.; Możeński, C.; Buszewski, B. Supercritical Fluid Extraction of Bioactive Compounds from Plant Materials. *J. AOAC Int.* **2017**, *100*, 1624–1635.

(14) Esquivel-Hernández, D. A.; Rodríguez-Rodríguez, J.; Cuéllar-Bermúdez, S. P.; García-Pérez, J. S.; Mancera-Andrade, E. I.; Núñez-Echevarría, J. E.; Ontiveros-Valencia, A.; Rostro-Alanis, M.; García-García, R. M.; Torres, J. A.*; et al.* Effect of Supercritical Carbon Dioxide Extraction Parameters on the Biological Activities and Metabolites Present in Extracts from Arthrospira platensis. *Marine drugs* **2017**, *15*.

(15) Aresta, M. *Carbon dioxide as chemical feedstock*; Green chemistry; Wiley-VCH: Weinheim, 2010.

(16) Pourmortazavi, S. M.; Hajimirsadeghi, S. S. Supercritical fluid extraction in plant essential and volatile oil analysis. *J. Chromatogr. A* **2007**, *1163*, 2–24.

(17) Alvarez-Sanchez, B.; Priego-Capote, F.; de Castro,M. D. L. Metabolomics analysis II. Preparation of biological samples prior to detection. *Trends Anal. Chem.* **2010**, *29*, 120–127.

(18) Tatsuya Ito; Miyako Masubuchi. Dereplication of microbial extracts and related analytical technologies. *J. Antibiot.* **2014**, *67*, 353–360.

(19) Seidel, V. Initial and Bulk Extraction of Natural Products Isolation. In *Natural products isolation,* 3rd ed. / edited by Satyajit D. Sarker, Lutfun Nahar; Sarker, S. D., Nahar, L., Eds.; Methods in molecular biology, 1064-3745 864; Humana Press: New York, 2012; pp 27–41.

(20) Zhang, L. Integrated Approaches for Discovering Novel Drugs From Microbial Natural Products. In *Natural Products*; Zhang, L., Demain, A. L., Eds.; Humana Press Inc: [New York], 2005; pp 33–55.

(21) Panter, F.; Krug, D.; Müller, R. Novel Methoxymethacrylate Natural Products Uncovered by Statistics-Based Mining of the *Myxococcus fulvus* Secondary Metabolome. *ACS Chem. Biol.* **2019**, *14*, 88–98.

(22) Zhang, F.; Braun, D. R.; Rajski, S. R.; DeMaria, D.; Bugni, T. S. Enhypyrazinones A and B, Pyrazinone Natural Products from a Marine-Derived Myxobacterium *Enhygromyxa sp*. *Marine drugs* **2019**, *17*.

(23) Surup, F.; Chauhan, D.; Niggemann, J.; Bartok, E.; Herrmann, J.; Koeck, M.; Zander, W.; Stadler, M.; Hornung, V.; Müller, R. Activation of the NLRP3 inflammasome by hyaboron, a new asymmetric boron-containing macrodiolide from the Myxobacterium *Hyalangium minutum*. *ACS Chem. Biol.* **2018**, *13*, 2981–2988.

(24) Gorges, J.; Panter, F.; Kjaerulff, L.; Hoffmann, T.; Kazmaier, U.; Müller, R. Structure, Total Synthesis, and Biosynthesis of Chloromyxamides: Myxobacterial Tetrapeptides Featuring an Uncommon 6-Chloromethyl-5-methoxypipecolic Acid Building Block. *Angew. Chem. Int. Ed. Engl.* **2018**, *57*, 14270–14275.

(25) Kjaerulff, L.; Raju, R.; Panter, F.; Scheid, U.; Garcia, R.; Herrmann, J.; Müller, R. Pyxipyrrolones: Structure elucidation and biosynthesis of cytotoxic myxobacterial metabolites. *Angew. Chem. Int. Ed.* **2017**, *56*, 9614–9618.

(26) Nadmid, S.; Plaza, A.; Garcia, R.; Müller, R. Cystochromones, unusual chromone-containing polyketides from the myxobacterium *Cystobacter* sp. MCy9104. *J. Nat. Prod.* **2015**, *78*, 2023–2028.

(27) Hoffmann, T.; Krug, D.; Bozkurt, N.; Duddela, S.; Jansen, R.; Garcia, R.; Gerth, K.; Steinmetz, H.; Müller, R. Correlating chemical diversity with taxonomic distance for discovery of natural products in myxobacteria. *Nat. Commun.* **2018**, *9*, 803.

(28) Hug, J. J.; Panter, F.; Krug, D.; Müller, R. Genome mining reveals uncommon alkylpyrones as type III PKS products from myxobacteria. *J. Ind. Microbiol. Biotechnol.* **2019**, *46*, 319–334.

(29) Panter, F.; Krug, D.; Baumann, S.; Müller, R. Self-resistance guided genome mining uncovers new topoisomerase inhibitors from myxobacteria. *Chem. Sci.* **2018**, *9*, 4898–4908.

(30) Okoth Dorothy A.; Hug, J. J.; Garcia, R.; Spröer, C.; Overmann, J.; Müller, R. 2-Hydroxysorangiadenosine: Structure and Biosynthesis of a Myxobacterial Sesquiterpene–Nucleoside. *Molecules (Basel, Switzerland)* **2020**, *25*.

(31) Oueis, E.; Klefisch, T.; Zaburannyi, N.; Garcia, R.; Plaza, A.; Müller, R. Two Biosynthetic Pathways in *Jahnella thaxteri* for Thaxteramides, Distinct Types of Lipopeptides. *Org. Lett.* **2019**, *21*, 5407–5412.

(32) Sester, A.; Winand, L.; Pace, S.; Hiller, W.; Werz, O.; Nett, M. Myxochelin- and Pseudochelin-Derived Lipoxygenase Inhibitors from a Genetically Engineered *Myxococcus xanthus* Strain. *J. Nat. Prod.* **2019**, *82*, 2544–2549.

(33) Dehhaghi, M.; Tan, V.; Heng, B.; Mohammadipanah, F.; Guillemin, G. J. Protective Effects of Myxobacterial Extracts on Hydrogen Peroxide-induced Toxicity on Human Primary Astrocytes. *Neuroscience* **2019**, *399*, 1–11.

(34) Lee, C.; Park, S.; Ayush, I.; Cho, K.; Kim, S. S.; Kang, I.; Choe, W.; Kim, Y.-S.; Yoon, K.-S. Effects of *Myxococcus fulvus* KYC4048 Metabolites on Breast Cancer Cell Death. *J. Microbiol. Biotechnol.* **2018**, *28*, 765–775.

(35) Bader, C. D.; Panter, F.; Müller, R. In depth natural product discovery - Myxobacterial strains that provided multiple secondary metabolites. *Biotechnol. Adv.* **2020**, *39*, 107480.

(36) Wenzel, S. C.; Müller, R. Myxobacteria—''microbial factories' for the production of bioactive secondary metabolites. *Mol. Biosyst.* **2009**, *5*, 567–574.

(37) Abbas, C. A.; Sibirny, A. A. Genetic control of biosynthesis and transport of riboflavin and flavin nucleotides and construction of robust biotechnological producers. *Microbiol. Mol. Biol. Rev.* **2011**, *75*, 321–360.

(38) Krug, D.; Zurek, G.; Revermann, O.; Vos, M.; Velicer, G. J.; Müller, R. Discovering the Hidden Secondary Metabolome of *Myxococcus xanthus*: a Study of Intraspecific Diversity. *Appl. Environ. Microbiol.* **2008**, *74*, 3058–3068.

(39) Hug, J. J.; Dastbaz, J.; Adam, S.; Revermann, O.; Koehnke, J.; Krug, D.; Müller, R. Biosynthesis of Cittilins, Unusual Ribosomally Synthesized and Post-translationally Modified Peptides from *Myxococcus xanthus*. *ACS Chem. Biol.* **2020**, *15*, 2221–2231.

(40) Trowitzsch, W.; Wray, V.; Gerth, K.; Höfle, G. Structure of myxovirescin A, a new macrocylic antibiotic from gliding bacteria. *J. Chem. Soc., Chem. Commun.* **1982**, 1340.

(41) Meiser, P.; Bode, H. B.; Müller, R. The unique DKxanthene secondary metabolite family from the myxobacterium *Myxococcus xanthus* is required for developmental sporulation. *Proc. Natl. Acad. Sci. U.S.A.* **2006**, *103*, 19128–19133.

(42) Jansen, R.; Reifenstahl, G.; Gerth, K.; Reichenberg, H.; Höfle, G. Myxalamide A,B,C und D, eine Gruppe homologer Antibiotika aus *Myxococcus xanthus* Mx x12 (Myxobacterales). *Liebigs Ann. Chem.* **1983**, 1081–1095.

(43) Kim, J.; Choi, J. N.; Kim, P.; Sok, D. E.; Nam, S. W.; Lee, C. H. LC-MS/MS Profiling-Based Secondary Metabolite Screening of *Myxococcus xanthus*. *J. Microbiol. Biotechnol.* **2009**, *19*, 51–54.

(44) Trowitzsch Kienast, W.; Gerth, K.; Reichenbach, H.; Höfle, G. Myxochromid A: Ein hochungesättigtes Lipopeptidlacton aus *Myxococcus virescens*. *Liebigs Ann. Chem.* **1993**, 1233–1237.

(45) Iwasa, K.; Takahashi, T.; Nishiyama, Y.; Moriyasu, M.; Sugiura, M.; Takeuchi, A.; Tode, C.; Tokuda, H.; Takeda, K. Online structural elucidation of alkaloids and other constituents in crude extracts and cultured cells of *Nandina domestica* by combination of LC-MS/MS, LC-NMR, and LC-CD analyses. *J. Nat. Prod.* **2008**, *71*, 1376–1385.

(46) Steinmetz, H.; Mohr, K. I.; Zander, W.; Jansen, R.; Gerth, K.; Müller, R. Indiacens A and B: prenyl indoles from the *myxobacterium Sandaracinus amylolyticus*. *J. Nat. Prod.* **2012**, *75*, 1803–1805.

(47) Helka Turunen. CO2-Balance in the Atmosphere and CO2-Utilisation: an engineering approach. Academic dissertation, University of Oulu, Linnanmaa, 2011.

(48) RAMSEY, E. D. *Analytical Supercritical Fluid Extraction Techniques*; Springer Netherlands: Dordrecht, 2012.

(49) Gerth, K.; Jansen, R.; Reifenstahl, G.; Höfle, G.; Irschik, H.; Kunze, B.; Reichenbach, H.; Thierbach, G. The myxalamids, new antibiotics from *Myxococcus xanthus*

(Myxobacterales). I. Production, physico-chemical and biological properties, and mechanism of action. *J. Antibiot.* **1983**, *36*, 1150–1156.

(50) Xiao, Y.; Gerth, K.; Müller, R.; Wall, D. Myxobacterium-produced antibiotic TA (myxovirescin) inhibits type II signal peptidase. *Antimicrob. Agents Chemother.* **2012**, *56*, 2014–2021.

(51) Meiser, P.; Weissman, K. J.; Bode, H. B.; Krug, D.; Dickschat, J. S.; Sandmann, A.; Müller, R. DKxanthene biosynthesis–understanding the basis for diversity-oriented synthesis in myxobacterial secondary metabolism. *Chem. Biol.* **2008**, *15*, 771–781.

(52) Hug, J. J.; Bader, C. D.; Remškar, M.; Cirnski, K.; Müller, R. Concepts and Methods to Access Novel Antibiotics from Actinomycetes. *Antibiotics* **2018**, *7*, 44.

Supporting Information

Supercritical Fluid Extraction Enhances Discovery of Secondary Metabolites from Myxobacteria

Chantal D. Bader[†], **Markus Neuber**[†], Fabian Panter[†], Daniel Krug[†] and Rolf Müller[†]*

* Corresponding author

[†] Department Microbial Natural Products, Helmholtz-Institute for Pharmaceutical Research Saarland (HIPS), Helmholtz Centre for Infection Research (HZI), German Center for Infection Research (DZIF, Partner site Hannover-Braunschweig) and Department of Pharmacy, Saarland University Campus E8.1, 66123 Saarbrücken (Germany)

Extract generation for statistical analysis and bioactivity profiling

Myxobacterial culture media

All culture media were prepared using deionized water and autoclaved at 121 °C, 2 bar for 20 min. Sterile-filtered Fe-EDTA and sterile-filtered Vitamin B_{12} were added after autoclaving of the medium. Cultivations were performed in triplicates as biological replicates.

Seed cultures

As seed culture, *M. xanthus* DK1622 was cultivated in CTT medium, MSr10575 in 2-SWT medium and MSr11367 in SHG-P medium, each in 100 mL culture volume in a 300 mL shaking flasks. The strains were grown at 30°C and 180 rpm on an orbitron shaker for three days prior to inoculation of the production cultures.

Production cultures

As production culture, *M. xanthus* DK1622 was cultivated in SHG-P medium, MSr10575 in 2-SWT medium and MSr11367 in PYGS medium, each in 400 mL culture volume in 2000 mL shaking flasks. The strains were grown at 30°C and 180 rpm on an orbital shaker for ten days prior to inoculation of the production cultures. Inoculation was performed using 5 % [v/v] of the seed cultures. To adsorb the metabolites Amberlite XAD16 resin was added to all production media to a volumetric concentration of 2 % [v/v]. At the end of fermentation, both resin and cells were harvested together by centrifugation (8000 rpm, 4 °C, 20 min).

Media recipes

Table S5.1 Medium recipe of CTT medium.

Ingredient	Supplier	Amount [mM]	pH adjusted to
Bacto Casitone	Difco	1.0 %	7.2 (KOH)
Tris-HCl		10.0	
KH_2PO_4		1.0	
$MgSO_4$ x 7 H_2O	Grüssing	8.0	

Table S5.2 Medium recipe of PYGS medium.

Ingredient	Supplier	Amount [%]	pH adjusted to
Potato starch	Sigma-Aldrich	1.0	7.6 (KOH)
Fresh baker's yeast	DHW	2.0	
Glucose	Roth	0.5	
$CaCl_2$ x 2 H_2O	VWR Chemicals	0.1	
$MgSO_4$ x 7 H_2O	Grüssing	0.1	
TRIS-HCl	Roth	11.9 (50 mM)	

Table S5.3 Medium recipe of 2-SWT medium.

Ingredient	Supplier	Amount [%]	pH adjusted to
Bacto tryptone	Difco	0.3	7.0 (KOH)
Soytone	BD	0.1	
Glucose	Roth	0.2	
Soluble starch	Roth	0.2	
Maltose monohy-drate	Roth	0.1	
Cellobiose	MP-Biomedicals	0.2	
$CaCl_2$ x 2 H_2O	VWR Chemicals	0.05	
$MgSO_4$ x 7 H_2O	Grüssing	0.1	
HEPES	Roth	10 mM	

Table S5.4 Medium recipe of SHG-P medium.

Ingredient	Supplier	Amount [%]	pH adjusted to
Corn flour	Sigma-Aldrich	2	7.5 (KOH)
Soluble starch	Roth	1	
Glycerol	Sigma-Aldrich	2	
$CaCO_3$		0.2	

Calculation of the Analytical GREEnness

SFE and UAE were compared regarding their environmental friendliness and human safety using the AGREE Analytical GREEnness calculator.[1] Here 12 principles of green analytical chemistry are transformed into a 0-1 scale, as shown below for both extractions. 1 would represent an optimal analytical chemistry process, whereas 0 represents a process which does not meet the criteria. Weight for all criteria was set to 2 to rank all criteria equally.

SF extraction

Analytical Greenness report sheet

29/09/2020 17:18:23

Criteria	Score	Weight
1. Direct analytical techniques should be applied to avoid sample treatment.	0.3	2
2. Minimal sample size and minimal number of samples are goals.	0.65	2
3. If possible, measurements should be performed in situ.	0.0	2
4. Integration of analytical processes and operations saves energy and reduces the use of reagents.	0.8	2
5. Automated and miniaturized methods should be selected.	1.0	2
6. Derivatization should be avoided.	1.0	2
7. Generation of a large volume of analytical waste should be avoided, and proper management of analytical waste should be provided.	0.17	2
8. Multi-analyte or multi-parameter methods are preferred versus methods using one analyte at a time.	1.0	2
9. The use of energy should be minimized.	0.5	2
10. Reagents obtained from renewable sources should be preferred.	0.5	2
11. Toxic reagents should be eliminated or replaced.	0.0	2
12. Operator's safety should be increased.	0.8	2

Figure S5.1 Analytical GREEnness evaluation of SFE.

UA extraction

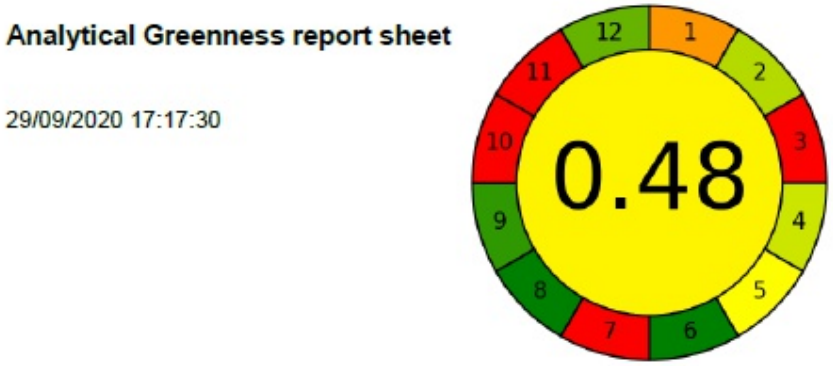

Criteria	Score	Weight
1. Direct analytical techniques should be applied to avoid sample treatment.	0.3	2
2. Minimal sample size and minimal number of samples are goals.	0.65	2
3. If possible, measurements should be performed in situ.	0.0	2
4. Integration of analytical processes and operations saves energy and reduces the use of reagents.	0.6	2
5. Automated and miniaturized methods should be selected.	0.5	2
6. Derivatization should be avoided.	1.0	2
7. Generation of a large volume of analytical waste should be avoided, and proper management of analytical waste should be provided.	0	2
8. Multi-analyte or multi-parameter methods are preferred versus methods using one analyte at a time.	1.0	2
9. The use of energy should be minimized.	0.91	2
10. Reagents obtained from renewable sources should be preferred.	0.0	2
11. Toxic reagents should be eliminated or replaced.	0.0	2
12. Operator's safety should be increased.	0.8	2

Figure S5.2 Analytical GREEnness evaluation of UAE.

All criteria influenced by sample preparation and subsequent analytical measurements are set to the same values, as those steps are the same for SF and UA extraction. For the two extraction procedures therefore main differences are found in criteria number 5 and 7, as

UAE is a fully manual process, whereas SFE is automated. Also the amount of waste generated is reduced for SFE, as at least 50% of the solvent used is CO_2 which can be recycled from other industrial processes. The difference of the total ranking of both extractions however is lowered as UAE requires less than 10% of the energy that is required for SFE (9).

Development of the UA extraction protocol

Extraction conditions

Classical solvent extraction (using one solvent stirring at room temperature) is still the most widespread extraction protocol used for natural product extraction from microorganisms. However, to the best of our knowledge there is no publication available, comparing the parameters chosen for solvent extraction of microorganisms used in recent years. This was only done for plant secondary metabolites, where the extraction procedures greatly differ due to the absence of media components. The UAE protocol used in this study we therefore developed adapted from the extraction protocols used for isolation of novel myxobacterial secondary metabolites and extract generation for comparison of biological functions in the past two years.[2–12] Except for one study, all used MeOH or acetone (or both) for the extraction, wherefore we decided to use a combination of both solvents. Concerning the solid/liquid ratio, those publications used between 4 and 20 % of extraction solvent related to the culture volume for compound isolation. However, as many publications do not mention the amount of solvent used per culture volume or solid mass at all, we decided to take the same amount of solvent as the culture volume, to guarantee exhaustive extraction. This may not represent the optimal method concerning "greenness", but we wanted to circumvent limiting the extraction efficiency by using not enough solvent. In most of the cases the extraction time chosen for compound extraction for subsequent isolation is also not mentioned, but for analytical extraction 60 minutes was the common timespan chosen per solvent, wherefore we took this as widely accepted time for extraction.

Extraction solvent

To investigate if MeOH and acetone really are the best solvents for extraction of myxobacterial secondary metabolites we carried out a targeted metabolomics comparison of extracts generated with the same solvents as previously used as co-solvents for SFE. For this purpose we re-grew the three myxobacterial strains used in our study in their respective media

(later on referred as batch 2) and extracted aliquots of 100 mg dry, pulverized pellet separately with 1.5 mL hexane, EtOAc, ^{i}PrOH, acetone or MeOH following otherwise the same conditions for extraction and analytical evaluation as used for UAE before. As those results stem from a second cultivation and the extracts were generated with a different volume of solvent used for extraction, intensity levels of the detected secondary metabolites as well as biological activities of those extracts cannot directly be compared to the results of the first batch and should be treated as a separate individual evaluation. The box plots showing extraction efficiency for secondary metabolites detectable in the extracts are shown in figure Figure S5.3Figure S5.22.

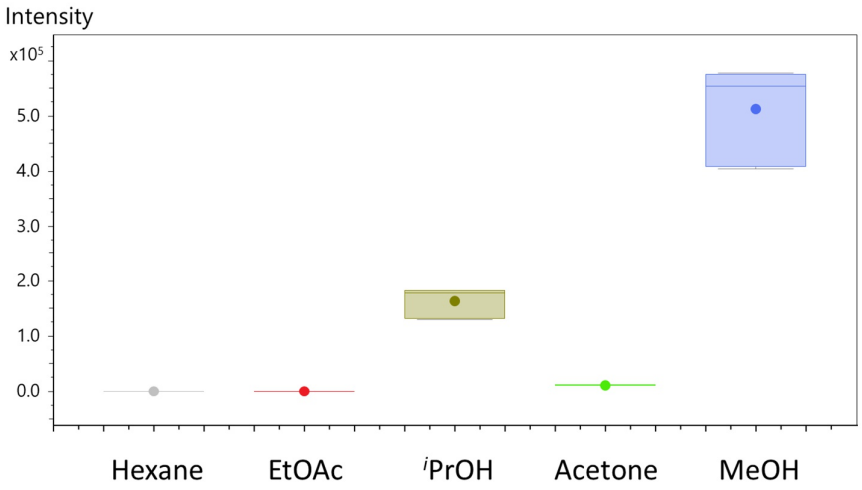

Figure S5.3 Box plot for cittilin A from *M. xanthus* DK1622 comparing different solvents for UAE.

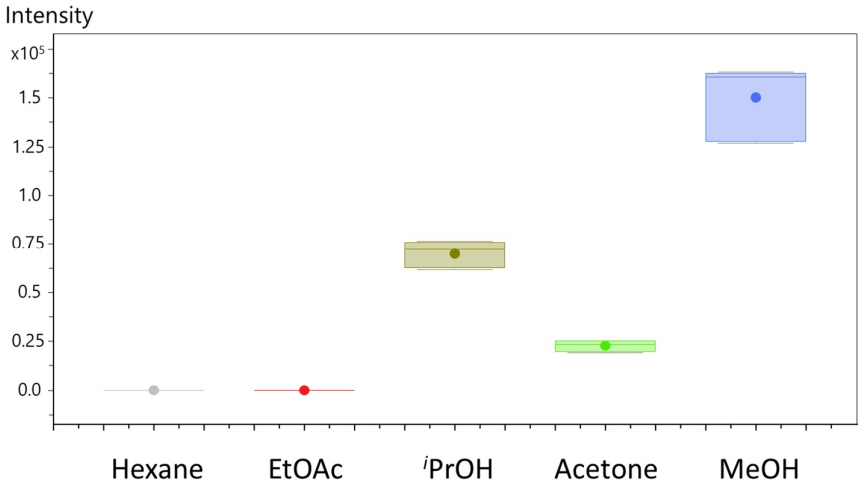

Figure S5.4 Box plot for riboflavin from *M. xanthus* DK1622 comparing different solvents for UAE.

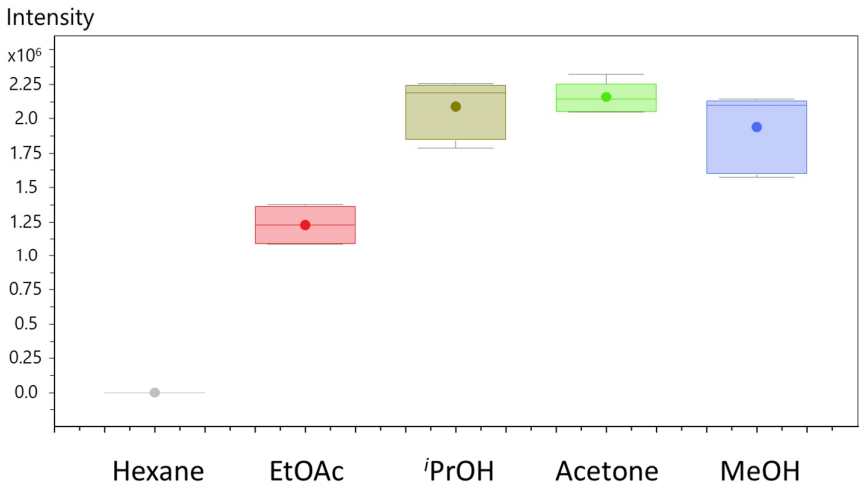

Figure S5.5 Box plot for myxovirescin A from *M. xanthus* DK1622 comparing different solvents for UAE.

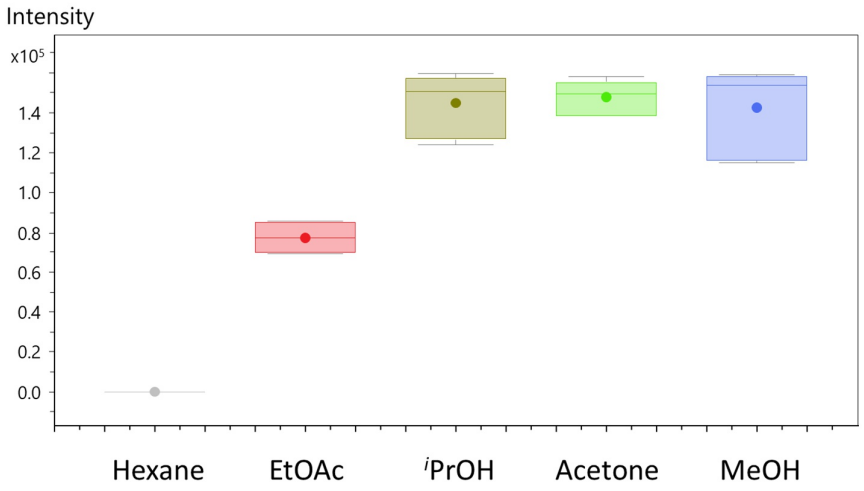

Figure S5.6 Box plot for myxovirescin B from *M. xanthus* DK1622 comparing different solvents for UAE.

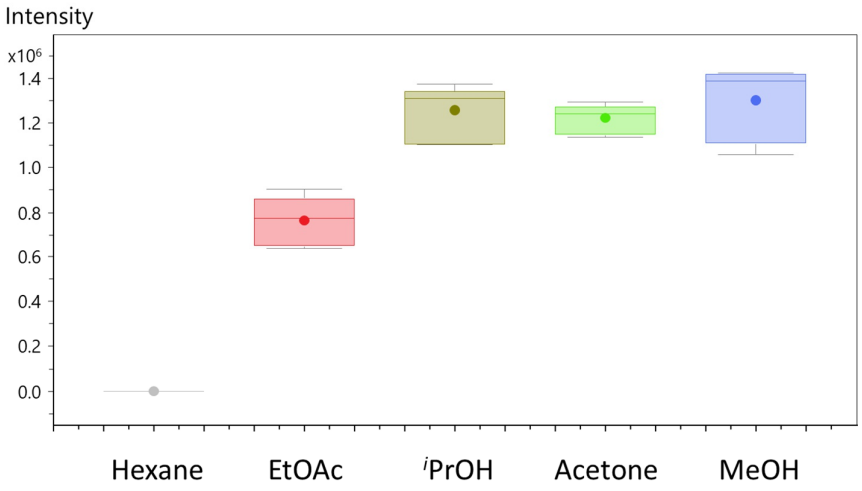

Figure S5.7 Box plot for myxovirescin C from *M. xanthus* DK1622 comparing different solvents for UAE.

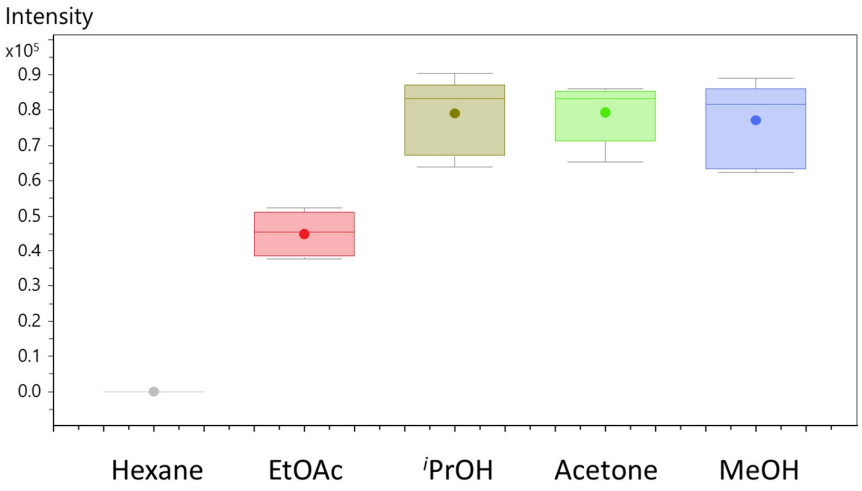

Figure S5.8 Box plot for myxovirescin G from *M. xanthus* DK1622 comparing different solvents for UAE.

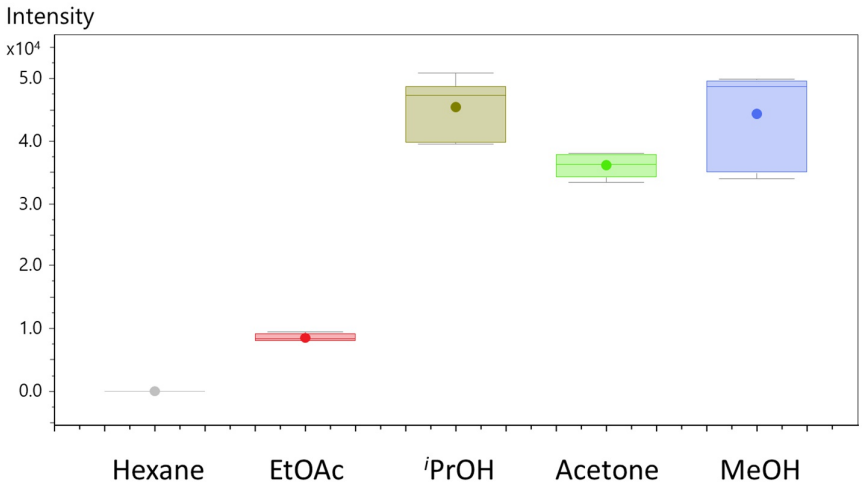

Figure S5.9 Box plot for myxovirescin variant KP641 from *M. xanthus* DK1622 comparing different solvents for UAE.

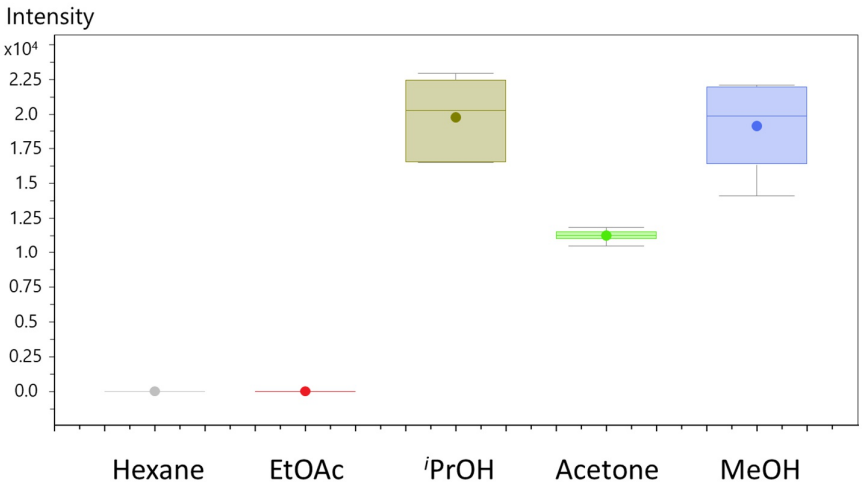

Figure S5.10 Box plot for chloroxanthic acid A from *M. xanthus* DK1622 comparing different solvents for UAE.

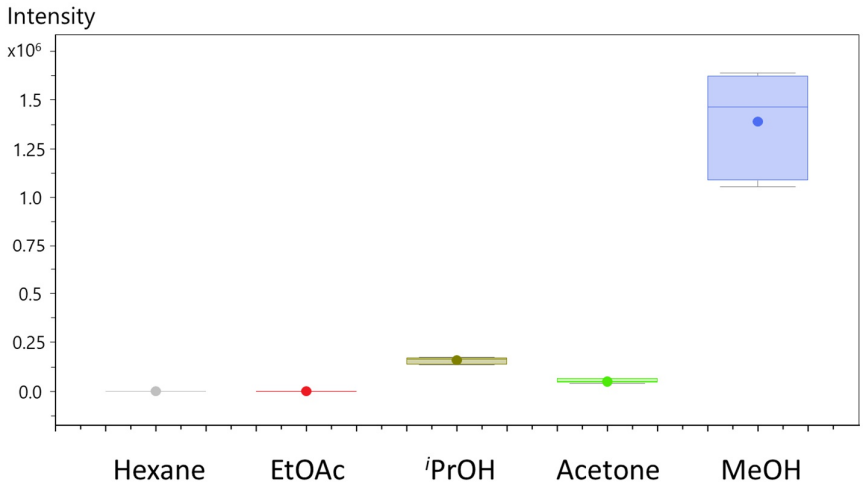

Figure S5.11 Box plot for DKxanthen 560 from *M. xanthus* DK1622 comparing different solvents for UAE.

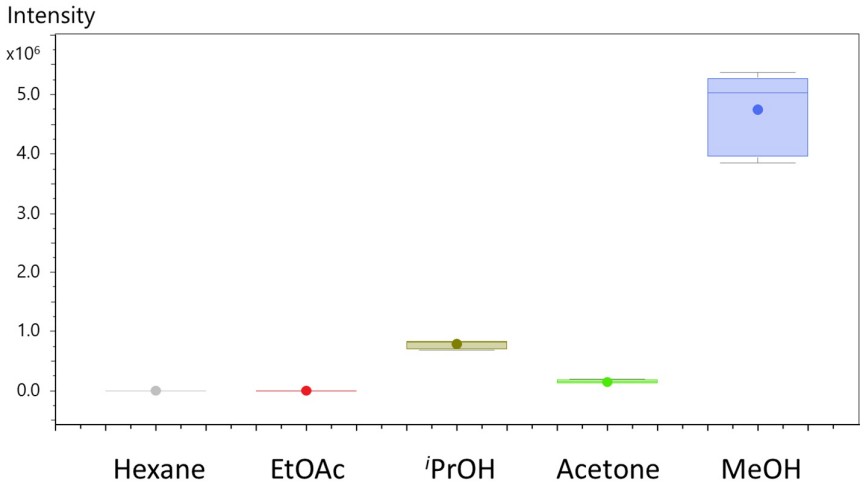

Figure S5.12 Box plot for DKxanthen 534 from *M. xanthus* DK1622 comparing different solvents for UAE.

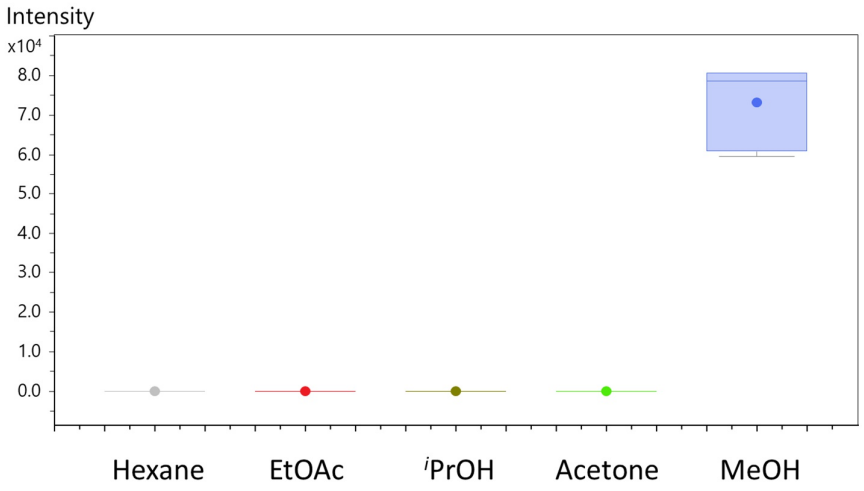

Figure S5.13 Box plot for DKxanthen 548 from *M. xanthus* DK1622 comparing different solvents for UAE.

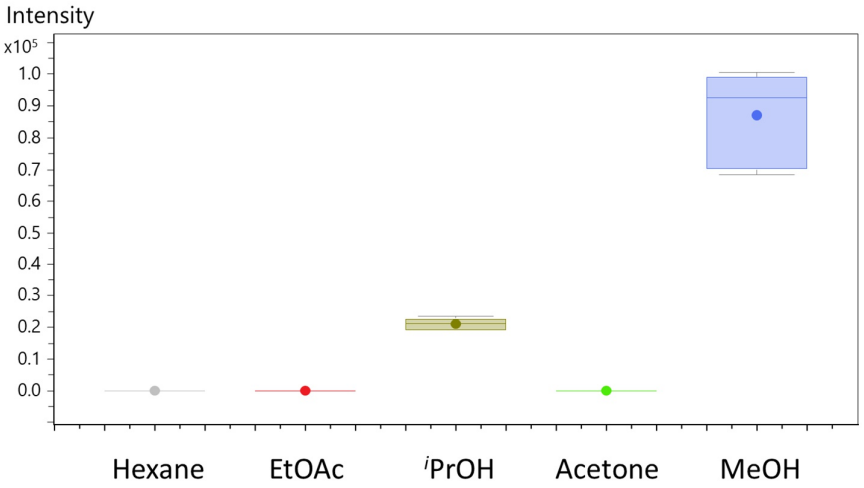

Figure S5.14 Box plot for DKxanthen 574 from *M. xanthus* DK1622 comparing different solvents for UAE.

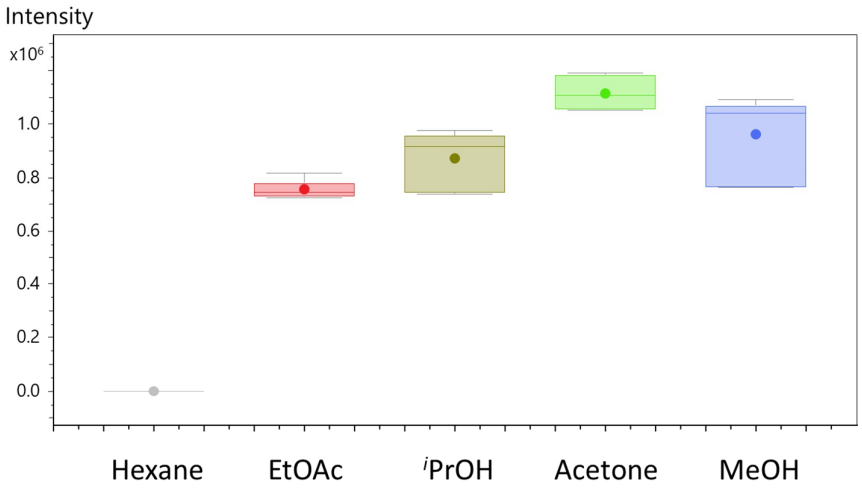

Figure S5.15 Box plot for myxalamid A from *M. xanthus* DK1622 comparing different solvents for UAE.

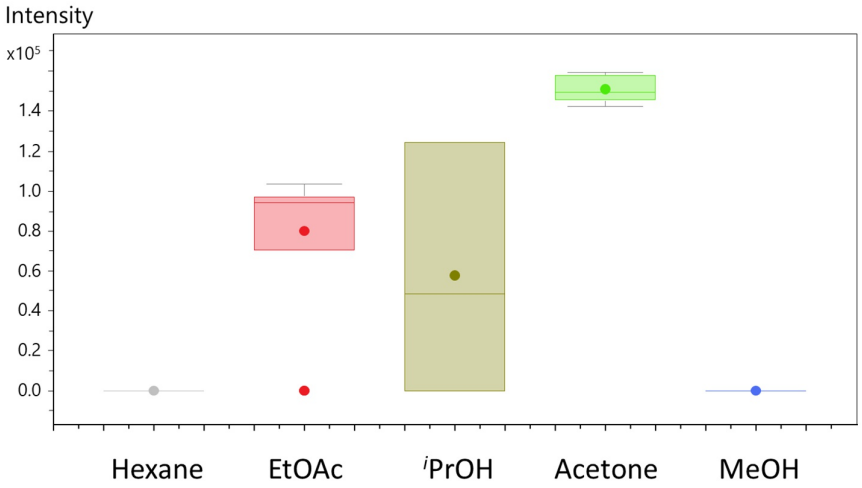

Figure S5.16 Box plot for myxalamid B from *M. xanthus* DK1622 comparing different solvents for UAE.

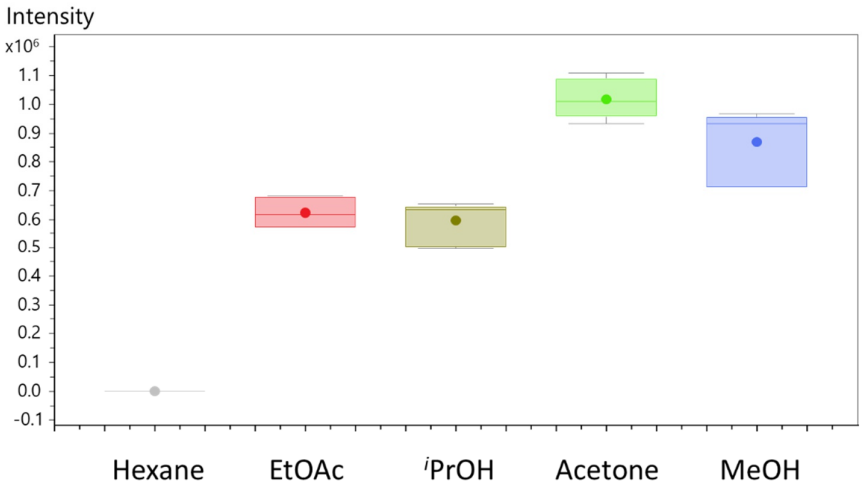

Figure S5.17 Box plot for myxalamid C from *M. xanthus* DK1622 comparing different solvents for UAE.

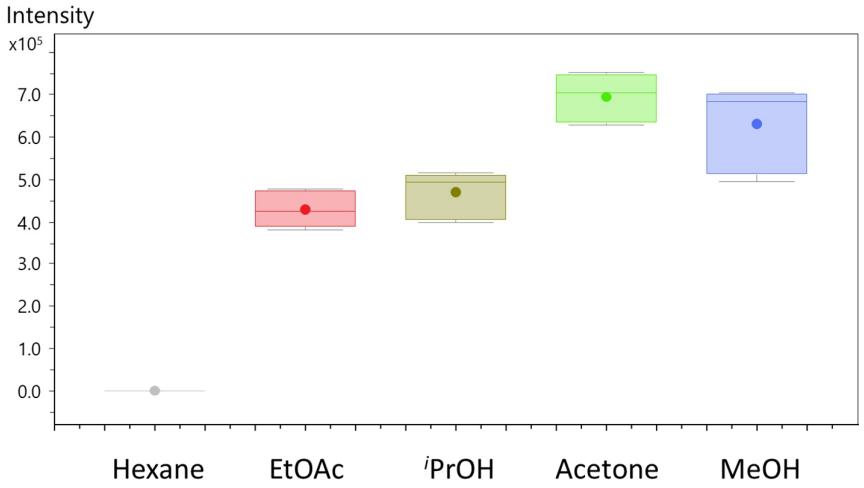

Figure S5.18 Box plot for myxalamid D from *M. xanthus* DK1622 comparing different solvents for UAE.

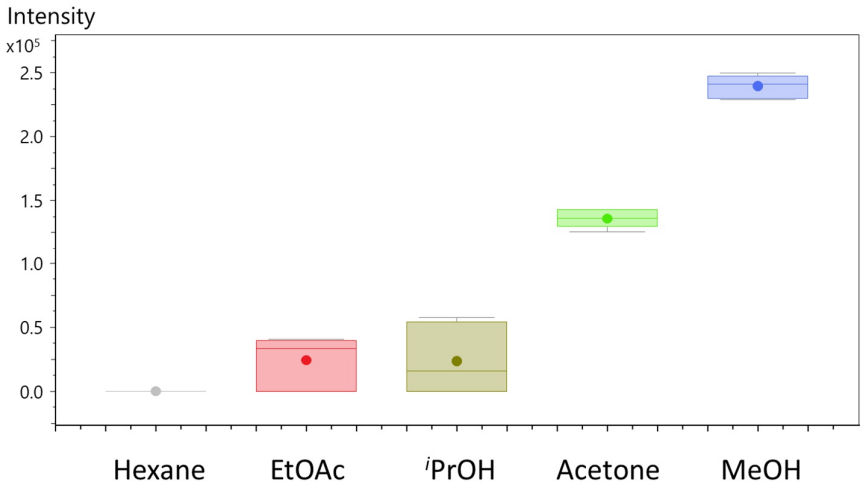

Figure S5.19 Box plot for myxochromid A3 from *M. xanthus* DK1622 comparing different solvents for UAE.

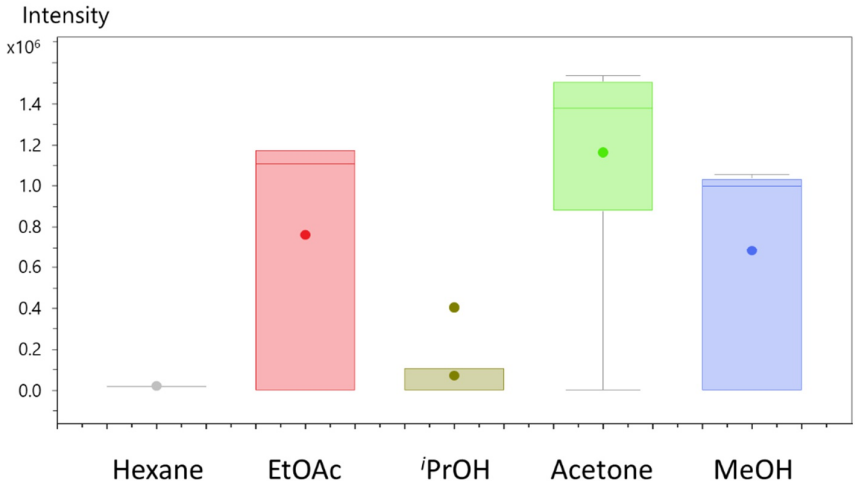

Figure S5.20 Box plot for indiacene A from MSr10575 comparing different solvents for UAE.

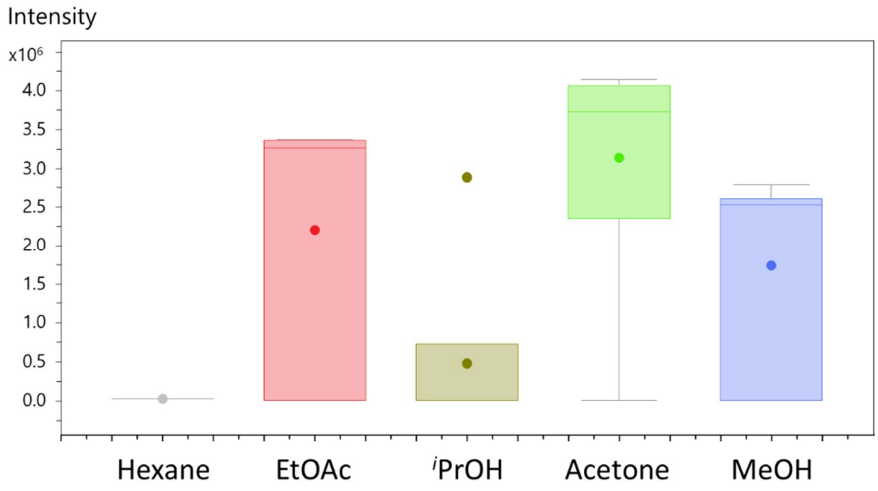

Figure S5.21 Box plot for indiacene B from MSr10575 comparing different solvents for UAE.

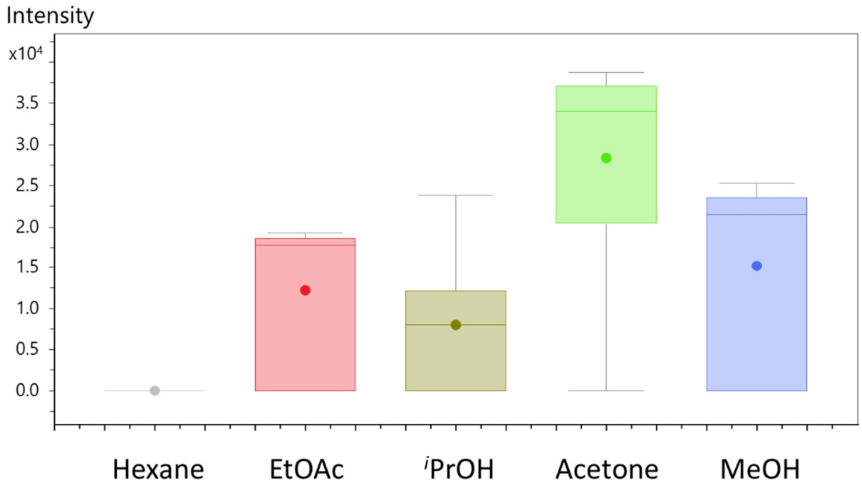

Figure S5.22 Box plot for terrestribisamid from MSr10575 comparing different solvents for UAE.

Our results support, that acetone and MeOH are indeed the best solvents for UA extraction in a targeted metabolomics workflow. In all cases they show equal if not superior extractability compared to the other three solvents. Myxochelin A, myxovirescin variant KP643, DKxanthen-520 and DKxanthen-526 could not be detected in the extracts were different solvents for UAE were evaluated, which may be caused by differences in production levels in between the two cultivation batches.

Antimicrobial activities of the UA extracts generated with different solvents

We evaluated the antimicrobial activities of the UA extracts generated with different solvents against a test panel of eight microbial strains. As reference we used a standard extract generated by consecutive extraction with MeOH and acetone (Std 2. Batch) comparable to the UA extract used for comparison with SFE. The antimicrobial activities of the different extracts are separately shown in figure Figure S5.23Figure S5.25 for the three myxobacterial strains.

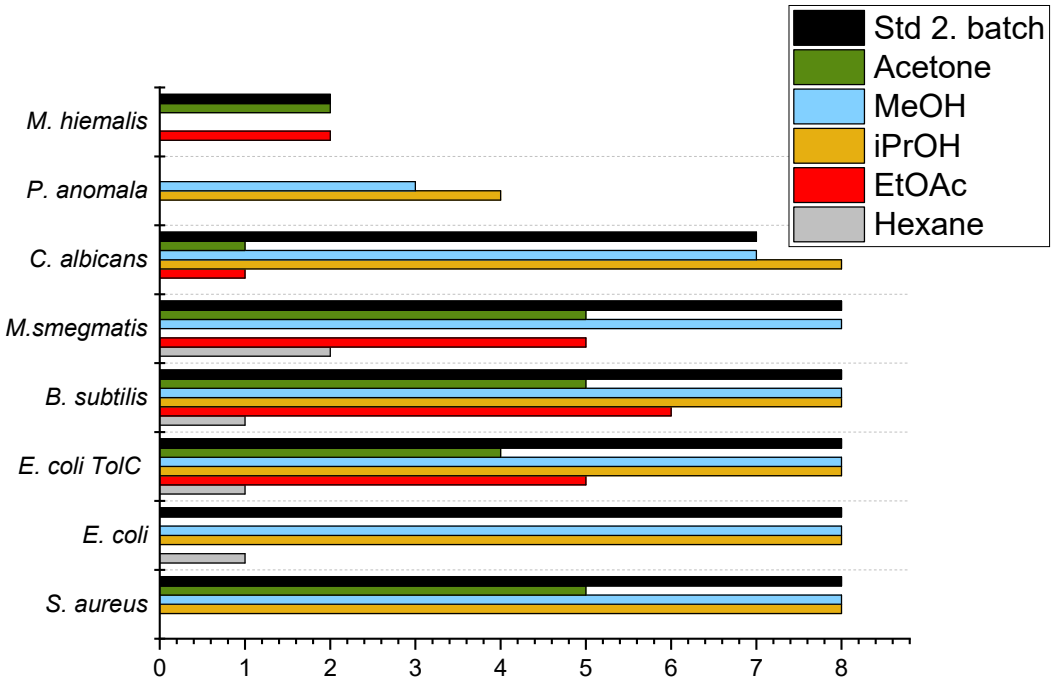

Figure S5.23 Antimicrobial activities of UA extracts from MSr10575 generated with different solvents.

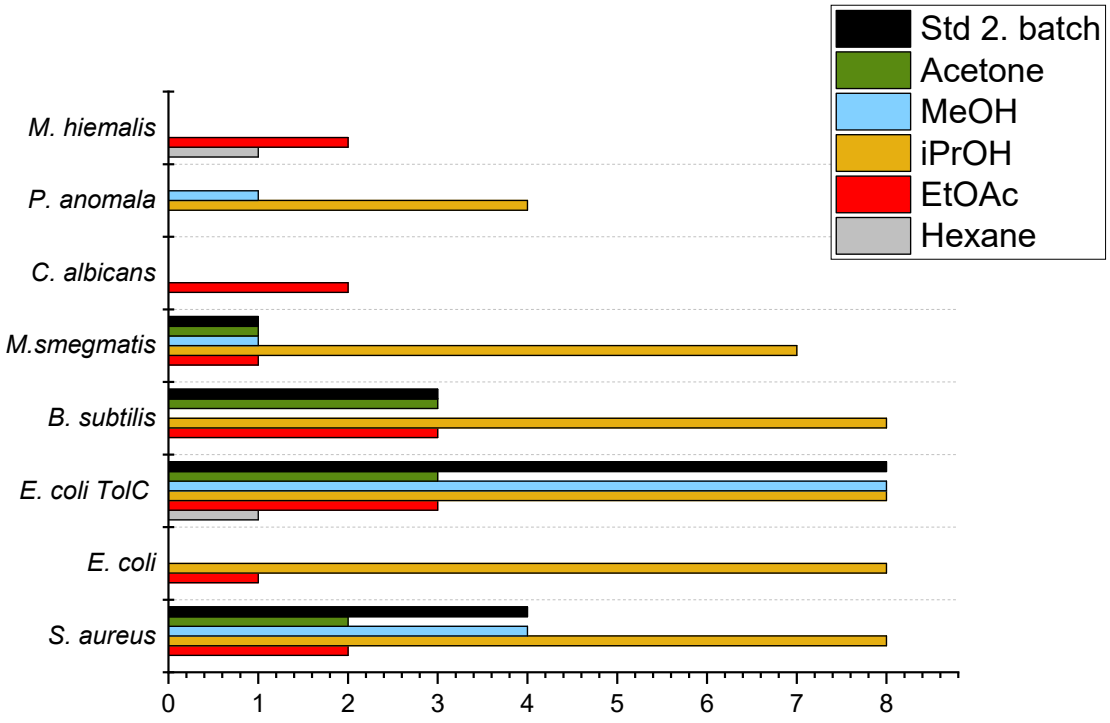

Figure S5.24 Antimicrobial activities of UA extracts from MSr11367 generated with different solvents.

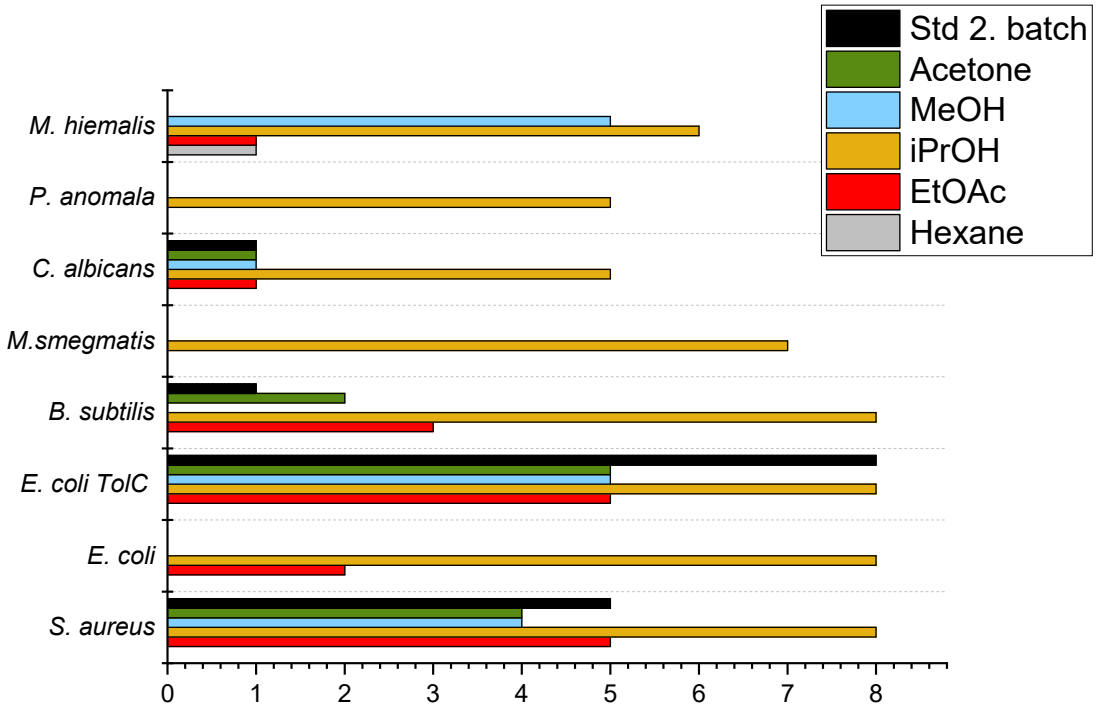

Figure S5.25 Antimicrobial activities of UA extracts from *M. xanthus* DK1622 generated with different solvents.

We observe similar effects on the antimicrobial activities when generating UA extracts with different solvents compared to SF extraction. We find higher activities of some of the extracts than the standard UA extracts, as well as some antimicrobial activities only detectable using specific solvents. Using a different solvent may therefore introduce some selectivity to the extraction process and generate extracts enriched in bioactive secondary metabolites, which highlights that limiting an extraction process to one solvent may hinder the detection of some antimicrobial activities or decrease the observed activity. We observe good antimicrobial activities of the ^{i}PrOH extracts for all three myxobacterial strains and even an activity of *M. xanthus* DK1622 extracts against *M. smegmatis* and *P. anomala*, not observable for any other solvent. This finding highlights ^{i}PrOH as interesting UA extraction solvent for bioactivity-guided isolation and structure elucidation of novel natural products, which is in contrast to the SF extraction. Here the ^{i}PrOH showed the lowest activities besides the pure CO_2 extracts. However, this finding for SFE may stem from the consecutive extraction protocol chosen, where biologically active secondary metabolites may already be extracted during the 20% EtOAc step.

Consecutive extraction

We were interested in comparison of UA extractions using single solvents with consecutive extractions comparable to the protocol performed with SFE. We therefore extracted an aliquot of *M. xanthus* DK1622 pellet first with hexane, then EtOAc, ^{i}PrOH, MeOH and finally with acetone. We also performed UA extraction with a mixture of an equal volume of each solvents as reference. The results for the six different secondary metabolite families detected in *M. xanthus* DK1622 extracts are shown in figure Figure S5.26Figure S5.31.

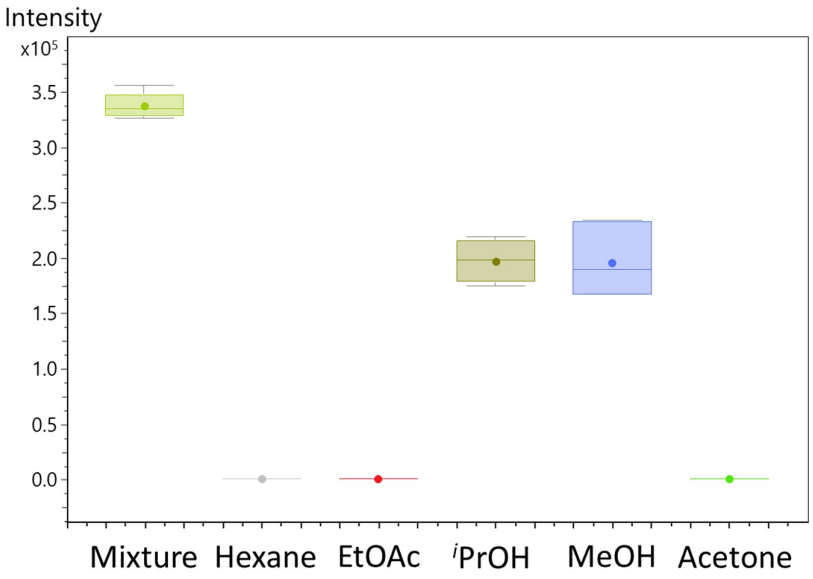

Figure S5.26 Box plot for cittilin A from *M. xanthus* DK1622 comparing consecutive extraction for UAE.

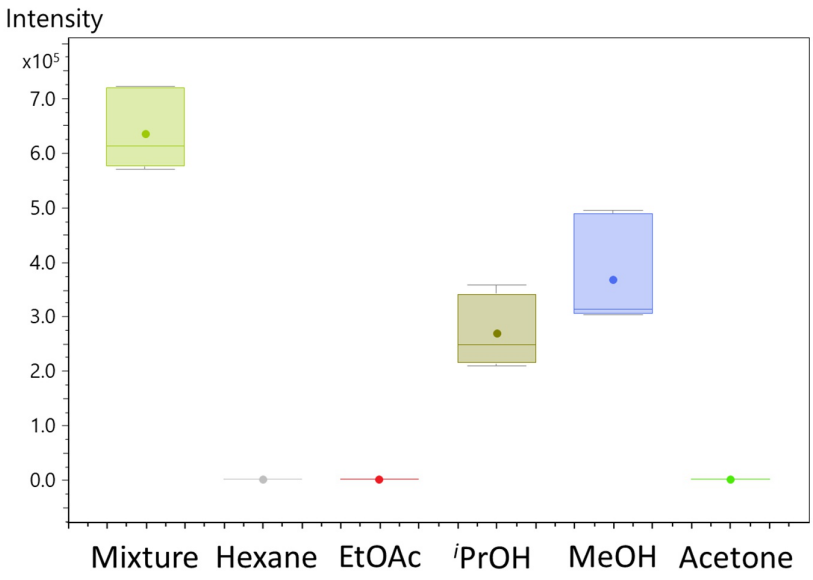

Figure S5.27 Box plot for DKxanthen 560 from *M. xanthus* DK1622 comparing consecutive extraction for UAE.

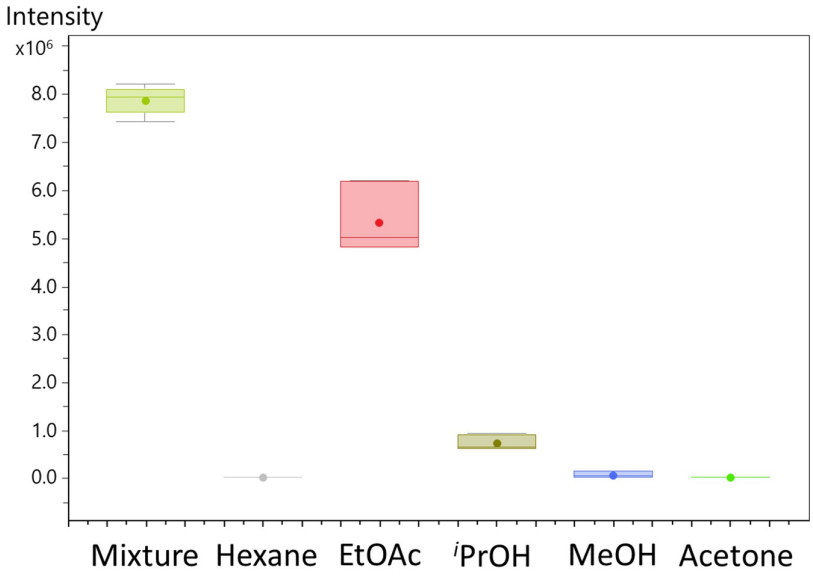

Figure S5.28 Box plot for myxalamid A from *M. xanthus* DK1622 comparing consecutive extraction for UAE.

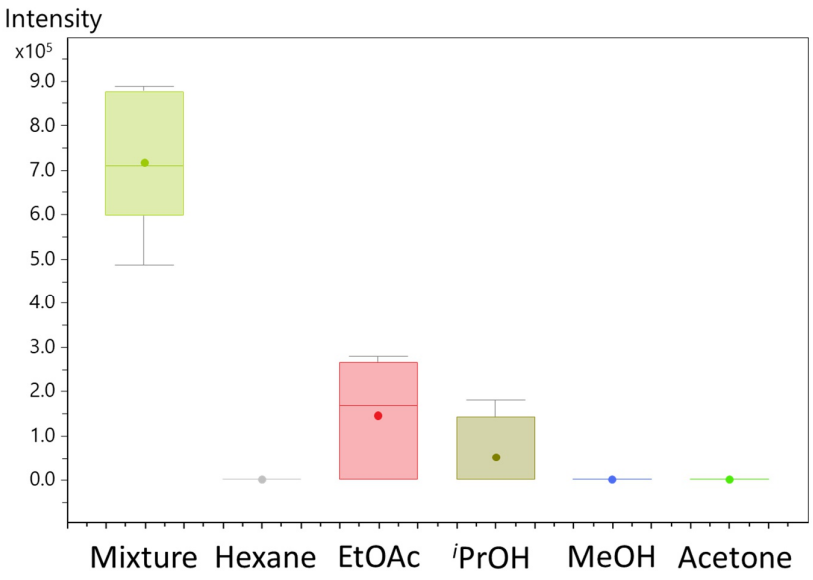

Figure S5.29 Box plot for myxochromid A3 from *M. xanthus* DK1622 comparing consecutive extraction for UAE.

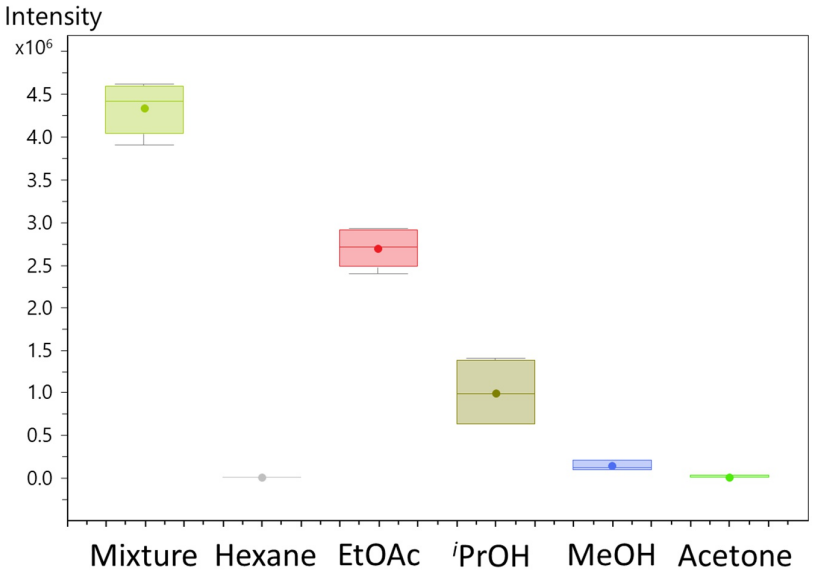

Figure S5.30 Box plot for myxovirescin A from *M. xanthus* DK1622 comparing consecutive extraction for UAE.

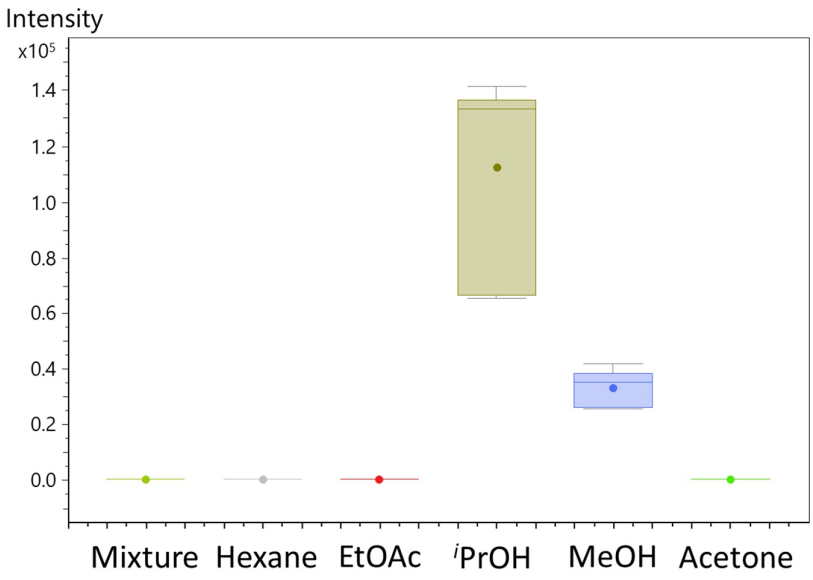

Figure S5.31 Box plot for riboflavin from *M. xanthus* DK1622 comparing consecutive extraction for UAE.

The secondary metabolite distribution when performing consecutive UA extraction with the five different solvents shows highly similar profiles compared to consecutive SF extraction. Secondary metabolites with a logP higher than 3 already show extraction with EtOAc, whereas secondary metabolites with a logP lower than 3 are mainly found in the ^{i}PrOH and MeOH extraction step. In contrary to SFE however, none of the metabolites was extractable under the most non-polar condition using hexane. All metabolites were already exhaustively extracted after the MeOH extraction step, as we were not able to detect any of them in the acetone extracts but have shown beforehand that different myxovirescin and myxalamid derivatives, as well as myxochromid A3 are extractable with acetone. Consecutive UA extraction is therefore also feasible for conducting a primary fractionation step during the extraction process, leading to enrichment of different secondary metabolites in the fractions based on their logP values.

Targeted metabolomics investigation of known myxobacterial secondary metabolites

Box plots of secondary metabolites extractable with SFE from *M. xanthus* DK1622

This chapter including figure Figure S5.32Figure S5.47 completes the box plots shown in figure Figure 5.1 in the main text for the remaining derivatives of each family of secondary metabolites produced by *M. xanthus* DK1622.

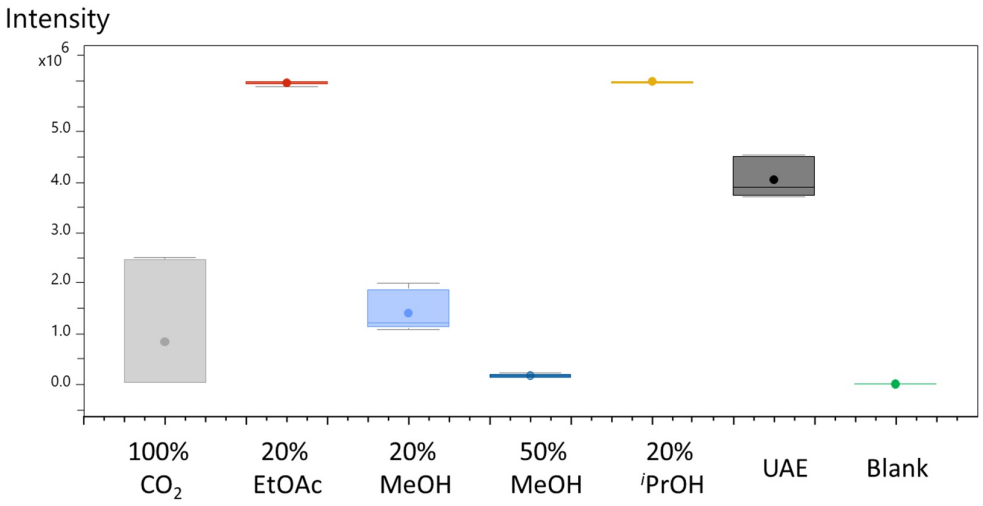

Figure S5.32 Box plot for riboflavin from *M. xanthus* DK1622 (SFE vs UAE).

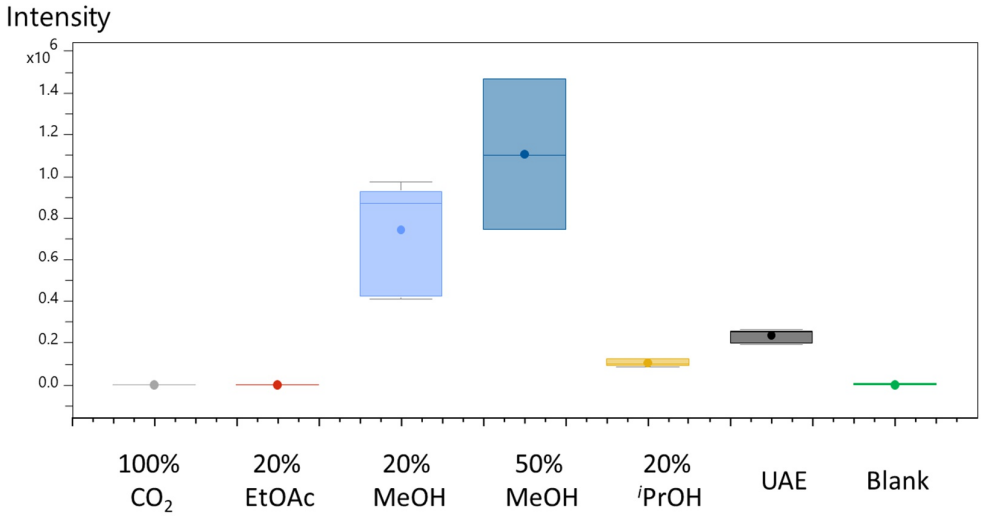

Figure S5.33 Box plot for chloroxanthic acid A from *M. xanthus* DK1622 (SFE vs UAE).

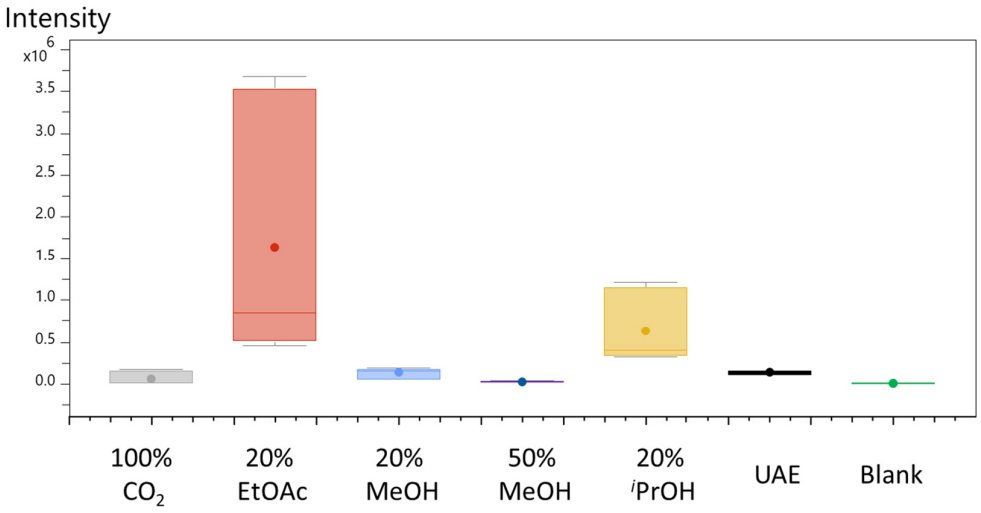

Figure S5.34 Box plot for myxovirescin variant KP643 from *M. xanthus* DK1622 (SFE vs UAE).

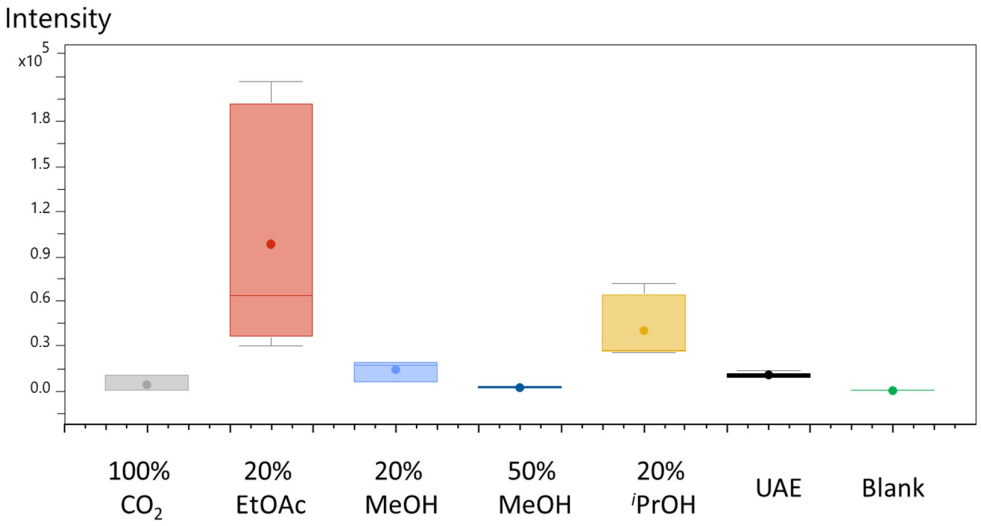

Figure S5.35 Box plot for myxovirescin variant KP641 from *M. xanthus* DK1622 (SFE vs UAE).

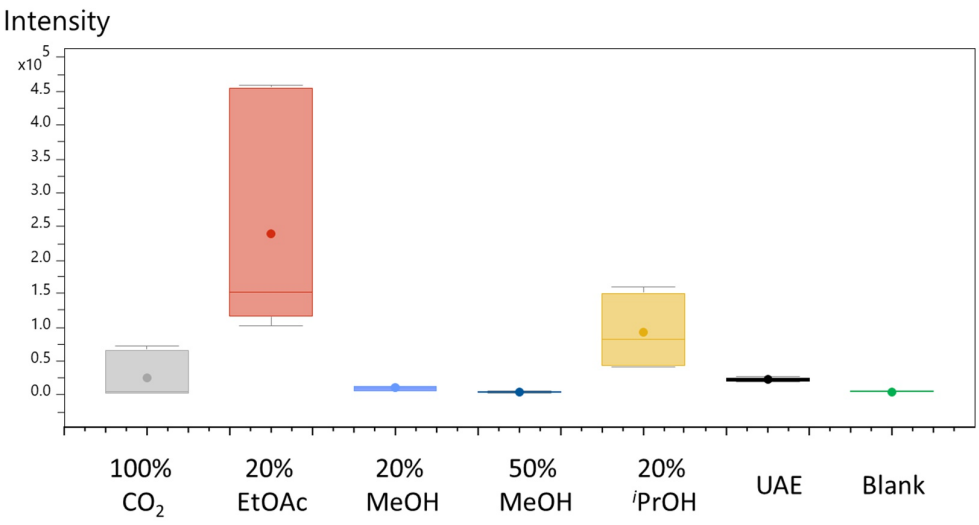

Figure S5.36 Box plot for myxovirescin B from *M. xanthus* DK1622 (SFE vs UAE).

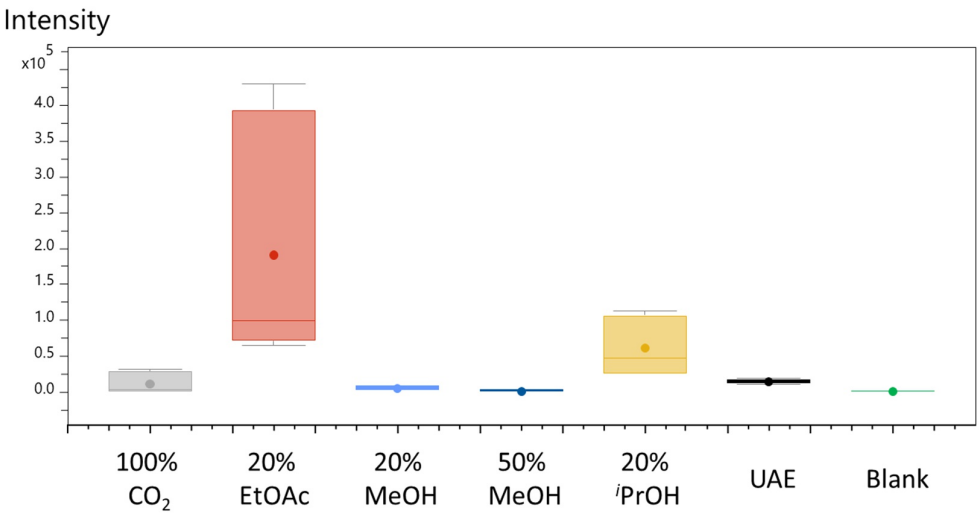

Figure S5.37 Box plot for myxovirescin C from *M. xanthus* DK1622 (SFE vs UAE).

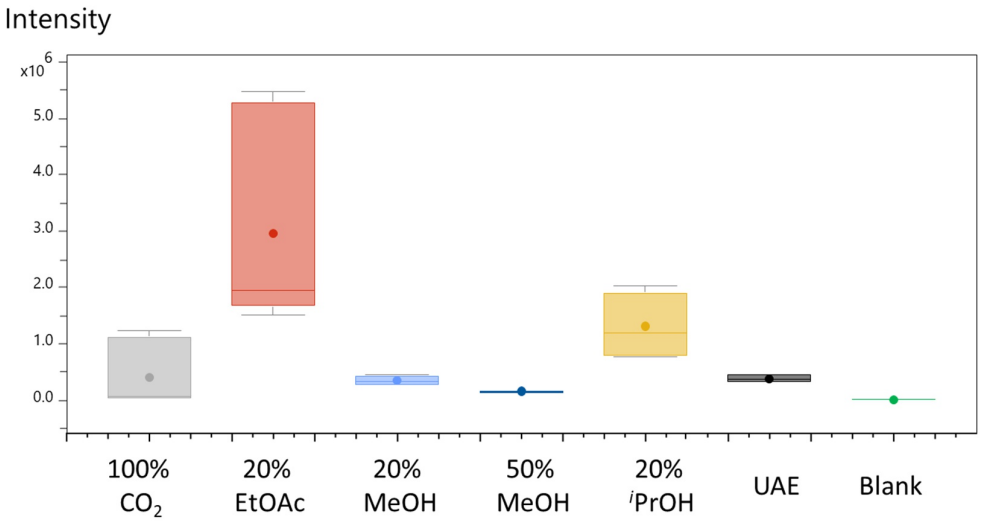

Figure S5.38 Box plot for myxovirescin G from *M. xanthus* DK1622 (SFE vs UAE).

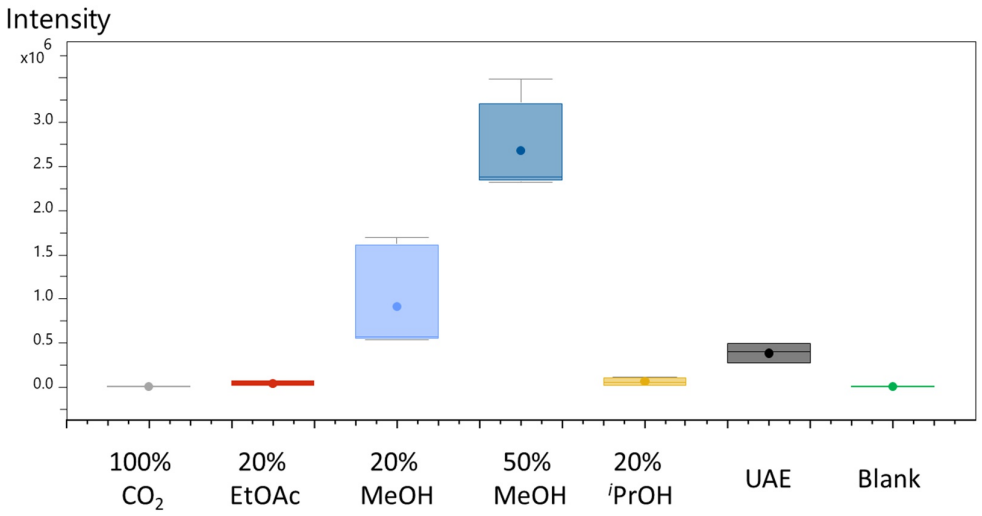

Figure S5.39 Box plot for DKxanthen 534 from *M. xanthus* DK1622 (SFE vs UAE).

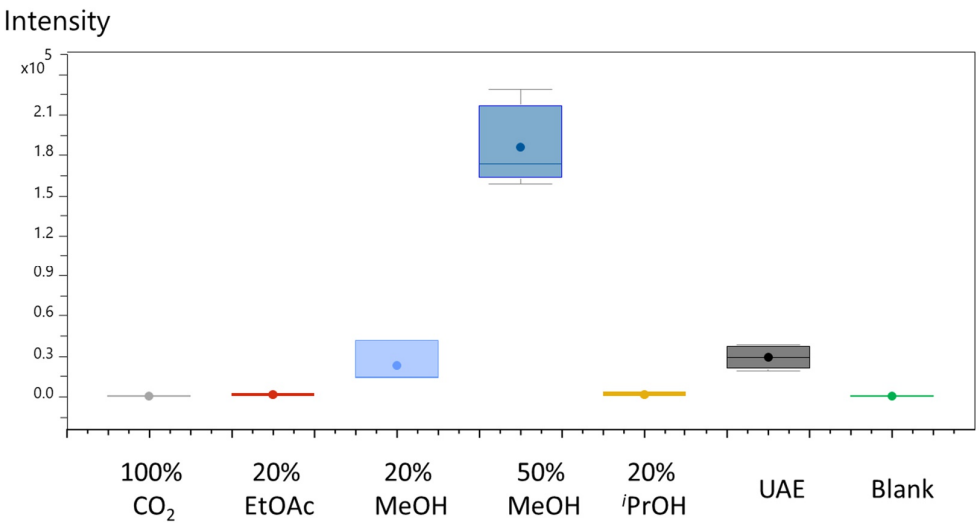

Figure S5.40 Box plot for DKxanthen 520 from *M. xanthus* DK1622 (SFE vs UAE).

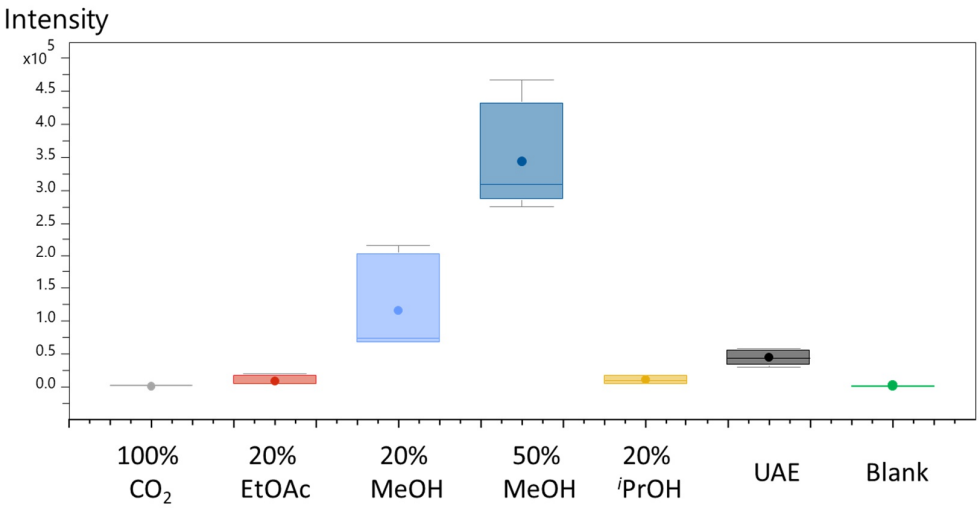

Figure S5.41 Box plot for DKxanthen 548 from *M. xanthus* DK1622 (SFE vs UAE).

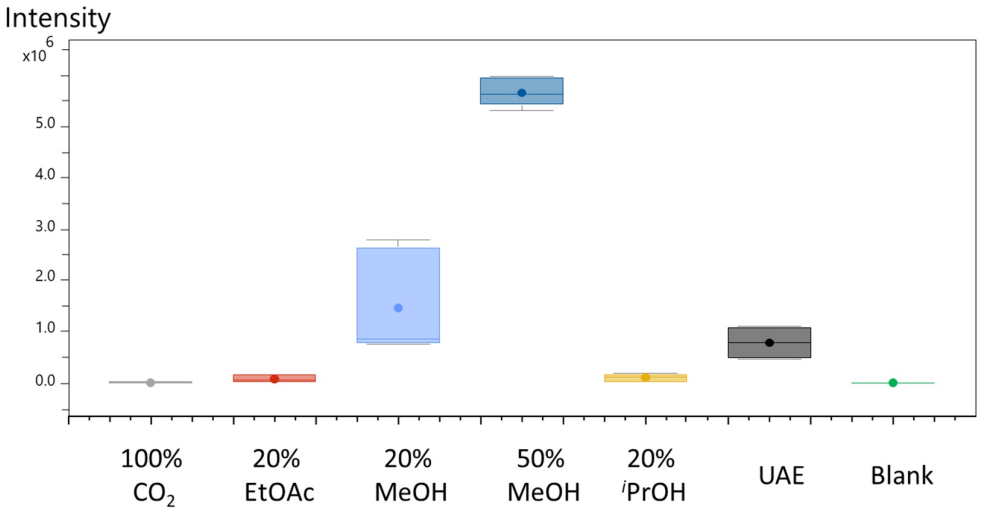

Figure S5.42 Box plot for DKxanthen 560 from *M. xanthus* DK1622 (SFE vs UAE).

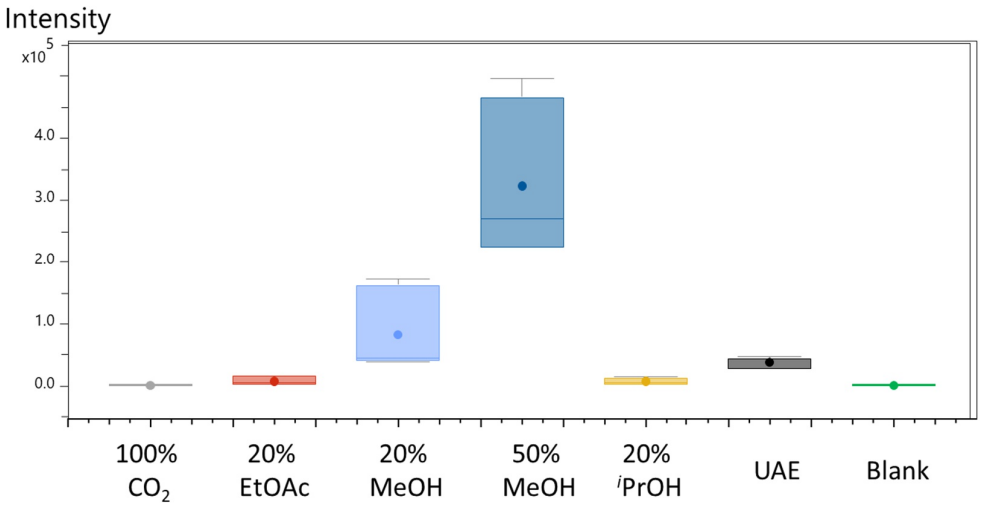

Figure S5.43 Box plot for DKxanthen 574 from *M. xanthus* DK1622 (SFE vs UAE).

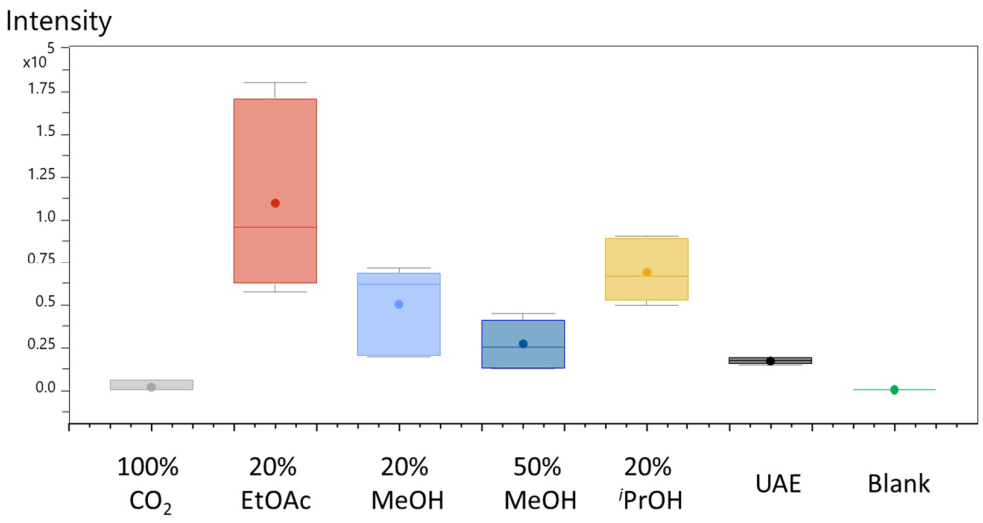

Figure S5.44 Box plot for DKxanthen 526 from *M. xanthus* DK1622 (SFE vs UAE).

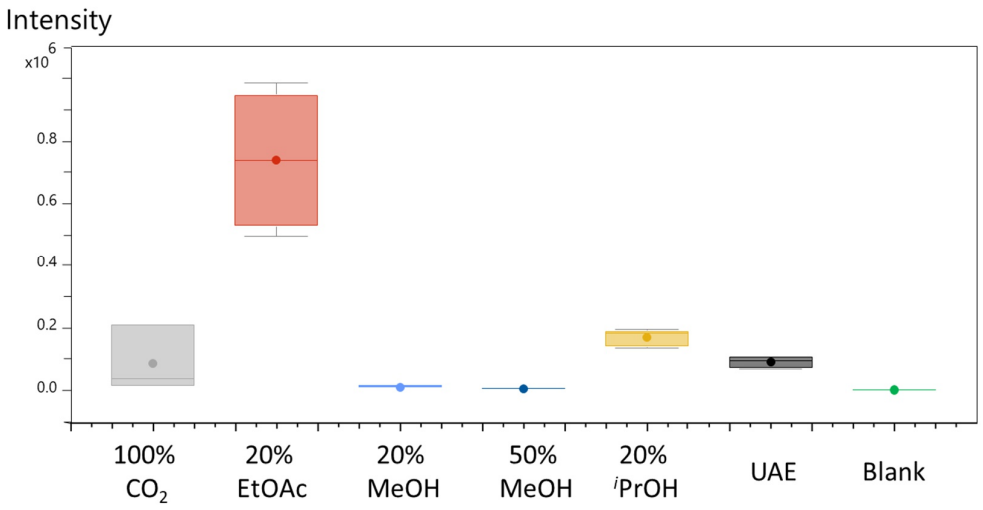

Figure S5.45 Box plot for myxalamid B from *M. xanthus* DK1622 (SFE vs UAE).

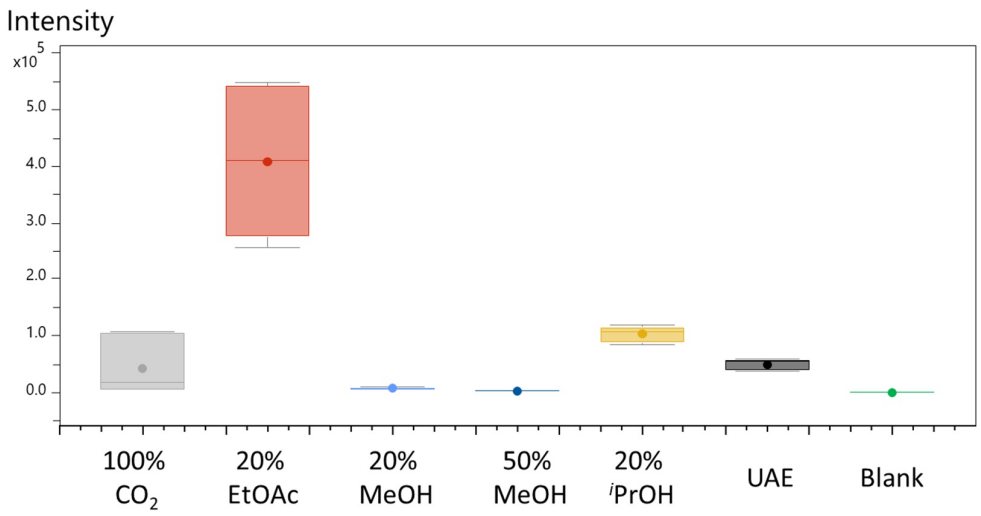

Figure S5.46 Box plot for myxalamid C from *M. xanthus* DK1622 (SFE vs UAE).

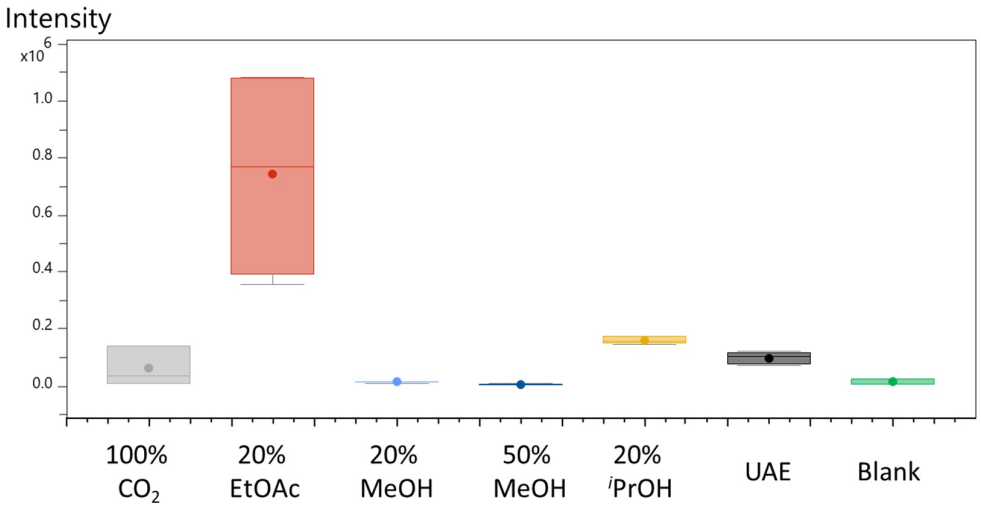

Figure S5.47 Box plot for myxalamid 430 from *M. xanthus* DK1622 (SFE vs UAE).

Box plots of secondary metabolites extractable with SFE from MSr10575

This chapter including figureFigure S5.48 completes the box plots shown in figure Figure 5.1 in the main text for the remaining derivatives of each family of secondary metabolites produced by MSr10575.

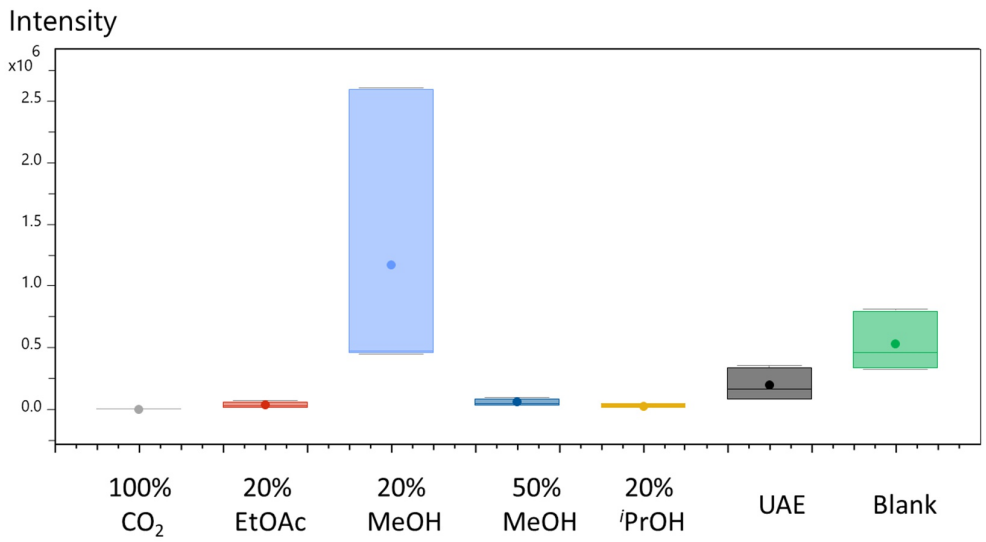

Figure S5.48 Box plot for indiacene B from MSr10575.

Non-targeted metabolomics investigation

Comparison of features detected in the UAE and SFE

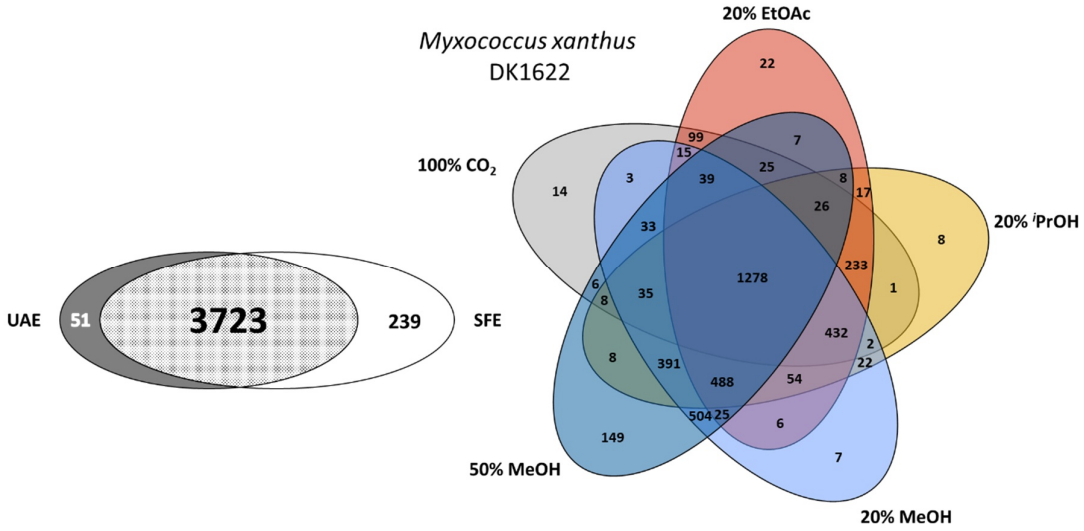

Figure S5.49 Euler diagrams for *M. xanthus* DK1622 Left-hand side: Features unique for UAE or SFE and features extractable with both methods. Right-hand side: Features found in the SF extracts from MSr10575 sorted by co-solvent used during the extraction process.

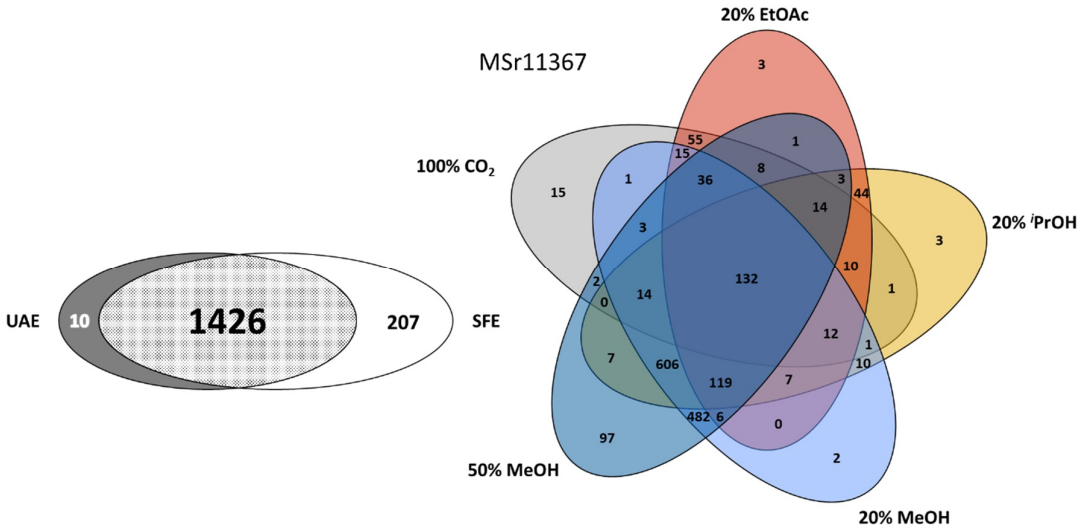

Figure S5.50 Euler diagrams for MSr11367. Left-hand side: Features unique for UAE or SFE and features extractable with both methods. Right-hand side: Features found in the SF extracts from MSr10575 sorted by co-solvent used during the extraction process.

Chlorinated metabolites from *M. xanthus* DK1622

Table S5.5 List of chlorinated molecular features detected with elevated intensities in the SF extracts.

	m/z meas.	Molecular Formula (M)	Intensity UAE/SFE [%]	RT
1	295.0848	C14H15ClN2O3	5	10.39
2	313.0954	C14H17ClN2O4	11	7.44
3	329.0459	C14H14Cl2N2O3	62	7.14
4	337.1682	C18H25ClN2O2	52	7.32
5	265.0741	C13H13ClN2O2	47	10.32
6	363.1474	C19H23ClN2O3	48	12.28
7	329.0459	C14H14Cl2N2O3	3	11.78
8	335.1526	C18H23ClN2O2	3	7.48
9	313.0954	C14H17ClN2O4	19	8.54
10	313.0954	C14H17ClN2O4	0	4.31
11	363.1475	C19H23ClN2O3	2	7.49
12	355.0616	C16H16Cl2N2O3	61	12.41
13	227.0584	C10H11ClN2O2	0	4.23
14	335.1162	C17H19ClN2O3	2	7.26
15	281.1055	C14H17ClN2O2	0	5.25
16	335.1162	C17H19ClN2O3	39	12.95
17	269.1055	C13H17ClN2O2	0	4.99
18	349.1318	C18H21ClN2O3	50	7.81
19	361.1319	C19H21ClN2O3	3	12.77
20	349.1319	C18H21ClN2O3	2	19.40
21	255.0534	C11H11ClN2O3	0	4.43
22	309.1368	C16H21ClN2O2	3	10.64
23	355.0616	C16H16Cl2N2O3	3	12.41
24	347.1164	C18H19ClN2O3	2	12.01
25	241.0741	C11H13ClN2O2	0	4.23

26	373.1319	C20H21ClN2O3	3	12.96
27	269.1054	C13H17ClN2O2	0	5.48
28	307.1211	C16H19ClN2O2	5	13.03
29	340.6873	C35H54ClN3O8	73	13.10
30	311.1525	C16H23ClN2O2	8	11.41

Isolation of myxobacterial natural products described in this study

Isolation of the indiacenes A and B from Sandaracinus strain MSr10575

Large scale cultivation and extraction

The *Sandaracinus* strain MSr10575 was fermented in 50 ml 2-SWT medium as a seed culture flasks on an Orbitron shaker at 160 rpm and 30°C. The translucid culture medium becomes orange and opaque after 7 to 11 days of fermentation. This pre-culture was used to inoculate 6 x 2L 2-SWT medium supplemented with 2% XAD-16 resin suspension in sterilized water in 6 x 5L baffled shake flasks on an Orbiton shaker at 160 rpm and 30°C. Fermentation was complete after 16 days. Cells and XAD-16 resin were harvested by centrifugation on a Beckmann Avanti J-26 XP with the JLA 8.1 rotor at 6000 rcf. Combined resin and cells were freeze dried and subsequently extracted using 2x 500 ml of a 2:1 mixture of methanol and chloroform. The combined extracts were concentrated on a rotary evaporator and partitioned between methanol and hexane. The indiacenes remained in the methanol phase, which was dried with a rotary evaporator and the residue partitioned between water and chloroform. The indiacenes retained in the chloroform phase, which was concentrated and stored in an air-tight glass vial at -20°C until further processing.

Centrifugal partition chromatography (CPC) pre-purification of the compounds

Pre-purification and fractionation of indiacene A and B was achieved by CPC. We used a Gilson CPC 100 device (Gilson purification S.A.S.) connected to a Varian ProStar Solvent delivery module and a Varian ProStar 2 Channel UV detector. Fraction collection is done with a Foxy Jr. auto sampler (Isco). Used biphasic solvent system is the buffered ARIZONA solvent system consisting of a 1:1:1:1 mixture of 10 mM Tris x HCl buffer pH 8.0 (Sigma), methanol (analytical grade, Fluka), EtOAc (analytical grade, Fluka) and hexane (analytical grade, Fluka). After equilibration of the system and loading of the sample, the

aqueous phase is used as a stationary phase for 40 min at 2 ml/min and a fraction size of 4 ml. The indiacenes elute simultaneously in fractions 35-55, that are pooled for fine purification.

Purification of indiacene A and B by HPLC

Purification of indiacene A and B was carried out using a Dionex Ultimate 3000 SDLC low pressure gradient system on a Waters Acquity CSH C18 250x10mm 5µm column with the eluents H_2O + 1% FA as A and ACN + 1% FA as B, a flow rate of 5 ml/min and a column thermostated at 30°C. Indiacene A and B are detected by UV absorption at 316 nm and purification is done by time dependent fraction collection. Separation is started with a plateau at 60% A for 2 minutes followed by a ramp to 24% A during 24 minutes and a ramp to 0% A during 1 minute. The A content is kept at 0% A for 2 minutes. The A content is ramped back to starting conditions during 30 seconds and the column is re-equilibrated for 2 minutes. After evaporation, the indiacenes A and B are obtained as orange solids.

Isolation of chloroxanthic acid A

Large scale cultivation and extraction

M. xanthus DK1622 was fermented in 50 ml CTT medium medium as a seed culture flasks on an Orbiton shaker at 160 rpm and 30°C. The translucid culture medium becomes dark yellow and opaque after 5 to 7 days of fermentation. This pre-culture was used to inoculate 3 x 300 mL SHG-P medium supplemented with sterile-filtered 7.5 µg/ml Fe-EDTA solution and 2% XAD-16 resin suspension in sterilized water in 3 x 1L shake flasks on an Orbiton shaker at 160 rpm and 30°C. Fermentation was complete after 10 days. Cells and XAD-16 resin were harvested by centrifugation on a Beckmann Avanti J-26 XP with the JLA 8.1 rotor at 6000 rcf. Combined resin and cells were freeze dried and subsequently extracted using SFE with 20% EtOAc as co-solvent. SFE parameters were consistent with the ones used for in the analytical setup (see “material and methods, extraction procedure” in the main text). The combined extracts were concentrated on a rotary evaporator and partitioned between methanol and hexane. Chloroxanthic acid A remained in the methanol phase, which was dried with a rotary evaporator and the residue partitioned between water and chloroform. Chloroxanthic acid retained in the chloroform phase, which was concentrated and stored in an air-tight glass vial at -20°C until further processing. Further isolation steps are described in the main text of the manuscript.

Structure elucidation of the natural products described in this study

Indiacene A and B

Crystallization conditions for indiacene A and B

The two indiacene secondary metabolites are dissolved in a minimal amount of methanol, transferred in a glass vial und kept in the fridge at 4°C without a lid. After two weeks, we see yellowish-orange needle shaped crystals appearing in the residual solvent. These crystals diffracted in a small molecule X-ray crystallograph, which allowed the acquisition of X-ray crystal structures. The data were collected at low temperature on a BrukerAXS X8Apex CCD diffractometer operating with graphite-monochromatized Mo Kα radiation. Frames of 0.5° oscillation were exposed; deriving reflections in the θ range of 2 to 27° with a completeness of ~99%. Structure solving and full least-squares refinement with anisotropic thermal parameters of all non-hydrogen atoms were performed using SHELX.[13] All relevant data concerning the crystal structures can be found in this section. Crystallographic data for the structure have been deposited with the Cambridge Crystallographic Data Centre, CCDC, 12 Union Road, Cambridge CB21EZ, UK. Copies of the data can be obtained free of charge on quoting the repository number CCDC 2035083 for indiacene A and 2035084 for indiacene B under www.ccdc.cam.ac.uk/data_request/cif.

Crystal structure parameters for indiacene A

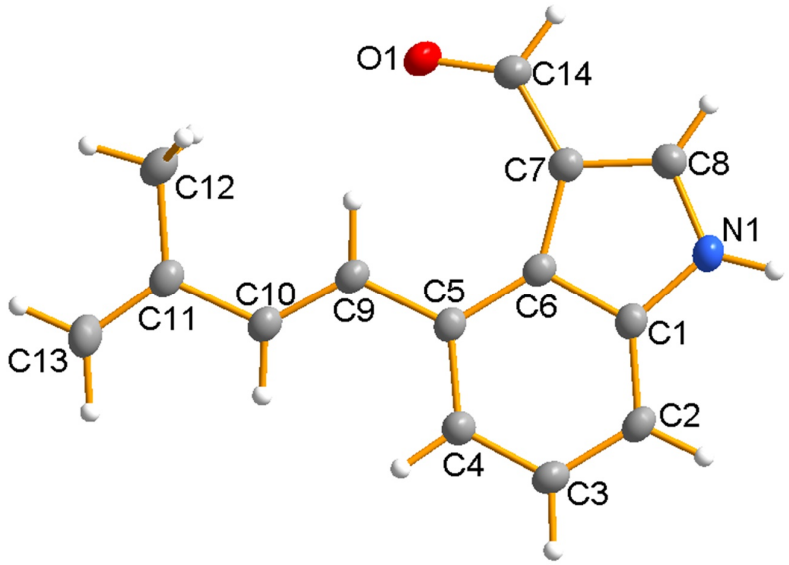

Figure S5.51 Electron density map calculated from the indiacene A diffraction pattern.

Empirical formula	$C_{14}H_{13}NO$
Formula weight	211.25 Da
Temperature	133(2) K
Wavelength	1.54178 Å
Crystal system	Orthorhombic
Space group	P $2_12_12_1$
Unit cell dimensions	a = 5.8884(3) Å α = 90°.
	b = 13.0563(6) Å β = 90°.
	c = 14.2977(6) Å γ = 90°.
Volume	1099.22(9) $Å^3$
Z	4
Density (calculated)	1.277 Mg/m^3
Absorption coefficient	0.635 mm^{-1}
F(000)	448
Crystal size	0.131 x 0.093 x 0.015 mm^3
Theta range for data collection	4.586 to 80.478°.

Index ranges	-	$7 \leq h \leq 7$, $-16 \leq k \leq 16$, $-18 \leq l \leq 18$
Reflections collected		21720
Independent reflections		2388 [R (int) = 0.0408]
Completeness to theta = 67.679°		99.4 %
Absorption correction		Semi-empirical from equivalents
Max. and min. transmission		0.7543 and 0.6472
Refinement method		Full-matrix least squares on F2
Data / restraints / parameters		2388 / 0 / 197
Goodness-of-fit on F2		1.072
Final R indices [I>2σ (I)]		R1 = 0.0278, wR2 = 0.0674
R indices (all data)		R1 = 0.0284, wR2 = 0.0679
Absolute structure parameter		0.08(8)
Largest diff. peak and hole		0.157 and -0.146 e.Å^{-3}

Table S5.6 Atomic coordinates (x 10^4) and equivalent isotropic displacement parameters (Å^2 x10^3) for indiacene A. U (eq) is defined as one third of the trace of the orthogonalized U^{ij} tensor.

	x	y	z	U(eq)
O(1)	6198(2)	5389(1)	2194(1)	29(1)
N(1)	6737(2)	4902(1)	5414(1)	25(1)
C(1)	4766(2)	5470(1)	5304(1)	22(1)
C(2)	3252(2)	5777(1)	5998(1)	25(1)
C(3)	1425(2)	6368(1)	5722(1)	26(1)
C(4)	1137(2)	6642(1)	4780(1)	24(1)
C(5)	2604(2)	6312(1)	4070(1)	21(1)
C(6)	4477(2)	5698(1)	4340(1)	20(1)
C(7)	6383(2)	5209(1)	3869(1)	23(1)
C(8)	7688(2)	4762(1)	4569(1)	26(1)
C(9)	2237(2)	6611(1)	3091(1)	23(1)
C(10)	369(2)	7090(1)	2772(1)	24(1)
C(11)	-22(2)	7416(1)	1807(1)	24(1)

C(12)	1745(3)	7184(1)	1081(1)	31(1)
C(13)	-1939(3)	7919(1)	1595(1)	32(1)
C(14)	7121(2)	5086(1)	2915(1)	25(1)

Table S5.7 Bond lengths [Å] and angles [°] for indiacene A.

bond lengths [Å]	
O(1)-C(14)	1.2303(18)
N(1)-C(8)	1.3434(19)
N(1)-C(1)	1.3864(17)
N(1)-H(5)	0.93(3)
C(1)-C(2)	1.3922(19)
C(1)-C(6)	1.4202(18)
C(2)-C(3)	1.382(2)
C(2)-H(1)	0.98(2)
C(3)-C(4)	1.4040(19)
C(3)-H(2)	0.98(2)
C(4)-C(5)	1.4010(19)
C(4)-H(3)	0.96(2)
C(5)-C(6)	1.4168(18)
C(5)-C(9)	1.4694(18)
C(6)-C(7)	1.4566(19)
C(7)-C(8)	1.390(2)
C(7)-C(14)	1.4410(18)
C(8)-H(4)	0.93(2)
C(9)-C(10)	1.3446(19)
C(9)-H(6)	1.01(2)
C(10)-C(11)	1.4621(18)
C(10)-H(7)	0.95(2)
C(11)-C(13)	1.341(2)
C(11)-C(12)	1.501(2)
C(12)-H(8)	1.00(2)

C(12)-H(9)	0.97(2)
C(12)-H(10)	0.98(2)
C(13)-H(11)	0.98(2)
C(13)-H(12)	1.02(2)
C(14)-H(13)	0.962(19)

bond angles in [°]

C(8)-N(1)-C(1)	108.69(11)
C(8)-N(1)-H(5)	127.6(15)
C(1)-N(1)-H(5)	123.2(15)
N(1)-C(1)-C(2)	127.55(12)
N(1)-C(1)-C(6)	108.79(11)
C(2)-C(1)-C(6)	123.66(12)
C(3)-C(2)-C(1)	117.11(12)
C(3)-C(2)-H(1)	122.8(12)
C(1)-C(2)-H(1)	120.1(12)
C(2)-C(3)-C(4)	120.71(13)
C(2)-C(3)-H(2)	119.3(11)
C(4)-C(3)-H(2)	120.0(11)
C(5)-C(4)-C(3)	122.81(13)
C(5)-C(4)-H(3)	120.2(12)
C(3)-C(4)-H(3)	117.0(12)
C(4)-C(5)-C(6)	117.16(12)
C(4)-C(5)-C(9)	121.18(12)
C(6)-C(5)-C(9)	121.64(12)
C(5)-C(6)-C(1)	118.46(12)
C(5)-C(6)-C(7)	136.21(12)
C(1)-C(6)-C(7)	105.31(11)
C(8)-C(7)-C(14)	117.92(13)
C(8)-C(7)-C(6)	106.12(12)
C(14)-C(7)-C(6)	135.96(12)

N(1)-C(8)-C(7)	111.05(13)
N(1)-C(8)-H(4)	121.9(13)
C(7)-C(8)-H(4)	127.1(13)
C(10)-C(9)-C(5)	124.51(12)
C(10)-C(9)-H(6)	119.3(12)
C(5)-C(9)-H(6)	116.2(12)
C(9)-C(10)-C(11)	125.74(13)
C(9)-C(10)-H(7)	121.3(12)
C(11)-C(10)-H(7)	113.0(12)
C(13)-C(11)-C(10)	119.29(13)
C(13)-C(11)-C(12)	121.72(13)
C(10)-C(11)-C(12)	119.00(13)
C(11)-C(12)-H(8)	109.8(12)
C(11)-C(12)-H(9)	113.3(13)
H(8)-C(12)-H(9)	105.8(18)
C(11)-C(12)-H(10)	112.7(13)
H(8)-C(12)-H(10)	106.6(17)
H(9)-C(12)-H(10)	108.1(18)
C(11)-C(13)-H(11)	120.5(13)
C(11)-C(13)-H(12)	122.1(13)
H(11)-C(13)-H(12)	117.5(18)
O(1)-C(14)-C(7)	128.65(13)
O(1)-C(14)-H(13)	117.8(12)
C(7)-C(14)-H(13)	113.6(12)

Table S5.8 Anisotropic displacement parameters ($Å^2 x\ 10^3$) for indiacene A.

	U^{11}	U^{22}	U^{33}	U^{23}	U^{13}	U^{12}
O(1)	32(1)	37(1)	19(1)	-4(1)	1(1)	2(1)
N(1)	28(1)	27(1)	21(1)	2(1)	-2(1)	2(1)
C(1)	25(1)	21(1)	20(1)	1(1)	-2(1)	-1(1)
C(2)	30(1)	28(1)	16(1)	0(1)	0(1)	-2(1)

C(3)	27(1)	30(1)	20(1)	-3(1)	2(1)	-1(1)
C(4)	24(1)	28(1)	21(1)	-2(1)	-1(1)	1(1)
C(5)	23(1)	22(1)	18(1)	-1(1)	-2(1)	-2(1)
C(6)	24(1)	20(1)	18(1)	-2(1)	0(1)	-3(1)
C(7)	26(1)	21(1)	22(1)	-1(1)	1(1)	0(1)
C(8)	27(1)	26(1)	25(1)	0(1)	1(1)	3(1)
C(9)	26(1)	24(1)	18(1)	-2(1)	0(1)	-2(1)
C(10)	27(1)	26(1)	19(1)	-1(1)	-1(1)	-1(1)
C(11)	29(1)	23(1)	19(1)	-2(1)	-3(1)	-5(1)
C(12)	38(1)	33(1)	21(1)	1(1)	2(1)	1(1)
C(13)	31(1)	40(1)	24(1)	3(1)	-7(1)	-2(1)
C(14)	26(1)	24(1)	23(1)	-4(1)	2(1)	1(1)

Table S5.9 Hydrogen coordinates (x 10^4) and isotropic displacement parameters ($Å^2$x 10^3) for indiacene A.

	x	**y**	**z**	**U(eq)**
H(1)	3520(30)	5582(16)	6649(15)	37(5)
H(2)	340(40)	6609(15)	6195(14)	31(5)
H(3)	-100(30)	7093(14)	4636(13)	29(4)
H(4)	9060(40)	4422(15)	4497(14)	31(5)
H(5)	7350(40)	4740(17)	5994(18)	44(6)
H(6)	3500(30)	6433(15)	2638(15)	34(5)
H(7)	-870(40)	7247(14)	3178(14)	33(5)
H(8)	1180(40)	7387(16)	451(15)	38(5)
H(9)	2110(40)	6461(17)	1035(15)	39(5)
H(10)	3160(40)	7562(17)	1183(15)	38(5)
H(11)	-2250(40)	8127(16)	946(16)	38(5)
H(12)	-3140(40)	8090(18)	2089(16)	44(6)
H(13)	8510(30)	4705(14)	2854(13)	29(4)

Crystal structure parameters for indiacene B.

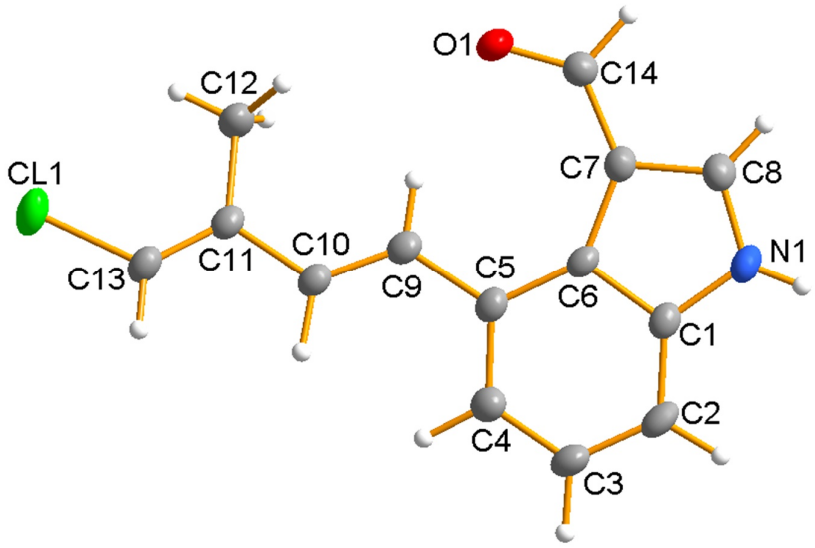

Figure S5.52 Electron density map calculated from the indiacene B diffraction pattern.

Empirical formula	$C_{14}H_{12}NOCl$
Formula weight	245.70 Da
Temperature	152(2) K
Wavelength	0.71073 Å
Crystal system	Orthorhombic
Space group	P $2_12_12_1$
Unit cell dimensions	a = 6.3460(4) Å α = 90°.
	b = 12.9149(9) Å β = 90°.
	c = 14.3042(10) Å γ = 90°.
Volume	1172.34(14) $Å^3$
Z	4
Density (calculated)	1.392 Mg/m^3
Absorption coefficient	0.307 mm^{-1}
F(000)	512
Crystal size	0.402 x 0.125 x 0.072 mm^3
Theta range for data collection	2.125 to 27.972°.
Index ranges	$-8 \leq h \leq 6$, $-17 \leq k \leq 17$, $-18 \leq l \leq 18$

Reflections collected	18425
Independent reflections	2822 [R (int) = 0.0561]
Completeness to theta = 25.242°	100.0 %
Absorption correction	Semi-empirical from equivalents
Max. and min. transmission	0.7456 and 0.7062
Refinement method	Full-matrix least squares on F2
Data / restraints / parameters	2822 / 0 / 202
Goodness-of-fit on F2	1.050
Final R indices [I>2σ (I)]	R1 = 0.0370, wR2 = 0.0723
R indices (all data)	R1 = 0.0575, wR2 = 0.0802
Absolute structure parameter -	0.04(4)
Largest diff. peak and hole	0.202 and -0.204 e.Å^{-3}

Table S5.10 Atomic coordinates (x 10^4) and equivalent isotropic displacement parameters (Å^{2}x 10^3) for in-diacene B. U (eq) is defined as one third of the trace of the orthogonalized U^{ij} tensor.

	x	y	z	U(eq)
Cl(1)	11853(1)	1972(1)	9149(1)	38(1)
N(1)	3467(4)	5208(2)	4042(2)	29(1)
O(1)	3466(3)	4533(2)	7232(1)	31(1)
C(1)	5331(4)	4676(2)	4181(2)	24(1)
C(2)	6890(5)	4457(2)	3531(2)	29(1)
C(3)	8591(5)	3891(2)	3837(2)	30(1)
C(4)	8723(5)	3551(2)	4760(2)	29(1)
C(5)	7209(5)	3795(2)	5431(2)	24(1)
C(6)	5458(5)	4387(2)	5135(2)	21(1)
C(7)	3569(4)	4814(2)	5570(2)	24(1)
C(8)	2447(5)	5286(2)	4855(2)	29(1)
C(9)	7399(5)	3444(2)	6405(2)	25(1)
C(10)	9116(5)	3022(2)	6782(2)	24(1)
C(11)	9310(5)	2687(2)	7758(2)	24(1)

C(12)	7397(5)	2682(3)	8369(2)	34(1)
C(13)	11212(5)	2404(2)	8038(2)	28(1)

Table S5.11 Bond lengths [Å] and angles [°] for indiacene B.

bond lengths [Å]	
Cl(1)-C(13)	1.733(3)
N(1)-C(8)	1.335(4)
N(1)-C(1)	1.382(4)
N(1)-H(5)	0.84(3)
O(1)-C(14)	1.237(3)
C(1)-C(2)	1.387(4)
C(1)-C(6)	1.418(4)
C(2)-C(3)	1.375(4)
C(2)-H(1)	0.99(3)
C(3)-C(4)	1.394(4)
C(3)-H(2)	1.01(3)
C(4)-C(5)	1.394(4)
C(4)-H(3)	1.03(3)
C(5)-C(6)	1.414(4)
C(5)-C(9)	1.470(4)
C(6)-C(7)	1.458(4)
C(7)-C(8)	1.387(4)
C(7)-C(14)	1.433(4)
C(8)-H(4)	0.92(3)
C(9)-C(10)	1.333(4)
C(9)-H(6)	0.96(3)
C(10)-C(11)	1.466(4)
C(10)-H(7)	1.05(3)
C(11)-C(13)	1.323(4)
C(11)-C(12)	1.496(4)
C(12)-H(8)	0.92(4)

C(12)-H(9)	1.00(4)
C(12)-H(10)	0.91(4)
C(13)-H(11)	0.99(3)
C(14)-H(12)	1.01(3)

bond angles in [°]

C(8)-N(1)-C(1)	109.1(2)
C(8)-N(1)-H(5)	128(2)
C(1)-N(1)-H(5)	123(2)
N(1)-C(1)-C(2)	128.0(3)
N(1)-C(1)-C(6)	108.5(2)
C(2)-C(1)-C(6)	123.5(3)
C(3)-C(2)-C(1)	117.0(3)
C(3)-C(2)-H(1)	124.7(16)
C(1)-C(2)-H(1)	118.2(16)
C(2)-C(3)-C(4)	121.1(3)
C(2)-C(3)-H(2)	118.5(17)
C(4)-C(3)-H(2)	120.2(17)
C(5)-C(4)-C(3)	122.7(3)
C(5)-C(4)-H(3)	118.7(17)
C(3)-C(4)-H(3)	118.5(17)
C(4)-C(5)-C(6)	117.2(2)
C(4)-C(5)-C(9)	121.8(3)
C(6)-C(5)-C(9)	121.0(3)
C(5)-C(6)-C(1)	118.4(2)
C(5)-C(6)-C(7)	136.3(2)
C(1)-C(6)-C(7)	105.3(2)
C(8)-C(7)-C(14)	117.6(3)
C(8)-C(7)-C(6)	105.9(2)
C(14)-C(7)-C(6)	136.4(2)
N(1)-C(8)-C(7)	111.1(3)

N(1)-C(8)-H(4)	121(2)
C(7)-C(8)-H(4)	128(2)
C(10)-C(9)-C(5)	125.2(3)
C(10)-C(9)-H(6)	118.9(18)
C(5)-C(9)-H(6)	115.8(18)
C(9)-C(10)-C(11)	125.1(3)
C(9)-C(10)-H(7)	120.4(14)
C(11)-C(10)-H(7)	114.4(14)
C(13)-C(11)-C(10)	116.5(3)
C(13)-C(11)-C(12)	124.2(3)
C(10)-C(11)-C(12)	119.3(3)
C(11)-C(12)-H(8)	110(2)
C(11)-C(12)-H(9)	111(2)
H(8)-C(12)-H(9)	103(3)
C(11)-C(12)-H(10)	110(2)
H(8)-C(12)-H(10)	111(3)
H(9)-C(12)-H(10)	112(3)
C(11)-C(13)-Cl(1)	125.5(2)
C(11)-C(13)-H(11)	124.4(17)
Cl(1)-C(13)-H(11)	110.0(17)
O(1)-C(14)-C(7)	128.6(3)
O(1)-C(14)-H(12)	115.5(17)
C(7)-C(14)-H(12)	115.9(17)

Table S5.12 Anisotropic displacement parameters ($Å^2 x\ 10^3$) for indiacene B.

	U^{11}	U^{22}	U^{33}	U^{23}	U^{13}	U^{12}
Cl(1)	39(1)	48(1)	27(1)	12(1)	-9(1)	-4(1)
N(1)	39(2)	29(1)	19(1)	3(1)	-4(1)	5(1)
O(1)	32(1)	40(1)	21(1)	1(1)	4(1)	4(1)
C(1)	30(2)	20(1)	20(1)	0(1)	-3(1)	-1(1)

C(2)	42(2)	31(2)	16(1)	-1(1)	0(1)	-2(1)
C(3)	32(2)	38(2)	20(1)	-3(1)	3(1)	-2(1)
C(4)	28(2)	34(2)	24(2)	-3(1)	-2(1)	1(1)
C(5)	27(2)	24(1)	20(1)	-1(1)	-3(1)	-2(1)
C(6)	27(2)	21(1)	16(1)	-1(1)	0(1)	-3(1)
C(7)	26(2)	23(1)	22(1)	0(1)	-3(1)	0(1)
C(8)	33(2)	27(2)	27(2)	1(1)	-3(1)	6(1)
C(9)	28(2)	27(2)	20(1)	-2(1)	0(1)	-1(1)
C(10)	28(2)	27(2)	18(1)	0(1)	0(1)	-1(1)
C(11)	31(2)	24(2)	18(1)	-2(1)	-1(1)	0(1)
C(12)	31(2)	46(2)	25(2)	6(1)	4(1)	5(2)
C(13)	33(2)	31(2)	20(1)	4(1)	-1(1)	-2(1)
C(14)	26(2)	25(2)	26(1)	-1(1)	0(1)	1(1)

Table S5.13 Hydrogen coordinates (x 10^4) and isotropic displacement parameters ($Å^2$x 10^3) for indiacene B.

	x	**y**	**z**	**U(eq)**
H(1)	6690(40)	4700(20)	2882(19)	23(7)
H(2)	9700(50)	3680(20)	3360(20)	32(8)
H(3)	9940(50)	3070(30)	4940(20)	39(9)
H(4)	1170(60)	5620(20)	4890(20)	35(9)
H(5)	3080(50)	5420(20)	3520(20)	36(9)
H(6)	6200(50)	3570(20)	6800(20)	36(9)
H(7)	10500(40)	2930(20)	6383(18)	24(7)
H(8)	6380(70)	2250(30)	8120(20)	63(13)
H(9)	6690(60)	3370(30)	8370(30)	60(11)

H(10)	7740(50)	2480(30)	8960(30)	50(10)
H(11)	12490(50)	2440(20)	7650(20)	34(9)
H(12)	1310(50)	5240(20)	6560(20)	31(8)

Chromatographic, mass spectrometric and NMR data of chloroxanthic acid A

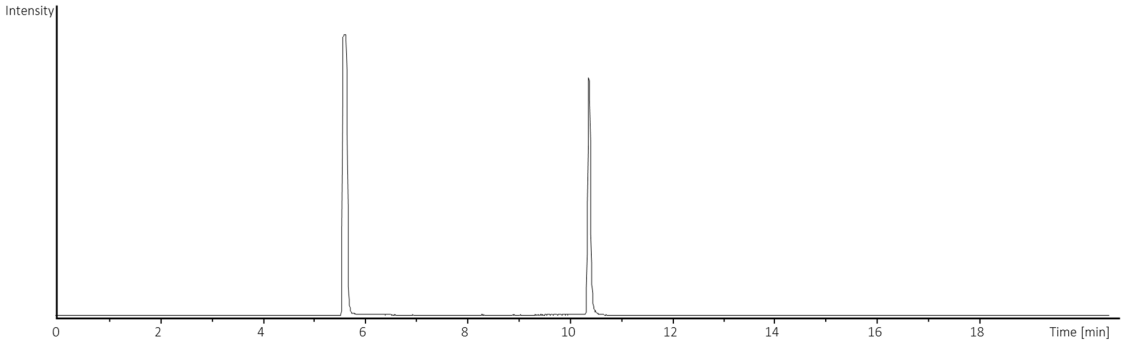

Figure S5.53 EIC at 295.08 for chloroxanthic acid A.

The two peaks visible in the EIC at 295.08 for chloroxanthic acid A likely derive from the *E/Z* isomers of chloroxanthic acid A, based on the high difference in retention time on rp-HPLC. As the double bond in position 9 is thermodynamically more stable and was determined to be in *E*-configuration based on the coupling constant of 16.1 Hz of proton 9, most likely those isomers derive from isomerization of the double bond in position 2 in aqueous solution. We only were able to generate NMR data for the mayor derivative, corresponding to the earlier eluting peak due to general low production of the compounds. In the NMR spectra we however are able to observe a second minor broad doublet at $\delta^1H = 6.46$ showing ca. 30% of the intensity of the mayor peak for proton 3. Therefore, we likely already observe a fast isomerization during NMR analysis in methanolic solution, although the isomers are nicely separable by semipreparative HPLC. The coupling constant of 8.4 Hz for the minor derivative points towards a *Z*-configuration of the minor and an *E*-configuration of the mayor isomer. Due to overlapping signals of the mayor proton signal at position 3 with the proton at position 13, the coupling constant of the proton belonging to the mayor isomer could not be determined.

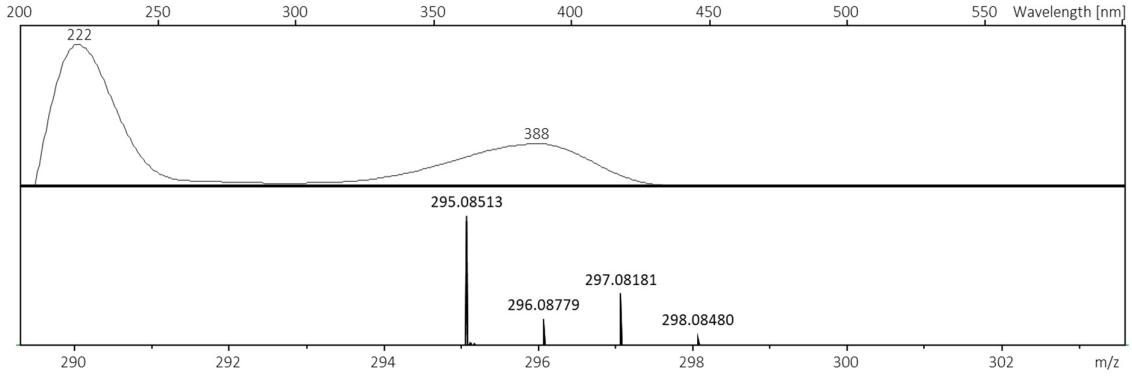

Figure S5.54 UV-absorption and isotopic pattern for $[M+H]^+$ of chloroxanthic acid A.

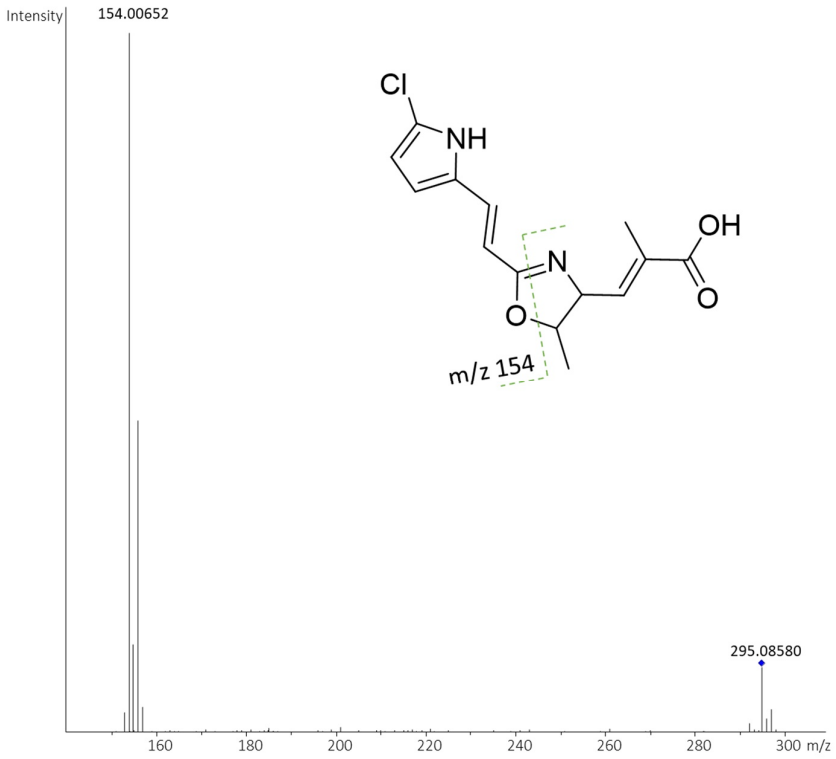

Figure S5.55 MS/MS Fragmentation pattern of chloroxanthic acid A.

Table S5.14 NMR signals of chloroxanthic acid A. Carbon numbers are shown in structure below.

Carbon No.	δ ^{1}H [ppm]	Multiplicity, *J* [Hz] and number of protons	δ ^{13}C [ppm]	COSY correla-tions	HMBC correla-tions
1	-	-	174.5	-	-
2	-	-	135.6	-	-
3	6.38	m*, 1H	136.9	4	-
4	4.55	dd, 1H, 9.3, 7.2	71.4	3,5	5,6,8
5	4.45	m, 1H	83.2	4,6	3,4,8
6	1.43	dd, 1H, nd	20.3	5	4,5
7	1.94	d, 1H, 1.44	14.0	-	1,2,3,4,5
8	-	-	166.9	-	-
9	6.18	d, 1H, 16.1	108.2	10	18,10,11
10	7.13	d, 1H, 16.2	131.8	9	8,9,11,12,13
11	-	-	129.8	-	-
12	6.03	d, 1H, 3.7	109.0	13	11,13,14
13	6.38	d*, 1H	115.6	12	10,11,12
14	-	-	120.3	-	-

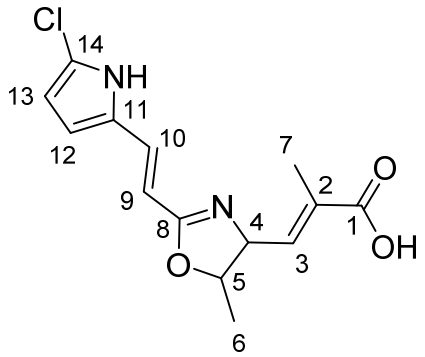

^{1}H NMR (700 MHz, METHANOL-d_4) δ ppm 1.41 - 1.44 (m, 4 H) 1.43 - 1.44 (m, 1 H) 1.94 (d, *J*=1.44 Hz, 2 H) 4.43 - 4.48 (m, 1 H) 4.43 - 4.48 (m, 1 H) 4.55 (dd, *J*=9.30, 7.18 Hz, 1 H) 4.53 - 4.57 (m, 1 H) 6.02 - 6.04 (m, 1 H) 6.03 (d, *J*=3.66 Hz, 1 H) 6.18 (d, *J*=16.09 Hz, 1 H) 6.35 - 6.41 (m, 1 H) 6.36 - 6.40 (m, 1 H) 6.36 - 6.40 (m, 1 H) 6.36 - 6.39 (m, 1 H) 6.37 - 6.39 (m, 1 H) 7.13 (d, *J*=16.18 Hz, 1 H)

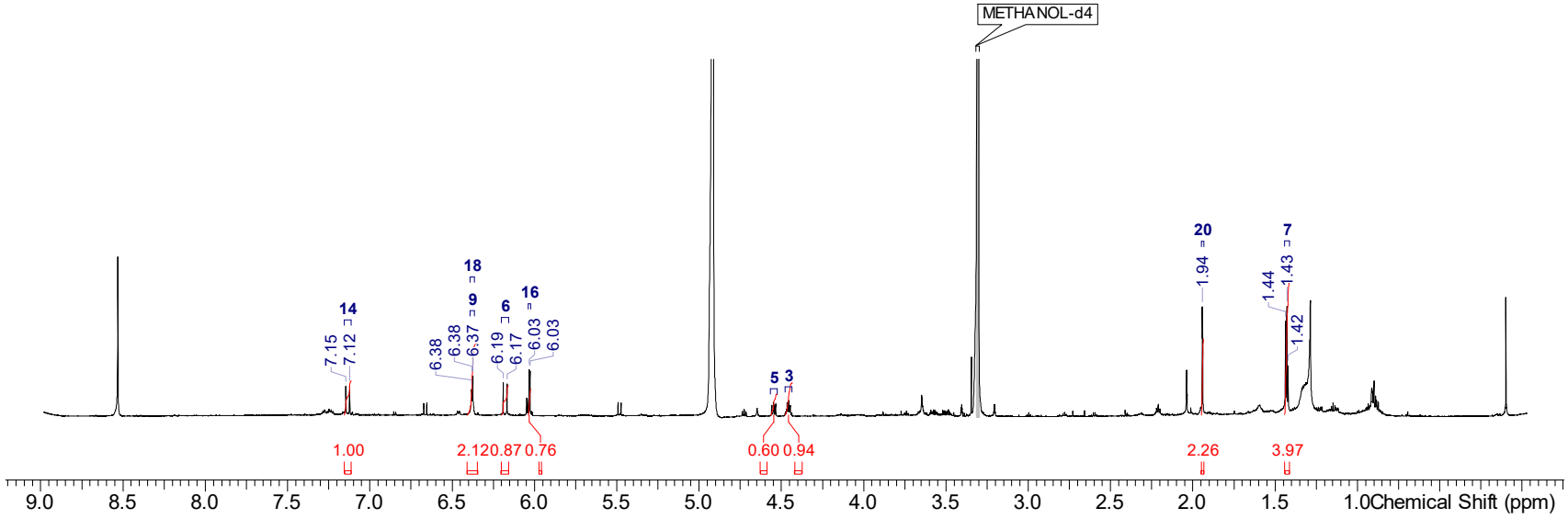

Figure S5.56 ^{1}H spectrum of chloroxanthic acid A in $MeOD_4$.

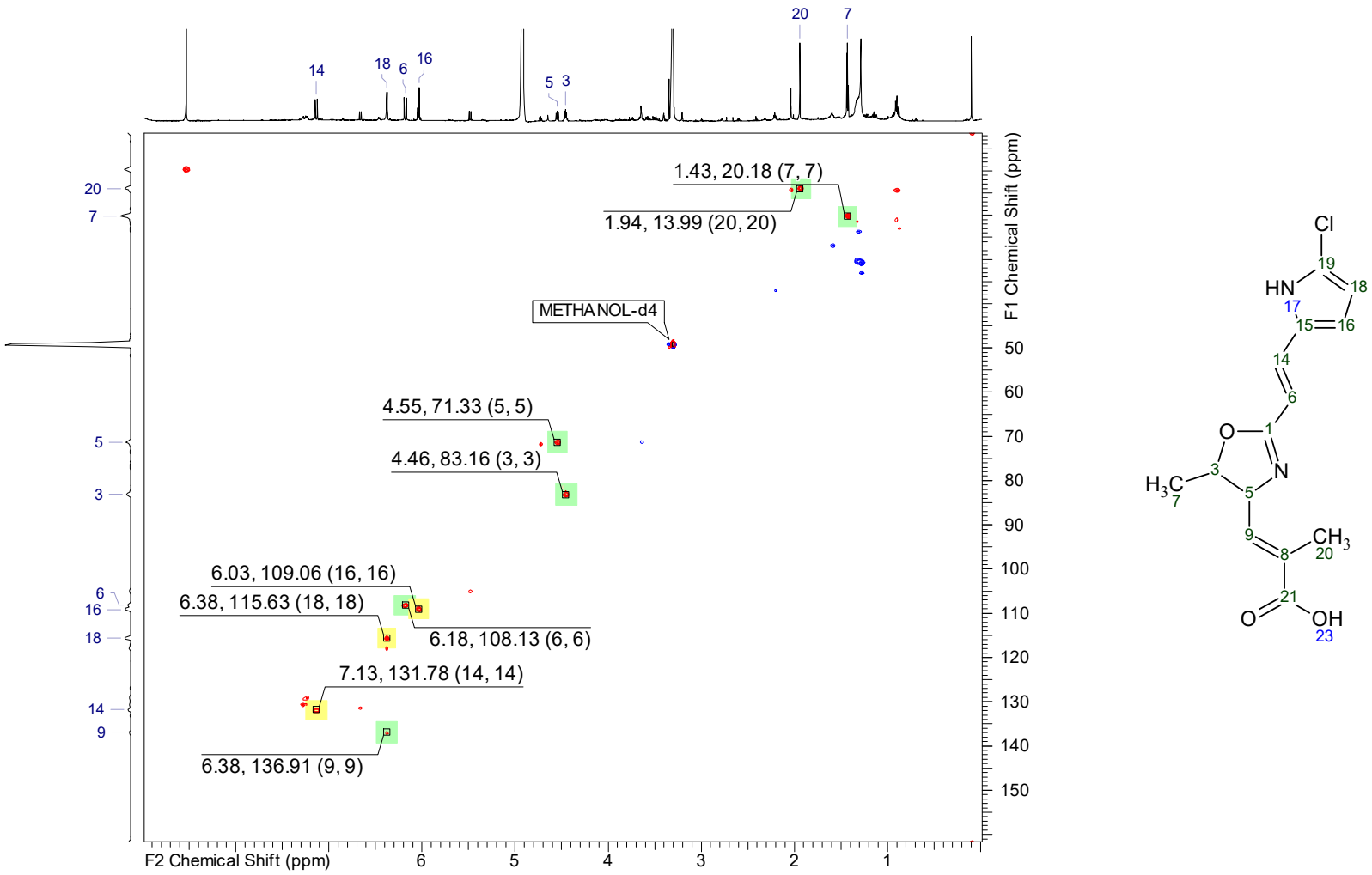

Figure S5.57 HSQC-dept-spectrum of chloroxanthic acid A in $MeOD_4$.

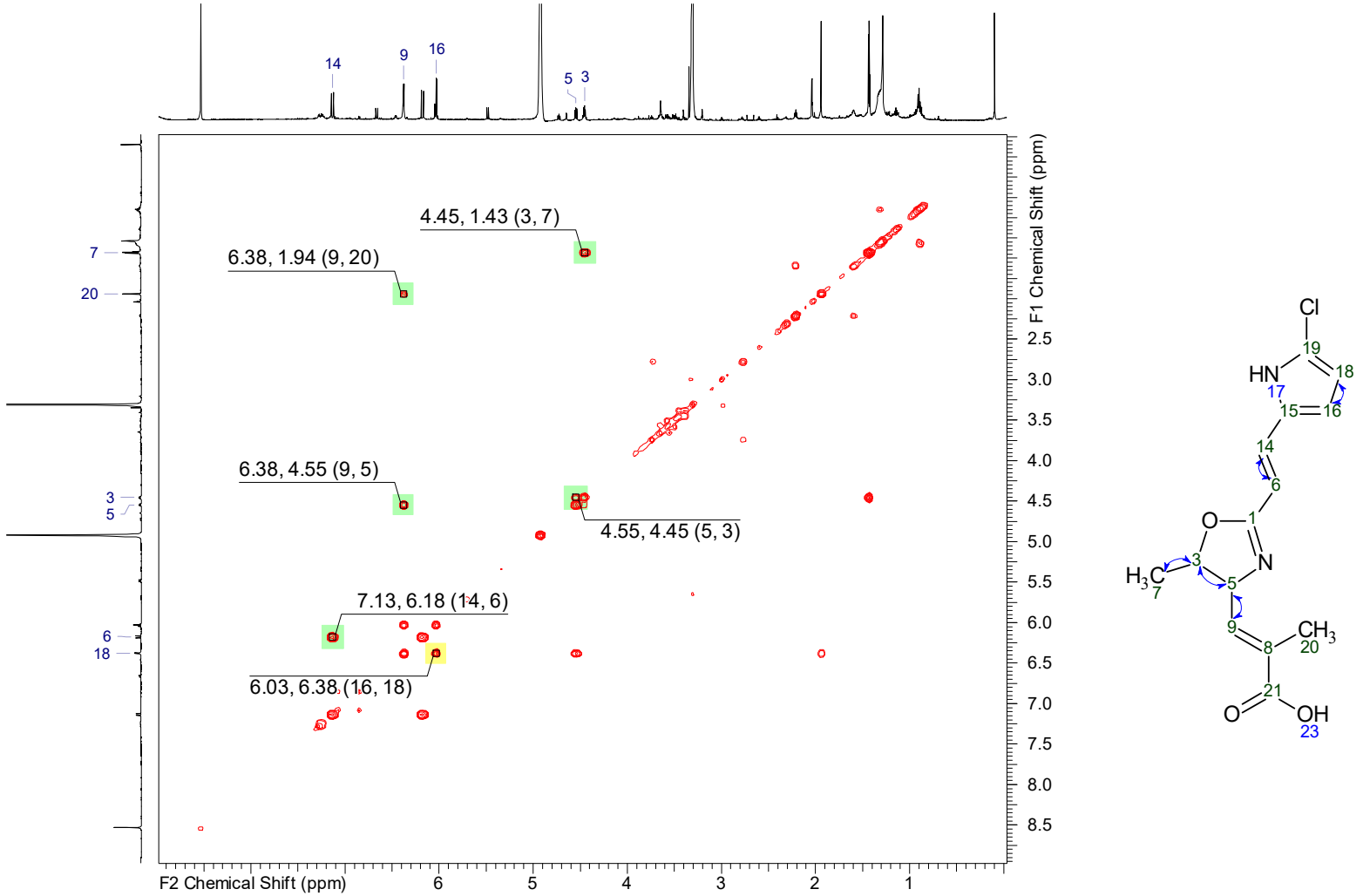

Figure S5.58 COSY-spectrum of chloroxanthic acid A in $MeOD_4$.

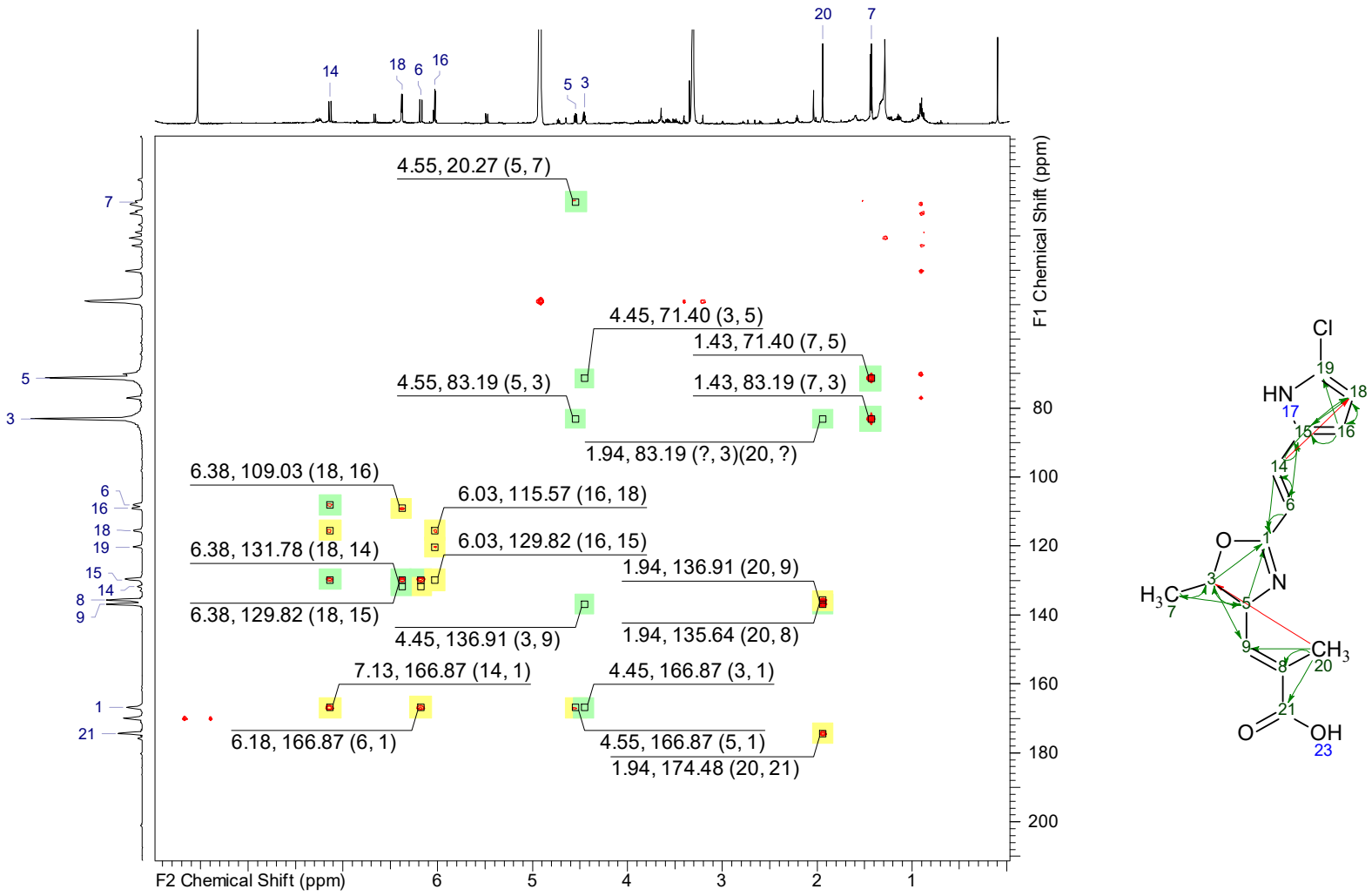

Figure S5.59 HMBC-spectrum of chloroxanthic acid A in $MeOD_4$.

References

(1) Pena-Pereira, F.; Wojnowski, W.; Tobiszewski, M. AGREE-Analytical GREEnness Metric Approach and Software. *Anal. Chem.* **2020**, *92*, 10076–10082.

(2) Hoffmann, T.; Krug, D.; Bozkurt, N.; Duddela, S.; Jansen, R.; Garcia, R.; Gerth, K.; Steinmetz, H.; Müller, R. Correlating chemical diversity with taxonomic distance for discovery of natural products in myxobacteria. *Nat. Commun.* **2018**, *9*, 803.

(3) Hug, J. J.; Panter, F.; Krug, D.; Müller, R. Genome mining reveals uncommon alkylpyrones as type III PKS products from myxobacteria. *J. Ind. Microbiol. Biotechnol.* **2019**, *46*, 319–334.

(4) Panter, F.; Krug, D.; Baumann, S.; Müller, R. Self-resistance guided genome mining uncovers new topoisomerase inhibitors from myxobacteria. *Chem. Sci.* **2018**, *9*, 4898–4908.

(5) Panter, F.; Krug, D.; Müller, R. Novel Methoxymethacrylate Natural Products Uncovered by Statistics-Based Mining of the *Myxococcus fulvus* Secondary Metabolome. *ACS Chem. Biol.* **2019**, *14*, 88–98.

(6) Zhang, F.; Braun, D. R.; Rajski, S. R.; DeMaria, D.; Bugni, T. S. Enhypyrazinones A and B, Pyrazinone Natural Products from a Marine-Derived Myxobacterium *Enhygromyxa sp*. *Marine drugs* **2019**, *17*.

(7) Gorges, J.; Panter, F.; Kjaerulff, L.; Hoffmann, T.; Kazmaier, U.; Müller, R. Structure, Total Synthesis, and Biosynthesis of Chloromyxamides: Myxobacterial Tetrapeptides Featuring an Uncommon 6-Chloromethyl-5-methoxypipecolic Acid Building Block. *Angew. Chem. Int. Ed. Engl.* **2018**, *57*, 14270–14275.

(8) Okoth Dorothy A.; Hug, J. J.; Garcia, R.; Spröer, C.; Overmann, J.; Müller, R. 2-Hydroxysorangiadenosine: Structure and Biosynthesis of a Myxobacterial Sesquiterpene–Nucleoside. *Molecules (Basel, Switzerland)* **2020**, *25*.

(9) Oueis, E.; Klefisch, T.; Zaburannyi, N.; Garcia, R.; Plaza, A.; Müller, R. Two Biosynthetic Pathways in *Jahnella thaxteri* for Thaxteramides, Distinct Types of Lipopeptides. *Org. Lett.* **2019**, *21*, 5407–5412.

(10) Dehhaghi, M.; Tan, V.; Heng, B.; Mohammadipanah, F.; Guillemin, G. J. Protective Effects of Myxobacterial Extracts on Hydrogen Peroxide-induced Toxicity on Human Primary Astrocytes. *Neuroscience* **2019**, *399*, 1–11.

(11) Lee, C.; Park, S.; Ayush, I.; Cho, K.; Kim, S. S.; Kang, I.; Choe, W.; Kim, Y.-S.; Yoon, K.-S. Effects of *Myxococcus fulvus* KYC4048 Metabolites on Breast Cancer Cell Death. *J. Microbiol. Biotechnol.* **2018**, *28*, 765–775.

(12) Korp, J.; Winand, L.; Sester, A.; Nett, M. Engineering Pseudochelin Production in *Myxococcus xanthus*. *Appl. Environ. Microbiol.* **2018**, *84*, e01789-18.

(13) Sheldrick, G. M. A short history of SHELX. *Acta Crystallogr. Sect. A* **2008**, *64*, 112–122.

Chapter 6

6. Discussion and Outlook

During this work, three different natural product mining approaches were carried out, leading to the discovery of several new compounds or derivatives of known substance families. Each compound family showed unique structural characteristics and biological activities. It was thus demonstrated that a comprehensive workflow including bioactivity-guided, genome- and metabolome-based approaches fuelled the identification and purification of specific metabolites. The establishment of alternative metabolic profiles with additional new metabolites was possible due to the implemented co-cultivation approach for myxobacteria. Moreover, in the case of *Sorangium sp.* MSr12523, the outcome of the metabolome changes was remarkable and led to the discovery of a myxobacterial derived alkyl-quinolone compound family with strong biological activity against *Mycobacterium tuberculosis* 7H37Ra. Solid-liquid cultivation with the Flow plate device yielded a mixed metabolic profile of *M. xanthus* DK1622 displaying characteristic features of both types of growth conditions. Extraction procedures using supercritical CO_2 in combination with the addition of medium-polar and polar co-solvents allowed the purification of myxobacterial SMs in higher yields and led to the discovery of a new compound family termed chloroxanthic acid. An innovative workup process enabled to utilise the benefits of comprehensive data assessment through in-depth application of emerging techniques to identify previously unknown myxobacterial secondary metabolites and led finally to their isolation and structural elucidation.

6.1 Obstacles in bioprospecting of microbial natural products

Antibiotic resistance has become a challenge for our public health and our society; it has allowed infectious diseases to once again become a threat to human health. Novel antibiotics that appear on the market are confronted with the emergence of resistant pathogens after a certain period of use[1]. Natural products (NPs) remain a promising source for novel chemical molecules which possess various intriguing biological activities[2]. Most of the antibiotics approved for medical use are products of microorganisms or are derived from their metabolic products, hence they are considered one of the most important reservoirs for the discovery of new lead structures for drugs[3]. As example, the introduction a new antibiotic to the market is the finish line of a process that can take up to 15 years and cost a 1-2

billion €. It is therefore important to reduce the major risks associated and not waste excessive time and resources. In the following, I will discuss several obstacles and bottlenecks on the bioprospecting pipeline of microbial-derived NPs.

The first hurdle is found in the discovery process that aims to identify novel compounds or lead structures suitable for drug development. However, there are some practical reasons which make the search for novel microbial natural products a challenging task. Re-discovering already known compounds from microbial extracts is most of what can happen in the early phase of bioprospecting. In the past, the bioactivity-guided approach was primarily used to discover antimicrobial substances, leading to this phenomenon[4]. For a long time, the focus was on isolating SMs that are produced in large quantities and thus are easy to obtain, the so-called "low hanging fruits", which very often turned out to be well-known. Therefore, the working step of so called “dereplication”, which is mostly based on HPLC-MS analysis, should be mandatory for all NP discovery surveys. The evaluation of MS^2 spectra and database searches play an important role in determining the elemental composition of analytes. In particular, the fragment pattern of the analyte helps with identification and can also provide a structural information’s by comparison with MS^2 reference spectra[5]. The implementation of an automated metabolomic networking workflow (Global Natural products Social Molecular Networking) and database search platform that allows metabolic networks to be generated represent a substantial gain for dereplication, particularly in the context of natural products research[6].

A second obstacle is the quality of bacterial isolates examined from soil samples that can be a limiting factor when it results in repeated isolation of nearly similar bacteria of the same genus. The bottleneck in the bioprospecting of bacteria is therefore rather the too selective isolation and subsequent screening of the containing bacterial strains within a sample. As one strategy for selecting bacteria for new antibiotic discovery in order to gain high hit rates of chemical novelty is to sample previously untapped or less sampled ecosystems, like the marine environment[1]. Only less than 2 % of the NPs originated from the deep sea environment and thus belong to the less studied ecosystems[7]. Nevertheless, the investigation of isolates from such ecosystems is not a guarantee for the lack of re-discovery of already known compounds. There is the possibility to investigate bacterial phyla that are known for their ability to produce SMs and select the less-investigated branches of those phyla. Studies showed a correlation between taxonomic distance and metabolic diversity and led to the conclusion that some natural product groups are preferentially found only in

certain genera[8]. Tapping into novel and untapped drug sources is essential for the success of antibiotic discovery and development, as previous strategies have failed and led to a stalemate in the current development pipeline[9].

A traditional bioprospective workflow is based usually on the "top-down" concepts starting with the biological and chemical characterisation of the produced bacterial metabolite. Based on bioinformatics and molecular biology, the genetic information on the biosynthetic potential of microorganisms could be expanded with the help of new available techniques and led to the "bottom-up" approach[10] (Figure 6.1).

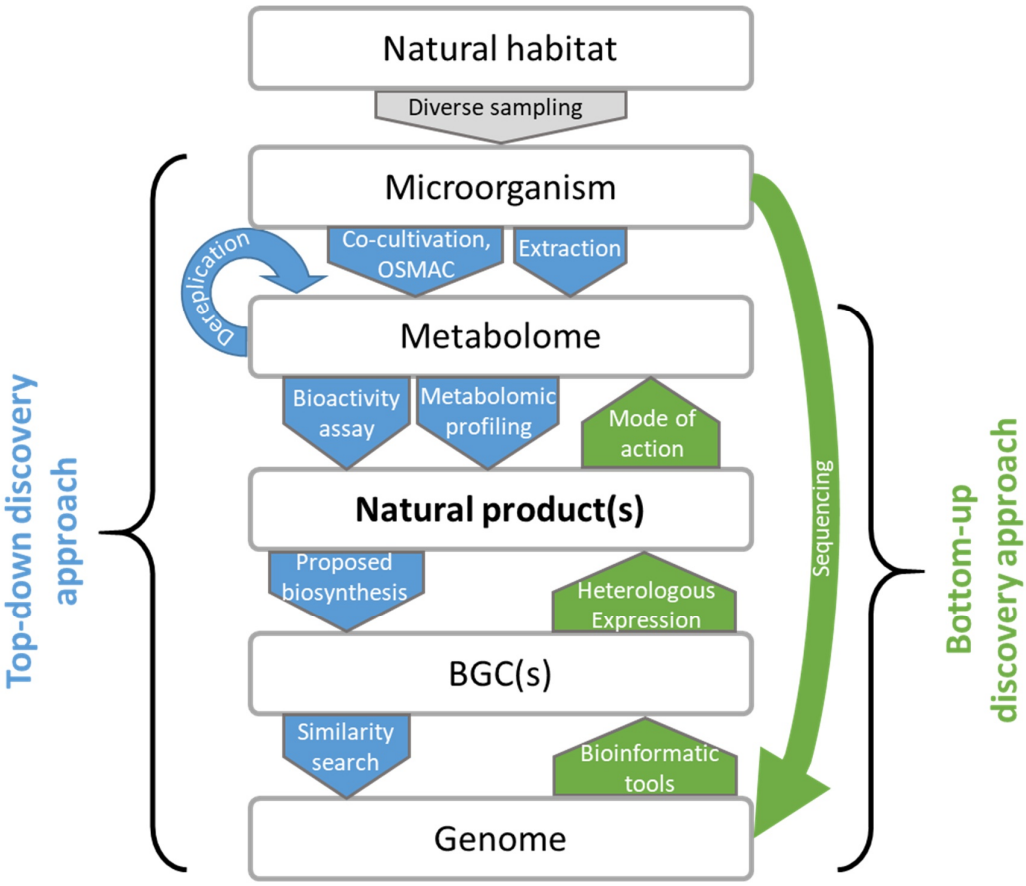

Figure 6.1 Schematic illustration of the bioprospective top-down and bottom-up workflow for NP discovery.

In addition, working with the bacteria can cause further hurdles in exploration, such as silent or non-expressed biosynthetic gene clusters (BGCs) or difficulties in cultivating of the microorganisms[11]. Several strategies have been established and applied to activate the non-expressed BGCs, such as co-cultivation, OSMAC (one strain many compounds) approach or molecular biology based techniques like heterologous expression or promoter

insertion[12]. In particular, the co-cultivation approach for *Sorangium sp.* MSr12523 demonstrated tremendous potential for altering the metabolite profile and is discussed in more detail in the section 6.2.2. Microbiological improvements in the cultivability of microbes and OSMAC approaches to influence the produced spectrum of NPs allow us to isolate bacteria and produce compounds that have not been accessible before[13,14]. In order to obtain further access to a broader spectrum of metabolites, an innovative mixed solid-liquid cultivation method was developed (see section 6.2.3).

In contrast to the “top down” strategy, the required genetic manipulation of a bacterium for e.g. promoter insertion in native host is more time-consuming and demands the genome sequence. Besides the bioinformatic tools to handle the vast amount of data, is the genomic access to microorganisms sometimes the limitation to apply such a genomic strategy successful. Bioinformatics tools as part of genome mining enable the identification and thereby access to silent gene clusters, which can be further manipulated by molecular biology techniques such as heterologous expression or promoter insertion[15]. AntiSMASH should be mentioned as a bioinformatics tool that facilitates the process of predicting potential BGC based on knowledge of already known gene clusters in bacterial genomes[16]. Such tool offers a great potential to gain more than an overview about the available biodiversity in particular strains. This also helps in the bioprospective selection of promising bacterial isolates in terms of the number of yet unknown BGCs to enhance the chances of NP discovery.

However, despite the top-down and bottom-up strategies mentioned above, ultimately the NPs need to be produced, extracted and purified in order to obtain sufficient material for structure elucidation and bioassays. Besides the microbial metabolite production, the extraction process is therefore an essential step for the successful discovery of novel NPs. As part of the investigation of new microbial NPs, a previously less explored extraction method using supercritical fluid CO_2 was selected and compared to a conventional method (see section 6.2.4).

Summarised, strategies for bioprospecting microbial natural products need to be adapted and more oriented towards the selection of organisms from more versatile ecosystems to accelerate the process of drug screening. Likewise, the identification of "truly" novel NPs needs to be pushed more through consequent dereplication, thereby rapidly eliminating the isolation of one of the numerous known compounds. Finding new sources to generate compounds that can be introduced into the drug development pipeline is more challenging than ever, but several promising approaches are within reach.

6.2 Selection of proven microbial producers of natural products

A different strategy to enlarge the possibility of antimicrobial hits in bioprospecting is to focus on bacteria of phylogenetic order that have been proven as be frequent producers antibiotics or bioactive molecules. Historically in the realm of bacteria, actinobacteria contribute the vast majority of bioactive molecules and are an indispensable source for commercially utilised antibiotics[17]. Among molecules that have become drugs, actinobacteria represented about 53% of discovered antibacterial compounds of microbial origin by the year 2002[18]. In particular, the genus *Streptomyces* belonging to actinobacteria is a producer of a high number of antibiotics. There are several statistical estimations that only 3% of the antibiotics produced by *Streptomyces* are discovered so far[19]. This proves that there are still a lot of potential antibiotics in actinobacteria, but they are not expressed among a large amount of known molecules, which makes discovery difficult due to false positive hits. Therefore, the above-mentioned dereplication strategy should gain further importance in the upcoming efforts to discover new antimicrobial molecules from actinobacteria.

An additional group of bacteria that harbours promising possibilities to produce novel compounds because of their high biosynthetic potential are myxobacteria. Members of this group are known to be remarkable producers of a number of new NPs and possess uncommonly large genomes with abundant biosynthetic gene clusters, most of them not yet linked to the respective molecules[18,20]. Myxobacterial large genomes are characterised by a high number of polyketide synthetases (PKS), non-ribosomal peptide synthetases (NRPS) and NRPS/PKS hybrid gene clusters and their physiological complexity (e.g. fruiting body formation) makes them unique in the bacterial kingdom[21,22]. A careful selection of bacterial strains can be regarded as an important strategy for exploiting improved biodiversity. Therefore, myxobacterial strains MSr12523, MSr11367, MSr11368 and MSr11954 studied in this work belong to a new phylogenetic clade of the suborder *Sorangineae* and revealed a greater taxonomic distance to already known bacterial members. However, with the knowledge that phylogenetic distances correlate with chemical diversity, isolation of myxobacteria from untapped habitats and subsequent genetic classification must be integrated to ensure that too many resources are not wasted on too similar strains.

Considering the large genome with its unexploited potential for new natural products, this becomes particularly important. The myxobacterial extract of *Sorangium sp.* MSr12523 demonstrated even now, after standard cultivation, effective antimicrobial activity against Gram-negative and Gram-positive pathogens. Dereplication process based on LC-MS data

revealed the presence of nocardamine, thuggacin and sorangicin as known natural compound classes. In addition, genome sequencing and subsequent analysis on the antiSMASH platform revealed the presence of 58 putative biosynthetic gene clusters there are linked to PKS and NRPS types. Only two BGCs (terpene and type I PKS) could be linked to previously known NP by a sequence similarity (> 85%) of the corresponding BGC. This indicates the enormous genetic potential of MSr12523 harboured in this strain to produce yet another variety of novel peptide- and/or polyketide NPs.

6.2.1 Activation of silent biosynthetic gene clusters

One problem is still that a strain alone carries much more potential for NP discovery than is actually accessible under standard cultivations and screening setups. Considering that a certain NP plays an evolutionary role in the habitat of their produces, it seems logical that the corresponding biosynthesis is only triggered by particular environmental stimuli and not enabled unconditionally. Several strategies to identify such inducers were successfully applied and led to the isolation of novel compounds, for example antibiotics, rare-earth elements or co-cultivation with other microorganisms[23–26]. Furthermore, the experimental setup of the cultivation, e.g. growth on agar or in liquid medium, showed an additional influence on the spectrum of the NPs produced[27]. In particular, due to the different growth behaviour of e.g. predatory myxobacteria swarming and gliding on surfaces versus unicellular suspension growth in liquid medium, there are fundamental differences in the regulation of expressed gene clusters[28,29].

It should be mentioned that heterologous expression as targeted approach of genome mining is an additionally promising strategy to access silent gene cluster. One major advantage of heterologous expression is its independence from the original host organism, because molecular biological tools to manipulate the host organism are frequently not available. Nevertheless, heterologous expression of a desired BGC is time-consuming technique and can cause problems with gene expression in the heterologous host platform[30]. For the present work, heterologous expression was not applied.

After the establishment of a co-cultivation approach of myxobacteria, different myxobacterial strains were selected to alter the metabolite spectrum. Three myxobacteria, MSr12523, MSr11954 and MSr11367, were selected due to their high number of unknown BGCs and their phylogenetically distance within the suborder *Sorangiineae*.

6.2.2 Co-cultivation approach – a path to alter the secondary metabolism

Co-cultivation intended to expand chemical diversity of the synthesised secondary metabolites (SMs) of microorganism. SMs on their own are engaged in inter- or intraspecies interactions in the producer's natural environment, but they are not essential for cell growth. The expression of such SMs is encoded in BGCs, which are inhibited until being activated by specific environmental factors, such as microbial interaction and physical stress from the natural habitat. Therefore, it is important to find a way activating “non-essential”/silent BGCs that are inherent in the genome of the microorganisms, which are often not expressed in axenic cultures.

Co-cultivation approaches convince with their simply designed experimental set-up (Figure 6.2) and are also effective in triggering silent BGCs of different microbial species[31]. However, the selection of the most potent microorganisms between producer and inducer strains remains unpredictable and a major challenge[32]. Another factor influencing the silent BGCs involves the type of co-cultivation, such as membrane-based techniques, solid surfaces or suspension growth of the respective microbes with each other, which is crucial for success or failure. In addition, co-cultures allows the real-time monitoring of bioactive SMs towards the microbial competition by the analysis of morphological changes or cell density in micro fluids[33]. Nevertheless, only few specific microbial combination between producer and partner (inducer) strain have been found that efficiently induce the production of novel SMs, such as antibiotics, antifungals, anticancer compounds, and siderophores[34,35].

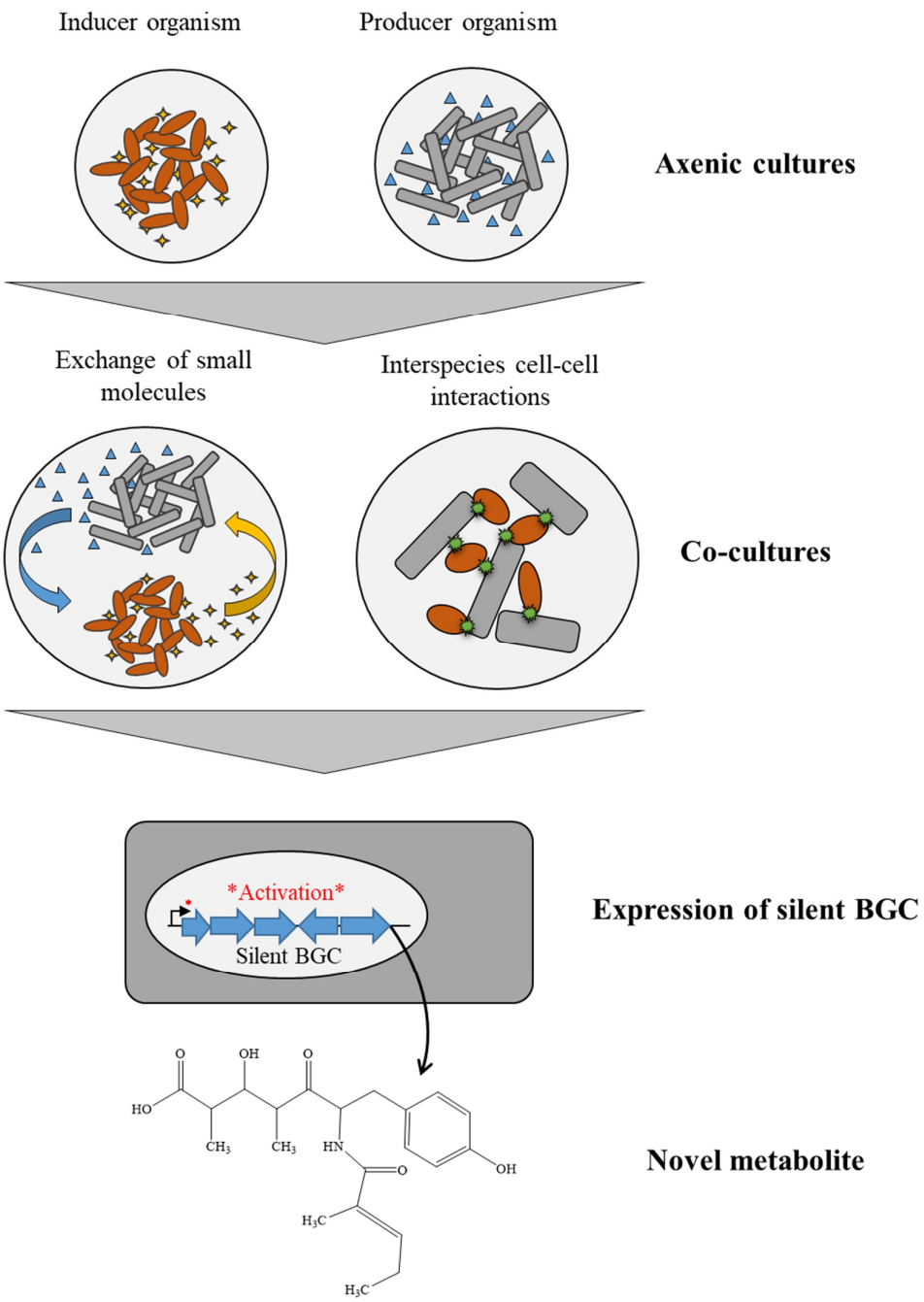

Figure 6.2: Production opportunities of secondary metabolites in co-culture leading to the activation of silent biosynthetic gene clusters (BGC) and formation of potentially novel SMs. Either the exchange of small molecules or the specific cell-cell interaction can trigger the production of new metabolites.

Myxobacterial co-cultivation with at least two different bacteria, including one myxobacterium as the production organism, have in the present work resulted in a remarkable outcome of additional metabolites from this comparatively simple approach. These secondary

metabolites discovered were from *Sorangium sp.* MSr12523 and showed structural characteristics of PKS and NRPS origin. Besides the influence of changed metabolic profiles after co-culturing with mycolic acid-containing bacterium (MACB) *T. pseudospumae*, also led to a remarkable alteration of the bioactive substances in the extract. Interestingly, the biological activity against *Mycobacterium smegmatis* mc² 155 to which the group of MACB also belongs, was particularly enhanced. This can be considered as a direct reaction that occurs during the microbial competition in the same liquid environment. The excretion of small molecules of the partner strain into the medium led to quorum sensing, that triggered the stimulation of certain pathways in the producer resulting in the activation of a promoter from silent BGCs. As a result, previously unexpressed putative BGCs are activated, which in response to signals from the partner strain then cause the synthesis of targeted metabolites against it. In the case of MACB, it is also conceivable that the bacterial cells establish cell–cell contact via the mycolic acid chains located in their outer cell membrane. The physiological encounter between *Sorangium sp.* MSr12523 and *T. pseudospumae* as a member of MACB then activated the previously silent BGC. Onaka *et. al.*[23] have demonstrated that such a phenomenon exists between different species of bacteria.

In summary, myxobacterial co-cultivation for the discovery of new SMs was employed for the first time in this work. The results obtained indicate the potential success of this method for the discovery of previously unseen compound classes and new chemical scaffolds, but the identification of the appropriate partner strain can be challenging in the sense that a straight-forward rationale for this selection cannot be established at the moment. Consequently, as there is not yet a suitable large-scale screening for myxobacteria that includes the co-cultivation approach, the myxobacterial production strains to be investigated should be carefully selected. It is therefore suggested to focus on phylogenetically more distinct species of the suborder *Sorangiineae*, *Nannocystineae* and *Cystobacterineae*. Furthermore, the bioinformatics tool antiSMASH can be helpful to reveal large discrepancies between the predicted number of BGCs and the determined amount of NP classes. Co-cultivation can also be considered as an effective approach for all microorganisms when genetic manipulation by using molecular biology techniques cannot be achieved.

6.2.2.1 Alkyl-quinolones from co-cultivation

Alkyl-quinolones (AQs) are a specific secondary metabolite class of *Pseudomonas* and *Burkholderia* genera and consist of a 4-quinolone core, usually substituted at position 2

with a variety of alkyl groups[36]. Already in 1940, a series of alkyl quinolones with remarkable antibiotic properties were isolated from *Pseudomonas aeruginosa* for the first time[37]. Recently, it became known that the Pseudomonas Quinolone Signal (PQS), an alkyl-quinolone derivative, plays an important role in bacterial communication and quorum sensing in *P. aeruginosa*[38].

MAQ derivative	R_1	R_2
MAQ-268	H	H
MAQ-302	Cl	H
MAQ-282	H	CH_3
MAQ-316	Cl	CH_3

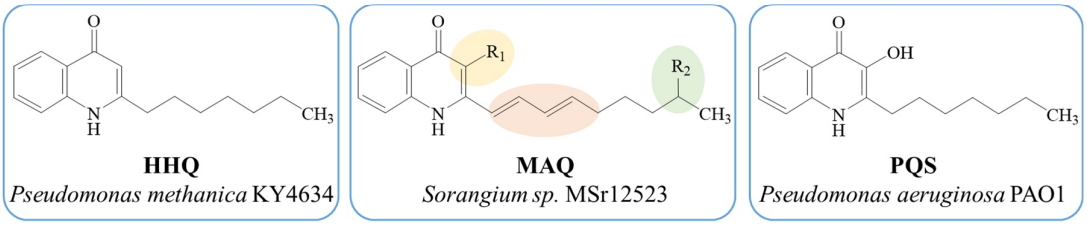

Figure 6.3: Chemical structures of a selection of alkyl-quinolones and their respective producing organism. Highlighted unique chemical characteristics of MAQs. HHQ – 2-heptyl-4-quinolone, MAQ – Myxobacterial alkyl-quinolone and PQS – Pseudomonas Quinolone Signal.

The myxobacterial alkyl-quinolones (MAQs) were identified by co-cultivation of *Sorangium sp.* MSr12523 with *T. pseudospumae* and axenic cultivation of changed media composition as part of a pleotropic approach. These MAQs show a close structural similarity to the well-known PQS and HHQ (Figure 6.3). Therefore, it is assumed that MAQ synthesis follows a comparable biosynthetic pathway as has already been published[39]. An unusual MAQ structural feature was found in the substitution at the C3 position by halogenation of the 4-quinolone core structure motif. Furthermore, there are additional modifications in the structure of the alkyl chain compared to HHQ and PQS. Nowadays, more than 57 different AQs have been isolated from bacteria belonging to the genera *Alteromonas*, *Pseudoalteromonas* and *Burkholderia*, thus indicating the ability to synthesise a vast portfolio of AQs derivatives[40]. Additionally, after genome sequencing of related myxobacterial *Sorangium sp.* (MSr11367, MSr11368, MSr11954), we found that there are phylogenetic differences between the strains compared to MSr12523. Interestingly, MAQ production was exclusively detectable in MSr12523, MSr11367, and MSr11368, which are genetically more closely related then MSr11954. Alongside their structural diversity, the AQs also bring with them a considerable number of biological effects. Based on the knowledge of the potential bioactivity, various assays were carried out in order to identify antimicrobial effects

against certain pathogens. The study of pyocyanin inhibition in *Pseudomonas aeruginosa* revealed that MAQ-302 (100 µM stock) achieved a maximum inhibition of 36% (data not shown). This result suggests the impact of MAQs on quorum sensing in Pseudomonas, which needs to be further investigated. Depending on the derivative, the MAQs exhibit remarkably potent antimycobacterial activity in the one-digit µM range. Unluckily, these MAQs also showed cytotoxic effects, but such effects might be addressed by semi- or total-synthesis of this compound class. As one result, anti-virulence PqsR-assay of our MAQs (-268, -282, -302, and -316) as inhibitors of quorum sensing of *Pseudomonas* showed only slight or no effect, depending on the derivative tested (data not shown). One hypothesis could be that the biological target of MAQs is predominantly found in myxobacteria and/or *Streptomyces*, but the structural similarity with the AQs of *Pseudomonas* and *Burkholderia* seems not to be coincidental.

To summarise, another producing AQ organism has been discovered, originating from the myxobacterial genus *Sorangium* by using the implemented co-cultivation approach[41]. So far, compounds belonging to the class of MAQs have not yet been tested for their effect against other myxobacteria. The MAQs could possibly serve as signal molecules and thus promote the biosynthesis of new compounds of further myxobacteria.

6.2.2.2 Thuggacin analogues from co-cultivation

The macrolide antibiotics known as thuggacins are moderately active against the causative agent of tuberculosis and produced by the myxobacterial strains *Sorangium cellulosum* So ce895 and *Chondromyces crocatus* Cm c5[42]. Some variants with different modified side chains, e.g. by hydroxylation, have already been discovered, but the core structures of the molecules show a considerable degree of similarity, except a few unique features (Figure 6.4).

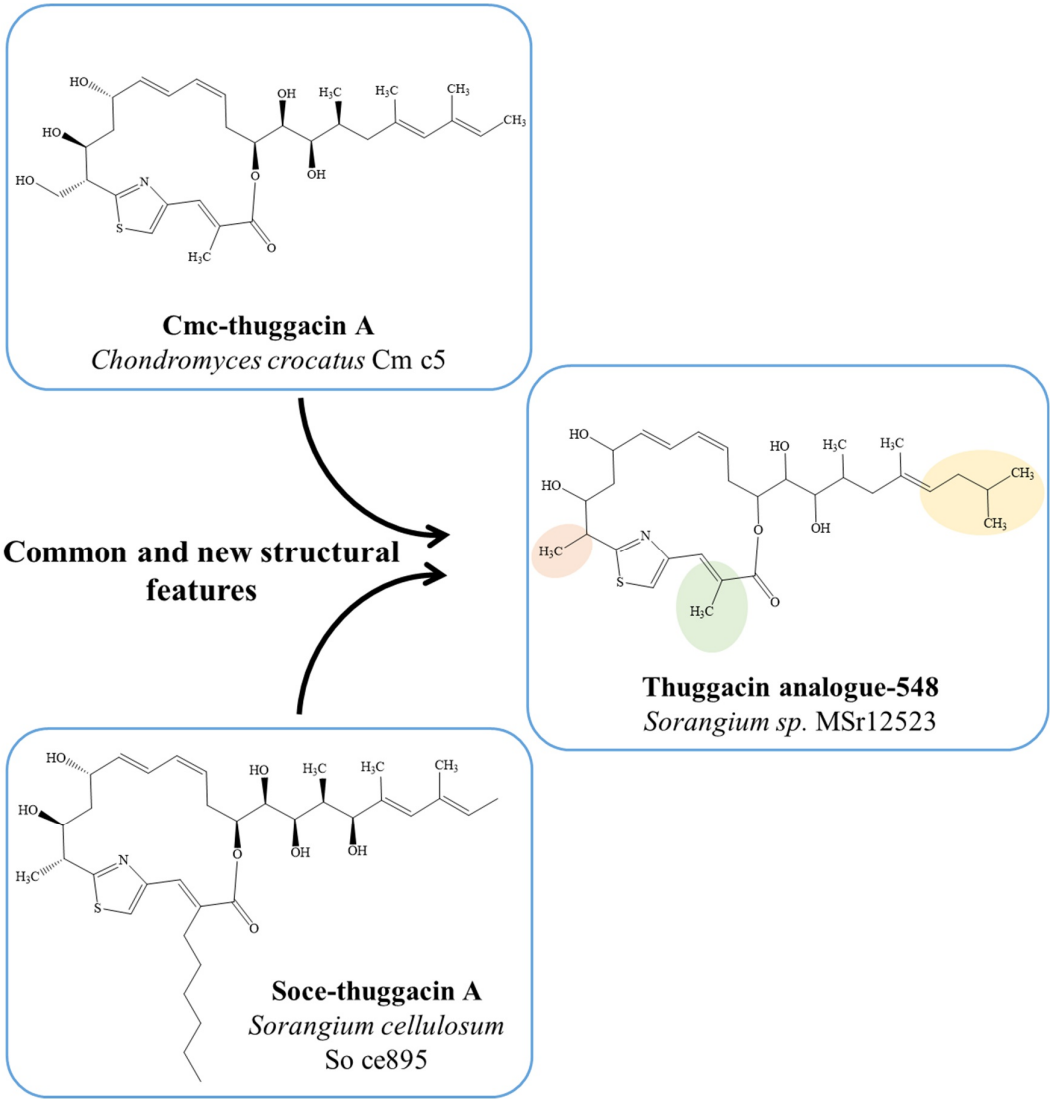

Figure 6.4: Chemical structures from the thuggacin family of *C. crocatus* Cm c5, *Sorangium sp.* MSr12523 and *S. cellulosum* So ce895. Unique chemical features highlighted for thuggacin analogue-548.

All elucidated structures of the new analogues (-548, -564, -566 and -578) possess an iso-valeryl-CoA starter unit that is incorporated at the start of the thuggacin assembly line in contrast to the previously described thuggacins. The relevant *thg1* (MSr12523) and *tugA* (Cm c5) genes show that they encode a different number of modules, which is probably related to an evolutionary development in this region. This leads to the assumption that Thg1 could be encoded by a version of *tugA* and *tgaA* (So ce895) genes.

Another important point to mention is that only thuggacin analogues-564, -566 and -578 which originate from the co-cultivation of MSr12523 and *T. soli* and *T. pseudospumae* contain the open–chain macrocyclic moiety, In addition and in contrast to the Soce-thuggacin A and analogue-548, these analogues did not show any antimycobacterial activity,

which may be explained by the opening of the macrocycle structure. Interestingly, the genus *Tsukamurella* belongs to the same order (*Mycobacteriales*) like *M. tuberculosis* 7H37Ra used to determine the antimycobacterial activity. It is considered a plausible hypothesis that during co-cultivation the partner strain *Tsukamurella* was recognised due to the cell–cell contact from *Sorangium sp.* MSr12523, triggering the respective BGC and leading to the biosynthesis of the thuggacin analogues as defence molecules in response[43,44]. As a defence strategy, *Tsukamurella* could then have secreted exoenzymes into the liquid environment for hydrolytic cleavage. This hypothesis is based on the fact that the open–chain macrocyclic moiety of the thuggacin analogues (-564, -566 and -578) were only detectable after co-cultivation with *Tsukamurella sp*. In contrast, in an axenic culture of *Sorangium sp.* MSr12523, there was only the thuggacin-548 observed with a cyclic configuration. The effect needs to be studied in more detail in future experiments. The addition of thuggacins to the culture of *Tsukamurella* might reveal potential bioactivity as well as provide evidence for a possible defence mechanism.

6.2.3 Innovative versus conventional cultivation systems

In the field of microbiology, for example, the term "OSMAC" (on strain many com-pounds) was created by Zeeck and co-workers at the turn of the 20th century[45]. However, the application of a variety of hundreds of unequal cultivation conditions or growth approaches to one single bacterium was done a very long time ago and enables the production of an altered set of microbial compounds that were previously inaccessible. The theory underlying the discrepancy between the number of SMs produced that could be observed and the number of BGCs encoding biosynthetic pathways was promoted by easier access to genome sequencing data[46].Some studies have already shown the influence on the metabolic profiles by altering media composition, pH, temperature, carbon sources, adding rare earth elements or elicitors, and comparing growth on solid and liquid environment[47–50].

The myxobacterial model organism *M. xanthus* DK1622, which is capable as known producer of nine different NP families[51–53], was selected to study the metabolic profiles in relation to growth on solid and in liquid environments. Several studies on this myxobacterium indicate complex regulation during solid surface behaviour, e.g. fruiting body formation[54,55], and the ability to adapt bacterial metabolome depending on the cultivation conditions in different life cycle stages applied[56]. In addition, *Hoffmann et. al.* discovered the homospermidine lipids as individual SMs only produced during fruiting body formation

growing under starving conditions on agar plate. The key limitation of that study was the isolation of pure substance from the solid-based cultivation system, which turned out to be a very laborious process and only small amounts of formed metabolites could be obtained[57].

Therefore, a new cultivation technique variant, the "Flow plate", was developed and used to investigate the possibility of easy access to specific metabolites that are predominantly synthesised during growth on solid-based cultivation systems such as agar plates. In principle, the cultivation of DK1622 with the Flow plate device enabled that individual produced metabolites diffused from the solid phase through a semi-permeable membrane into the liquid phase, where they accumulated. Notably, the known myxobacterial homospermidine lipids were only detected in the upper solid part of the flow plate and apparently were unable to diffuse through the semi-permeable membrane. Furthermore, the number of identified metabolites in the extracts after flow plate cultivation shows that improved growth conditions for the agar were achieved by the additional liquid phase. Thereby, the occurrence of a mixed DK1622 metabolic profile was evidenced by non-targeted metabolomics data analysis, which showed significant overlap of metabolites produced in both the solid-based (on agar) and liquid-based cultivation.

The exemplary semi-quantification of three different myxobacterial metabolites showed that even a low production level of the Flow plate device leads in an almost equal yield of the myxovirescin C, because the growth surface is more than twofold larger. In order to achieve an almost similar growth surface of the Flow plate, at least four agar plates are necessary. For a similar production yield of homospermidine-522 and cittilin A, three and thirteen agar plates, respectively, would need to be used to produce these particular metabolites in the same cultivation time. It should be noted that these calculations are based on a fixed extract concentration of 5 mg/mL and do not consider the absolute amounts of the extracts obtained from each experiment. Moreover, the Flow plate device enables different production yields depending on the metabolite, which can be used to improve accessibility to less abundant SMs for purification followed by structure elucidation and bioactivity testing.

In conclusion, the established solid-liquid cultivation platform offers the possibility of increased yields at comparable metabolite production levels, as well as the opening up of the SMs produced, both when growing on solid phase and on liquid medium. In particular, the execution of parallel cultivations with the same myxobacterium with variable conditions

can provide a deeper insight into the opportunities of the Flow plate device. A further development to the following Flow plate prototype is already in the pipeline, manufactured with 3D printing technology[58] playing a central role (Figure 6.5). One of the most important issues is the selection of the appropriate printing material, and its physical and chemical properties must be able to resist the sterilisation process. However, the versatility of use and the rapid implementation of design changes represent a tremendous opportunity for this technology in the field of biotechnological applications.

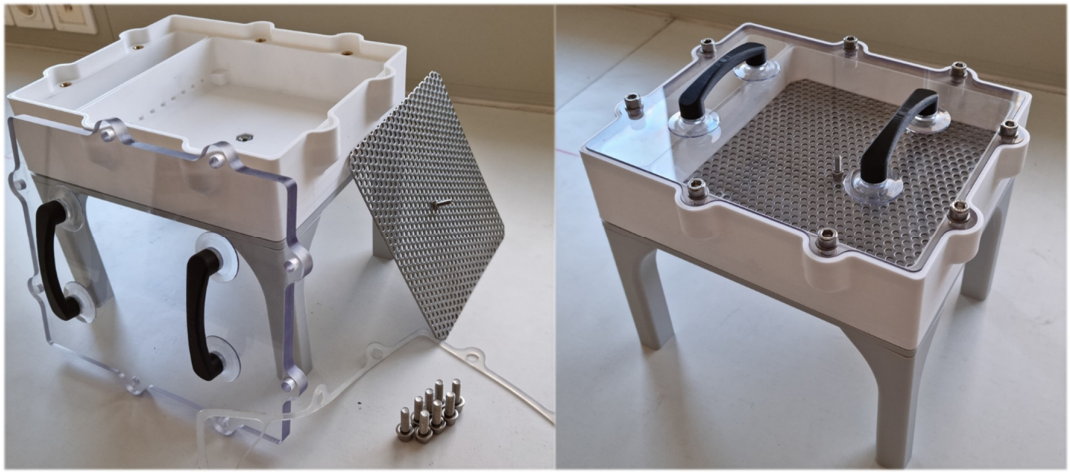

Figure 6.5: Second prototype of the Flow plate manufactured via 3D printing in co-operation with working group of Michael Wahl from Umwelt-Campus Birkenfeld[59].

6.2.4 Access to natural products - a question of the extraction process

Alongside the successful isolation and cultivation of microorganisms, the extraction process to obtain as many dissimilar SMs as possible across a diverse spectrum of chemical diversity is one of the most crucial steps in the discovery of NPs. If the extraction process is insufficient, i.e. the amount of metabolite is too poor or the chemical selectivity is too imbalanced, there is a discrepancy between formed and detected SMs. Today, there are more than a dozen different extraction methods available (e.g. maceration, acid-base extraction, percolation, ultrasound-assisted solvent, soxhlet extraction), which can be used with polar and non-polar solvents as well as in mixtures of them, according to the starting material for purification of the desired target compounds[60–63]. Every isolation and purification workflow must be preceded by extraction/release of the NPs from the natural source material.

Access to NPs of microbial natural products is impeded by the production yields and the complex mixture of SMs, which is usually lower than that of plants[64]. Likewise, there are

also differences at the production level of SMs between individual genera of actinobacteria. As an example, members of *Streptomyces* and *Myxococcales* are known for their SM formation and are characterised by highly different production rates. In a dedicated part of this work, supercritical fluid extraction (SFE) was implemented as opposed to conventional ultrasound-assisted extraction (UAE) as a microbial isolation technique for SMs. Due to their unique physiochemical properties, SFE offers a promising, as yet unexplored extraction technique for the search for new natural products from microbial metabolome.

In particular, the extraction efficiency depends on the physicochemical properties of supercritical CO_2 and the good yield of obtained metabolites emphasises these extraction methods. During the extraction with supercritical fluid is it possible to achieve a broad range of polarity in combination with a number of co-solvents, resulting in improved extraction conditions. It is therefore important to estimate the polarity of the SMs to be extracted in order to match the most appropriated co-solvent. Considering this extraction procedure with supercritical CO_2, in addition to the extraction of the bacterial SMs, a degree of selectivity can be achieved by the choice of solvent. Such a selective extraction step within the overall extraction process can increase the concentration of metabolites in the resulting fraction, fraction, making some metabolites accessible in the first place. As example, chloroxanthic acid A could be only isolated from the well-studied model organism *M. xanthus* DK1622 after application of supercritical fluid based extraction. Moreover, some antimicrobial activities have been observed only in SF extracts of MSr11367, while no activity was detected in the ultrasound-assisted extracts.

In summary, the concentration of particular metabolites in the extracts achieved with SFE enables isolation and structure elucidation without the requirement to upscale the culture volume in selected cases. This fact is particularly important for myxobacteria, which often exhibit a reduction in metabolite production when cultivation conditions are changed during upscaling. Thus, the SFE additionally opens up access to those microbial natural substances that cannot be reached with conventional extraction methods.

6.3 Final conclusion

Overall, this work underlines how complex the topic of natural product discovery is at present and highlights the significant challenges still waiting for us. At the same time, the presented studies provide an outlook towards alternative strategies in order to avoid some of the limitations of existing methods for the discovery of natural products. In light of the diverse roles that secondary metabolites play in the natural habitat of a microorganism it appears plausible to consider co-cultivation as an emerging strategy. Besides their extraordinary life cycle, myxobacteria are excellent manufacturers of an exciting diversity of natural products families. The combination of techniques applied in this thesis reinforces the notion that to date these interesting soil residents are still underestimated as producers of natural products.

6.4 References

(1) Schneider, Y. K. Bacterial Natural Product Drug Discovery for New Antibiotics: Strategies for Tackling the Problem of Antibiotic Resistance by Efficient Bioprospecting. *Antibiotics* **2021**, *10*.

(2) Cragg, G. M.; Newman, D. J. Natural products: a continuing source of novel drug leads. *Biochim. Biophys. Acta* **2013**, *1830*, 3670–3695.

(3) Pettit, R. K. Small‐molecule elicitation of microbial secondary metabolites. *Microb. Biotechnol.* **2011**, *4*, 471–478.

(4) Becker, H.; Scher, J. M.; Speakman, J.-B.; Zapp, J. Bioactivity guided isolation of antimicrobial compounds from *Lythrum salicaria*. *Fitoterapia* **2005**, *76*, 580–584.

(5) Dührkop, K.; Fleischauer, M.; Ludwig, M.; Aksenov, A. A.; Melnik, A. V.; Meusel, M.; Dorrestein, P. C.; Rousu, J.; Böcker, S. SIRIUS 4: a rapid tool for turning tandem mass spectra into metabolite structure information. *Nat. Methods* **2019**, *16*, 299–302.

(6) Wang, M.; Carver, J. J.; Phelan, V. V.; Sanchez, L. M.; Garg, N.; Peng, Y.; Nguyen, D. D.; Watrous, J.; Kapono, C. A.; Luzzatto-Knaan, T.*; et al.* Sharing and community curation of mass spectrometry data with Global Natural Products Social Molecular Networking. *Nat. Biotechnol.* **2016**, *34*, 828–837.

(7) Skropeta, D. Deep-sea natural products. *Natural product reports* **2008**, *25*, 1131–1166.

(8) Hoffmann, T.; Krug, D.; Bozkurt, N.; Duddela, S.; Jansen, R.; Garcia, R.; Gerth, K.; Steinmetz, H.; Müller, R. Correlating chemical diversity with taxonomic distance for discovery of natural products in myxobacteria. *Nat. Commun.* **2018**, *9*, 803.

(9) Lewis, K. New approaches to antimicrobial discovery. *Biochem Pharmacol* **2017**, *134*, 87–98.

(10) Luo, Y.; Cobb, R. E.; Zhao, H. Recent advances in natural product discovery. *Curr. Opin. Biotechnol.* **2014**, *30*, 230–237.

(11) Zhang, G.; Li, J.; Zhu, T.; Gu, Q.; Li, D. Advanced tools in marine natural drug discovery. *Curr. Opin. Biotechnol.* **2016**, *42*, 13–23.

(12) Pérez, J.; Muñoz-Dorado, J.; Braña, A. F.; Shimkets, L. J.; Sevillano, L.; Santamaría, R. I. *Myxococcus xanthus* induces actinorhodin overproduction and aerial mycelium formation by *Streptomyces coelicolor*. *Microb. Biotechnol.* **2011**, *4*, 175–183.

(13) Zhang, L.; An, R.; Wang, J.; Sun, N.; Zhang, S.; Hu, J.; Kuai, J. Exploring novel bioactive compounds from marine microbes. *Antimicrobials* **2005**, *8*, 276–281.

(14) Pan, R.; Bai, X.; Chen, J.; Zhang, H.; Wang, H. Exploring Structural Diversity of Microbe Secondary Metabolites Using OSMAC Strategy: A Literature Review. *Front. Microbiol.* **2019**, *10*, 294.

(15) Covington, B. C.; Xu, F.; Seyedsayamdost, M. R. A Natural Product Chemist's Guide to Unlocking Silent Biosynthetic Gene Clusters. *Annu. Rev. Biochem.* **2021**, *90*, 763–788.

(16) Medema, M. H.; Blin, K.; Cimermancic, P.; Jager, V. de; Zakrzewski, P.; Fischbach, M. A.; Weber, T.; Takano, E.; Breitling, R. antiSMASH: rapid identification, annotation and analysis of secondary metabolite biosynthesis gene clusters in bacterial and fungal genome sequences. *Nucleic Acids Res.* **2011**, *39*, W339-W346.

(17) Jose, P. A.; Jha, B. New Dimensions of Research on Actinomycetes: Quest for Next Generation Antibiotics. *Front. Microbiol.* **2016**, *7*, 1295.

(18) Bérdy, J. Bioactive Microbial Metabolites. *J Antibiot* **2005**, *58*, 1–26.

(19) Watve, M. G.; Tickoo, R.; Jog, M. M.; Bhole, B. D. How many antibiotics are produced by the genus Streptomyces? *Arch. Microbiol.* **2001**, *176*, 386–390.

(20) Müller, R.; Wink, J. Future potential for anti-infectives from bacteria - How to exploit biodiversity and genomic potential. *Int. J. Med. Microbiol.* **2014**, *304*, 3–13.

(21) Erol, Ö.; Schäberle, T. F.; Schmitz, A.; Rachid, S.; Gurgui, C.; El Omari, M.; Lohr, F.; Kehraus, S.; Piel, J.; Müller, R.*; et al.* Biosynthesis of the myxobacterial antibiotic corallopyronin A. *ChemBioChem* **2010**, *11*, 1235–1265.

(22) Gemperlein, K.; Zaburannyi, N.; Garcia, R.; La Clair, J.; Müller, R. Metabolic and Biosynthetic Diversity in Marine Myxobacteria. *Mar. Drugs* **2018**, *16*, 314.

(23) Onaka, H.; Mori, Y.; Igarashi, Y.; Furumai, T. Mycolic acid-containing bacteria induce natural-product biosynthesis in *Streptomyces* species. *Appl. Environ. Microbiol.* **2011**, *77*, 400–406.

(24) Zhu, H.; Sandiford, S. K.; van Wezel, G. P. Triggers and cues that activate antibiotic production by actinomycetes. *J. Ind. Microbiol. Biotechnol.* **2014**, *41*, 371–386.

(25) Tanaka, Y.; Hosaka, T.; Ochi, K. Rare earth elements activate the secondary metabolite-biosynthetic gene clusters in Streptomyces coelicolor A3(2). *J. Antibiot.* **2010**, *63*, 477–481.

(26) Scherlach, K.; Hertweck, C. Triggering cryptic natural product biosynthesis in microorganisms. *Org. Biomol. Chem.* **2009**, *7*, 1753–1760.

(27) Crüsemann, M.; O'Neill, E. C.; Larson, C. B.; Melnik, A. V.; Floros, D. J.; da Silva, R. R.; Jensen, P. R.; Dorrestein, P. C.; Moore, B. S. Prioritizing natural product diversity in a collection of 146 bacterial strains based on growth and extraction protocols. *J. Nat. Prod.* **2017**, *80*, 588–597.

(28) Bode, H. B.; Müller, R. Secondary metabolism in myxobacteria. In *Myxobacteria: Multicellularity and differentiation*; Whitworth, D., Ed.; ASM Press: Chicago, 2007; pp 259–282.

(29) Wenzel, S. C.; Müller, R. The impact of genomics on the exploitation of the myxobacterial secondary metabolome. *Nat. Prod. Rep.* **2009**, *26*, 1385–1407.

(30) Huo, L.; Hug, J. J.; Fu, C.; Bian, X.; Zhang, Y.; Müller, R. Heterologous expression of bacterial natural product biosynthetic pathways. *Nat. Prod. Rep.* **2019**, *36*, 1412-1436.

(31) Reen, F. J.; Romano, S.; Dobson, A. D. W.; O'Gara, F. The Sound of Silence: Activating Silent Biosynthetic Gene Clusters in Marine Microorganisms. *Mar. Drugs* **2015**, *13*, 4754–4783.

(32) Kim, J. H.; Lee, N.; Hwang, S.; Kim, W.; Lee, Y.; Cho, S.; Palsson, B. O.; Cho, B.-K. Discovery of novel secondary metabolites encoded in actinomycete genomes through coculture. *J. Ind. Microbiol. Biotechnol.* **2021**, *48*.

(33) Wu, M.-H.; Huang, S.-B.; Lee, G.-B. Microfluidic cell culture systems for drug research. *Lab on a chip* **2010**, *10*, 939–956.

(34) Meschke, H.; Walter, S.; Schrempf, H. Characterization and localization of prodiginines from *Streptomyces lividans* suppressing *Verticillium dahliae* in the absence or presence of *Arabidopsis thaliana*. *Environ. Microbiol.* **2012**, *14*, 940–952.

(35) Hoshino, S.; Wong, C. P.; Ozeki, M.; Zhang, H.; Hayashi, F.; Awakawa, T.; Asamizu, S.; Onaka, H.; Abe, I. Umezawamides, new bioactive polycyclic tetramate macrolactams isolated from a combined-culture of Umezawaea sp. and mycolic acid-containing bacterium. *J Antibiot* **2018**, *71*, 653–657.

(36) Reen, F. J.; McGlacken, G. P.; O'Gara, F. The expanding horizon of alkyl quinolone signalling and communication in polycellular interactomes. *FEMS Microbiol. Lett.* **2018**, *365*.

(37) Hays, E. E.; Wells, I. C.; Katzman, P. A.; Cain, C. K.; Jacobs, F. A.; Thayer, S. A.; Doisy, E. A.; Gaby, W. L.; Roberts, E. C.; Muir, R. D.*; et al.* Antibiotic substance produced by *Pseudomonas aeruginosa*. *J. Biol. Chem.* **1945**, *159*, 725–750.

(38) Pesci, E. C.; Milbank, J. B.; Pearson, J. P.; McKnight, S.; Kende, A. S.; Greenberg, E. P.; Iglewski, B. H. Quinolone signaling in the cell-to-cell communication system of *Pseudomonas aeruginosa*. *Proc. Natl. Acad. Sci. USA* **1999**, *96*, 11229–11234.

(39) Klaus, J. R.; Coulon, P. M. L.; Koirala, P.; Seyedsayamdost, M. R.; Déziel, E.; Chandler, J. R. Secondary metabolites from the *Burkholderia pseudomallei* complex: structure, ecology, and evolution. *J. Ind. Microbiol. Biotechnol.* **2020**, *47*, 877–887.

(40) Sams, T.; Baker, Y.; Hodgkinson, J.; Gross, J.; Spring, D.; Welch, M. The Pseudomonas Quinolone Signal (PQS). *Isr. J. Chem.* **2016**, *56*, 282–294.

(41) Ochi, K.; Hosaka, T. New strategies for drug discovery: activation of silent or weakly expressed microbial gene clusters. *Appl. Microbiol. Biotechnol.* **2013**, *97*, 87–98.

(42) Buntin, K.; Irschik, H.; Weissman, K. J.; Luxenburger, E.; Blöcker, H.; Müller, R. Biosynthesis of thuggacins in myxobacteria: comparative cluster analysis reveals basis for natural product structural diversity. *Chem. Biol.* **2010**, *17*, 342–356.

(43) Hoshino, S.; Ozeki, M.; Wong, C. P.; Zhang, H.; Hayashi, F.; Awakawa, T.; Morita, H.; Onaka, H.; Abe, I. Mirilactams C-E, Novel Polycyclic Macrolactams Isolated from Combined-Culture of *Actinosynnema mirum* NBRC 14064 and Mycolic Acid-Containing Bacterium. *Chem. Pharm. Bull.* **2018**, *66*, 660–667.

(44) Asamizu, S.; Ozaki, T.; Teramoto, K.; Satoh, K.; Onaka, H. Killing of Mycolic Acid-Containing Bacteria Aborted Induction of Antibiotic Production by *Streptomyces* in Combined-Culture. *PLoS ONE* **2015**, *10*, e0142372.

(45) Bode, H. B.; Bethe, B.; Höfs, R.; Zeeck, A. Big effects from Small Changes: Possible Ways to Explore Nature's Chemical Diversity. *ChemBioChem* **2002**, *3*, 619–627.

(46) Cimermancic, P.; Medema, M. H.; Claesen, J.; Kurita, K.; Wieland Brown, L. C.; Mavrommatis, K.; Pati, A.; Godfrey, P. A.; Koehrsen, M.; Clardy, J.*; et al.* Insights into secondary metabolism from a global analysis of prokaryotic biosynthetic gene clusters. *Cell* **2014**, *158*, 412–421.

(47) Kawai, K.; Wang, G.; Okamoto, S.; Ochi, K. The rare earth, scandium, causes antibiotic overproduction in *Streptomyces* spp. *FEMS Microbiol. Lett.* **2007**, *274*, 311–315.

(48) Biarnes-Carrera, M.; Breitling, R.; Takano, E. Butyrolactone signalling circuits for synthetic biology. *Curr. Opin. Chem. Biol.* **2015**, *28*, 91–98.

(49) Sánchez, S.; Chávez, A.; Forero, A.; García-Huante, Y.; Romero, A.; Sánchez, M.; Rocha, D.; Sánchez, B.; Avalos, M.; Guzmán-Trampe, S.*; et al.* Carbon source regulation of antibiotic production. *J. Antibiot.* **2010**, *63*, 442–459.

(50) Vandermolen, K. M.; Raja, H. A.; El-Elimat, T.; Oberlies, N. H. Evaluation of culture media for the production of secondary metabolites in a natural products screening program. *AMB Express* **2013**, *3*, 71.

(51) Cortina, N. S.; Krug, D.; Plaza, A.; Revermann, O.; Müller, R. Myxoprincomide: a natural product from *Myxococcus xanthus* discovered by comprehensive analysis of the secondary metabolome. *Angew. Chem. Int. Ed. Engl.* **2012**, *51*, 811–816.

(52) Volz, C.; Krug, D.; Müller, R. *Myxococcus xanthus* ist Mikrobe des Jahres 2020: Leben und Überleben im Boden. *Biologie in unserer Zeit* **2020**, *50*, 424–432.

(53) Krug, D.; Zurek, G.; Revermann, O.; Vos, M.; Velicer, G. J.; Müller, R. Discovering the Hidden Secondary Metabolome of *Myxococcus xanthus*: a Study of Intraspecific Diversity. *Appl. Environ. Microbiol.* **2008**, *74*, 3058–3068.

(54) Huntley, S.; Hamann, N.; Wegener-Feldbrügge, S.; Treuner-Lange, A.; Kube, M.; Reinhardt, R.; Klages, S.; Müller, R.; Ronning, C. M.; Nierman, W. C.*; et al.* Comparative Genomic Analysis of Fruiting Body Formation in Myxococcales. *Mol. Biol. Evol.* **2011**, *28*, 1083–1097.

(55) Bode, H. B.; Ring, M. W.; Schwär, G.; Kroppenstedt, R. M.; Kaiser, D.; Müller, R. 3-Hydroxy-3-methylglutaryl-coenzyme A (CoA) synthase is involved in the biosynthesis

of isovaleryl-CoA in the myxobacterium *Myxococcus xanthus* during fruiting body formation. *J. Bacteriol.* **2006**, *188*, 6524–6528.

(56) Meiser, P.; Bode, H. B.; Müller, R. The unique DKxanthene secondary metabolite family from the myxobacterium *Myxococcus xanthus* is required for developmental sporulation. *Proc. Natl. Acad. Sci. U.S.A.* **2006**, *103*, 19128–19133.

(57) Hoffmann, M.; Auerbach, D.; Panter, F.; Hoffmann, T.; Dorrestein, P. C.; Müller, R. Homospermidine Lipids: A compound class specifically formed during fruiting body formation of *Myxococcus xanthus* DK1622. *ACS Chem. Biol.* **2018**, *13*, 273–280.

(58) Shahrubudin, N.; Lee, T. C.; Ramlan, R. An Overview on 3D Printing Technology: Technological, Materials, and Applications. *Procedia Manuf.* **2019**, *35*, 1286–1296.

(59) te Heesen, H.; Wahl, M.; Bremer, M.; Huwer, A.; Messemer, J. Heterogene Einsatzfelder der generativen Fertigung. *Industrie Management* **2020**, *2020*, 25–29.

(60) King, J. W. Modern supercritical fluid technology for food applications. *Annu. rev. food sci. technol.* **2014**, *5*, 215–238.

(61) Sharma, B. R.; Kumar, V.; Gat, Y.; Kumar, N.; Parashar, A.; Pinakin, D. J. Microbial maceration: a sustainable approach for phytochemical extraction. *3 Biotech* **2018**, *8*.

(62) Rao, G. Optimization of ultrasound-assisted extraction of cyanidin 3-rutinoside from litchi (*Lichi chinensis* Sonn.) fruit pericarp. *Anal. Methods* **2010**, *2*, 1166.

(63) Delazar, A.; Nahar, L.; Hamedeyazdan, S.; Sarker, S. D. Microwave-assisted extraction in natural products isolation. *Methods Mol. Biol.* **2012**, *864*, 89–115.

(64) Olano, C.; Lombo, F.; Mendez, C.; Salas, J. A. Improving production of bioactive secondary metabolites in actinomycetes by metabolic engineering. *Metab. Eng.* **2008**, *10*, 281–292.